

# Physicochemical Problems of Mineral Processing

---

Index No. 32213X



ISSN 1643-1049

46

2011

# Physicochemical Problems of Mineral Processing 46 (2011)

## **Instructions for preparation of manuscripts**

It is recommended that the following guidelines be followed by the authors of the manuscripts:

- Original papers dealing with the principles of mineral processing and papers on technological aspects of mineral processing will be published in the journal which appears once a year
- The manuscript can be sent to the Editors for reviewing any time of year
- The manuscript should be written in English. For publishing in other languages an approval of the editor is necessary
- Contributors whose first language is not the language of the manuscript are urged to have their manuscript competently edited prior to submission
- The manuscript should not exceed 10 pages
- There is a 80 USD fee for printing the paper. No fee is required for the authors participating in the Annual Symposium on Physicochemical Problems on Mineral Processing
- Manuscripts and all correspondence regarding the symposium and journal should be sent to the editor.

## **Address of the Editorial Office**

Wrocław University of Technology  
Wybrzeże Wyspiańskiego 27, 50-370 Wrocław, Poland  
Institute of Mining Engineering  
Laboratory of Mineral Processing

Location of the Editorial Office:

pl. Teatralny 2, Wrocław, Poland  
phone: (+48 71) 320 68 79, (+48 71) 320 68 78  
fax: (+48 71) 344 81 23

jan.drzymala@pwr.wroc.pl  
zygmunt.sadowski@pwr.wroc.pl  
andrzej.luszczkiewicz@pwr.wroc.pl  
pawel.nowak <ncnowak@cyf-kr.edu.pl>

[www.minproc.pwr.wroc.pl/journal](http://www.minproc.pwr.wroc.pl/journal)

**Physicochemical Problems  
of Mineral Processing  
46 (2011)**

[www.minproc.pwr.wroc.pl/journal](http://www.minproc.pwr.wroc.pl/journal)

WROCLAW 2011

Editors

Jan Drzymała editor-in-chief  
Zygmunt Sadowski  
Andrzej Łuszczkiewicz  
Paweł Nowak

Editorial Board

Ashraf Amer, Wiesław Blaschke, Marian Brożek, Stanisław Chibowski, Tomasz Chmielewski, Beata Cwalina, Janusz Girczys, Andrzej Heim, Jan Hupka, Teofil Jesionowski, Andrzej Konieczny, Janusz Laskowski, Kazimierz Małyśa, Andrzej Pomianowski (honorary chairman), Stanisława Sanak-Rydlewska, Jerzy Sablik, Kazimierz Sztaba (chairman), Barbara Tora, Tadeusz Tumidajski

Technical assistance

Przemysław B. Kowalczyk

The papers published in the Physicochemical Problems of Mineral Processing journal are abstracted in Chemical Abstracts, Thomson Reuters (Science Citation Index Expanded, Materials Science Citation Index, Journal Citation Reports), Coal Abstracts, Google Scholar and other sources

This publication was supported in different forms by  
Komitet Górnictwa PAN  
(Seksja Wykorzystania Surowców Mineralnych)  
Akademia Górniczo-Hutnicza w Krakowie  
Politechnika Śląska w Gliwicach  
Politechnika Wroclawska

ISSN 1643-1049

OFICyna WYDAWNICZA POLITECHNIKI WROCLAWSKIEJ  
WYBRZEŻE WYSPIAŃSKIEGO 27, 50-370 WROCLAW, POLAND

## CONTENTS

R. Modrzewski, P. Wodziński, <i>Grained material classification on a double frequency screen</i> .....	5
M. Watanabe, P.B. Kowalczyk, J. Drzymala, <i>Analytical solution of equation relating maximum size of floating particle and its hydrophobicity</i> .....	13
T. Chmielewski, R. Kaleta, <i>Galvanic interactions of sulfide minerals in leaching of flotation concentrate from Lubin concentrator</i> .....	21
R. Ciccu, I. Kursun, <i>Potential advances in flotation by using water jets</i> .....	35
J. Aromaa, <i>Electrochemical dissolution of synthetic heazlewoodite (<math>Ni_3S_2</math>)</i> .....	51
W. Janusz, A. Sędlak, <i>Specific adsorption of carbonate ions at the hematite /aqueous electrolyte solution interface</i> .....	65
W. Janusz, E. Skwarek, <i>Adsorption of Ca(II) and Fe(III) ions at the <math>SnO_2</math>/electrolyte solution interface</i> .....	73
A. Pilarska, T. Jesionowski, <i>Synthesis of MgO in magnesium hydroxide carbonatisation process</i> .....	83
A. Taşdemir, H. Özdağ, G. Önal, <i>Image analysis of narrow size fractions obtained by sieve analysis - an evaluation by log-normal distribution and shape factors</i> .....	95
H.A.M. Ahmed, <i>Dry versus wet upgrading of nepheline syenite ores</i> .....	107
M. Ulewicz, E. Radzymińska-Lenarcik, <i>Transport of metal ions across polymer inclusion membrane with 1-alkylimidazole</i> .....	119
S. Pietarsaari, L. Rintala, J. Aromaa, <i>The application of public geological data in description of raw materials for hydrometallurgical processes</i> .....	131
T.P. Olejnik, <i>Milling kinetics of chosen rock materials under dry conditions considering strength and statistical properties of bed</i> .....	145
J. Gęga, W. Walkowiak, <i>Leaching of zinc and manganese from used up zinc-carbon batteries using aqueous sulfuric acid solutions</i> .....	155
A.M. Amer, <i>Kinetics of hydrometallurgical extraction of sulfur from Egyptian el-Maghara coal deposits</i> .....	163
V. Soltanmohammadi, M. Noaparast, A.H. Kohsari, F. Zamani, <i>Influence of flotation parameters on decreasing sulfur and phosphorus content of Gol-e-Gohar iron ore concentrate</i> .....	173

D.K. Szponder, K. Trybalski, <i>Determination of progressive research methodology of using modern measuring devices to determine physical, chemical and mineralogical properties of raw materials and mineral wastes</i> .....	191
K. Ochromowicz, T. Chmielewski, <i>Solvent extraction in hydrometallurgical processing of Polish copper concentrates</i> .....	207
A. Obraniak, T. Gluba, <i>A model of granule porosity changes during drum granulation</i> .....	219
L. Rintala, K. Lillkung, J. Aromaa, <i>The use of decision and optimization methods in selection of hydrometallurgical unit process alternatives</i> .....	229
A. Korkosz, M. Niewiadomski, J. Hupka, <i>Investigation of properties of swimming pool water treatment sediments</i> .....	243
Y. Abali, S.U. Bayca, K. Arisoy, A.I. Vaizogullar, <i>Optimization of dolomite ore leaching in hydrochloric acid solutions</i> .....	253
M. Lundström, J. Aromaa, O. Forsén, <i>Microscopy and XRD investigations of the product layer formed during chalcopyrite leaching in copper(II) chloride solutions</i> .....	263
F. Ciesielczyk, T. Jesionowski, <i>Characterisation of highly dispersed magnesium silicates prepared from silica sols and selected magnesium salts</i> .....	279
B. Gajda, A. Skrzypczak, M.B. Bogacki, <i>Separation of cobalt(II), nickel(II), zinc(II) and cadmium(II) ions from chloride solution</i> .....	289
A.A. El-Midany, S.S. Ibrahim, <i>The interfacial role of compatibilizers to improve mechanical properties of silica-polypropylene composites</i> .....	295
Dr. Eng. Zofia Blaschke - a tribute on her 70th birthday .....	307
Professor Andrzej Krysztafkiewicz, Ph.D., D.Sc. (1947-2010).....	315

Remigiusz MODRZEWSKI\*, Piotr WODZIŃSKI\*

## GRAINED MATERIAL CLASSIFICATION ON A DOUBLE FREQUENCY SCREEN

*Received April 10, 2010; reviewed; accepted May 5, 2010*

The present study demonstrates the results of research carried out at the Department of Process Equipment, Technical University of Lodz, devoted to double-frequency screens. Process investigations were aimed at determination of efficiency and capacity of an experimental screen on a semi-commercial scale. The project assumptions of an industrial machine were presented.

*keywords: screening, screen, sub-sieve, grained material, grain classes*

### 1. INTRODUCTION

Construction of well performing industrial screen is a challenging and difficult task. Our present investigations were aimed to determine efficiency and capacity of a semi-commercial screen. The tests were carried out using an experimental stand (Wodziński, 1997) (Fig. 1), which consisted of charging hopper 1, a riddle with a sieve 2, an upper driving vibrator 3 of rotational speed  $\omega_1$ , bottom driving vibrator 4 of rotational speed  $\omega_2$ , spring suspension 5 mounted at the lifting construction and a

---

\* Łódź University of Technology, ul. Wólczajska 175, 90-924 Łódź, Poland, wodzinsk@wipos.p.lodz.pl

container for above-screen product 6 and under-screen product 7.

The screen has a possibility of vibrator set-up change from 0 to 380 mm in respect of the centre (Fig. 2). A change of the vibrator spacing causes a change of oscillation path angle of screen  $\beta$ .

In the course of process investigations three different configurations were applied:

- vibrators arranged one under another in the centre of the riddle,  $\beta=0^\circ$  (Fig. 2a)
- vibrators spaced in respect of the centre by 110 mm,  $\beta=27,5^\circ$  (Fig. 2b)
- vibrators spaced in respect of the centre by 380 mm,  $\beta=61^\circ$  (Fig. 2c).

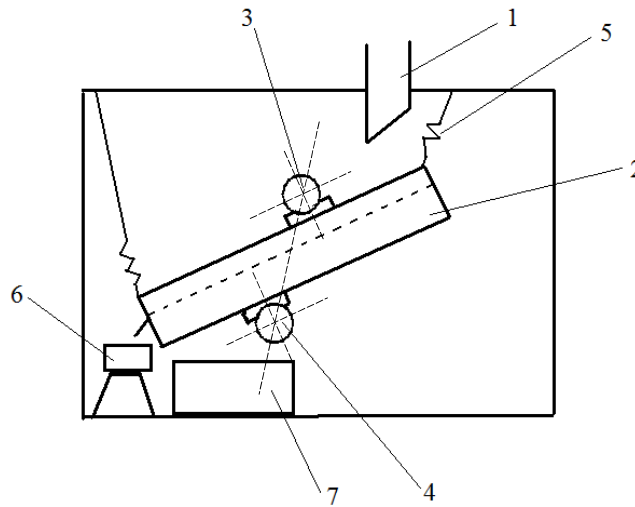


Fig. 1. Experimental screen

The experimental stand is equipped with an inverter being the system of vibrators' control. The inverter allows for the change of current frequency which makes it possible to attain various rotational speeds of vibrators. This enables to change the direction of vibrators' shafts rotation. The control panel contains two separate regulators for the upper and bottom engine. The maximum rotational speed possible to be obtained using the control panel is equal to 1500 rpm.

In the course of investigations the speed and direction of only one vibrator were altered. This was the bottom vibrator ( $\omega_2$ ). On the other hand, the upper engine ( $\omega_1$ ) was set on the maximum rotational speed and was not subjected to any modifications.

In the course of investigations the following machine operation parameters were changed:

- intensity of feed inflow
- rotational speed of bottom vibrator (4 variants were investigated:  $\omega_2 = \omega_{\max}$ ,  $\omega_2 = 2/3 \cdot \omega_{\max}$ ,  $\omega_2 = 1/2 \cdot \omega_{\max}$  and  $\omega_2 = 1/3 \cdot \omega_{\max}$ )
- the rotation direction of the bottom vibrator (to the right or to the left)

- the exciting force of the upper vibrator (3 variants were examined:  $F_1 = F_{\max}$ ,  $F_1 = 50\% F_{\max}$  and  $F_1 = 25\% F_{\max}$ )
- electro-vibrators arrangement in respect of the centre ( $\beta=0^\circ$ ,  $\beta=27,5^\circ$  and  $\beta=61^\circ$ ).

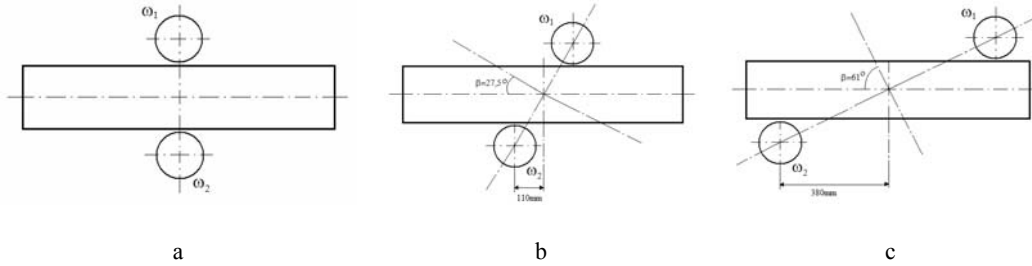


Fig. 2. Vibration engines layout

## 2. PROCESS INVESTIGATION

Loose material utilized for investigations was as follows: agalite (a model material of spherical grains), sand (irregular grains) and marble aggregate (sharp-edged grains). The material had been prepared beforehand, i.e. it had been screened in laboratory shakers, so the half of feed mass was the upper fraction and the other half was the bottom fraction. The granulometric composition was the same for all materials applied.

Screening efficiency ( $\eta$ ) and screening capacities ( $Q$  and  $q$ ) were calculated according to the following formulas (Banaszewski, 1990; Sztaba, 1993; Dietrych 1962):

- screening efficiency

$$\eta = \frac{m_d}{m_n \cdot K_d} [-] \quad (1)$$

- screening capacity

$$Q = \frac{m_n}{t_1} \quad [\text{kg/s}] \quad (2)$$

$$q = \frac{m_n}{t_1 \cdot S} \quad [\text{kg/m}^2 \cdot \text{s}] \quad (3)$$

$$S = B \cdot L \quad [\text{m}^2] \quad (4)$$

where

$m_d$  – mass of bottom product [kg]

$m_n$  – mass of feed = 30 kg

$K_d$  – bottom class fraction in feed = 50%

$t_1$  – the time of material pouring out [s]

$L$  – the length of screen's sub-sieve = 1.325 m

$B$  – width of screen's sub-sieve = 0.295 m

$S$  – surface of screen's sub-sieve = 0.39 m<sup>2</sup>.

The results of investigations are presented in the form of efficiency–capacity dependences. The example diagrams 3 - 8 allow to assess how the ratio of rotational speeds of driving vibrators changes influence the process of screening.

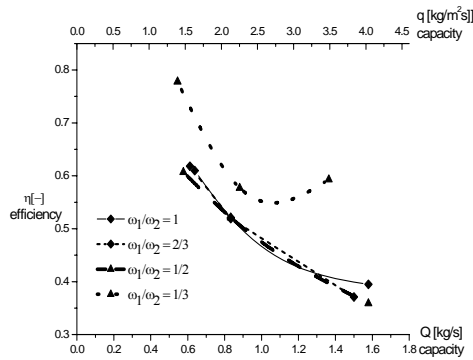


Fig. 3. Results for setting  
 $\beta = 0^\circ$ ,  $\alpha = 20^\circ$ ,  $F = 2$  kN

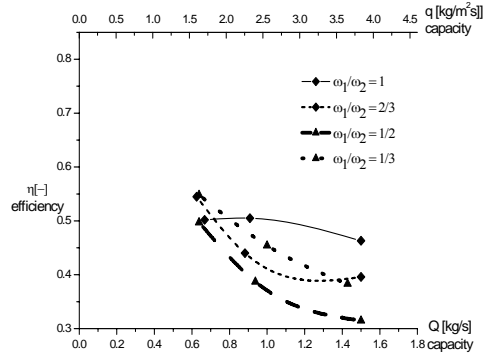


Fig. 4. Results for setting  
 $\beta = 0^\circ$ ,  $\alpha = 20^\circ$ ,  $F = 1$  kN

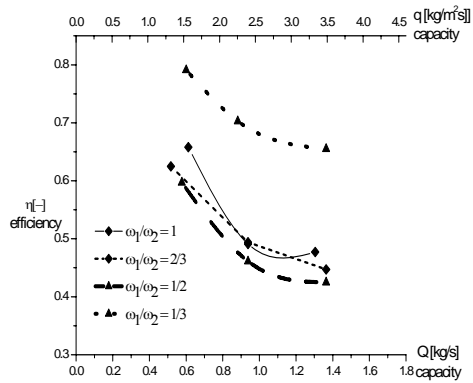


Fig. 5. Results for setting  
 $\beta = 0^\circ$ ,  $\alpha = 20^\circ$ ,  $F = 0.5$  kN

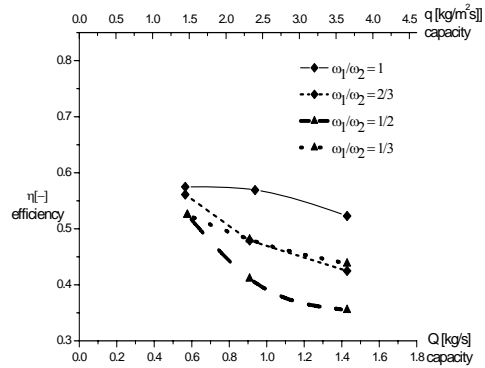


Fig. 6. Results for setting  
 $\beta = 27,5^\circ$ ,  $\alpha = 20^\circ$ ,  $F = 1$  kN

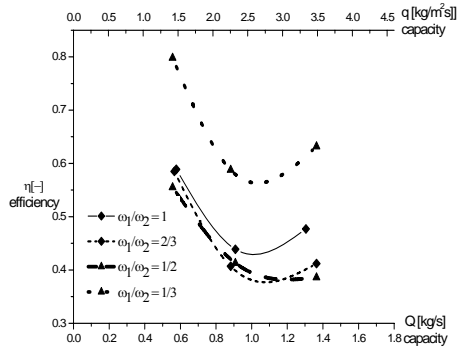


Fig. 7. The results for the following settings  
 $\beta = 27.5^\circ$ ,  $\alpha = 20^\circ$ ,  $F = 0.5$  kN

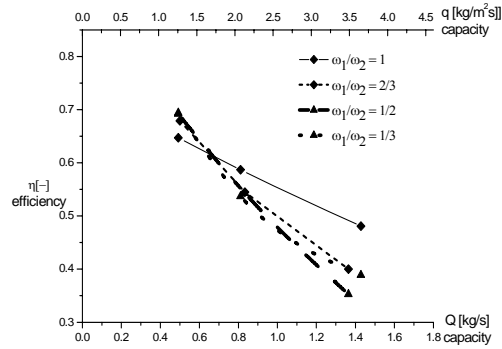


Fig. 8. Results for setting  
 $\beta = 61^\circ$ ,  $\alpha = 20^\circ$ ,  $F = 2$  kN

### 3. DEFINING PROJECT ASSUMPTIONS

The analysis of the obtained investigation results allowed to define the range of optimal operation parameters of a double screen (Table 1), which will shorten and simplify the subsequent stage of work being the screen investigation on an industrial scale.

Table. 1. The most beneficial operation parameters of a double-screen

Inclination angle of a sieve	Engine spacing	Exciting forces	Angular velocity ( $\omega_1/\omega_2$ ratio)
20°	0	1/4	1/3
	0	1/4	-1/3
	1/3	1/4	1/3
	1/3	1/4	-1/3
	max	1/4	1/3
	max	1/4	-1/3

Optimization of the drive operation is carried out through the regulation of the vibrators rotational frequency, their exciting force and mutual location as well as the direction of rotations. Based on the examination, it may be stated that:

- countercurrent synchronization of vibrators is better from the process point of view
- application of vibrators of considerable power is not economically justified
- location of vibrators with regard to the mass centre does not affect the process

- screen drive system allows to obtain a complex sieve motion which, in turn, enables to attain high screening efficiency
- double-frequency screen should be assigned to the screening of finely grained materials and those which are screened with difficulty due to the fact that the machine brings about intensive loosening of material on the sieve
- condition of proper operation of the screen is to ensure the rigidity of the sieve on the plane of vibration trajectories.

The phenomenon of driving vibrators self-synchronization (Modrzewski and Wodziński, 2009) enables to simplify the construction of the screen because it is not necessary to apply any devices which would trigger the synchronization. Self-synchronization is a durable phenomenon. In the course of the measurements the motion once appeared in trajectories, depends exclusively upon the configuration of the driving system.

The construction of the line-elliptic screen allows the application of all known construction elements of the screening machines which makes it easier to apply this screen practically in industry.

#### 4. INDUSTRIAL DOUBLE FREQUENCY SCREEN

Based on the investigations discussed in the present study the project assumptions for construction of a double frequency screen devoted to a sand mine in Inowłodz (Mikrosil Company, Poland) were prepared. The machine is characterized by a screen inclination angle  $\alpha = 18^\circ$  in respect of the level. The angle of screen paths is  $\beta = 0^\circ$ . The screen is equipped with a 3-deck riddle in which there are mounted screens of the hole size of,  $l_1 = 2.4$  mm,  $l_2 = 1.5$  mm and  $l_3 = 0.7$  mm. Screen size is: length  $L = 4.0$  m, width  $B = 1.5$  m.

For the drive of the machine, an axial rotational and modular vibrator of static moment from 100 to 210 Nm (from 10 to 21 kGm) was applied. This is the main vibrator located between the second and third screen deck. An electrovibrator (an unbalanced engine) being the second rotational vibrator, is located above the riddle. This is an electrovibrator of nominal rotations of  $1460 \text{ min}^{-1}$  and characterized by the operation moment equal to 900 kGm and the static moment equal to 450 kGm.

The process of screening will be conducted under dry or wet conditions applying water spray (Wolff, 1979). A charging–water hopper should be located under the screen for collecting the finest product (under-screen product) whereas above-screen products from all screen decks should be collected by chutes mounted to the lifting construction. The height of screening product collection points over hardened bed should make it possible to install there typical ribbon conveyors dedicated to collection of screening products. The integral equipment of the screen is the control

panel comprising drive control elements (inverters, contactors, safety devices, etc.).

The double-frequency screen is a multi-variant machine, which means that it may be constructed in various construction versions. The scheme of a prototype screen is presented in Fig. 9. Vibrating mass of the screen WH3–1.5x4.0 is equal to 4500 kg. The whole installation is presented schematically in Fig. 10.

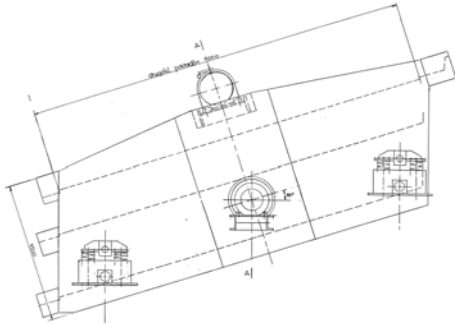


Fig. 9. Double frequency screen WH3-1.5 x 4.0

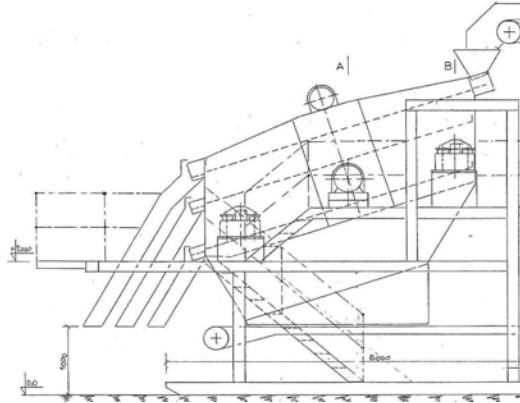


Fig. 10. Double frequency screen installation

## 5. CONCLUSIONS

The main feature of the double-frequency screen is the possibility of free configuration of the inertia drive and thus the possibility of its compliance with the requirements set by the process of screening of a given granular material. This screen is a universal screen based on the experience gained so far on the structure and exploitation of screening machines. Furthermore, this screen is characterized by a uniform distribution of the oscillating masses which does not take place in the case of the constructions which have been known up to the present moment.

## ACKNOWLEDGMENTS

This study was performed as a part of chartered assignment W-10/12/2010/Dz.St.

## REFERENCES

- BANASZEWSKI T., 1990. *Przesiewacze*, Wydawnictwo „Śląsk”, Katowice  
 WODZIŃSKI P., 1997. *Przesiewnie i przesiewacze*, Wydawnictwo Politechniki Łódzkiej, Łódź

- SZTABA K., 1993. *Przesiewanie*, Śląskie Wydawnictwo Techniczne, Katowice
- DIETRYCH J., 1962. *Teoria i budowa przesiewaczy*, Wydawnictwo Górniczo – Hutnicze, Katowice
- WOLFF K., 1979. *Systemsiebboden für Siebmaschinen*, Aufbereitungs Technik, Essen
- MODRZEWSKI R., WODZIŃSKI P., 2010. *The results of process investigations of a double-frequency screen*, Physicochem. Probl. Miner. Process., 44, 169-178

**Modrzewski, R., Wodziński, P.,** *Klasyfikacja materiałów ziarnistych na przesiewaczu dwuczęściowym*, Physicochem. Probl. Miner. Process., 45 (2011) 5-12, (w jęz. ang), <http://www.minproc.pwr.wroc.pl/journal>

Niniejsza praca prezentuje wyniki programu badawczego prowadzonego w Katedrze Aparatury Procesowej Politechniki Łódzkiej, poświęconego przesiewaczom dwuczęściowym. Badania procesowe miały na celu określenie sprawności i wydajności przesiewacza doświadczalnego w skali półtechnicznej. Do napędu przesiewacza stosowane są dwa wibratory rotacyjne o jednakowych lub niejednakowych momentach statycznych. Jak sama nazwa wskazuje jest to przesiewacz, który charakteryzuje się dwiema różnymi prędkościami obrotowymi tych wibratorów napędowych. Konstrukcja przesiewacza umożliwia regulację wszystkich podstawowych parametrów pracy maszyny, w szczególności takich jak: nachylenie rzeszota względem poziomu, ustawienie silników względem środka rzeszota, siły wymuszające wytwarzane przez silniki oraz prędkości obrotowe tych silników.

Głównym celem niniejszego opracowania jest przedstawienie wyników badań procesowych tego przesiewacza dla różnych konfiguracji napędu, w postaci graficznych zależności sprawnościowo-wydajnościowych. Na ich podstawie zostały opracowane założenia projektowe maszyny przemysłowej

*słowa kluczowe: przesiewanie, przesiewacz, sito, materiał ziarnisty, klasy ziarnowe*

Masahiro WATANABE\*, Przemyslaw B. KOWALCZUK \*\*, Jan DRZYMALA \*\*

## **ANALYTICAL SOLUTION OF EQUATION RELATING MAXIMUM SIZE OF FLOATING PARTICLE AND ITS HYDROPHOBICITY**

*Received April 2, 2010; reviewed; accepted June 20, 2010*

An analytical form of the equation relating particle hydrophobicity, expressed as the so-called contact angle, and the maximum size of spherical particle able to float with a bubble is presented. The starting equation, which is based on the balance of forces operating at the moment of particle detachment from a bubble, can be solved only numerically. In this paper the third-degree polynomial equation is transformed into an analytical trigonometric function. Although there are several roots of the equation, practically only one is valid for the detachment contact angle calculation.

*keywords: flotation, flotometry, contact angle, particle size, cubic equation*

### 1. INTRODUCTION

Well designed flotation experiments can be used for determination or estimation of different properties of the system. One of them is the so-called contact angle which reflects the hydrophobicity of particles. The procedure of contact angle determination is based on measuring the maximum size of floating particles and using equations, which result from a balance of forces at the moment of particle-bubble rupture. It was applied in the particle levitation technique (Li et al., 1993), bubble-capture-by-particles method (Hanning and Rutter, 1989) and Hallimond cell flotation experiments (Drzymala, 1994). The method, also called flotometry (Konovalov and Tikhonov, 1982; Drzymala and Lekki, 1989), provides a detachment contact angle being

---

\* 4-28-1 Minami-Sakasai, Kashiwa-shi, Chiba 277-0043, Japan, [mwsqp@yahoo.co.jp](mailto:mwsqp@yahoo.co.jp)

\*\* Wrocław University of Technology, Wybrzeże Wyspińskiego 27, 50-370 Wrocław, Poland, [przemyslaw.kowalczuk@pwr.wroc.pl](mailto:przemyslaw.kowalczuk@pwr.wroc.pl), [jan.drzymala@pwr.wroc.pl](mailto:jan.drzymala@pwr.wroc.pl)

equivalent to the advancing contact angle, which can be simply recalculated into the equilibrium (Young's) contact angle.

The derivation of the equation relating the maximum size of floating spherical particle and hydrophobicity of the particle starts with the balance of forces involved in the process. Assuming that the main adhesive force is the capillary force  $F_\sigma$  and that the detachment occurs when the capillary force reaches maximum  $F_{\sigma(\max)}$  (Scheludko et al. 1976, Drzymala, 1994), the balance (Fig. 1) is:

$$F_{\sigma(\max)} - F_w - F_e - F_a = 0 \quad (1)$$

where  $F_w$  is the weight of particle partially immersed (due to attachment to the bubble) in a liquid,  $F_e$  denotes the excess force, and  $F_a$  stands for different forces generated during movement of bubbles with the attached particles, both immersed in the liquid medium.

Another assumption regarding the adhesive forces in the balance was proposed by Nguyen (2003, 2004). Since it is based on non-existing forces such as the weight of a completely immersed particle, this approach does not seem to be correct.

The maximum capillary force at the moment of particle detachment from the bubble,  $F_{\sigma(\max)}$ , is expressed by the equation:

$$F_{\sigma(\max)} = \pi r_{\max} \sigma (1 - \cos \theta_d), \quad (2)$$

where  $\sigma$  is liquid surface tension,  $r_{\max}$  maximum radius of floating spherical particle,  $\theta_d$  angle of detachment of particles from bubble (equivalent to the advancing contact angle) and  $\pi$  is 3.14.

The weight of the particle partially immersed in water  $F_w$  is in fact equal to  $F_g - F_b$ , where  $F_g$  is the gravity force and  $F_b$  is the buoyancy:

$$F_w = \frac{4}{3} \pi r_{\max}^3 \rho_p g - \pi r_{\max}^3 \rho_w g \left[ \frac{2}{3} + \cos(\theta_d/2) - \frac{1}{3} \cos^3(\theta_d/2) \right], \quad (3)$$

where  $\rho_w$  is density of liquid,  $\rho_p$  density of particle,  $g$  acceleration due to gravity while  $r_{\max} \leq R$ .

The excess force  $F_e$  is defined as  $(F_p - F_h)$ , where  $F_p$  is an additional pressure inside the bubble and  $F_h$  stands for the hydrostatic pressure and is given by:

$$F_e = F_p - F_h = \pi r_{\max}^2 (1 - \cos \theta_d) (\sigma/R - R \rho_w g), \quad (4)$$

where  $R$  is bubble radius.

There are also hydrodynamic forces in the system. Their list includes inertia, drag, diffusive, and other forces (Morris and Matthesius, 1988). For practical purpose it was proposed by Schulze (1993), and later by Ralston (Gontijo et al., 2007), to combine the hydrodynamic forces into one effective acceleration force,  $F_a$ . The mathematical formula for the effective acceleration force is not well established. Gontijo et al.

(2007) used:

$$F_a = \frac{4}{3} \pi r^3 \rho_p a \quad (5)$$

where  $a$  is the acceleration of particle in the external flow field. Another expression in which  $\rho_p - \rho_w$  instead of  $\rho_p$  in Eq. (5) was used by Mitrofanov et al. (1970) while Koch and Noworyta (1992) used  $\rho_p + f\rho_w$  instead of  $\rho_p$  in Eq. (5) (where  $f$  is a constant). Since the acceleration force does not depend on contact angle, the inversion of the numerical equation into the analytical form does not require, during the derivation, the knowledge of the detailed expression for  $F_a$ .

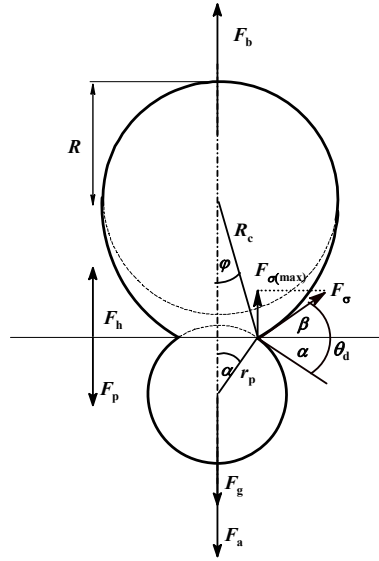


Fig. 1. Particle-bubble aggregate at the moment of particle detachment when the contact angle becomes detachment angle  $\theta_d$ .  $F_\sigma$  denotes capillary force,  $\alpha$  central angle,  $\beta$  angular inclination of meniscus at the three-phase contact,  $\varphi$  central angle at the bubble center,  $R_c$  bubble curvature,  $r_p = r_{\max}$ . Other symbols are explained in the text

Taking into account expressions for appropriate forces one gets the following equation:

$$\pi r_{\max} \sigma (1 - \cos \theta_d) - \left\{ \frac{4}{3} \pi r_{\max}^3 \rho_p g - \pi r_{\max}^3 \rho_w g \left[ \frac{2}{3} + \cos(\theta_d/2) - \frac{1}{3} \cos^3(\theta_d/2) \right] \right\} - \pi r_{\max}^2 (1 - \cos \theta_d) (\sigma/R - R \rho_w g) - F_a = 0. \quad (6)$$

Analytical solution of Eq. (6) for  $r_{\max}$  can be easily obtained since it becomes a quadratic equation of  $r_{\max}$  after division by  $r_{\max}$ . On the other hand is it much more difficult to solve Eq. (6) for  $\theta_d$  because it assumes a cubic form. The solution of Eq. (6) is presented in this paper.

## 2. SOLUTION

In Eq. (6) the detachment angle occurs as  $\theta_d$  and  $\theta_d/2$ . Therefore, we have to use the double-angle formula for cosine,  $\cos \theta_d = 2\cos^2(\theta_d/2) - 1$ . Substituting this into Eq. (6), we obtain a cubic equation:

$$X^3 + 3AX^2 - 3X - 3A + 2B = 0, \quad (7)$$

where

$$X = \cos(\theta_d / 2) \quad (0 < X < 1), \quad (8)$$

$$A = \frac{2\sigma(1 - r_{\max} / R)}{r_{\max}^2 \rho_w g} + \frac{2R}{r_{\max}} \quad (2 \leq A), \quad (9)$$

$$B = 1 + 2 \cdot \frac{\rho_p - \rho_w}{\rho_w} + \frac{3F_a}{2\pi r_{\max}^3 \rho_w g} \quad (1 < B). \quad (10)$$

The ranges of  $X$ ,  $A$  and  $B$  are due to  $0^\circ < \theta_d < 180^\circ$ ,  $r_{\max} \leq R$  and  $\rho_w < \rho_p$ , respectively. Analytical solutions of cubic equations are known, therefore we are able to solve Eq. (7) for  $X$  and then calculate  $\theta_d$ , because  $\theta_d = 2\arccos X$ .

To eliminate the second-degree term in Eq. (7), we put

$$X = Y - A, \quad (11)$$

and next we get a reduced cubic equation:

$$Y^3 - 3(A^2 + 1)Y + 2(A^3 + B) = 0. \quad (12)$$

To solve Eq. (12) one can use either algebraic or trigonometric solution. Since both provide the same results, only the algebraic path is presented in this paper.

Equation (12) can be solved by a well-known cubic formula (Bewersdorff, 2006; Cox, 2004; Dickson, 1914; King, 1996; Rotman, 2000; Rotman, 2007; Uspensky, 1948):

$$Y = \sqrt[3]{-(A^3 + B) + \sqrt{D}} \cdot \left(-\frac{1}{2} + \frac{\sqrt{3}}{2}i\right)^{j-1} + \sqrt[3]{-(A^3 + B) - \sqrt{D}} \cdot \left(-\frac{1}{2} - \frac{\sqrt{3}}{2}i\right)^{j-1} \quad (13)$$

where  $j=1, 2, 3$ , and  $D$  denotes the discriminant, in our case defined as:

$$D = (A^3 + B)^2 - (A^2 + 1)^3, \quad (14)$$

which can be either zero or positive, or even negative. Using Eq. (13), taking into account the signs of  $D$ , we have 3·3, that is 9, solutions.

For  $D = 0$  or  $B = (A^2 + 1)^{3/2} - A^3$ , it is known that there are three real roots of a

reduced cubic equation and at least two of them are equal. The roots of Eq. (7) are given by:

$$X_{Z1} = -2\sqrt{A^2 + 1} - A, \quad (15)$$

$$X_{Z2} = X_{Z3} = \sqrt{A^2 + 1} - A, \quad (16)$$

where Z denotes that  $D$  is zero.  $X_{Z1}$  is negative while  $X_{Z2}$  and  $X_{Z3}$  are within the range of  $0 < X < 1$  (Fig. 2).

For  $D > 0$  or  $B > (A^2 + 1)^{3/2} - A^3$ , a reduced cubic equation has one real root and two imaginary roots. The real root of Eq. (7), in which we are interested, is given by:

$$X_{P1} = -\sqrt[3]{A^3 + B - \sqrt{(A^3 + B)^2 - (A^2 + 1)^3}} - \sqrt[3]{A^3 + B + \sqrt{(A^3 + B)^2 - (A^2 + 1)^3}} - A \quad (17)$$

where P denotes that  $D$  is positive. The expression for  $X_{P1}$  clearly indicates that  $X_{P1}$  is negative and should be rejected. Discussion on the imaginary roots  $X_{P2}$  and  $X_{P3}$  is omitted.

For  $D < 0$  (called the *casus irreducibilis*) or  $B < (A^2 + 1)^{3/2} - A^3$ , there are three distinct real roots and Eq. (13) leads to the following equation (Bewersdorff, 2006; Dickson, 1914; King, 1996; Uspensky, 1948):

$$Y_{Nj} = 2\sqrt{A^2 + 1} \cos \left[ \frac{\phi}{3} + \frac{2(j-1)\pi}{3} \right] \quad (j = 1, 2, 3), \quad (18)$$

where N denotes that  $D$  is negative, and  $\phi$  is defined as:

$$\phi = \arccos \left[ -\frac{A^3 + B}{(A^2 + 1)^{3/2}} \right] \quad (\phi < \pi). \quad (19)$$

As  $\phi$  is in the second quadrant, it can be shown that  $X_{N2}$ :

$$X_{N2} = 2\sqrt{A^2 + 1} \cos \left( \frac{\phi}{3} + \frac{2\pi}{3} \right) - A, \quad (20)$$

is outside the range of  $0 < X < 1$ .  $X_{N1}$  and  $X_{N3}$  are:

$$X_{N1} = 2\sqrt{A^2 + 1} \cos \frac{\phi}{3} - A, \quad (21)$$

$$X_{N3} = 2\sqrt{A^2 + 1} \cos \left( \frac{\phi}{3} + \frac{4\pi}{3} \right) - A, \quad (22)$$

and their boundary is  $X_{Z2}$  or  $X_{Z3}$ .  $X_{N1}$  is always in the range of  $0 < X < 1$  and provides detachment angles between  $0^\circ$  and  $180^\circ$ . On the other hand  $X_{N3}$  yields different values from  $X_{N1}$  for a given set of  $A$  and  $B$ , and may be in the range of  $0 < X < 1$ , or  $X < 5^{1/2} - 2$  precisely, providing detachment angles greater than  $152.69^\circ$ . Such a large



## 3. CONCLUSION

The flotometric equation delineates flotation and relates the maximum size of floating particle with its hydrophobicity expressed as detachment contact angle. The flotometric equation is based on the balance of forces involved in flotation and can be utilized after solving it by iterative methods. In this work the flotometric equation, being a third-degree polynomial of  $\cos(\theta_d/2)$ , was transformed into analytical form which is much easier to handle. For the particle size and hydrophobicity encountered in flotation parameter  $B$  is usually smaller than  $(A^2+1)^{3/2}-A^3$  and thus the final form of the equation relating detachment contact angle and the maximum size of floating particle is given by the equation being a combination of Eqs (23) and (8–10)

$$\theta_d = 2 \arccos \left\{ \cos \left[ \frac{1}{3} \arccos \left[ - \frac{\left( \frac{2\sigma(1-r_{\max}/R) + 2R}{r_{\max}^2 \rho_w g} + 1 \right)^3 + 1 + 2 \cdot \frac{\rho_p - \rho_w}{\rho_w} + \frac{3F_a}{2\pi r_{\max}^3 \rho_w g}}{\left( \left( \frac{2\sigma(1-r_{\max}/R) + 2R}{r_{\max}^2 \rho_w g} + 1 \right)^2 + 1 \right)^{3/2}} \right] \right] - \left( \frac{2\sigma(1-r_{\max}/R) + 2R}{r_{\max}^2 \rho_w g} + 1 \right) \right\}$$

This analytical equation can be used for many further applications, especially involving derivations.

## ACKNOWLEDGMENTS

The authors thank professor Shuji Owada of Waseda University for his valuable idea of application of analytical approach to solve the flotometric equation. Financial support by the Polish Statutory Research Grant (343-165) is also greatly acknowledged.

## REFERENCES

- BEWERSDORFF, J., 2006. *Galois Theory for Beginners: A Historical Perspective*. American Mathematical Society, Providence, Chap.2.
- BIRKHOFF, G., MAC LANE, S., 1965. *A Survey of Modern Algebra, third ed.* Macmillan, New York, pp.90–91.
- CHAU, T.T., 2009. *A review of techniques for measurement of contact angles and their applicability on mineral surfaces*. Miner. Eng. 22, 213–219.
- COX, D.A., 2004. *Galois Theory*, John Wiley & Sons, Hoboken, Chap.1.
- DICKSON, L.E., 1914. *Elementary Theory of Equations*, John Wiley & Sons, New York, Chap.3.
- DRZYMALA, J., 1994. *Characterization of materials by Hallimond tube flotation. Part 2: maximum size of floating particles and contact angle*. Int. J. Miner. Process. 42, 153–167; Erratum, Int. J. Miner. Process. 43, 135.

- DRZYMALA, J., LEKKI, J., 1989. *Flotometry — another way of characterizing flotation*. J. Colloid Interface Sci. 130, 205–210.
- GONTIJO, C. de F., FORNASIERO, D., RALSTON, J., 2007. *The limits of fine and coarse particle flotation*. Can. J. Chem. Eng. 85, 739–747.
- HANNIG, R.N., RUTTER, P.R., 1989. *A simple method of determining contact angles on particles and their relevance to flotation*. Int. J. Miner. Process. 27, 133–146.
- KING, R.B., 1996. *Beyond the Quartic Equation*, Birkhäuser, Boston, Chap.5.
- KOCH, R., NOWORYTA, A., 1992. *Mechanical processing in chemical engineering*, WNT Warszawa (in Polish).
- KONOVALOV, S.A., TIKHONOV, O.N., 1982. *Flotometric analysis using the variation principle in the regularisation method*. Izv. VUZ. Tsvetnaya Metallurgiya 25, No.1, 100–104 (in Russian); English summary, Sov. Non-ferr. Met. Res. 10, 65.
- MITROFANOV, S.I., YATSENKO, N.N., KUROCHKINA, A.V., 1970. *Determining the critical inertial forces causing mineral particles to detach from air bubbles*. Tsvetnye Metally 43, No.8, 87–89 (in Russian); English translation, Sov. J. Non-ferr. Met. 11, No.8, 85–87.
- MORRIS, R.M., MATTHESIU, G.A., 1988. *Froth flotation of coal fines: The influence of turbulence on cell performance*. J. S. Afr. Inst. Min. Metall. 88, 385–391.
- NGUYEN, A.V., 2003. *New method and equations for determining attachment tenacity and particle size limit in flotation*. Int. J. Miner. Process. 68, 167–182.
- NGUYEN, A.V., SCHULZE, H.J., 2004. *Colloidal Science of Flotation (Surfactant Science Series, vol. 118)*, Marcel Dekker, New York, Part 5: *Stability of bubble-particle aggregates*, Chap.23–24.
- ROTMAN, J.J., 2000. *A First Course in Abstract Algebra*, second ed., Prentice Hall, Upper Saddle River, Chap.4.
- ROTMAN, J.J., 2007. *Journey into Mathematics: An Introduction to Proofs*, Dover Publications, Mineola, Chap.4.
- SCHELUDKO, A., TOSHEV, B.V., BOJADJIEV, D.T., 1976. *Attachment of particles to a liquid surface (capillary theory of flotation)*. J. Chem. Soc. Faraday Trans. I 72, 2815–2828.
- SCHULZE, H.J., 1993. *Flotation as a heterocoagulation process: possibilities of calculating the probability of flotation*. In: *Coagulation and Flocculation. Theory and Applications*, B. Dobias (Ed.) Marcel Dekker, New York, pp.321–353.
- TIGNOL, J.-P., 1988. *Galois' Theory of Algebraic Equations*, Longman Scientific & Technical, Harlow, Chap.6.
- USPENSKY, J.V., 1948. *Theory of Equations*, McGraw-Hill, New York, Chap.5.

**Watanabe, M., Kowalczyk, P.B., Drzymala, J.,** *Analityczne rozwiązanie równania wiążącego maksymalny rozmiar flotującego ziarna i jego hydrofobowość*, Physicochem. Probl. Miner. Process., 46 (2011) 13-20, (w jęz. ang), <http://www.minproc.pwr.wroc.pl/journal>

W pracy została przedstawiona analityczna forma równania wiążącego maksymalny rozmiar flotującego ziarna i jego hydrofobowość, wyrażoną jako kąt zwilżania. Równanie to, zwane fotometrycznym, oparte jest na bilansie sił działających w układzie ziarno-pęcherzyk powietrza-ciecz w momencie zerwania ziarna i do tej pory rozwiązywane było tylko numerycznie. Rozpatrywane równanie fotometryczne, posiadające postać wielomianu trzeciego stopnia, zostało przedstawione jako funkcja trygonometryczna, dla której istnieje tylko jedno rozwiązanie.

*słowa kluczowe: flotacja, flotometria, kąt zwilżania, ziarno grube, wielomian, równanie kubiczne*

Tomasz CHMIELEWSKI\*, Rafał KALETA\*\*

## **GALVANIC INTERACTIONS OF SULFIDE MINERALS IN LEACHING OF FLOTATION CONCENTRATE FROM LUBIN CONCENTRATOR**

*Received April 30, 2010; reviewed; accepted June 22, 2010*

Measurements of the rest potential of copper sulfide electrodes and pyrite, present in copper ores and concentrates from Lubin Concentrator, have been carried out. Moreover, measurements of sulfide-sulfide contact potential and galvanic current were also performed using deoxygenated sulphuric acid solutions as well as the solutions saturated with oxygen and containing Fe(III) ions. Significant galvanic interactions were observed for sulfide couples exhibiting high potential difference, particularly when copper sulfides were short-circuited with pyrite. According to mineralogical data for Lubin polymineral copper concentrate, chalcocite and bornite are dominating with chalcopyrite and covellite as minor copper minerals. Expected is advantageous affect of pyrite in promoting the kinetics of copper leaching from Lubin concentrate as a result of observed galvanic interactions between pyrite and copper sulfides.

*keywords: copper concentrate, sulfide electrode, galvanic interactions*

### 1. INTRODUCTION

Polish copper deposits, known as LGOM (Lubin-Glogow Copper Basin, SW Poland) exhibit unique, sedimentary nature (Rydzewski, 1996; Konstantynowicz, 1990) and consist of three lithological ore fractions: dolomitic, sandstone, and shale. The shale fraction exhibits the highest concentrations of copper and accompanying metals (Ag, Ni, Co, Zn, Pb, V, Mo etc.) and simultaneously is the most troublesome material in the flotation circuits (Tomaszewski, 1995; Łuszczkiewicz, 2000; 2004).

---

\* Wrocław University of Technology, Faculty of Chemistry, Wybrzeże Wyspiańskiego 27, 50-340 Wrocław, Poland, [tomasz.chmielewski@pwr.wroc.pl](mailto:tomasz.chmielewski@pwr.wroc.pl)

\*\* KGHM Polska Miedź S.A., ul. M. Skłodowskiej-Curie 48, 59-301 Lubin

Moreover, the shale fraction reveals the fine dissemination of metal-bearing sulfides in the carbonate matter and in the black shale-clay rocks that form the majority of the gangue. Such a fine dissemination of copper and other metals sulfides in the carbonateorganic matrix considerably reduces susceptibility of the ore to both effective liberation and subsequent upgrading by means of flotation. At present observed is an increase of quantity of shale-clay and carbonate fractions in flotation feeds, which are known as mostly hard-to-treat in flotation circuits. According to the latest data (Kubacz and Skorupska, 2007) the content of shale fraction in Lubin deposit may already reach as much as 25 % and is expected to increase in coming years.

A complex and very unique mineralogical and chemical composition of the Polish copper ores, mined from the LGOM sedimentary deposits, is the principal reason for copper, silver and other metals losses to flotation tailings (Łuszczkiewicz, 2000; 2004). The metals losses are found to be particularly high in Lubin Concentrator. Additionally, the presence and elevated content of shale create numerous technical, economical and ecological issues both in flotation and in flash smelting.

Selective liberation of fine metal-bearing mineral particles from the host matrix would be the only way to enhance metals recovery in flotation. However, it appears to be in-effective in the existing milling circuits. Consequently, the hydrophilic gangue-sulfide intergrowths seriously reduce both the flotation selectivity and metal grade in the concentrate (Łuszczkiewicz et al., 2006). Therefore, it can be concluded that the existing beneficiation technologies currently applied for processing of the Polish copper ores have already reached the limit of their technological efficiency and require substantial alterations (Chmielewski and Charewicz, 2006; Łuszczkiewicz and Chmielewski, 2006; Konopacka et al., 2007).

According to the KGHM technological data, the techniques of copper production, currently used at KGHM have to be considerably modified in order to enhance or at least to maintain their efficiency. It has also been generally acknowledged that the application of modern hydro- or biometallurgy becomes a potential alternative and necessity in the Polish copper industry to reverse unfavorable trends in flotation results, particularly at Lubin Concentrator (Grotowski, 2007). Flotation – smelting – refining processes, currently used at KGHM, became not enough efficient for acceptably high recovering of Cu and accompanying metals (Ag, Ni, Zn etc), due to the decline of ore grade and decrease of its quality. Moreover, cobalt and zinc are totally lost.

The application of atmospheric leaching, preceded by non-oxidative carbonates decomposition, is recently considered as an alternative or as a complimentary process for processing of shale flotation by-product which is hardly to beneficiate using existing techniques. This approach, presented by a group of authors from Wroclaw University of Technology within the research program of BIOSHALE project (Chmielewski and Charewicz, 2006; Chmielewski, 2007), primarily involves separation of the most

troublesome ore fraction (shale containing middlings) and introduction of hydrometallurgical methods for their alternative effective processing.

Another, recently discussed approach comprises the application of atmospheric or pressure leaching for processing of the Lubin copper sulfide concentrates. Lowering the concentrate grade may simultaneously result in a significant increase of metals recovery. Application of alternative hydrometallurgical processing of such a concentrate may lead to increasing production of copper, silver, lead, nickel, zinc and cobalt. The last two elements are totally lost in current technologies.

The copper flotation concentrates produced at Lubin Concentrator are of polymetallic and polymineral composition. They contain chalcocite ( $\text{Cu}_2\text{S}$ ) and bornite ( $\text{Cu}_5\text{FeS}_4$ ) as dominating copper sulfides, whereas chalcopyrite ( $\text{CuFeS}_2$ ) and covellite ( $\text{CuS}$ ) are minor minerals (KGHM, 2007; Łuszczkiewicz, 2009). Moreover, in recent years was also observed an increasing content of pyrite ( $\text{FeS}_2$ ), which appeared to be a beneficial component in terms of mechanism alteration and enhancing the kinetic of copper leaching. Electrochemical nature of sulfides flotation (Chanturiya and Vigdergauz, 2009) and leaching along with electrocatalytic properties of pyrite has already been described (Majima and Peters, 1968; Nowak et al., 1984; Holmes and Crundwell, 1995) and used for leaching of copper sulphidic concentrates in the Galvanox Process (Dixon and Mayne, 2007), where finely ground  $\text{FeS}_2$  is added to the leaching slurry to intensify the process in a galvanic manner, by facilitating the charge transfer from the oxidant to dissolved sulfide. The presence of numerous sulphidic copper, iron, zinc and lead minerals in the feed to leaching can advantageously result in mutual electrochemical interactions caused by different potentials attained by sulfides in leaching conditions. These interactions have already been examined for conditions of non-oxidative leaching of the Lubin shale middlings (Kowalczyk and Chmielewski, 2010) and are expected to result in significant acceleration of copper leaching.

In this work results of laboratory investigations performed for electrodes prepared from natural copper sulfides and pyrite, which are dominating minerals in the Lubin copper flotation concentrate are presented. Sulphuric acid solutions, deoxygenated, oxygenated and containing Fe(III) ions, simulating the leaching conditions, were applied. Investigated were rest potentials, contact potentials and galvanic contact currents for selected mineral couples of highest potentials differences. The results were interpreted in terms of leaching kinetics of the Lubin concentrate in acidic oxygenated Fe(III) solutions.

## 2. AIM OF THE WORK

Examination of electrochemical phenomena existing during non-oxidative and oxidative leaching of the copper sulfide concentrate provides enormous amount of basic information important for both future leaching kinetics and leaching mechanism.

The following mineralogical and electrochemical aspects have been examined for sulfide minerals present in the Lubin flotation concentrate:

- mineralogical evaluation of the feed in terms of possible mutual impacts of various sulfides contained in the concentrate,
- evaluation of electrochemical control of non-oxidative and oxidative leaching using oxygen and Fe(III) ions,
- correlation of measured rest potentials of sulfides with their leachability in sulphuric acid solutions,
- selection of sulfide-sulfide systems exhibiting strongest galvanic interactions under leaching conditions,
- indication of possible electrode processes on sulfides during leaching,
- quantitative evaluation of galvanic interactions by means of measurements of contact potentials and contact currents for selected sulfide systems.

### 3. EXPERIMENTAL

#### 3.1. ELECTRODES AND MEASUREMENTS

The sulfide electrodes applied in reported measurements have been prepared from handpicked samples of natural copper sulfides and pyrite from Polish LGOM copper deposits. A sample of individual mineral was initially cut and ground to the near rectangular shape of about 0.5 – 1 cm<sup>3</sup>. Electrical contact between the mineral specimen and copper wire was made using silver-impregnated conducting epoxy resin. Subsequently, the contacted sample was mounted in epoxy resin and after hardening the working face of the electrode was ground and polished using emery paper.

The solutions were prepared from analytical grade reagents (sulfuric acid, iron(III) sulphate, gaseous oxygen and argon). Rest potential of sulfide electrodes was measured and recorded versus Ag, AgCl, KCl<sub>sat</sub> electrode ( $E_h = +0.197$  V), which was connected to a thermostated measuring cell with a Luggin capillary. The solution was either deoxygenated with argon to simulate non-oxidative conditions, or saturated with oxygen in the presence of Fe(III) ions, to simulate oxidative leaching conditions. Galvanic currents were recorded under different conditions, after connecting two selected electrodes with electrical wire.

#### 3.2. CHEMICAL AND MINERALOGICAL CHARACTERIZATION OF THE LUBIN CONCENTRATE

The copper flotation concentrate was taken from a commercial flotation circuit of the Lubin Concentrator (ZWR Lubin) in the form of water slurry. Mineralogical composition of the Lubin concentrate, compared with Polkowice and Rudna concentrates is shown in Table 1. Table 2 indicates the chemical composition of the Lubin concentrate.

Table 1. Mineralogical composition of the copper flotation concentrates at the KGHM concentrators (mean values for 2007-2008, Luszczkiewicz, 2009)

Concentrator mean data 2007-2008	Bornite	Chalcocite, digenite	Chalco- pyrite	Pyrite, marcasite	Covellite	Sphalerite	Tennan- tite	Galena
Lubin	33.1	14.5	26.1	17.4	3.5	1.8	2.0	1.9
Polkowic e	13.6	55.5	12.0	10.9	3.7	1.2	1.5	1.6
Rudna	24.8	40.4	7.2	15.0	5.8	3.1	1.5	2.3

The Polish flotation copper concentrates from all three concentrators: Lubin, Rudna and Polkowice exhibit the dominating content of chalcocite and bornite, the easiest-to-leach copper sulfides. This is a unique and exceptionally beneficial attribute of the Polish copper concentrates with regard to their potential application for hydrometallurgical treatment. The content of chalcopyrite – most refractory copper mineral, is rather insignificant, except of the Lubin deposit, where chalcopyrite content is about a half of that of chalcocite and bornite.

Table 2. Chemical composition of the Lubin flotation concentrate (sample taken on 01. Sept., 2007)

Component	Content in concentrate
Cu	15.64%
Ag	840 ppm
Zn	4600 ppm
Co	1216 ppm
Ni	216 ppm
Pb	2.15%
C <sub>org</sub>	10.18%
S	10.8%

In contrary to the Polkowice and Rudna concentrate, Lubin concentrate is rather poor in terms of copper content (KGHM, 2007) and its quality is hardly accepted for flash smelting. Moreover, both concentrate grade and metal recovery have been remarkably decreasing in recent period. According to the latest data, copper content in the Lubin concentrate decreased to less than 15% (KGHM, 2009) whereas copper recovery at the Lubin concentrator has recently fallen to only 85.9% (KGHM, 2009). However, the Lubin concentrate is the richest in silver (850 ppm) and exhibits

evidently elevated content of Zn, Co, Ni and Pb (Table 2). Recovery of these metals is currently reported either as very low while cobalt and zinc are not recovered at all.

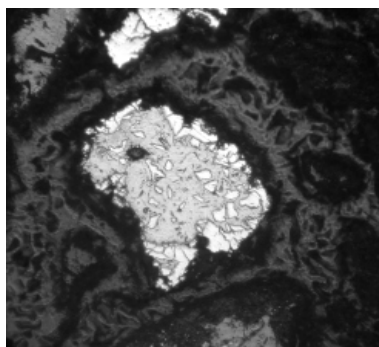


Fig. 1a. Intergrowths of pyrite (light) with chalcopyrite (gray). Reflected light, magnification ~ 120x

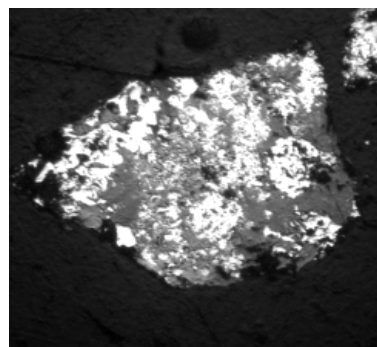


Fig. 1b. Intergrowths of pyrite (light) with covellite (dark gray). Reflected light, magnification ~120x

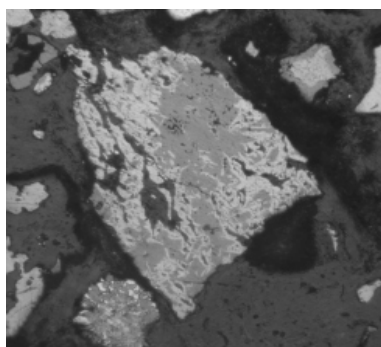


Fig. 1c. Intergrowths of chalcopyrite (gray) with bornite (dark gray). Reflected light, magnification ~ 120x

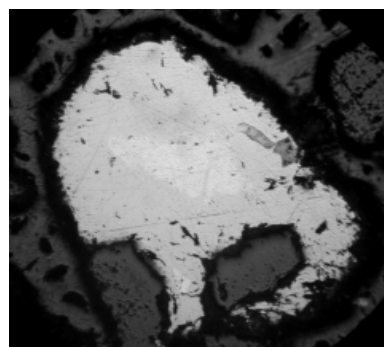


Fig. 1d. Intergrowths of chalcopyrite (light gray) with chalcocite (dark gray). Reflected light, magnification ~ 120x

## 4. RESULTS AND DISCUSSION

### 4.1. REST POTENTIALS OF SULFIDE ELECTRODES

In order to compare different conducting and electrochemical properties of investigated sulfides, their resistivity, type of semiconductivity and rest potentials, reported in literature (Hiskey and Wadsworth, 1981; Mehta and Murr, 1983) and measured in this work in deoxygenated with argon sulphuric acid solutions with concentration of  $50 \text{ g/dm}^3$  the data are presented in Tables 3 and 4. A very good

correlation can be observed for rest potential measured in this work and found from the literature data (Hiskey and Wadsworth, 1981; Paramguru, 2002).

Earlier literature data discussed the effect of electrochemical properties of sulfides and their mutual galvanic interactions on flotation efficiency and selectivity (Kocabag and Smith, 1985; Majima, 1968; Biegler et al., 1977; Peters and Majima, 1968).

Table 3. Conducting properties and rest potentials of selected copper sulfides and pyrite (Hiskey and Wadsworth, 1981)

Mineral	Resistivity, $\Omega\text{m}$	Semiconductivity type	Rest potential, mV (SHE)
Pyrite	$0.1 - 3 \cdot 10^{-2}$	n, p	630
Chalcopyrite	$0.2 - 9 \cdot 10^{-3}$	n	530
Chalcocite	$10^{-2} - 10^{-5}$	p	440
Covellite	$10^{-4} - 10^{-6}$	p	420
Copper	$1.7 \cdot 10^{-8}$	metallic conductor	340

According to the data shown in Tables 3 and 4, chalcocite can be recognized as electrochemically the most active mineral among all copper sulfides, exhibiting the lowest rest potential (+151 mV vs. Ag,AgCl). Bornite with the rest potential of +195 mV, is only slightly less active than chalcocite. In contrary, covellite, exhibiting potential of +290 mV, and chalcopyrite, exhibiting the highest rest potential (+330 mV) among copper sulfides, are the least active or most refractory in terms of leachability. Pyrite was found to reveal the highest rest potential among all examined sulfides. Its potential was found to be + 434 mV (Ag, AgCl).

Table 4. Results of measurements of rest potentials of sulfide electrodes (at 25°C) and literature data (Mehta and Murr, 1983)

Mineral	Measured rest potential mV, (Ag, AgCl)	Rest potential (literature) mV, (Ag, AgCl) (Mehta and Murr, 1983)
Chalcocite	+ 151	+ 183
Bornite	+ 195	+ 223
Covellite	+ 290	+ 253
Chalcopyrite	+ 330	+ 363
Pyrite	+ 434	+ 464

From measured rest potential of copper sulfides and pyrite (Table 4) we can anticipate galvanic interactions between minerals, because those of evidently higher potential (pyrite, chalcopyrite) will play the role of a cathode (reduction of oxygen or

iron(III) ions) whereas minerals of lowest potential (chalcocite, bornite) will be dissolved anodically with a considerably elevated rate.

From the measurements of the rest potential the following galvanic couples were set up for further measurements of contact potentials and galvanic current:

- |   |                           |   |                     |
|---|---------------------------|---|---------------------|
| – | chalcopyrite – chalcocite | – | pyrite – chalcocite |
| – | chalcopyrite – chalcocite | – | pyrite – bornite    |
| – | chalcopyrite – chalcocite | – | pyrite – covellite. |

#### 4.2. REST POTENTIALS OF SULFIDES DURING LEACHING

Rest potentials of a platinum electrode and selected sulfide electrodes as well as sulfide – pyrite couples were recorded in  $\text{H}_2\text{SO}_4$  solution ( $50 \text{ g/dm}^3$ ) at temperatures 25, 50, 70, and 90°C. Figures 2 and 3 exhibit experimental data collected at 70°C. Non-oxidative conditions were simulated by deoxygenation of the solution with argon. Gaseous oxygen and iron(III) ions of concentration of  $1 \text{ g/dm}^3$  were used to create oxidative conditions. It is well seen from potential – time plots that an apparent decrease in sulfide electrode potential reflects non-oxidative conditions. Within the period of 20 minutes the rest potential of chalcocite and bornite electrodes decreases about 100 mV. Such a potential observed under non-oxidative conditions is too low for dissolution of copper from its sulfidic form.

When gaseous oxygen was introduced to the solution, an increase of the rest potential was recorded (Figs 2 and 3). This indicates a very slow minerals digestion. When iron(III) ions were present, the increase of potential was very evident, even at very low Fe(III) concentration, applied for presented measurements. This is a clear evidence that Fe(III) ion is a considerably much better leaching agent than oxygen, due to their faster reduction on sulfides surfaces in comparison to oxygen.

After copper sulfide electrodes were coupled with the pyrite electrode, the observed increase of the rest potential in the presence of oxygen and iron(III) ions was found to be more evident (Figs 4 and 5) due to expected electrochemical interactions (Table 4). This is the result of formation of galvanic couples between more noble pyrite, which was a cathode, and covellite or chalcopyrite, which were anodes in the galvanic pyrite - covellite and pyrite - chalcopyrite couples.

After introduction of oxygen under atmospheric pressure only a slight increase of potential was observed for platinum, chalcocite (about 20 mV) and bornite (about 50 mV) electrodes. An increase of the potential of sulfide electrode above the rest potential observed under non-oxidative conditions results in anodic dissolution of the mineral. For covellite, chalcopyrite and pyrite the increase of the rest potential in the presence of oxygen was rather insignificant.

The most noticeable raise of the rest potential of all examined sulfides and platinum was caused by iron(III) ions. Even if the Fe(III) concentration was as low as

1 g/dm<sup>3</sup>, the effect of this oxidant was very strong. This clearly explains why the presence of iron(III) in the oxidative leaching systems for copper sulfides is therefore strongly recommended.

The increase of the rest potential of sulfide minerals was observed to be very stable when oxygen was present in the solution as an oxidation agent for regeneration of Fe(II) to Fe(III). The presence of iron(III) ions and dissolved oxygen as regeneration agent is also recently considered for leaching of sulfide concentrates and by-products from flotation circuits at KGHM. For Fe(III) – O<sub>2</sub> system. For this system is observed the highest leaching recovery of copper from sulfidic ores and concentrates under atmospheric conditions (Chmielewski, 2009). The selection of a proper feed for hydrometallurgical processing, accepted by technical and economical factors, will be analysed and extensively investigated from year 2010 to 2013 within the HYDRO comprehensive research project financed by National Center of Research and Development, performed currently at the Faculty of Chemistry, Wrocław University of Technology.

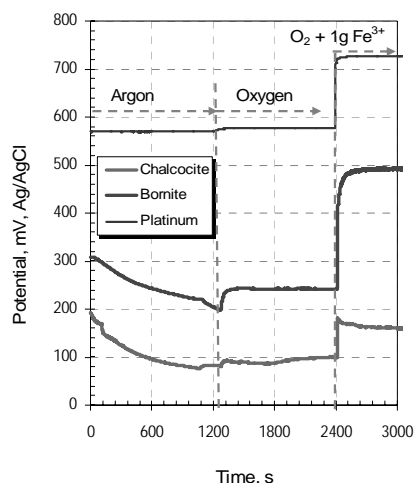


Fig. 2. Potential – time plot for bornite, chalcocite and Pt electrodes in sulphuric acid solutions: deoxygenated, oxygenated and in the presence of iron(III) ions at 70°C

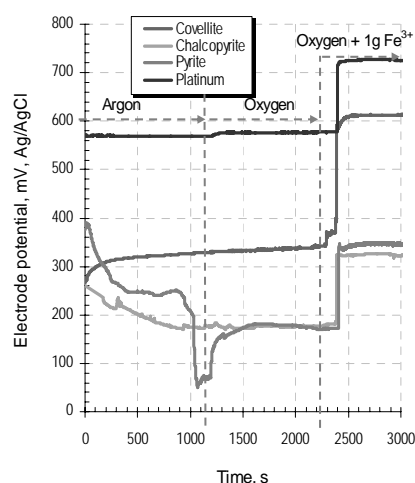


Fig. 3. Potential – time plot for chalcocopyrite, covellite, pyrite and Pt electrodes in sulphuric acid solutions: deoxygenated, oxygenated and in the presence of iron(III) ions at 70°C

The highest increase of the potential of sulfide electrodes was detected after introduction of iron(III) to the solution (Figs 2 and 3). The elevation of the potential was observed to be very stable, since simultaneous regeneration of Fe(II) to Fe(III) takes place in the presence of oxygen. This undoubtedly explains the reason of application of Fe(III) + oxygen system as the most effective for leaching of copper sulfides. When the copper minerals were coupled with pyrite, known as most noble sulfide, the observed contact potential was evidently higher than for single electrodes (Figs 4 and 5).

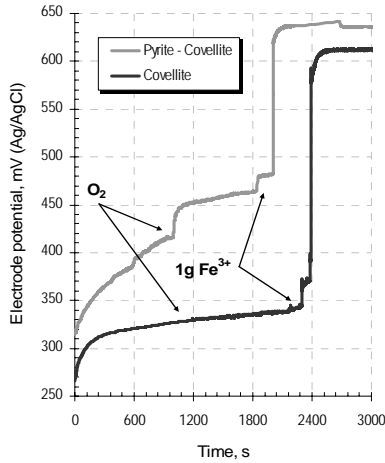


Fig. 4. Potential – time plot for covellite and covellite-pyrite couple in sulphuric acid solutions: deoxygenated, oxygenated and in the presence of iron(III) ions at 70°C.

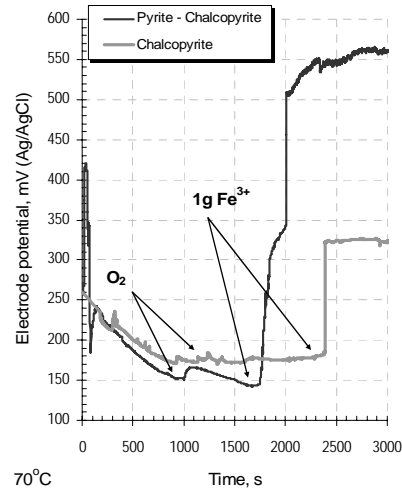


Fig. 5. Potential – time plot for chalcopyrite and chalcopyrite-pyrite couple in sulphuric acid solutions: deoxygenated, oxygenated and in the presence of iron(III) ions at 70°C

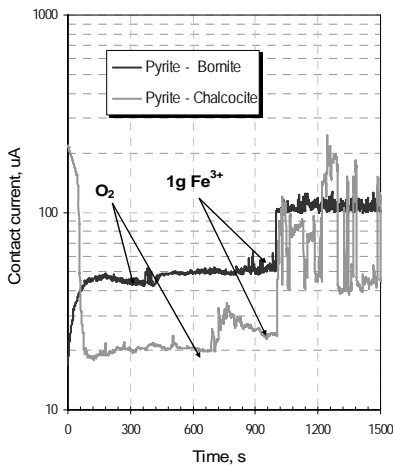


Fig. 6. Contact currents for galvanic systems: pyrite-bornite and pyrite - chalcocite (effect of oxygen and Fe(III))

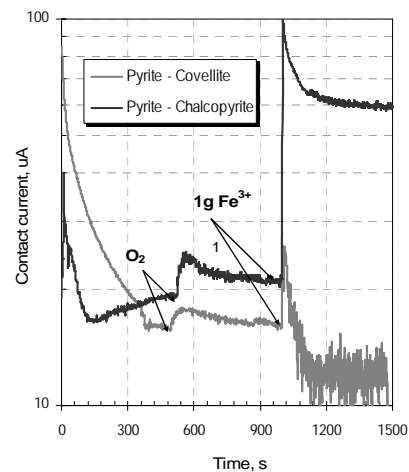


Fig. 7. Contact currents for galvanic systems: pyrite-covellite and pyrite - chalcopyrite (effect of oxygen and Fe(III))

The most significant effect of galvanic couples on the kinetics of anodic dissolution of copper sulfides can be reported from galvanic current measurements for copper sulfide electrodes short-circuited with pyrite electrode (Figs 6–9). The recorded galvanic current reflected the possible leaching rate of copper sulfides. It is clearly visible from the current – time plots that the contact current for pyrite-bornite couple was about 10-fold higher than that for the chalcopyrite-bornite couple.

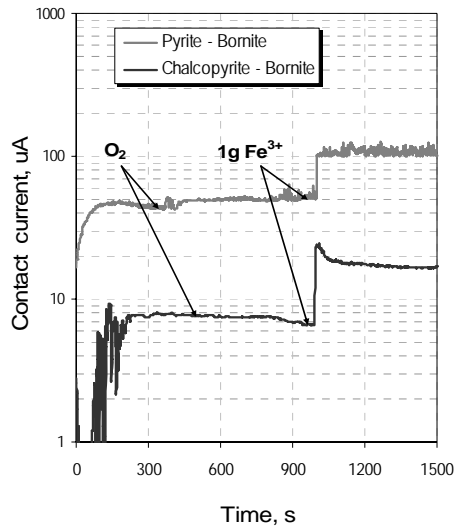


Fig. 8. Contact currents for galvanic systems: pyrite-bornite and chalcopyrite – bornite (effect of oxygen and Fe(III))

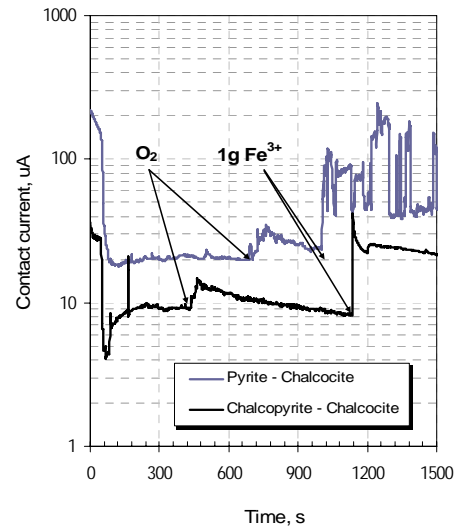


Fig. 9. Contact currents for galvanic systems: pyrite-chalcocite and pyrite chalcopyrite - chalcocite (effect of oxygen and Fe(III))

## 5. CONCLUSIONS

Shrinking of copper resources along with declining of copper ores quality and simultaneous increase of demand for the metal in the World leads to the commencement of exploitation of those copper resources, which in the past were not enough attractive and not mined. As a result of changing circumstances, novel hydrometallurgical techniques have been recently introduced for recovering of copper and accompanying metals from those resources, which remained as not applicable for flotation/smelting due to the complex character of ores and of a small scale of mining. The role of hydrometallurgy has been evidently growing in recent years and the need of application of hydrometallurgy in technological circuits at KGHM has also recently appeared.

It can be concluded that polymetallic and polymineral character of the Lubin concentrate, particularly the dominating bornite-chalcocite copper mineralization is advantageous in terms of excellent leachability. Moreover, elevated content of pyrite and chalcopyrite as well as the presence of numerous intermineral contacts, can substantially facilitate atmospheric leaching of the concentrate in sulphuric acid solutions containing oxygen and Fe(III) ions as leaching agents. This was confirmed in this work by mineralogical analyses, measurements of rest potentials of single mineral electrodes and potential changes of coupled copper minerals and pyrite. The measurements of contact currents between copper sulfides short - circuited with pyrite

clearly indicates that relatively high content of pyrite in the Lubin concentrates may be beneficial if the concentrates were used as a feed for oxidative leaching with oxygenated acidic solutions of Fe(III).

## REFERENCES

- BIEGLER T., RAND O.A.J., WOODS R., 1977: Oxygen reduction on sulfide minerals. In: Trends in Electrochemistry, (Bockris J.O.M., Rand D.A.J. and Welch B.J., Eds.), Plenum Press, N.Y.
- CHANTURIJA V.A., VIGDERGAUZ V.E. 2009, Electrochemistry of Sulfides, Theory and Practice of Flotation, Ore and Metals, Moscow 2009.
- CHMIELEWSKI T., 2009. Atmospheric leaching of shale middlings as an alternative for technological alterations at the Lubin Concentrator, Proceedings of XII Seminar „Hydrometallurgical Methods and Production Development at KGHM Polska Miedź SA”, Lubin 17 February 2009: 38-54 (in Polish).
- CHMIELEWSKI T., 2007: Atmospheric leaching of shale by-product from Lubin concentrator, Physicochem. Probl. Miner. Process., 41: 337-348.
- CHMIELEWSKI T., CHAREWICZ W., 2006, Hydrometallurgical processing of shale middlings from technological circuits of Lubin Concentrator, In: Perspectives for applying bioleaching Technology to process shale-bearing copper ores, BIOPROCOP'06, Lubin 2006, KGHM Cuprum, Wrocław 2006: 125-145.
- DIXON D.G., MAYNE D.D., 2007: Galvanox – a novel galvanically assisted atmospheric leaching technology for copper concentrates, Proc. Copper/Cobre 2007 Conference, Toronto (Canada), Riveros P., et al., eds., Vol. IV (1), CIM Montreal, Canada: 191.
- GROTOWSKI A., 2007: Possibilities and perspectives for implementation of hydrometallurgical methods in KGHM Polska Miedź S.A., Proc. VIII International Conference on Non-ferrous Ore Processing, Wojcieszycze (Poland), May 21-23, KGHM Cuprum Wrocław 2007, 29-46.
- HISKEY, J.B., WADSWORTH, M.E., 1981. In: M. Kuhn (Ed.), Process and fundamental considerations in selected hydrometallurgical systems, SME-AIME, New York: 303.
- HOLMES P.R., CRUNDWELL F.K., 1995: Kinetic aspects of galvanic interactions between minerals during dissolution, Hydrometallurgy 39: 353-375.
- KGHM 2007, Monograph of KGHM “Polska Miedź” SA., Piestrzynski A., Ed., KGHM Cuprum CBR, Wrocław.
- KGHM, 2009, unpublished data.
- KOCABAG D., SMITH M.R., 1985: The effect of grinding media and galvanic interactions upon the flotation of sulfide minerals, in: Proc. Symp “Complex Sulfides – Processing of Ores, Concentrates and By-products”, (Zunkel A.D., et al Eds.), WBD, Indialantic, USA: 55-77 .
- KONIECZNY A, KASIŃSKA-PILUT E, PILUT R., 2009: Technological and technical problems in mineral processing of Polish copper ores at Division of Concentrators KGHM “Polska Miedź” SA, IX International Conference on Non-Ferrous Ore Processing, ICNOP Łądek Zdrój, 18 – 20 May 2009:11-21 (in Polish).
- KONOPACKA Z., LUSZCZKIEWICZ A., CHMIELEWSKI T., 2007: Effect of non-oxidative leaching on flotation efficiency of Lubin Concentrator Middlings, Physicochem. Probl. Miner. Process., 41: 275-289.
- KONSTANTYNOWICZ-ZIELIŃSKA J. 1990, Petrography and genesis of copper-bearing shales of Foresudetic Monocline, Rudy i Metale Nieżelazne, R.35(5-6): 128-133 (in Polish).
- KOWALCZUK P. B. and CHMIELEWSKI T. 2010. Changes of electrode potential in the non-oxidative leaching, Physicochem. Probl. Miner. Process., 44 (2010): 115-126.
- KUBACZ N., SKORUPSKA B. 2007, Evaluation of the effect of organic carbon on concentration and

- smelting processes. Proc. VIII International Conference on Non-ferrous Ore Processing, Wojcieszycze (Poland), May 21-23, KGHM Cuprum Wrocław 2007: 157-166.
- ŁUSZCZKIEWICZ A. 2004, Analysis and evaluation of floatability of the ore exhibiting elevated content of black shale. Report of Investigations, Archive of Institute of Mining Engineering, Laboratory of Mineral Processing, Wrocław University of Technology, Wrocław, October 2004
- ŁUSZCZKIEWICZ A., 2000, Utilisation of black shale copper ore fraction from Lubin – Głogów Copper Basin, in: Proc. Conf. “Modern Aspects of Copper Ore Processing in Poland”, Polkowice, 16 November 2000, Committee of Mining, Polish Academy of Sciences and KGHM Polska Miedź SA: 137-156.
- ŁUSZCZKIEWICZ A., CHMIELEWSKI T., 2006, Technology of chemical modification of by-products in copper sulphidic ore flotation systems, *Rudy i Metale Nieżelazne*, R-51: 2-10.
- ŁUSZCZKIEWICZ A., DRZYMAŁA J., 2009, Possibility of reduction of lead, arsenic and organic carbon content in copper concentrates. *Physicochem. Probl. Miner. Process.*, 44th Seminar, Niepołomice, Plenary lecture (in Polish), unpublished.
- ŁUSZCZKIEWICZ A., KONOPACKA Z., DRZYMAŁA J., 2006, Flotation of black shales from Lubin copper ores. In: Perspectives for applying bioleaching Technology to process shale-bearing copper ores, BIOPROCOF'06, Lubin 2006, KGHM Cuprum, Wrocław 200, 29-47.
- MAJIMA H., PETERS E. 1968: Electrochemistry of sulfide dissolution in hydrometallurgical systems, *Proc. Int. Mn. Proc. Congress.*, Leningrad: 13.
- MAJIMA H., 1969: How oxidation affects selective flotation of complex sulfide ores, *Can. Met. Quart.*, 8(3): 111-117.
- MEHTA, A.P., MURR, L.E., 1983. Fundamental studies of the contribution of galvanic interaction to acid-bacterial leaching of mixed metal sulfides. *Hydrometallurgy*, 9: 235-256.
- NOWAK P., KRAUSS E., POMIANOWSKI A. 1984: The electrochemical characteristics of the galvanic corrosion of sulfide minerals in short-circuited model galvanic cell, *Hydrometallurgy*, 12, 95-110.
- PARAMGURU R.K., 2002: Electrochemical Aspects in Some of the Hydrometallurgical Processes, *Mineral Processing and Extractive Metallurgy Review*, 23: 65-100.
- PETERS E., MAJIMA H., 1968: Electrochemical reactions of pyrite in acid perchlorate solutions, *Can. Met. Quart.*, 7: 111-117.
- RYDZEWSKI A., ŚLIWIŃSKI W., 2007, Lithology of deposit rocks. In: Monograph of KGHM “Polska Miedź” SA, Piestrzyński A., Ed., KGHM Cuprum CBR, Wrocław, Lubin, 111-115.
- TOMASZEWSKI J., 1985, Problems of rational utilization of copper polymetallic ores from Fore-sudetic Monocline, *Physicochem. Probl. Miner. Process.*, 17: 131-141 (in Polish).

**Chmielewski, T., Kaleta, R.,** *Oddziaływania galwaniczne minerałów siarczkowych podczas ługowania koncentratu flotacyjnego z ZWR Lubin*, *Physicochem. Probl. Miner. Process.*, 46 (2011) 21-34, (w jęz. ang), <http://www.minproc.pwr.wroc.pl/journal>

Przedstawiono wyniki pomiarów potencjału spoczynkowego elektrod wykonanych z siarczków miedzi i pirytu, obecnych w rudach i koncentratkach ZWR Lubin. Ponadto, wykonano pomiary potencjałów zwarcia układów siarczek-siarczek oraz prądów zwarcia wybranych par siarczków w odtlenionych roztworach kwasu siarkowego oraz w roztworach natlenionych i zawierających jony Fe(III). Obserwowano wyraźne oddziaływania między siarczkami różniącymi się znacznie wartością potencjału spoczynkowego, zwłaszcza, gdy siarczki miedzi były w kontakcie z pirytem. Zgodnie z danymi mineralogicznymi dla koncentratu Lubin chalkozyn i bornit są dominującymi siarczkami

miedzi, natomiast zawartość chalkopirytu i covellinu jest wyraźnie niższa. Można stąd oczekiwać korzystnego dla ługowania wpływu oddziaływania pirytu na ługowanie przejawiający się wzrostem szybkości ługowania miedzi w wyniku oddziaływań galwanicznych w układach pirit – siarczki miedzi.

*słowa kluczowe: koncentrat miedzi, elektrody siarczkowe, oddziaływania galwaniczne*

Raimondo CICCU \*, Ilgin KURSUN \*\*

## POTENTIAL ADVANCES IN FLOTATION BY USING WATER JETS

*Received April 26, 2010; reviewed; accepted June 22, 2010*

Some mineral processing problems are not yet satisfactorily solved by the current technology, especially those based on the use of mechanical energy for comminution and separation. The use of mechanical energy has certain inherent drawbacks such as wear of machinery components and limitation in the speed of moving parts to avoid risk of failure under the severe working conditions encountered in the industrial processes. Waterjet can contribute to overcoming such disadvantages since it allows to transfer energy without contacts between solid materials (no wear) and it is suitable for generating high velocity streams in air or in water even at relatively low pressures. The potential benefits of waterjet technology are particularly interesting in flotation where the size and speed of the air bubbles, that depend on the shear velocity induced by agitation, are a critical aspect for the optimization of the separation results (recovery and selectivity) and the reduction of the running cost items (wear and energy consumption).

*keywords: waterjet, flotation, coal flotation, comminution*

### 1. INTRODUCTION

The possibility of taking advantage of the power of water in mining and mineral beneficiation is known since early times, although only very few instances of the application of this technology can be found in the industrial practice. In Spain Romans used to disintegrate the gold-bearing soft formations by means of water streams forced to flush down the slope of the hills against the ore (*ruina montium*). The flow of suspended particles was then allowed to settle along appropriate channels where heavier gold particles could be separated by gravity from the washed-away barren

---

\* DIGITA, University of Cagliari, Italy, [ciccu@unica.it](mailto:ciccu@unica.it)

\*\* Department of Mining Engineering, Istanbul University, 34320 Istanbul, Turkey, [ilginkur@istanbul.edu.tr](mailto:ilginkur@istanbul.edu.tr)

sand.

Much later, the same principle has been employed for digging the ore during the *gold rush* as well as for coal production in underground mines, using low pressure, high flowrate monitors.

More recently, attempts were made for winning hard rocks by means of high pressure water cannons, although the productivity was poor due to the discontinuity of the operation.

Today the interest in waterjet technology is considerably increased and widely expanded owing to the development of suitable systems capable of generating a variety of jets for specific applications in different fields of science and engineering.

The performance of the jet can be enhanced by the addition into the water stream of suitable components like, for instance, soluble polymers for improving the coherence of the jet over longer distances, and/or abrasives for increasing the erosion capability when cutting hard materials. Accordingly, a water jet can represent an efficient tool, alone or in combination with other actions of different nature (mechanical, chemical, thermal, electric) for piercing, drilling, cutting, kerfing, milling, fracturing, crushing, and cleaning any kind of solid material, to the characteristics of which the jet can be properly tailored, as well as for carrying, stirring, emulsifying, aerating, breaking, and blending multiphase mixtures.

## 2. STATE OF THE ART IN FLOTATION

### 2.1. PROBLEMS ENCOUNTERED WITH CURRENT TECHNOLOGY

Froth flotation is the dominating mineral beneficiation technique and has achieved great commercial success. This process has also found many applications in other industrial fields where physical separation of materials is needed like, for instance, water cleaning and decontamination, elimination of foreign materials from molten metals, and so on.

However, its process efficiency is often limited to a narrow particle size range of approximately 10-100  $\mu\text{m}$  (Tao, 2005).

It is a well known fact that separation performance of traditional flotation machines gradually deteriorates as particle size decreases, resulting in a poor recovery, unsatisfactory quality of the product and a high specific consumption of energy and reagents, when very finely ground materials, let's say below few microns, are treated.

### 2.2. BUBBLE POPULATION FEATURES

The formation of air bubbles into the pulp is the necessary requirement for the development of the flotation process. Collection efficiency increases if the bubbles are

well dispersed into the cell meaning that, for a given volume of injected air, bubble size should be as small as possible at the moment of their generation, merging later then into larger bubbles due to coalescence phenomena for the uplift of attached mineral particles.

From the analysis of the conditions governing the dispersion of the bubbles in flotation cells with mechanical agitation it emerges that their average size decreases if: i) the surface tension at the liquid-gas interface increases, ii) a more intense turbulence into the liquid phase is achieved and iii) air is injected into the pulp at higher velocity (Klassen and Mokrousov, 1963).

Studies on the effects of the gas phase have shown that in flotation, like in other gas-liquid mass transfer processes, the rate of mineral recovery is intimately linked to the bubble size distribution in the flotation vessel.

It is widely recognised that particle-bubble collision, attachment and detachment, bubble collapse, insufficient buoyancy action for heavier floatable particles and the undesired mechanical draw of gangue slimes are the most critical steps in the flotation process. All these aspects require a careful knowledge and control of the hydrodynamics in the flotation cell.

A scientific approach to the problem enables to meet the growing need to design larger and more efficient flotation cells to treat the lower grade and more finely disseminated ores that are currently being mined in the world.

### 2.3. AVAILABLE KNOWLEDGE

#### 2.3.1. IMPORTANCE OF BUBBLE SIZE

Many researchers have been dealing with the problem concerning air bubble generation and hydrodynamics into flotation cells.

It is generally agreed upon that the scant flotation recovery of very fine particles is mainly due to the low probability of bubble-particle collision, while the main reason for poor flotation recovery of coarse particles is the high probability of detachment of particles from the bubble surface. Fundamental analysis indicates that use of smaller bubbles is the most effective approach to increase the probability of collision and reduce the probability of detachment (Tao, 2005). The same statement has been made by other authors.

It has been experimentally proven that the degree of aeration of the pulp in the form of small bubbles increases linearly with the relative velocity of the two interacting fluids (air and water) whereas it is inversely proportional to the so-called capillary elasticity, i.e. the ratio between surface tension and bubble diameter.

While a reduction in surface tension always plays an outstanding role in the process, on the other hand it is also clear that, at equal surface tension, a good dispersion chiefly depends on the shear friction between the liquid and the gaseous

phase, i.e. on the degree of turbulence right in the region of bubble formation.

The amount of friction, strictly related to the transfer of momentum, is given by the well known general equation:

$$F = A K (-\Delta V)^2, \quad (1)$$

where  $F$  is the friction force,  $A$  the contact surface,  $K$  a constant,  $\Delta V$  is the equilibrium velocity, i.e. the difference between the actual velocity of one of the phases at a given point and that which would theoretically be reached under the same conditions if it were in a state of steady flow with the other phase (Loncin, 1961).

Further confirmation of the importance of bubble size distribution can be found in a comparison study of column flotation technologies for cleaning Illinois coal: generation of small bubbles can be promoted by increasing the shear rate of the fluid at the bubble nucleation site.

In the same study it is underlined that the addition of larger amounts of frother in order to further reduce bubble size can be detrimental to selectivity as a result of increased water recovery from the pulp to the froth. Therefore, reducing bubble size by increasing the shear rate should be regarded as a better choice in terms of selectivity, although this alternative could result in a somewhat higher energy consumption (Honaker, 1994).

The successful achievements of column flotation technology especially in the case of fine particles is due to the fact that the external bubble generators used in column flotation produce smaller bubbles with higher degree of uniformity than conventional flotation cells. Consequently, a significant increase in the rate of coal recovery from the pulp can be achieved owing to the larger overall amount of bubble surface area for a given aeration rate, available for the capture of floatable particles.

### 2.3.2. HYDRODYNAMICS OF MULTIPHASE FLOW IN THE CELL

Different concepts have been developed in the attempt to improve the chances of bubble-particle attachment. For example, one approach utilizes a complete froth column. Other techniques utilize packing or baffles to reduce turbulence, thereby, decreasing the probability of a particle escaping without bubble contact. The use of self-induced air and the generation of uniform microbubbles are novel concepts of other column technologies.

Ahmed and Jameson (1985) reported an almost one-hundred-fold increase in the rate of fine quartz flotation when the average bubble size in their batch flotation cell was reduced from 655 to 75  $\mu\text{m}$ , and Yoon and Luttrell (1989) showed theoretically that the probability of contact between particles and bubbles in flotation varies as the inverse of the bubble size raised to a power of between 1 and 2.

An obvious consequence of any attempt to enhance the probability of collision between the air bubbles and the particles is that the retention time required to achieve a high recovery decreases considerably even 2 to 3 times less, like in the case of the

Jameson Cell. The overall carrying capacity of the froth in ton/hr of product increases accordingly (Honaker, 1994).

### 2.3.3. MODELLING THE FLOTATION PROCESS

From the above it emerges that a careful study of bubble features is of a paramount importance for the optimization of flotation performance.

To this end a number of models have been proposed. However, the traditional approach to modelling gas dispersion in mechanical flotation cells has generally not involved micro-properties such as bubble size distribution, but has rather dealt with macroscopic properties of the system.

A more sophisticated attempt to describe the bubble population balance in both the space and time domains allows to predict the Sauter mean bubble diameters in a mechanical flotation cell which is treated as two separate, statistically homogeneous zones: the impeller zone and the bulk tank zone (Sawyer et al., 1998).

Balance functions for the rates of bubble breakage, coalescence, recirculation and inlet-outlet events are proposed based on classical chemical engineering research in two- and three-phase fluid mixing systems.

The reliability of mathematical models can be better assessed with the assistance of observation techniques capable of sizing accurately a large number of bubbles. A technique consisting in exposing a stream of bubbles to a progressive scan camera has been used to study the effect of several physical and chemical variables on bubble size in laboratory scale flotation cells (Grau, 2006).

### 2.3.4. EFFECT OF TURBULENCE

Experimental results of a research aimed at purifying molten aluminium indicate that turbulence may enhance the flotation rate of non-metallic inclusions to bubbles significantly. Possible flow phenomena responsible for such effects are investigated. Only the smaller eddies contribute to an enhanced turbulent deposition of inclusions whereas the eddies in the spectrum larger than the bubble diameter can only displace the bubble.

The bubble size and the collection conditions at the bubbles may change considerable with rotor speed. Turbulence may increase the collection efficiency by more than 100-fold compared to laminar conditions (Gammelsæter et al., 1997).

The hydrodynamic conditions prevailing in the flotation cells can be modified mainly by altering the impeller speed and aeration conditions, as well as the frother concentration.

The aeration rate has a profound impact on bubble generation because the bubble size increases with an increase of the air flow rate entering the flotation cell. The aeration rate seems to determine to a large extent the size, shape and behaviour of the

aerated cavities formed behind the blades of the rotor of the cell.

The U.S. Bureau of Mines examined the influence of turbulence on the fine bubble flotation of fine-sized (minus 40 micrometer) galena in order to improve flotation efficiency. While improved flotation response was obtained with intense agitation, the effect of bubble size was small. These results matched the model's predicted response for fine particle flotation (Spears and Jordan, 1989).

#### 2.3.5. EFFECT OF FROTHER ADDITION

With increasing frother concentration, the degree of bubble coalescence decreases, while at a particular frother concentration, known as the critical coalescence concentration (CCC) bubble coalescence is totally hindered. The experimental results also indicate that frothers appear to affect the break-up process or bubble generation. (Grau, 2006)

At frother concentrations beyond CCC, bubble size is no longer determined by coalescence but depends on the sparger geometry and hydrodynamic conditions.

The results show that probability of collection increases rapidly with decreasing bubble size, and the values are in good agreement with the theoretical collision probabilities predicted from Weber and Paddock's analysis (Yoon and Luttrell, 1989).

Coalescence can be prevented at frother concentrations exceeding the critical coalescence concentration (CCC). The foamability tests indicate that stability of foams under dynamic conditions is determined by bubble coalescence (Cho and Laskowski, 2002).

The ultimate size of bubbles in a flotation cell is an outcome of competing processes: coalescence of bubbles and adsorption of the surfactant on their surface. Formation of highly developed initial interface due to break-up of the gas phase is an indispensable condition for stabilizing bubble size at a lower size level (Kondrat'ev and Bochkarev, 1998).

#### 2.3.6. INSIGHT INTO THE MECHANISM INVOLVED IN FLOTATION

The basic mechanism of gas dispersion under highly turbulent conditions has been dealt with by a number of researchers. In mechanically agitated, aerated vessels, such as flotation cells, air introduced into the cell accumulates in low pressure cavities behind the impeller blades and bubbles are sheared off the cavities by the impeller's rotation (Tatterson, 1991). These bubbles are further broken under the turbulent conditions in the impeller region and are then dispersed throughout the cell by the pumping action of the impeller. In the bulk region of the cell, bubble motion is controlled by the surrounding fluid circulatory motion and by the bubble's inherent buoyancy. Bubbles in this region may collide and coalesce, re-circulate back to the impeller region, or rise out of the cell. The equilibrium bubble size distribution in the

cell is ultimately dictated by all the events taking place in the cell, in particular by the relative rates of bubble breakage and bubble coalescence in the cell.

Investigations into bubble coalescence reported in the literature have isolated the coalescence rate by eliminating the contribution of bubble breakage to the equilibrium bubble size distribution. This has been done either by employing very quiescent bubble columns where the rate of bubble breakage was negligible, or by sparging bubbles into the system that were too small to be broken up by the impeller.

It is evident that both coalescence and breakage are complex, interdependent phenomena that are influenced by the instantaneous state of the system, in systems such as the mechanical flotation cell, where both bubble breakup and coalescence are taking place.

### 3. WATERJET POTENTIAL IN FLOTATION

#### 3.1. LABORATORY EXPERIMENTS

##### 3.1.1. STARTING POINT OF THE RESEARCH

As pointed out above, poor results are generally achieved in the treatment of slimes using conventional methods. Since fine size fractions below 0.5 mm can together represent a significant portion of the plant's feed, the development of suitable technologies for an efficient recovery of their valuable mineral content may give a considerable contribution to the economic balance of the beneficiation process. Froth flotation can be regarded as the most attractive technique for treating such slimes.

In order to create the most favourable conditions for the full development of collection and separation mechanisms, a new approach has been devised and tested, according to which agitation is produced using high velocity water jets generated through a suitable nozzle configuration (Carbini et al., 1996; 1998; Chudacek et al., 1997).

In mechanically agitated conventional flotation cells impellers are used for creating the conditions for achieving the highest differential velocity between the liquid and the gaseous phases, thus enhancing the pulp aeration. There the differential velocity is that established at the rim of the rotor between the incoming air and the layer of stirred water (Ciccu and Kursun, 2010).

However, in spite of using suitable devices like a facing stator with the goal of improving the effect, differential velocity commonly achieved in mechanical cells does not exceed few metres per second.

On the basis of these considerations, the possibility of applying a different concept in the attempt to increase substantially the differential velocity was an intriguing opportunity to investigate.

Collection efficiency improves if the bubbles are well dispersed into the cell

meaning that, for a given volume of injected air, bubble size should be as small as possible at the moment of their generation. Then controlled coalescence into large bubbles can ensure sufficient buoyancy while avoiding rupture phenomena due to thinning of the interface film.

To this end, the chances offered by waterjet seemed very attractive for a number of reasons such as

- possibility of generating a high velocity water streams, at least one order of magnitude higher than with mechanical impellers, even at relatively low pressures,
- high turbulence into the vessel owing to the feasibility of producing a number of superimposing whirls by suitably modifying the arrangement of the nozzles,
- smaller initial bubbles issuing from calibrated holes right below the waterjet nozzle,
- even distribution of the bubbles inside the vessel (Fig. 1).

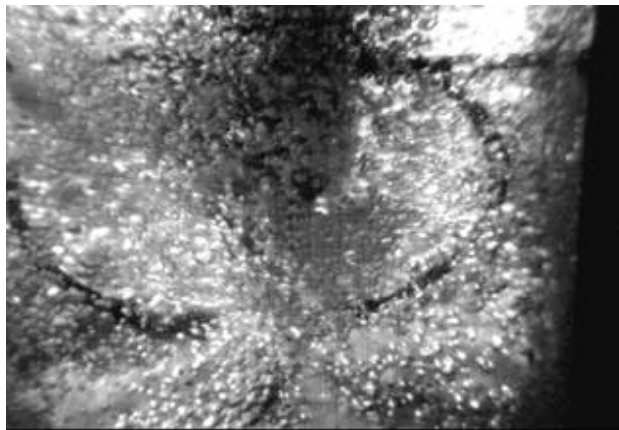


Fig. 1. Features of bubble produced with waterjet agitation

A high-velocity water jet is capable of carrying a considerable power (up to some hundreds of kW) concentrated in a small space (less than  $1 \text{ mm}^2$ ). When this beam of energy is injected into a vessel filled with still water the shear velocity can be very high, by at least an order of magnitude greater depending on the hydraulic parameters (pressure and flowrate).

### 3.1.2. LABORATORY EQUIPMENT

A prototype of the waterjet-agitated flotation cell named ‘Hydrojet’ has been designed and built. It consists of a cylindrical vessel, about  $10 \text{ dm}^3$  in volume provided

with a hemispherical bottom screen for the discharge of the reject through a central outlet. Froths are eliminated through a chute in the upper section of the cylindrical body (Carbini et al., 1998).

The efficiency of the flotation process depends highly on the initial contact between the air bubble and the mineral particle. To enhance this contact, the nozzle arrangement inside the flotation cell has been devised to achieve good mixing between the suspended solids and the dispersing air. A sketch of the laboratory equipment is shown in Fig. 2.

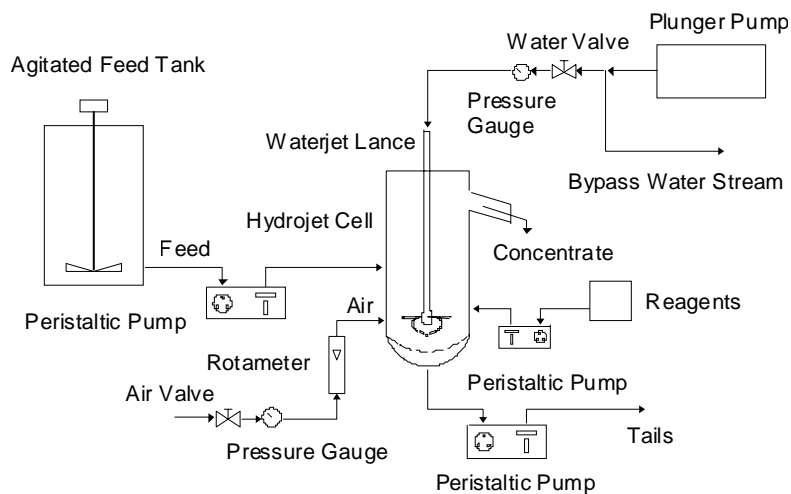


Fig. 2. Sketch of the Hydrojet cell laboratory equipment

## 3.2. RESULTS

### 3.2.1. PROOF OF THE HYDROJET CONCEPT

Parallel series of flotation tests have been carried out with waterjet or with a conventional impeller (M&M), using the same cylindrical cell under common experimental conditions for the unbiased comparison of the results. Experiments were made on samples of a run-of-mine coal, a barite crude ore and a sphalerite sample with quartz gangue.

### 3.2.2. COAL FLOTATION

The high-rank coal utilised for the flotation tests, coming from the Walsum mine (Germany) was dry ground to below 0.3 mm. The kinetics of the process with waterjet

or with mechanical agitation was studied by varying the solids feed rate. Technical results (fuel recovery and quality of the separation products) as a function of residence time are summarised in Fig. 3. Recovery with waterjet is considerably higher than that achieved with mechanical agitation. Results are better using only two jets, although the quality of the product is slightly worse. For achieving the same recovery a 2.5-fold longer residence time is needed with mechanical agitation (Agus et al., 1998).

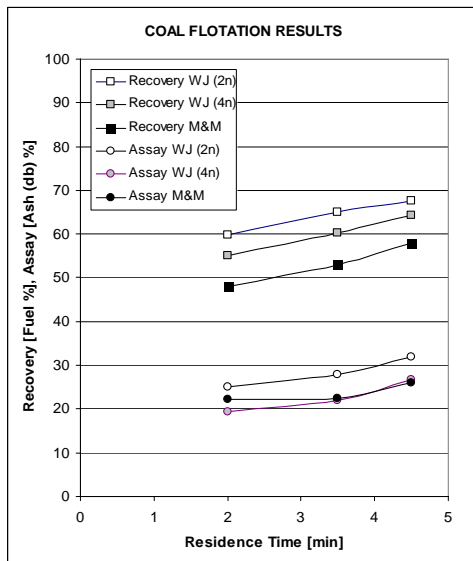


Fig. 3. Rougher flotation of Walsum coal. Fuel recovery and ash content in the product versus residence time. Frother concentration (MIBC) was  $9.7 \text{ g/dm}^3$

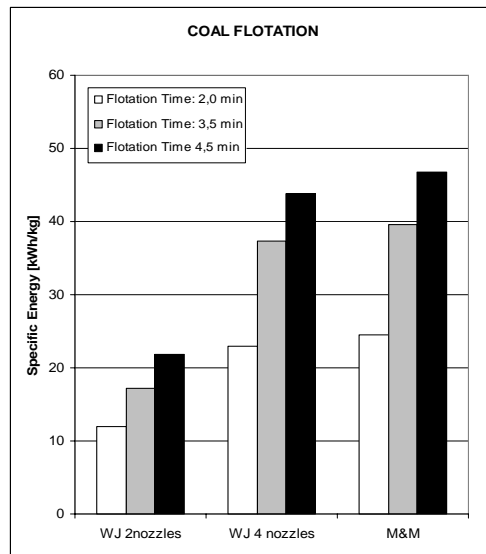


Fig. 4. Specific energy consumption in coal flotation experiments

A further advantage offered by the Hydrojet cell is a considerable reduction in energy consumption, as shown in Fig. 4, where specific energy per kg of recovered coal is represented at variable residence time. Compared with the conventional cell, specific energy with four 0.3 mm jets is almost the same but it becomes less than half if only two jets are used, which is also the most favourable condition for separation (Carbini et al., 2007).

### 3.2.3. FLOTATION OF INDUSTRIAL MINERALS

The sample used for the experiments, dry ground to below 0.2 mm, contained about 45%  $\text{BaSO}_4$ , the main gangue components being limestone, silica and iron

oxides. Results of rougher flotation are summarised in Fig. 5.

The following aspects are worth underlining:

- BaSO<sub>4</sub> recovery with waterjet is somewhat higher than that achieved with mechanical agitation at any dosage of collector, although with lesser evidence than for coal (Carbini et al., 1998)
- BaSO<sub>4</sub> content in the concentrate is slightly higher with waterjet in spite of using half the power
- results do not improve by doubling the jet flowrate using four 0.3 mm nozzles instead of two at equal pressure
- the presence of an optimum value for pressure can be identified around 9 MPa for the laboratory model, although it can be higher for larger cells.

The above findings are of great interest for the future development of the concept and the improvement in the design and operation of waterjet cells.

#### 3.2.4. SULFIDE FLOTATION

The zinc sulphide ore used for the new series of experiments originates from a Sardinian mine and averages about 9.5 % Zn, ground to below 0.2 mm.

In order to put into a better evidence the expected advantages achievable by using water jets, flotation tests have been carried out using the same cylindrical vessel, hosting the waterjet nozzle head (Hydrojet cell) or the conventional impeller (Minemet), under common experimental conditions concerning the reagents used and their dosage, the solids feed rate and mass concentration, the residence time (3.5 min) and the air flow rate

Results of the comparative tests between Minemet and Hydrojet cell carried out according to the above described procedure are summarised in Fig. 6, where Zn recovery and Zn grade of the rougher concentrate are plotted against air rate.

It is worth underlining that both Zn recovery and Zn concentrate grade with the Hydrojet cell are well higher (by more than 10 percent points, and by about 2-3 points, respectively) than those achieved with mechanical agitation at any pulp aeration conditions, while the metal loss in the tailings is significantly lower (by at least 2 points).

All the curves are almost parallel showing that the difference in results is essentially due to the kind of agitation. This achievement fully corroborates the results already obtained with coal and barite and further confirms the superior flotation selectivity when using waterjet.

It seems that optimum operating pressure is around 8-10 MPa, giving a jet velocity at the nozzle of about 100 m/s. An increase in pressure beyond that level at equal hydraulic power using smaller nozzles does not appear very profitable. However it is likely that higher pressure will be needed in the scale-up of the system.

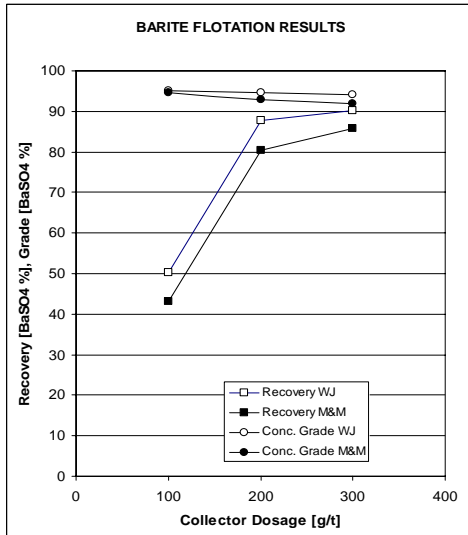


Fig. 5. Rougher flotation recovery and concentrate grade with water jet and with mechanical agitation as a function of collector dosage

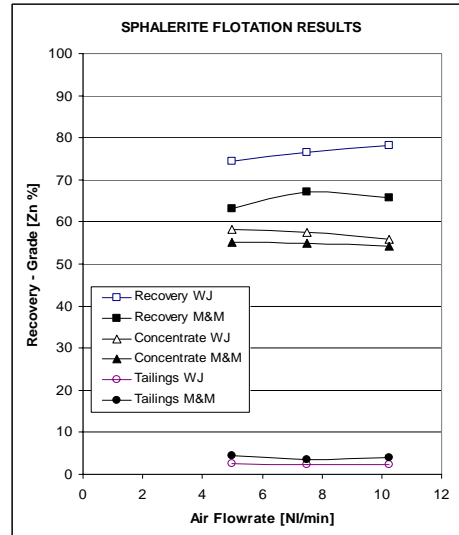


Fig. 6. Rougher flotation recovery and concentrate grade with water jet and with mechanical agitation as a function of collector dosage

### 3.3. DISCUSSION

Based on the outcome of the experimental tests, the following considerations can be drawn concerning the scientific explanation of the observed results.

#### 3.3.1. GRADE OF THE PRODUCT

The quality of the floated products is always better when waterjet is used for agitation and bubble generation for coal, sulfide and barite ores. It is believed that this is due to the more favourable size distribution of the bubbles (mean value and dispersion parameter). In order to support this statement in a quantitative way it should be necessary to characterize the bubble features with suitable measurements. For this purpose, a specific research project has been undertaken at the University of Cagliari using the Particle Image Velocimetry (*PIV*) optical technique, that allows to measure displacement with time (and hence the velocity) of individual particles starting from a sequence of images taken at very small time intervals.

Floatable mineral particles are uplifted only if buoyancy prevails over the attached weight. If particles are well liberated by comminution, selectivity should be good irrespective of bubble size. However, this is not true for mixed particles: provided that the attachment strength is sufficient, a single large bubble will carry a particle even if

the gangue component largely prevails, thus polluting the product, whereas this is avoided in the case of small bubbles that may attach to the same particle, making flotation more selective, especially for coarser particles.

### 3.3.2. FLOTATION RECOVERY

The higher recovery, observed in the experiments with waterjet agitation, can be explained by the fact that bubble-particle collision probability is enhanced because the bubbles are smaller (and hence much higher in number for a given overall air flow), faster and much better distributed inside the cell than in the case of mechanical agitation. Moreover larger bubbles are more likely to break before reaching the froth layer, thus losing the attached particles. The use of a suitable number of nozzles conveniently placed in the inner space of the cell allows to optimise bubble distribution by multiplying the generation points while avoiding the backwards draw of the bubble stream towards the rotor where an air vortex is formed.

### 3.3.3. THROUGHPUT CAPACITY

Owing to faster development of collection mechanism, a shorter flotation time is needed for achieving a given recovery level when resorting to waterjet for bubble generation. This is a considerable advantage concerning the economic issues of a beneficiation process.

### 3.3.4. ENERGY CONSUMPTION

In spite of the fact that waterjet is generally regarded as an energy consuming technology, specific energy required in this particular application is relatively low. In fact, for attaining a shear velocity tenfold higher than the peripheral velocity of conventional rotors, a relatively low pressure is needed, thus limiting the overall hydraulic power of the jets per unit volume of the flotation vessel. Wear is also quite insignificant due to the absence of components subject to consumption in presence of abrasive minerals.

### 3.3.5. CONCLUDING REMARKS

Separation performance of available flotation machines gradually deteriorates as particle size decreases, resulting in low recovery, unsatisfactory quality of the product and a high specific consumption of energy and reagents. The use of water jets generated at moderate pressure can be considered as a suitable way for improving the required conditions for the full development of flotation mechanisms, especially in the

case of very finely ground ores.

The following advantages can be predicted with the further improvement and the industrial scale-up of the technology, compared to conventional methods:

- more favourable bubble features
- efficient control of the agitation pattern by optimising the nozzle arrangement and using fan jets
- higher recovery and better separation selectivity especially for the fine particle sizes
- less energy consumption using lower pressures
- reduced wear (no rotating parts are involved)
- expected higher capacity per unit volume of the cell owing to faster flotation kinetics
- waterjet can be the base for the design of a new sparger device in column flotation.

#### 4. CONCLUSION

A jet of water issued at high velocity from a calibrated nozzle can be used in a variety of applications owing to its unique capability of carrying a high power concentrated in a very small space. The potential is considerably increased by the possibility of incorporating a load of abrasive particles into the jet. However, although this technology is still applied in many fields of rock and stone engineering (excavation, slotting, cutting, drilling, surface finishing) no commercial instances can be found in the areas of mineral comminution and separation. This is due to the high level of maturity reached by conventional methods and equipment, the use of which enables the efficient solution of most mineral processing problems. However waterjet can offer new opportunities for improving the performance of conventional machines on one side as well as for designing and implementing new solutions.

#### REFERENCES

- AGUS M., CARBINI P., CICCU R., GHIANI M., SATTA F., TILOCCA C., 1998, *Flotation of coal fines using high shear water*, Proc. XIII International Coal Preparation Congress, Brisbane, Australia, October 1998.
- AHMED, N., JAMESON, G.J., 1985, *The Effect of Bubble Size on the Rate of Flotation of Fine Particles*. Int J. of Min. Proc., vol. 14, 1985. pp. 195-215.
- BISWAL, K, REDDY, P. S. R., BHAUMIK, S. K., 2009, *Bubble size distribution in a flotation column*, The Canadian Journal of Chemical Engineering Volume 72 Issue 1, Pages 148- 152, Published

Online: 27 Mar 2009.

- CAPESE, C.E., MC IHINNEY, A.E., MC KEEVER, R.E., MESSER, L., 1976, *Application of spherical agglomeration to coal preparation*. Proc. VII Int. Coal Prep. Congress, Sydney, May 1976.
- CARBINI, P., CICCUCI, R., GHIANI, M., SATTI, F., TILOCCA, C., 1998, *A new concept in flotation technology*, Proc. 5<sup>th</sup> Pacific Rim International Conference on Water Jet Technology, New Delhi, India, Vijay M.M, Babu N.R. and Yahiro T (eds), Allied Publishers Ltd, New Delhi, pp. 295-301.
- CARBINI, P., CICCUCI, R., GHIANI, M., SATTI, F., TILOCCA, C., 1998, *Flotation of barite fines with the new Hydrojet cell*, Proc. 7<sup>th</sup> International Mineral processing Symposium Innovations in Mineral and Coal Processing, Istanbul 1998
- CARBINI, P., CICCUCI, R., GHIANI, M., SATTI, F., TILOCCA, C., 2001, *Flotation of a sulphide ore using high velocity water jets* Proc. VI SHMMT/XVIII ENTMMME, Rio de Janeiro 2001 pp. 5
- CARBINI, P., CICCUCI, R., GHIANI, M., SATTI, F., TILOCCA, C., 2007, *Advances in Coal Flotation Technology*, Proc. Third Int. Conf. on Clean Coal Technologies for our Future, Cagliari May 2007, 15 pp.
- CHEN, H.T., MIDDLEMAN, S., 1967, *Drop size Distribution in Agitated Liquid-Liquid Systems*. A.I.C.H.E. Journal, vol. 13, 1967. p. 989.
- CHO, Y. S., LASKOWSKI, J. S., 2002, *Effect of flotation frothers on bubble size and foam stability*, Int. J. Miner. Process. 64 (2002) pp. 69-80
- CHUDACEK M.W., MARSHALL S.H., FISHERA M.A., BURGESS J., BURGESS F.L., 1997, *Super-scavenging of zinc from tailings by the FASTFLOT process*, Proc. of the XX Int. Mineral Processing Congress, Aachen, Germany, Hoberg H.(ed.), GDMB, Clausthal-Zellerfeld, Germany, Vol. 3, pp. 275-284
- CICCUCI, R., KURSUN, I. 2010, *Potential Advances in Mineral Processing and Flotation by Using Water Jets*, 18th Proceedings of BHRG Conferences on Waterjetting, Austria, pp.485-494.
- GAMMELSAETER, R., BECH, K., JOHANSEN, S.T., 1997, *Enhanced flotation of inclusions to bubbles due to turbulence*, Proc.TMSINC 97, pp. 11
- GRAU, R.A., 2006, *Dissertation for the degree of doctor of science in technology Helsinki University of Technology*.
- HONAKER, R. Q. et al., 1994, *A comparison study of column flotation technologies for cleaning Illinois coal*, Report ICCI Project Number: 93-1/5.1A-IP DOE Grant Number: DE-FC22-92PC92521, 1994
- KLASSEN, V.I., MOKROUSOV, V.A., 1963. *Formation of air bubbles*, An Introduction to the Theory of Flotation, Butterworths, London, 1963, pp. 443-463.
- KOH, P. T. L., MANICKAM, M., SCHWARZ, M. P., 2010, *CDF simulation of bubble-particle collisions in mineral flotation cells*, Minerals Engineering Volume 23, Issue 1, Pages 1-64.
- KONDRAT'EV, S.A., BOCHKAREV, G.R., 1995, *Intensification of aeration processes in flotation of sulphide ores*, *Journal of Mining Science* Vol. 31 (6), pp. 454-458.
- SAWUERR, F., DEGLON, D.A., O'CONNOR, C.T., 1998, *Prediction of bubble size distribution in mechanical flotation cell*, The Journal of the South African Institute of Mining and Metallurgy July/August 1998 pp. 179-186.
- SPEARS, D.R., JORDAN, C.E., 1989, *The effect of turbulence on the flotation rate of galena when using fine bubbles*, Advances in Coal and Mineral Processing Using Flotation, SME 1989, pp.8.
- TAO, D., 2005, *Role of bubble size in flotation of coarse and fine particles- a review*. Separation Science and Technology, vol. 39 (4), pp. 741-760.
- TATTERSON, G.B., 1991, *Fluid Mixing and Gas Dispersion in Agitated Tanks*. McGraw-Hill.
- YOON, R.H., LUTTRELL, G.H., 1989, *The Effect of Bubble Size on Fine Particle Flotation*, Minerals Processing and Extractive Metallurgy Review, vol. 5, pp. 101-122.

**Ciccu, R., Kursun, I.,** *Możliwości usprawnienia flotacji przez użycie strumieni wodnych*, Physicochem. Probl. Miner. Process., 46 (2011) 35-50, (w jęz. ang), <http://www.minproc.pwr.wroc.pl/journal>

Niektóre problemy występujące w przeróbce kopalin jak dotąd nie są rozwiązane przez obecnie stosowane technologie, zwłaszcza te oparte na użycie energii mechanicznej. Stosowanie energii mechanicznej ma wady takie jak zużycie części maszyn oraz ograniczona prędkość części ruchomych z powodu unikania ryzyka awarii w wyniku trudnych warunków pracy. Strumienie wodne mogą przyczynić się do przezwyciężenia tych trudności poprzez transfer energii bez kontaktu pomiędzy częściami wykonanych z materiałów stałych (brak tarcia) i są one wygodne dla generowania wysokich prędkości strumienia powietrza oraz wody przy względnie niskich ciśnieniach. Możliwe korzyści ze stosowania strumieni wodnych mogą mieć miejsce zwłaszcza we flotacji, gdzie rozmiar i prędkość pęcherzyków powietrza zależy od prędkości ścinania wywoływanej agitacją jako krytyczny aspekt optymalizacji wyników separacji (uzysk i selektywność). Pozwoli to także na redukcję rosnących kosztów zużycia części oraz oszczędność energii.

*słowa kluczowe: strumienie wodne, flotacja, flotacja węgla, rozdrabnianie*

Jari AROMAA \*

## ELECTROCHEMICAL DISSOLUTION OF SYNTHETIC HEAZLEWOODITE ( $\text{Ni}_3\text{S}_2$ )

*Received May 20, 2010; reviewed; accepted June 23, 2010*

The aim of the study was to examine the dissolution kinetics of synthetic heazlewoodite and the formation of elemental sulfur by electrochemical methods. Anodic polarisation curves, potentiostatic measurements and cyclic voltammetry were carried out in 1 N sulfuric acid at temperature 25°C. The anodic dissolution of heazlewoodite proceeds in two stages. At potentials below 600 mV vs. SCE heazlewoodite is only converted to higher sulfides such as millerite NiS. At higher potential the reaction products dissolve forming first other sulfides and elemental sulfur and later other sulfides, elemental sulfur and sulfate. The percentage of sulfides in the reaction products was high even at high potentials. The formation of elemental sulfur was not seen to hinder dissolution of the sulfide. The part of sulfur oxidized to sulfate increased with increasing potential. Up to 900 mV only elemental sulfur was formed, at 1000 mV 10% of sulfur was oxidized to sulfate and at 1600 mV 90% of the sulfur was sulfate.

*keywords: Nickel sulfide, dissolution, reaction mechanism, sulfur formation*

### 1. INTRODUCTION

Nickel is a transition element that exhibits a mixture of ferrous and nonferrous metal properties. Nickel forms several natural sulfides of which heazlewoodite ( $\text{Ni}_3\text{S}_2$ ) is the most nickel-rich compound. The other stable compounds found in sulfide ores are godlevskite ( $\text{Ni}_7\text{S}_6$ ), millerite (NiS), polydymite ( $\text{Ni}_3\text{S}_4$ ) and vaesite ( $\text{NiS}_2$ ). The bulk of the nickel comes from laterites where the principal ore minerals are

---

\* Aalto University, Department of Materials Science and Engineering, PO Box 16200, FIN-00076 Aalto, Finland, jari.aromaa@tkk.fi

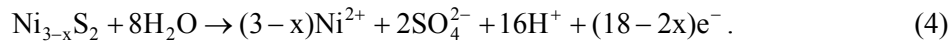
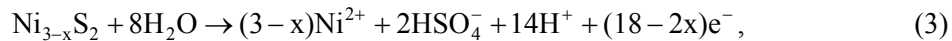
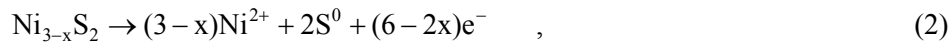
nickeliferous limonite (Fe,Ni)O(OH) and garnierite (a hydrous nickel silicate), or magmatic sulfide deposits where the principal ore mineral is pentlandite (Ni,Fe)<sub>9</sub>S<sub>8</sub> (Kuck, 2010). Heazlewoodite is sometimes found in nickel ores but it is a main component in smelted nickel matte (Muir et al., 2006; Palant et al., 2008).

Mineral sulfides are non-stoichiometric and they contain impurities. Therefore they have crystal defects that affect sulfide electrical properties. Heazlewoodite is a metallic conductor. This is based on the location of d-electrons that do not participate in the formation of chemical bonds. In sulfide minerals, sulfur occurs at its lowest oxidation state, -2. The metals have usually oxidation state +2. In several compounds the electroneutrality would not be fulfilled if there were not anion-anion bonds that decrease the net oxidation state of anions or cation-cation bonds that decrease the oxidation level of cations (Vaughan et al., 1978).

The usual hydrometallurgical route for the extraction of metals from sulfides requires oxidation of sulfur in the compound to either elemental sulfur or sulfate. Oxidation of sulfur to higher oxidation states (0, +2, +4 and +6) can occur if the redox-potential of the oxidant in solution, e.g. O<sub>2</sub>, Fe<sup>3+</sup>, is higher than the equilibrium potential of the sulfide. Basing on leaching studies of natural and synthetic heazlewoodite and nickel converter matte, the dissolution of heazlewoodite proceeds in two stages (Buckley et al., 1991; Ghali et al., 1981; Laig-Hörstebrook, 1969; Power, 1982; Price et al., 1982). In the first stage nickel is released from the sulfide structure and a reaction product layer forms. In this reaction product layer the ratio of metal atoms to sulfur atoms is less than the 1.5 of heazlewoodite. This is also known as conversion of heazlewoodite to higher sulfides. Heazlewoodite dissolves in the first stage after reaction (1) releasing nickel ions



In the second stage the reaction product layer dissolves after reactions (2)-(4) depending on the oxidation potential and pH



The formation of the reaction product layer can hinder the dissolution of the sulfide. This is due to slower transfer of oxidant and metal ions through the reaction product layer. The formation of the reaction product layer according to reaction (1) begins at potentials 200 to 0 mV vs. SCE (Buckley and Woods, 1991; Laig-Hörstebrook, 1969; Power, 1982; Wong et al., 2001). The reaction product layer can dissolve chemically, which indicates that the chemical bonds in the reaction product are weaker than in normal sulfide (Power, 1982). The reaction product layer breaks

down at potentials 500-800 mV vs. SCE (Ghali et al., 1981; Price and Davenport, 1982). The formation of the reaction product layer has been considered as a region of semipassivation as Ni<sup>2+</sup> slowly diffuses from the sulfide lattice to form a series of increasingly sulfur-rich nickel sulfides (Muir and Ho, 2006). Formation of NiS and Ni<sup>2+</sup> has also been related to oxidation peaks at 900 mV and 1100 mV vs. SCE, respectively (Wong and Tian et al., 2001). Formation of elemental sulfur has been the cause of decrease of current at potentials above 1100-1200 mV. Complete dissolution of the sulfides requires potentials above 1500 mV (Muir and Ho, 2006). Analysis of activation energies in perchloric acid shows that at potentials below 100-200 mV vs. SCE the dissolution is controlled by charge transfer or chemical step and at potentials above 800-900 mV the dissolution becomes mass transfer controlled. A mixed control prevails at potentials 200-800 mV vs. SCE (Knuutila, 1988).

Heazlewoodite has been used as model compound to study the electrochemical leaching of nickel from sulfide minerals. During chemical or electrochemical dissolution of sulfide minerals, sulfur may remain in amorphous form enveloping gradually the dissolving particles. Then, the dissolution is hindered and the diffusion of ions through the amorphous sulfur layer finally ceases. Sulfur may also be oxidized to sulfate, which increases the consumption of reagents or energy. In this paper the dissolution kinetics and sulfur formation as a function of oxidation potential have been studied.

## 2. EXPERIMENTAL

Heazlewoodite was synthesized in vacuum quartz ampoules as described by Vaughan and Craig, 1978. The materials were 10 μm nickel powder with minimum 99.5% purity (Merck 12277) and sulfur powder (JT Baker 0335). The theoretical composition of the ampoule charge was 60.0031 wt. percent of Ni and 39.9969 wt. percent of S. Nickel powder was pressed to 3 cm<sup>2</sup> round pieces using 8 ton hydraulic press and treated at 500°C in hydrogen atmosphere for one hour. Sulfur was pressed to 1 cm<sup>2</sup> pieces using hand press. The mineral synthesis was done at 400°C for three days, slowly raised (50°C / 12 hours) to 700°C, followed by treatment at 700°C for another three days and slow cooling (30°C/12 hours) to room temperature. The synthesized mineral was characterized by chemical analysis and XRD. The Ni<sub>3</sub>S<sub>2</sub> sample contained 70.4 wt. percent of Ni and 29.6% of S and corresponds to 56.5 wt. percent of Ni. The sulfide is slightly metal-deficient. No other phases than Ni<sub>3</sub>S<sub>2</sub> were detected.

The experiments were carried out in a three-electrode cell with electrolyte volume of 800 cm<sup>3</sup> (Fig. 1). The counter electrode was a platinum sheet with dimensions of 20 mm x 15 mm. The electrode potential was measured using Haber-Luggin capillary and liquid junction. The reference electrode was Radiometer type K401 saturated calomel

electrode (SCE). The SCE was put in Agar-Agar gel in a separate beaker to protect the electrode. All the measured potentials in this paper are presented in the SCE scale, i.e. +242 mV vs. SHE.

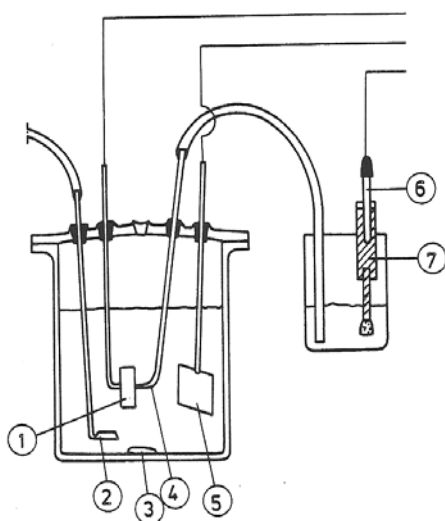


Fig. 1. Electrochemical test cell. 1 – Sulfide sample, 2 – Gas purging, 3 – Magnetic stirrer, 4 – Luggin capillary, 5 – Counter electrode, 6 – Reference electrode, 7 – Protecting gel

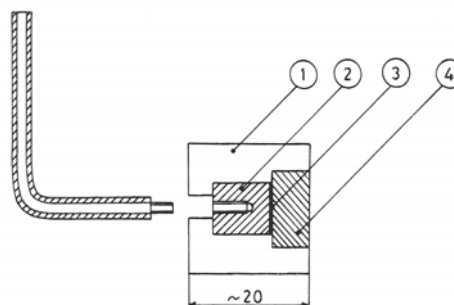


Fig. 2. The sample mounting. 1 – Epoxy resin, 2 - Copper backing plate, 3 – Graphite or silver glue, 4 - Sulfide sample

Pieces of synthetic heazlewoodite were attached with graphite glue to copper backing plate and mounted in non-conductive epoxy resin (Fig. 2). The use of threaded copper backing plate allowed removal of the current conducting wire from the sample for XRD and SEM analyses.

The electrolyte was 1 N sulfuric acid (Merck 731) solution. All tests were done at room temperature. The electrolyte was purged with nitrogen (AGA 99.99% N<sub>2</sub>) for two hours before the experiment and purging continued during the experiment. A magnetic stirrer was used during nitrogen purging and experiments. The corrosion potentials fluctuated, but after the five minute period the potentials were fairly constant in the range from -420 to -360 mV vs. SCE. The electrochemical experiments, which included anodic polarisation curves, cyclic voltammetry and potentiostatic measurements, were carried out with an automatic electrochemical measurement system developed at the Helsinki University of Technology, Laboratory of Corrosion and Material Chemistry (Aromaa, 1988). Metal ion contents of the electrolytes in potentiostatic leaching experiments were measured with the Perkin-Elmer 372 atom absorption spectrometer (AAS).

### 3. RESULTS

The anodic polarisation measurements were carried out to gain general information on dissolution characteristics of the sulfide mineral, while the cyclic voltammetry measurements gave more detailed information on reaction stages, mechanisms and behavior of sulfur. The potentiostatic leaching experiments gave more data on the kinetics of dissolution.

#### 3.1. RESULTS

A general leaching behavior of the sulfide mineral was examined using anodic polarization measurements. Anodic sweeps were started at the corrosion potential and the samples were polarized stepwise at scan rate 20 mV/min up to gas evolution region, i.e. 2000 mV vs. SCE.

An example of the polarization curve is shown in Fig. 3. The polarization curves show three different reaction stages, i.e. two dissolution reactions of the sulfide including phase transformation (stage I) and decomposition of the sulfide to higher sulfides or to nickel and elemental sulfur (stage II and III). At the reaction stage III the oxidation of sulfur to sulfate may also occur. These reactions are followed by oxygen evolution at the anode. The reactions occur at the potential ranges of 0-500 mV (I), 700-1200 mV (II) and above 1300 mV (III), respectively. This anodic behavior agrees with the behaviour presented in literature (Buckley and Woods, 1991; Ghali et al., 1981; Muir and Ho, 2006; Power, 1982; Price and Davenport, 1982).

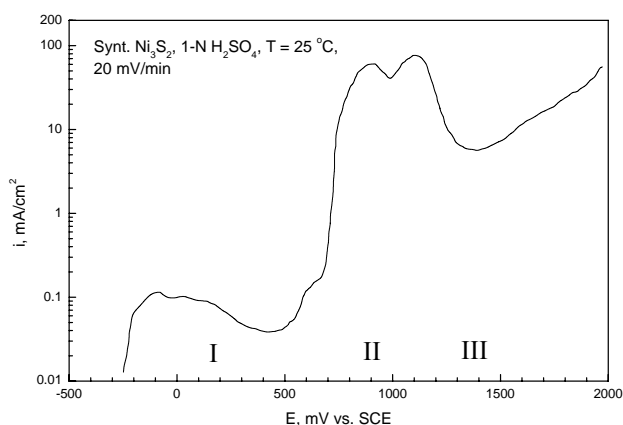


Fig. 3. Anodic polarisation curve of synthetic  $Ni_3S_2$  in 1 N  $H_2SO_4$ ,  $dE/dt = 20$  mV/min.

Stage I - dissolution by mineral transformations, Stage II - dissolution by oxidation of mineral sulfur to higher sulfides or elemental sulfur, and Stage III - dissolution by oxidation of sulfur to elemental sulfur or sulfate

## 3.2. CYCLIC VOLTAMMETRY MEASUREMENTS

The cathodic maximum potential in the cyclic voltammetry measurements was set to a constant potential of -500 mV and the anodic maximum potential was altered between +300 and +900 mV (Figs. 4 and 5). The measurements were carried out clockwise starting at the corrosion potential of the mineral. The elemental sulfur formed in anodic dissolution reaction is reduced to  $H_2S$  during the following cathodic sweep. The reduction peak can be seen in the potential range of -100 to -400 mV. The reduction peak is mostly due to reduction of elemental sulfur to hydrogen sulfide, but as side reactions can happen reductive leaching of heazlewoodite or higher sulfides (Filmer, 1981; Filmer et al., 1980). As the anodic maximum potential increases, the peak of reduction to hydrogen sulfide becomes larger. This means that at higher anodic potentials more sulfide has dissolved, even in this rapid experiment.

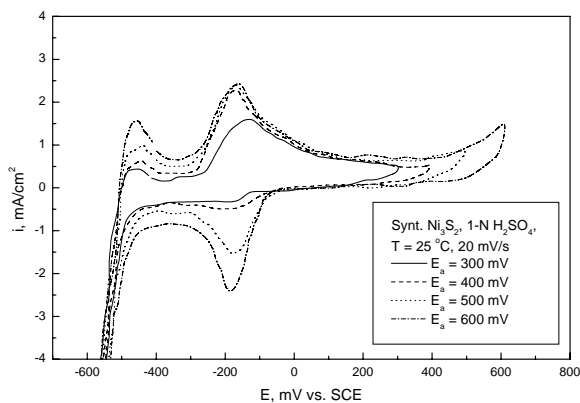


Fig. 4. Cyclic voltammograms of heazlewoodite in 1 N H<sub>2</sub>SO<sub>4</sub>, T = 25 °C, dE/dt = 20 mV/s, second cycles, anodic max. potentials 300, 400, 500 and 600 mV

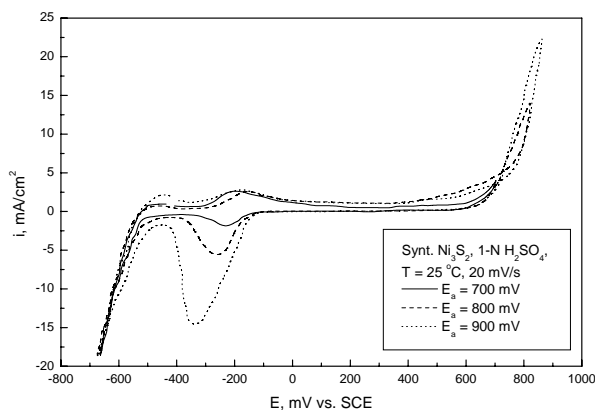


Fig. 5. Cyclic voltammograms of heazlewoodite in 1 N H<sub>2</sub>SO<sub>4</sub>, T = 25 °C, dE/dt = 20 mV/s, second cycles, anodic max. potentials 700, 800 and 900 mV

The charge of both anodic dissolution ( $q^+$ ) and cathodic  $H_2S$  reduction reaction ( $q^-$ ) is integrated from the corresponding peak areas (Figs. 4 and 5). The ratio of cathodic reduction charge of sulfur and the anodic charge of dissolution were integrated from the steady state cycles. Figure 6 shows that at low anodic maximum potentials the ratio of anodic to cathodic charges is high. At low anodic potentials the reaction products do not contain much of compounds that are reduced to hydrogen sulfide. As the anodic maximum potential increases, the ratio becomes smaller. At potentials between 600 and 700 mV the reaction product layer breaks down and elemental sulfur is formed as anodic dissolution product. At higher anodic potentials sulfur is oxidized to elemental sulfur and sulfate and the  $q^+/q^-(H_2S)$  ratio is fairly constant (approximately 3).

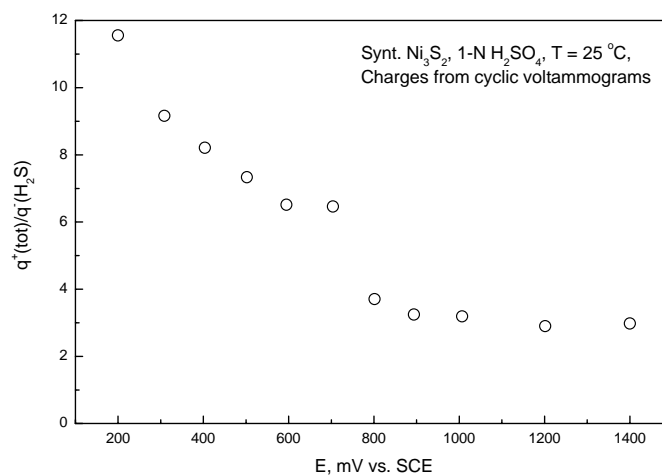


Fig. 6. Ratio of anodic and cathodic charges calculated by integration of cyclic voltammograms. As the anodic maximum potential increases, more reaction products which can be reduced to hydrogen sulfide, are formed

### 3.3. POTENTIOSTATIC MEASUREMENTS

Potentiostatic leaching experiments were carried out at potential range from -200 to 1600 mV. According to the polarisation curves, several different anodic leaching reactions can be observed at this potential range. The potentiostatic tests were done for 15 minutes to 1.5 hours depending on the potential used. At lowest potentials the test times were longest.

Current densities from the potentiostatic curves at different potentials are shown in Figure 7. The times are 0 s, 60 s and 900 s. The current density at  $t = 0$  s is determined by assuming inverse relationship of square root of current density with time. The relationship was quite well for potentials below 1400 mV. The shapes of the plots in

Figure 7 correspond good with the shape of the anodic polarization curve. The rapid decrease in current density at potentials below 600 mV supports the general trend that formation of higher sulfides leads to semi-passive state. The decrease in current density with time at 1300 mV can result from passivating sulfide formation. At higher potentials the increase in current density is due to disintegration of the sulfide and oxygen evolution. Gas evolution on sample surface was seen at this potential.

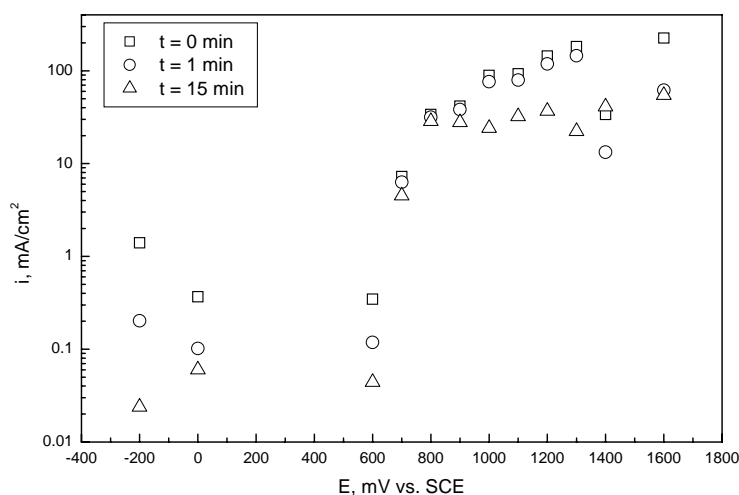


Fig. 7. Current densities from short potentiostatic tests

Even longer potentiostatic experiments were done to grow reaction product layers for analysis. In these tests the polarization times were 4 to 150 hours, again longest polarization times were used for lowest potentials. In these tests solution samples were taken for AAS analysis and the amount of dissolved nickel was determined. The reaction product layer was analyzed by cathodic reduction as in cyclic voltammogram using sweep rate 5 mV/s. The anodic charge was then calculated using the analyzed nickel concentration after Faraday's law and cathodic charge from integration of the reduction peak.

Figure 8 shows the ratio of anodic charge of the potentiostatic test and theoretical anodic charge calculated from nickel analysis. At the lowest potential (600 mV) there can be chemical dissolution in addition to the potentiostatic leaching. However at potentials of 700-900 the ratio is close to 1 indicating that all of the anodic current has been consumed in releasing of nickel. At potentials of 1100 mV and above the ratio is constant and slightly less than 1.5. The calculated charge ratio means that at potentials equal to 700-900 mV the current efficiency for nickel leaching is close to 100% but decreases to ~70% at 1100 mV and above. At this potential range part of the anodic current has been consumed in other reactions. According to reactions (2)-(4) this can be due to oxidation of sulfur to sulfate ions.

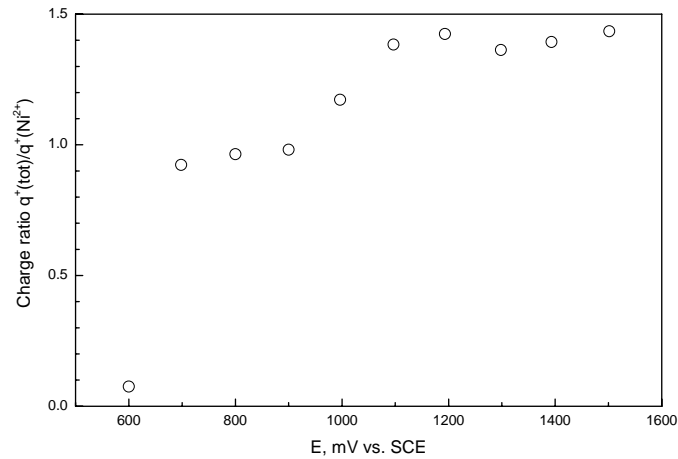


Fig. 8. Ratio of total anodic charge to theoretical nickel charge. At potentials of 700-900 mV the whole anodic current is consumed in nickel leaching and at potentials of 1100 mV and above part of sulfur is oxidized to sulfate

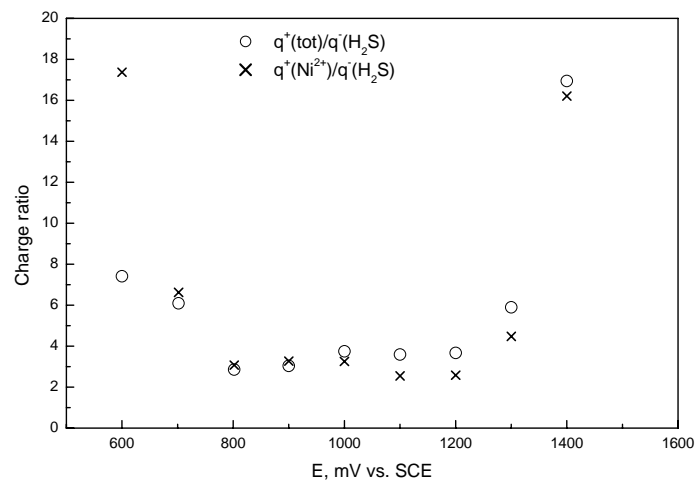


Fig. 9. Ratio of total anodic charge and theoretically calculated nickel charge to charge consumed in cathodic reduction of reaction products

By analysing the anodic charges and theoretical nickel charges vs. cathodic reduction of the reaction product layer further information on the oxidation of sulfur to sulfate was found. As shown in Fig. 9, the ratio of both anodic to cathodic charge increases at low potentials and at high potentials. At the potential range from 800 to 1200 mV the ratio is approximately 3, but little less for  $\text{Ni}^{2+}$  ratio at the higher potentials. The nickel ratio is higher than total charge ratio at low potentials and at

high potentials the ratio is vice versa. At potentials below 800 mV the high nickel ratio indicates that some of nickel has been released by chemical reactions. At potentials above 1000 mV some of the anodic charge has been consumed by other reactions than nickel dissolution.

### 3.3. XRD-ANALYSIS OF REACTION PRODUCTS

The surfaces of heazlewoodite samples were analyzed with XRD after potentiostatic leaching tests. The surfaces of fresh samples, samples left in open circuit potential, and samples polarized to potentials below 600 mV vs. SCE were greenish yellow. With microscope it was possible to see thin long cracks. When the reaction product layer disintegrates at potentials range of 600-900 mV the surface becomes black. At potentials over 1300 mV the grain boundaries of the sulfide become etched and the reaction product layers become loose.

As the sample is polarized to anodic potentials the heazlewoodite reacts to higher sulfides and when the potential is high enough, these reaction products from elemental sulfur, and finally also sulfates, are seen. Table 1 shows a compilation of XRD analyses. For a fresh untested sample only heazlewoodite was found. For an unpolarized sample left in test solution for 24 hours only heazlewoodite was seen. When the sample was polarized to the anodic direction ( $\approx 200$  mV overpotential) several higher sulfides were detected. At potential of 600 mV elemental sulfur was seen and at potential of 1000 mV also peaks of nickel sulfate were seen. The sulfate peaks can also result from crystallization of released nickel and sulfate anions of the test electrolyte.

Table 1. XRD-analysis of unreacted sample and samples polarized to constant potential for hours

Sample	Ni <sub>3</sub> S <sub>2</sub>	Ni <sub>7</sub> S <sub>6</sub>	NiS	Ni <sub>3</sub> S <sub>4</sub>	NiS <sub>2</sub>	S <sup>0</sup>	NiSO <sub>4</sub>
Untested	x						
Unpolarized	x						
E = -200 mV	x	x	x	x	x		
E = 200 mV	x	x	x	x	x		
E = 600 mV	x	x	x	x	x	x	
E = 1000 mV	x	x	x	x	x	x	x
E = 1400 mV	x	x	x	x	x	x	x

## 4. DISCUSSION

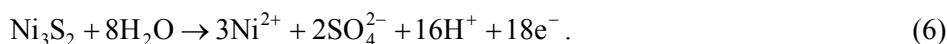
From a phase diagram of the Ni-S system a number of intermediates could have been anticipated. From this, it is predicted that dissolution of nickel from Ni<sub>3</sub>S<sub>2</sub> can proceed through the following series of phases: Ni<sub>3</sub>S<sub>2</sub> → Ni<sub>7</sub>S<sub>6</sub> → NiS → Ni<sub>3</sub>S<sub>4</sub> → NiS<sub>2</sub>. The anodic polarization curves (Fig. 3) showed the known behavior with three

different reaction mechanisms: At low potentials up to 600 mV mineral transformation, at intermediate potentials of 700-1200 mV formation of elemental sulfur and at high potentials above 1300 mV disintegration of the sulfide with formation of elemental sulfur and sulfate. XRD analysis of reaction product layers showed all the different intermediate sulfides.

At the low potential range of mineral transformation reactions, the reaction rates are too slow for meaningful leaching. The current densities of 0.01-0.1 mA/cm<sup>2</sup> at the low potential range correspond to dissolution rate of 0.03-0.25  $\mu$ m/hour for complete dissolution to nickel and sulfur. The oxidation potential must be high enough to dissolve all the higher sulfides and form elemental sulfur in order to get useful dissolution rates. Analysis of anodic and cathodic charges suggests that elemental sulfur formation begins at approximately 800 mV vs. SCE.

The charges from potentiostatic tests show that at potentials of 900 mV and below all the anodic charge is used in nickel dissolution. At higher potentials some of the charge is consumed in other reactions. Cyclic voltammograms show that the amount of reducible species in reaction products increases with increasing potential up to about 800 mV vs. SCE. At potentials from 800 to 1400 mV the ratio of anodic charges to cathodic charges is approximately 3. The charges calculated from potentiostatic tests followed by cathodic reduction of the reaction product layer also show that at potentials of 800-1200 mV the ratio of anodic charges to cathodic charges are approximately 3. Analysis of charges consumed in potentiostatic leaching and reduction of the corresponding reaction product layers indicate that disintegration of reaction product layer begins at 1200 mV.

Assuming that at the intermediate potential range the dissolution of heazlewoodite proceeds by reaction (2), i.e. the reaction products are nickel ions ( $3xNi^{2+}$ ) and elemental sulfur ( $2xS^0$ ), the ratio of anodic nickel release to cathodic sulfide reduction to hydrogen sulfide is 1.5. At this potential range the calculated charge ratio is close to 3. This means that part of the sulfur in the reaction product layer has not been reduced or the sulfur is in form that cannot be reduced. Two main causes can explain the charge ratio: the intermediate sulfides formed at low potentials are not reacting to hydrogen sulfide and at high potentials part of the elemental sulfur has been oxidized to sulfate and that can not be reduced. By simplifying heazlewoodite dissolution reactions (2) and (4) to (5) and (6) estimations of the reaction products can be done:



At potentials of 700-900 mV the current efficiency of nickel is close to 100% so only formation of intermediate sulfides and elemental sulfur can happen, (reactions (1) and (5)). At higher potentials current efficiency of nickel is less than 100% and so also sulfate formation (6) happens. By using the anodic total charge  $q^+(\text{tot})$ , anodic charge

calculated from nickel analysis  $q^+(\text{Ni}^{2+})$  and cathodic reduction charge  $q^-(\text{H}_2\text{S})$ , the relation between intermediate sulfide, elemental sulfur and sulfate can be calculated:

- elemental sulfur formation =  $q^-(\text{H}_2\text{S})$
- intermediate sulfide formation =  $q^+(\text{tot}) - 1.5 \cdot q^-(\text{H}_2\text{S})$
- sulfate formation =  $q^+(\text{tot}) \cdot [1 - \eta(\text{Ni}^{2+})]$ .

When calculating at potentials above 900 mV the sulfate charge is calculated first using current efficiency of nickel and intermediate sulfides and sulfur charges are calculated using the remaining total charge. The percentages of charges consumed in formation of different reaction products at different potentials are shown in Figure 10. The relative charges comply with expected behavior in that less elemental sulfur and more sulfates are formed at higher potentials. Somewhat unexpected was a high percentage of intermediate sulfides at high potentials as it was expected that sulfide disintegration with sulfate formation would be the main reaction.

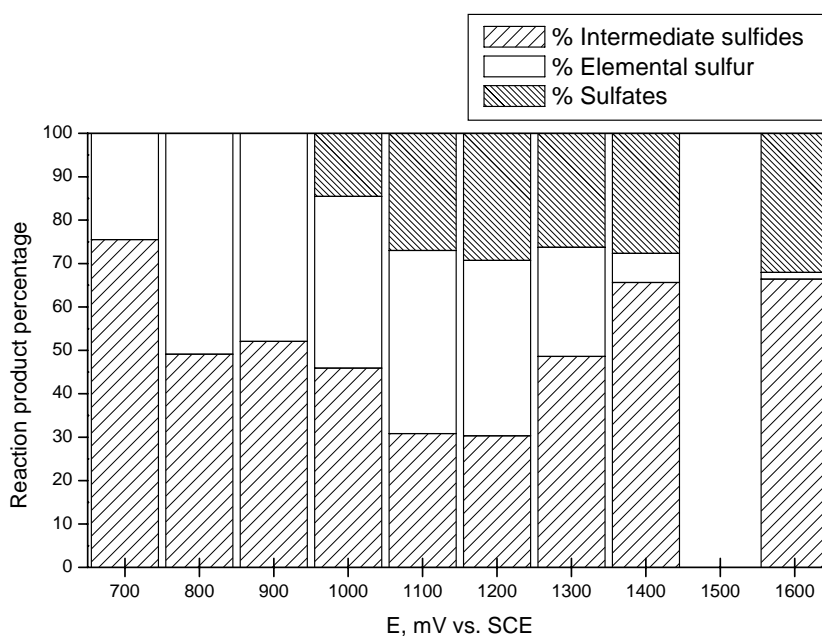


Fig. 10. Percentages of reaction products calculated from measured charges. Note that no test was done at  $E = 1500$  mV

When the formation of intermediate sulfides is excluded from the reaction products it is possible to estimate the percentages of elemental sulfur and sulfate. The ratio of elemental sulfur to sulfate decreases with increasing potential. Up to 900 mV only sulfur is formed. At 1000 mV there is 90% elemental sulfur and 10% sulfate but at 1600 mV only 10% sulfur and the rest is sulfates.

## 5. CONCLUSIONS

The synthetic heazlewoodite dissolves anodically with three different reaction mechanisms as presented in literature. They were interpreted as up to 600 mV mineral transformations, at intermediate potentials of 700-1200 mV formation of elemental sulfur and at high potentials, above 1300 mV disintegration of the sulfide with formation of elemental sulfur and sulfate.

The analysis of potentiostatic tests and cyclic voltammograms revealed that the formation of reaction products is not as clear as predicted by the polarization curves. Formation of intermediate sulfides continues even at the highest potentials tested. From 30 to 75% of the charge is consumed in formation of intermediate sulfides with minimum at 1100-1200 mV. Up to 900 mV only sulfur is formed. At 1000 mV there is 90% elemental sulfur and 10% sulfates but at 1600 mV only 10% sulfur and the rest is sulfates.

## REFERENCES

- AROMAA, J. (1988). Automatization of Electrochemical Experiments Using a Microcomputer, Lic.Tech. Thesis, Helsinki University of Technology, 115 p. (in Finish)
- BUCKLEY, A. & WOODS, R. (1991). Electrochemical and XPS studies of the surface oxidation of synthetic heazlewoodite (Ni<sub>3</sub>S<sub>2</sub>). *Journal of Applied Electrochemistry* 21: pp. 575-582.
- FILMER, A. (1981). The non-oxidative dissolution of nickel mattes in aqueous solutions. *Journal of the South African Institute of Mining and Metallurgy*(3): pp. 74-84.
- FILMER, A. & NICOL, M. (1980). The non-oxidative dissolution of nickel sulphides in aqueous acidic solutions. *Journal of the South African Institute of Mining and Metallurgy*(12): pp. 415-424.
- GHALI, E., MERIC, C. & DEROO, D. (1981). Electrodisolution de la heazlewoodite in milieu chlorhydrique. *Journal of Applied Electrochemistry* 11: pp. 153-163.
- KNUUTILA, K. (1988). Anodic dissolution behaviour of heazlewoodite (Ni<sub>3</sub>S<sub>2</sub>) in perchloric acid solution. Doctoral Thesis, Helsinki University of Technology, 72 p.
- KUCK, P. (2010). Nickel Statistics and Information. Retrieved 18.4.2010, from [minerals.usgs.gov/minerals/pubs/commodity/nickel/index.html](http://minerals.usgs.gov/minerals/pubs/commodity/nickel/index.html)
- LAIG-HÖRSTEBROCK, H. (1969). Electrochemisches Verhalten von Metallsulfidanoden. Dr.-Ing. Thesis, TU Berlin, p.
- MUIR, D. & HO, E. (2006). Process review and electrochemistry of nickel sulphides and nickel mattes in acidic sulphate and chloride media. *Transactions of the Institute of Mineral and Metallurgy C* 115(2): pp. 57-65.
- PALANT, A., BRYUKVIN, V., VINETSKAYA, T. & MAKARENKOVA, T. (2008). Kinetics of Ni<sub>3</sub>S<sub>2</sub> Sulfide Dissolution in Solutions of Sulfuric and Hydrochloric Acids. *Russian Metallurgy (Metally)*(1): pp. 22-24.
- POWER, G. (1982). The electrochemistry of nickel sulfides - 2Ni<sub>3</sub>S<sub>2</sub>. *Electrochimica Acta* 27(3): pp. 359-364.
- PRICE, D. & DAVENPORT, W. (1982). Anodic reactions of Ni<sub>3</sub>S<sub>2</sub>, b-NiS and nickel matte. *Journal of Applied Electrochemistry* 12: pp. 281-290.
- VAUGHAN, D. & CRAIG, J. (1978). Mineral chemistry of metal sulfides. Cambridge, Cambridge University Press. 493 p.

WONG, J., TIAN, M., JIN, W. & HE, Y. (2001). Speciation of Sulfidic Nickel by Carbon Paste Electrode Voltammetry. Determination of Ni<sub>3</sub>S<sub>2</sub> in Solid Mixtures. *Electroanalysis* 13(16): pp. 1355-1359.

**Aromaa, J.**, *Elektrochemiczne roztwarzanie syntetycznego hezelwudytu (Ni<sub>3</sub>S<sub>2</sub>)*, *Physicochem. Probl. Miner. Process.*, 46 (2011) 51-64, (w jęz. ang), <http://www.minproc.pwr.wroc.pl/journal>

Przedmiotem pracy były badania kinetyki roztwarzania syntetycznego hezelwudytu oraz tworzenia się siarki w tym procesie, z zastosowaniem metod elektrochemicznych. Badania prowadzone były w 1 N kwasie siarkowym, w temperaturze 25°C, metodami: potencjostatyczną, krzywych polaryzacyjnych oraz woltamperometrii cyklicznej. Roztworzenie anodowe hezelwudytu przebiega dwustopniowo. Przy potencjałach poniżej 600 mV hezelwudyty przechodzi w siarczki o wyższej zawartości siarki, na przykład mileryt (NiS). Przy wyższych potencjałach hezelwudyty ulega roztwarzaniu, tworząc siarczki o wyższej zawartości siarki i siarkę, a następnie siarczki o wyższej zawartości siarki, siarkę i siarczany, przy czym przy wyższych potencjałach obserwowano tworzenie się większej ilości siarczków o wyższej zawartości siarki. Nie zaobserwowano negatywnego wpływu tworzenia się siarki elementarnej na przebieg procesu roztwarzania. Ilość tworzących się siarczanów wzrasta wraz ze wzrostem potencjału. Poniżej potencjału 900 mV tworzy się siarka elementarna, przy potencjale 1000 mV 10% siarki ulega utlenieniu do siarczanów, a przy potencjale 1600 mV do siarczanów ulega utlenieniu aż 90% siarki.

*słowa kluczowe: siarczek niklu, roztwarzanie, mechanizm reakcji, tworzenie siarki*

Władysław JANUSZ\*, Anna SĘDŁAK\*

## **SPECIFIC ADSORPTION OF CARBONATE IONS AT THE HEMATITE /AQUEOUS ELECTROLYTE SOLUTION INTERFACE**

*Received May 2, 2010; reviewed; accepted June 25, 2010*

A study on adsorption of carbonate ions at the  $\alpha$ -Fe<sub>2</sub>O<sub>3</sub>/aqueous solution of NaClO<sub>4</sub> interface is presented. The concentration range of carbonate ions was from  $1.00 \cdot 10^{-6}$  to  $1.00 \cdot 10^{-3}$  M. The shape of carbonate ion adsorption plot vs. pH is characteristic for anions adsorption onto metal oxides and is called "adsorption envelope". To prevent carbon dioxide access to the solution, all measurements were conducted in a special chamber in nitrogen atmosphere.

*keywords: carbonate ions, adsorption, hematite*

### 1. INTRODUCTION

Adsorption of ions at the metal oxide/electrolyte solution interface results in changes of charge density distribution in the electrical double layer in such system. The triple layer model of the electrical double layer assumes that the cation specific adsorption leads to an increase of negatively charged groups (SO<sup>-</sup>Ct<sup>+</sup>) at the surface, whereas adsorption of anions causes an increase of positively charged groups (SOH<sub>2</sub><sup>+</sup>An<sup>-</sup>) (James and Parks, 1982; Schindler, 1981). Practical application is the most important aspect for experimental study of properties of the electrical double

---

\* Department of Radiochemistry and Colloid Chemistry, Maria Curie- Skłodowska University, Pl. M.C. Skłodowskiej 3, 20-031 Lublin, Poland, [wladyslaw.janusz@poczta.umcs.lublin.pl](mailto:wladyslaw.janusz@poczta.umcs.lublin.pl)

layer (edl). Zeta potential measurements give important information concerning the properties of the diffuse part of the edl. Very interesting aspects of ion adsorption at the metal oxide/electrolyte solution interface are systems where anions that form bidentate surface complexes and multivalent cations are presented (Collins et al., 1999).

Hematite is a commonly occurring natural form of iron oxide (Davis and Bhatnagar, 1995). Synthetic iron oxide pigments are of great economical importance due to their stability and their relatively low production costs (Eggleston and Stack, 2003). In order to obtain precise experimental results, the measurements were carried out on  $\alpha$ -Fe<sub>2</sub>O<sub>3</sub> with rigorously defined properties (Schwertmann and Cornell 1991).

Adsorption of ions at the metal oxide/water solution interface and its influence on edl is well described in literature. However in real dispersed systems, for instance in many technological processes and aqueous environment, the solid phase as well as of solution are rich in many organic and inorganic impurities.

## 2. MATERIALS AND METHODS

All measurements were carried out with hematite prepared according to the Matijevic's procedure (Matijevic, 1993) (acidic hydrolysis of FeCl<sub>3</sub>). The powder specific surface, determined by the Braunauer-Emmet-Teller (BET) method (nitrogen adsorption - desorption) was 63.5 m<sup>2</sup>/g. Polydispersity coefficient (PCS method) was 0.22, meaning that the investigated hematite was monodispersed. X-ray diffraction data confirmed its crystalline structure. NaOH and sodium carbonate were supplied by Polskie Odczynniki Chemiczne (Gliwice, Poland) and NaClO<sub>4</sub> by Aldrich. They were dispersed in doubly-distilled water. The surface charge of hematite was calculated by comparison of the potentiometric titrations curve of the oxide suspension and background electrolyte. The titrations of oxide suspensions were carried out in a thermostatic Teflon vessel in free of CO<sub>2</sub> nitrogen atmosphere at 25°C with 0.1°C accuracy using Julabo Refrigerated/Heating Circulator model F10 kept in a special chamber that isolated the titration vessel from the outer environment. During experiments nitrogen pressure in the chamber was slightly higher than that outside the chamber.

The measurements were performed using a PHM 240 Radiometer Research pH-meter with a glass and calomel reference electrode. The whole titration procedure (e.g. addition of titrant by Dosimat 665) and data acquisition from the pH-meter during measurement was computer-controlled. Potentiometric titration was carried out with the use of an automatic burette (Dosimat 665, Metrohm). For adsorption and potentiometric titration experiments the sample of  $\alpha$ -Fe<sub>2</sub>O<sub>3</sub> (1.0 g) was added to 50 cm<sup>3</sup> of solution.

The background electrolyte concentrations were  $1.00 \cdot 10^{-1}$ ,  $1.00 \cdot 10^{-2}$  and

$1.00 \cdot 10^{-3} \text{ M}$  respectively. The concentration range of carbonate ions in the system was from  $1.00 \cdot 10^{-6}$  to  $1.00 \cdot 10^{-3} \text{ M}$ . The adsorption measurements of carbonate ions from the  $\text{NaClO}_4$  solution were carried out with  $^{14}\text{C}$  isotope as the radiotracer. The radioactivity of samples was measured by the LS5000 TD Beckman beta counter. The pH range was from 3 to 10.

The  $\zeta$  potential measurements were carried out for concentration of electrolyte ranging from  $1.00 \cdot 10^{-6}$  to  $1.00 \cdot 10^{-3} \text{ M}$  using the Malvern 3000 Standard Zetasizer. Each measurement of the  $\zeta$  potential was repeated five times.

### 3. RESULTS AND DISCUSSION

The surface charge is formed on the metal oxide as a result of ionization and complexation reactions of surface hydroxyl groups. Surface charge density as a function of pH is very important feature of surface properties of metal oxide/electrolyte solution systems. The  $\text{pH}_{\text{pzc}}$  position depends on the alkaline-acidic character of the surface hydroxyl groups. For hematite this parameter is from 7.0 to 9.0 (Kosmulski, 2001).

The surface charge density dependence on pH for the  $\alpha\text{-Fe}_2\text{O}_3$ /aqueous  $\text{NaClO}_4$  solution indicates that the  $\text{pH}_{\text{pzc}}$  is equal to 8.53. However, the  $\zeta$  potential shows that  $\text{pH}_{\text{iep}} = 8.7 - 9.0$  (Fig. 1). The difference between these values may arise from  $\alpha\text{-Fe}_2\text{O}_3$  particle size fractions used in the potentiometric titration and electrophoretic measurements. In the latter method fine particles was used while in the potentiometric titrations fine particles as well as hematite aggregates were applied.

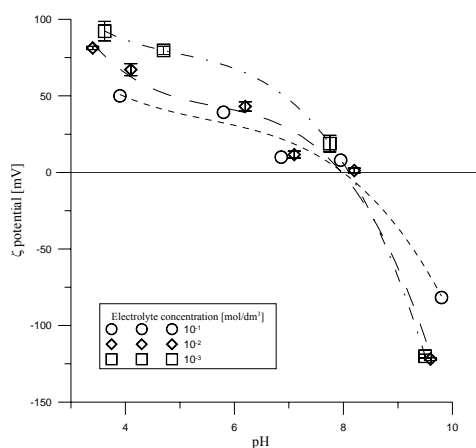


Fig. 1.  $\zeta$  potential of  $\alpha\text{-Fe}_2\text{O}_3$  as a function of pH

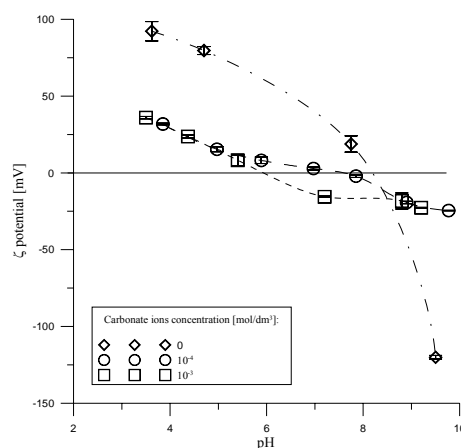


Fig. 2.  $\zeta$  potential of  $\alpha\text{-Fe}_2\text{O}_3$  as a function of pH in  $1.00 \cdot 10^{-3} \text{ M}$   $\text{NaClO}_4$  solution in the presence of carbonate ions

The  $\zeta$  potential of  $\alpha$ -Fe<sub>2</sub>O<sub>3</sub> as a function of pH in the presence of carbonate ions is shown in Fig. 2. One can see that the isoelectric point of  $\alpha$ -Fe<sub>2</sub>O<sub>3</sub> is equal to pH=8.3 in the absence of carbonate ions and is shifted towards lower pH in the presence of carbonate ions with the increase of their concentration. At the initial concentration of  $1.0 \cdot 10^{-3}$  M carbonate ions the pH<sub>iep</sub> is equal to 6.2.

Specific adsorption of anions at the metal oxide/electrolyte interface leads to a decrease of pH<sub>iep</sub> due to the increase of concentration, complexed by anions, positively charged groups at the  $\alpha$ -Fe<sub>2</sub>O<sub>3</sub>/electrolyte interface and simultaneous decrease of concentration of ionized positively charged forms. Because the diffuse layer charge is proportional to the algebraic sum of negatively and positively charged groups, the decrease of concentration of positively charged groups leads to majority of negative charged ones, and decrease of zeta potential making a shift of pH<sub>iep</sub> towards lower pH.

The adsorption densities and equilibrium concentrations of carbonate ions as a function of pH are depicted in Figs 3, 4, 5 and 6.

The initial concentration of carbonate ions was from  $1.00 \cdot 10^{-3}$  M to  $1.00 \cdot 10^{-6}$  M respectively. The shapes of adsorption of carbonate ions plot vs. pH are characteristic for anions adsorption onto metal oxides and are called “adsorption envelope”. One can observe an increase of adsorption and decrease of concentration of carbonate ions with a decrease of pH of the electrolyte. Such progress of adsorption is characteristic for specific anion’s adsorption onto metal oxides. The edge of adsorption moves to acidic environment with the increase of the concentration of carbonate ions. It means that carbonate ions adsorption may go through exchange of hydroxyl groups with inner-sphere complex formation or through decreasing hydrogen ions population with outer-sphere complex formation.

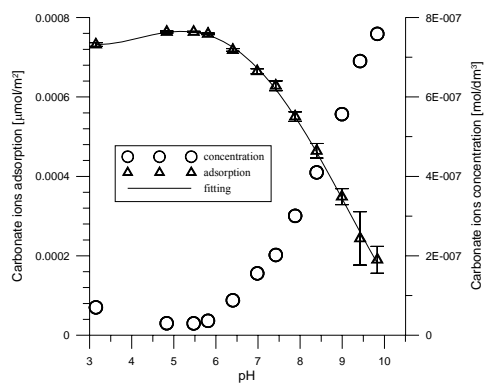


Fig. 3. Adsorption density as a function of solution pH for  $\alpha$ -Fe<sub>2</sub>O<sub>3</sub>/1.00·10<sup>-3</sup> M NaClO<sub>4</sub> + 1.00·10<sup>-6</sup> M HCO<sub>3</sub><sup>-</sup> system. Fitting curve for pK = 3.685 and n = 0.46

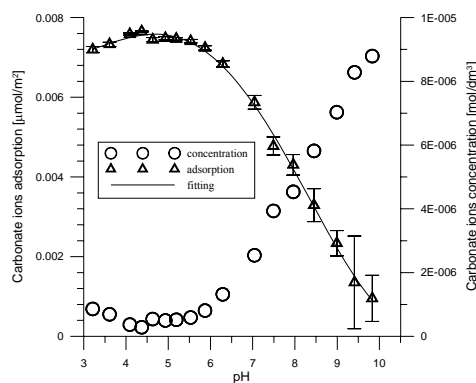


Fig. 4. Adsorption density as a function of solution pH for  $\alpha$ -Fe<sub>2</sub>O<sub>3</sub>/1.00·10<sup>-3</sup> M NaClO<sub>4</sub> + 1.00·10<sup>-5</sup> M HCO<sub>3</sub><sup>-</sup> system. Fitting curve for pK = 3.685 and n = 0.46

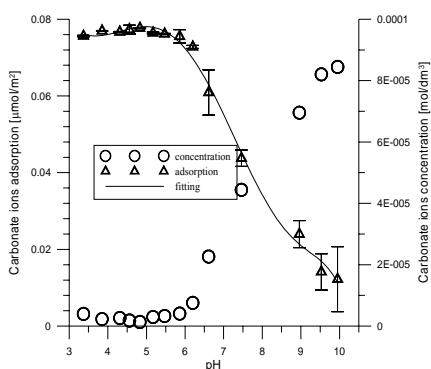


Fig. 5. Adsorption density as a function of solution pH for  $\alpha\text{-Fe}_2\text{O}_3/1.00 \cdot 10^{-3} \text{ M NaClO}_4 + 1.00 \cdot 10^{-4} \text{ M HCO}_3^-$  system. Fitting curve for  $\text{pK} = 3.684$  and  $n = 0.52$

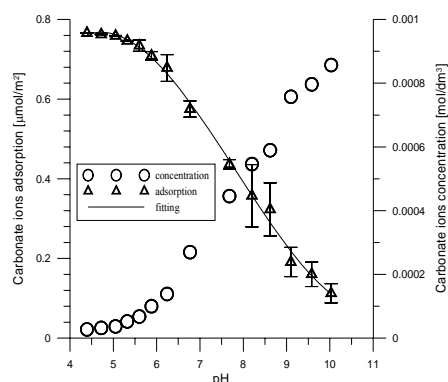


Fig. 6. Adsorption density as a function of pH solution for  $\alpha\text{-Fe}_2\text{O}_3/1.00 \cdot 10^{-3} \text{ M NaClO}_4 + 1.00 \cdot 10^{-3} \text{ M HCO}_3^-$  system. Fitting curve for  $\text{pK} = 3.685$  and  $n = 0.46$

Table 1. Parameters calculated from adsorption data

Initial concentration of carbonate ions mol/dm <sup>3</sup>	pK	n	pH <sub>50%</sub>	ΔpH <sub>10-90%</sub>
1.00·10 <sup>-6</sup>	3.685	0.46	8.025	4.175
1.00·10 <sup>-5</sup>	3.685	0.46	8.049	4.107
1.00·10 <sup>-4</sup>	3.684	0.52	8.172	3.706
1.00·10 <sup>-3</sup>	3.685	0.46	8.025	4.175

where: pK – is the constant of the reaction; n – is the number of OH<sup>-</sup> released per carbonate ion; pH<sub>50%</sub> and ΔpH<sub>10-90%</sub> - are the parameters of edge of adsorption

Table 2. Comparison of specific surface of hematite before and after adsorption measurements

Parameter	Hematite	Hematite after carbonate ions adsorption	
		Initial concentration 1.0·10 <sup>-4</sup> M	Initial concentration 1.0·10 <sup>-3</sup> M
BET surface area	63.5 m <sup>2</sup> /g	125.2 m <sup>2</sup> /g	127.9 m <sup>2</sup> /g
BJH cumulative adsorption surface area of pores between 1.7nm<d<300nm	0.2 cm <sup>3</sup> /g	0.4 cm <sup>3</sup> /g	0.4 cm <sup>3</sup> /g
BJH cumulative desorption surface area of pores between 1.7nm<d<300nm	0.2 cm <sup>3</sup> /g	0.4 cm <sup>3</sup> /g	0.4 cm <sup>3</sup> /g

One can see that the values of equilibrium constants do not depend on the initial concentration of carbonate ions. It means that there is no influence of the electrostatic component on adsorption. The quantity of freed OH<sup>-</sup> ions is also unchanged and is smaller than 1. As a consequence the adsorption edge parameters are constant. From

these data one can conclude that alkaline iron carbonates can be formed on the  $\alpha$ - $\text{Fe}_2\text{O}_3$  surface.

In order to verify the changes that took place on the surface of the oxide after adsorption, iron oxide was examined and the results were compared. One can conclude from Table 2 that not only BJH cumulative adsorption surface area of pores but also BET surface area increased. It can be explained by the formation of carbonate layer on the surface of  $\alpha$ - $\text{Fe}_2\text{O}_3$ .

Figure 7 shows changes in the size distribution of hematite after adsorption of carbonate ions. These results were confirmed by the AFM (Atomic Force Microscopy) method (Fig. 8).

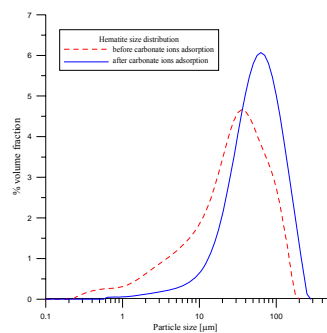


Fig. 7. Size distribution of hematite before and after adsorption measurements by Static Light Scattering

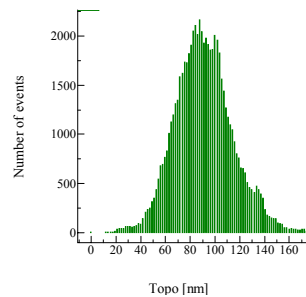
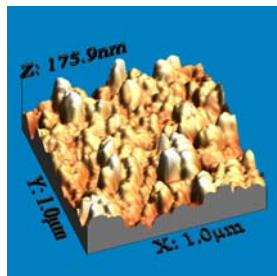


Fig. 8a. 3D image and roughness histogram before adsorption of carbonate ions

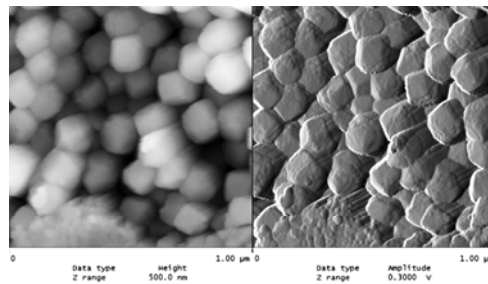


Fig. 8b. AFM pictures of hematite samples before adsorption of carbonate ions

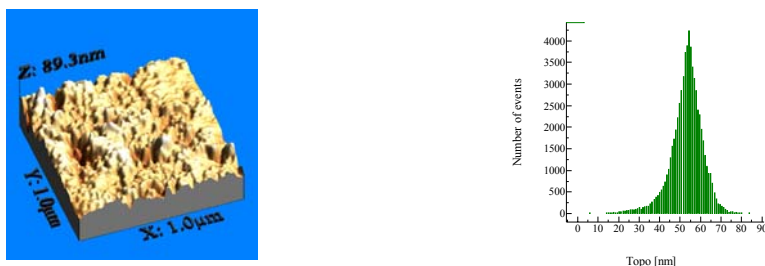


Fig. 8c. 3D image and roughness histogram after adsorption of carbonate ions

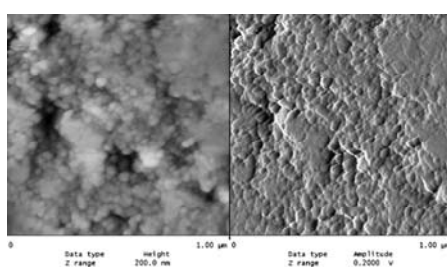


Fig. 8d. AFM pictures of hematite samples after adsorption of carbonate ions

Comparing the above results one can conclude that there are clear differences in shape and size of hematite crystallites. Hematite sample after adsorption is more crumbled and crystallites are more oval in the shape. The surface becomes smoother. It was confirmed by the RSM roughness parameter equal to 23.4 before and to 8.1 after adsorption measurements.

The IR spectroscopy revealed that two new peaks were present after adsorption measurements. The broad and intense band at  $3444\text{ cm}^{-1}$  can be ascribed to the stretching mode of hydroxyl group and water molecule. The peaks at  $1320 - 1630\text{ cm}^{-1}$  correspond to stretching mode in the carbonate molecule (Frost and Dickfos, 2007, Ferretto and Glisenti, 2008; de Faria and Lopes, 2007).

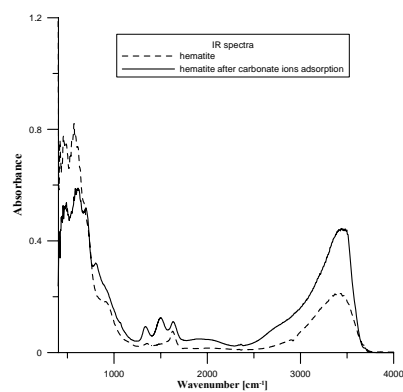


Fig. 9. IR spectra of hematite before and after adsorption measurements

### 3. CONCLUSIONS

Carbonate ions adsorption leads to an exchange of surface hydroxyl with carbonate groups that causes an increase of negatively charged groups on the hematite surface and, in consequence, a decrease of  $\zeta$ . The shapes of the carbonate ions adsorption vs. pH plot are characteristic for anions adsorption onto metal oxides and are called "adsorption envelope". One can observe an increase of adsorption and decrease of concentration of carbonate ions in solution with a decrease of pH of the electrolyte. Carbonate ions cause also changes of the surface properties of the oxide.

### REFERENCES

- DAVIS, P., BHATANAGAR, V., Adsorption of cadmium and humic acid onto hematite, *Chemosphere*, vol. 30, 2 (1995) 243-256.
- EGGLESTON, C.M., STACK, A.G., The Structure of Hematite (001) Surfaces in Aqueous Media: Scanning Tunneling Microscopy and Resonant Tunneling Calculations of Co-Existing O and Fe Terminations, *Geochimica et Cosmochimica Acta*, 67 (2003) 985 – 1000.
- DE FARIA, D.L.A., LOPES, F.N., Heated goethite and natural hematite: can Raman spectroscopy be used to differentiate them?, *Vibrational Spectroscopy*, 45 (2007) 117 – 121.
- FERRETTO, L., GLISENTI, A., Study of the surface acidity of an hematite powder, *Journal of Molecular Catalysis A: Chemical*, 187 (2002) 119-128.
- FROST, R.L., DICKFOS, M., Synthesis and vibrational spectroscopic characterization of nickel containing aurichalcite, *Polyhedron*, 26 (2007) 4503 – 4508.
- FROST, R.L., DICKFOS, M., Raman and infrared spectroscopic study of the anhydrous carbonate minerals shortite and barytocalcite, *Spectrochimica Acta Part A*, 71 (2008) 143 – 146.
- KOSMULSKI, M., *Chemical Properties of Material, Surfaces Surfactant*, Sci. Ser., vol. 102, Marcel Dekker, New York, 2001.
- MARCZEWSKI, A.W., Kinetics and equilibrium of adsorption of organic solutes on mesoporous carbons, *Applied Surface Science*, 253 (2007) 5818–5826.
- MATIJEVIC, E., Preparation and properties of uniform size colloids, *Chemistry of Materials*, 5 (1993) 412.
- SCHWERTMANN, U., CORNELL, R.M., *Iron oxides in the laboratory: Preparation and characterization*, VCH Publishers 1991.

**Janusz, W., Sędlak, A.,** Adsorpcja specyficzna jonów węglanowych na granicy faz hematyt/roztwór elektrolitu., *Physicochem. Probl. Miner. Process.*, 46 (2011) 65-72, (w jęz. ang), <http://www.minproc.pwr.wroc.pl/journal>

Adsorpcja jonów węglanowych powoduje zwiększenie negatywnie naładowanych grup powierzchniowych obecnych na powierzchni hematytu i w konsekwencji spadek potencjału dzeta. Kształt krzywych adsorpcji jest charakterystyczny dla adsorpcji anionów na tlenkach metali. Obserwowane są ponadto zmiany we właściwościach powierzchniowych, np. wzrost powierzchni właściwej hematytu po adsorpcji jonów węglanowych, zmiany w rozkładzie ziarnowym, czy zmiany w widmach IR.

*słowa kluczowe: jony węglanowe, hematyt, adsorpcja*

Władysław JANUSZ\*, Ewa SKWAREK\*

## ADSORPTION OF Ca(II) AND Fe(III) IONS AT THE SnO<sub>2</sub>/ELECTROLYTE SOLUTION INTERFACE

*Received May 7, 2010; reviewed; accepted June 25, 2010*

Adsorption of Ca(II) and Fe(III) ions at the SnO<sub>2</sub>/NaCl solution interface as well as the effect of adsorption on the structure of electrical double layer were presented in this paper. The influence of ionic strength, pH and presence of ions on adsorption of Ca(II) and Fe(III) at the SnO<sub>2</sub>/NaCl solution interface were also investigated. Adsorption was investigated in the pH range of 2 to 10. The zeta potential, surface charge density, adsorption density, pH<sub>50%</sub> and ΔpH<sub>10-90%</sub> parameters for different concentrations of carrying electrolyte were presented. The adsorption reaction constants involving the surface hydroxyl groups were determined using the numerical optimization method.

*keywords:* SnO<sub>2</sub>, electrical double layer, surface charge density, zeta potential, Ca(II) adsorption, Fe(III) adsorption

### 1. INTRODUCTION

Tin is a chemical element which is not widely spread in the Earth's crust ( $4 \cdot 10^{-3}$  wt. %). There are few more than ten minerals containing tin and the most important is cassiterite (tin dioxide SnO<sub>2</sub>), a source of tin as well as other tin compounds (Bielański, 1998). Tin dioxide has been used for a long time in ceramics, sensors for environment pollutants control in chromatographic detectors as well as catalysts (Dobrzański and Zawadzki, 1981). Tin dioxide has also been used in production of

---

\* Department of Radiochemistry and Colloid Chemistry, Maria Curie- Skłodowska University, Pl. M.C. Skłodowskiej 3, 20-031 Lublin, Poland, [wladyslaw.janusz@poczta.umcs.lublin.pl](mailto:wladyslaw.janusz@poczta.umcs.lublin.pl)

semiconducting solar cells (Suppan, 1997). Since present natural resources of tin are small, the role of tin recycling increases significantly. Control of stability of tin dioxide dispersion during enrichment process is very important and this is possible by means of changes of electrokinetic potential that depends on concentration of potential determining and specifically adsorbing ions (Janusz et al., 2007). Adsorption or desorption of calcium and iron ions on the SnO<sub>2</sub> surface is related not only to the hydrogen ions concentration but also to the surface potential. Adsorption has a great influence on the surface potential and through it, on SnO<sub>2</sub> particles aggregation and heteroaggregation with other particles. The multivalent ions can be adsorbed specifically on one or two surface sites (hydroxyl groups) of metal oxide surface via hydrogen exchange, but number of sites usually occupied by a single ion is smaller than two (Schindler et al., 1981). Adsorption of such ions may lead to formation of inner-sphere or, when the adsorbed cation is separated from the surface by a water molecule, outer-sphere complexes. Usually a sharp increase of cations adsorption from 0 to 100%, with an increase of pH of the electrolyte, is observed. This relationship is called “the edge of adsorption” Robertson and Leckie (1997) proposed very useful parameters to characterize it:

- $d(pMe)/d(pH)$  – parameter that shows the activity of cations; must vary when pH of the solution changes to maintain the constant adsorption of the cations
- $pH_{50\%}$  - the value of pH when 50% of the initial concentration of cations is adsorbed; this parameter characterizes the position of adsorption edge on the pH scale
- $pH_{10-90\%}$  - the range of pH where the adsorption changes from 10 to 90%; it characterizes the slope of the edge.

Heavy metal cations belong to ions possessing a great adsorption affinity for mixed oxide surfaces and create inner-sphere complexes. The DLM (double layer) and TLM (triple layer) models describe specific adsorption of ions. According to the DLM, the specific adsorption of ions is possible with the creation of the inner-sphere complexes, where ions are situated inside the surface plane. According to the TLM (model SCM, site binding), also adsorption of background electrolyte ions may be considered as specific and nonspecific. The ions, taking part in the ionization and complexation reactions, increase the surface charge density on the oxide and adsorb specifically, but those in the diffusion part of the electrical double layer (EDL) are adsorbed nonspecifically (Hayes and Katz, 1996). In the present paper we report the influence of ionic strength, pH and presence of ions on the adsorption of Ca(II) and Fe(III) and the structure of the EDL at the SnO<sub>2</sub>/electrolyte interface. Adsorption measurements are complemented with the surface charge density and  $\zeta$  potential determinations. The effect of Ca(II) and Fe(III) adsorption on the properties of the EDL is discussed. To determine the constants of surface reaction by numerical optimization, the ion adsorption data and triple layer model of the EDL were used.

## 2. EXPERIMENTAL

Experiments were carried out using a commercial SnO<sub>2</sub> sample purchased from Aldrich Chemical Company. The roentgen diffraction analysis revealed a rutile type structure of the studied dioxide. The size distribution analysis by the photo correlation spectroscopy (PCS) method showed that particle sizes ranged from 300 nm to >3000 nm and the arithmetic mean diameter of the particles was 458 nm. The specific surface of the SnO<sub>2</sub> sample determined by nitrogen desorption was 7.4 m<sup>2</sup>/g. The BJH (Barret, Joyner, Halenda) analysis of the isotherm obtained by adsorption-desorption of nitrogen did not reveal micropores in the examined SnO<sub>2</sub> sample.

Adsorption densities of Ca(II) and Fe(III) ions were measured using a radiotracer technique with <sup>45</sup>Ca and <sup>55</sup>Fe radioisotopes supplied by Polatom (Świerk, Poland). Specific adsorption of Ca(II) and Fe(III) ions at the /SnO<sub>2</sub> interface was studied as a function of Ca(II) and Fe(III) ions concentration, NaCl concentration and pH. The initial concentration of Ca(II) and Fe(III) ions ranged from 10<sup>-6</sup> to 10<sup>-3</sup> M, pH was changed from 2.0 to 10.0. NaCl solution was used as a background electrolyte. The adsorption measurements were complemented by potentiometric titration of SnO<sub>2</sub> suspensions and electrokinetic measurements.

Adsorption and surface charge measurements were carried out simultaneously in a thermostated Teflon vessel at 25°C. To eliminate the influence of CO<sub>2</sub> all potentiometric measurements were performed under nitrogen atmosphere. pH values were measured using a PHM240 Research pH-meter (G202C and K401 electrodes). The surface charge density was calculated from the difference between the amounts of added acid or base to obtain the same pH value of suspension as for the background electrolyte.

The zeta potential of SnO<sub>2</sub> dispersions was determined by electrophoresis with Zetasizer 3000 by Malvern. Diluted SnO<sub>2</sub> suspensions containing 100 ppm of solids in the electrolyte solution were used. Before measurements the suspensions were dispersed using Sonicator XL2020 made by Misonix.

## 3. RESULTS AND DISCUSSION

The characteristic parameter of the EDL for the tin dioxide (SnO<sub>2</sub>)/NaCl system is the shift of the point of zero charge (pH<sub>pzc</sub>) with the background electrolyte concentration which decreases from 4.8 for 0.001 M NaCl to 4.0 for 0.1 M NaCl. This effect is caused by specific adsorption of cation. The pH<sub>iep</sub> shifts from 4.5 for the solution 0.1 M to 4.0 for 0.001 M NaCl. The ionization constants, calculated from the charge density as a function of pH and electrolyte concentration, are pK<sub>a1</sub>=0.154, pK<sub>a2</sub>=7.984 and the complexation constants are pK<sub>Cl</sub>=1.765, pK<sub>Na</sub>= 5.173.

3.1. SPECIFIC ADSORPTION OF CA(II) IONS AT THE SnO<sub>2</sub>/NaCl SOLUTION INTERFACE

Specific adsorption of multivalent/heavy ions at the metal oxide/electrolyte solution interface significantly influences the EDL structure. Influence of calcium ions on the EDL of the SnO<sub>2</sub>/electrolyte solution interface has been presented by Ardizzone and Trasatti (1996). In this paper a comprehensive study on the influence of calcium ions Ca(II) adsorption on the EDL properties for the tin dioxide/electrolyte solution interface is presented. Figure 1 presents a dependence of characteristic parameters of the adsorption edge on the initial Ca(II) concentration for the SnO<sub>2</sub>/0.1 M NaCl solution system. The position of the adsorption edge, characterized by pH<sub>50%</sub>, shifts from pH 4.2 to pH 5.5 for the 0.001 M NaCl concentration. With the increase of initial Ca<sup>2+</sup> ions concentration, the adsorption edge slightly flattens, as indicated by parameter pH<sub>10-90%</sub>. For more concentrated NaCl solution the shift of the Ca<sup>2+</sup> ions adsorption edge in the SnO<sub>2</sub>/electrolyte solution system is more complicated due to competition in Na<sup>+</sup> and Ca<sup>2+</sup> ions adsorption.

Figure 2 shows the adsorption isotherms as the log-log plot for adsorption versus concentration at the SnO<sub>2</sub>/0.1M NaCl interface for three selected pH values (5, 7 and 9). A linear approximation of the log-log adsorption vs. concentration plot, indicated by a dashed line, for the lowest concentration shows that the slope of the straight line differs distinctly from 1, being a characteristic value for the isotherms based on either Henry or Langmuir equations. It means that these isotherms cannot be used for this system and quantitative description of adsorption requires taking into consideration interactions connected with the presence of double electric layer or energetic heterogeneity of the surface. The surface charge density at the SnO<sub>2</sub>/NaCl electrolyte interface in the presence of Ca(II) ions for 0.001M NaCl is shown in Fig. 3.

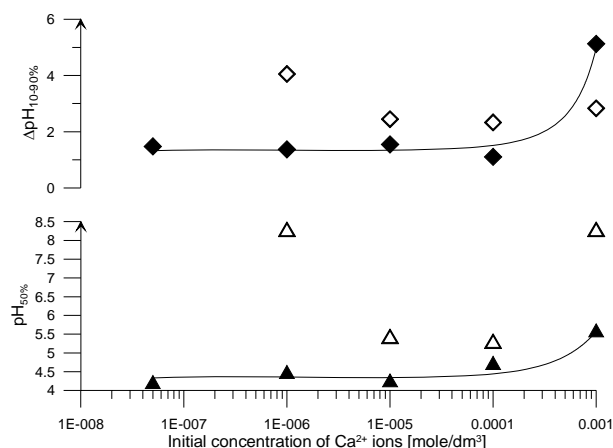


Fig. 1. Parameters of adsorption edge vs. initial concentration of Ca<sup>2+</sup> ions for the SnO<sub>2</sub>/0.001 M NaCl solution system. Closed symbols - 0.001 M NaCl, open symbols - 0.1 M NaCl

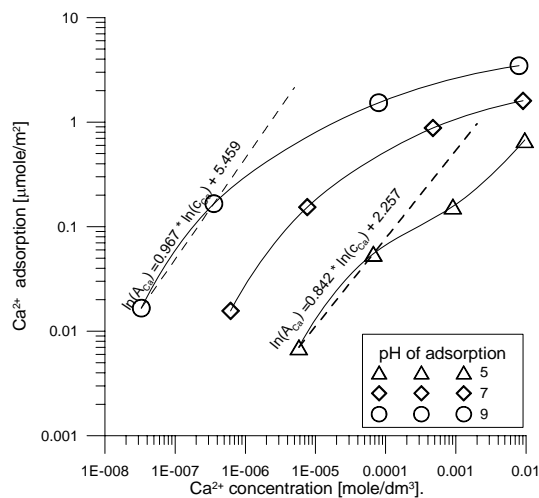


Fig. 2. Ca<sup>2+</sup> adsorption isotherms for the SnO<sub>2</sub>/0.1 M NaCl solution system

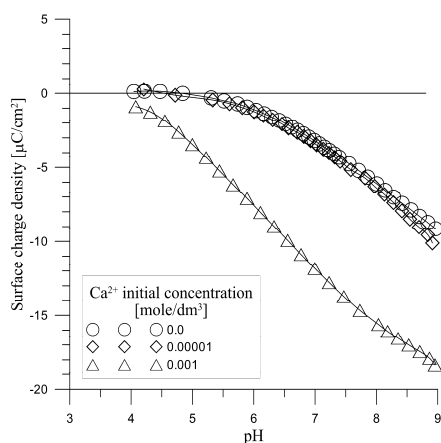


Fig. 3. Surface charge density as a function of pH in the presence of Ca<sup>2+</sup> for the SnO<sub>2</sub>/0.001M NaCl solution system

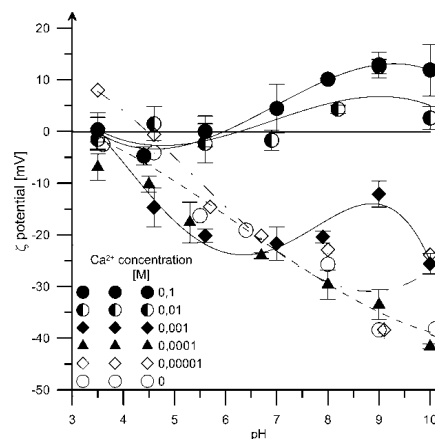


Fig. 4. Zeta potential vs. pH and initial Ca<sup>2+</sup> concentration for SnO<sub>2</sub>/0.1 M NaCl solution system

As result from Fig. 3, at a low initial concentration of Ca(II) ions, there is no effect of Ca<sup>2+</sup> ions adsorption on the surface charge density at the SnO<sub>2</sub>/NaCl solution interface because one can expect that for the adsorption density of 0.17 μmol/m<sup>2</sup> for the initial concentration of 10<sup>-4</sup> M Ca<sup>2+</sup> at pH>7, assuming that one Ca<sup>2+</sup> ion replaces on the SnO<sub>2</sub> surface one hydrogen atom in one hydroxyl group, it should cause a surface charge density decrease by about 1.6 μC/cm<sup>2</sup>. When the initial concentration of Ca<sup>2+</sup> ions exceeds 10<sup>-3</sup> M, then a significant decrease of the surface charge density and a shift of pH<sub>pzc</sub> towards lower values of pH are observed. This is a result of negatively charged groups formation due to complexation of calcium ions by the

surface hydroxyl groups. Reaction of calcium ions proceeds via release of  $H^+$  ions from the surface hydroxyl groups. This causes an exchange of the  $H^+$  ions of the hydroxyl groups with  $Ca^{2+}$  ions. The dependence shown in Fig. 3 indicates that  $Ca^{2+}$  ions are partially absorbed onto ionized ( $\equiv SnO^-$ ) or complexed ( $\equiv SnO^-Na^+$ ) and partially onto  $\equiv SiOH$  groups with  $H^+$  ions release.

Similarly, adsorption of  $Ca^{2+}$  ions from the solution of low initial concentrations of  $Ca^{2+}$  ions did not bring about within the experimental error any change of  $\zeta$  potential. When the initial concentration of  $Ca^{2+}$  ions is equal to 0.001 M NaCl, then an increase of zeta potential above pH=7 is observed. For higher initial concentrations the charge reversal point (CR2) (change from negative to positive values of zeta potential) was observed. This is caused by a considerable compensation of the electric charge by the  $Ca^{2+}$  ions in the compact part of the electrical double layer. The calcium ion, being adsorbed onto one hydroxyl group, introduces two charge units into the compact layer of EDL.

Using adsorption density of  $Ca^{2+}$  ions as a function of pH the equilibrium constants for the reactions of  $Ca^{2+}$  ions in the  $SnO_2/0.001$  M NaCl solution system (Eqs 1 and 2) were calculated by the method proposed by Schindler (1976), taking into account the ionized and complexed forms at the  $SnO_2$  surface:

$${}^*K_1^S = \frac{[H^+][\equiv SO^-Me^{2+}]}{[Me^{2+}][\equiv SOH]} \frac{\gamma_H\gamma_1}{\gamma_{Me}\gamma_0} \times \exp\left(\frac{e(2\psi_1 - \psi_H)}{kT}\right) \quad (1)$$

$${}^*\beta_{21}^S = \frac{[H^+]^2[(\equiv SO^-)_2Me^{2+}]}{[Me^{2+}][\equiv SOH]^2} \frac{\gamma_H^2\gamma_2}{\gamma_{Me}\gamma_0^2} \times \exp\left(\frac{e(2\psi_2 - \psi_H)}{kT}\right) \quad (2)$$

where:  $\gamma_1$ ,  $\gamma_2$  – activity coefficients of  $\equiv SOH^{(z-1)+}$  and  $(\equiv SO)_2H^{(z-2)+}$  groups,  $\psi_1$ ,  $\psi_2$  – denotes potentials in the planes of adsorption of  $Me^{2+}$  bounded to  $\equiv SOH^{(z-1)+}$  and  $(\equiv SO)_2H^{(z-2)+}$  surface species, respectively,  $\gamma_0$  – activity coefficients of  $\equiv SOH$  group,  $\gamma_H$  – activity coefficients of  $H^+$  ions,  $\gamma_{Me}$  – activity coefficients of metal cation,  $k$  – Boltzmann constant. The values of the reaction constants determined by a numerical optimization procedure are collected in Table 1.

Table 1. Reaction constants for adsorption involving one and two hydroxyl groups in 0.1M NaCl aqueous solution

$C_{Ca}$ , mol/dm <sup>3</sup>	pK <sub>i</sub>	pK <sub>B</sub>
0.000001	4.0	6.0
0.00001	3.88	6.0
0.0001	3.13	0.0
0.001	3.42	4.9
0.01	5.99	0.0

3.2. SPECIFIC ADSORPTION OF Fe(III) IONS AT THE SnO<sub>2</sub>/NaCl SOLUTION INTERFACE

Distribution of iron(III) ions in aqueous solutions analyzed by Baes and Mesmer (1976) shows that hydrolysis starts at pH about 1 and Fe(OH)<sub>2</sub><sup>+</sup> appears at pH=1. From pH 3 to 6 the main form of iron(III) ions is Fe(OH)<sub>2</sub><sup>+</sup>, then from pH 6 to 9 it is replaced with Fe(OH)<sub>3</sub> and over that value of pH with Fe(OH)<sub>4</sub><sup>-</sup>. These charged species may interact with the surface of tin dioxide electrically and chemically.

For high iron salt concentrations in weakly acidic solutions one may expect appearance of solid iron hydroxide whose solubility product is 10<sup>-38.6</sup>. A study of iron(III) ions adsorption on SiO<sub>2</sub> carried out by Schindler et al. (1976) showed that the adsorption edge for iron ions occurs in the largely acidic environment (pH<sub>50%</sub>=2.0). They assumed that iron ion adsorbs on the silica gel surface exchanging from 1 hydrogen atom at pH=1 to about 2 at pH=2. Fe(III) ions adsorb on the metal oxide forming the so-called inner sphere complexes, located in the surface plane. Due to the assumption  $\psi_1 = \psi_H$ , the exponential term in Eqs 1 and 2 is equal to 1. In such a case the equilibrium constants can be calculated using the adsorption data and neglecting the electrostatic interaction, for example using the James et al. (1975) model. The values of equilibrium constants of nonstoichiometric exchange are collected in Table 2.

Table 2. Nonelectrostatic model parameters for Fe(III) ions adsorption at the SnO<sub>2</sub>/electrolyte solution interface (James et al., 1975)

C <sub>Fe</sub> mol/dm <sup>3</sup>	pK <sub>n</sub>	n <sub>H+</sub>	pH <sub>50</sub>
0.000001	5.356±1.011	2.89	1.973
0.00001	4.555±0.160	2.75	2.103
0.0001	1.439±0.145	1.64	2.239
0.001	-0.258±0.092	0.81	1.645

As can be seen from Table 2, the reaction equilibrium constants decrease with the increase of the initial concentration. A similar decrease is found for the number of released hydrogen ions (smaller than 3 for the lowest concentration). The number of hydrogen ions released at the highest concentration is surprisingly low. The characteristic parameter for the adsorption edge (pH<sub>50%</sub>) is also shown in Table 2. Its value grows with the initial Fe(III) concentration towards higher pH values, but not for the highest iron ions concentration. This shift is not as large as that for Ca(II) ions, where pH<sub>50%</sub> of the adsorption edge is over pH=4. Figure 5 depicts the iron ions adsorption isotherms for the selected pH values, that is pH=3, pH=5, pH=7. According to the previous prerequisites, the isotherms shape indicates that precipitation occurs at higher iron ions concentrations (Hayes et al., 1996).

Figure 6 shows the dependence of charge density on pH in the presence of Fe(III) ions. Iron ions adsorption in the solution with the initial concentration of 10<sup>-4</sup> M

Fe(III) causes accumulation of negatively charged groups at the surface (in comparison with the system in which iron ions are absent). In addition, an increase of surface concentration of negatively charged groups is observed with the pH increase, which indicates change in the form of the adsorbed Fe(III) ions (formation of surface hydroxyl complexes of Fe ions). Iron ions at the initial concentration of  $10^{-3}$  M, as mentioned before, causes precipitation of iron compounds and growth of iron ions consumption. Figure 7 shows a contribution of individual complex forms on the  $\text{SnO}_2$  surface as a function of pH for the initial concentration of Fe ions equal to  $10^{-4}$  M.

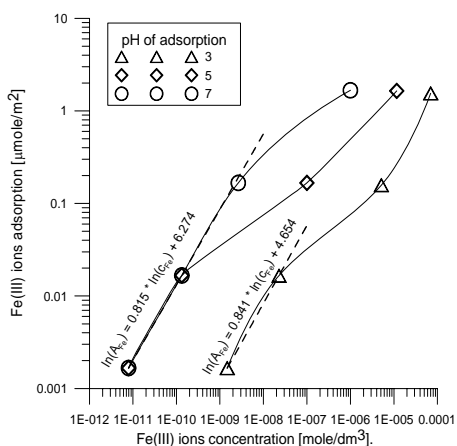


Fig. 5. Fe(III) ions adsorption as a function of Fe(III) equilibrium concentration at the  $\text{SnO}_2/0.1$  M NaCl solution interface

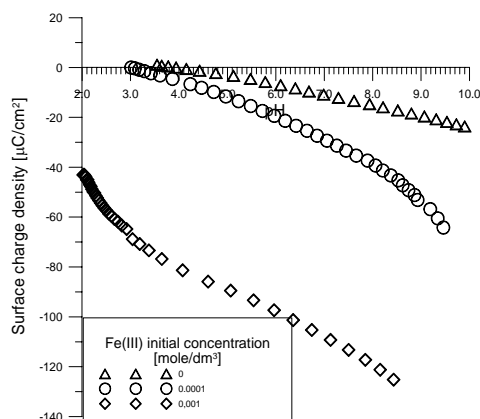


Fig. 6. Surface charge density as a function of pH in the presence of Fe(III) for the  $\text{SnO}_2/0.1$  M NaCl solution interface

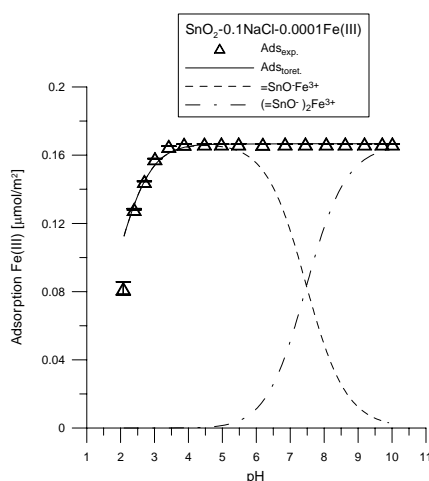


Fig. 7. Adsorption density of Fe(III) ions for the  $\text{SnO}_2/0.1\text{M}$  NaCl- $0.0001\text{M}$  Fe(III) solution system

For Fe ions of the initial concentration of  $10^{-4}$  M and pH=6 the form of Fe adsorbed on one hydroxyl group dominates while at pH=8 and over the dominating form is Fe adsorbed on two groups. This effect may result from iron ions abundance at a low equilibrium concentration, which is more beneficial for the adsorption on two groups than on one. The above statement is based on the Schindler model, taking adsorption on one and two hydroxyl groups into account (Schindler et al., 1981).

### 3. CONCLUSIONS

The investigations carried out in this paper can be summed up as follows.

1. The electrical double layer for the SnO<sub>2</sub>/NaCl solution system can be characterized by the point of zero charge,  $\text{pH}_{\text{pzc}}$ , which shifts with the electrolyte concentration and increases from 4.8 for 0.001 M NaCl to 4.0 for 0.1 M NaCl. This effect is caused by specific adsorption of cation ( $\text{Na}^+$ ). The  $\text{pH}_{\text{iep}}$  shifts from 4.5 for 0.1 M NaCl solution to 4.0 for 0.001 M NaCl.

2. The ionization constants, calculated from the charge density dependence on pH and electrolyte concentration, are  $\text{pK}_{\text{a1}}=0.154$ ,  $\text{pK}_{\text{a2}}=7.984$ . The complexation constants are  $\text{pK}_{\text{Cl}}=1.765$ ,  $\text{pK}_{\text{Na}}=5.173$ , respectively.

3. Calcium ions adsorbing on the tin dioxide surface release hydrogen ions. The number of ions released depends on pH and calcium ions concentration.

4. The adsorption isotherms for Ca(II) ions reveal mutual interactions of ions in the adsorption layer. The direction coefficient of the isotherm for the log-log plot of adsorption vs. the balance equilibrium concentration is lower than 1.

5. The adsorption of calcium ions on one hydroxyl group from the solution of high Ca(II) concentrations causes overcharging the EDL condensed layer leading to the positive  $\zeta$  potential over  $\text{pH}_{\text{pzc}}$ , and even under alkaline conditions.

6. Fe(III) ions, up to 0.0001M, are absorbed on the tin dioxide releasing hydrogen ions ( $\text{H}^+$ ). An increase of negatively charged groups density on the surface takes place.

7.  $\text{Fe}^{+3}$  adsorption edge at the tin dioxide/electrolyte solution interface occurs in acidic environment at pH about 2.

8. Precipitation of iron hydroxide on the tin dioxide surface occurs at the initial concentration of 0.001 M Fe(III) ions.

### REFERENCES

- ARDIZZONE S., TRASATTI S. (1996), Interfacial Properties of Oxides with Technological Impact in Electrochemistry, *Adv. Colloid Interface Sci.*, 64, 173-251.
- BAES C.F. and MESMER R.E., *The Hydrolysis of Cations*, Wiley-Interscience, New York (1976).
- BIELAŃSKI A. *Podstawy chemii nieorganicznej* Wydawnictwa Naukowe PWN część 3, Warszawa (1998).

- DOBRZAŃSKI B., ZAWADZKI S. (1981). Gleboznawstwo, Państwowe Wydawnictwa Rolnicze i Leśne, Warszawa
- HAYES K.F., KATZ L.E., (1996) Application of X-ray absorption spectroscopy for Surface Complexation modeling of Metal Ion Sorption in: Physics and Chemistry of Mineral Surfaces, Ed. P.V. Brady, CRC Press, New York, pp 147-224.
- JAMES R.O, STIGLICH P.J., and HEALY T.W., (1975) Characterization of Aqueous Colloids by Their Electrical Double –Layer and Intrinsic Surface Chemical Properties Disc. Faraday Soc., 59, 142.
- JANUSZ W., SKWAREK E., ZARKO V.I., GUN'KO V.M., (2007), *Structure of electrical double layer at the  $Al_2O_3$ - $SiO_2$ /electrolyte solution interface*, Physicochem. Probl. Miner. Process. 41, 215-225.
- SCHINDLER P.W., FÜRST B., DICK R., WOLF P.U., (1976) Ligand properties of silanol groups J. Colloid Interface Sci. 55-469.
- SUPPAN, P. Chemia i Światło, PWN, Warszawa (1997).
- ROBERTSON A.P., LECKIE J.O., (1997) Cation binding predictions of surface complexation models: effects of pH, ionic strength, cation loading, surface complex and model fit, J. Colloid Interface Sci. 88, 444.

**Janusz, W., Skwarek, E.,** *Adsorpcja jonów Ca(II) i Fe(III) na granicy faz  $SnO_2$ /roztwór elektrolitu*, Physicochem. Probl. Miner. Process., 46 (2011) 73-82, (w jęz. ang), <http://www.minproc.pwr.wroc.pl/journal>

Cyna i jej związki mają szereg praktycznych i istotnych zastosowań od wielu lat. Obecnie zasoby naturalne cyny są nieduże. Szacuje się, że wystarczą na około 40 lat. Dlatego należy podjąć próbę odzysku cyny z materiałów zawierających ten pierwiastek. Przeprowadzono pomiary adsorpcji jonów wapnia i żelaza, dla jego różnych stężeń początkowych, w funkcji pH dla układu  $SnO_2$ /roztwór NaCl. Kształt krzywej adsorpcji w funkcji pH ma postać krawędzi adsorpcji. Wzrost stężenia początkowego jonów Ca(II) i Fe(III) powoduje przesunięcie krawędzi w kierunku zasadowym w skali pH. Wyznaczono charakterystyczne parametry krawędzi adsorpcji tj.  $pH_{50\%}$  i  $\Delta pH_{10-90\%}$ . W oparciu o zależność adsorpcji od pH obliczono również stałe adsorpcji jonów Ca(II) i Fe(III). Zależność gęstości ładunku powierzchniowego od pH w obecności jonów Ca(II) i Fe(III) jest w dobrej korelacji z zależnością adsorpcji jonów Ca(II) i Fe(III) od pH. Adsorpcja jonów Ca(II) i Fe(III) na powierzchni  $SnO_2$  prowadzi do wzrostu stężenia grup ujemnie naładowanych

*słowa kluczowe:  $SnO_2$ , podwójna warstwa elektryczna, gęstość ładunku powierzchniowego, potencjał dzeta, adsorpcja Ca(II), adsorpcja Fe(III)*

Agnieszka PILARSKA\*, Teofil JESIONOWSKI\*

## SYNTHESIS OF MgO IN MAGNESIUM HYDROXIDE CARBONATISATION PROCESS

*Received June 10, 2010; reviewed; accepted July 1, 2010*

A method for synthesis of magnesium oxide by calcination of magnesium carbonate, obtained by carbonisation of magnesium hydroxide with carbon dioxide, is presented and the products obtained are characterised. The influence of the following experimental conditions on the final product properties was established: pH of the reaction medium, mode and rate of reagents supply. The final products were characterised by determination of their dispersion properties, wettability profiles (with water), specific surface area (BET), size and volume of pores. The products were identified by the X-ray diffraction method. The results proved a significant influence of the reaction conditions on the physicochemical parameters of the final magnesium oxide.

*keywords: MgO, precipitation, carbonisation process, particle size distribution, surface morphology, wettability, adsorptive properties*

### 1. INTRODUCTION

Due to its great mechanical resistance and thermal stability magnesium oxide is applied as catalyst or catalyst support (Choudhary, 1997; Ruckenstein, 1997; Xu, 2008). It is also a promising sorbent of pollutants of different types (Gulkowa, 2004). Thanks to its unique basic character magnesium oxide and its derivative make a specific class of substances of similar properties, similarly as the classes of acidic,

---

\* Poznan University of Technology, Institute of Chemical Technology and Engineering  
Pl. M. Skłodowskiej-Curie 2, PL-60965 Poznan, Poland [teofil.jesionowski@put.poznan.pl](mailto:teofil.jesionowski@put.poznan.pl), phone  
:+48(61)6653720, fax :+48(61)6653649

neutral or amphoteric sorbents such as aluminium oxide, zeolites, silica and activated carbon.

The magnesium oxide features, highly desirable for the above applications, are mesoporosity and large specific surface area (Choudhary, 2004; Gulkova 2004). According to an interesting suggestion given by (Przepiórski, 2009) the control of porous structure in carbon materials appears as one of the most important aspects of adsorbents design. The adsorbing substances should be characterised by diversity of pores.

Many methods of obtaining microporous and mesoporous carbon materials have been described in literature. Mesoporous carbon materials can be obtained by thermal decomposition of a carbon precursor mixed with MgO or other magnesium-containing components like acetate or citrate.

Magnesium oxide is most often obtained by thermal decomposition of magnesium hydroxide (Green 1983), organic (Chhor, 1995; Thomas 1997) and inorganic salts (including hydrogencarbonate) (Botha, 2001), magnesium carbonate (Choudhary, 2004; Morozow, 2003) and containing it minerals (Yildirim, 2010). It has been proved that magnesium oxide obtained from magnesium carbonate is catalytically active. Morozow (2003) and other authors reported experimental studies on thermal decomposition of magnesium carbonate to magnesium oxide, including analysis of structural and textural characterisation of the intermediate and final products (XRD, BET). At particular stages of calcination conducted usually in the range 20÷800°C, the degree of decomposition was evaluated by DTA and TG methods. An important observation was that different DTA or TG curves were obtained for products synthesised from the same substrates but under different conditions, i.e. the time and temperature of calcination.

This paper presents a method for obtaining magnesium oxide by thermal decomposition of magnesium carbonate precipitated in our laboratory from magnesium hydroxide and carbon dioxide in a gas form. The influence of parameters of precipitation on the properties of the final product was analysed and the final product was characterised.

## 2. EXPERIMENTAL

Magnesium carbonate was obtained as a result of carbonisation of magnesium hydroxide ( $\text{Mg}(\text{OH})_2$ , POCh SA) with  $\text{CO}_2$  in the gas form (see Fig. 1). Precipitation was performed in a reactor of 500 cm<sup>3</sup> in capacity, equipped with a high-speed stirrer of Eurostar digital type made by IKA-Werke GmbH. Carbon dioxide was introduced to a suspension of magnesium hydroxide by a peristaltic pump ISM833A made by Ismatec, or in parallel with the suspension to the water system, at the rate of 1÷6 dm<sup>3</sup>/min, for 3h, until getting pH=8 and stirred at 1800 rpm. The reaction was conducted at 20 or 40°C, using the suspension at the concentration of 5%. The

precipitated magnesium carbonate was dried (105°C, for ~8h) and then calcined at either 300, 600 or 950°C, for 1.5 h to get magnesium oxide as a final product using programmable oven (Controller P320 MB1, Nabertherm GmbH).

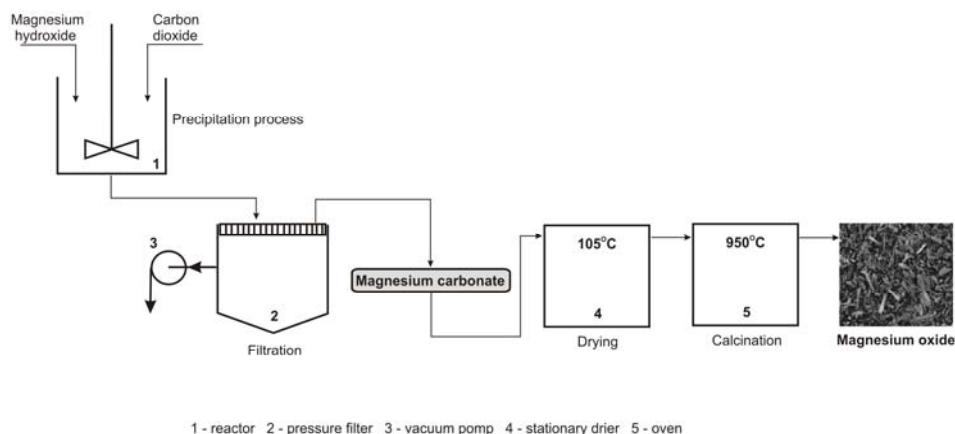


Fig. 1. Technological scheme of the process of precipitation of magnesium carbonate from magnesium hydroxide and carbon dioxide

The samples were characterised by determination of bulk density and particle size distributions using Zetasizer Nano ZS and Mastersizer 2000 made by Malvern Instruments Ltd, permitting measurements of particle diameters in the range from 0.6 to 6000 nm (NIBS method) and 0.2-2000  $\mu\text{m}$  (diffraction laser scattering technique). Crystalline structures of selected magnesium oxides were studied by the WAXS method. The X-ray patterns were taken with the help of a computer-controlled horizontal diffractometer TUR M-62, equipped with a HZG-3 type goniometer. The wettability of magnesium oxide with water samples obtained was estimated by using a tensiometer K100 made by Krüss. To characterise the texture of selected MgO samples, the nitrogen adsorption-desorption isotherms were analysed to determine the specific surface area (BET), pore volume and pore diameter (calculated by the BJH method). The isotherms were taken by ASAP 2020 instrument made by Micromeritics Instruments Co.

### 3. RESULTS AND DISCUSSION

At the first stage of the experiment, samples of magnesium carbonate were precipitated according to the following procedure:  $\text{CO}_2$  was introduced to a 5% suspension of magnesium hydroxide placed in the reactor at the rates in the range from 2 to 5  $\text{dm}^3/\text{min}$  at 20 or 40°C. The intermediate products were subjected to calcination

to get magnesium oxide samples. The final samples obtained are characterised in Table 1.

Table 1. Physicochemical and dispersive properties of magnesium oxide precipitated by introducing CO<sub>2</sub> to a 5% suspension of magnesium hydroxide

Sample No.	Precipitation process conditions		Physico-chemical and dispersive properties				
	Flow rate (dm <sup>3</sup> /min)	Temperature (°C)	Bulk density (g/dm <sup>3</sup> )	Diameter (nm) from Zetasizer Nano ZS	Diameter (µm) from Mastersizer 2000		
					d(0.1)	d(0.5)	d(0.9)
1	2	20	109	459÷2300	2.30	8.20	24.55
2		40	138	122÷2300 4150÷5560	3.09	8.87	42.58
3	3	20	120	615÷2300	2.88	7.77	25.98
4		40	125	122÷255 295÷2300 4150÷5560	3.25	9.67	32.83
5	4	20	160	91÷5560	2.78	16.01	46.03
6		40	171	164÷531 615÷5560	2.93	17.02	47.03
7	5	20	167	91÷255; 295÷1720	2.78	16.32	46.82
8		40	182	79÷342 459÷4150 4800÷5560	3.72	20.05	48.76

The physicochemical properties of magnesium oxide samples (1-8), obtained under conditions specified above, were found to be significantly depended on the rate of CO<sub>2</sub> supply and temperature of the process. The products obtained at relatively low rates of CO<sub>2</sub> supply (2 and 3 dm<sup>3</sup>/min) were characterised by rather small bulk densities from 109 to 125 g/dm<sup>3</sup>, and the lower values of densities were obtained when the process was run at 20°C. When the rate of CO<sub>2</sub> supply was increased to 4 and 5 dm<sup>3</sup>/min, the product density increased to 182 g/dm<sup>3</sup> (sample 8, 5 dm<sup>3</sup>/min, 40°C). A similar relation was observed for particle diameters. They were smaller for the low rates of CO<sub>2</sub> supply and at 20°C (samples 1 and 3). According to the results of measurements with Mastersizer 2000, in sample the contribution of particles of diameters not greater than 2.30 µm in the sample is 10%, the contribution of those of diameters below 8.20 µm is 50% and the contribution of those of diameters not greater than 24.55 µm is

90%. For the products obtained at 40°C a tendency to formation of particles of greater diameters was observed. For the rates of CO<sub>2</sub> supply of 4 and 5 dm<sup>3</sup>/min, the process of particle agglomeration developed irrespective of the temperature applied. The magnesium oxide samples precipitated under such conditions (samples 5÷8) were characterised by relatively high values of  $d(0.9)$  up to 48.76 µm.

Figs 1 and 2 present the particle size distributions and SEM photographs of MgO samples 1 and 3, showing the most beneficial physico-chemical properties. The curves in Figs 1a and 2a display monomodal bands covering similar ranges of particle diameters, from 615 to 2300 nm and from 459 to 2300 nm, respectively. The similar dispersion, morphology and microstructure of the samples are confirmed by the SEM photograph, revealing the dominant presence of longitudinal crystallites of irregular form.

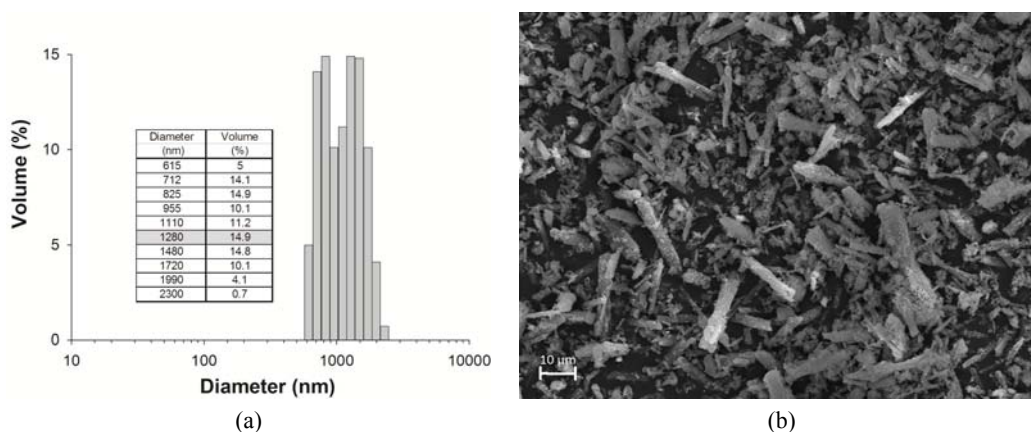


Fig. 1. (a) Particle size distribution (Zetasizer Nano ZS) and (b) SEM photograph of magnesium oxide (sample 1) precipitated when CO<sub>2</sub> was introduced to magnesium hydroxide suspension at the rate of 2 dm<sup>3</sup>/min, at 20°C

Particle size distributions of samples 1, 2, 3 from the micrometric range are similar and vary from 1 to 79 µm. As to the particles bringing the maximum volume contributions, for sample 1 the maximum volume contribution of 6.3% is brought by the particles of 6.6 µm in diameter, whereas for samples 2 and 3 by particles of greater diameters. In sample 2 the maximum volume contribution of 6.7% comes from the particles of 11.5 µm in diameter. The character of the particle size distribution curve obtained for sample 4 proves its variable dispersion. Two maxima in the particle size distribution pattern imply the dominance of particles of diameters in the micrometric and nanometric ranges.

At the second stage of study the final samples were obtained when both substrates were simultaneously introduced into the water system.

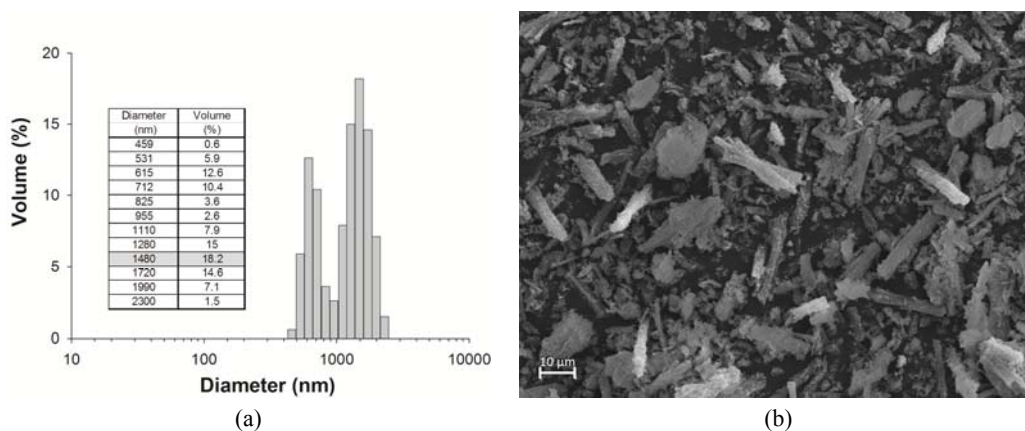


Fig. 2. (a) Particle size distribution (Zetasizer Nano ZS) and (b) SEM photograph of magnesium oxide (sample 3) precipitated when  $\text{CO}_2$  was introduced to magnesium hydroxide suspension at the rate of  $3 \text{ dm}^3/\text{min}$ , at  $20^\circ\text{C}$

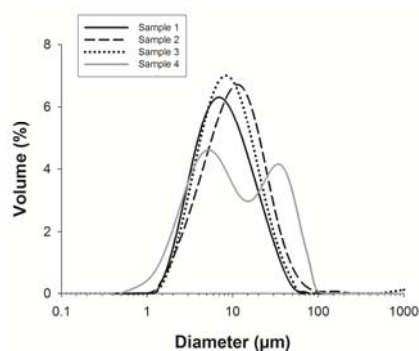


Fig. 3. Particle size distribution (Mastersizer 2000) of magnesium oxide samples 1, 2, 3 and 4 precipitated when  $\text{CO}_2$  was introduced to magnesium hydroxide suspension at the rate of 2 and  $3 \text{ dm}^3/\text{min}$ , respectively

Bulk densities of samples 9-16 (Table 2) obtained when the two reagents were introduced simultaneously, are close to those of the samples obtained when  $\text{CO}_2$  was introduced to magnesium hydroxide suspension and are higher for the process carried out at  $40^\circ\text{C}$  and for higher rates of the reagents supply. For example, the bulk density of sample 9 is  $138 \text{ g/cm}^3$ , while that of sample 16 is  $171 \text{ g/cm}^3$ . The diameters of particles from the nanometric range (measured with Zetasizer Nano ZS), irrespectively of the precipitation conditions, vary from 255 nm to 5560 nm. Some differences in the dispersion and morphology of the samples were revealed by the results of particle size diameters from the micrometric range (Mastersizer 2000). Analysis of  $d(0.9)$  values indicated greater tendency towards formation of agglomerates for the samples precipitated at  $40^\circ\text{C}$ , similarly to the samples obtained in the first stage of the study.

Smaller agglomerates are observed in the samples obtained in the process run at 20°C and at higher rates of the reagents supply. The latter observation is true only for the samples obtained at the second stage of the experiment, i.e. for simultaneous supply of reagents. Among all samples of magnesium oxide obtained in the first and in the second stages of the experiment, the particles of the smallest diameters were obtained for sample 15 (Mastersizer 2000). In this sample 10% volume was taken by the particles of diameters not greater than 1.58  $\mu\text{m}$ , 50% volume was taken by those of diameters below 4.04  $\mu\text{m}$  and 90% volume was taken by those of diameters below 13.59  $\mu\text{m}$ .

Figures 4a and 5a show the particle size distributions of samples 13 and 15 corresponding to the diameters of particles from the nanometric range. For these two samples the ranges of particle diameters are comparable with maxima at 5560 nm. The SEM photographs in Figs. 4b and 5b reveal inhomogeneity of the samples and much greater diameters of agglomerates in sample 13.

Table 2. Physicochemical and dispersive properties of magnesium oxide obtained for simultaneous supply of CO<sub>2</sub> and 5% suspension of magnesium hydroxide

Sample No.	Precipitation process conditions		Physico-chemical and dispersive properties				
	Flow rate (dm <sup>3</sup> /min)	Temperature (°C)	Bulk density (g/dm <sup>3</sup> )	Diameter (nm) from Zetasizer Nano ZS	Diameter ( $\mu\text{m}$ ) from Mastersizer 2000		
					d(0.1)	d(0.5)	d(0.9)
9	2	20	138	91-5560	2.27	9.47	36.61
10		40	144	142-5560	2.63	16.11	50.08
11	3	20	141	164-5560	2.27	13.65	40.63
12		40	146	122-5560	3.08	20.49	53.70
13	4	20	156	164-5560	2.39	9.48	29.54
14		40	158	142-5560	2.55	9.93	44.51
15	5	20	161	91-5560	1.58	4.04	13.59
16		40	171	255-5560	1.87	5.71	40.39

The particle size distribution profiles presented in Fig. 6 can be assigned to two groups according to dispersion. The first group includes samples 15 and 16 in which the maximum volume contribution of 7% and 5.6% is brought by the particles of diameter of 3.8  $\mu\text{m}$ . The band obtained for sample 15 is relatively narrow, which means that this sample is relatively homogeneous (Fig. 5b). The bands corresponding to samples 13 and 14 are wider and the maximum volume contributions in them are brought by particles of greater diameters.

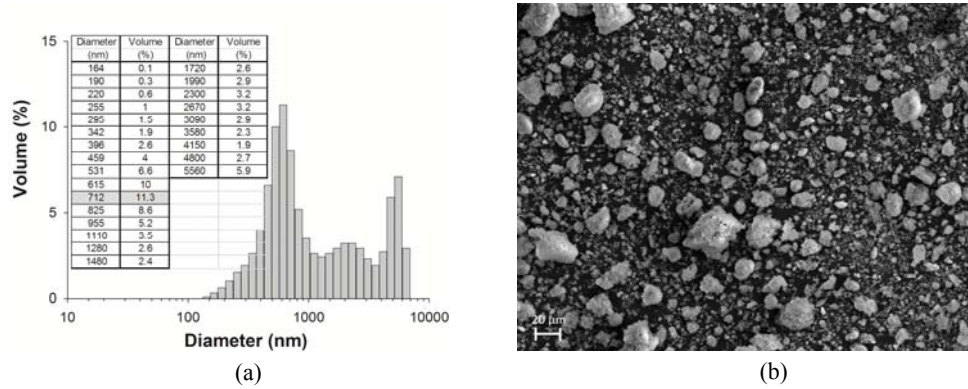


Fig. 4. (a) Particle size distribution (Zetasizer Nano ZS) and (b) SEM photographs of sample 13 precipitated at simultaneous supply of the reagents at the rate of 4 dm<sup>3</sup>/min at 20°C

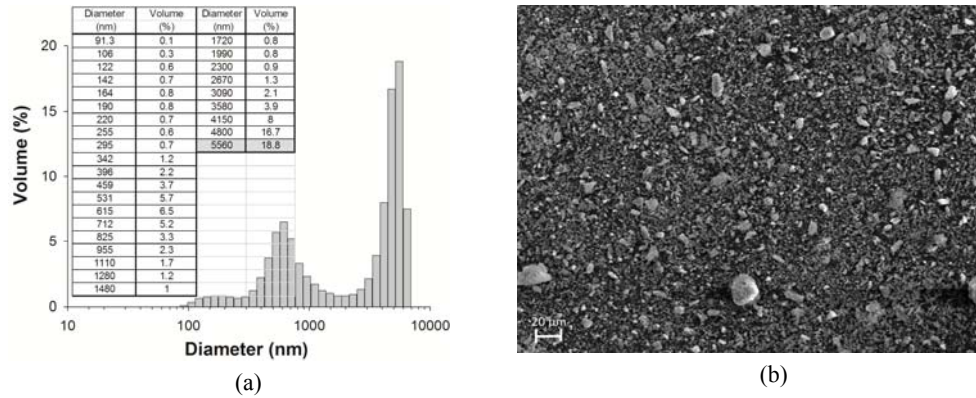


Fig. 5. (a) Particle size distribution (Zetasizer Nano ZS) and (b) SEM photograph of magnesium oxide sample 15, precipitated upon simultaneous introduction of reagents at the rate of 5 dm<sup>3</sup>/min at 20°C

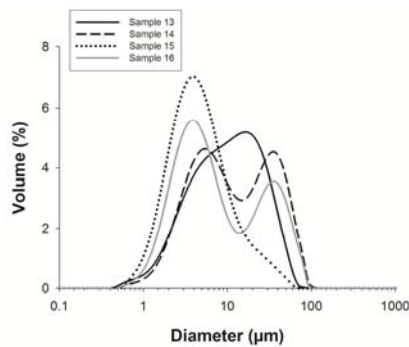


Fig. 6. Particle size distribution (Mastersizer 2000) for samples 13 and 14 precipitated upon simultaneous supply of the reagents at the rate 4 dm<sup>3</sup>/min and for samples 15 and 16 precipitated in the same mode of reagents supply at the rate of 5 dm<sup>3</sup>/min

According to WAXS results, undertaken to identify the samples with the X-RAYAN program, the samples obtained after calcination of magnesium carbonates (intermediate products) were synthetic magnesium oxides of crystalline structure. Figure 7 presents typical of the crystalline MgO phase diffraction maxima for samples 1 and 15.

Selected samples were also characterised as to the wettability with water. Figure 8 presents wettability profiles recorded for samples 1, 2, 15 and 16. The greatest tendency to absorb water (the highest hydrophilicity) was noted for sample 1, (0.95 g), precipitated upon introduction of CO<sub>2</sub> to magnesium hydroxide suspension. The lowest tendency to absorb water showed sample 15 (0.70 g), obtained upon simultaneous supply of reagents. All samples absorbed characteristic the amount of water during similar time (165-185 s) after which the mass of the samples got stabilized.

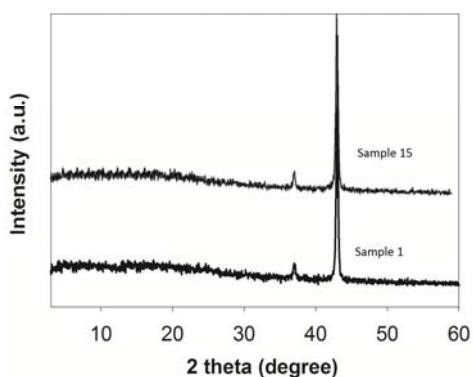


Fig. 7. X-ray diffraction patterns of selected magnesium oxides (samples 1, 15)

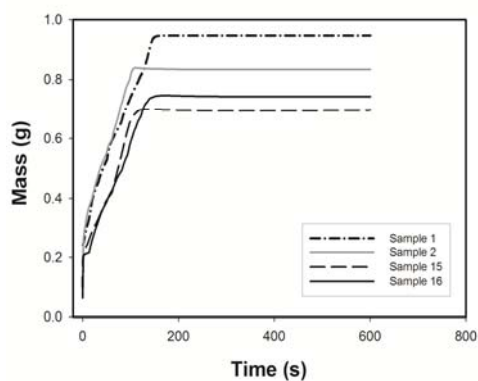


Fig. 8. Profile of wettability with water obtained for selected magnesium oxides (samples 1, 2, 15, 16)

Table 3. Adsorptive properties of selected magnesium oxide samples precipitated under different precipitation process conditions

Sample No.	BET surface area (m <sup>2</sup> /g)	Pore volume (cm <sup>3</sup> /g)	Pore size (nm)
1	15.2	0.01	3.0
3	21.2	0.15	28.5
13	18.7	0.01	2.7
15	17.5	0.01	2.9

To check the potential use of the oxides as adsorbents and catalysts, their adsorption capacity was determined on the basis of nitrogen adsorption-desorption

isotherms. Figure 9 presents the isotherms recorded for sample 3. With increasing relative pressure the volume of nitrogen adsorbed systematically increased to reach at  $p/p_0=1$  a maximum value of  $100 \text{ cm}^3/\text{g}$ .

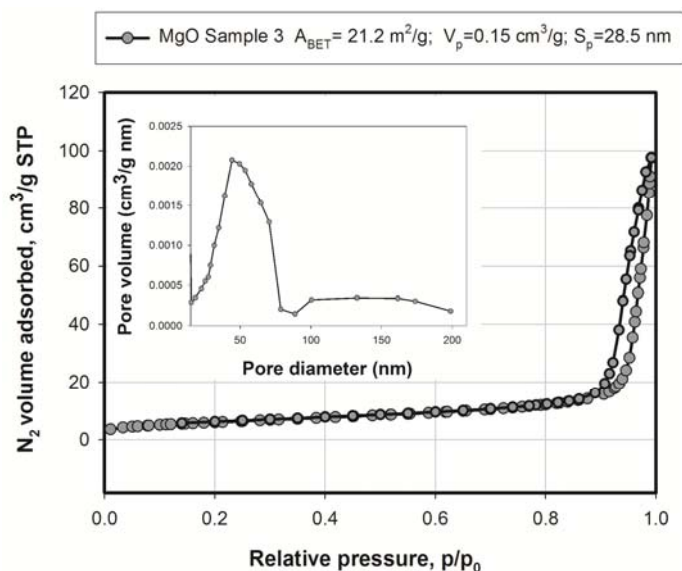


Fig. 9. Nitrogen adsorption-desorption isotherm and pore density distribution of sample 3

Analysis of the isotherms of nitrogen adsorption and desorption recorded for samples 1, 3, 13, 15 permitted determination of specific surface area, pore volume and pore diameters (table 3). All samples have relatively low specific surface area ranging from  $15.2$  to  $21.2 \text{ m}^2/\text{g}$ . The best adsorption properties were found for sample 3. According to the pore size of about  $28.5 \text{ nm}$ , this sample is classified as mesoporous.

### 3. CONCLUSION

The proposed method of obtaining MgO from  $\text{MgCO}_3$  precipitate using magnesium hydroxide and carbon dioxide, permits getting magnesium oxide of desired dispersive, morphological and adsorption properties by controlling the conditions of synthesis. The magnesium oxide samples obtained revealed a significant tendency towards formation of secondary agglomerations. Sample 15 was found to have the particles from the micrometric range of the smallest diameter of  $13.59 \mu\text{m}$ . This sample was precipitated at  $20^\circ\text{C}$  upon simultaneous supply of reagents at the rate of  $5 \text{ dm}^3/\text{min}$ . The same sample also showed the smallest tendency to absorb water. The samples obtained in the experiment, when  $\text{CO}_2$  was supplied to magnesium hydroxide suspension, were characterised by better dispersion properties when lower rates of

supply were applied. The optimum temperature of the process was found to be 20°C as the magnesium oxide samples, precipitated at that temperature, were generally lighter and less agglomerated. The majority of samples obtained were characterised by small adsorption activity. Sample 3, found to have the largest pore diameters of 28.5 nm, was obtained upon CO<sub>2</sub> introduction to magnesium hydroxide suspension at the rate of 3 dm<sup>3</sup>/min at 20°C.

## REFERENCES

- BOTHA A., STRYDOM C.A., 2001, Preparation of a magnesium carbonate from magnesium hydroxide, *Hydrometallurgy*, 62, 175-183.
- CHHOR K., BOCQUET J.F., POMMIER C., 1995, Synthesis of submicron magnesium oxide powders, *Mat. Chem. Phys.*, 40, 63-68.
- CHOUDHARY V.R., RANE V.R., PANDIT M.Y., 1997, Comparison of alkali metal promoted MgO catalysts for their surface acidity/basicity and catalytic activity/selectivity in the oxidative coupling of methane, *J. Chem. Tech. Biotechnol.*, 68, 177-186.
- CHOUDHARY V.R., PATASKAR S.G., ZOPE G.B., CHAUDHARI P.N., 2004, Surface properties of magnesium oxide obtained from basic magnesium carbonate: Influence of preparation conditions of magnesium carbonate, *J. Chem. Tech. Biotechnol.*, 64, 407-413.
- GREEN J., 1983, Calcination of precipitated Mg(OH)<sub>2</sub> to active MgO in the production of refractory and chemical grade MgO, *J. Mater. Sci.*, 18, 637-651.
- GULKOVA D., SOLKOVA O., ZDRAZIL M., 2004, Preparation of MgO catalytic support in shaped mesoporous high surface area form, *Micropor. Mesopor. Mat.*, 76, 137-149.
- MOROZOV S.A., MALKOV A.A., MALYGIN A.A., 2003, Synthesis of porous magnesium oxide by thermal decomposition of basic magnesium carbonate, *Russ. J. Gen. Chem.*, 73, 37-42.
- PRZEPIÓRSKI J., KAROLCZYK J., TAKEDA K., TSUMURA T., TOYODA M., MORAWSKI A.W., 2009, Porous carbon obtained by carbonization of PET mixed with basic magnesium carbonate: pore structure and pore creation mechanism, *Ind. Eng. Chem. Res.*, 48, 7110-7116.
- RUCKENSTEIN E., HU Y.H., 1997, The effect of precursor and preparation conditions of MgO on the CO<sub>2</sub> reforming of CH<sub>4</sub> over NiO/MgO catalysts, *Appl. Catal. A-Gen.*, 154, 185-205.
- THOMAS H., EPPLE M., RELLER A., 1997, Magnesium diolates as precursors for MgO: A low-temperature route, *Thermochim. Acta*, 3375, 195-200.

**Pilarska, A., Jesionowski, T.,** *Otrzymywanie MgO w procesie karbonizacji wodorotlenku magnezu*, *Physicochem. Probl. Miner. Process.*, 46 (2011) 83-94, (w jęz. ang), <http://www.minproc.pwr.wroc.pl/journal>

Przedstawiono badania nad otrzymywaniem tlenku magnezu z użyciem wodorotlenku magnezu i ditlenku węgla metodą karbonizacji. Otrzymany węgiel magnezu poddano termicznemu rozkładowi, prowadzonemu stopniowo w odpowiednich warunkach temperaturowych do uzyskania produktu finalnego – tlenku magnezu. W reakcji strącania uwzględniono następujące warunki eksperymentalne: pH medium reakcyjnego, temperaturę, sposób i szybkość dozowania reagentów. Określono właściwości dyspersyjne oraz profile zwilżalności w układach wodnych tlenku magnezu. W celu sprawdzenia charakteru adsorpcyjnego wytworzonych produktów wyznaczono wielkość powierzchni właściwej BET,

wielkość i objętość porów. Ponadto produkt poddano identyfikacji metoda rentgenograficzną. Dowiedziono istotnego wpływu warunków prowadzenia procesu na parametry fizykochemiczne otrzymanego MgO oraz wyłoniono produkty o najbardziej reprezentatywnych właściwościach.

*słowa kluczowe: MgO, precipitacja, carbonatyzacja, skład ziarnowy, morfologia powierzchniowa, zwilżalność, właściwości adsorpcyjne*

Adem TAŞDEMİR\*, Hüseyin ÖZDAĞ\*, Güven ÖNAL\*\*

## IMAGE ANALYSIS OF NARROW SIZE FRACTIONS OBTAINED BY SIEVE ANALYSIS - AN EVALUATION BY LOG-NORMAL DISTRIBUTION AND SHAPE FACTORS

*Received May 5, 2010; reviewed; accepted July 7, 2010*

In this research, a pure quartz sample was subjected to sieve analysis and nine narrow size fractions were obtained. Polished sections were prepared from the representative samples of each fraction and were examined by image analysis (IA) to determine particle size distributions (PSDs) of fractions. Both size and shape measurements were made on individual quartz particles. Mean Feret diameter ( $d_F$ ) and three shape factors measurements, namely chunkiness ( $Ch$ ), roundness ( $R$ ) and form factor ( $FF$ ), were carried out. This study showed that majority of particles in sieved fractions lied outside the nominal openings of the sieves. PSDs in all narrow sieve fractions were found to obey the log-normal distribution function. If number-based distribution of a system is found to be log-normal, the distribution of the derived diameters is also log-normal with the same geometric standard deviation. The number-based means obtained by IA were transformed to the volume (mass)-based means by using this property. The means of number- and volume (mass)-based IA sizes before and after correction by shape factors were compared with their corresponding geometric sieve means. Among the shape factors,  $FF$  was found as the most relating factor of sieve and IA sizes. The average of mean  $FF$  values of all size fractions was equal to 0.78. Reciprocal of this value (1.29) was very close to the slope of 1.28 obtained from the volume (mass)-based means of IA versus geometric sieve means relation. This result suggests that the slopes of the lines can provide a measure of differences between sieving and IA and this was related to  $FF$  values for quartz when  $d_F$  was used as IA size.

*keywords: particle size distribution, image analysis, sieving, log-normal distribution, shape factor*

\* Eskişehir Osmangazi University, Dept. of Mining Engineering, Division of Mineral Processing, 26480, Eskişehir-Turkey, atadem@ogu.edu.tr, Tel: +90 222 239 37 50 ext:3438

\*\* Istanbul Technical University, Faculty of Mines, Dept. of Minerals Engineering, İstanbul-Turkey

## 1. INTRODUCTION

The quantification of particle size and shape is problematic for researchers because descriptive single parameter measurements of particle morphology do not exist (Meloy, 1984). For a very specific material, a single method of determining size and shape can be sufficient to describe differences between individual particles of that material. However, a combination of methods is often required to provide more precise quantification of the size and shape parameters (Haughton and Amidon, 1992).

There are many different methods available for particle size and shape analysis. Size characterization is simple for spherical particles. For irregular particles it is not, and therefore the assigned size depends on the method of measurement. A comparison of results obtained from different particle size measurement methods is often required. Therefore, it is necessary to determine conversion factors between the methods when it is needed.

Despite a long and successful use in most applications, sieving is still neither a precise nor accurate technique of particle-size measurement. When particle size distribution (PSD) parameters are calculated from the sieve analysis, it is generally assumed that the distributions within the sieve fractions are linear (normal distribution) and produce a mean particle size equal to the average of the sieve intervals or that a more proper number is the geometric mean of these two apertures (Carstensen and Dali, 1999).

Among the methods used for size characterization, microscopy based image analysis (IA) is the only commonly used method in which individual particles are viewed and measured. An advantage of this method is that both various sizes as well as qualitative and quantitative shape information can be obtained simultaneously.

Particle size, like other variables in nature, tends to follow well-defined mathematical laws in its distribution. PSDs have been described by relations between particle mass and size, volume and size, number and size, and number and mass. Different mathematical formulas and approaches have been suggested to express relations against size, and total mass/volume/number is given against increasing size (mass/volume/number) of undersize and to make distribution curves linear, especially the size distribution. PSDs of fragmented geological materials have been described previously by at least seven relations between mass/volume/number and mass/size of fragments (Blenkinsop, 1991).

One major difficulty remaining with the image analysis is that the primary PSDs are number-based. This means that a direct comparison of results from IA with sieving, which yields mass-based size distributions, is generally not possible. In order to compare IA and sieve results, it is necessary to transform the IA results into volume (mass)-based distributions.

The log-normal law is frequently found with particulate systems. Since the particle

size is plotted on a logarithmic scale, the presentation of data on a log-probability graph is particularly useful when the range of size is large (Allen, 1997; Svarovsky, 1981). The other usefulness of the log-normal distribution is that if the number distribution of a particulate system is found log-normal, the mass distribution is also log-normal with the same geometric standard deviation (Allen, 1997). Therefore, the other mean sizes and their distributions can be determined by using this property. This method was applied successfully for determination of unbroken grain size distribution of bonded chromites (Taşdemir et al., 1997; Taşdemir and Bozkurt, 2007; Taşdemir, 2008) and the other different types of chromite ores (Taşdemir, 2008).

In this research, PSDs and shape factors of narrowly sieved size fractions of quartz sample were determined for polished sections which were prepared from nine sieved fractions by using IA. The mean Feret diameters were used as the IA size and its PSDs of sieve fractions were evaluated statistically. It was found that all PSDs of size intervals obeyed the log-normal distribution function very well. Using the log-normal distribution properties, number-based means of size fractions were converted into volume (mass)-based means and these IA means were compared with their geometric means of sieve intervals before and after correction by three shape factors, namely chunkiness ( $Ch$ ), roundness ( $R$ ) and form factor ( $FF$ ).

## 2. MATERIAL AND METHOD

### 2.1. SAMPLE PREPARATION

This paper presents a comparison of two different methods of measuring particle size distribution of a glass quality quartz sample. Natural quartz is often used as a reference mineral in most mineral processing studies including comminution, flotation, etc. Therefore, a pure quartz sample from Çine/Aydın (Turkey) was chosen and used in the experiments. The quartz sample produced for the glass production was supplied from the Ak Mining Co. The representative sample of quartz was sieved using sieve series including 600, 500, 400, 300, 212, 150, 106, 75, 53 and 38  $\mu\text{m}$  in sizes.

The sieve analysis was initially carried out manually by wet sieving until there was no particle passage under the sieves. At the end of sieving, each sieve was subjected to ultrasonic bath for cleaning. This process also allowed the particles, especially elongated particles trapped between the in the sieve apertures, to pass through the sieve.

The sieve diameter of a particle is usually defined as a geometric mean of openings of the last sieve through which the particle passes and the sieve on which it is retained (Kennedy and Koh, 1961). This is the sieve diameter definition that will be used here. Geometric means of sieve intervals were calculated as:

$$D[S,50] = \sqrt{D^i \cdot D^{i-1}}, \quad (1)$$

where  $D^i$  is the upper sieve size through which a particle can pass and  $D^{i-1}$  is the sieve aperture that the particle cannot pass.

Representative samples of dried powders of each sieve fractions were prepared as polished sections by using low viscosity epoxy resin which was mixed with appropriate amount of hardener. The air bubbles which occurred while stirring the epoxy resin/hardener mixture were removed by vacuum. After pouring a small amount of this mixture into a molding assembly, the particles of each narrow-sieved fraction were carefully poured into resin/hardener mixture in the mounting cup where the particles slowly sunk. After ensuring all the surfaces of the particles were wet and particle completely settled, the powders and the resin were stirred, to have them thoroughly mixed. The entrapped air bubbles during this process were also removed by vacuum. Since the epoxy-hardener mixture used cures over eight hours, enough time was given to all grains without preferred orientation on the polished section surface. As a result, the particles on the surface of the polished sections were randomly oriented and laid in their most stable positions. A grinding and polishing flow sheet was developed and applied successfully for the polished sections of coarse and fine sieve fractions.

## 2.2. SIZE AND SHAPE MEASUREMENTS BY IMAGE ANALYSIS

The size and shape measurements on polished sections of sieve fractions were performed with a Leco 2001 image analyzer. Two-dimensional images of quartz particles were produced by Olympus reflected light microscopy associated with the image analyzer. Each particle was measured individually.

In this research, the measurements such as area ( $A$ ), perimeter ( $P$ ) and Feret diameter  $d_F$ , which is the distance between two parallel lines tangent to the projected cross-section in eight different directions, i.e. at angular resolution of  $22.5^\circ$  were performed on the individual quartz particles. In this study. The Mean Feret diameter calculated by averaging these eight measures was used as the IA size. Also, comparisons between  $D[S,50]$  and the mean size values, which were obtained from multiplying the mean IA sizes of sieve fractions with their corresponding mean of shape factors, namely chunkiness ( $Ch$ ), roundness ( $R$ ) and form factor ( $FF$ ), were carried out. These shape factors were calculated as:

$$\text{Chunkiness}(Ch) = [\text{Width}(W), \text{min.Feret}] / [\text{Feret length perpendicular to } W], \quad (2)$$

$$\text{Roundness}(R) = (4\pi A) / (P^2), \quad (3)$$

$$\text{Form Factor}(FF) = \sqrt{R}. \quad (4)$$

## 2.3. LOG-NORMAL DISTRIBUTION

The probability density function  $f(x)$  of the log-normal distribution is given by the following equation (Al-Thyabat and Miles, 2006):

$$f(x) = \frac{1}{\ln x \ln \sigma_g \sqrt{2\pi}} \exp\left[-\frac{(\ln x - \ln x_g)^2}{2 \ln^2 \sigma_g}\right], \quad (5)$$

where  $x$  is the particle size.

The log-normal distribution is a two-parameter function (geometric mean,  $\ln x_g$  and geometric standard deviation  $\ln \sigma_g$ ). The parameters of the log-normal distribution can be calculated by the following equations (Ang and Tang, 1975; Koch and Link, 1970):

$$\ln x_g = \ln \mu - \frac{1}{2} \ln^2 \sigma_g, \quad (6)$$

$$\ln \sigma_g = \sqrt{\ln\left(\frac{\sigma^2}{\mu^2} + 1\right)}, \quad (7)$$

where  $\mu$  is the normal arithmetic mean of distribution and  $\sigma$  is the standard deviation of the distribution.

If the measured data points show a pattern of linearity in log probability drawing paper, then they can be considered to follow the log-normal distribution.

## 2.4. RELATIONS BETWEEN MEAN SIZES FOR THE LOG-NORMAL DISTRIBUTION

Since the PSDs measured by an image analysis system are number-based, the geometric mean calculated by Eq. (6) is the geometric mean of number distribution ( $\ln x_{gN}$ ). If a number distribution is found to obey log-normal distribution, length, surface and volume means are calculated by using the same geometric standard deviation found for number distribution. Details of the derivation of these formulas can be found in details in the literature (Allen, 1997 and Svarovsky, 1981). Once a number geometric mean and geometric standard deviation of a log-normal distribution are determined, mean of number-length and volume (mass) means can be calculated by using the following formulas:

$$\ln x_{NL} = \ln x_{gN} + \frac{1}{2} \ln^2 \sigma_g, \quad (8)$$

$$\ln x_{VM} = \ln x_{gN} + 3.5 \ln^2 \sigma_g. \quad (9)$$

Equations (8) and (9) were used as number-based and volume (mass)-based means of log-normal distribution, respectively.

### 3. RESULTS

#### 3.1. PROPERTIES OF PSDS IN NARROWLY SIEVED FRACTIONS

The PSDs of all sieve fractions of the quartz sample were first evaluated and tested by normal distribution because narrowly sized PSDs are expected to be normally distributed (Carstensen and Dali, 1999). However, it was found that the PSDs of sieved fractions were not neatly normal. The PSDs of sieve fractions are plotted on a log-normal scale plot and resulting graph is presented in Fig. 1. It can be clearly seen, that the data points of size fractions show an appropriate pattern of linearity (Fig. 1), and thus they can be considered to follow the log-normal pattern very well. The log-normal distribution plots of sieve intervals do not deviate from the linearity and provides straight lines for the entire range of measured grain sizes. Coefficients of determination ( $R^2$ ) were over 0.99 for all sieve fractions. These results suggest that the properties of log-normal distribution can be applied easily to the PSDs of all fractions to obtain various mean diameters and their distributions.

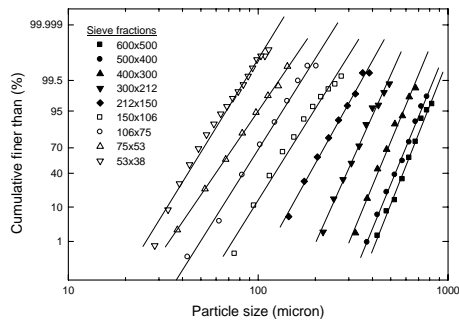


Fig. 1. Size distributions of sieve fractions plotted on log-normal drawing paper

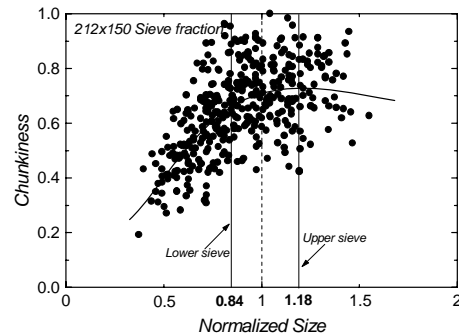


Fig. 2. Chunkiness-normalized size domain for 212x150  $\mu\text{m}$  size fraction

In Fig. 2, chunkiness shape factor against size domain where the information on shape with respect to size for an individual particle can be obtained is presented for 212x150  $\mu\text{m}$  size fraction as an example. Similar results were also obtained for other narrow sieve fractions. In this figure, the width values of individual particles (smallest Feret size) were normalized by the geometric mean of the sieve fraction. It is seen clearly that all of the particles are not within their sieve ranges and actual particle size limits are not confined in this region. This figure also shows different shape properties of particles that are found in the same sieve interval. Particles that were found in the defined sieve range were more regular than other particles. The particles that were smaller than the sieve size limit were more irregular since they had comparatively smaller chunkiness values, i.e. were more elongated. However, the particles which were larger than the sieve ranges were more regular in the shape as the particles lied

inside the nominal sieve openings. According to this finding, the particles within a sieve interval might have many different particle shapes, and the *PSDs* of narrowly sieved fractions were wider than the sieve limits and were not narrowly distributed.

### 3.2 STATISTICAL PARAMETERS OF LOG-NORMAL DISTRIBUTION AND EVALUATION WITH SHAPE FACTORS

In this study geometric means of sieve fractions ( $D[S,50]$ ), arithmetic mean of mean Feret diameters ( $\mu$ ) and standard deviation ( $\sigma$ ) obtained by the IA for each sieve fraction were found. For each sieve interval, ( $\mu$ ) and ( $\sigma$ ) parameters were converted to number geometric means ( $\ln x_{gN}$ ) and geometric variances ( $\ln^2 \sigma_g$ ) by using Eqs. (6) and (7) to find the log-normal distribution parameters. The  $x_{NL}$  and  $x_{VM}$  values were calculated by using Eqs. (8) and (9). Also means of *Ch*, *R* and *FF* shape factors of each sieve fraction were determined by Eqs. (2-4). The statistical data of the nine sieve intervals for size and shape are shown in Table 1. According to these results, the mean particle shapes varied in sieve fractions and were not constant, indicating that they were generally size dependent. Both number- and volume (mass)-based IA means of all sieve intervals are larger than the calculated  $D[S,50]$ .

Table 1. Statistical parameters of mean Feret diameters and mean shape factors measured in narrowly sieved intervals by IA

Sieve fractions, $\mu\text{m}$	Geometric means $D[S,50]$	$\mu$	$\sigma$	$\ln x_{gN}$	$\ln \sigma_g$	$x_{NL}$	$x_{VM}$	<i>Ch</i>	<i>R</i>	<i>FF</i>	
600x500	547.72	610.94	94.69	6.40	0.16	611.64	658.24	0.74	0.56	0.75	
500x400	447.21	557.58	91.85	6.31	0.17	557.78	606.69	0.71	0.61	0.78	
400x300	346.41	443.67	74.59	6.08	0.16	443.65	481.05	0.73	0.61	0.78	
300x212	252.19	309.07	55.68	5.72	0.18	309.08	339.58	0.72	0.62	0.79	
212x150	178.33	201.46	44.22	5.28	0.21	201.38	230.07	0.65	0.59	0.76	
150x106	126.10	129.59	32.69	4.84	0.24	129.48	153.25	0.65	0.61	0.78	
106x75	89.16	91.98	21.93	4.49	0.23	91.97	108.09	0.63	0.62	0.78	
75x53	63.05	66.34	18.06	4.16	0.27	66.34	81.53	0.64	0.58	0.75	
53x38	44.88	45.29	10.65	3.79	0.22	45.24	52.26	0.65	0.69	0.83	
								Mean	0.68	0.61	0.78
								1/Mean	1.47	1.64	1.29

The plots of  $x_{NL}$  and  $x_{VM}$  versus  $D[S,50]$  are shown in Figs (3-6). It should be noticed that the slope values on all plots in the figures were obtained from simple linear equations but the results were presented as log-log graphs for all plots given here to see the differences more clearly for the smaller sieve fractions. There was a simple linear correlation between  $D[S,50]$  and  $x_{NL}$  as well as  $x_{VM}$  sizes in all cases. These basic relations gave straight lines. The slopes of the lines may provide a measure of the discrepancy between the IA sizes and sieve sizes.

For investigation of possible relations between calculated shape factors and  $x_{NL}$  as well as  $x_{VM}$  slopes value, the number- and volume (mass)-based IA sizes were multiplied by their corresponding shape factor values and their means were compared with the corresponding  $D[S,50]$ . The slopes obtained before and after correction were evaluated as the deviations from the ideal 1:1 line.

Figs (3) and (4) give the  $x_{NL}$  and  $x_{VM}$  IA means against their corresponding  $D[S,50]$ , respectively. The values obtained from  $x_{NL}$  and  $x_{VM}$  calculations deviated from the 1:1 line with slopes of 1.21 (Fig. 3) and 1.28 (Fig. 4), respectively.

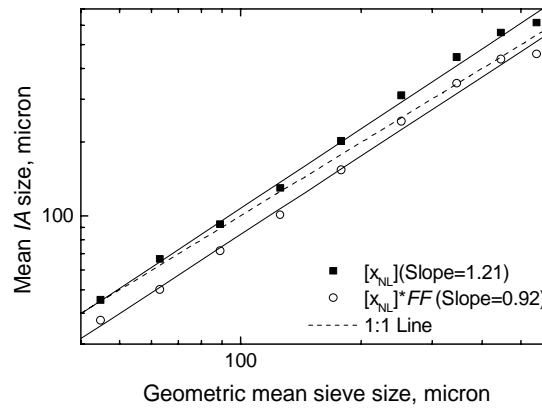


Fig. 3. Relationship between number-based IA means versus mean sieve sizes (■) and corrected number-based IA means by  $FF$  shape factor against geometric mean of sieve fractions (○)

After correction with the  $FF$  values, the deviations are smaller and have the values of 0.92 (Fig. 3) and 0.97 (Fig. 4) for  $x_{NL}$  and  $x_{VM}$  respectively. The close proximity of the deviation for  $x_{VM}$  to the ideal slope (1) shows that the volume (mass)-based values transformed from the log-normal distribution and corrected by  $FF$  agrees closely with that of sieving. The reciprocal of the average of the mean  $FF$  values of all sieve fractions was found as 1.29 (Table 1), which was very close to the slope value calculated before the correction by the shape factors for the  $D[S,50]$  versus  $x_{VM}$  plot (1.28) (Fig. 2). In a previous work, geometric mean of the minimum Feret (width) and maximum Feret (length) were used as the IA size and compared with the  $D[S,50]$  (Taşdemir et al., 2009). The slope was 1.23 for the sieve size means against the

volume (mass)-based means which were calculated in a different manner from this study. It was found that the mean Feret diameter ( $d_F$ ) gave better results than the previous work and improved the results.

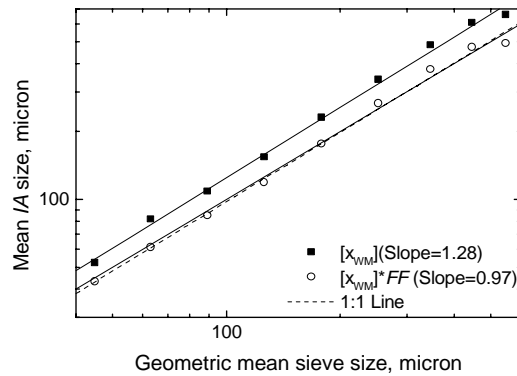


Fig. 4. Relationship between volume (mass)-based IA means versus mean sieve sizes (■) and corrected volume (mass)-based IA means by  $FF$  shape factor against geometric mean of sieve fractions (○)

The IA values corrected by  $Ch$  and  $R$  versus  $D[S,50]$  are given in Fig. 5 and Fig. 6, respectively. The result was also good when the  $x_{NL}$  and  $x_{VM}$  values were multiplied with their corresponding  $Ch$  values since the slopes were 0.90 and 0.96 for these relations, respectively, and the deviations from the 1:1 line were quite small (Fig. 5). But these results were not as good as the one which was obtained by using the  $FF$  values since fewer points were on the 1:1 line. In addition, neither the mean  $Ch$  (0.69) nor reciprocal of the  $Ch$  value (1.47) of sieve fractions give an approximate value of the slope as in the  $FF$ .

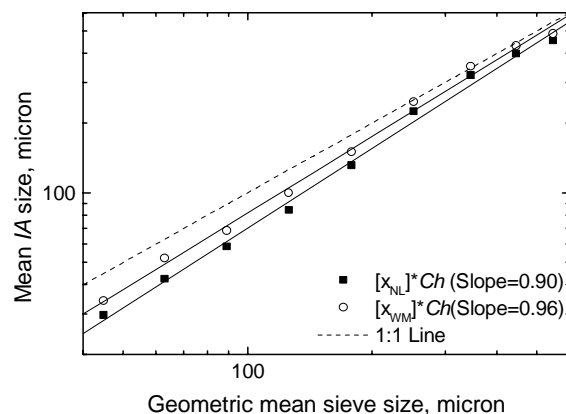


Fig. 5. IA means corrected by  $Ch$  against geometric mean of sieve fractions for number-based means (■) and volume(mass)-based means (○)

After correction of the IA results by  $R$  values of particles, the slopes were 0.70 and 0.75 for the  $x_{NL}$  and  $x_{VM}$  means respectively and the deviations were larger than the ones which were obtained by the  $FF$  and  $Ch$  factors. Although the relations were also linear, when  $R$  was used as a correction factor, there were no points on the 1:1 line and the points were very far from the 1:1 line in both cases (Fig. 6). From these results, the differences between IA of polished section and sieving for quartz sample can be attributed to the effects of particle shape and this relation is related mostly to the  $FF$  of particles.

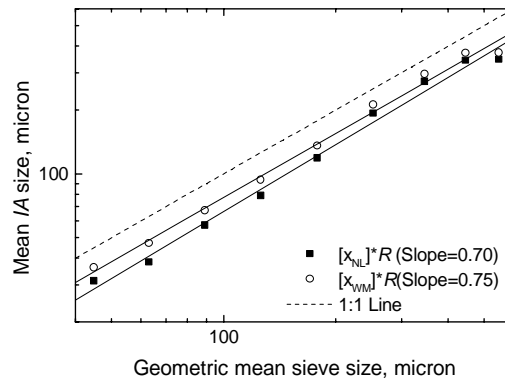


Fig. 6. IA means corrected by  $R$  against geometric mean of sieve fractions for number-based means (■) and volume (mass)-based means (○)

#### 4. CONCLUSION

In this work, particle size and shape measurements of narrowly sieved fractions were measured on polished sections for pure quartz by using image analysis. Mean Feret diameter and three shape factors namely chunkiness, roundness and form factor, were obtained for individual particles in the sections. The PSDs of all sieve fractions were found to obey the log-normal distribution, not normal distribution as expected. The number-based distributions were converted into volume (mass)-based distributions by log-normal distribution properties and their means were compared with the geometric means of sieve intervals before and after correction by the shape factors.

This study was also focused on the possible conversion of factor between the IA size measured on polished sections of particulate materials and sieve size by using measured shape factors. It was concluded that the mass-based means multiplied by the  $FF$  values of sieve fractions gave the best results with the geometric sieve means. The slope of the mass-based means against sieve means was 1.28 and this value was very near to reciprocal of the mean value of  $FF$  shape factors of all sieve fractions (1.29).

## REFERENCES

- ALLEN, T., 1997. Powder Sampling and Particle Size Determination, in: Particle Size Measurement, Volume 1, Scarlet, B. and Jimbo, G. (ed), 682 p.
- AL-THYABAT, S. and MILES, N. J., 2006. An Improved Estimation of Size Distribution from Particle Profile Measurements, Powder Technology, 166: 152-160.
- ANG, A. H. S. and TANG, W. H., 1975. Probability Concepts in Engineering Planning and Design, John Wiley and Sons, New York.
- BLINKINSOP, T. G., 1991. Cataclasis and Process of Particle Size Distribution, PAGEOP, 136: 59-86.
- CARSTENSEN, J. T. and DALI, M., 1999. Particle Size Distributions in Mesh Cuts and Microscopically Estimated Volumetric Shape Factors, Drug Development and Industrial Pharmacy, 25/3: 347-352.
- HAUGHTON, M. E. and AMIDON, G. E., 1992. Microscopic Characterization of Particle Size and Shape: An Inexpensive and Versatile Method, Pharmaceutical Research, 9: 856-859.
- KENNEDY, J. F. and KOH, R. C. Y., 1961. The Relation Between The Frequency of Sieve Diameters and Fall Velocities of Sediment Particles, Journal of Geophysical Research, 66/12: 4233.
- KOCH, G. S. and LINK, R. F., 1970. Statistical Analysis of Geological Data, John Wiley and Sons, New York.
- MELOY, T. P., 1984. Particulate Characterization: Future Approaches, Handbook of Powder Science and Technology, Fayed, M. E. and Otten, L. (ed), 69-98.
- SVAROSKY, L., 1981. Characterization of Particles Suspended in Liquid, Solid-Liquid Separation, Second Edition, Svarovsky, L. (ed), pp 9-32.
- TAŞDEMİR, A., ÖNAL, G., BOZKURT, R. and DOĞAN, M. Z., 1997. "Particle Size Determination of Unbroken Banded Chromite Ore by Image Analyzer" Proceedings of XX International Mineral Processing Congress, Aachen-Germany, p. 131-139.
- TAŞDEMİR, A. and BOZKURT, R., 2007. Grain Size Determination of Karaburhan Banded Chromite Ore Prior to Comminution, Dumlupınar Üniversitesi Fen Bilimleri Enstitüsü Dergisi, 14: 87-96 (Turkish text).
- TAŞDEMİR, A., ÖZDAĞ, H. and ÖNAL, G., 2009. Comparison of Geometric Mean Sizes Obtained by Image Analysis and Sieving and Their Correlation, 4 th Asian Particle Technology Symposium, New Delhi-India, pp APT2009/74.
- TAŞDEMİR, A., 2008. Evaluation of Grain Size Distribution of Unbroken Chromites, Minerals Engineering, 21: 711-719.

**Taşdemir, A., Özdağ, H., Önal, G.,** *Analiza obrazu wąskich klas ziarnowych otrzymanych za pomocą analizy sitowej – ocena z użyciem log-normalnej dystrybucji oraz współczynnika kształtu*, Physicochem. Probl. Miner. Process., 46 (2011) 95-106, (w jęz. ang), <http://www.minproc.pwr.wroc.pl/journal>

Próbki czystego kwarcu poddano analizie sitowej w celu wydzielenia dziewięciu wąskich klas ziarnowych. Klasy te użyto do przygotowania zglądów, które analizowano za pomocą komputerowej analizy obrazu (IA) w celu wyznaczenia składu ziarnowego (PSDs) każdej klasy. Określano zarówno rozmiar jak i współczynniki kształtu poszczególnych ziarn. Dokonano pomiarów średniej średnicy Fereta ( $d_F$ ) oraz trzech współczynników kształtu (krępość  $Ch$ , zaokrąglenie  $R$ , wskaźnik kształtu  $FF$ ). Wykazano, że wymiary większości ziarn frakcji z analizy sitowej znajdowały się poza nominalnymi rozmiarami sit. PSDs wszystkich wąskich klas ziarnowych można było opisać log-normalną funkcją rozkładu. Jeżeli oparta na liczbie ziarn dystrybucja spełnia rozkład log-normalny, wynikająca średnica

jest także opisywana funkcją log-normalną z tym samym geometrycznym odchyleniem standardowym. Średnie średnice oparta o liczbę ziarn, otrzymana za pomocą IA, zostały przeliczone na średnią objętościową (masową). Oznacza to, że wymiary oparte o liczbę i objętość (masę) IA przed i po korekcie za pomocą współczynnika kształtu były porównywalne z ich odpowiednimi geometrycznymi średnimi średnicami sitowymi. Stwierdzono, że wśród współczynników kształtu, wskaźnik  $FF$  okazał się najlepszy dla powiązania rozmiaru sitowego z rozmiarem z IA. Średnia wartość  $FF$  dla wszystkich frakcji wyniosła 0.78. Odwrotność tej liczby (1.29) jest bardzo bliska nachyleniu 1.28 otrzymanemu z średniej średnicy objętościowej IA wykreślonej jako funkcja geometrycznej średniej średnicy sitowej. Sugeruje to, że nachylenie tych zależności może dostarczyć miary różnicy wyników otrzymanych z przesiewania a z IA. Wyjaśniono to wartościami  $FF$  kiedy  $d_F$  jest użyte jako rozmiar oparty o IA.

*słowa kluczowe* skład ziarnowy, komputerowa analiza obrazu, przesiewanie, dystrybucja log-normalna, współczynnik kształtu

Hussin A. M. Ahmed\*

## DRY VERSUS WET UPGRADING OF NEPHELINE SYENITE ORES

*Received April 20, 2010; reviewed; accepted July 10, 2010*

Under strict specifications regarding its iron, alumina, and alkali contents, nephelyine syenite has a wide range of applications as filler, pigment and extender besides its usage in glass and ceramic industries. Kingdom of Saudi Arabia has huge nepheline syenite deposits in SAWDA mountain. Unfortunately, the ore is of low grade as to its high iron content (7.68% Fe<sub>2</sub>O<sub>3</sub>) and low alumina (17.38% Al<sub>2</sub>O<sub>3</sub>), and thus cannot be used in any of the previously mentioned industries as mined. This paper aims at investigating the amenability of processing the ore to meet market specifications. In the investigation two different technologies, dry and wet, are considered. The first is magnetic separation as a dry upgrading technique while the second is flotation as the wet upgrading technique. In applying magnetic separation technique the cross belt dings magnetic separator was used. The main studied variables were applied field intensity, separator belt speed, feed rate, and feed size, while the collector dosages were tested for upgrading the ore by flotation technology in a Denver D-12 flotation cell. The obtained results showed that magnetic separation can never produce nepheline concentrates having Fe<sub>2</sub>O<sub>3</sub> less than 0.85%. It was also found that at optimum flotation conditions the nepheline concentrates have Fe<sub>2</sub>O<sub>3</sub> content not less than 0.40%. However, combining the two techniques i.e. applying flotation under optimum conditions for cleaning of the previously obtained magnetic concentrate resulted in a final concentrate of 0.09% Fe<sub>2</sub>O<sub>3</sub> with Al<sub>2</sub>O<sub>3</sub> content of 23.58%. The produced concentrate can be used in many industrial applications, especially in glass and ceramics production.

*keywords: nepheline syenite, magnetic separation, flotation, glass and ceramics*

---

\* Mining Engineering Department, Faculty of Engineering, King Abdulaziz University, P.O. Box 80204, Jeddah 21589, Kingdom of Saudi Arabia

## 1. BACKGROUND

Nepheline syenite is an igneous rock. It may be formed in alkali-rich rock magma deficient in silica or by metasomatic nephelinization processes. Nepheline syenite rocks are composed essentially of nepheline, sodic plagioclase (usually albite or oligoclase) and microcline but in varying proportions, with small amounts of biotite, hornblende, magnetite, pyroxene, muscovite, sodalite, garnet, zircon, apatite, ilmenite, calcite, pyrite and zeolites or some of them as impurities or iron-bearing minerals (Guillet, 1994). The main nepheline syenite reserves are located in the former USSR, Norway, Canada, and recently Turkey (Harben, 1995). In Norway the proven nepheline syenite reserves exceed 400 Tg (teragrams, million tons). In Canada, Idusmin Co. has published a reserve figure of 240 Tg of nepheline syenite found in Blue Mountain area. Reserves of the rock in Turkey, was recently estimated and was found over 1 Pg (pentagrams or billion tons) (Gulsoy, 1994). Reserves of other countries are typically much smaller; however, there is a little information about their possible economic significance. In Egypt for example, the main nepheline syenite deposits are located in the southern sector of the Eastern Desert, south Idfu-Mersa Alam road with estimated reserves of approximately 100 Tg (El Ramely et al., 1971; Dardir et al., 1994). In the Kingdom of Saudi Arabia nepheline syenite deposits exist mainly in SAWDA mountain which is located 7 km to the east of EL Aqbaa Gulf and 35 km south of ALhaql port. The proven reserves of the ore have not been evaluated but the report prepared by Collin (1994) for the Saudi Ministry of Petroleum and Mineral Resources showed that the ore deposits cover an area of 7 square kilometers. Considering this fact, one can expect an average ore reserve of not less than 90 Mg assuming an ore thickness of 3 m.

In many industrial applications, feldspar and nepheline syenite are largely interchangeable (Burat et al., 2006). Compared to feldspars, nepheline syenite has a higher alkali/alumina ratio and therefore is considered as a challengeable competitor for feldspars (Gulsoy et al., 1994). In this aspect Esposito et al. (2005) stated that *“Compared to pure feldspars, the advantages coming from the use of nepheline-syenite are: (i) the content of potassium and sodium is higher,  $K_2O + Na_2O$  is about 9–12% in feldspars, whereas it is larger than 14% in nepheline syenite, and (ii) the melting temperature is generally lower than that of potassium-feldspar, which always contains other phases, such as quartz, which shifts the melting point to higher temperatures”*. In ceramics, the low fusing temperature and high fluxing capacity of the nepheline syenite allow for a vitrifying agent by producing an early glassy phase that binds other constituents of the mix. Applications for nepheline syenite as extender, pigments and fillers, have been pioneered in Canada. Finely-ground nepheline syenite is especially used as inert filler in paints, both latex and alkalid systems, for use in high traffic areas, as metal primers, wood stains, sealers and undercoats (Guillet, 1994). In plastics, nepheline syenite is used as inert, low cost

mineral filler in polyvinyl chloride (PVC), epoxy, and polyester resin systems. Because it exhibits a low resin demand, high filler loadings are possible, permitting reduced requirements for more expensive components (Guillet, 1994).

Regarding the required specifications for each application one can say nepheline syenite used for glassmaking should be a sandy sized product falling within the range of 40 to 200 mesh (Harben, 1995). Its iron content should not exceed 0.1% Fe<sub>2</sub>O<sub>3</sub> while alumina and alkali should be as high as possible, typically at least 23 and 14%, respectively (Harben, 1995).

On the other hand, nepheline syenite for the ceramics industry should be finely-ground, typically into products of 200, 270, and 400 mesh (Harben, 1995). Summary of the above background reflects the wide range of industrial applications of nepheline syenite deposits after achieving the required specifications.

Unfortunately, the Saudi nepheline syenite at Sawda Mountain contains high iron content and low alumina assay which makes it not suitable for industrial applications. As a result, this investigation is devoted to study the amenability of the ore to upgrading to meet specifications needed for different industrial applications.

## 2. EXPERIMENTAL

### 2.1. FEED PREPARATION

Nepheline syenite feeds were prepared to suit the applied upgrading technique. The sample was firstly subjected to primary and secondary crushing leading to a product of 100% -3.36 mm. In the subsequent size reduction stages a “Wedag” rod mill was used to produce -0.25 or -0.125 mm as separate feeds for magnetic separation, where the mill was fed with the -3.36 mm secondary crushed ore. It was operated in a batch closed-circuit with a screen (0.25 mm or 0.125 mm) according to intended produced feed. The operating conditions of the mill were as follows: dry bases, 9 grinding rods and 15 min batch grinding time. On the other hand, preparation of the finer feeds (-0.075 mm) for flotation purposes was conducted by regrinding the rod mill fine product (-0.125 mm) in a ball mill working in wet bases at 50% solid by weight. To achieve the targeted size, the mill was operated in a closed circuit with a 0.075 mm screen. The produced flotation feed was deslimed using a rig hydrocyclone giving a cut size of 25 µm. Finally, grinding of the cleanest magnetic concentrate for further cleaning by flotation was achieved by using a porcelain planetary mill.

### 2.2. CHARACTERIZATION OF ORE SAMPLES

The ore was characterized physically and chemically. The first was accomplished by size analyses of the crushed and ground products while the second was achieved by running complete chemical analyses. Complete chemical analysis of the original and

final produced samples for determining  $\text{Fe}_2\text{O}_3$ ,  $\text{SiO}_2$ ,  $\text{CaO}$ ,  $\text{MgO}$ ,  $\text{Al}_2\text{O}_3$ ,  $\text{Na}_2\text{O}$  and  $\text{K}_2\text{O}$  was conducted by X-ray fluorescence. For routine chemical analysis in the optimization tests Fe in the form of  $\text{Fe}_2\text{O}_3$  was determined applying a standard method of dissolution of the samples using HCl or  $\text{HNO}_3$ . Iron contents in the dissolved samples were determined using Perkin Elmer Atomic Adsorption (Suzan et al., 2002).

### 2.3. MAGNETIC SEPARATION TESTS

These tests were designed to check the possibility of dry upgrading of the ore, where water was used neither in the previous feed preparation steps nor in the separation stage. Two series of magnetic separation tests were carried out. The first series was performed on samples ground to 100% -0.250 mm while the second series were carried out using feed samples 100% less than 0.125 mm. The “Dings” cross-belt magnetic separator was used in both cases. The separator used in this investigation is a “pick-up” separator with an auxiliary permanent magnet for the separation of ferromagnetic material. The head of the electromagnet reaches a maximum magnetic field of 1.3 T (13 kGauss) at a minimum air gap of 3 mm. Optimization of the main parameters affecting the separation process included verification of magnetic field strength, feed rate and feed size. In studying the effect of feed rate mono or, sometimes multiple particle layer were applied. The feed rate was calculated from equation adopted by Negm et al. (2000). Moreover, cleaning of the concentrate was repeated sometimes.

### 2.4. FLOTATION TESTS

The -0.075 + 0.025 mm prepared flotation feed was cleaned in a “Denver D-12” flotation machine at a pulp density of 67-70% solid and motor speed of 2500 rpm for 10 min. Reverse flotation of iron-bearing contaminants from the nepheline syenite samples were then carried out in the laboratory using a “Denver D-12” subaeration flotation cell. The used collector was a mixture of the “Cyanamid” aeropromoters 801 and 825 (1:1 by weight mixture) of commercial grade from local market. For each test, 250 g batches of the -0.075+0.025 mm feed were used and conditioned with  $\text{H}_2\text{SO}_4$  or NaOH for 5 min for pH control. Other operating conditions were adjusted at their optimum values determined by Abouzied et al. (2000), where the optimum conditions were as follows: 25% solid pulp density, pH~4, frother Aerofrother 65 at a dosage of 0.1 kg/Mg. After adjusting all the parameters, the aeration was started, followed by manual skimming of the froth for about 10 min, which usually denotes demineralized froth. Both floated and sink products were collected, dried and analyzed for their iron contents.

2.5. COMBINED MAGNETIC SEPARATION-FLOTATION OF SAMPLES

Cleaning of the non-magnetic nepheline syenite concentrate was carried out by flotation, under the predetermined optimum dosage of the studied collector mixture. Cleaner concentrate were collected, dried, weighed and analyzed. The final product from this series was subjected to complete chemical analyses.

3. RESULTS

3.1. CHARACTERIZATION OF NEPHELINE SYENITE SAMPLE

Table 1 shows results of the complete chemical analysis of the original nepheline syenite sample. It indicates that the ore is of low grade and out of market specifications for glass and ceramics production. This is because of its low alumina content (17.38% compared with at least 23%), its high iron content (7.68%  $Fe_2O_3$ ) compared to minor iron contents for glass and ceramics manufacture. Similarly, its alkali content is 14.59% on the border line to market specifications, which is 14%. As a result its upgrading becomes a must.

Table 1. Complete chemical analysis of the considered nepheline syenite sample

Constituent	SiO <sub>2</sub>	Al <sub>2</sub> O <sub>3</sub>	Fe <sub>2</sub> O <sub>3</sub>	CaO	MgO	Na <sub>2</sub> O
%	56.82	17.38	7.68	0.97	0.20	9.23
Constituent	K <sub>2</sub> O	TiO <sub>2</sub>	P <sub>2</sub> O <sub>5</sub>	S	Cl	L.O.I
%	5.36	0.09	0.01	0.02	0.05	1.55

Figure 1 shows some of the physical and chemical characteristics of the primary crushed nepheline syenite sample. From this Figure it is clear that a general unimodal representation is exhibited with  $d_{50}$  of 2 mm. Meanwhile, chemical analysis of the different size fractions shows, more or less, an even distribution of Al<sub>2</sub>O<sub>3</sub> and Fe<sub>2</sub>O<sub>3</sub> indicating no separation of individual mineral components due to preferential hardness.

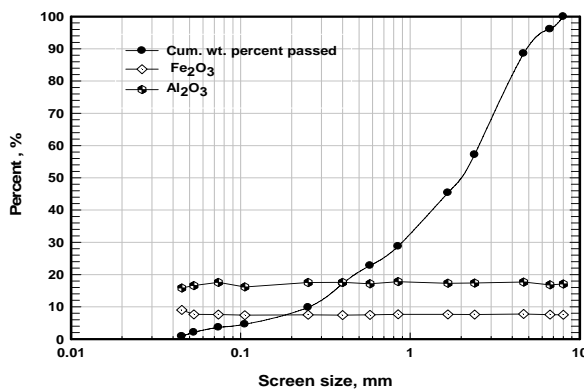


Fig. 1. Size distribution and chemical analyses of primary crushed nepheline syenite sample

Results of further size reduction of the sample are shown in Table 2. It shows that near 50 % of the sample is in the size cut of  $-0.211 + 0.125$  mm. Chemical analyses of the different size fractions indicated that the finest fraction ( $-0.045$  mm) has the highest iron content (10%).

Table 2. Size distribution and chemical analyses of the ground nepheline syenite considered sample

Screen size, mm	Wt. percent retained	Cum. Wt. percent passed	Assay in a given fraction, %		Recovery in a given fraction, %	
			Fe <sub>2</sub> O <sub>3</sub>	Al <sub>2</sub> O <sub>3</sub>	Fe <sub>2</sub> O <sub>3</sub>	Al <sub>2</sub> O <sub>3</sub>
-0.25+0.211	12.84	100	6.99	17.59	11.81	13.10
-0.211+0.125	44.7	87.16	7.27	17.67	42.74	45.82
-0.125+0.106	12.44	42.46	7.29	16.93	11.94	12.22
-0.106+0.075	12.51	30.02	8.05	16.84	13.24	12.22
-0.075+0.053	7.03	17.51	8.24	16.74	7.63	6.83
-0.053+0.045	5.56	10.48	8.42	16.55	6.16	5.34
-0.045	4.92	4.92	10.00	15.61	6.47	4.45
Head	100		7.60	17.24	99.99	99.98

### 3.2. MAGNETIC SEPARATION RESULTS

The magnetic separator belt speed is an important parameter because it determines the residence time of the feed particles in the magnetic field. Figure 2 shows the effect of changing belt speed of the "Dings" magnetic separator on the separation process, considering a feed rate as single particle layer of the first feed (100%  $-0.25$  mm) at applied magnetic field of 1 T. It illustrates that increasing the belt speed leads to improvement of the nonmagnetic fraction yield but this is in expense of its quality as its iron content increases. However, at a belt speed of 2 m/min, which is the optimum, only 42.6% of the iron is recovered in the non magnetic product (concentrate). This means that about 47.4% of the iron content was rejected in the tail product (magnetic fraction). The overall poor results obtained in this series maybe attributed to the wide size range of the feed, and thus, the calculated monolayer particle is not accurate.

Changing the feed rate (number of feed layers) on the belt at its optimum speed and under the same operating conditions applied in the previous series resulted in deterioration of the separation process due to the shielding effect (Fig. 3). This has, in fact, a major effect on the quality of the concentrate and the capacity of separator as well. Results indicate that at a four-particle layer feed (48 kg/hr), a concentrate having 6.73% Fe<sub>2</sub>O<sub>3</sub> was obtained, i.e. only 15.34% of iron-bearing impurities were rejected. This indicates that the optimum feed rate for this size is 12 kg/hr, which implies a monolayer feed. However, the hitherto unsatisfactory obtained results lead to investigating the effect of increasing the magnetic field strength to its maximum of

1.3 T by increasing the applied current to 3 A, under the predetermined optimum conditions and entering the previous feed in two modes. The first is as it is (100% - 0.25 mm) and the second is after its desliming using a 0.045 mm screen followed by repetitive cleaning until no change in the concentrate weight. The obtained results are shown in Table 3. It can be noticed that a relative improvement in the quality of the concentrate is achieved. This is because the iron content the first feed (100% -0.25) was decreased to 2.63% Fe<sub>2</sub>O<sub>3</sub>, i.e about 70.8% removal of magnetic impurities and the iron content of the second feed (-0.25+0.045 mm) was 1.96 % without cleaning achieving ~ 73% removal of the original feed iron. It is also clear that the fifth cleaning cycle of the second product lead to a remarkable improvement in its quality where the iron content of this product is 1.33% which means iron removal of approximately 81%. The improved obtained results confirm the shielding effect of coarse particles and necessity using much narrower size feeds with this kind of separators.

However, this was taken into consideration when studying the finer feed (-0.125). Figure 4 shows that using the deslimed fine feed (-0.125 + 0.045 mm) at monolayer feed rate and a magnetic field intensity of 1 T an optimum belt speed of 4 m/min is noticed. At this speed, a nonmagnetic fraction of ~1% Fe<sub>2</sub>O<sub>3</sub> can be obtained achieving an overall iron removal of 73%, with an iron recovery in the non-magnetic fraction of 11% and the rest of the iron was previously rejected with the slimes (-0.045 fraction).

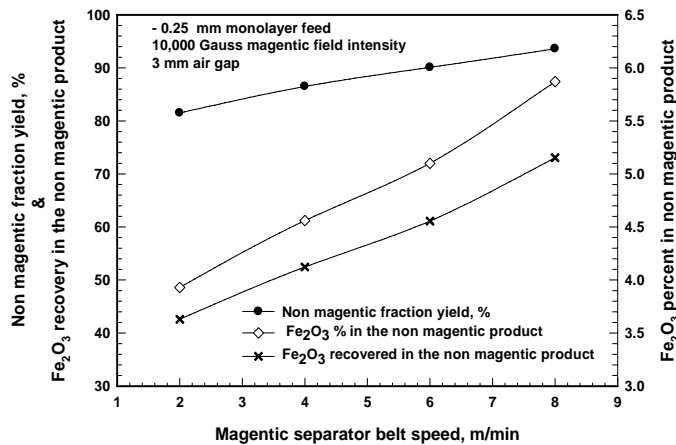


Fig. 2. Effect of the main belt speed of the "Dings" cross belt magnetic separator on the quantity and quality of nepheline syenite concentrate

Using this deslimed fine feed i.e. -0.125 +0.045 mm, under a monolayer feed rate, belt speed of 4 m/min, and maximum field strength of 1.3 T with three repetitive

cleaning cycles resulted in an appreciable decrease in the iron content of the concentrate to 0.85%  $\text{Fe}_2\text{O}_3$ , corresponding to air removal of 77% (Table 4). The obtained results are in agreement with some published results regarding upgrading of a similar Egyptian nepheline syenite ore (Abouzeid et. al., 2000; Suzan et al., 2002)

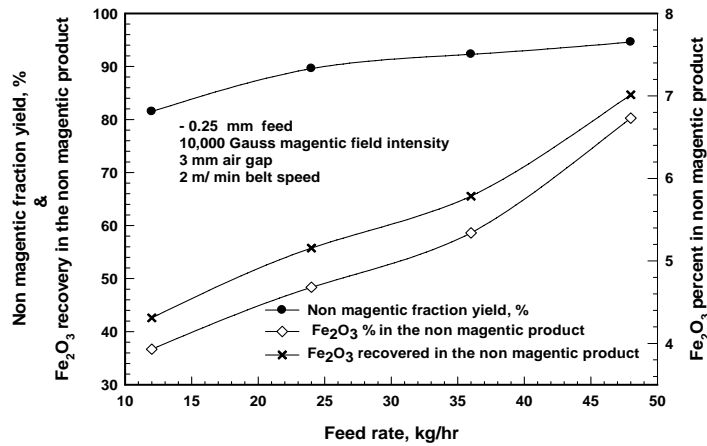


Fig. 3. Effect of the feed rate of "Dings" cross belt magnetic separator on the quantity and quality of nepheline syenite concentrate

However, one can conclude that, within the aforementioned limits of experimentation, it was not possible to produce high quality nepheline syenite concentrates by dry upgrading using magnetic separators only.

Table 3. Separation of the considered nepheline syenite sample (-0.25+0.045mm) at maximum field strength (1.3 T) using the "Dings" cross belt magnetic separator

Feed size, mm	Product	Wt., %	$\text{Fe}_2\text{O}_3$	
			Ass., %	Rec., %
-0.25	Conc.	83.67	2.63	29.22
	Tail	16.33	32.64	70.78
	Total	100	7.53	100
-0.25+0.045	Conc.	79.83	1.96	20.78
	Tail	15.25	36.06	73.03
	Total	95.1	7.43	93.81
-0.25+0.045 With 5 cleaning cycles	Conc.	74.76	1.33	13.2
	Tail	20.34	29.85	80.63
	Total	95.1	7.43	93.83

Table 4. Separation and cleaning of fine deslimed nepheline syenit feed at maximum magnetic field strength of "Dings" cross belt separator

Feed size, mm	product	Wt. %	Fe <sub>2</sub> O <sub>3</sub>	
			Ass. %	Rec. .%
-0.125+0.045 with 3 cleaning cycles	Conc.	70.63	0.85	7.97
	Tail	18.9	30.6	76.8
	Total	89.53	7.13	84.77

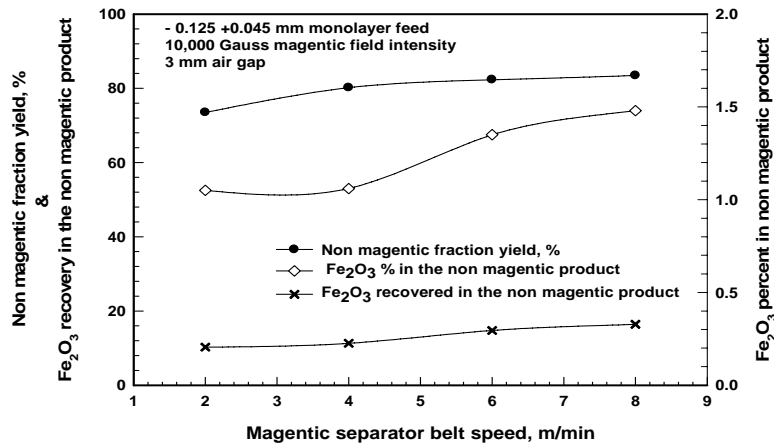


Fig. 4. Effect of main belt speed of "Dings" cross belt magnetic separator on the quantity and quality of nepheline syenite concentrate considering deslimed finer feed (-0.125+0.045 mm)

### 3.3. FLOTATION RESULTS

Figure 5 illustrates the effect of dosage of Cynamid 801 and 825 as a collector on the quantity and quality of the nepheline syenite concentrate obtained by flotation under the operating parameters listed in the bottom left corner of the graph. It can be easily noticed that the greater the collector dosage the better is the produced concentrate regarding its quality and quantity. However, collector dosages higher than 2.5 kg/Mg have no credible effect either on the quality or quantity of the obtained concentrate. At this dosage, approximately 61% by weight of the original sample is yielded as concentrate having 0.4% Fe<sub>2</sub>O<sub>3</sub>. In this way, the iron recovered in the concentrate is only 4% of the iron contained in the original sample. The amount of iron rejected in the flotation tailings and slimes represents a good success regarding the separation process. But still the targeted specifications for marketable nepheline concentrates are not met yet. As a result further upgrading will be introduced in the next section.

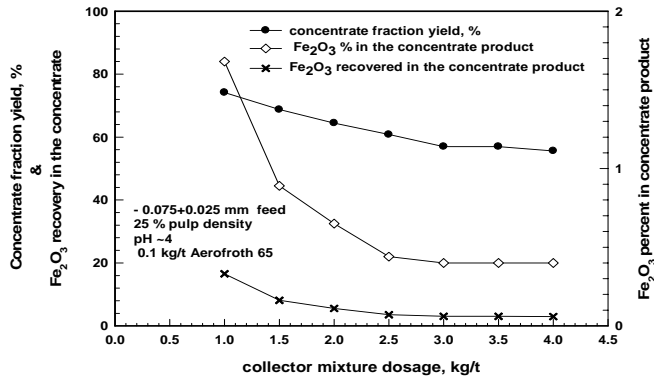


Fig. 5. Effect of dosage of Cynamid 801 and 825 as a collector on the quantity and quality of nepheline syenite concentrate

### 3.4. COMBINED MAGNETIC SEPARATION-FLOTATION OF SAMPLES

The cleanest nepheline syenite concentrate obtained from the finer feed (-0.125+0.045 mm), shown in Table 4, was ground in a planetary mill and was considered as a new flotation feed. It was tested under the same optimum conditions mentioned in the flotation section. The Cynamid mixture was added stepwise. The final obtained concentrate results obtained at collector dosage of 2 kg/Mg is shown in Table 5. It reflects a concentrate of high quality regarding its iron content (0.09% Fe<sub>2</sub>O<sub>3</sub>).

To ensure the quality of the produced concentrate regarding its content from other constituents, it was subjected to complete chemical analyses. Results are shown in Table 6. The results confirm the high quality of the produced concentrate and its amenability to be applied in different industries.

Table 5. Combined magnetic separation-flotation results of nepheline syenite

Feed size, mm	product	Wt. %	Fe <sub>2</sub> O <sub>3</sub>	
			Ass. %	Rec. %
-0.075 at 2 kg/Mg Cyanamid mixture (step wisely added)	Conc.	55.43	0.09	0.66
	Tail	15.1	3.62	7.31
	Total	70.53	0.85	7.97

Table 6. Complete chemical analysis of the cleanest nepheline syenite concentrate obtained by combined magnetic separation - flotation

Constituent	SiO <sub>2</sub>	Al <sub>2</sub> O <sub>3</sub>	Fe <sub>2</sub> O <sub>3</sub>	Na <sub>2</sub> O	K <sub>2</sub> O
%	59.43	23.58	0.09	10.16	6.31

## 4. CONCLUSIONS

From the presented results the following conclusions can be drawn:

- the Saudi nepheline syenite from the Sawda Mountains, is a low grade ore and as mined beyond market specifications due to its high iron and low alumina contents,
- upgrading the ore applying a single technique either on dry basis (magnetic separation) or wet basis (flotation) can never lead to a marketable concentrate product,
- the cleanest concentrate that can be obtained in case of dry upgrading of the ore, by magnetic separation only, contains not less than 0.85% iron in the form of  $\text{Fe}_2\text{O}_3$ ,
- wet upgrading of the ore applying flotation technology and using 2.5 kg/Mg of Cyanamid 801 and 825 mixtures as a collector can lead to a concentrate having 0.4%  $\text{Fe}_2\text{O}_3$  or more,
- cleaning of the concentrate obtained at the optimum conditions of magnetic separation, by flotation results in a final concentrate of high quality regarding its iron, alumina and alkali contents (0.09%, 23.58%, 16.47% for  $\text{Fe}_2\text{O}_3$ ,  $\text{Al}_2\text{O}_3$  and  $\text{Na}_2\text{O} + \text{K}_2\text{O}$ , respectively).

## REFERENCES

- NEGM, A.A., BOULOS, T., AHMED, H.A.M., 2000, *Beneficiation of nepheline syenite ore for glass and ceramics industries* 8<sup>th</sup> Int. Min. Proc. Symposium, Antalya, Turkey, 16-18 Oct. 2000.
- RAMSAY C.R., DRYSDALL, A.R., Clark, M.D., 1986, *Felsic plutonic rocks of the Midyan region, Kingdom of Saudi Arabia—I. Distribution, classification and resource potential*, J. Afr. Earth. Sci. 4, pp. 63-77.
- COLLIN, R.R., 1994, *Mineral Resources of Saudi Arabia* unpublished report, prepared for the Ministry of Petroleum and Mineral Resources.
- DARDIR, A.A., ABU-ZEID, K.M. Amin, H.M., 1994, *Ceramics, Glass and Refractories Ores in Egypt from the Economic Conception*, Proceedings of the 4th Mining, Petroleum and Metallurgy Conference, Assiut, Egypt.
- EL-RAMLY, M.F., BUDAROUV, I., HUSSIEN, A.A., 1971, *Alkalino Rocks of South Eastern Desert of Egypt*, Geological Survey of Egypt, Cairo, Egypt.
- BURAT, F., KANGAL, O., ONAL, G., 2006, *An alternative mineral in the glass and ceramic industry: nepheline syenite*, Miner. Eng. 19, pp. 370–371.
- GUILLET, R.G., 1994, *Nepheline Syenite Beneficiation for Different Application*, Industrial Minerals and Rocks, 6th edition, Senior editor: Carr, D.D, SME of AIME, Colorado, 1994.
- GULSOY, O.Y., ERGUN, S.L., KULAKSIZ, S., 1994, *Beneficiation of Nepheline Syenite in Turkey*, Proceedings of the 4<sup>th</sup> Mining, Petroleum and Metallurgy Conference, Assiut, Egypt.
- HARBEN, P.W., 1995, *The Industrial Minerals Handbook*, Second Edition, Metal Bulletin, London.
- ESPOSITO, L., SALEM, A., TUCCI, A., GUALTIERIC, A., JAZAYERI, S.H., 2005, *The use of nepheline-syenite in a body mix for porcelain stoneware tiles*” Ceramics International 31, 233–240.

- NEGM, T., ABOUZIED, A.Z., BOULOS, T.R., AHMED, H.A.M., 2000, *Nepheline syenite processing for glass and ceramic industries*, Physicochem. Probl. Miner. Process. 34, pp. 5-16.
- IBRAHIM, S.S., AHMED, H.A.M., BOULOS, T.R., 2002, *Dry magnetic separation of nepheline syenite ores*, Physicochem. Probl. Miner. Process. 36, pp. 173-183.

**Ahmed, H.A.M.**, *Wzbogacanie na sucho i na mokro sjenitów nefelinowych.*, Physicochem. Probl. Miner. Process., 46 (2011) 107-118, (w jęz. ang), <http://www.minproc.pwr.wroc.pl/journal>

Nefelin sjenitowy ma zastosowanie jako wypełniacz, pigment oraz jako składnik szkła i ceramiki. Królestwo Arabii Saudyjskiej ma duże złoża nefelinu sjenitowego, które występują w Górach Sawda. Są one jednak niskiej jakości, ze względu na wysoką zawartość żelaza (7.68% Fe<sub>2</sub>O<sub>3</sub>) oraz niską zawartość Al<sub>2</sub>O<sub>3</sub> (17.38%). W pracy badano ich wzbogacanie metodą magnetyczną na sucho i flotacyjną na mokro. Badano wpływ natężenia pola magnetycznego, prędkość taśmy, prędkości podawania nadawy oraz uziarnienia, a flotację prowadzono w maszynie Denver D-12 badając zużycie kolektora. Separacja magnetyczna pozwala na otrzymywanie koncentratów nefelinowych posiadających jednak więcej niż 0.85% Fe<sub>2</sub>O<sub>3</sub>, podczas gdy flotacja mogła dostarczać koncentratów zawierających nie więcej niż 0.40% Fe<sub>2</sub>O<sub>3</sub>. Łącząc obie techniki tj. dokonując flotacji w optymalnych warunkach uprzednio wzbogacanego na sucho materiału, otrzymano końcowy koncentrat zawierający 0.09% Fe<sub>2</sub>O<sub>3</sub>, przy zawartości Al<sub>2</sub>O<sub>3</sub> wynoszącej 23.58%. Otrzymane koncentraty mogą być użyte w wielu przemysłach, zwłaszcza do produkcji szkła i ceramiki.

*słowa kluczowe: nefelin sjenitowy, separacja magnetyczna, flotacja, szkło, ceramika*

Małgorzata ULEWICZ\*, Elżbieta RADZYMIŃSKA-LENARCIK \*\*

## TRANSPORT OF METAL IONS ACROSS POLYMER INCLUSION MEMBRANE WITH 1-ALKYLIMIDAZOLE

*Received May 14, 2010; reviewed; accepted July 10, 2010*

The facilitated transport of copper(II), zinc(II), cobalt(II), and nickel(II) ions across polymer inclusion membranes (PIMs), which consist of cellulose triacetate as polymeric support, *o*-nitrophenyl pentyl ether as plasticizer and 1-alkylimidazole as ion carrier was reported. PIM was characterized by using atomic force microscopy (AFM) technique. The results show that Cu<sup>2+</sup> can be separated very effectively from others heavy and transition metal cations as Zn<sup>2+</sup>, Co<sup>2+</sup>, and Ni<sup>2+</sup> (at concentration of 10<sup>-3</sup> M each). Alkyl substituents in position 1 of imidazole ring have an effect on hydrophobic properties and the initial flux of the transported metal ions. Also, the influence of the chloride ions concentration on the separation process was investigated. To explain the mechanism of membrane transport the diffusion of metal ions complexes with 1-alkylimidazole was also measured.

*key words: polymer inclusion membrane (PIM), ions separation, copper(II), zinc(II), nickel(II), cobalt(II), 1-alkylimidazole*

### 1. INTRODUCTION

Presently, for separation of nonferrous metals from water solutions and industrial waste water on laboratory scale, membrane techniques are more and more often used. A liquid membrane constitutes a distinct organic phase that separates two other water phases. In terms of their construction, membranes are divided into: bulk liquid

---

\* Department of Metal Extraction and Recirculation, Czestochowa University of Technology, 42-200 Czestochowa, Armii Krajowej 19, ulewicz@mim.pcz.czyst.pl

\*\* Department of Inorganic Chemistry, University of Technology and Life Sciences, Seminaryjna 3, 85-326 Bydgoszcz, elaradz@utp.edu.pl

membranes (BLM), supported liquid membranes (SLM), emulsion liquid membranes (ELM), and polymer inclusion membranes (PIM).

Membrane processes are distinguished by a better use of the ion carrier (extractant) existing in the organic phase (membrane), compared to the traditional extraction system. The proper selection of the carrier is decisive for the effectiveness of the liquid membrane. High separation selectivity factors are achieved, when a chosen carrier shows high affinity with respect to one of the components of the feeding solution. As metal ion carriers in the membrane processes, the same organic substances as those used in extraction processes are employed in the membrane processes (Walkowiak et al., 2002). For the separation of nonferrous ions in the liquid membrane transport process both classical and new types of carriers are used (Nghiem et al., 2006). The review on application of macrocyclic compound as ion carriers in a liquid membranes were presented by Ulewicz (2008) as well as Walkowiak and Kozłowski (2009).

Hayashi et al. (2003) reported on the selective proton-driven transport of lead(II) ions in presence of nonferrous cations ( $\text{Cu}^{2+}$ ,  $\text{Cd}^{2+}$ ,  $\text{Zn}^{2+}$ ,  $\text{Ni}^{2+}$ ) across polymer inclusion membranes with proton diionizable polyethers bearing different alkyl chain lengths (from  $-\text{C}_7\text{H}_{15}$  to  $-\text{C}_{16}\text{H}_{33}$ ). The transport selectivity of PIM with polyether bearing  $-\text{C}_8\text{H}_{17}$  alkyl chain was as follows:  $\text{Pb}^{2+} > \text{Cu}^{2+} > \text{Cd}^{2+} > \text{Zn}^{2+} > \text{Ni}^{2+}$ . Ulewicz et al. (2004) investigated competitive transport of Zn(II), Cu(II), and Cd(II) ions from aqueous chloride source phase through polymer inclusion membranes containing side-armed lariat ether-type derivatives of diphosphaza-16-crown-6 as ion carrier. It was found that the initial fluxes of all investigated cations increase with acidity of the feed phase and the selectivity order was as follows:  $\text{Cd(II)} > \text{Zn(II)} > \text{Cu(II)}$ .

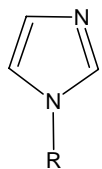
The cations:  $\text{Zn}^{2+}$ ,  $\text{Pb}^{2+}$ ,  $\text{Cu}^{2+}$ ,  $\text{Ni}^{2+}$ ,  $\text{Co}^{2+}$  and  $\text{Cd}^{2+}$  are transported across PIMs containing azocrown and thioazocrown imidazole derivatives were investigated by Ulewicz et al. (2007, 2009). A linear decrease in the values of the initial metal ions transport fluxes was observed with the increase in the hydrophilic-hydrophobic balance (HLB) index of the imidazole crown ether derivatives. The transport selectivity of PIM with azocrown imidazole was as follows:  $\text{Pb(II)} > \text{Zn(II)} > \text{Cu(II)} > \text{Co(II)} > \text{Ni(II)} > \text{Cd(II)}$ . Recently, pyrrole azocrown ethers in ordinary bulk membrane system were also found to preferentially transport lead(II) from equimolar mixture of  $\text{Co}^{2+}$ ,  $\text{Ni}^{2+}$ ,  $\text{Cu}^{2+}$ ,  $\text{Zn}^{2+}$ ,  $\text{Cd}^{2+}$ ,  $\text{Ag}^+$  and  $\text{Pb}^{2+}$  ions (Luboch et al., 2006).

The present article deals with a competitive transport of copper(II), zinc(II), cobalt(II), and nickel(II) ions from a dilute aqueous solutions using PIM doped with 1-alkylimidazoles. The initial fluxes and selectivity coefficients of copper(II), zinc(II), cobalt(II) and nickel(II) ions transport across PIM doped with 1-alkylimidazole from aqueous source phase containing equimolar mixture of all metals are investigated too. The effects of chloride ions concentration in source phase upon the efficiency and selectivity Cu(II) ions transport is reported.

## 2. EXPERIMENTAL

### 2.1. REAGENTS

The inorganic chemicals, i.e. copper(II), zinc(II), nickel(II), and cobalt(II) chlorides were of analytical grade and were purchased from POCh (Gliwice, Poland). The organic reagents, i.e. cellulose triacetate (CTA), *o*-nitrophenyl phenyl ether (*o*-NPPE) and dichloromethane were also of analytical grade and were purchased from Fluka and used without further purification. The 1-alkylimidazole were synthesized by Skrzypczak according to the procedure described in (Pernak et al. 1987).

	No	R-	pKa
	<u>1</u>	-C <sub>6</sub> H <sub>13</sub>	7.30
	<u>2</u>	-C <sub>7</sub> H <sub>15</sub>	7.32
	<u>3</u>	-C <sub>8</sub> H <sub>17</sub>	7.34
	<u>4</u>	-C <sub>9</sub> H <sub>19</sub>	7.39
	<u>5</u>	-C <sub>10</sub> H <sub>21</sub>	7.43

### 2.2. POLYMER INCLUSION MEMBRANE PREPARATION

The membranes were prepared according to the procedure reported in the previous paper (Ulewicz et al., 2007). A solution of cellulose triacetate as the support, plasticizer and 1-alkylimidazole as ion carrier in dichloromethane was prepared. A specified portion of this solution was poured into a membrane mould comprised of a 9.0 cm diameter glass ring placed on a glass plate with cellulose triacetate - dichloromethane glue. After slow solvent evaporation overnight the resulting membrane was peeled off from the glass plate by immersion in cold water. Then, the membrane was soaked for 12 hours in distilled water to achieve their homogeneity. Two samples of membrane were cut from the same membrane film for duplicate transport experiments.

### 2.3. TRANSPORT STUDIES

Transport experiments were carried out in a permeation module cell described in our earlier paper (Ulewicz et al., 2007). The membrane film (surface area of 4.9 cm<sup>3</sup>) was tightly clamped between two cell compartments. Both, i.e. the source and receiving aqueous phases (45 cm<sup>3</sup> each) were mechanically stirred at 600 rpm. The receiving phase was deionized water. The PIM transport experiments were carried out

at the temperature of  $20 \pm 0.2^\circ \text{C}$ . Small samples ( $0.1 \text{ cm}^3$  each) of the aqueous receiving phase were removed periodically via a sampling port with a syringe and analyzed to determine cation concentrations by atomic absorption spectroscopy method (AAS Spectrometer, Solaar 939, Unicam). The source phase pH was kept constant ( $\text{pH} = 6.0$ ) and controlled by pH meter (pH meter, CX-731 Elmetron, with combine pH electrode, ERH-126, Hydromet, Poland). The permeability coefficient ( $P$ , m/s) of metal ions across polymer membranes was described by the following equation (Danesi, 1984-85):

$$\ln\left(\frac{c}{c_i}\right) = -\frac{A}{V} \cdot P \cdot t, \quad (1)$$

where  $c$  is the metal ions concentration (M) in the source aqueous phase at some given time,  $c_i$  is the initial metal ions concentration in the source phase,  $t$  is the time of transport (s),  $V$  is volume of the aqueous source phase ( $\text{m}^3$ ), and  $A$  is an effective area of membrane ( $\text{m}^2$ ).

A linear dependence of  $\ln(c/c_i)$  in the source phase versus time was obtained and the permeability coefficient was calculated from the slope of the straight line that fits the experimental data. The initial flux ( $J_i$ ) was determined as equal to:

$$J_i = P \cdot c_i. \quad (2)$$

The selectivity coefficient ( $S$ ) was defined as the ratio of initial fluxes for  $M1$  and  $M2$  metal ions, respectively:

$$S = J_{i,M1} / J_{i,M2}. \quad (3)$$

The reported values correspond to the average values of three replicates, with the standard deviation within 5%.

### 3. RESULT AND DISCUSSION

The most significant factor determining metal ions transport across a liquid membrane are the properties of an ion carrier and its acidity or basicity strength. The imidazole ring is a stable molecule that according to Pearson's HSAB principle is ranged among intermediate class of bases. Although its basicity is by an order of magnitude lower than that of ammonia, imidazole forms more stable complexes with metal ions belonging to the intermediate class of Pearson's acids (Schaeckers et al., 2004). Alkyl substituents at position 1 of the imidazole ring distinctly affect hydrophobic properties of the molecule and weakly strengthen its basicity (Lenarcik and Ojczenasz, 2002) ( $\text{pK}_a = 7,165 + n \cdot 0.0222$ ). Hence, 1-alkylimidazoles have been used as extractants of a number of metal ions, in particular those classified as intermediate HSAB acids (Cuprey, 1974).

Table 1. Initial fluxes, selectivity order and selectivity coefficients for competitive transport of Cu(II), Zn(II), Co(II), and Ni(II) ions across PIM doped with 1-alkylimidazole; membrane: 2.6 cm<sup>3</sup> *o*-NPPE /1g CTA and 1.0 M carriers calculated on plasticizer

Carrier	Metal ions	J, $\mu\text{mol}/\text{m}^2\cdot\text{s}$	$S_{\text{Cu(II)/Me(II)}}$
<b>1</b>	Cu(II)	4.28	Cu(II) > Zn(II) > Co(II) > Ni(II) 3.7    17.8    35.7
	Zn(II)	1.17	
	Co(II)	0.24	
	Ni(II)	0.12	
<b>2</b>	Cu(II)	4.48	Cu(II) > Zn(II) > Co(II) > Ni(II) 3.6    9.0    26.4
	Zn(II)	1.26	
	Co(II)	0.25	
	Ni(II)	0.17	
<b>3</b>	Cu(II)	5.41	Cu(II) > Zn(II) > Co(II), Ni(II) 3.2    21.6
	Zn(II)	1.70	
	Co(II)	0.25	
	Ni(II)	0.25	
<b>4</b>	Cu(II)	5.74	Cu(II) > Zn(II) > Ni(II), Co(II) 3.1    19.8
	Zn(II)	1.88	
	Co(II)	0.29	
	Ni(II)	0.29	
<b>5</b>	Cu(II)	6.36	Cu(II) > Zn(II) > Ni(II) $\geq$ Co(II) 3.0    14.8    15.5
	Zn(II)	2.15	
	Co(II)	0.36	
	Ni(II)	0.41	

The initial fluxes and selectivity coefficients of copper(II), zinc(II), cobalt(II) and nickel(II) ions transport across PIM doped with 1-alkylimidazole from aqueous source phase containing equimolar mixture of all metals is shown in Table 1. The copper(II) ions were transported with a highest rate, and the selectivity order for carrier **1** and **2** was as follows: Cu(II) > Zn(II) > Co(II) > Ni(II), whereas for **3** - **5** Cu(II) > Zn(II) > Ni(II), Co(II). The initial flux of copper(II) transport increases in the order **1** < **2** < **3** < **4** < **5**. The observed trend is in accordance with increasing size of the -R groups on ring imidazole structure. The maximum value of the initial flux for Cu(II) ions was equal to 6.36  $\mu\text{mol}/\text{m}^2\cdot\text{s}$  (for **5**).

The stability constants of all the 1-alkylimidazole complexes with Cu(II) are constant and independent of the alkyl chain length and  $\text{p}K_a$  of the 1-alkylimidazole base (Radzaminska-Lenarcik, 2007). Stabilities of the Co(II), Zn(II), and Ni(II) complexes have been found to increase with increasing alkyl chain length of 1-alkylimidazoles (Lenarcik and Ojczenasz, 2004; Lenarcik and Kierzkowska, 2004; Lenarcik and Rauckyte, 2004). These dependences are lineal. Straight line parameters illustrating the dependence of the  $\log \beta_n$  of Co(II), Ni(II), and the Zn(II) complexes

with 1-alkylimidazoles as a function of the carbon atoms ( $n$ ) in the group of alkyl chain in 1-alkylimidazole are presented in the Table 2.

Table 2. Comparison of the stability constants  $\beta_n$  of Co(II), Ni(II), Cu(II), and Zn(II) complexes with 1-alkylimidazoles

$\log \beta_n$	Co(II)	Ni(II)	Cu(II)	Zn(II)
$\log \beta_1$	$y = 0.302n + 1.653$	$y = 0.161n + 2.631$	4.15	$y = 0.229n + 1.986$
$\log \beta_2$	$y = 0.342n + 3.592$	$y = 0.164n + 5.290$	7.57	$y = 0.229n + 4.500$
$\log \beta_3$	$y = 0.377n + 4.881$	$y = 0.164n + 7.233$	-	$y = 0.229n + 6.700$
$\log \beta_4$	$y = 0.434n + 5.780$	$y = 0.166n + 8.653$	-	-

Stability constants of the Cu(II) complexes are considerably higher than those of Co(II), Ni(II), and Zn(II). This may be explained in terms of a larger contribution of the  $\pi_{M \rightarrow L}$  back donation to interaction of Cu(II) with the imidazole ring (Radzymińska-Lenarcik, 2008). The 1-alkyl substituent does not significantly affect either polarization of the imidazole ring or the energy of its antibonding  $\pi$  orbitals (Sundberg and Martin, 1974). It can thus be assumed that the contribution of the  $\pi_{M \rightarrow L}$  bonding is invariable in the Cu(II) complexes with all the 1-alkylimidazoles. The initial fluxes of Zn(II) ions increase more rapidly than Co(II) and Ni(II) ions with increase of  $pK_a$  carriers. The values of the diffusion coefficient of metal complex in the membrane as well as the constant rate of reaction are the factors showing whether the given process is controlled by diffusion in the membrane or by indirect (mixed) kinetics, i.e. the state, in which the rates of diffusion process and chemical reaction are comparable. In this way in the next step, the diffusion coefficient ( $D_o$ ) of the metal-complex across the membrane doped with 1-hexylimidazole was calculated according to the procedure reported in the previous paper (Ulewicz et al., 2010). In Fig. 1, the correlation graphs  $[Me^{2+}]_i - [Me^{2+}]_t$  versus time of metal ions transport from different mixture solutions across PIM doped with carrier **1** is presented. The diffusion coefficient of Me(II) was calculated, substituting  $D_o = d_o / \Delta_o$ , where  $d_o$  is the thickness of the membrane (0.0025 cm) and  $\Delta_o$  could be evaluated by plotting  $[Me^{2+}]_i - [Me^{2+}]_t$  vs. time. Obtained values of diffusion coefficients are presented in Table 3. Also, the corrected (normalized) membrane diffusion coefficient  $D_{o,n}$ , which considers the morphological features inside the membrane ( $\varepsilon$ - porosity and  $\tau$  - tortuosity), calculated from equation described by Salazar-Alvarez et al. (2005):  $D_{o,n} = D_o \cdot (\varepsilon / \tau)$ , are presented in this Table. The porosity ( $\varepsilon$ ) as well as roughness ( $R_q$ ) of the membrane were calculated using atomic force microscopy (AFM). Figure 2 shows an AFM image of PIM's with carrier **1** in three-dimensional form with format of 1.0 x 1.0  $\mu m$  and example histogram for measurement. The distribution of the carrier in the

investigated membrane after evaporation of the dichloromethane is homogeneous on the entire surface. The porosity and roughness for PIM doped with **1** is 24.2% and 3.9 nm, respectively. This value of roughness is comparable with that found for polymer membrane with thioazocrown derivative imidazole ( $R_q$  equal 3.3-5.3) reported by Ulewicz et al. (2009) and for membrane with D2EHPA prepared by Salazar-Alvarez et al. (2005), which is equal to 4.6 nm. The membrane tortuosity was determined from the relationship developed by Wolf and Strieder (1990):  $\tau = 1 - \ln \varepsilon$  and was equal to 2.42 (for  $\varepsilon = 0.242$ ). Values of diffusion coefficient determined in this study (Table 3) are comparable with presented in literature data for different membranes and are in the range  $10^{-6}$  to  $10^{-12}$   $\text{cm}^2/\text{s}$  showing that the limiting step of the process is transfer of metal complex across membrane barrier.

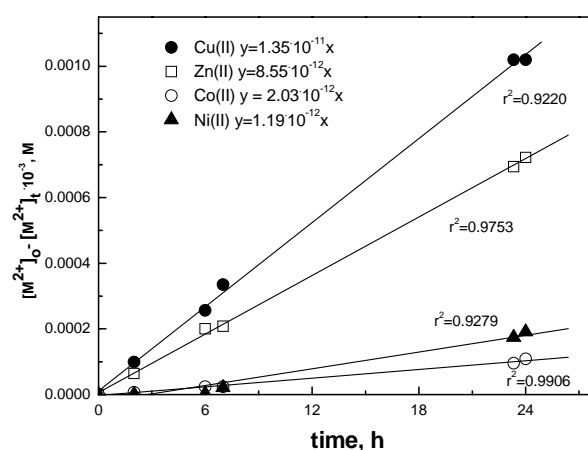


Fig. 1. Relation of  $[\text{Me}^{2+}]_i - [\text{Me}^{2+}]_t$  plotted vs. time for  $\text{Cu}^{2+}$ ,  $\text{Zn}^{2+}$ ,  $\text{Co}^{2+}$  and  $\text{Ni}^{2+}$  transport across PIM membrane doped with 1.0 M carrier **1**. Conditions of experiment as in Table 1

Table 3. Permeability and diffusion coefficients normalized for competitive transport of  $\text{Cu}(\text{II})$ ,  $\text{Zn}(\text{II})$ ,  $\text{Co}(\text{II})$ , and  $\text{Ni}(\text{II})$  ions through PIM with **1**

Cations	$P$ , m/s	$\Delta_o$ , s/m	$D_o$ , $\text{cm}^2/\text{s}$	$D_{o,n}$ , $\text{cm}^2/\text{s}$
$\text{Cu}^{2+}$	$4.28 \cdot 10^{-3}$	$10^{6.86}$	$3.44 \cdot 10^{-11}$	$4.17 \cdot 10^{-10}$
$\text{Zn}^{2+}$	$1.17 \cdot 10^{-3}$	$10^{7.06}$	$2.18 \cdot 10^{-11}$	$2.64 \cdot 10^{-10}$
$\text{Co}^{2+}$	$0.24 \cdot 10^{-3}$	$10^{7.69}$	$5.17 \cdot 10^{-12}$	$6.26 \cdot 10^{-11}$
$\text{Ni}^{2+}$	$0.12 \cdot 10^{-3}$	$10^{7.92}$	$3.03 \cdot 10^{-12}$	$3.67 \cdot 10^{-11}$

In the next step, the influence of chloride ions concentration in the source phase on the transport of metal ions was investigated. As seen from Table 4, the permeability coefficients of Cu(II) ions decrease only slightly upon increasing chloride-ion concentration in the source phase. Whereas the permeability coefficient of the Zn(II), Co(II), and Ni(II) ions increases with an increase of chloride ions concentration, in particular those of the Zn(II) ions. On the other hand, the selectivity coefficients of Cu(II)/Zn(II) decreases with  $\text{Cl}^-$  concentration increase in the source phase. The lowest value of the selectivity coefficient Cu(II)/Zn(II) was equal to 1.4 for 1.0 M of  $\text{Cl}^-$  in the source phase. For compound **1** the selectivity coefficients of Cu(II)/Co(II) and Cu(II)/Ni(II) were 11.4; 14.4; for 0.5 and 2.8 for 1.0 M  $\text{Cl}^-$ , respectively. Among all of the cations studied, only Cu(II) has the propensity for deformation of the coordination sphere owing to the Jahn-Teller effect (Bersuker, 1972; Gažo et al., 1976) (this being favourable for the process).

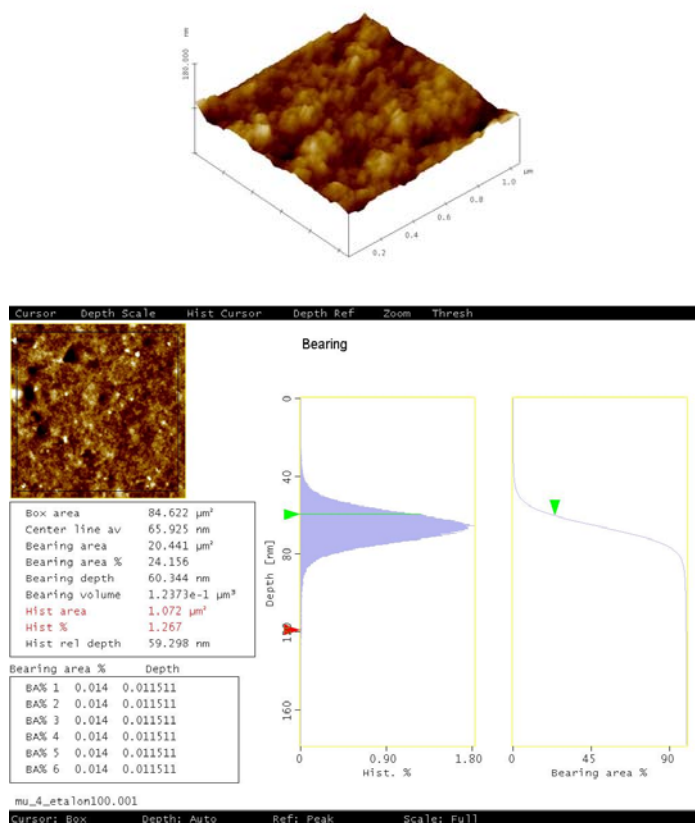


Fig. 2. 3D-view atomic force microscopy for PIM with carrier **1** and example histogram

A necessary condition for the transfer a metal ion through PIM is its complexation with 1-alkylimidazole. Permeability coefficients ( $P$ ) of the cations are fairly compatible with stability constants of their 1-alkylimidazole complexes (Table 2 and 4). Elongation of the alkyl chain of the 1-alkylimidazole molecule results in the volume of the donor molecule thus increasing the probability of formation of the Zn(II) and Cu(II) complexes according to the equation:



The phenomenon increases the  $P$  value and at the same time suppresses selectivity coefficients of Cu(II)/Zn(II) and Cu(II)/Co(II). Addition of the chloride ions to the feeding phase enables formation of the  $MCl$  and  $MCl_2$  complexes, especially with the Cu(II) and Zn(II) ions. Those complexes are more dissociableness. This phenomenon increases permeability coefficient  $P$  and suppresses selectivity coefficient.

Table 4. The permeability coefficients for transport of Cu(II), Zn(II), Co(II), and Ni(II) ions across PIM with **1** vs. the concentration of  $Cl^-$  in the source phase; membrane:  $2.6 \text{ cm}^3$  *o*-NPPE /1g CTA and 1.0 M carriers **1** calculated on plasticizer

Metal ions	Permeability, $P$ , m/s		
	-	0.5 M	1.0 M
Cu(II)	$4.28 \cdot 10^{-3}$	$3.75 \cdot 10^{-3}$	$2.94 \cdot 10^{-3}$
Zn(II)	$1.17 \cdot 10^{-3}$	$1.38 \cdot 10^{-3}$	$2.14 \cdot 10^{-3}$
Co(II)	$2.43 \cdot 10^{-4}$	$3.28 \cdot 10^{-4}$	$1.04 \cdot 10^{-3}$
Ni(II)	$1.19 \cdot 10^{-4}$	$2.61 \cdot 10^{-4}$	$1.28 \cdot 10^{-3}$

### 3. CONCLUSION

The 1-alkylimidazoles under study can be used for separation of the Cu(II) ions from an equimolar mixture of the Cu(II), Zn(II), Co(II) and Ni(II) ions in the transportation process across PIM. With elongation of the chain length of substituent - R in the imidazole ring, the initial flux of the ions increases, but the separation coefficients decrease. The highest flux of the Cu(II) ions was noticed for carrier **5**,

whereas the highest separation coefficient for compound **1**. It was also proved that an increase in chloride-ion concentration in the source phase resulted in the increase in the permeability coefficients which attained their top values at 1.0 M concentration of the chloride ions. The permeability coefficient of the Cu(II) ions from solutions with 1.0 M chloride-ion concentration was  $2.94 \cdot 10^{-3}$  m/s. The rate limiting step in transport of  $\text{Cu}^{2+}$  across PIM doped with **1** can be the diffusion coefficient of the carrier-cation complex across the membrane. The studied PIM membrane exhibit good stability described with the Danesi thermodynamical model.

## REFERENCES

- BERSUKER I.B., *Elektronnoe strojenie i svojstva koordinacijonnych sojedinej*, Wyd. Chimia, Leningrad 1972 (in Russian).
- CUPREY, M.E. (1974) *N-Imidazole compounds and their complex metal derivatives*. US Patent, 3,843,667, October 22.
- du PREEZ, J.G.H.; GERBER, T.I.A.; EGDE, W.; MTOTYWA, V.L.V.; van BRECHT, J.A.M. (2001) *Nirtogen Reagents in Metal Ion Separation. XI. The Synthesis and Extraction Behavior of a New NS Imidazole Derivative*. Solvent. Extr. Ion Exch. 19, 143-154.
- DANESI P.R., (1984-85) *Separation of metal species by supported liquid membranes*, Sep. Sci. Technol., 19, 857-894.
- GAŽO J., BERSUKER I.B., GARAJ J., (1976) *Plasticity of the coordination sphere of copper(II) complexes, is manifestation and causes*, Coord. Chem. Rev., 19, 253-297.
- LENARCIK, B.; OJCZENASZ, P. (2002) *The influence of the size and position of the alkyl groups in alkylimidazole molecules on their acid – base properties*. J. Heterocyclic Chem. 39, 287-290.
- LENARCIK B., OJCZENASZ P., (2004) *Investigation of the Stability Constants of Co(II) Complexes with a Homologous Series of 1-Alkylimidazoles in Aqueous Solution by Using a Partition Method with Several Solvents*, Sep. Sci. Technol, 39, 199-226.
- LENARCIK B., KIERZKOWSKA A., (2004) *The Influence of Alkyl Length on Stability Constants of Zn(II) Complexes with 1-Alkylimidazoles in Aqueous Solutions and Their Partition Between Aqueous Phase and Organic Solvent*, Sol. Extr. Ion Exch., 22, 449-471.
- LENARCIK B., RAUCKYTE T., (2004) *The Influence of Alkyl Length on Extraction Equilibria of Ni(II) Complexes with 1-Alkylimidazoles in Aqueous Solution/Organic Solvent Systems*, Sep. Sci. Technol., 39, 3353-3372.
- LUBOCH, E., WAGNER-WYSIECKA, E., FAINERMAN-MELNIKOVA M., LINDOY L. F., BIERNAT J.F., (2006) *Pyrrole azocrown ethers. Synthesis, complexation, selective lead transport and ion-selective membrane electrode studies*, Supramol. Chem., 18, 593.
- NGHIEM L.D., MORNANE P., POTTER, I.D., PERERA, J.M., CATTRALL, R.W., KOLEV, S.D. (2006), *Extraction and transport of metal ions and small organic compounds using polymer inclusion membranes (PIMs)*, J. Membrane Sci., 281, 7-41.
- HAYASHI R., HAYASHITA T., YOSHIKAWA T., HIRATANI K., BARTSCH R.A., TERAMAE N., (2003) *Design of a polymer inclusion membrane having proton- ionisable polyether carriers and their separation function of lead ions*, Bunseki Kagaku, 52, 755-765.
- PERNAK J., KRYSINSKI J., SKRZYPCZAK A., (1987) *Bakterizide wirkung von iminiumverbindungen*, A. Tenside Surfact. Det., 24, 276-286.
- RADZYMIŃSKA-LENARCIK E., (2007) *The influence of the alkyl chain length on extraction equilibrium of Cu(II) complexes with 1-alkylimidazoles in aqueous solution/ organic solvent systems*. Solvent Extr. Ion Exch. 25, 53-64.

- RADZYMIŃSKA-LENARCIK, E., (2008) Search for the possibility of utilizing the differences in complex-forming capacities of alkylimidazoles for selective extraction of some metal ions from aqueous solutions. *Pol. J. Chem. Technol.*, 10, 73-78.
- SUNDBERG R.J., MARTIN B.R., (1974) Interaction of Histidine and other Imidazole Derivatives with Transition Metal Ions in Chemical and Biological System, *Chem. Rev.*, 74, 471-517
- SCHAEKERS, J.M.; du PREEZ, J.G.H. (2004) Solvent extraction mixture comprising substituted imidazole or benzimidazole for the purification of groups of base metals. US Patent, US 2004/0208808 A1, October 21.
- SALAZAR-ALVAREZ G., BAUTISTA-FLORES A. N., SAN MIGUEL E.R., MUHAMMED M., GYVES, (2005) Transport characterization of a PIM system used for the extraction of Pb(II) using D2EHPA as carrier, *J. Membr. Sci.*, 250, 247-257.
- ULEWICZ M., KOZŁOWSKI C.A., WALKOWIAK W., (2004) Removal of Zn(II), Cd(II) and Cu(II) ions by polymer inclusion membrane with side-armed diphosphaza-16-crown-6-ethers, *Physicochem. Probl. Miner. Process*, 38, 2004, 131-138
- ULEWICZ M. (2008), Application of macrocyclic compounds to the transport of Zn(II), Cd(II) and Pb(II) ions cross the polymer inclusion membrane (PIM), *Polish J. Chem.*, 82, 1237-1244.
- ULEWICZ M., LESINSKA U., BOCHENSKA M., (2010), Transport of lead across polymer inclusion membrane with *p*-tert-butylcalix[4]arene derivative, *Physicochem. Probl. Miner. Process.*, 44, 245-256.
- ULEWICZ M., SZCZYGELSKA –TAO J., BIERNAT J.F., (2007) Transport of Zn(II), Cd(II) and Pb(II) across polymer inclusion membrane doped with imidazole azocrown ethers, *Desalination*, 214, 352-364.
- ULEWICZ M., SZCZYGELSKA –TAO J., BIERNAT J.F., (2009) Selectivity of Pb(II) transport across polymer inclusion membranes doped with imidazole azothiacrown ethers, *J. Membr. Sci.*, 344, 32-38.
- WALKOWIAK W., ULEWICZ M., KOZŁOWSKI C.A., (2002) Application of macrocyclic compounds for metal ions separation and removal – a review, *Ars Separatoria Acta*, 1, 87-98
- WALKOWIAK W., KOZŁOWSKI C. (2009), Macrocyclic carriers for separation of metal ions in liquid membrane processes – a review, *Desalination*, 240, 186-197.
- WOLF J.R., STRIEDER W., (1990) Toruosities for a random fiber bed: overlapping, parallel cylinders of several radii, *J. Membr. Sci.*, 49, 103-115.

**Ulewicz, M., Radzyńska-Lenarcik, E.,** Transport jonów metali przez polimerową membranę inkluzyjną z 1 alkylimidazolem, *Physicochem. Probl. Miner. Process.*, 46 (2011) 119-130, (w jęz. ang), <http://www.minproc.pwr.wroc.pl/journal>

Zbadano selektywność transportu jonów Cu(II), Zn(II), Co(II) i Ni(II) ( $c_{Me}=0,001M$ , każdy) przez polimerowe membrany inkluzyjne składające się z trójocianu celulozy (suportu), eteru o-nitrofenylooktylu (plastyfikatora) i przenośnika jonów (1 alkylimidazole). Polimerowa membrana została scharakteryzowana przy pomocy mikroskopii sił atomowych (AFM). Wykazano, że podstawnik alkilowy w pozycji 1 pierścienia imidazolu zmieniając własności hydrofobowe przenośnika wpływa na strumień początkowy transportu jonów metali. Wartości strumienia początkowego transportu jonów przy użyciu przenośnika **1** i **2** maleją w szeregu: Cu(II) > Zn(II) > Co(II) > Ni(II), natomiast dla **3** - **5** w szeregu: Cu(II) > Zn(II) > Ni(II), Co(II). Strumień transportu Cu(II) wzrasta w szeregu użytych przenośników: **1** < **2** < **3** < **4** < **5**, osiągając najwyższą wartość 6,36  $\mu\text{mol}/\text{m}^2\cdot\text{s}$  (dla **5**). Na selektywność

transportu wpływ również stężenie jonów chlorkowych w fazie zasilającej. Czynnikiem limitującym szybkości transportu  $\text{Cu}^{2+}$  przez PIM jest współczynnik dyfuzji kompleksu przenoszonego kationu przez membranę.

*słowa kluczowe: polimerowa membrana inkluzyjna, separacja jonów, miedź(II), cynk(II), nikiel(II), kobalt(II), 1-alkilimidazol*

Satu PIETARSAARI \*, Lotta RINTALA\*, Jari AROMAA\*

## THE APPLICATION OF PUBLIC GEOLOGICAL DATA IN DESCRIPTION OF RAW MATERIALS FOR HYDROMETALLURGICAL PROCESSES

*Received April 28, 2010; reviewed; accepted July 12, 2010*

This paper describes a method for getting the geological, mineralogical and geochemical information from an ore deposit or prospect area and its ore body. The information is needed to select a suitable hydrometallurgical processing method. Usually the first step is to go through expensive and time-consuming field explorations and a number of rock sample analyzing processes. By using existing public deposit information for that purpose, it could be possible to save time and money. A literature study was done about possible sources of public geological information related to world's ore mineral deposits. The study included also a couple of experimental cases where the information-searching procedure was tested in practice. The test minerals were gold and lateritic nickel. The results of the tests show that there are different kinds of mineral deposit databases and that in most cases it is possible to find the needed information. It was found that there are benefits in this type of information gathering system, but there are also some downsides such as the reliability of information.

*keywords: mineral, ore deposit, database, hydrometallurgy*

### 1. INTRODUCTION

When choosing a suitable hydrometallurgical processing method for an ore body, certain important geological features should be known first. These include deposits geology and ore body mineralogy and geochemistry. The methods for getting all the geological information needed are field and laboratory explorations, which are usually expensive and time consuming. Field tests include geological surveying, geophysical

---

\* Aalto University, Department of Materials Science and Engineering, PO Box 16200, FIN-00076 Aalto, Finland. email: jari.aromaa@tkk.fi

explorations, drill core sampling and the core sample analysing with different methods (Papunen et al., 1986). The drill core sampling is the most expensive exploration method, but it is also the most important method (Grönholm et al., 2006). The chemical analysis together with the mineral composition analysis is the most important information when choosing the hydrometallurgical processing method. Both of these analyses are performed from the core samples. Some of the core sample material is pulverised for the chemical analysis and some of the core sample is made into thin sections for mineralogical analysis and polished sections for resources approximation (Papunen et al., 1986). All these studies have to be done before there is any confirmation of the processing ability of the ore body in question.

The above-mentioned situation usually creates problems in mining companies' point of view, because they have to invest on research that does not necessarily result in financial benefit. There is always a possibility that the ore mineral or the valuable metal in the deposit is locked with the host rock in the way that is impossible to liberate it economically with the methods available. However, in some cases there could be another way to get the geological information needed to make decisions for processing methods. The more accurate and more expensive geological explorations and surveys could then be done after suitable hydrometallurgical process alternatives have been selected based on geological information.

This article describes a data-mining study related to geological information. The main idea of the research was to find out public information sources, such as deposit or mineral databases, where to look for the geological information needed. Another aim was to explore the promising information sources and evaluate their usability as help in choosing a hydrometallurgical process. This part is focussed on geological information using the existing documentation in the databases. The research included also experimental cases where the information-searching procedure was tested in practice. Possible problems that occurred during the testing and the reliability and the quality factors that should be considered when using the information found were discussed.

There are different kinds of mineral and deposit databases made about old ore deposits and prospects. It became clear that in most cases it is possible to get the information needed, not necessarily in directly from the databases, but through them by using the database as search portal. Their main benefit is economical, as the information gathered through the databases does not require new fieldwork. There are few risks such as the age and reliability of the information, but the risks can be properly taken into account.

## 2. PUBLIC SOURCES FOR GEOLOGICAL INFORMATION

There are different types of possible sources of deposit or prospect information such as scientific articles written about deposit areas, official exploration and survey

reports and deposit or mineral databases. The last one contains usually all kinds of references to the other two information types in its reference list. This makes the databases very good starting places for searching the information, as they are more like search engines.

Deposit or mineral databases are usually public and freely accessible in the internet, containing variable amount geological, geographical and other general information about the deposits and prospects that are in the database. Almost every country, continent or groups of countries have their own databases, which are usually created and administrated by geological surveys or similar organizations. In some cases, mining companies are also connected to the maintenance of the databases. The main goal of the databases is to make geological information public and easier to find for everybody. Table 1 contains the most usable freely accessible databases discussed in this work and a short description of the type of the database. The internet addresses of the databases are listed in the reference list of this article.

There were also databases worth mentioning that are not listed in Table 1, because they were either liable to charge or created with language other than English. They are South African Mineral Deposits Database (Samindaba), African-European Georesources Observation System (AEGOS), which will be completed in 2011 and Info Terre made by BRGM, which is France's leading public institution involved in the Earth Science field for the sustainable management of natural resources, surface and subsurface risks (BRGM 2008). It is also very positive that the databases are continuously improved and new databases will probably be created.

### 3. GENERAL USABILITY OF DATABASES

Almost all of the databases have many other functions than just being a search engine for deposit information. However, in this case that was the main interest, so it was convenient to make the evaluations based on how suitable and easy to use they are when searching the original exploration reports written from the deposits. This means, how easy it was to find the reference lists from the deposits and to locate the listed material in readable form. Table 2 shows the results of the evaluation. As the results indicate, most of the databases are very suitable for this kind of information retrieval.

The optimal database for the information retrieval described in this paper fulfils following characteristics: The database must give out sufficient amount general information about a deposit such as commodities, host rocks, deposit type, reserves, resources, geographical coordinates etc. Most important, the reference list should be presented so that it is easy to find and comprehend, because that is the source material to get the information needed.

Table 1. Databases found in the original research

Database	Description
FODD - Fennoscandian ore database	Database found from the web site of the Geological survey of Finland (GTK). It contains all the deposits in the Fennoscandian area. It has been created together with the Geological Surveys of Finland, Sweden, Norway and Russia.
MRDS - Mineral Resources On-Line Spatial Data	Database created and administrated by The United States Geological Survey (USGS). It contains deposit information all around the world, also industrial mineral deposits.
ACP – African, Caribbean and Pacific group of states mining data bank	Database contains information about all deposits from African, Caribbean and Pacific states.
GECO - Geology for an ECONomic sustainable development of Congo	A small mineral database that is limited to the copper – cobalt and uranium minerals from the Katanga copper belt and extended by some other species that can be of special importance for identifying specific stratigraphical or structural entities.
GEMS- Geographic Exploration and Mining Services	Database created and administrated by the Geological Survey of Ireland. It contains all the possible information available in public about deposits in Ireland.
BGS - British Geological Survey	From the web site of the British Geological Survey can be found number of different databases (GeoIndex). They cover all of the geology of the British Islands.
TIS -Titles Information System	Database made by The Northern Territory Geological Survey of Australia (NTGS). It is created for public reporting of The Northern Territory's ore deposits. There is also list of other databases in the web site.
DODEX – Geoscience Greenland	Database of the deposits in Greenland. The database is only a search engine for the exploration rappers.
Geology of India - Map Service	A database made by Geological Survey of India. It contains information about ore deposits of India and other geological information.
GERM - The Geological Resource Map of New Zealand	A mineral database made by GNS science, a New Zealand government research organization. The database contains all the ore deposits in New Zealand.
(GeoVIEW.WA) Interactive Geological Map Australia	A database made by the Geological Survey of Western Australia (GSWA) that contains all of the deposits in Western territory of Australia.
SARIG - South Australian Resources Information Geoserver	A mineral database made by PIRSA (Primary Industries and Resources SA), which is The Minerals and Energy Division in South Australian government.

Table 2. Databases evaluation for suitability for information retrieval.  
Scale I = very poor, II = poor, III = moderate, IV = good, V = very good

Database	User interface	Suitability for the information retrieval
FODD - Fennoscandian Ore Database	Map	V
MRDS - Mineral Resources On-Line Spatial Data	Map	IV
ACP - Mining data bank	Map	III
GECO - Geology for an ECONomic sustainable development of Congo	Map and Text editor	II
GEMS- Geographic Exploration and Mining Services	Map	IV
British Geological Survey	Map	II
Tis -Titles Information System	Map	Needs a registration in order to function properly
DODEX - Geoscience Greenland	Text editor for retrieval of reports	V
Geology of India - Map Service	Map	IV
Interactive Geological Map (GeoVIEW.WA) Australia	Map	IV
SARIG – South Australian Resources Information Geoserver	Text editor	V
GERM - The Geological Resource Map of New Zealand	Map	II

#### 4. GEOLOGICAL INFORMATION AND SEARCHING PROCEDURE

##### 4.1. GEOLOGICAL INFORMATION AND ITS USE

The information that hydrometallurgist needs when making decision about processing regards geology, mineralogy and geochemistry of the deposit. In this case, geology means the information about the host rocks, main metals, deposit structure, shape etc. Geological properties have a big impact on the whole mining project, because the chosen excavation method is usually based on them (Papunen et al.,

1986), but those methods are not considered in this article. From mineralogy, it is important to know at least what kind of minerals the host rock consists of and how the valuable metals are combined with the host rock. For example, are they in small or large disseminations within the host rock or as an element in the composition of the minerals in the host rock? The purpose of the geochemical analysis is to specify the elemental composition of the minerals in the host rock. This is probably the most informative data for a hydrometallurgist. However, knowing only the elemental compositions of the minerals is not enough, because there are plenty of minerals that have the same elemental composition, but the elements are combined together with different chemical bonds and the minerals have different structures. Hydrometallurgist needs specifically the information how the elements are bonded and this is obtainable by connecting the geochemical data with the mineralogy.

During the evaluation of an ore body, the three main datasets include size, chemical analysis and mineralogy of the ore body. The size and chemical analysis of the ore body will determine what kind of leaching techniques can be used. Large ore bodies with low-grade ores are best leached with dump, heap or vat leaching. Rich ore bodies that can be concentrated are best treated with reactor leaching. In some cases, it is not economical to mine and transport the ore then in-situ leaching can be considered. The selection of the leaching technique depends on the metal content and particle size of the ore body, with or without pre-treatment steps (Fig. 1).

The intergrowth of minerals will affect the selection of leaching technique (Fig. 2). In cases where the minerals are easily separated by mechanical methods, the selection of leaching technique and leaching chemistry has more freedom. In cases where mechanical separation of minerals is difficult the leaching must be based on dissolving all minerals in order to get the valuable metals in solution.

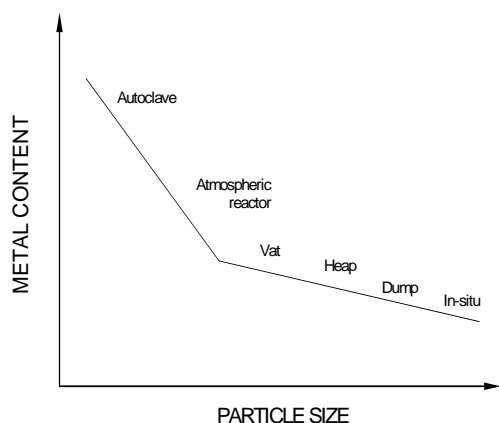


Fig. 1. Alternative leaching techniques depending on particle size and metal content of the raw material

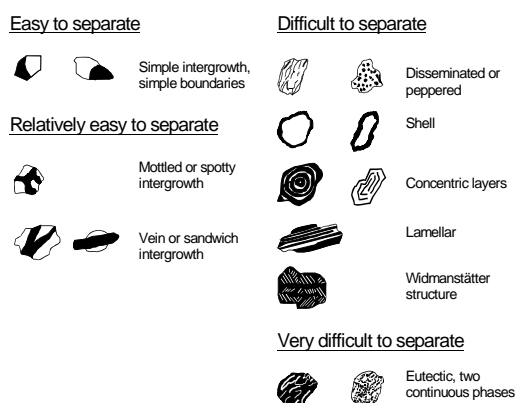


Fig. 2. Basic intergrowth patterns of minerals, after (Hayes, 1985)

The chemical and mineralogical analysis of the ore body will determine the leaching chemistry to be used. The task of the leaching step is to liberate wanted metals from the minerals and, as far as possible, keep the unwanted metals in their compounds. Depending on the compounds in the ore body (*i.e.* minerals), oxidizing or reducing and acid or alkaline chemistry can be used. The aims for selection of the leaching chemistry are to maximize mineral dissolution rate and to ensure that the dissolved metal remains as cation or complex for the subsequent purification steps. The electron configuration of the mineral allows some preliminary alternatives for selection of leaching chemistry (Hayes, 1985):

- minerals of the s-block, *i.e.* chlorides, carbonates or sulfates of alkaline or earth alkaline metals are usually easily dissolved in water
- minerals of the 3d-block are oxides or sulfides of Fe, Co, Ni, Cu, Zn, Cr, Mn and Ti. Oxides are dissolved in acids and sulfides with acid oxidative leaching
- minerals of the 4d- and 5d-block include for example Zr, Nb, Ta, Mo and noble metals. The oxides of the block are leached with strong acids or alkalis. Noble metals are leached with oxidative leaching and complexing agent. Sulfides are leached with oxidative leaching and sometimes an autoclave is needed
- minerals of the 4f-block include for example rare earth metals. They are often leached from phosphates or carbonates. The 5f-block minerals are radioactive and for example, uranium is leached from oxide with acid
- the p-block includes minerals of Al, Sn and Pb. The oxides of Al are leached with alkali. The sulfides are processed with zinc sulfides or Cu-Ni-Fe-sulfides.

#### 4.2. SEARCHING PROCEDURE

It might be convenient to start the information search from the databases, but as it turned out in the progress of the research, they are mostly just search engines for the details. It also became clear that the geochemical analyses were in every case unavailable directly from the database. In order to get the analyses it was necessary to go through the reference material listed in the database.

Although the references are not necessarily accessible through the database or in Internet, there still are usually mentioned journals which contain the articles or places where to look for the exploration reports.

Figure 3 shows a flow chart of the procedure used in the information retrieval. The procedure is as follows:

- search the wanted deposit or prospect from the database, view the information given there, and gather all the usable data such as the reference list
- try to find the references in readable form and again gather all usable data. If all the needed information has been found, the mission is completed
- if the references did not answer all questions, try to find the secondary

references, which are the references of the reference articles found through the database.

The information retrieval procedure was found to be effective. A very good strategy for finding the reference material is to use for example Google Scholar search engine. Another strategy for reference material is to use library services, but in that case, it should be a library specialized in the field. The information retrieval procedure does not always give the desired results as it turned out in one of the research's experimental cases. In the next chapters three of the experimental cases are presented; one in which all the information needed was found very easily and one where it was not found at all. In the third one the information was eventually found, but it was not easy.

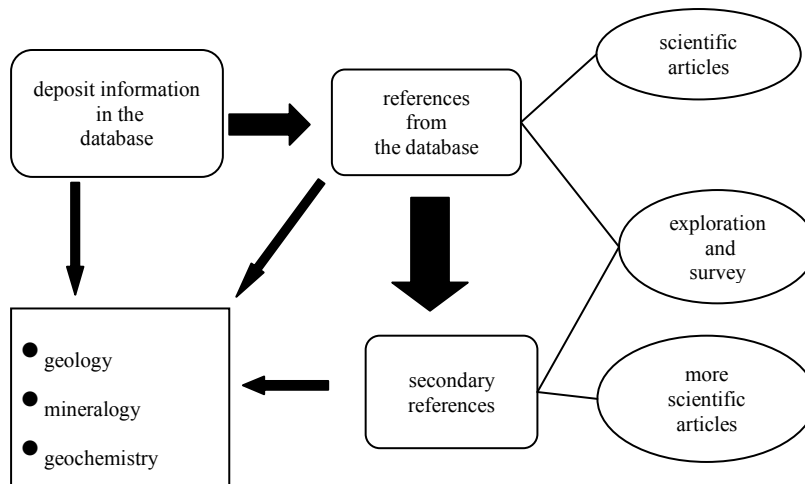


Fig. 3. Flow chart for the retrieval of geological information

#### 4.3. FIRST CASE: MOUNT DAVIES NICKEL PROSPECTS 1-3

The first case is lateritic nickel, for which information was found quite easily. There were three Mount Davies Nickel prospects found through SARIG-database (Sarig 1, 2009) in the same area of South Australia (Fig. 4). They were named as prospect 1, 2 and 3. Although the information given by the database was rather limited, it actually described how the nickel was bonded with the other basic elements of the host rock. Other good feature in this database was that the exploration reports and the articles written about the prospects were directly accessible through a web link found under the general information of the database.

For the Mount Davies Nickel prospects 1-3 almost all the needed information was found very quickly and without any difficulties. Only the chemical analyses in the

exploration reports, as they turned out to be, were partial, but probably informative enough.

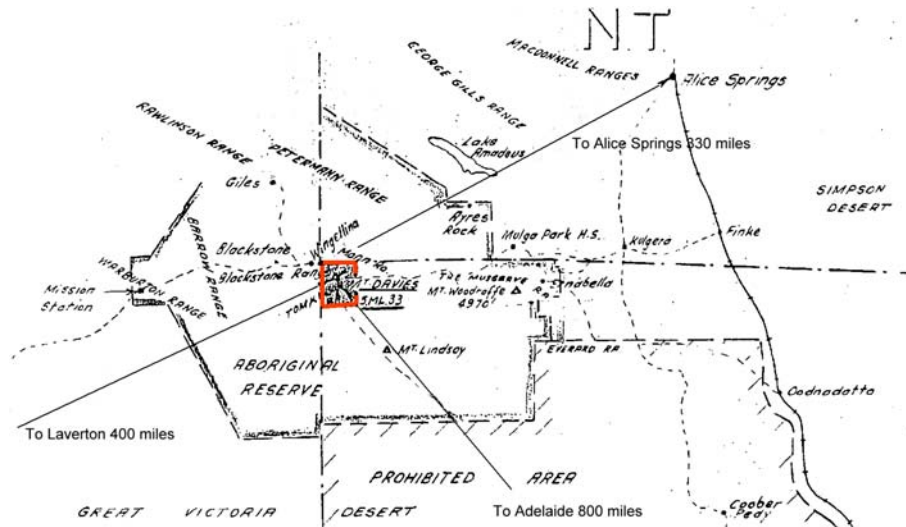


Fig. 4. The location of the Mount Davies Nickel prospects. The prospects 1-3 are located in the red square (Thompson et al., 1960)

#### 4.4. SECOND CASE: RED MOUNTAIN LATERITE

The second case is also about lateritic nickel, but in this case search results were quite poor. Red Mountain Laterite is a lateritic nickel deposit (Ridenour, 2009) in California, USA, (Fig. 5). The MRDS database, from where it was found, offered some basic information such as geographical location, size of the deposit, list of the rock types, commodities and references.

The retrieval of the more detailed information was left to be found in the reference material. However, in this case those references were nowhere to be found in readable form. There were indications that the articles and exploration reports do exist, as links were found through Google Scholar, but the publications were not found in downloadable form. Other search channels came also out empty. They would probably have been available in the archives of the offices that had made the explorations and surveys, but to get them from there was not possible in this work.

#### 4.5. THIRD CASE: NEAR ROUND HILL

The third case is a gold deposit, where at first no information was found in the database. Near Round Hill is a gold deposit in the shear zone of the Round Hill in

New Zealand (de Ronde et al., 2000). The GERM-database through which the near Round Hill-deposit was found did not give any other information about the deposit than is shown in Table 3. No reference material was mentioned and there was no other search portal on the web sites of the Geological Survey of New Zealand.

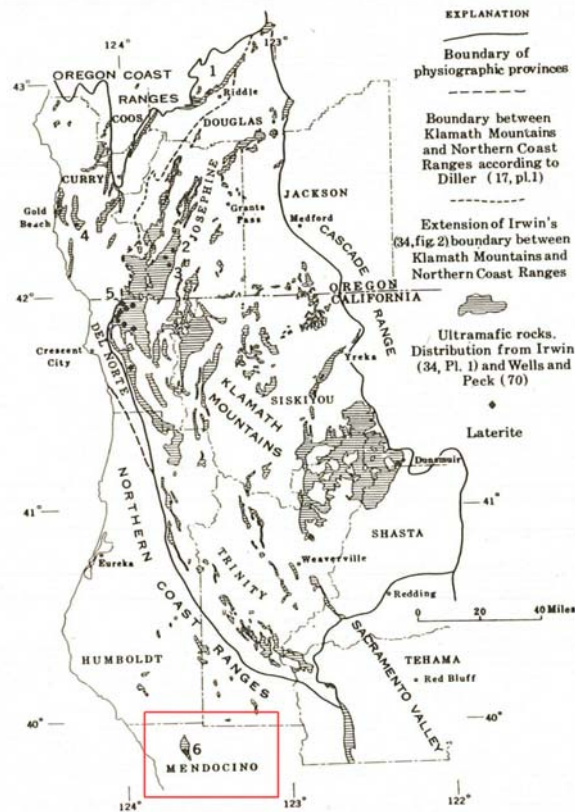


Fig. 5. Map of N.W. California and S.W. Oregon showing physiographic provinces, distribution of ultramafic rocks and locations of lateritic deposits. Rounded with red rectangle is the location of the Red Mountain Laterite (No. 6) (Hotz, 1964)

This kind of situation was actually quite promising for further research, because in this case only other channels and search engines were left in order to find more information. First search engine that was used was Google Scholar and it found a reference of an article that was originally published in the *Economic Geology* journal (de Ronde et al., 2000). It was a research about finding evidences about magmatic ore fluids. The article itself was found with no difficulties through library services. Although the article was not primarily about the deposit exploration in the sense of finding gold and referring the progression of the exploration, it still gave usable geological and mineralogical information. However, the chemical analyses results

shown were evidences about gases and fluids that might have been in the ore before crystallizing and their composition, as it was the articles main theme. On the other hand, the information about the fluids might also be quite interesting from hydrometallurgy point of view.

Table 3. The information sheet from GERM-database about near Round Hill gold deposit (Germ 1, 2010)

Summary Details for D46/e26	
Lat/Long	46°21'10.6''S 167°49'53.9''E
NZMG Coordinate	(D46) 2112200 5415999 (New Zealand Map Grid)
Site Name	near Round Hill
Compiled Date	20-Jul-1987
Site Type	outcrop (LI)
NZGS File Number	263
Commodities	Metals (ME): Aluminium, Antimony, Chromium, Cobalt, Copper, Gold, Iron, Lead, Magnesium, Manganese, Mercury, Molybdenum, Nickel, Platinum, Silver, Titanium, Tungsten, Uranium, Vanadium, Zinc
Feature Commodities	Gold, Platinum

## 5. DISCUSSION

The procedure of retrieval of geological information and using the information found has advantages but there are also disadvantages and risks. The advantages of this method are savings in time and money in the stage where alternative processing methods are evaluated. However, the savings in time and overall costs depend on the quality of the information found and how the information can reduce necessary explorations. The real benefit in using public information is that the new explorations are done only after processing alternatives are narrowed. The explorations are targeted to verify the geological data needed for the process alternatives.

There are important factors that should be taken into account when using the public information and results. These factors include the credibility and reliability of the database, its articles and exploration reports, and the age of the exploration and surveys made. The database can be trusted when the creator and administrator is known. As known authorities usually administer the public databases, credibility is seldom a risk. The articles are scientifically valid when they have been published in some of the known scientific journals. Reports can usually be trusted when known authorities or companies have done them. The age of the articles and reports can affect the quality of the information. Older publications have often less accurate information

than the newer ones, simply because today more research methods are available and their accuracy is better.

One criterion for a reliable report is that the report has been made using some known reporting standard, such as JORC-code or NI-34 101. JORC-code is an ore deposit reporting standard created by The Joint Ore Reserves Committee of The Australasian Institute of Mining and Metallurgy (JORC-code, 2004). NI-43 101 is a reporting standard or rule created by Canadian Securities Administrators (CSA) (FORTUNA, 2010; CSA, 2005). In addition, Committee for Mineral Reserves International Reporting Standards (CRIRSCO, 2006) has recently taken an interest in the reliability of exploration reports and have a vision for creating a single, worldwide standard for public reporting of ore deposits and prospect (CRIRSCO, 2006). However, it is always crucial to understand the subject of the article or the purpose of the explorations, because that might have an impact on the real usability of the information. For example, a survey made to estimate a deposit for a certain metal can lack information about other valuable metals that have come to interest tens of years after the survey has been done.

Overall, it is easy, time saving and economical to have the preliminary research done by searching public sources using the method described here, as it needs only one person to do the work. The disadvantage in this method is that it is not guaranteed that enough information will be found. Some fieldwork has to be done in every case.

## 6. CONCLUSION

The findings of this work show that the many different kinds of public information is available about ore deposit. They also indicated strongly that some of those public information sources could be used as preliminary information sources. It also became clear that the internet based ore and mineral databases are in most of the cases used just as search engines for the specific information needed, such as the geology, mineralogy and geochemistry of a deposit. It turned out that in many cases the valuable information that can be get from the database is the list of the references, where the deposit information is taken from.

However, the most important thing to remember is to never trust blindly the information found in the internet. The results of explorations, which have been done by some unknown party for a different purpose than the information is now needed, are seldom useful. In those cases, the information is only usable as preliminary and no important decisions shall be made based on them.

## REFERENCES

- BRGM - Service Ressources minérales. (2008). What is AEGOS? (cited 9.2.2010)  
<http://www.brgm.fr/brgm/aegos/what.htm>.
- CSA - Canadian Securities Administrators Staff Notice 43-302.(2005), Chapter 5, Rules and Policies -

- NATIONAL INSTRUMENT 43-101 STANDARDS OF DISCLOSURE FOR MINERAL PROJECTS. Section 7. <http://www.spsc.gov.sk.ca/ssc/files/nat-noti/43-302amendedjan24-03.pdf>.
- DE RONDE, C. E. J., FAUTRE, K., BRAY, C. J. (2000). Round Hill Shear Zone-Hosted Gold Deposit, Macraes Flat, Otago, New Zealand: Evidence of a Magmatic Ore Fluid. *Economic Geology and the Society of Economic Geologists*. Vol. 95, s.1025-1048.
- FORTUNA - Fortuna Silver Mines INC. What is National Instrument 43-101? <http://www.fortunasilver.com/s/NI43-101Explanation.asp> (cited 28.1.2010).
- GERM 1 (2010), - <http://data.gns.cri.nz/minerals/germ/buildframe.jsp>.
- GRÖNHOLM, S., AVIOLA, R., KINNUNEN, K.A., Eds. (2006). *Retkeilijän kiviopas*. Geologian tutkimuskeskus. Edita Prima Oy.
- HAYES, P., (1985). *Process selection in extractive metallurgy*. Hayes Publishing, Brisbane, 406 p.
- HOTZ, P. E. (1964). Nickeliferous laterites in southwestern oregon and Northwestern California. *Economic geology and the society of economic geologists*. Vol. 59, s. 355-396.
- JORC-code (2004) The Joint Ore Reserves Committee of The Australasian Institute of Mining and Metallurgy, Australian Institute of Geoscientists and Minerals Council of Australia (JORC). JORC Code - Australasian Code for Reporting of Exploration Results, Mineral Resources and Ore Reserves. 5th ed., s.2-31, [http://www.jorc.org/jorc\\_code.asp](http://www.jorc.org/jorc_code.asp)
- PAPUNEN, H., HAAPALA, I., ROUHUNKOSKI, P., Eds (1986). *Suomen Malmigeologia Metalliset Malmiesiintymät*. Suomen Geologia Seura r.y. Mänttä, 317 p.
- RIDENOUR, J., Red Mountain Laterite. [http://tin.er.usgs.gov/mrds/show-mrds.php?dep\\_id=10140214](http://tin.er.usgs.gov/mrds/show-mrds.php?dep_id=10140214), Updated 6.5.2009 (sited 24.11.2009).
- SARIG 1. - <http://www.minerals.pir.sa.gov.au/sarig>, updated 1.8.2009 (cited 25.11.2009).
- THOMPSON B. P., MIRIAMS R. C. (1960) Regional geology and Nickel exploration in the Mann 4 miles sheet and adjoining areas. Rap.No.659.

#### DEPOSIT DATABASES INTERNET ADDRESSES

- FODD: <http://geomaps2.gtk.fi/website/fodd/viewer.htm>
- MRDS: <http://mrdata.usgs.gov/mineral-resources/mrds-us.html>
- ACP: [http://mines.acp.int/html/accueil\\_en.html](http://mines.acp.int/html/accueil_en.html)
- GECO: <http://www.gecoproject.org/?page=minerals&>
- GEMS: <http://www.mineralsireland.ie/Available+Exploration+Data/Exploration+report+search.htm>
- BGS: <http://www.bgs.ac.uk/GeoIndex/index.htm>
- TIS: <http://dmetis.nt.gov.au/tis/OLQ.ASP?WCI=Main&WCE=getPageSize&WCU=>
- DODEX: <http://jupiter.geus.dk/Dodex/pages/search.jsf>.
- Geology of India - Map Service: [http://www.portal.gsi.gov.in/public\\_html/gis/Guest/viewer.htm](http://www.portal.gsi.gov.in/public_html/gis/Guest/viewer.htm).
- GERM: <http://data.gns.cri.nz/minerals/germ/buildframe.jsp>.
- GeoVIEW.WA: <http://www.dmp.wa.gov.au/7113.aspx#7116>.
- SARIG: <http://www.minerals.pir.sa.gov.au/sarig>

**Pietarsaari, S., Rintala, L., Aromaa, J.,** *Zastosowanie ogólnodostępnych danych geologicznych w opisie surowców dla procesów hydrometalurgicznych*, *Physicochem. Probl. Miner. Process.*, 46 (2011) 131-144, (w jęz. ang), <http://www.minproc.pwr.wroc.pl/journal>

Artykuł opisuje metodę pozyskiwania danych geologicznych, geochemicznych i mineralogicznych dla złóż rud i obszarów poszukiwania złóż. Informacje te są potrzebne w celu ustalenia optymalnych metod przeróbki hydrometalurgicznej. Pierwszym etapem w takim przypadku są zwykle kosztowne

i długotrwałe badania geologiczne połączone z licznymi analizami próbek skał. Można zaoszczędzić dużo czasu i pieniędzy posługując się w tym celu ogólnie dostępnymi informacjami na temat złóż. Przeprowadzono literaturowe poszukiwania ogólnodostępnych danych geologicznych na temat światowych złóż minerałów. W pracy opisano również kilka przykładów praktycznego zastosowania opisanych procedur poszukiwania informacji. Przykłady te dotyczyły minerałów laterytowych niklu oraz złota. Rozważane przykłady pokazały, że istnieje wiele różnych baz danych o złożach minerałów i w większości przypadków można znaleźć niezbędne dane. Stwierdzono, że korzystanie z tego typu metod może przynieść korzyści, trzeba się jednak liczyć z ograniczoną wiarygodnością tak pozyskanych informacji.

*słowa kluczowe: mineral, złoża, ruda, hydrometalurgia, bazy danych*

Tomasz P. OLEJNIK\*

## **MILLING KINETICS OF CHOSEN ROCK MATERIALS UNDER DRY CONDITIONS CONSIDERING STRENGTH AND STATISTICAL PROPERTIES OF BED**

*Received May 15, 2010; reviewed; accepted July 15, 2010*

The article presents the results of investigations concerning the analysis of milling kinetics of chosen rock materials taking into consideration their strength properties. Investigations were carried out for a mill operating on a semi-industrial scale. Milling was conducted in a periodical mode using grinding media differing in diameters. Mineral raw materials differing in terms of crystallographic structure were subjected to grinding. The process of milling was carried out for quartzite, granite and greywacke. Input fraction of ground material was of size 5 – 8 mm. Grain strength from particular size fractions and its influence on the process kinetics were determined. Grinding rate of particular size fractions and basic parameters used in the theory of statistical moments were calculated.

*keywords: ball mill, specific grinding rate, moments theory*

### 1. INTRODUCTION

The mechanism of grinding is based on division of solid grains into grains of smaller size and the process is caused by internal or external loadings, exceeding the strength limit and damaging atomic and molecular bonds (Blumenauer and Pusch, 1981). As each material cracking in the zone of loading precedes deformation, the process of grinding requires a supply of indispensable quantities of energy, this quantity being conditioned by deformation, tensile properties of deformed material and the type of loading. Grain cracking requires overcoming cohesive forces in cracking planes (exposed to external forces) and increasing the distance between elementary particles. The phenomenon under scrutiny may be brought about by

---

\* Faculty of Process and Environmental Engineering, Technical University of Lodz, Wolczanska 213, 90-094 Lodz, tolejn@p.lodz.pl

normal stresses – tensile or tangential stresses.

The process of grinding in ball mills is determined by a complex character of grinding media influence on the ground material. The main geometrical dimensions of mill's drum, grinding media size and the type of their movement have an impact on grinding rate and final composition of grinding products. The process of grinding takes place due to the complex interaction of grinding media with ground material being located between those media and the internal surface of the drum. Grains of ground material located in those areas are ground and sheared with an opportunity of a crushing mechanism (Lynch, 1974; Shipway and Hutchings, 1993). Conditions of energy transfer from grinding media to grains are defined by the energy level of mill's working elements. Potential energy is regarded as a basic energy level under the Earth gravity. Therefore, a measure of grinding media energy level is the ratio of their dynamic forces to gravity forces or the ratio of kinetic to potential energy. A complex mechanism of grinding media interaction with feed determines the course of a grinding process and the final grain size product composition. Using mathematical tools, which are applied to the theory of statistical moments, one may describe the influence of ball composition change on the change of skewness and flattening coefficients (Heim and Olejnik 1997). Thus, there is a possibility of grain size product composition and the grinding time to be predicted based on percentage fraction of balls of appropriate diameters. Change of process conditions determining the change of milling products grain size composition may shorten substantially the milling time. The situation under scrutiny is desirable due to a purely economical aspect of grinding process and each action shortening the time necessary for obtaining the required product grain size has a direct influence on the costs of the whole process. Low practical efficiency of a milling process, forces to search for optimal process parameters considering the energy input to obtain shortest milling time. The effects of milling in a ball mill were analyzed from such a point of view and taking into account grain resistance to normal stresses and statistical moment distributions in the analysis of the results.

The aim of investigation was to compare the influence of process condition and properties of raw material on specific grinding rate. Grain size distribution function, determined by process parameters, has a key impact on main factors used in statistical moment theory. A relationship between statistical parameters and process conditions may carry on to simpler expression describing milling process.

## 2. PROCESS AND EQUIPMENT PARAMETERS OF MILLING

The process of milling was carried out under dry conditions. Milling was conducted for three mineral materials: quartzite, greywacke and granite. Raw material came from the Lower Silesia region. Quartzite is a dense, hard, metamorphic rock

composed almost exclusively of quartzite grains. Silica content ( $\text{SiO}_2$ ) in this rock is more than 99%. This is the so-called typical quartzite. Greywacke is a sedimentary clastic multi-component rock rich in chippings of various finely crystalline rocks (above 25% of dendrite material). Granite is a lithic, acidic, magmatic-intrusive rock, medium or thickly crystalline rock of clearly crystalline structure displaying a visible joint in three perpendicular directions. These three raw material differed in mechanical properties and grain structure. Investigations of milling kinetics were carried out for a semi-industrial mill. Basic technical data about the mill is summarized in Table 1. Basic data concerning feed mass and physical properties of ground materials are summarized in Table 2. Raw materials of graining from 5 to 8 mm were used for milling.

Table 1. Basic parameters of a semi-industrial mill

Internal diameter, m	0.5
Total capacity, $\text{m}^3$	0.112
Rotation frequency $n$ , $\text{min}^{-1}$	31
$V/V_{\text{mill}}$ , - (feed volume/mill capacity)	0.30
$n/n_{\text{kr}}$ , -	0.54

Table 2. Basic feed properties

Raw material	Bulk density $\text{kg/m}^3$	Bulk density after thickening $\text{kg/m}^3$	Mean feed density $\text{kg/m}^3$	Feed mass kg
Quartzite	1236	1298	1267	45
Greywacke	1268	1324	1296	45
Granite	1394	1410	1402	45

Charge of the mill (grinding media and feed) was determined for circa 30% of mill capacity. The process of milling was conducted in a periodical mode using balls of different diameters. Ball sets, differing in diameters, are presented in Table 3. Total mass of balls applied for milling was about 41 kg. Feed sampling was performed every 30 minutes, collecting mass of about 0.6 kg for the grain size analysis. The samples were subjected to a grain size analysis using a laser grain size analyzer ANALYSETTE 22 (FRITSCH). Additionally, a screen analysis was carried out.

Table 3. Ball specification for particular compositions

Series	A	B	C	D
Ball diameter, mm	Ball mass, kg / Number of contact points			
10	-	6 / 27588	1 / 6424	-
20	-	12.3 / 11176	12.5 / 11363	11 / 9999
30	-	12.3 / 2035	12.5 / 2068	15 / 2475
40	-	10 / 671	15 / 1001	15 / 1001
60	40 / 512	-	-	-
Total	40 / 512	40.6 / 50611	41 / 14432	41 / 13475

### 3.RESULT

Based on the grain size analysis, grinding rates of particular size fractions were calculated using the author's computer program. To perform calculations, Gardner and Austin's formula (Eq. 1) was applied for discrete values of fractions assuming an ideal mixing of ground material (Lowrison, 1974; Heim and Olejnik, 2006).

$$\frac{\Delta w_i(t)}{\Delta t} = -S_i w_i(t) + \sum_{j=1, i>1}^{i-1} S_j b_{i,j,t} \cdot w_j(t), \quad (1)$$

where  $w_i(t)$ ,  $w_j(t)$  are weight fraction of particles  $i$  or  $j$  after grinding time  $t$ ;  $S_i$ ,  $S_j$  specific grinding rate (distribution parameter) of particles in fraction  $i$  or  $j$ ,  $s^{-1}$ ;  $b_{i,j,t}$  particle size distribution function and  $t$  is time grinding, s.

Based on the knowledge of grain size composition, mean grain size was calculated using the following formula:

$$d_s = \sum_{i=1}^n d_{si} \cdot x_i, \quad (2)$$

where  $d_{si}$  denotes mean (arithmetic) particle size in size fraction  $i$ , mm;  $x_i$  is mass fraction of particles in size fraction  $i$ .

The example values of rate coefficients  $S_i$  of particular size fractions for ball set A are summarized in Table 4. The results of grain size analysis were used for calculation of skewness and flattening of distributions, applying for this purpose the tools utilized in the theory of statistical moments (Heim and Olejnik, 1997). Equations defining modified flattening coefficients  $K_{1m}$  and skewness coefficients  $K_{2m}$ , were defined using Eqs 3 and 4.

$$K_{1m} = \frac{M_4 - (M_2)^2}{M_4}, \quad (3)$$

$$K_{2m} = \frac{M_3}{M_2^{3/2} + |M_3|}. \quad (4)$$

Central moments  $M$  of the second, third and fourth order ( $k$ ) present in Eqs 3 and 4 were derived as follows:

$$M_k = \sum_{i=1}^n (d_{xi} - d_s)^k \cdot x_i. \quad (5)$$

Selected grains of particular size fractions were subjected to a destructive test in which compressive loading was applied. Crushing tests were performed using an INSTRON device. The data containing the values of crushing forces and grain deformations during tests were processed statistically. Example values of compressive forces and resulting destructive stresses in grains of ground minerals are shown in Table 5.

Table 4. Grinding rates of particular grain size fractions for milling with ball set A

	Quartzite	Greywacke	Granite
$d_s$	$S_{ik} [\text{min}^{-1}]$	$S_{is} [\text{min}^{-1}]$	$S_{ig} [\text{min}^{-1}]$
2.5	0.00267	0.00244	0.0215
1.8	0.0095	0.00221	0.0151
1.5	0.015	0.00115	0.0172
1.32	0.044	0.00372	0.017
1.13	0.045	0.00306	0.0174
0.9	0.0563	0.00291	0.0201
0.4	0.101	0.0198	0.0457

Analyzing the process of grinding of chosen mineral materials, one may notice a considerable influence of their structure on the process kinetics. For granite, characterized by a clear joint, a detrimental influence of grinding media causes a rapid change of mean grain size. The consequence of this fact is obtaining high values of grinding rate (Table 4) for all the investigated grain size ranges. For the size fraction of granite between 2 and 3 mm, the greatest mean forces destroying grains existed. Their value is equal to more than 270 N. In the course of granite grain destructive tests, mean destructive forces and mean grain size tended to decrease. For the smallest grains from the range of 0.5 to 0.8 mm the destructive forces were equal to slightly more than 26 N. Simultaneously, for the whole range of grain size variability, the approximate values of destructive stresses were measured. The value of above-

mentioned stresses was in the range from 13.27 MPa (for grains from the range 1.6 to 2 mm) and to 48 MPa for the smallest size fractions. Different values of destructive forces and corresponding destructive stresses were observed for quartzite and greywacke.

Table 5. Values of destructive forces and stresses of investigated raw materials

Grain size class mm	Mean destructive force, N	Mean destructive stresses, MPa	Raw material
3 ÷ 2	244.1	12.44	Quartzite
	279.4	14.01	Granite
	412	21.01	Greywacke
2 ÷ 1.6	144.8	14.24	Quartzite
	135	13.27	Granite
	348	34.2	Greywacke
1.6 ÷ 1.4	94.62	13.39	Quartzite
	118	16.7	Granite
	132.3	18.73	Greywacke
1.4 ÷ 1.25	60.71	11.01	Quartzite
	126.4	22.93	Granite
	124.6	17.46	Greywacke
1.25 ÷ 1.0	45.49	11.45	Quartzite
	108.9	27.4	Granite
	71.22	18.31	Greywacke
1.0 ÷ 0.8	34.46	13.55	Quartzite
	57.66	22.67	Granite
	84.86	33.37	Greywacke
0.5 ÷ 0.8	26.39	19.88	Quartzite
	74.98	48.72	Granite
	36.13	27.45	Greywacke

For the analyzed process conditions, grinding rates  $S_i$ , are for granite by one order greater when compared to quartzite and greywacke. After milling time equal to 200 minutes, mean grain size was equal to less than 0.5 mm.

Quartzite has a different composition. This is a clastic rock composed of quartzite grains very densely packed and silica bound. Therefore, the rock is characterized by a low susceptibility to grinding. In the investigated range of grain size (Table 5), very similar values of destructive stresses were obtained. For coarse grains (up to 1 mm) the values were equal to 12.44 MPa whereas for grains below 1 mm destructive stresses increased to the value above 19 MPa. A constant decrease of normal force values causing destructive stresses is intriguing. For the greatest grains from the range

of 2 to 3 mm, the destructive force is equal to 244.1 N. A decrease of the grain size causes a decrease of destructive force to the value of 26.39 N for grains from the range of 0.5 to 0.8 mm. The increase of destructive stresses accompanied by a simultaneous decrease of loading may be elucidated by an increase of grain structure deformations without losing material cohesion. For greater grains, it is possible for a soft binder to occur, weakening material structure, then, a very homogenous material is obtained for smaller grains subjected to the grinding process.

The observed diversification, in terms of susceptibility of investigated raw materials to grinding, may inspire one to apply a differing composition and size as well as ball mass. Quartzite, composed of hard grains, depending on size fraction, displays a different susceptibility to grinding. Therefore, grain size has a relevant meaning for achieving an appropriate state of destructive stresses. For coarse grains, the main mechanism causing crushing of raw material will be impact reaction of grinding media whereas for the smallest grains tangential forces may decide about the grinding rate. For greater fractions grinding media should display appropriately high kinetic energy, capable of overcoming internal cohesive forces acting between grains of the raw material. When grinding is carried out with balls that have the same diameter, then greater values of specific grinding rate occur for the smallest grains. In such a case, grinding media of a considerable size and mass in comparison with the smallest grain size fraction may evoke tangential destructive stresses being appropriately high. In the case of greywacke being very similar to sandstones in terms of structure, destructive stresses obtained for the investigated size fractions attain similar values.

The analysis of grinding rate inspires to state that the mechanism of impact grinding occurs in case of all investigated raw materials. However, its effect is greater in the case of greater grains, whereas smaller grains are ground mainly by means of a grinding mechanism.

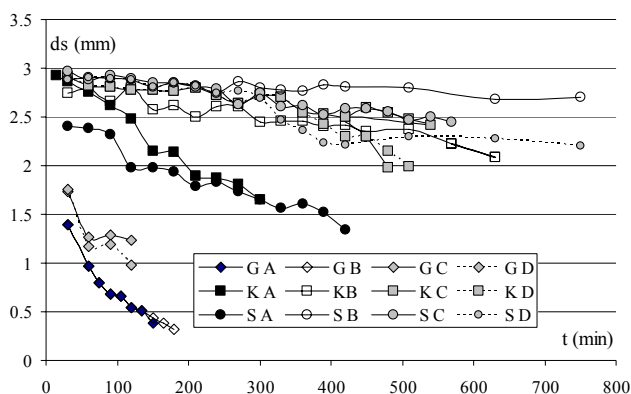


Fig. 1. Change of mean grain size  $d_s$  with in time: granite – G, quartzite – K and greywacke - S for four ball compositions (A, B, C, and D)

As a matter of fact, grinding of large grains causes the formation of the smallest fraction but it does cause the movement of destroyed grains to the finest grain fraction. Grinding, which is longer in time may decrease the size of coarse grains to such an extent that they move to the neighbouring size fraction. The consequence of the grain strength change accompanied by their mean size change was that varying milling time was necessary. For the investigated raw materials, grinding times and corresponding change of mean grain size  $d_s$ , are shown in Fig. 1. The application of balls of series A, for all raw materials contributed to a considerable shortening of the grinding time. For quartzite displaying a more homogenous structure, when compared to greywacke and granite, diversification of ball composition produced no considerable influence on the change of mean grain size. In spite of change of the mean size, quartzite grains are of similar strength. For raw materials containing soft, hard and resistant inclusions and soft binder, a change of ball compositions brings about an increase of destructive interactions for balls of smaller diameter. Distribution of skewness coefficients  $K_{2m}$  and flattening coefficients  $K_{1m}$ , is shown in Figure 2.

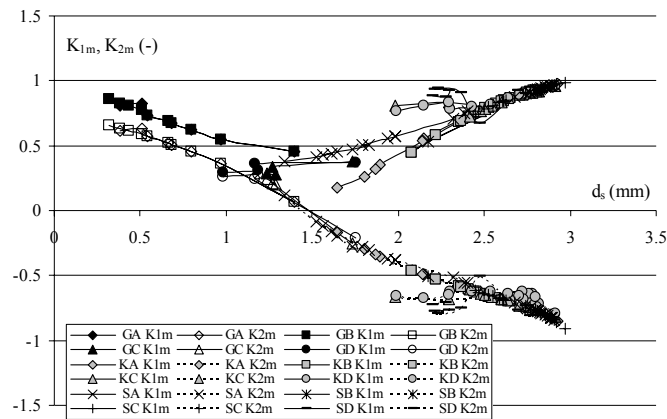


Fig. 2. Change of values of modified flattening coefficient  $K_{1m}$  and skewness coefficient  $K_{2m}$  for investigated raw materials. Symbols: G - granite, K - quartzite and S - greywacke. A, B, C and D denote ball compositions

The application of changing ball compositions contributes to the fact, that for certain mean grain size, one may obtain distributions similar to a normal distribution and grains are more monodispersive. Obtaining small grinding times for granite and, what is connected with this, a rapid change of the mean grain size causes high changeability of skewness and flattening coefficients. This is reflected in occurrence of a considerable number of grains differing in terms of size and causing the fact that grain distributions are characterized by high changeability (skewness). Obviously, the analysis of process kinetics as well as its influence on statistical distributions should consider destructive ball interactions and bed strength properties changing in the

course of milling. The aforementioned problem should be a subject of further investigations.

#### 4. CONCLUSION

Based on the results obtained in this work the following conclusions can be drawn:

- grinding rate of chosen size fractions may depend on the magnitude of normal forces occurring at the contact point of grinding media with ground raw materials
- grinding kinetics is determined by grain resistance to destructive stresses depending on the structure of ground raw material
- differing ball size may influence substantially predominant mechanisms of grain grinding
- ball composition has a considerable impact on the values of skewness and flattening coefficients of grain size distributions.

#### ACKNOWLEDGMENTS

This study was carried out within research project no. N N208 0773 33, financed by the State Committee for Scientific Research in the years 2007-2010.

#### REFERENCES

- BLUMENAUER H., PUSCH G., 1981, Technische Bruchmechanik. VEB Deutscher Verlag für Grundstoffindustrie, Leipzig.
- HEIM A., OLEJNIK T., 1997, *Opis kinetyki procesu rozdrabniania niektórych materiałów skalnych za pomocą teorii momentów*; Zesz. Nauk. PŁ, Inż. Chem.; 779; z. 21, s. 101.
- HEIM A., OLEJNIK T.P. (2006), Proceedings of Fifth World Congress on Particle Technology; Swan and Dolphin Resort, Orlanado, 18-13.
- LOWRISON G. C. (1974), Crushing and grinding. Butterworth, London.
- LYNCH A.J.(1974), Mineral crushing and grinding circuits, Oxford, New York.
- SHIPWAY P.H., HUTCHINGS I.M.(1993), Phil. Magaz., A, **67**, 1389-1404.

**Olejnik, T.P.**, *Kinetyka mielenia wybranych materiałów skalnych z uwzględnieniem wytrzymałości oraz własności statystycznych nadawy*, Physicochem. Probl. Miner. Process., 46 (2011) 145-154, (w jęz. ang), <http://www.minproc.pwr.wroc.pl/journal>

Artykuł przedstawia rezultaty badań kinetyki mielenia, wybranych materiałów skalnych, z uwzględnieniem ich własności wytrzymałościowych. Badania prowadzono dla półprzemysłowego

młyna kulowego. Przemiał realizowano w trybie okresowym, używając mielników o zróżnicowanych wymiarach. Materiał skalny różnił się budową krystalograficzną. Mielenie przeprowadzono dla kwarcytu, granitu oraz szarogłazu. Nadawa charakteryzowała się początkową frakcją rozmiarową z przedziału 5 – 8 mm. Zbadano wytrzymałość ziarn, należących do poszczególnych frakcji rozmiarowych, oraz jej wpływ na kinetykę procesu. Obliczono szybkość przemiału poszczególnych frakcji rozmiarowych oraz rozkłady wielkości matematycznych, wykorzystywanych w teorii momentów statystycznych.

*słowa kluczowe: młyn kulowy, szybkość właściwa rozdrabniania, teoria momentów*

Jerzy GĘGA\*, Władysław WALKOWIAK \*\*

## LEACHING OF ZINC AND MANGANESE FROM USED UP ZINC-CARBON BATTERIES USING AQUEOUS SULFURIC ACID SOLUTIONS

*Received May 10, 2009; reviewed; accepted July 15, 2010*

Zinc-carbon and alkaline zinc-manganese dioxide batteries are widely used for powering small appliances as they have favorable electrical properties/price ratio. Due to a large amount of these batteries sold every year they are a considerable secondary source of zinc and manganese. A hydrometallurgical method of recovering those metals seems to be attractive.

In this paper leaching tests have been presented to evaluate the leaching behavior of Zn and Mn and their compounds of interests under different conditions such as solid/liquid ratio (weight of sample/leaching solution volume), sulfuric acid concentrations, temperature and time of leaching. The acid concentration was investigated in the range of 0.2 to 5.0 M and the leaching time was from 30 minutes to 5 hours. The tests were carried out in temperature range of 20 – 80°C.

It was shown that the leaching recovery of zinc and manganese increases with increasing sulfuric acid concentration up to 2.0 M and zinc is dissolved under these conditions, whereas only around 50% of manganese is recovered. It was found that the rate of zinc leaching is higher than that of manganese and the rate of both reactions is increasing with temperature as well as with a decrease of the solid/liquid ratio.

*keywords: used up batteries, zinc, manganese, leaching, sulfuric acid*

---

\* Czestochowa University of Technology, Department of Chemistry, J.H. Dabrowskiego 69, 42-201 Czestochowa, Poland, [gega@wip.pcz.pl](mailto:gega@wip.pcz.pl)

\*\* Wroclaw University of Technology, Department of Chemical Metallurgy, Wybrzeze Wyspianskiego 27, 50-370 Wroclaw, Poland, [wladyslaw.walkowiak@pwr.wroc.pl](mailto:wladyslaw.walkowiak@pwr.wroc.pl)

## 1. INTRODUCTION

Presently economical and environmental requirements impose a development of effective and inexpensive methods for recovering of valuable metals from secondary sources. Zinc-carbon and alkaline zinc-manganese dioxide batteries are widely used as they have good electrical properties/price ratio. Due to large amount of these batteries selling every year they can be thought over as a considerable secondary source of Zn and Mn. The comparison of price changes for zinc and manganese over last three years are shown in Fig. 1. A hydrometallurgical method of recovering those metals seems to be attractive. Recycling process of zinc-carbon and alkaline-manganese batteries should be developed to achieve environmental conservation as well as the effective utilization of metal resources.



Fig. 1. The comparison of price changes for zinc and manganese over last three years (www.infomine.com)

Several methods to recover metal values from used up batteries based on pyrometallurgical or hydrometallurgical technologies can be found in the literature. The pyrometallurgical method consists basically of selective volatilization of metals at elevated temperatures followed by condensation. The examples of such processes are BATREC, SNAM-SAVAN, SAB-NIFE and INMETCO (Bernardes et al., 2004; Espinosa et al., 2004; Kosarga et al., 2006; Salgado et al., 2003). Except of the BATREC process, the other methods are commonly used to recover cadmium from Ni-Cd batteries by volatilisation at temperatures around 900°C. On the other hand, the BATREC process recycles zinc and mercury from zinc-carbon and alkaline batteries at 1500°C. Highly pure zinc is obtained when no Ni-Cd batteries are present and treated because zinc and cadmium are not selectively volatilised in the furnace. Therefore, a classification step is necessary. Generally, pyrometallurgical routes do

not require batteries dismantling, however applied operations are very energy consuming and some emissions of dust and gases are expected.

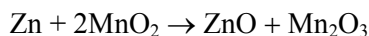
The hydrometallurgical routes are commonly found more economical and efficient than pyrometallurgical methods. The metal separation routes based on hydrometallurgical operations are characterised by lower energy consumption, higher metal selectivity and no air pollution, as there are no particles produced. However, some pre-treatment steps are necessary to improve metal dissolution rates in the aqueous phase, like batteries sorting, dismantling, magnetic separation and leaching. The examples of hydrometallurgical processes being in commercial use could be BATENUS (Fröhlich and Sewing, 1995), and MODIFIED ZINCEX (Martin et al., 2001). These processes differ basically in the metal separation method used to treat the obtained leach liquor. The BATENUS process can treat any type of batteries, except of button cells that contain high mercury levels. After leaching with sulfuric acid, zinc present in the liquor can be separated by solvent extraction (SX) while copper, nickel and cadmium can be selectively separated by an ion exchange (IX) technique and manganese is precipitated as  $\text{MnCO}_3$ . The MODIFIED ZINCEX process uses solvent extraction to produce a high quality zinc electrolyte solution suitable for producing zinc or zinc sulfate. Zinc extraction from the leaching liquor (PLS – pregnant leach solution) is performed with di-2-ethylhexyl phosphoric acid (D2EHPA) as extractant. Manganese is left in the raffinate and then is crystallized as  $\text{MnSO}_4$ .

Although a few of hydrometallurgical methods of processing of spent batteries are already in use there is still a need for new methods providing higher efficiency and lower operational costs. This paper presents results of leaching tests of spent zinc-carbon and alkaline zinc-manganese dioxide batteries with sulfuric acid solutions.

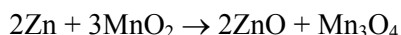
## 2. EXPERIMENTAL PROCEDURE

### 2.1. BATTERIES

Zinc-carbon and alkaline zinc-manganese dioxide batteries are popular and widely used. Detailed description of their construction can be found elsewhere (Linden and Reddy, 2001). The zinc-carbon battery consists of a zinc can (serves as the battery container and anode), a manganese dioxide cathode and an electrolyte of ammonium chloride and/or zinc chloride dissolved in water. Carbon (acetylene black) is mixed with manganese dioxide to improve conductivity and retain moisture and compressed under pressure to form a bobbin. The bobbin is the positive electrode and is also called black mix, depolarizer or cathode. A carbon rod, serving as the current collector for the positive electrode is inserted into the bobbin. The battery is inserted into a steel can with plastic separator. As the battery is discharged, the zinc is oxidized and the manganese dioxide is reduced. A simplified overall battery reaction can be written as:



Although the alkaline zinc-manganese dioxide battery uses the same anode and cathode material, its construction is quite different. The active materials in these batteries are manganese dioxide, an aqueous alkaline electrolyte, and powdered zinc metal. The electrolyte is a concentrated solution of KOH (usually 35 to 52%). Powdered zinc is used for the anode to provide a large surface area for reduced current density and to distribute solid and liquid phases more homogeneously. The components are inserted into a steel can. A simplified overall battery reaction can be written as:



In our research AA (R6) of different manufacturers were used. All batteries were dismantled. After separation of iron scrap, plastic and paper, the remaining part of battery was cut and crushed into small parts below 5 mm in size and then dried for 24 hours and ground. All the tests were carried out using homogeneous samples of this material. The average content of the main components of the mixture were determined by atomic absorption spectrometry after dissolution of the sample in aqua regia and are presented in Table 1. The obtained values correspond to those which can be found in literature (Bartolozzi et al., 1995; Salgado et al., 2003)

Table 1. Metal components content of investigated batteries

Battery type	Component contents (%)					
	Zn	Mn	K	Fe	Co	Ni
Zn-C	5.20	23.10	-	0.50	0.01	0.01
Alkaline	18.0	29.85	7.55	1.42	0.01	0.01

## 2.2. LEACHING TESTS

The two major components of the used up batteries are metallic zinc and manganese dioxide. An analysis of E-pH diagrams for the Zn-H<sub>2</sub>O and Mn-H<sub>2</sub>O systems (Fig. 2) allows to choose the leaching system. According to data presented in Fig. 2, in strongly acidic solutions, both zinc and manganese should be present in the form of divalent ions. In the case of manganese, it can also be in the form of solid MnO<sub>2</sub>. Therefore, acids seem to be suitable for leaching of used up Zn-MnO<sub>2</sub> batteries. Among them, sulfuric acid is attractive due to its accessibility and low price. For that reason leaching experiments were carried out using sulfuric acid solutions.

In each test a sample 2.0 g of the battery was leached in appropriate volume of H<sub>2</sub>SO<sub>4</sub> solutions of suitable concentrations in a thermostatic beaker under mechanical stirring at the rate of 600 rpm. Preliminary tests have shown that the rates above 500 rpm do not influence the rate of leaching. During and at the end of the experiments, samples of the leached pulp were taken and separated by filtration. The concentration

of metal ions in the leach aqueous solutions was determined by atomic absorption spectrometry (AAS).

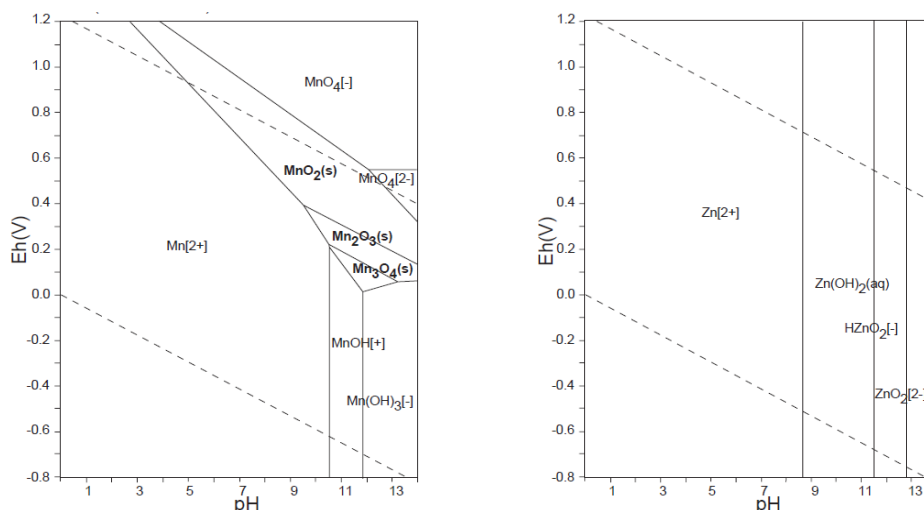


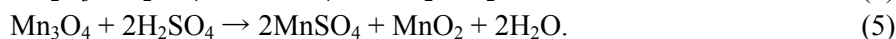
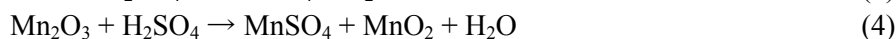
Fig. 2. E-pH diagrams for the Zn-H<sub>2</sub>O and Mn-H<sub>2</sub>O systems (Atlas of Eh-pH diagrams, 2005)

### 3. RESULTS AND DISCUSSION

The effect of four factors, i.e. H<sub>2</sub>SO<sub>4</sub> concentration, reaction time, temperature as well as solid to liquid ratio on metal leaching from the used up zinc carbon and zinc-manganese alkaline batteries was studied. Leaching of zinc and manganese as a function of time for two selected concentrations of sulfuric acid are shown in Figs 3a (2.0 mol dm<sup>-3</sup>) and 3b (0.2 mol dm<sup>-3</sup>). Taking into consideration that zinc occurs in batteries as a metal or metal oxide the following reactions can be written:



Manganese can be detected as MnO<sub>2</sub> and Mn<sub>2</sub>O<sub>3</sub> depending on a discharge level of the battery. The following leaching reaction are expected:



A relationship between metals leaching and sulfuric acid concentration at 20°C and after 1 hour of leaching is shown in Fig. 4. Leaching of zinc depended highly on the H<sub>2</sub>SO<sub>4</sub> concentration up to about 2.0 mol dm<sup>-3</sup>, but the leaching of manganese does not

depend so strongly on  $\text{H}_2\text{SO}_4$ . A further increase of acid concentration does not cause of leaching efficiency increase of metals. However, after 1 hour of leaching the percentage of leached zinc was slightly above 60% for alkaline and about 55% for zinc-carbon batteries. Leaching efficiency of manganese was always smaller than that for zinc. It is undoubtedly caused by the presence of  $\text{MnO}_2$  produced in reactions (4) and (5) which is insoluble in sulfuric acid solutions. The percentage of leached manganese does not exceed 20%.

The only way to increase the leaching efficiency is to increase the temperature of leaching process. The effect of temperature on the leaching efficiency of zinc and manganese was studied using 2M  $\text{H}_2\text{SO}_4$  and solid/liquid ratio equal to 100 at leaching time equal to 1 hour. The results are shown in Fig. 5.

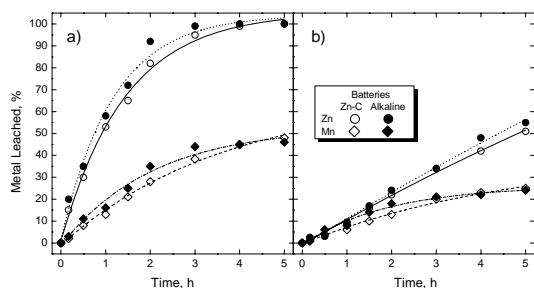


Fig. 3. Leaching efficiency of zinc and manganese in sulfuric acid solutions as a function of time.  $\text{H}_2\text{SO}_4$  concentration: 2.0 mol  $\text{dm}^{-3}$  (a) and 0.2 mol  $\text{dm}^{-3}$  (b), temperature: 20°C, solid/liquid ratio: 1:100

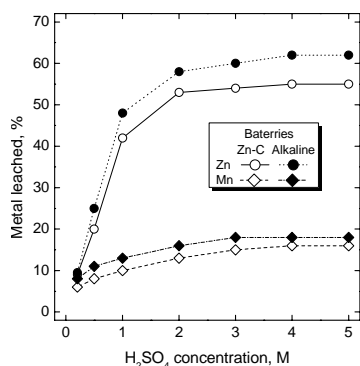


Fig. 4. Leaching efficiency of zinc and manganese as a function of sulfuric acid concentration. Temperature: 20°C, solid/liquid ratio: 1:100, process time: 1 hour

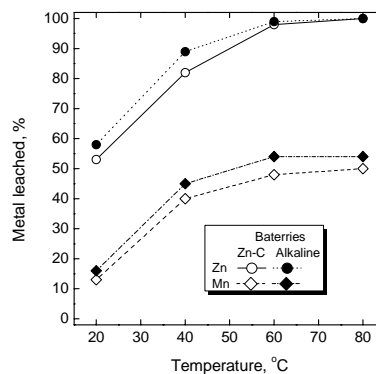


Fig. 5. Leaching efficiency of zinc and manganese as a function of process temperature.  $\text{H}_2\text{SO}_4$  concentration: 2.0 mol  $\text{dm}^{-3}$ , solid/liquid ratio: 1:100, process time: 1 hour

The results presented in Fig. 5 indicate that in the case of Zn-Mn batteries only about 55% of zinc and 16% of manganese can be leached at 20°C. In the same conditions the leaching efficiency for alkaline batteries were slightly higher and were

about 62% and 18% for zinc and manganese, respectively. The leaching efficiency of the both metals increased with increase in leaching temperature up to 60°C. Further increase in temperature did not show any significant increase in the recovery of zinc as well as manganese. At the temperature of 60°C all amount of zinc and zinc oxide was leached but only about 50% of manganese compounds were leached. This is because of the insoluble  $\text{MnO}_2$  presence of in sulfuric acid solutions.

The effect of solid/liquid ratio on the leaching efficiency of zinc (i.e. higher leached metal) was studied in the range of 1:20 to 1:200. The experimental conditions were 2.0 M  $\text{H}_2\text{SO}_4$ , and 60°C. The results of leaching are presented in Fig. 6 as the relationships between leaching efficiency and leaching time for fixed solid/liquid ratio. The results indicate that the leaching efficiency of zinc is similar for both type batteries and increases with increase of ratio of solid to liquid, i.e. from about 80% for 1:20 to 100% for 1:100 and 1:200.

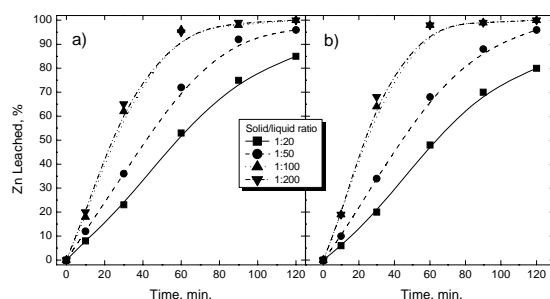


Fig. 6. Leaching efficiency of zinc in 2.0 M sulfuric acid solutions as a function of time and solid/liquid ratio for zinc-carbon (a) and zinc-manganese alkaline (b) spent batteries. Temperature of process: 60°C

Based on the above experimental results, the final optimum conditions for leaching process were determined to be 2.0 M sulfuric acid, a process temperature of 60°C and a solid to liquid ratio of 1:100. Under these conditions 100% of zinc and about 50% of manganese could be leached in the time of 1 hour.

#### 4. CONCLUSION

Due to a large amount of zinc-carbon and alkaline batteries selling every year they are a promising secondary source of zinc and manganese. This paper discusses and demonstrates the alternative use of leaching with sulfuric acid as Zn and Mn recovery process from batteries. The results of the examinations indicate that the method of leaching with sulfuric acid for an acid concentration of 2.0 M  $\text{H}_2\text{SO}_4$ , liquid/solid ratio of 1:100 and temperature of 60°C is suitable for recovering of almost 100% of Zn as the aqueous solution of  $\text{ZnSO}_4$ . However, in these conditions only about 50% of manganese could be transferred into solution, what is caused probably by the insoluble  $\text{MnO}_2$  formation during leaching process of manganese compounds. To solve this problem leaching with a moderate reductive agent (like glucose,  $\text{Cl}^-$  ions,  $\text{SO}_2$ , hydrogen peroxide etc.) can be used. This study will be a subject of next papers.

## REFERENCES

- Atlas of Eh-pH diagrams. Intercomparison of thermodynamic databases. Geological Survey of Japan Open File Report No.419. National Institute of Advanced Industrial Science and Technology, May 2005, available via [www.gsj.jp/GDB/openfile/files/no0419/openfile419e.pdf](http://www.gsj.jp/GDB/openfile/files/no0419/openfile419e.pdf)
- BARTOLOZZI, M., BRACCINI, G., BONVINI, S., MARCONI, P.F., 1995. Hydrometallurgical recovery process for nickel-cadmium spent batteries. *Journal of Power Sources* 55, 247-250.
- BERNARDES, A.M., ESPINOSA, D.C.R., TENÓRIO, J.A.S., 2004. Recycling of batteries: a review of current processes and technologies. *Journal of Power Sources* 130, 291-298.
- ESPINOSA, D.C.R., BERNARDES, A.M., TENÓRIO, J.A.S., 2004. An overview on the current processes for the recycling of batteries. *Journal of Power Sources* 135, 311-319.
- FRÖHLICH, S., SEWING, D., 1995. The BATENUS process for recycling mixed battery waste. *Journal of Power Sources* 57, 27-30.
- KOSARGA, E., WALKOWIAK, W., GEGA, J., 2006. Hydrometalurgiczne metody wydzielenia metali ze zużytych baterii i akumulatorów. *Przemysł Chemiczny* 85, 249-253.
- LINDEN, D., REDDY, T.B., 2001. *Handbook of Batteries* McGraw-Hill, New York, NY, USA.
- MARTIN, D., GARCIA, M.A., DIAZ, G., FALGUERAS, J., 2001. A new zinc solvent extraction application: Spent domestic batteries treatment plant. In: Cox, M., Hidalgo, M., Valiente, M. (Eds.), *International Solvent Extraction Conference (ISEC'99)*. Society of Chemical Industry (SCI), Barcelona, Spain, pp. 201-206.
- SALGADO, A.L., VELOSO, A.M.O., PEREIRA, D.D., GONTIJO, G.S., SALUM, A., MANSUR, M.B., 2003. Recovery of zinc and manganese from spent alkaline batteries by liquid-liquid extraction with Cyanex 272. *Journal of Power Sources* 115, 367-373.

**Gęga, J., Walkowiak, W.,** *Ługowanie cynku i manganu z zużytych baterii cynkowo-węglowych z użyciem roztworów kwasu siarkowego*, *Physicochem. Probl. Miner. Process.*, 46 (2011) 155-162, (w jęz. ang), <http://www.minproc.pwr.wroc.pl/journal>

Elektrochemiczne ogniwa cynkowo-węglowe oraz alkaliczne cynkowo-manganowe są obecnie najczęściej stosowanymi źródłami zasilania małowatowych urządzeń elektrycznych powszechnego użytku przede wszystkim z powodu korzystnego stosunku ceny do parametrów elektrycznych. Biorąc pod uwagę dużą ilość sprzedawanych corocznie ogniw tego rodzaju i stosunkowo krótki okres ich użytkowania mogą stanowić one znaczące wtórne źródło cynku i manganu oraz ich związków.

W prezentowanej pracy przedstawiono wyniki ługowania zużytych ogniw  $Zn-MnO_2$  za pomocą roztworów kwasu siarkowego(VI). Badano wpływ na efektywność ługowania takich parametrów, jak: stężenie kwasu, temperatura, czas prowadzenia procesu oraz stosunek fazy stałej do ciekłej (masa próbki poddawanej ługowaniu do objętości roztworu ługującego). Stężenie kwasu siarkowego(VI) zmieniano w zakresie od 0,2 do 5,0 M, a ługowanie prowadzono w czasie od 30 minut do 5 godzin. Temperatura procesu była zmieniana w zakresie od 20 do 80°C.

Stwierdzono, że stopień wyługowania cynku i manganu wzrasta ze wzrostem stężenia kwasu do wartości 2,0 M. W tych warunkach uzyskano całkowite wyługowanie cynku przy jednoczesnym ok. 50% wyługowaniu manganu. Szybkość ługowania cynku była większa od szybkości ługowania manganu a w obydwu przypadkach wzrost temperatury oraz zwiększanie stosunku fazy stałej do ciekłej powodowały zwiększenie szybkości ługowania.

*słowa kluczowe: zużyte baterie, cynk, mangan, ługowanie, kwas siarkowy(VI)*

Ashraf M. AMER\*

## KINETICS OF HYDROMETALLURGICAL EXTRACTION OF SULFUR FROM EGYPTIAN EL-MAGHARA COAL DEPOSITS

*Received December 15, 2009; reviewed; accepted July 19, 2010*

Tests were carried out to determine pyrite dissolution, present in coal, in aqueous sulfuric acid and oxygen as an oxidant. The main objective is the evaluation of oxidative treatment in acidic media focused on the elimination of pyrite from coal. The influence of several parameters such as temperature, acid, and oxygen pressure concentrations were investigated. It was found that the dissolution curves for pyritic sulfur follow the kinetic model of the shrinking core model, with diffusion through the solid product of the reaction as the controlling stage. Additional tests show a preferential release of iron from pyrite leaving a “polysulfide” or “metal deficient” layer. Results also indicate that in aqueous solutions of 0.5 M of H<sub>2</sub>SO<sub>4</sub> at 150°C and with increase in the oxygen pressure, pyrite dissolution increases around 50%.

*keywords: kinetics, extraction, sulfur, coal, Egypt*

### 1. INTRODUCTION

Coal is a complex and heterogeneous material incorporating a variety of minerals in different forms, where silicates and carbonates constitute the major ash-forming minerals. The principal sulfur-bearing minerals in coal are pyrite and marcasite. Other sulfide minerals, elemental sulfur and calcium as well as iron sulfates are found as minor constituents, while a considerable portion of the sulfur content may be organic in the form of alkyl and aryl thiols. Organic sulfur level ranges commonly from about

---

\*Environmental Science Dept., Faculty of Science, Alexandria Univ., ashrafamer0408@yahoo.com

0.3 to 2.0%, whereas the pyritic sulfur content may be from about 0.8 to 6%. Pyrite may be present in a wide variety of forms ranging from large grains to micron size crystallites (Wheelock and Markuszewski, 1981). When coal is burned, various sulfur forms are converted to gaseous oxides which are emitted to the atmosphere. Sulfur oxides upon reacting with atmospheric water form sulfuric acid which eventually causes acid rain. Coal is also used in the manufacture of steel, where the presence of high sulfur content is also deleterious in steel making. Therefore, coal desulfurization is important for protection of the environment and for producing metallurgical quality coals.

The conventional coal cleaning techniques are usually used for removal of coarsely liberated pyritic sulfur. However, since pyrite in most coals exists in fine sizes, advanced coal cleaning technology is required to effectively separate pyritic sulfur from coal. Removal of sulfur and ash by coal preparation methods is more economical than removing the ash and sulfur from boiler products. Desulfurization of coal is carried out through chemical processing using different leachants (iron and copper sulfate) and oxidizing agents such as  $H_2O_2$  and  $O_2$  (Mixon and Vermeulen 1981; Prasassarakich and Pecharanond, 1992; Yaman et al., 1995; Prayuenyong, 2002). Flotation and microbial beneficiation have been considered the most potential techniques for desulfurizing coal (Nikitin et al., 1981; Mistrik et al., 1982; Petukhov et al., 1988; Ichinose et al., 1988; Sen et al., 1991; Setfanova et al., 1991; Choudhry and Aplan, 1992; Dogan and Celedk; 1992). Both flotation and microbial beneficiation partially separate pyritic sulfur from coal, while organic sulfur, which is chemically bound to the organic structure, can be removed only through chemical reaction. Additional problems of separation by flotation result from similarity in the surface properties of unweathered coal and fresh coal pyrite. An efficient sulfur removal is difficult to be reached since both materials are hydrophobic. Chemical desulfurization is a promising technique for removal of both inorganic and organic sulfur. In this investigation desulfurization of Maghara coal is achieved through leaching with diluted sulfuric acid under oxygen pressure to convert pyrite into water-soluble sulfate form. The effect of temperature, sulfuric acid concentration, and oxygen partial pressure upon leaching of pyritic sulfur as well as kinetics of the leaching process have been studied.

## 2. EXPERIMENTAL

### 2.1. MATERIALS AND APARATUS

Maghara coal deposits are considered as the largest and the only economical coal deposits in Egypt (Al Far, 1966; Adindani, 1970; Nakhala, 1990; Said, 1991). The average results of proximate analysis on the dry basis of the studied representative coal samples are given in Table 1.

Table 1. Average results of proximate analysis on dry basis in wt. percent of studied coal samples

Constituents	Proximate chemical analysis wt. %
Volatiles	53.80
Ash	9.20
Fixed carbon	36.00
Calculated	100.00

Table 1 indicates that the Maghara coal is of a high-volatile bituminous rank with low to medium grade.

All pressure oxidation tests were conducted in a 2 dm<sup>3</sup> autoclave with titanium internal parts to resist acid corrosion. The experimental setup and procedure were similar to those described previously (Papangelakis et al., 1991; Amer, 2001). The acidity was fixed at 0.5 M H<sub>2</sub>SO<sub>4</sub> throughout the experiments and the temperature range investigated was from 120 to 160°C. The partial pressures of O<sub>2</sub> varied from 0.5 to 2.0 MPa. Pyrite dissolution was followed by iron analysis with atomic absorption spectrophotometer. For the calculation of the pyrite conversion, correction factors were applied to account for the volume and mass losses due to sampling, so the following formula was used:

$$X = \frac{(C_1 V_1 + A_1) 10^{-6} \cdot M_{\text{FeS}_2}}{m \cdot M_{\text{Fe}}} \quad (1)$$

where  $X$  denotes conversion of FeS<sub>2</sub>,  $C_1$  iron concentration (kg m<sup>-3</sup>),  $V_1$  volume of leaching solution prior to its sampling (m<sup>3</sup>),  $A_1$  total amount of iron withdrawn with previous samples (kg),  $M_{\text{FeS}_2}$  molecular mass of pyrite (g mol<sup>-1</sup>),  $M_{\text{Fe}}$  molecular mass of iron (g mol<sup>-1</sup>),  $M$  mass of charged coal (kg).

### 3. RESULT AND DISCUSSION

#### 3.1. PETROGRAPHIC STUDY

A petrographic examination of the polished section of the studied coal samples revealed the following:

- Maghara coal samples are rich in liptinite maceral group mainly in the form of thick and/or thin walled cuticles. Pyrite grains are well observed by its yellowish colour and isotropism as euhedral to subhedral crystals and/or aggregate of fine grained framboidal pyrite associated with coal forming microlithotypes,
- study of ash by transmitted light revealed that iron oxides, mainly in the form of reddish to brownish hematite, are observed as fine to coarse grains.

### 3.2. X-RAY DIFFRACTION STUDY

From X-ray diffraction of the Maghara coal ash (Fig. 1) it is evident that the diagnostic peaks of hematite at "d" values 0.269 nm and 0.252 nm have maximum intensities. This ascertains a high percentage of pyrite in the Maghara coal. It is worth to mention that the presence of hematite in the Maghara coal ash is due to mainly complete combustion of pyrite associated with its coal forming lithotyes (Gaigher, 1983).

### 3.3. INFRA-RED SPECTRAL ANALYSIS

The infra-red (IR) absorption spectrum is a useful and quick method that can be used for analysis of most organic compounds, including coal and kerogen-rich shales. The interpretation of IR spectra (Griddle et al., 1980), displayed in Fig. 2, has revealed the following results:

- organic groups comprise free (OH) at  $3660-3420\text{ cm}^{-1}$ , H-bonded (OH) at  $3530-3480\text{ cm}^{-1}$ ,
- inorganic ions include the groups of silicates mainly as kaolinite at  $1050-1035\text{ cm}^{-1}$  and  $930\text{ cm}^{-1}$ , carbonates, such as calcite or dolomite, at  $1460-1445\text{ cm}^{-1}$ ,  $790\text{ cm}^{-1}$  and  $690\text{ cm}^{-1}$ , and oxides in the form of hematite at  $530\text{ cm}^{-1}$ , and quartz at  $465\text{ cm}^{-1}$ .

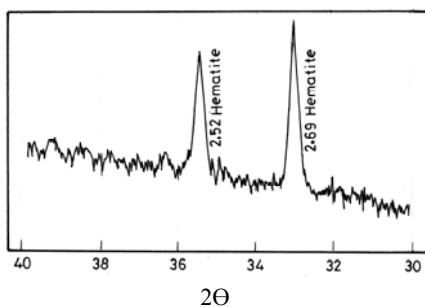


Fig. 1. X-ray diffraction of studied coal ashes showing characteristic hematite peaks

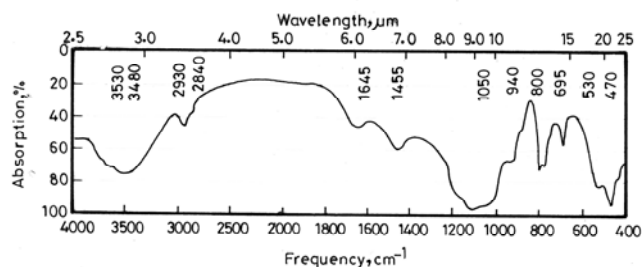
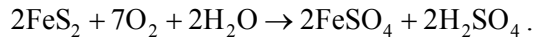
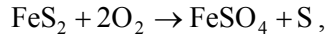


Fig. 2. Infrared absorption spectra of Maghara coals

3.4. PRESSURE OXIDATION OF PYRITE

The oxidation of pyrite may be represented by two main reactions:



An examination was made to study the effect of the following variables on the kinetics of oxidation of pyrite present in studied coal and on the distribution of products: temperature 120-160°C, oxygen partial pressure 0.5-2.0 MPa, initial acid concentration 0.1-0.6 M, pulp density 2-8% solids.

3.5. EFFECT OF TEMPERATURE

Rate for oxidation experiments at temperature from 120-160°C are shown in Fig. 3. The temperature coefficient of the rate corresponds to an activation energy of 55.9 kJ/mol. This value is consistent with 46.2 9 kJ/mol determined by Mckey and Halpern (1958) for the rate of oxidation of pyrite. The rate law for the oxidation of pyrite can be represented by

$$\frac{-d[\text{FeS}_2]}{dt} = K \cdot A_{\text{FeS}_2} \cdot P_{\text{O}_2} , \tag{1}$$

where  $[\text{FeS}_2]$  is the concentration of pyrite ( $\text{kg m}^{-3}$ ),  $A_{\text{FeS}_2}$  surface area of coal ( $\text{m}^2$ ),  $P_{\text{O}_2}$  oxygen partial pressure in MPa.

The experimental data lead to the following expression for  $k$

$$k = 0.125 \exp[-13.300/RT] . \tag{2}$$

Varying temperature has a marked effect on the distribution of sulfur oxidation products. With increasing temperature the formation of sulfuric acid was favored at the expense of elemental sulfur.

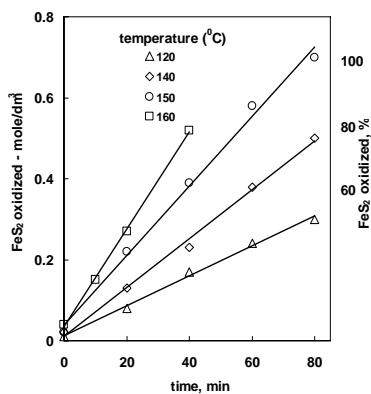


Fig. 3. Oxidation of coal pyrite in 0.5 M H<sub>2</sub>SO<sub>4</sub> at 1 MPa of O<sub>2</sub> at various temperatures

## 3.6. EFFECT OF OXYGEN PARTIAL PRESSURE

Rate plots of a series of experiments in which the oxygen partial pressure was varied from 0.5 to 2.0 MPa are shown in Fig. 4. The slopes of these plots were found to be directly proportional to the oxygen partial pressure (Fig. 5).

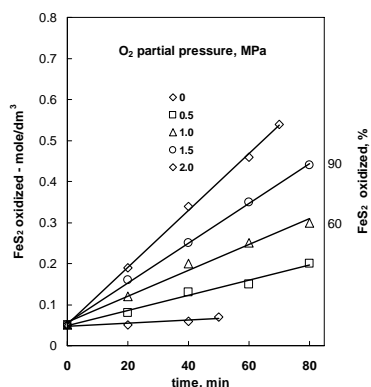


Fig. 4. Oxidation of coal pyrite at 0.5 M  $\text{H}_2\text{SO}_4$ , 150°C at various  $\text{O}_2$  pressure partial pressure

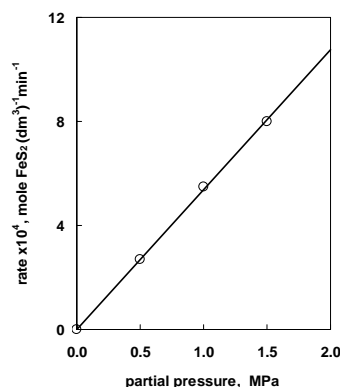


Fig. 5. Dependence of oxidation rate of coal pyrite at 150°C on  $\text{O}_2$  pressure

## 3.7. EFFECT OF INITIAL ACID CONCENTRATION

The results of experiments made with solutions containing different initial concentrations of  $\text{H}_2\text{SO}_4$  ranging from 0 to 0.6 M are shown in Fig. 6. The most marked effect of this variation is on the distribution of sulfur products. With increasing acid concentration all sulfur in the pyrite and organic forms is oxidized to sulfate, which appears as ferrous and ferric sulfates and sulfuric acid.

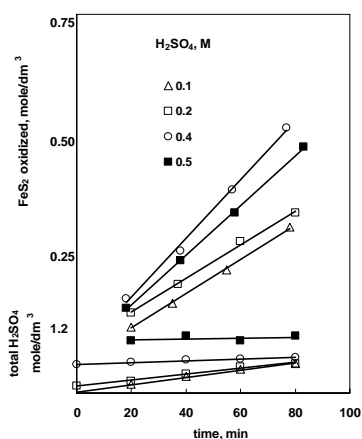


Fig. 6. Effect of initial  $\text{H}_2\text{SO}_4$  concentration on oxidation of coal pyrite at 150°C and 1 MPa of  $\text{O}_2$

3.8. EFFECT OF SURFACE AREA AND PULP DENSITY

The effect of specific surface area and pulp density of the studied coal are shown by the linear rate plots in Figs. 7 and 8. The rate of the reaction between pyrite present in coal with  $H_2SO_4$  in the presence of oxygen appears to be determined by heterogeneous process on the pyrite surface. The distribution of sulfur oxidation products appears to be substantially the same for all the experiments. On the other hand the Fe(III) to Fe(II) ratio is independent of the specific surface area of coal and increases with the pulp density used. This can be explained by the fact that the rate of oxidation of Fe(II) to Fe(III) is of second order. Thus, higher coal concentration favor the formation of Fe(III). It might be expected that the resulting reduction in the size of the coal particles would be accompanied by an increase in surface area which would lead to progressive reduction in the rate as the reaction proceeded. The simplest explanation of this is that leaching is accompanied by an increase in surface roughness which compensates for the reduction in surface area. Microscopic examination of some pyrite crystals present in coal subjected to desulfurization revealed degree of surface etching which provides a support for this interpretation.

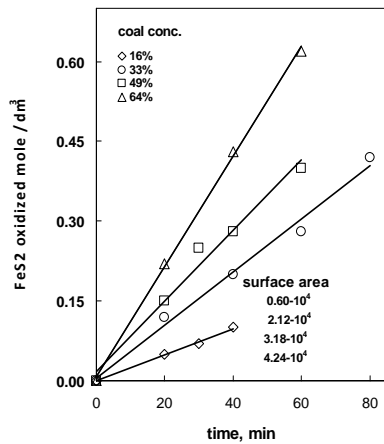


Fig. 7. Effect of pulp density and surface area on oxidation vs. leaching time of coal pyrite at 0.5 M  $H_2SO_4$ , 150°C and 1 MPa of  $O_2$

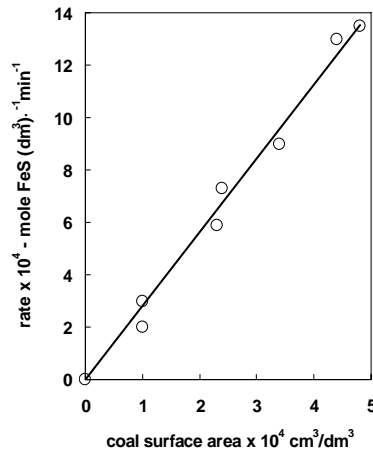
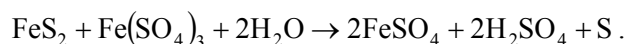


Fig. 8. Dependence of rate of oxidation at 150°C and 1 MPa of  $O_2$  on coal surface area

3.9. EFFECT OF ADDITION OF Fe(II) AND Fe(III) SULFATES

Since ferrous and ferric sulfate accumulate in the solution during leaching of pyrite, it was considered to examine their possible effect on the reaction. It is seen that after leaching time of about 50 min Fe(II) was completely reduced while some  $FeS_2$  was oxidized and leached. The reaction involved in oxidation of pyrite by ferric

sulfate is presumably represented by:



It might be expected that addition of  $\text{FeSO}_4$  or  $\text{Fe}(\text{SO}_4)_3$  to the solution accelerates oxidation of pyrite by  $\text{O}_2$ .

### 3.10. EFFECT OF COPPER SULPHATE

An addition of copper sulfate to the leaching solution was found to have very little effect on the rate of pyrite oxidation and on the distribution of the sulfur oxidation products. However, a definite trend could be noted in direction of an increased Fe(III) to Fe(II) ratio as the  $\text{CuSO}_4$  concentration is increased (Fig. 9). It is also of interest to note that  $\text{CuSO}_4$  does not catalyze the direct oxidation of  $\text{FeS}_2$  by  $\text{O}_2$ . It previously had been suggested that such catalysis might result from the mechanism involving the replacement of  $\text{CuSO}_4$  by  $\text{FeS}_2$  as follows:

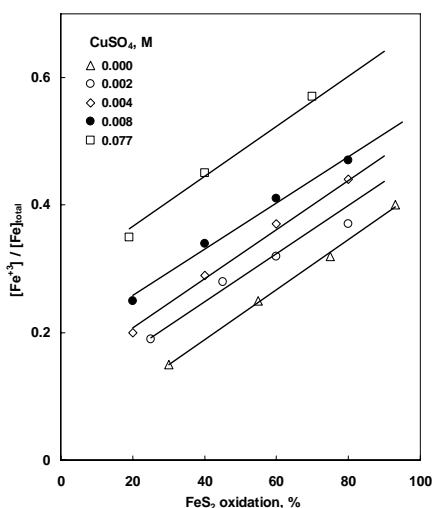
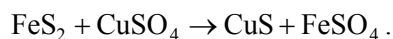


Fig. 9. Effect of  $\text{CuSO}_4$  on  $\text{FeS}_2$  oxidation at 0.5 M  $\text{H}_2\text{SO}_4$ , 150°C and 1 MPa of  $\text{O}_2$  partial pressure

### 3. CONCLUSIONS

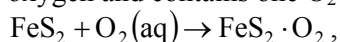
A number of conclusions concerning the mechanism of the Maghara coal desulfurization may be derived from the foregoing results:

- rate-determining step in the oxidation of pyritic sulfur is apparently a heterogeneous process on the pyrite surface,
- desulfurization of coal increases with increasing temperature and oxygen partial pressure where 96% of sulfur present in coal is removed at 150°C in 0.5 M after

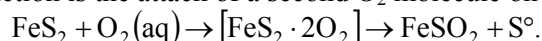
60 min of leaching,

- a plausible mechanism for coal desulfurization is consistent with the observed kinetics, and might involve a sequence of steps:

1) fast, O<sub>2</sub> is chemisorbed rapidly on the pyrite surface which is always covered by a monolayer of oxygen and contains one O<sub>2</sub> molecule at each FeS<sub>2</sub> site



2) slow, the reaction is the attack of a second O<sub>2</sub> molecule on an O<sub>2</sub> covered site



#### REFERENCES

- ADINDANI, A., SHAKOV, R.A., 1970, *The occurrences of coal and some geological features of the Mesozoic and Paleozoic sediments in Egypt*, Geol. Surv. Egypt. September, 67-86.
- AL-FAR, D.M., 1966, *Geology and coal deposits of Gabal El Maghara Northern Sinai*, G.S.E. Cairo, paper 37, 59.
- Amer, A.M.; (2001); *Kinetics of acid Pressure Leaching of Mechanically Activated Cassiterite Concentrate*, ERZMETALL, 54, No. 9, 446-49.
- CHOUHRY, V, APLAN, F.F., 1992, *Pyrite depression during coal flotation*, Aust. Miner. Metall. Process. 9(2), 51-6.
- DOGAN, M.Z., CELEDK, M.S., 1992, *Latest developments in coal desulfurization by flotation and microbial beneficiation*, 3rd Mining, Petroleum and Metallurgy Conf. 2-4, Feb 1992, Cairo, Vol. I, 385-393.
- GAIGHER, J.L., 1983, *Quantitative X-ray diffraction for the determination of minerals in South African coal production samples*, Proc. 1st Cong. App. Mineralogy, p. 163-168.
- GRIDDLE, W.L., ELLIS, G.P., 1980, *Spectral and chemical characteristics of organic compounds*, 2<sup>nd</sup> ed. John Wiley, John Wiley, N.Y., 1980, p. 115.
- ICHINOSE, T., SHOJIMA, T., SATO, S., NAKAMURA, A, 1998, *Flotation of fine coal powders*. J. (1988) JPN. 63, 104, 668.
- MCKAY, D.R., HALPERN, J., 1958, *A kinetic study of the oxidation of pyrite in aqueous suspension*. Trans. Met. Soc. AIME, 6, 301-8.
- MISTRİK, E.J., HREBACKA, J., VİCHA, V., 1982, *Flotation of coal, ores and minerals*, Pol. Pat. 109, 239,
- MIXON, D.A., VERMEULEN, T., 1981, *Oxydesulfurization of coal by acidic iron sulfate*. Energy Res 6(23).
- NAKHLA, F.M., 1990, *Utilization of Maghara coal for energy development and metallurgical*, Coke Energy Research Center, Fac-Eng. Cario Univ., 9, p. 159.
- NIKITIN, I.N., PREOBRAZHENSKII, B.P., LYODOV, V.V., 1981, *Improvements in methods for the bonification of coal sludges*. Ugol' Ukr. (USSR), 3,44-5.
- PAPANGELAKIS, V.G., DEMOPOULOS, G.P., 1991, *Acid pressure oxidation of pyrite: reaction kinetics*, Hydrometallurgy. 26, 309-325
- PETUKHOV, V.N., MUSAVIROV, R.S., NADOGREI, E.P., ZHURKINA, I.P., AKSEENOVA, M.G., 1988, *Methods of flotation of coal*, Russian. Pat. 1, 391, 712.
- PRASASSARAKICH, P., PECHARANOND, P, 1992, *Kinetics of coal desulfurization in aqueous copper (II) sulfate*. Fuel 71(8), 929- 933.
- PRAYUENYONG, P., 2002, *Coal biodesulfurization processes*. Songklanakarin J. Sci. Technol., 24(3), 493-507.

- SAID, R., , 1990: *Geology of Egypt*, First Edition, . Balkema: Rotterdam,
- SEN, K., CHAKRABORTY, D.K., ROY, S.K., Ghose, E ; 1991, *Developments in fine coal flotation for future*. Fuel Sci. Technol, 10(1-2) S.1991, 35-8.
- STEFANVOVA, V., GENEVSK, T., STEFANOV, B., BAKARDZHIEV, N, 1991, *Technological aspects of coal flotation waste utilization in flash smelting*, Erz Metal 44(11) P.1991, 538-41.
- WHEELLOCK, T.D., MARKUSZEWSKI, R., 1991, *Chemistry and physics of coal utilization*, Ed. Coer, B.R. and Petrakis, L., American Inst. of Physics, New York, R.,1991 p357-387.
- YAMAN, S., MERICBOYU, A.E., KUCUKBAYRAK, S., 1995, Chemical coal desulfurization research in Turkey. Fuel Science and Technology International, 13(1), research in Turkey. Fuel Science and Technology International, 13(1), 49-58.

**Amer, A.M.**, *Kinetyka hydrometalurycznej ekstrakcji siarki z węgla pochodzącego ze złoża El-Maghara w Egipcie*, Physicochem. Probl. Miner. Process., 46 (2011) 163-172, (w jęz. ang), <http://www.minproc.pwr.wroc.pl/journal>

Przeprowadzono badania w celu określenia rozpuszczalności pirytu obecnego w węglu. Roztworzenie prowadzono za pomocą kwasu siarkowego oraz tlenu jako utleniacza. Głównym celem badań była ocena procesu utleniania pirytu w roztworach kwaśnych w celu usunięcia go z węgla. Badano wpływ temperatury oraz stężenia kwasu, a także ciśnienia tlenu. Stwierdzono, że rozpuszczanie siarki pirytowej zachodzi według modelu "shrinking core" z dyfuzją przez ciało stałe jako reakcją kontrolującą. Dodatkowe badania wykazały, że uprzywilejowane uwalnianie się jonów żelaza z pirytu pozostawia warstwę polysiarczku lub warstwę zubożonej w metal. Otrzymane wyniki wskazują, że w wodnych roztworach 0.5 M H<sub>2</sub>SO<sub>4</sub> w temperaturze 160°C i ze wzrostem ciśnienia tlenu rozpuszczanie pirytu wzrasta około 50%, oraz że zachodzi "degradacja" tlenu z powodu obecności jonów żelaza w strukturze węgla.

*słowa kluczowe: kinetyka, ekstrakcja, siarka, węgiel, Egipt*

Vahid SOLTANMOHAMMADI\*, Mohammad NOAPARAST\*\*, Amir Hossein KOHSARI\*\*, Farshid ZAMANI\*\*\*

## INFLUENCE OF FLOTATION PARAMETERS ON DECREASING SULFUR AND PHOSPHORUS CONTENT IN THE GOL-e-GOHAR IRON ORE CONCENTRATE

*Received April 30, 2010; reviewed; accepted July 21, 2010*

Gol-e-Gohar iron complex, one the largest iron concentrate producer, is located in the Kerman Province in Iran. The ore suffers from elevated S and P content equal to 0.5% S and 0.08% P, respectively, while the steel industrial permitted limit is 0.1% S and 0.05% P. The main source of S and P are pyrite and apatite. In this work it was attempted to decrease the S and P content in concentrate using reversed flotation with xanthates, in which pyrite floated while fine apatite particles were entrained with water. The liberation degree for pyrite in the -75+53  $\mu\text{m}$  size fraction was 65%. The influence of such parameters as type and dose of collector, frother and depressant, solid content, pH, impeller speed, frothing time, conditioning time and desliming, on S and P removal were investigated. The best results were achieved with desliming. The collector, frother and dispersant doses were 50g/Mg of KAX, 60g/Mg of MIBC and 200g/Mg of sodium silicate at pulp pH=8 and 6 minutes of conditioning time. Under best conditions, with desliming, a concentrate with acceptable grades of Fe (70.24%), S (0.041%), and P (0.043%) were obtained. The recovery of Fe was 95.11% while sulfur removal 92.24%. The effect of different size fractions and two-stage flotation were also studied. The result showed that in +45  $\mu\text{m}$  and also -38  $\mu\text{m}$  size fractions, S and P contents were below or near the permitted limit. It was postulated that +45  $\mu\text{m}$  size fraction was the most convenient for flotation while -38  $\mu\text{m}$  was the best for removal with water flow. With 100 g/Mg of KAX and one-stage flotation, S content was 0.191% while in two-stage flotation it was reduced to 0.097%.

*keywords: iron ore, Gol-e-Gohar concentrator, sulfur removal, phosphorus removal*

\* Mining Engineering Department, Yazd University, Yazd, Iran

\*\* School of Mining Engineering, Un. College of Eng., University of Tehran, noparast@ut.ac.ir.

\*\*\* Head of R&D Division, Gol-E-Gohar iron ore concentrator, Sirjan

## 1. INTRODUCTION

Gol-e-Gohar iron ore complex (Kerman Province, Iran) is one the largest iron concentrate producers and is located 50 km southwest of the Sirjan City. The complex with about 1200 Tg (teragrams) reserves of iron ores provides production of 5 Tg/year of concentrates. The Gol-e-Gohar iron ore concentrate suffers from high content of S (0.5%) and to some extent P (0.08%), which are higher than permitted limit of 0.1% S and 0.05% P (Svoboda, 2004). Therefore, it is very important to remove and/or decrease the sulfur and phosphorus contents from the Gol-e-Gohar concentrate. In this work concentrate samples from this plant were processed to find out the optimum conditions for eliminating S and P.

Pyrite is the main source of sulfur. There are usually three types of pyrites: a) separated from magnetite, b) associated with magnetite, and c) inclusion in magnetite. Phosphorus is normally observed as apatite in fractions finer than 20  $\mu\text{m}$  (Jafarzadeh et al., 1995). Floatability of pyrite is fair and micro-particles of apatite follow water flow. Therefore, to decrease S and P content in the Gol-e-Gohar concentrate a reverse flotation was implemented.

In this work different experiments were performed to achieve optimum values of various parameters involved in flotation including consumption of collector, frother and depressant, pulp solids content, pH, conditioning and flotation times. The role of desliming in sulfur and phosphorus removal was also studied.

## 2. MINERALOGICAL STUDIES

Mineralogical studies were carried out prior to processing. To do this X-ray diffraction (XRD) analysis and polished and thin sections were employed. Elemental studies indicated the presence of Fe, S, P and iron oxides. Contents of iron and iron oxides were analyzed by titration and the X-ray fluorescence (XRF) analysis. The results obtained from XRD showed that magnetite is the main phase and hematite as well as goethite were present also in the sample, but not as much as magnetite. Calcite, pyrite and chlorite were the other minerals. Thin and polished sections studies showed that the main minerals were magnetite and hematite with small amounts of goethite, chlorite, pyrite, calcite, quartz and apatite, chalcopyrite and pyrrhotite.

Pyrite was observed as separated from magnetite, associated with magnetite, and inclusions in magnetite. In some cases, because of alteration, pyrite was converted to goethite. Chalcopyrite and pyrrhotite contents were very low and they occurred as inclusion in magnetite. Figure 1 shows contacts between pyrite and magnetite while Fig. 2 illustrates inclusion of pyrrhotite in magnetite. To determine minerals liberation size and comminution size (grinding limit), the liberation degree of minerals were

measured in size fractions of -150+75 and -75+53  $\mu\text{m}$  (Table 1). There can be seen that in the size fraction of -75+53  $\mu\text{m}$  65% of pyrite was liberated. Therefore, this size (av. 68 micrometers) was considered as the grinding limit ( $d_{80}$  of grinding product). Although in size fraction of -53+45  $\mu\text{m}$ , about 80% of magnetite was liberated, but this size was too fine to be considered as grinding size and would produce significant amount of slimes.

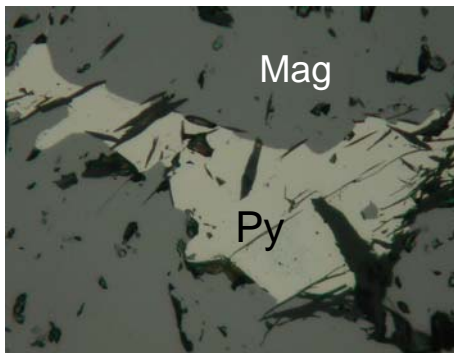


Fig. 1. Pyrite (Py) and magnetite (Mag) contact

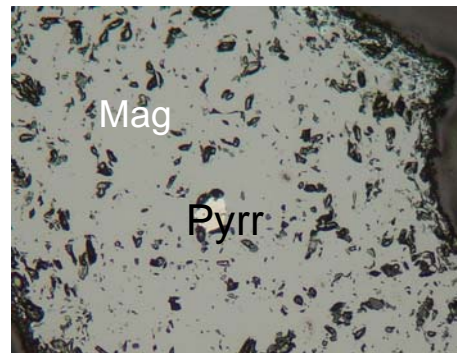


Fig. 2. Pyrrhotite (Pyrr) inclusions in magnetite (Mag)

Table 1. Liberation studies results

Minerals	-150+75 $\mu\text{m}$	-75+53 $\mu\text{m}$
Magnetite-hematite-goethite	80.5%	-
Pyrite	38.8%	65%
Calcite	40.0%	63%

### 3. ELEMENTAL ANALYSIS

Elemental analyses were applied on two samples: i) to have the feed contents, and ii) size fractions distribution. Results obtained for the feed content showed 67.75% Fe, 17.8% FeO, 0.5% S, and 0.08% P. The contents of S and P were higher than acceptable values of 0.1% S and 0.05% P. For elemental analysis in various size fractions about 250 g samples were screened from -150+106 down to -38  $\mu\text{m}$ , and then mass retained in each size fraction was analyzed for Fe, S, and P. Figures 3-5 present changes of Fe, S and P contents in different size fractions.

According to Fig. 3, the lowest Fe content, referred to ranges finer than 38  $\mu\text{m}$ , and the higher ones were those of size ranges of 53 to 90  $\mu\text{m}$ . In addition, the lowest content of S is for the size range over 106  $\mu\text{m}$  (Fig. 4). It should be noted that the content of S was increasing with the decreasing size. According to Fig. 5, the

maximum content of P was in size fractions finer than 38  $\mu\text{m}$  and the lowest in -90+75  $\mu\text{m}$ .

#### 4. SAMPLE PREPARATION

The weight of initial sample of the Gol-e-Gohar concentrate was about 60 kg. Then, 57 of one-kilogram samples were prepared by sequential rifling approach. One of the representative samples was divided into halves. One of these 500 g samples was then screened. Figure 6 shows the size distribution of a sample which  $d_{80}$  was less than 400  $\mu\text{m}$ , and 60% of particles were finer than 200  $\mu\text{m}$ . It can be observed that 30% of sample was finer than 90  $\mu\text{m}$ .

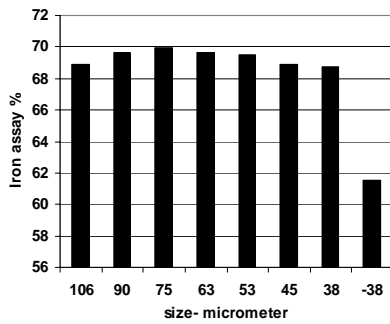


Fig. 3. Variation of Fe content versus size

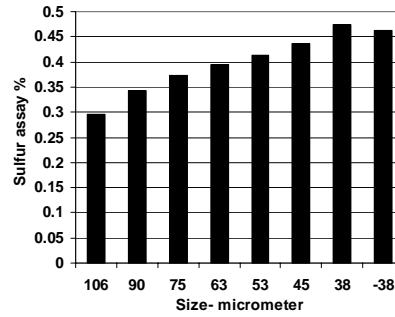


Fig. 4. Variation of S content versus size

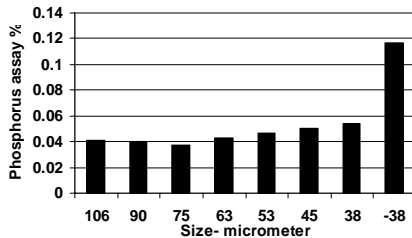


Fig. 5. Variation of P content versus size

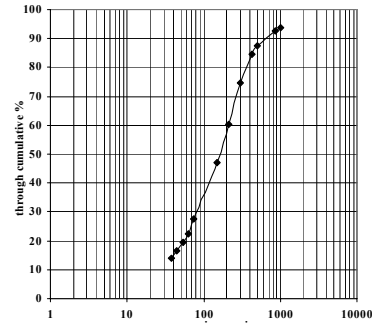


Fig. 6. Size distribution of head sample

#### 5. SIZE REDUCTION PROCESS

The target of size reduction was firstly to liberate valuable minerals from the gangue, and then determination of the best size distribution for concentration. Therefore, four tests were performed in a wet rod milling. Table 2 presents the

specification of used rod mill, in which the grinding times were 5, 10, 15, and 20 minutes. The results of these tests are illustrated in Fig. 7. Wet rod milling was applied for two reasons: i) lower slime production, ii) wet character of flotation.

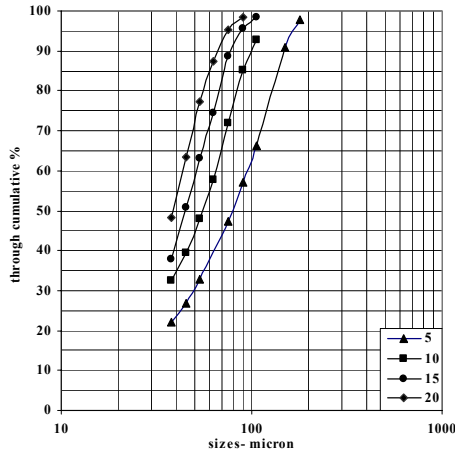


Fig. 7. Size distribution of grinding products

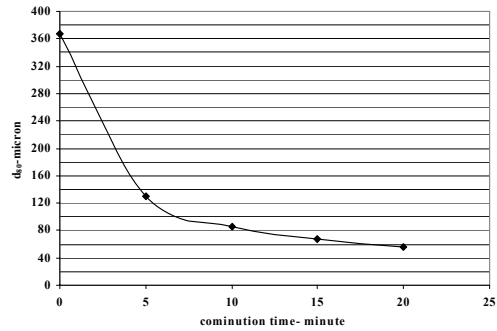


Fig. 8.  $d_{80}$  values of grinding products

As it is observed in Fig. 7, after 5, 10, 15, and 20 minutes of grinding, the  $d_{80}$  values of products were 130, 86, 68 and 56  $\mu\text{m}$ , respectively. Figure 8 shows a diagram with  $d_{80}$  values of the products versus different grinding times.

Thus, the pyrite liberation size is  $-75+53 \mu\text{m}$  (av. 68  $\mu\text{m}$ ) and 15 min was selected as the optimum grinding time while the pulp solid percent in grinding 50%.

Table 2. The specification of used rod mill

Mill		Rods		
D-L, mm	rpm (65% of Cs)	Rod No.	D-L, mm	W, g
200-250	61	18	24-245	15710

## 6. FLOTATION EXPERIMENTS

Pyrite is the main source of sulfur in the magnetic concentrate of Gol-e-Gohar iron ores. In the presence of oxygen, xanthates combine with pyrite and forms dixanthogen making pyrite floatable (Rao, 2003). Due to this fact and low content of pyrite in comparison with oxide iron minerals, the reverse flotation approach was implemented for pyrite, to decrease the sulfur contents in the Gol-e-Gohar concentrate. Because of the presence of apatite in fine sizes, reverse flotation of pyrite could decrease P content as well. In this paper selection of optimum flotation conditions were based on

concentrate quality and sulfur removal. In some cases, obtained contents and recoveries did not yield desired values, therefore a separation efficiency index was implemented (Wills and Napier-Munn, 2006).

## 7. REAGENTS SELECTION

In reverse flotation of pyrite, various reagents such as collector, frother and depressant can be used. Among sulphhydryl anionic collectors, which are common in beneficiation of sulfides (Wills and Napier-Munn, 2006), xanthates are most suitable for pyrite flotation because of their collecting power, wide range of flotation pH and low cost (Vijayendra, 1995). In the experiments three xanthates: potassium amyl (KAX), sodium ethyl (NaEX) and sodium isopropyl ( $Z_{11}$ ) xanthates were utilized. In addition, two different frothers: pine oil and methyl isobuthyl carbinol (MIBC) were considered and the latter was selected for experiments due to its higher solubility, greater stability, better purity and economics (Vijayendra, 1995). Sodium silicate was used as a depressant of oxide minerals and slimes (Parekh and Miller, 1999; Bulatovic, 2007). The initial conditions of reverse flotation are presented in Table 3.

Table 3. Initial conditions of reverse flotation

Comminution time, min	15
Collector doze, g/Mg	200
MIBC, g/Mg	200
$Na_2SiO_3$ , g/Mg	500
Conditioning time, minute	6
Frothing time, minute	3
pH	7
Solid content, %	20
Speed, rpm	1500

## 8. TYPE AND DOZE OF COLLECTOR

To investigate the effect of type and doze of collector in decreasing of S content, KAX, NaEX, and  $Z_{11}$  collectors were used in the doze of 50, 100, 150, 200 and 250 g/Mg. The obtained results are presented in Table 4. They indicate that the iron content is in the range of 68-69% with 99% of recovery. The content of S was 0.15%. Under best conditions with 50g/Mg of KAX, 70% of S rejection was achieved. The content of S was higher than the permitted limit of 0.1%, and therefore, to reach this level, other conditions had to be adjusted.

In all the tests the content of P was higher than permitted limit of 0.05%. In comparison with other xanthates, influence of KAX on decreasing P content was more

distinctive. Due to a high sulfur removal 50 g/Mg of KAX was selected as the best dose. Figures 9-10 illustrate S content and removal vs. collector consumption.

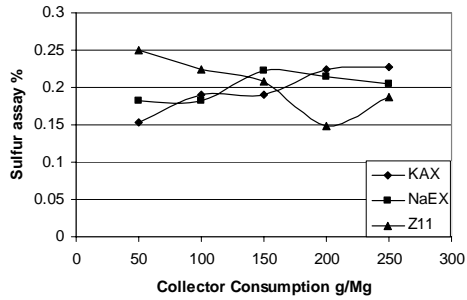


Fig. 9. Effect of collector doze on S content

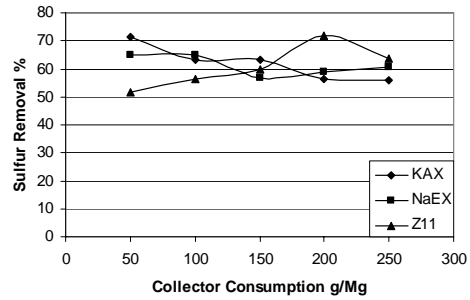


Fig. 10. Effect of collector doze on S removal

Table 4. Results of flotation tests with KAX, NaEX and Z<sub>11</sub>

Collector	Consumption, g/Mg	Concentrate content, %			Iron recovery, %	Sulfur removal, %
		Fe	S	P		
KAX	50	68.24	0.153	0.070	99.5	70.4
	100	68.03	0.191	0.070	99.7	63.1
	150	68.65	0.190	0.065	99.1	63.4
	200	68.97	0.225	0.070	99.0	56.3
	250	68.94	0.227	0.070	98.9	55.8
NaEX	50	68.35	0.183	0.070	99.4	64.8
	100	68.05	0.182	0.068	99.6	65.0
	150	67.85	0.223	0.075	99.9	56.7
	200	68.78	0.214	0.073	99.2	58.7
	250	68.45	0.205	0.073	99.4	60.8
Z <sub>11</sub>	50	68.72	0.250	0.073	99.0	51.8
	100	68.12	0.225	0.071	99.7	56.5
	150	68.48	0.208	0.073	99.5	59.6
	200	68.55	0.149	0.071	98.8	71.9
	250	68.57	0.187	0.072	99.3	63.7

### 9. EFFECT OF FROTHER

To consider the effect of frother consumption, 20, 60, 100, 140 and 200 g/Mg of MIBC, and KAX (50 g/Mg) were tested. The results are presented in Table 5. The content of Fe and its recovery are around 68% and 99%. However, in all the tests, S content was higher than permitted limit of 0.1%, and under the best condition was with the consumption of 60 g/Mg of MIBC. In latter test, the S content and its removal

was obtained as 0.157% and 69.7%, respectively. In addition, P content decreased to 0.06% which was just 0.01% higher than the permitted limit of 0.05%. Figures 11-12 illustrate S content and removal vs. MIBC consumption. The diagram shows that with increasing MIBC consumption S content increases and its removal decreases.

Table 5. Results of flotation tests with MIBC

Consumption g/Mg	Concentrate content, %			Iron recovery, %	Sulfur removal, %
	Fe	S	P		
20	68.54	0.184	0.059	99.2	64.4
60	68.07	0.157	0.059	99.7	69.7
100	68.37	0.204	0.061	99.4	60.5
140	68.50	0.184	0.058	99.1	64.6
200	68.78	0.214	0.073	99.2	58.7

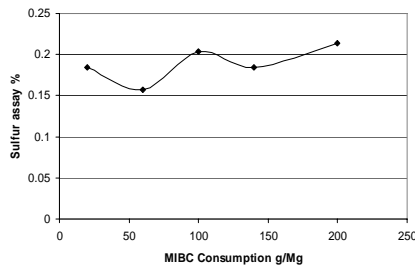


Fig. 11. Effect of frother dose on S content

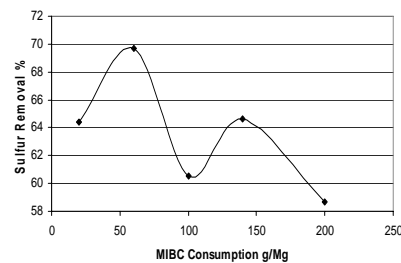


Fig. 12. Effect of frother dose on S removal

## 10. EFFECT OF DEPRESSANT

In different flotation tests  $\text{Na}_2\text{SiO}_3$  was used as: i) depressant of silicate and oxide minerals (Parekh and Miller, 1999; Bulatovic, 2007), ii) dispersant of slimes. The influence of various amounts of  $\text{Na}_2\text{SiO}_3$  was investigated on S decreasing using 0, 200, 300, 400 and 500 g/Mg. The obtained results are presented in Table 6.

Table 6. Results of flotation tests with  $\text{Na}_2\text{SiO}_3$ 

Consumption g/Mg	Concentrate content, %			Iron recovery, %	Sulfur removal, %
	Fe	S	P		
0	69.55	0.248	0.058	97.8	54.0
200	68.41	0.200	0.060	99.3	61.8
300	68.25	0.203	0.058	99.5	61.2
400	68.40	0.248	0.058	99.3	52.9
500	68.37	0.252	0.059	99.3	51.6

In the absence of  $\text{Na}_2\text{SiO}_3$ , the content of iron was 69.55% and the recovery 97.8%. The results in Table 8 indicate that the presence and/or absence of sodium silicate does

not have any remarkable effects on sulfur removal. However, it was observed that the best values were achieved using 200 g/Mg of  $\text{Na}_2\text{SiO}_3$ . Figures 13-14 illustrate S content and its removal vs.  $\text{Na}_2\text{SiO}_3$  consumption. Figure 13 shows that increasing with  $\text{Na}_2\text{SiO}_3$ , S content decreased at first and then increased to nearly constant amount. Figure 14 shows that also S removal increased at first, and then reached a constant level.

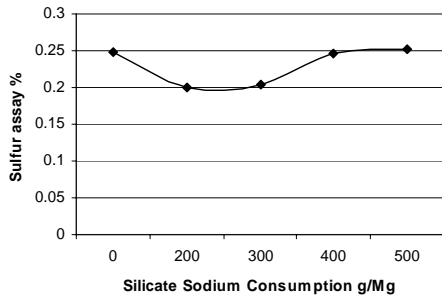


Fig. 13. Effect of  $\text{Na}_2\text{SiO}_3$  dose on S content

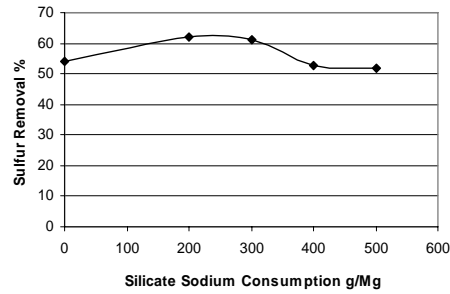


Fig. 14. Effect of  $\text{Na}_2\text{SiO}_3$  dose on S removal

### 11. IMPELLER SPEED

Increasing impeller speed caused fine bubbles production. Thus, the possibility of particles contacts with bubbles was increased leading to increased recovery. It should be noted that very high impeller speed causes the bubbles to be blown, and therefore the recovery drops accordingly. The role of impeller speed was studied at 1350, 1500 and 1650 rpm. The results of these tests were presented in Table 7. They indicate that the Fe contents and recoveries are around 68% and 99%, respectively. The most unsuitable test to decrease S content was at 1350 rpm. It was observed that at 1500, and 1650 rpm, the removal of sulfur was increased. To select the best impeller speed, the Schulz separation efficiency index (SE) was also employed (Wills and Napier-Munn, 2006). The results of these tests and separation efficiency estimation showed that at 1500 rpm, the SE values were higher than those of other speeds. Therefore, 1500 rpm was selected as the most suitable value for impeller speed. It should be mentioned that the P content obtained from the test at 1500 rpm was higher than the permitted limit of 0.05% in all three experiments.

Table 7. Results of different impeller speed tests

Speed, rpm	Concentrate content, %			Fe recovery, %	S removal, %	SE
	Fe	S	P			
1350	68.1	0.311	0.057	99.6	42.4	-
1500	68.4	0.200	0.060	99.3	61.8	57.8
1650	68.4	0.211	0.056	99.1	62.5	51.8

## 12. FROTHING TIME

By increasing frothing time the recovery increases. The trend of this increase follows exponential function. Different experiments were carried out to consider the effect of frothing time on sulfur decrease, iron content and recovery. The frothing time was 1<sup>st</sup>, 3<sup>rd</sup> and 7<sup>th</sup> min of flotation. The results obtained from these experiments are shown in Figs 15-16. It was observed that with increasing frothing time, the content of S in concentrate decreased, and its removal accordingly increased. Therefore, the best frothing time was 7 minutes.

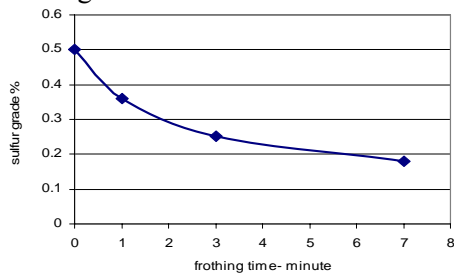


Fig. 15. Frothing time versus S content

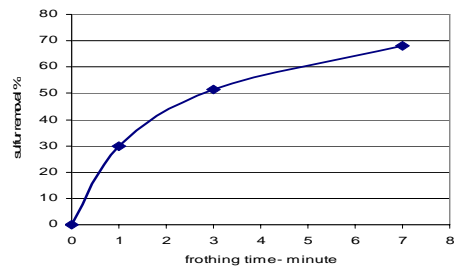


Fig. 16. Frothing time versus S removal

## 13. EFFECT OF pH

The influence of pulp pH on S removal was studied in acidic, neutral and alkaline environments, and the results are shown in Table 8. The natural pH of pulp was 8, and thus no regulator was added, but sulfuric acid was used in other tests to adjust the pH.

Table 8. Effect of pH on sulfur removal

pH	Concentrate content, %			Iron recovery, %	Sulfur removal, %
	Fe	S	P		
5	67.85	0.293	0.058	99.9	46.0
6	68.00	0.174	0.057	99.7	67.7
7	69.40	0.158	0.058	99.1	70.7
8	69.00	0.113	0.057	99.4	79.2

According to Table 8, by increasing pH, the content of iron increased and its recovery decreased. In addition, the content of sulfur decreased and its removal increased. The optimum value for pH was achieved at natural pH=8, and the content of sulfur and its recovery were 0.113% and 79.2%, respectively. Increasing pH did not have any significant effects on decreasing P content and under the best condition its amount was decreased to 0.057%, which is higher than the permitted limit. Figures 17 and 18 illustrate S content and removal versus pH, respectively. Trend of the diagram shows that by increasing pH, S content decreases and its removal increases.

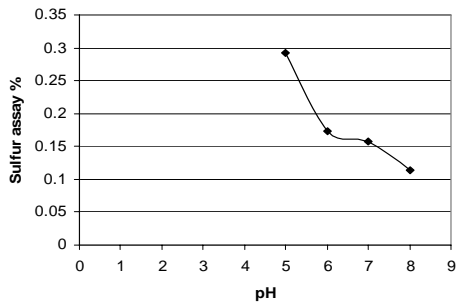


Fig. 17. Effect of pH on S content

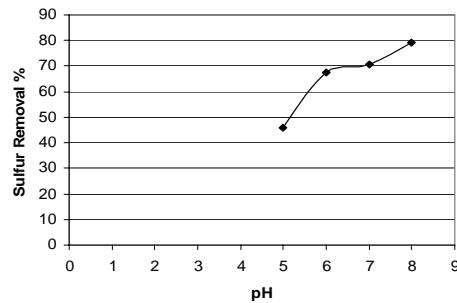


Fig. 18. Effect of pH on S removal

### 13. EFFECT OF SOLID CONTENT

Solids content in any pulp shows a direct relation with ore density. The amount of the weight solid content could be from 10 to 15% for light minerals such as coal, and higher than 35% for heavy minerals such as galena and sphalerite (Vijayendra, 1995). In order to obtain optimum flotation results, the solids content has to be in a certain range. Economically it is 30-35% (Vijayendra,1995; Parekh and Miller, 1999).

In this project, the weight of solids was tested between 20 and 36%, and the results are presented in Table 9. According to this Table, the content of iron in different experiments and for various solids content was approximately nearly the same and showed very small variation from 68.6 to 69.0%. By increasing the solids content, S content increased and then decreased, so at the solids content of 36% the S content decreased to 0.08% and its removal recovery increased to 85.5%. Since the content of sulfur at the solids content of 36% was less than permitted level, this value was selected as the optimum for the solids. The P content was approximately similar in all tests, and at the solids content of 36% reached 0.052%, which is very near to the permitted level.

Figures 19-20 illustrate S content and its removal vs. solid content, respectively. Figure 19 shows that by increasing solids content, S content increased at first and then decreased. Also Fig. 20 indicates that S removal decreased at first and then increased.

Table 9. Results of solid content tests

Solid content, %	Concentrate content %			Iron recovery, %	Sulfur removal, %
	Fe	S	P		
20	69.0	0.113	0.057	98.4	79.2
25	68.6	0.134	0.055	99.0	75.0
31	68.9	0.115	0.056	97.8	78.29
36	68.8	0.080	0.052	98.4	85.5

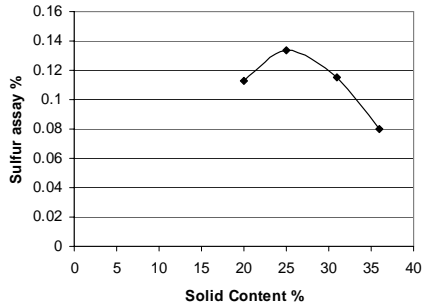


Fig. 19. Effect of solid content on S content

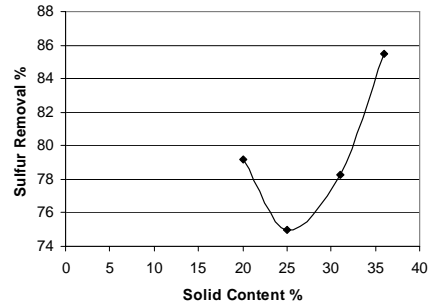


Fig. 20. Effect of solid content on S removal

#### 14. CONDITIONING TIME

To verify the effect of conditioning time on flotation, it was reduced to 25% (25% less than initial time, Table 3), for each reagent. Then, the content of S and its removal were studied. The results obtained for 4.5 and 6 min as the conditioning time are shown in Table 10. The content of sulfur increased from 0.08% to 0.113%, which was 0.013% (small discrepancy) higher than the permitted limit (0.1%). The content of P also increased. Thus, 6 minutes was the best time for conditioning.

Table 10. Results of two conditioning time tests

Time, min	Concentrate content %			Iron recovery %	Sulfur removal %
	Fe	S	P		
4.5	68.5	0.113	0.056	98.8	79.5
6	68.8	0.080	0.052	98.4	85.5

#### 15. EFFECT OF DESLIMING

The aim of desliming was to study: i) direct influence on decreasing S and P contents, and ii) effect on flotation. We attempted to separate particles finer than 10  $\mu\text{m}$  using hydrocyclone and then flotation experiments were performed on deslimed samples. In the first test, the sample was ground for 15 minutes in a rod mill. The product of mill was then deslimed with a hydrocyclone to remove particles finer than 10  $\mu\text{m}$ . The samples of feed, overflow and underflow of hydrocyclone were analyzed for Fe, S, and P content. The results are presented in Table 11.

It is observed that desliming did not have any significant effect on decreasing S content, but P content decreased to 0.05%, which is in the acceptable range. It can be

concluded that the main part of apatite existed in the undersize size fractions and the weight of slimes (-10 μm) is 7% of the initial sample weight. Next, the deslimed sample was floated to verify the influence of flotation on the deslimed sample. The conditions of this test are shown in Table 12, and the results in Table 13. The recovery of Fe was 98.5% with 69.5% Fe in the concentrate. The content of S reached 0.088%, which was less than the limit, and with 80.6% of S removal. The content of P decreased to an acceptable limit of 0.049%. Frothing time was reduced to 3 minutes.

Table 11. Results of desliming test (first test)

Products	Fe, %	S, %	P, %	Weight, %
Feed	67.75	0.500	0.080	100
Underflow	67.91	0.440	0.052	89.9
Overflow	48.95	0.564	0.107	7.35
Lost	-	-	-	2.75

Table 12. Conditions of flotation test (first test)

Collector (g/Mg)	KAX 50
Frother (g/Mg)	MIBC 60
Depressant (g/Mg)	Sodium silicate 500
Solid content %	20
Pulp pH	7
Conditioning time (minute)	6
Frothing time (minute)	3
Impeller speed (rpm)	1500

Table 13. Results of deslimed sample flotation (first test)

Products	Fe%	S%	P%	Iron recovery %	Sulfur removal %
Feed	67.91	0.440	0.052	98.50	80.57
Concentrate	69.45	0.088	0.049		
Tail	27.21	12.236	0.077		

Table 14. Results of desliming (second test)

Products	Fe, %	S, %	P, %	Weight, %
Feed	67.75	0.500	0.080	100
Underflow	68.00	0.454	0.051	89.4
Overflow	50.00	0.548	0.103	7.4
Lost	-	-	-	3.2

Table 15. Results of deslimed sample flotation (second test)

Products	Fe, %	S, %	P, %	Iron recovery %	Sulfur removal, %
Feed	68.00	0.454	0.051	95.11	92.24
Concentrate	70.24	0.041	0.043		
Tail	41.66	8.54	0.104		

The procedure of the second test was identical with the first one: 15 minutes of rod milling, and then a hydrocyclone was used to deslime the ground sample to remove particles finer than 10  $\mu\text{m}$ . The results of desliming are presented in Table 14, which indicates that desliming did not have any direct effect on the S while P content decreased to 0.05%. In the next step, the deslimed sample was floated, but some parameters were different from the those of the first test. In this experiment, the solids content in the pulp was 44% (in first test 20%), and pH was 8 (in first test 7). Moreover, the consumption of sodium silicate decreased from 500 to 200 g/Mg and the other parameters were identical with the first test (Table 12). The results achieved in this test are presented in Table 15. It was observed that flotation of deslimed sample decreased the S content to 0.041%, which was remarkably less than permitted limit of 0.1% with sulfur removal of 92.24%. The content of Fe was 70.24% with 95.11% of recovery. The content of phosphorus reached 0.043% (less than permitted level 0.05%). It was found that increasing solids content, pulp pH, and decreasing  $\text{Na}_2\text{SiO}_3$  consumption, yielded very significant results, particularly S elimination.

In this work effect of size fraction and two-stage flotation (rougher+cleaner) on S and P content reduction were also studied which are presented in following section.

## 16. EFFECT OF FLOTATION ON S AND P REDUCTION IN SIZE FRACTIONS

Prior to running flotation experiments, contents of S and P in the head sample, S content in all size fractions, and P content in the -38  $\mu\text{m}$  fraction were higher than their permitted limits. The flotation test yielded a considerable decrease of the S and P content in all size fractions. The greatest decrease occurred in -38  $\mu\text{m}$  and the least in -45+38  $\mu\text{m}$  size fractions, respectively. Figures 21 and 22 present the results of the flotation experiments. The lowest contents of S are obtained in the -63+53  $\mu\text{m}$  and the highest in the -45+38  $\mu\text{m}$  size fractions. It should be noted that except of -45+38  $\mu\text{m}$  fraction, the S and P contents are near to or below of the desired limits in other fractions. It could be postulated that the decrease of the S and P content in the -38 size fraction is due to the fineness of particles in this size class which causes their easily removal by water flow. It seems that +45  $\mu\text{m}$  particles have enough capability to float while -45+35 fraction is not too fine to be removed by water flow (as -38  $\mu\text{m}$  particles). These facts are presented in Fig. 22. They indicate that the P content is

around 0.05% before flotation in all size fractions coarser than 45  $\mu\text{m}$ , and it is around 0.05% for the -45+38  $\mu\text{m}$  fraction, but it is high for the -38  $\mu\text{m}$  size fraction (about 0.12%).

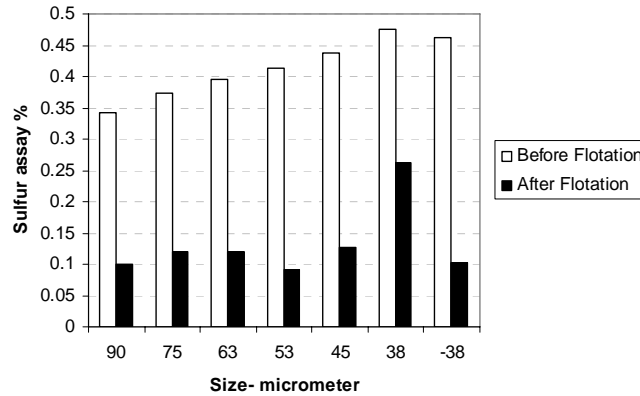


Fig. 21. Effect of flotation on S content in different fractions

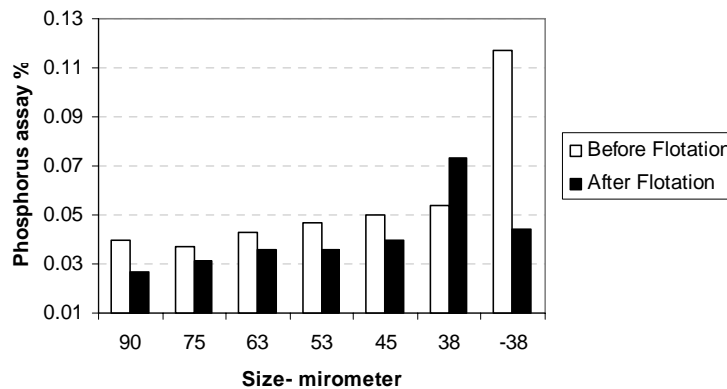


Fig. 22. Effect of flotation on P content in different fractions

### 17. EFFECT OF TWO STAGE FLOTATION

Table 4 presents results of a flotation test using 100g/Mg of KAX. In this test the content of S reached 0.191% which is more than the accepted limit. In a next step, it was considered to perform the flotation tests in two stages. In each test 50g/Mg of KAX was used, and concentrate of the first test was used as the feed of the second test (cleaner). In this cleaner test 50g/Mg KAX, 40g/Mg MIBC, 500g/Mg sodium silicate,

20% solids content of the were used in a 2 dm<sup>3</sup> Denver flotation cell with 1500 rpm at pH=7. The new approach yielded better results than the one-stage flotation test. Table 4 shows that by using 100 g/Mg KAX, S content was 0.191% with 63.1% recovery, while using twice 50 g/Mg of KAX in two tests, the S content reached 0.097% with 81.88% recovery, and P content nearly reached the desired limit.

Table 16. Results of two-stage flotation tests

Stage	Material	content %			Iron recovery %		Sulfur removal %	
		Fe%	S	P	initial	overall	initial	overall
1	Feed	67.75	0.5	0.080	99.49	-	70.45	-
	Product	68.24	0.153	0.070				
	Tail	27.5	8.241	0.114				
2	Feed	68.24	0.153	0.070	98.99	98.49	38.67	81.88
	Product	68.66	0.097	0.056				
	Tail	43.48	1.81	0.159				

## 18. CONCLUSION

The iron ore concentrate of the Gol-e-Gohar complex contains high amount of sulfur and phosphorus. Their contents were 0.5% S and 0.08% P, respectively, which were higher than the steel industrial permitted limit of 0.1% S and 0.05% P. The major sources of S and P are pyrite and apatite. To decrease the sulfur and phosphorus content in the concentrate, reverse flotation of pyrite in the presence of xanthates was used. In reverse flotation, pyrite was floated and apatite particles were entrained with the froth product water. Prior to the flotation tests, mineralogical and size reduction studies were carried out. Results indicated that pyrite liberation (65%) was achieved in the size fraction of -75+53  $\mu\text{m}$ . Therefore, the average size of 68  $\mu\text{m}$  was considered as the target size for grinding. In order to achieve this size, 15 minutes of rod milling was needed. To yield the optimum condition, role of various parameters such as type and doze of collector, frother and depressant, solid content, pH, impeller speed, frothing time, conditioning time and desliming were investigated. The results obtained in two procedures, with and without desliming, are given in Table 17. The best results were obtained applying 50 g/Mg of KAX, 60 g/Mg of MIBC and 200 g/Mg of sodium silicate, pulp pH=8, and conditioning time 6 minutes. Other conditions are presented in Table 17, which shows that desliming produced better results than without desliming, leading to a decrease of sulfur and phosphorus contents in the concentrate.

In addition, some experiments were performed to investigate the influence of particles size and two-stage flotation, which showed that in the +45 and -38  $\mu\text{m}$

fractions, sulfur and phosphorus content are near to the permitted limits, but in the -45+38  $\mu\text{m}$  fraction those were too high. It was postulated that for convenient flotation, +45  $\mu\text{m}$  particles, and -38  $\mu\text{m}$  fraction removal with water flow should be used. Results indicated that consumption of 100 g/Mg of KAX in two-stage (50+50) flotation, S and P contents could be reduced to 0.097% and 0.056% (near the permitted limit), while the same collector dose in one-stage flotation, the content were 0.191% and 0.070%, respectively.

Table 17. Optimum flotation results

State		Without desliming	With desliming
Solid content, %		36	44
Frothing time, min		7	3
Elemental contents of product, %	Fe	68.80	70.24
	S	0.080	0.041
	P	0.052	0.043
Iron recovery, %		98.43	95.11
Sulfur removal, %		85.50	92.24

## REFERENCES

- BULATOVIC, S.M., 2007, *Handbook of Flotation Reagents: Chemistry, Theory and Practice: Flotation of Sulfides Ores*, Vol. 1, Elsevier, Amsterdam.
- JAFARZADEH, A., QURBANI, M., PEZESHKPOR, M., 1995, *Iran Geology-Iron Ores*, Iran Geology Organization, Tehran, Iran.
- PAREKH, B.K., MILLER, J.D., 1999, *Advances in Flotation Technology*, SME Publishers, New York.
- RAO, S.R., 2003, *Surface Chemistry of Froth Flotation* 2<sup>nd</sup> Edition (1<sup>st</sup> Edition by Leja, J.), Marcel Dekker.
- SVOBODA, J., 2004, *Magnetic Techniques for the treatment of minerals*, Kluwer Academic Publishers, Boston.
- VIJAYENDRA, H.G., 1995, *Handbook on Mineral Dressing*, Vikas Publishsing House PVT Ltd., New Delhi.
- WILLS, B.A., NAPIER-MUNN, T., 2006, *Wills' Mineral Processing Technology*, 7<sup>th</sup> Edition, Butterworth Heinemann, Boston.

**Soltanmohammadi, V., Noaparast, M., Kohsari, A.H., Zamani, F.,** *Wpływ parametrów flotacji na zmniejszenie zawartości siarki i fosforu w koncentraty żelaza z Gol-e-Gohar*, Physicochem. Probl. Miner. Process., 46 (2011) 173-190, (w jęz. ang), <http://www.minproc.pwr.wroc.pl/journal>

Kombinat Gol-E-Gohar znajdujący się w Iranie w prowincji Kerman jest jednym z największych producentów koncentratów żelaza. Wykorzystywana ruda ma nadmierną zawartość siarki (0.5%) oraz fosforu (0.08%) gdyż dozwolona ich ilość wynosi 0.1% S oraz 0.05% P. Głównym źródłem siarki i fosforu w rudzie są piryt oraz apatyt. W tej pracy podjęto próbę zmniejszenia zawartości S i P stosując flotację. Podczas flotacji ksantogenianami flotuje piryt, podczas gdy drobne ziarna apatytu są wynoszone mechanicznie z wodą piany. Stopień uwolnienia pirytu w klasie  $-75+53 \mu\text{m}$  wynosił 65%. Badano wpływ takich parametrów jak typ i dodatek kolektora, spieniacza, depresantu, zawartości części stałych, pH, prędkości mieszania, czasu pienienia, czasu kondycjonowania oraz odszlamiania na usuwanie S oraz P. Najlepsze wyniki osiągnięto przez odszlamianie. Ilości kolektora, spieniacza oraz depresantu wynosiły 50 g/Mg KAX, 60 g/Mg MIBC oraz 200 g/Mg krzemianu sodu. pH pulpy było 8, a czas kondycjonowania wynosił 6 minut. W tych warunkach, z odszlamianiem, otrzymano koncentrat zawierający kwalifikowane zawartości składników: 70.24% Fe, 0.041% S oraz 0.043% P. Uzysk Fe wynosił 95.11%, a uzysk siarki w odpadzie osiągnął 92.24%. Badano także wpływ różnych klas ziarnowych oraz dwustopniowej flotacji na obniżenie zawartości S oraz P. Wyniki wskazywały, że dla frakcji większych niż 45 mikrometrów oraz mniejszych niż  $38 \mu\text{m}$  zawartości S oraz P były poniżej lub blisko dozwolonych ilości. Postuluje się, że frakcja  $+45 \mu\text{m}$  jest najbardziej odpowiednia do flotacji, a frakcja  $-38 \mu\text{m}$  do usuwania z wodą.

*słowa kluczowe: Gol-e-gohar, usuwanie siarki, usuwanie fosforu*

Dominika Katarzyna SZPONDER\*, Kazimierz TRYBALSKI\*

## **DETERMINATION OF PROGRESSIVE RESEARCH METHODOLOGY OF USING MODERN MEASURING DEVICES TO DETERMINE PHYSICAL, CHEMICAL AND MINERALOGICAL PROPERTIES OF RAW MATERIALS AND MINERAL WASTES**

*Received May 10, 2010; reviewed; accepted July 25, 2010*

Currently, in science, rapid development in the use of new research methods takes place. Examples of these methods are scanning electron microscopy, x-ray diffraction analysis, thermal analysis performed using derivatograph, grain size analysis performed using laser particulate measuring instruments, density measurements using gas pycnometers and measurements of specific surface area carried out using the Blaine detector. These methods can be used in almost any field of science dealing with solids. Modern methods are also used in studies of properties of raw materials and mineral wastes. Further studies, using the above and other advanced testing methods will create comprehensive testing procedures for mineral raw materials and waste.

The paper presents progressive research methodology of using modern measuring devices to determine physical, chemical and mineralogical properties of fly ashes. In the theoretical part the characteristics of different research methods and the principles of operation of test equipment were described. In the practical part the methodology and exemplary results were presented.

*keywords: fly ash, mineralogical properties, x-ray diffraction, x-ray microanalysis; thermal analysis, laser size analysis; gas pycnometry, surface area*

---

\* Department of Mineral Processing and Environmental Protection, Faculty of Mining and Geoengineering, AGH University of Science and Technology, Al. Mickiewicza 30, 30-059 Krakow, Poland. Email: dominika.szponder@gmail.com, trybal@agh.edu.pl

## 1. INTRODUCTION

So far in the laboratory studies of physical and physicochemical properties of raw materials, mining waste and power industry waste traditional research methods were used (such as petrographic and mineralogical studies, sieve analysis, enrichment analysis, determination of magnetic and electrostatic properties). In addition, to determinate coal properties extra research methods were used (such as determination of moisture, ash content, sulphur content, volatile matter content, analysis of heating values).

Scientific development, which took place in the last century in many fields of science dealing with solids, allowed to create more accurate methods of research. These methods can be used in studies of properties of raw materials and mineral waste. The results of such tests are used to assess feasibility of enrichment of raw minerals, technological processes and feasibility of utilization and treatment of waste.

Among these methods of measurement, the greatest potential for use has X-ray diffraction analysis, scanning electron microscopy, X-ray microanalysis, thermal analysis, grain size analysis, gas pycnometry and Blaine analysis. These methods have many applications. A few of them are presented below.

Scanning Electron Microscopy (SEM) and Energy Dispersive Spectrometers (EDS) were, for instances, used to analyze the solid reaction products of reduction of ilmenite pellets under a CO-N<sub>2</sub> gas mixture. With these methods metallic Fe with small amount of Ti dissolved in it and titanium oxides were found in the solid reaction products. However, no formation of nitride phases was found under most conditions (Zhao et al., 2008).

X-ray diffraction (XRD) and differential thermal analysis (DTA) for instance were used to identify physical properties and mineral and chemical composition of bentonite from different calcium bentonite deposits in Turkey. The bentonite was used to produce desiccant clay (Bulut et al., 2008).

Laser particle size analysis was used for high resolution on-line measurement of particle size distribution in highly concentrated ore slurries (Jenny et al., 2008).

Blaine specific surface area tester, laser size analyzer, scanning electron microscope (SEM) and X-ray diffraction analyzer (XRD) were used to determinate the working mechanism of High Pressure Grinding Rolls (HPGR) and to optimize grinding, balling and firing processes parameters (Pan et al., 2008).

A wide range of publications point to the fact that modern research methods are widely applicable, not only in mineralogy and geology, but also in raw materials and mineral waste properties studies (Mo and Fournier, 2007; Erol et al., 2007; Kutchko and Kim, 2006; Maenami et al., 2004; Chaowasakoo and Sombatsompop, 2007; Styszko-Grochowiak et al., 2004; Bouzoubaâ et al., 1998; Sarbak et al., 2004; Blaha et al., 2008; Inaba and Matsumoto, 1999; Zaenia et al. 2010). Further studies, using these

methods, will create comprehensive testing procedures for mineral raw materials and waste on laboratory scale. Then, these procedures can be applied for in situ measurements of variable properties of raw materials, products and waste on industrial scale. The test procedure will be helpful in continuous evaluation of the properties of raw materials, products and wastes in processing plants. This will allow to improve enrichment technology, to increase the yield of useful components and to find the most economic means of disposal of waste.

## 2. METHODS AND MATERIALS

In this paper, systematics of modern research methods and opportunities of using these methods to determinate physical and chemical properties of raw materials and mineral waste is presented. Characteristics of these methods as well as the possibility of their use to measure and quantify properties of mineral waste materials are shown on the example of fly ashes.

### 2.1. METHODS

#### 2.1.1. STRUCTURAL AND PHASE X-RAY DIFFRACTION ANALYSIS (XRD)

In this method, X-ray of known wavelength is used to test unknown crystalline phases. In X-ray phase analysis the most frequently used technique is the powder method, performed using diffractograms (X-ray apparatus). Polycrystalline samples in the form of powdered mineral or rock and monolithic samples of fine-grained and fine-crystalline minerals (i.e. fly ash), are tested by this method. This method is based on an assumption that a sample consists of grains oriented in random way. A limited number of these grains is located relative to a monochromatic X-ray beam that falls on the sample, in such a way that the specified crystal planes (hkl) satisfy the Bragg condition for wave interference. Each crystalline phase is attributed to crystal planes that are filled in a specified way with atoms or ions forming that phase. Each substance is characterized by a corresponding deviation from the original direction of incidence of the interference beam. The interference beam is recorded on a film (film technique) or by using a Geiger or scintillation counter (diffractometer, counter technique). The result of the test, using the powder method, is a record of spectra in form of diffraction pattern. The diffraction pattern plots the diffractive extremes. It is the basis for the identification of the crystalline phases contained in the sample. The diffraction pattern is obtained in numerical and graphical forms. The mineral composition of the sample and the percentage of individual phases are identified

automatically using appropriate software that includes directories of characteristic values for each phase. The result of testing is a complete qualitative and quantitative analysis of the mineral composition of tested samples (Kędzior et al., 2003; Ahuja and Jespersen, 2009; Chancey et al., 2010; Jiang et al., 2007; Koukouzas et al., 2009).

### 2.1.2. SCANNING ELECTRON MICROSCOPY (SEM)

It is currently the most common modern method used for observing and testing microstructures. In the scanning microscope, an electron spot beam bombards the sample. The beam produces emission of secondary electrons through a linear sweep of the sample's surface. Thus, the sample emits a variety of signals. The signals are recorded by detectors and converted sequentially into an image of the test samples or X-ray spectrum (Goldstein et al., 2003).

Signals that generate information about the properties of the samples can be divided into groups: secondary electron emissions (topography, morphology and crystalline structure of the sample, distribution of potential and intensity of electric and magnetic fields in the sample); backscattered electron emissions (topography and morphology of the sample, the distribution of magnetic domains in the sample, composition contrast); auger electron emissions (chemical analysis of surface layers of the sample, measurement of local potentials in the sample); cathodoluminescence (recombination processes in material, identification of impurities, additives and structural heterogeneity) and characteristic X-ray emission (qualitative and quantitative chemical analysis of the material) (Goldstein et al., 2003; Krawczykowska, 2007; Gomes, et al., 1999; Hsieh and Tsai, 2003; O'Keefe et al., 2000; Sarbak et al., 2004; Słówko et al., 2002).

### 2.1.3. COMPLEX THERMAL ANALYSIS

This is a two step method. The analysis is performed using derivatograph. In the first step, changes in mass of the sample during the cooling or heating are measured as a function of time. As a result of this measurement graphs showing the curves of DTG (Differential Thermogravimetric Curve) and TG (Thermogravimetric Curve) are plotted. The second step is called Differential Thermal Analysis (DTA Curve). In this step the difference between temperature of the test sample and a reference substance, in relation to time or temperature, is measured. The samples and the reference substance are in the same conditions, and their heating or cooling is strictly controlled. Comprehensive thermal analysis methods allow to trace the reactions taking place at pre-selected temperature intervals. The type of the reaction (dehydration, oxidation, degradation, polymorphic transformation, sintering, melting, etc.) can be specified as a result of the interpretation and comparison the DTA, DTG and TG curves. The

analysis of the TG and DTG curves allows for accurate quantitative determination of these reactions and processes (qualitative analysis and quantitative assessment of processes). This method provides information on crystallization of phases, recrystallization of minerals and compounds, amount of heat needed for the synthesis of products, quality and quantity of newly formed compounds or loss in weight of the material (Nocuń-Wczelik, 2003; Guo et al., 1998; Moreno et al., 2005; Wyrwicki, 2004).

#### 2.1.4. GAS PYCNOMETRY DENSITY ANALYSIS

This method is used to determine accurate density of the test materials. Density is determined by the measurement of the weight of the sample (carried out by an analytical balance) and the measurement of the sample volume (performed by a gas pycnometer). In gas pycnometry, the volume of solids is determined by measuring the volume of gas, which is displaced by the test sample, from a calibrated measure. The substances used as a medium have properties similar to the properties of perfect gas. These substances neither react with the test material nor adsorb on the material surface (e.g. helium) (Ahuja and Jespersen, 2006; Thipse et al., 2002).

#### 2.1.5. BLAINE SPECIFIC SURFACE AREA ANALYSIS

Measurements of the specific surface area are carried out by the Blaine detector. In this device the gas flow through a layer of compacted formulation is measured (method of permeability). This method is based on the properties of laminar (viscous) flow (Poiseuille-type) through a porous layer. Measurement is performed for two substances - the standard sample and the test sample. The results are relative and depend on the standard sample used in the experiment. To obtain the absolute value of the specific surface area it is necessary to make additional calculations (Rymon-Lipiński and Zborowski, 1978; Kordek et al., 2005; Tosun, 2006).

#### 2.1.6. LASER PARTICLE SIZE ANALYSIS

Grain size analysis, performed using a laser particulate measuring instrument, gives a full assessment of the composition of the fine-grained sample. Particle size analysis, in the device of this type, is based on measuring the intensity of coherent laser light scattering by the grains in suspension. When the laser light encounters the population of grains, the volumetric distribution of grain sizes is expressed by the intensity of light scattered on them. Refraction angle of the laser beam is higher on smaller grains than on larger grains. Diffraction pattern, which is formed in that way, is identified by

a system of sensors, while the received signals are used to calculate the particle size distribution (Trybalski et al., 2004). During particle size analysis, the frequency of occurrence of selected size grades is determined. The results of particle size analysis are presented as tables or graphs (e.g. histogram - the percentage of the grains which sizes are contained in the selected size grades; cumulative curve - is a continuous function, that shows the contents of particles with diameters smaller or larger than the selected diameter  $D$  in the tested material; particle size distribution curve – differentiate cumulative curve, equivalent of probability density). In order to characterize the size distribution of grains (similar to Gaussian distribution) such parameters as average value (median), standard deviation and modal value (mode) are defined. When the particle size distribution is different than Gaussian distribution, additional parameters such as asymmetry factor and flattening coefficient are determined (Bolewski et al., 1981; Jones et al., 2006; Styszko-Grochowiak et al., 2004).

## 2.2. MATERIALS

Fly ash is an artificial puzzolana that is produced as a result of combustion of coal. It leaves a pulverized, fuel-fired furnace with flue gases. It takes the form of fine mineral dust from light to dark grey in colour and consists primarily of silicon oxides, aluminium oxides and iron oxides. In addition, it contains a variety of trace elements and small amount of unburned carbon (Kasprzyk and Pietrykowski, 2007).

Fly ashes from Power Plant BOT Opole SA (sample designated as Sample O) and from Thermal-Electric Power Station "Cracow" SA (sample designated as Sample L) were used in the studies. Samples were collected from the fly ash retention tanks. Samples (approximately 1 kg) were collected with a probe (with an inside diameter of 80 mm and a length of 1,500 mm), from the hopper of retention tank, at the time of gravitational movement of material. The collected samples were an averaged mixture of ash produced in these plants.

## 3. RESULTS AND DISCUSSION

This publication aims to systematize the knowledge on modern research methods and measuring equipment that is used to determine the physical, chemical and mineral composition of solids. It also shows their applicability to measure properties of various types of raw materials and mineral waste. Therefore, the samples of different types of the fly ashes were examined. Based on laboratory studies, usability of these research methods and measuring equipment to determine the properties of raw materials and mineral waste was evaluated.

## 3.1. CHARACTERISTICS OF MINERAL COMPOSITION

## 3.1.1. STRUCTURAL AND PHASE ANALYSIS - X-RAY DIFFRACTION ANALYSIS (XRD)

To determine the mineral composition of the samples the X-ray phase analysis was used. The powder method was used because sample contained only small particles. The results of X-ray analysis of Sample L and Sample O are shown in Table 1 and Table 2.

Table 1. Mineralogical composition of fly ash by X-ray analysis – Sample L

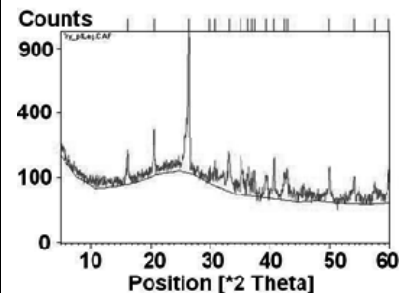
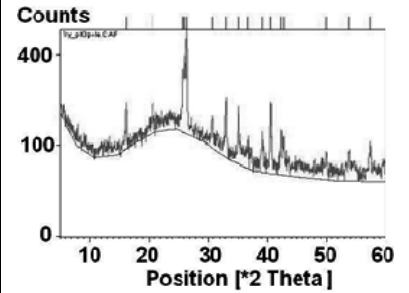
	Mass [%]	Compound Name	Scale	Chemical formula
	49	Quartz	0.896	SiO <sub>2</sub>
	47	Mullite, syn.	0.202	Al <sub>5.65</sub> Si <sub>0.35</sub> O <sub>9.175</sub>
	4	Calcite	0.069	(Mg <sub>0.129</sub> Ca <sub>0.871</sub> )CO <sub>3</sub>

Table 2. Mineralogical composition of fly ash by X-ray analysis – Sample O

	Mass [%]	Compound Name	Scale	Chemical formula
	25	Quartz	0.906	SiO <sub>2</sub>
	6	Hematite	0.199	Fe <sub>2</sub> O <sub>3</sub>
	62	Mullite, syn.	0.501	Al <sub>4.984</sub> Si <sub>1.016</sub> O <sub>9</sub>
7	Dolomite	0.195	CaMg(CO <sub>3</sub> ) <sub>2</sub>	

It can be concluded that the fly ash from Sample L belongs to group of siliceous fly ashes containing a significant amount of aluminium compounds. The main component of this fly ash is silicate that occurs in the form of quartz (gangue) and mullite (aluminosilicate, carbonaceous shale and refractory clay. Quartz in fly ash has similar use as natural mineral aggregates of similar composition, while mullite makes fly ash highly flame resistant. In addition, mineralogical composition of this fly ash is supplemented by calcium carbonate and magnesium carbonate, that affect its binding properties. Sample O belongs to the siliceous-aluminum ashes group, which contains small quantities of calcium in the form of dolomite. It consists of a large quantity of synthetic mullite, which was formed as a result of burning coal that contains mainly

aluminosilicates, and slate and clay as the waste rock. Another component of the sample that is present in large quantities is quartz. It is a component of many types of gangue, with different characteristics and origins. The test sample contained also dolomite, which affects its binding properties. In addition, the composition of the fly ash is supplemented by a certain amount of iron in the form of hematite, which is a valuable component of the supplemental material for the production of clinker, cement and ceramics.

As it was demonstrated in this studies, X-ray analysis, carried out by diffraction patterns, can be used to accurately determine mineralogical composition of almost any raw mineral or mineral waste. However, tested substance must be in form of powder. The result of testing is a complete qualitative and quantitative analysis of the mineral composition of samples.

### 3.2. CHARACTERISTICS OF CHEMICAL COMPOSITION

Chemical properties of samples were determined by using two research methods – scanning electron microscopy and thermal analysis.

#### 3.2.1. ELEMENTAL COMPOSITION AND SURFACE MORPHOLOGY - SCANNING ELECTRON MICROSCOPY

To determine the elemental composition and morphology of samples scanning electron microscopy (SEM) was used. Figures 1 to 8 present the scanning microscopic images and diffraction patterns of samples of fly ashes.

The scanning microscopy proved that Sample L and Sample O are fine-grained fly ashes (grain 1 - 100  $\mu\text{m}$ ) (Figs 1 and 2). These fly ashes contained grains of various sizes and shapes. The shape and size of grains depend on its chemical composition. Both samples are dominated by spherical grains with a smooth surface (pirospherical (Fig. 3), cenosphical (Fig. 4), and plerospherical (Fig. 5)), single (Fig. 4 and 5) or combined into agglomerates (Fig. 3). In Figures 3a and 3b, the results of point microanalysis performed on the surface of this kind of grains (No. 1 and No. 2 in Fig. 3) are plotted. They consist mainly of silicon, aluminium and oxygen (mineralogical composition – silicate glass, quartz -  $\text{SiO}_2$ , mullite -  $3\text{Al}_2\text{O}_3 \cdot 2\text{SiO}_2$ ).

Other grains can be divided into three groups. First contains grains of irregular shape, which cement spherical grains or form a crust on their surface. This grains are composed of magnesium carbonate, calcium carbonate, sodium carbonate, potassium carbonate (calcite and dolomite) (Figs 6 and 6a). The second group of grains contains spherical grains made of crystals with a structural fabric. It contains iron, titanium and other metals (hematite) (Figs 7 and 7a). In the last group irregular in shape, very porous with rounded or sharp-edged borders, grains can be found. Such grains contain unburned coal (Figs 8 and 8a).

These studies show that the scanning microscope with an X-ray microanalyzer can be used to obtain information about sample morphology and grains amount, type, shape and elemental composition. These factors have a significant impact on properties of the sample. These measurements can be used for all raw materials and mineral wastes, not only in the powder forms, but also in the form of microsections or cuts. Due to this analysis, the elemental composition, the chemical and physical properties of almost all minerals, can be determined.

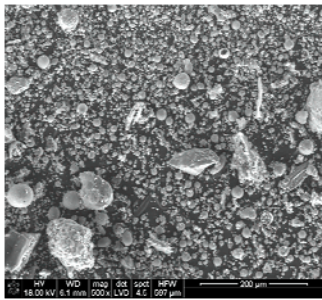


Fig. 1. General view of Sample L

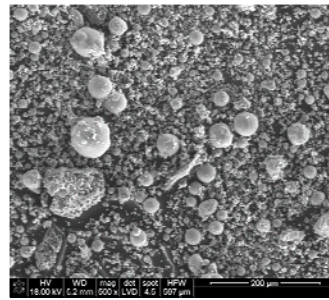


Fig. 2. General view of Sample O

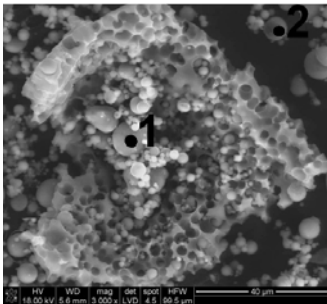


Fig. 3. Agglomerate– Sample O

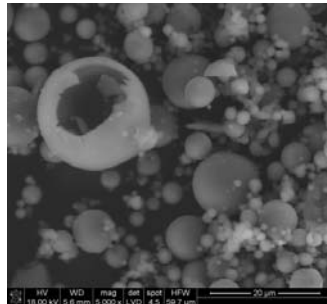


Fig. 4. Cenospherical grain – Sample L

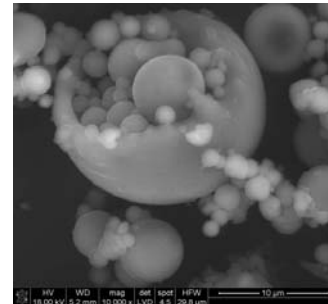


Fig. 5. Plerospherical grain – Sample O

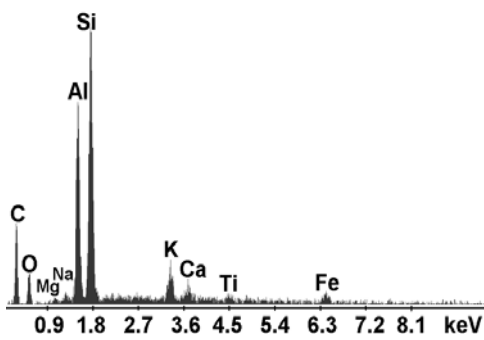


Fig. 3a. X-ray microanalysis at point No. 1 in Fig. 3

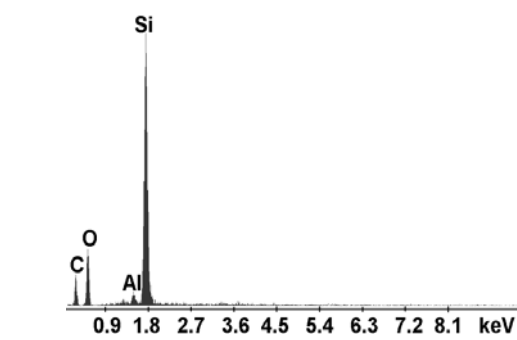


Fig. 3b. X-ray microanalysis at point No. 2 in Fig. 3

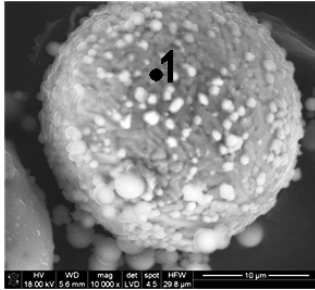


Fig. 6. Spherical grains made of crystals with structural fabric – Sample L

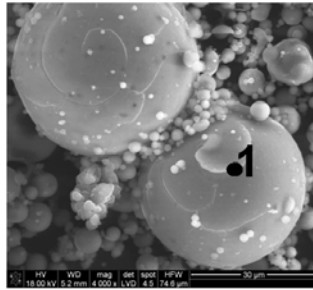


Fig. 7. Smooth surface grains with crust on surface – Sample O

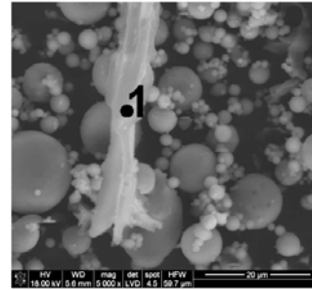


Fig. 8. Grains of irregular shape, containing carbon – Sample L

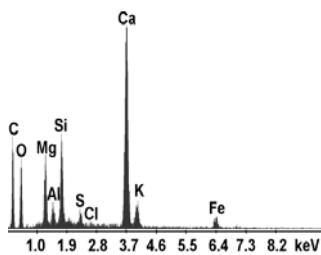


Fig. 6a. X-ray microanalysis at point No. 1 in Fig. 6

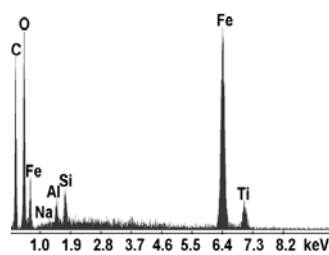


Fig. 7a. X-ray microanalysis at point No. 1 in Fig. 7

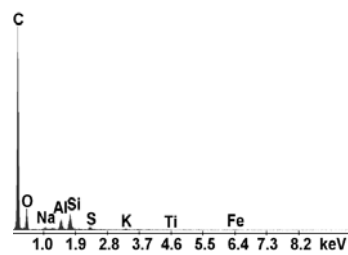


Fig. 8a. X-ray microanalysis at point No. 1 in Fig. 8

### 3.2.2. QUANTITATIVE AND QUALITATIVE DETERMINATION OF CHEMICAL PROCESSES - THERMAL ANALYSIS

Thermal analysis was used to determine chemical reactions taking place during cooling or heating of the sample. The results of thermal analysis of Sample L and Sample O are shown in Figs 9 and 10.

Based on the analysis of the results obtained in studies using derivatograph, during heating of the test sample, chemical reaction of oxidation of residual carbon occurred producing carbon dioxide ( $\text{CO}_2$ ). The percentage of carbon remaining in Sample L, after combustion in power plants, is 3.5 wt% of fly ash. The percentage of carbon remaining in Sample O is 3 wt% of fly ash.

Research, carried out by this method, allows tracing the reactions taking place in the material during cooling or heating. A comparison and interpretation of DTA, DTG and TG curves provided information about the type of reaction that takes place. The analysis of the TG and DTG curves was used to determine quantitatively this reaction. The behaviour of raw materials and mineral wastes under different conditions of temperature, their frost resistance and their behaviour during combustion or burning,

can be specified through this analysis. These factors are very important and they are used on a wide scale in selection of ways and methods of utilization of raw materials and mineral wastes.

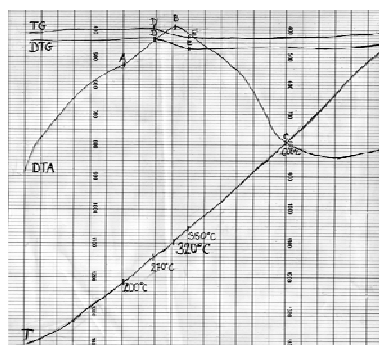


Fig. 9. Derivatograph – Sample O

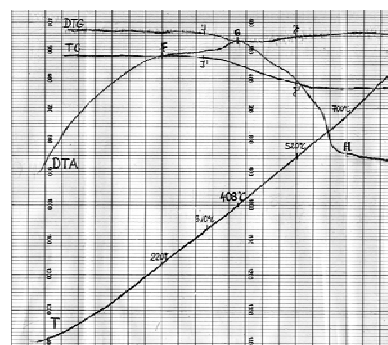


Fig. 10. Derivatograph – Sample L

### 3.3. PHYSICAL PROPERTIES

Basic physical properties of the samples were determined by using research methods such as density analysis (gas pycnometer), specific surface area analysis (Blaine detector) and grain size analysis (laser particle size analyzer).

#### 3.3.1. DENSITY ANALYSIS – GAS PYCTOMETER

The density of the samples was determined by measuring weight of the sample (carried out by analytical balance) and the measurement of sample volume (performed by helium pycnometer). The results of density analysis of Sample L and Sample O are presented in Table 3.

Table 3. Density and specific surface

Sample	Density, g/cm <sup>3</sup>	Specific surface area, cm <sup>2</sup> /g
Sample L	2.2529	3233.7
Sample O	2.1847	3523.5

Both samples have similar densities. The density results from chemical and mineralogical compositions of the tested samples. The value is closed to the average densities of minerals that build the investigated ashes.

The measurement of density is a basic test carried out for all the waste and raw materials used in building industry, mining industry as well as in mineral processing. This test is often performed and it allows to select an appropriate composition of the mixtures used in manufacture of building materials, fillings etc.

### 3.3.2. SPECIFIC SURFACE AREA ANALYSIS – BLAINE DETECTOR

The Blaine detector was used to determine specific surface area. The results of specific surface area analysis of Sample L and Sample O are shown in Table 3.

Specific surface areas are similar for both samples. Literature specific surface area of fly ashes is 2500 - 6000 cm<sup>2</sup>/g (Giergiczny, 2002; Małolepszy and Tkaczewska, 2007). Both tested fly ashes have specific surface area that classifies them into the group of fly ashes with developed specific surface area (fine-grained, porous and spherical grain).

Measurement of specific surface area is a basic study carried out for all waste and raw materials that are used in mining and mineral processing. The specific surface area is particularly important in determining the properties of cements. It is also important in the case of use of fly ash in the manufacture of ceramics, concrete, filling, road embankments, and even in agriculture.

### 3.3.3. GRAIN SIZE ANALYSIS – LASER PARTICLE SIZE ANALYZER

Laser particle size analyzer was used to determine grain size distribution. The results of the grain size analysis of Sample L and Sample O are shown on Figs 11 and 12.

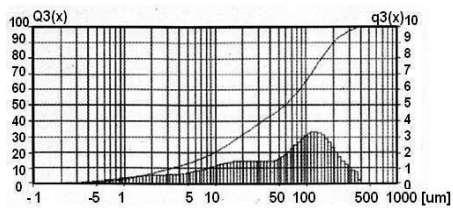


Fig. 11. Particle size analysis of Sample L

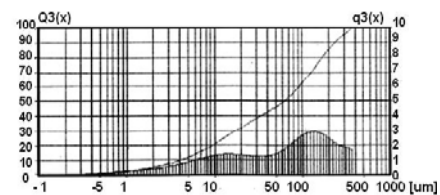


Fig. 12. Particle size analysis of Sample O

The results of grain size distribution of Sample L present size of grains that is in the range of 0 to 420 μm. Only about 3% of grains are smaller than 1 μm while 99% of grains are smaller than 340 μm, and 80% are smaller than 150 μm. It may be said that the fly ash is considered as fine-grained material. The grain size distribution of Sample L has a maximum of approximately 126 μm. It has average value of 57 μm and the standard deviation of 9 μm. Sample O has similar grain size distribution. The volume of grains is in the range of 0 to 360 μm. Only about 2.5% of grains are smaller than 1 μm, while 99% of grains are smaller than 350 μm, and 80% of them are smaller than 170 μm (fine-grained material). The grain size distribution of Sample O has one maximum approximately from 125 to 138 μm. It has average value from 58 to 62 μm and the standard deviation of 10 μm. Both fly ashes can be used as a raw material for the manufacture of many ceramic materials, cements, concretes, fillings, plastics

without further fragmentation, but its use in the manufacture of artificial aggregates or in agriculture is limited.

An accurate determination of the grain size distribution in loose raw materials and mineral wastes has extraordinary meaning in the selection of methods for their utilization in industry in which they can be used. It is particularly important when these materials are used in the mining, building, roads, ceramic and agriculture industry.

#### 4. CONCLUSION

An article presents progressive research methodology of using modern measuring devices to determine physical, chemical and mineralogical properties of fly ash. It also shows that this methodology allows to describe most important properties of tested material. The results allow to determine the direction of utilization of fly ash.

Although, the article discusses the application of different methods and measuring devices for analyzing samples of fly ash (a mineral substance with a very fine particles), most of these methods can be also used in studies of physical and chemical properties of other minerals.

The tests show that each of methods taken separately give only a part of the characteristics of investigated materials. These methods in parallel studies complement and confirm each other and allow for full characterization of the physical, chemical and mineralogical properties of various raw materials, waste and products. The results obtained by various methods overlap or act as input for other, e.g. elemental composition of the sample obtained in the point X-ray microanalysis (scanning microscope) corresponds to elemental composition determined by X-ray apparatus (elements, in the form of specific minerals).

Further studies, using the above and other advanced testing methods, will create comprehensive testing procedures for mineral raw materials and waste on a laboratory scale. Then, these procedures can be applied for in situ measurements of various properties of raw materials, products and waste on an industrial scale.

#### ACKNOWLEDGEMENTS

This article was carried out within the statutory work No. 11.11.100.276.

#### REFERENCES

- AHUJA, S., JESPERSEN, N., 2006. *Modern Instrumental Analysis*, Elsevier, New York.
- BLAHA, U., SAPKOTA, B., APPEL, E., STANJEK, H., RÖSLER, W., 2008. Micro-scale grain-size analysis and magnetic properties of coal-fired power plant fly ash and its relevance for environmental magnetic pollution studies, *Atmospheric Environment*, Vol. 42, No. 36, pp. 8359-8370.

- BOLEWSKI, A., KUBISZ, J., ŻABIŃSKI W., 1981. Mineralogia ogólna, Wydawnictwo Geologiczne: Warszawa.
- BOUZOUBAÂ, N., ZHANG, MH., BILODEAU, A., MALHOTRA, V.M., 1998. Laboratory-produced high-vol. fly ash blended cements: physical properties and compressive strength of mortars, *Cement and Concrete Research*, Vol. 28, No. 11, pp. 1555-1569.
- BULUT, G., CHIMEDDORJ, M., PEREK, K. T., ERSEVER, G., ESENLİ, F., 2008. Bentonite Calcium-interactions in Desiccant Clay Production, in *Proceedings of XXIV International Mineral Processing Congress* (ed: Duo, W D, Yao, S C, Hang, W F, Cheng, Z L and Long, H), pp. 3237-3240, (Beijing China).
- CHANCEY, RT, STUTZMAN, P, JUENGER, MCG and FOWLER, DW, 2010. Comprehensive phase characterization of crystalline and amorphous phases of a Class F fly ash, *Cement and Concrete Research*, Vol. 40, No. 1, pp. 146-156.
- CHAUWASAKOO, T and SOMBATSONPOP, N, 2007. Mechanical and morphological properties of fly ash/epoxy composites using conventional thermal and microwave curing methods, *Composites Science and Technology*, Vol. 67, No. 11-12, pp. 2282-2291.
- EROL, M, KÜÇÜKBAYRAK, S and ERSOY-MERİÇBOYU, A, 2007. Characterization of coal fly ash for possible utilization in glass production, *Fuel*, Vol. 86, No. 5-6, pp. 706-714.
- GIERGICZNY, Z., 2002. Popiół lotny aktywnym składnikiem cementu, IV Sympozjum Naukowo-Techniczne: Reologia w technologii betonu, Gliwice.
- GOLDSTEIN, J., NEWBURY, D.E., JOY, D.C., LYMAN, C.E., ECHLIN, P, LIFSHIN, E, SAWYER, L C, MICHAEL, J R, 2003. *Scanning Electron Microscopy and X-ray Microanalysis*, 3rd ed. (Plenum Press: New York).
- GOMES, S., FRANÇOIS, M., ABDELMOULA, M., REFAIT, Ph., PELLISSIER, C., EVRARD, O., 1999. Characterization of magnetite in silico-aluminous fly ash by SEM, TEM, XRD, magnetic susceptibility, and Mössbauer spectroscopy, *Cement and Concrete Research*, Vol. 29, No. 11, pp. 1705-1711.
- GUO, R.Q., VENUGOPALAN, D., ROHATGI, P.K., 1998. Differential thermal analysis to establish the stability of aluminum-fly ash composites during synthesis and reheating, *Materials Science and Engineering A*, Vol. 241, No. 1-2, pp. 184-190.
- HSIEH, Y.M., TSAI, M.S., 2003. Physical and chemical analyses of unburned carbon from oil-fired fly ash, *Carbon*, Vol. 41, No. 12, pp. 2317-2324.
- INABA, K., MATSUMOTO, K., 1999. The development of the measurement of particle concentration using a commercial laser diffraction particle size analyzer, *Advanced Powder Technology*, Vol. 10, No. 1, pp. 89-103.
- JENNY, G., PANKEWITZ, A., BEHRENS, C., 2008. High Resolution On-line Particle Size Distribution Analyses on Highly Concentrated Ore Slurries in *Proceedings of XXIV International Mineral Processing Congress* (ed: Duo, W D, Yao, S C, Hang, W F, Cheng, Z L and Long, H), pp. 2523-2534, (Beijing China).
- JIANG, J., Xu, X., WANG, J., YANG, S. and ZHANG, Y., 2007. Investigation of basic properties of fly ash from urban waste incinerators in China, *Journal of Environmental Sciences*, Vol. 19, No. 4, pp. 458-463.
- JONES, M.R., MCCARTHY, A., BOOTH, A.P.P.G., 2006. Characteristics of the ultrafine component of fly ash, *Fuel*, Vol. 85, No. 16, pp. 2250-2259.
- KASPRZYK, K. and PIETRYKOWSKI, P., 2007. Wykorzystanie popiołów lotnych w gospodarce [online], Zakład Spalania i Detonacji, Politechnika Wrocławska. Available from: <[http://www.spalanie.pwr.wroc.pl/badania/popioły/popioły\\_go.htm](http://www.spalanie.pwr.wroc.pl/badania/popioły/popioły_go.htm)> [Accessed: 10 April 2007].
- KĘDZIOR, A, TRYBALSKI, K, KONIECZNY, A, 2003. Zastosowanie nowoczesnych metod badawczych w inżynierii mineralnej, *Inżynieria Mineralna*, Vol.3.
- KORDEK, J., KĘPYS, W. and PALUCH, D., 2005. Powierzchnia właściwa proszków, porównanie wyników oznaczeń bezpośrednich z wynikami obliczonymi na podstawie składu ziarnowego, *Zeszyty Naukowe. Górnictwo / Politechnika Śląska*, Vol. 266, pp. 81-89.

- KOUKOUZAS, N., WARDB, C.R., PAPANIKOLAOU, D., LI, Z., KETIKIDIS, C., 2009. Quantitative evaluation of minerals in fly ashes of biomass, coal and biomass-coal mixture derived from circulating fluidised bed combustion technology, *Journal of Hazardous Materials*, Vol. 169, No. 1-3, pp. 100-107.
- KRAWCZYKOWSKA, A., 2007. Rozpoznawanie obrazów w identyfikacji typów rud i ich właściwości w produktach przeróbki rud miedzi, PhD thesis (unpublished), AGH University of Science and Technology, Kraków.
- KUTCHKO, B.G., and Kim, A.G., 2006. Fly ash characterization by SEM-EDS, *Fuel*, Vol. 85, No. 17-18, pp. 2537-2544.
- MAENAMI, H., Isu, N., ISHIDA, E.H., MITSUDA, T., 2004. Electron microscopy and phase analysis of fly ash from pressurized fluidized bed combustion, *Cement and Concrete Research*, Vol. 34, No. 5, pp. 781-788.
- MAŁOLEPSZY, J., TKACZEWSKA, E., 2007. Wpływ frakcji ziarnowej krzemionkowych popiołów lotnych na proces hydratacji i właściwości cementu, V Konferencja Naukowo-Techniczna: Zagadnienia materiałowe w inżynierii lądowej MATBUD'2007, Kraków.
- MO, X., FOURNIER, B., 2007. Investigation of structural properties associated with alkali-silica reaction by means of macro- and micro-structural analysis, *Materials Characterization*, Vol. 58, No. 2, pp. 179-189.
- MORENO, N., QUEROL, X., ANDRÉS, J.M., STANTON, K., TOWLER, M., NUGTEREN, H., JANSSEN-JURKOVICOVÁ, M., JONES, R., 2005. Physico-chemical characteristics of European pulverized coal combustion fly ashes, *Fuel*, Vol. 84, No. 11, pp. 1351-1363.
- NOCUŃ-WCZELIK, W. (ed.), 2003. *Laboratorium materiałów wiążących AGH Uczelniane Wydawnictwa Naukowo-Dydaktyczne*: Kraków).
- O'KEEFE, C.A., WATNE, T.M. and HURLEY, J.P., 2000. Development of advanced scanning electron microscopy techniques for characterization of submicron ash, *Powder Technology*, Vol. 108, No. 2-3, pp. 95-102.
- PAN, J., ZHU, D.Q., XIONG, S.A. and MENDES, V., 2008. Improving the Pelletization of Refractory Hematite by High Pressure Grinding Rolls. In *Proceedings of XXIV International Mineral Processing Congress* (ed: Duo, W D, Yao, S C, Hang, W F, Cheng, Z L and Long, H), pp. 2857-2865 (Beijing China).
- RYMON-LIPIŃSKI, T. and ZBOROWSKI, J., 1978. *Fizykochemiczne metody badań w ceramice* (AGH Uczelniane Wydawnictwa Naukowo-Dydaktyczne: Kraków).
- SARBAK, Z., STAŃCZYK, A. and KRAMER-WACHOWIAK, M., 2004. Characterisation of surface properties of various fly ashes, *Powder Technology*, Vol. 145, No. 2, pp. 82-87.
- SŁÓWKO, W., DRZAZGA, W. and KLUBIŃSKI, G., 2002. Quantitative characterization of surface topography in scanning electron microscopy, *Inżynieria Materiałowa*, Vol. XXIII, No. 2, pp. 69-72.
- STYSZKO-GROCHOWIAK, K., GOŁAŚ, J., JANKOWSKI, H. and KOZIŃSKI, S., 2004. Characterization of the coal fly ash for the purpose of improvement of industrial on-line measurement of unburned carbon content, *Fuel*, Vol. 83, No. 13, pp. 1847-1853.
- THIPSE, S.S., SCHOENITZ, M. and DREIZIN, E.L., 2002. Morphology and composition of the fly ash particles produced in incineration of municipal solid waste, *Fuel Processing Technology*, Vol. 75, No. 3, pp. 173-184.
- TOSUN, K., 2006. Effect of SO<sub>3</sub> content and fineness on the rate of delayed ettringite formation in heat cured Portland cement mortars, *Cement and Concrete Composites*, Vol. 28, No. 9, pp. 761-772.
- TRYBALSKI, K., KĘDZIOR, A. and KRAWCZYKOWSKI, D., 2004. Urządzenia i metody pomiarowe uziarnienia w polskich zakładach przeróbki rud metali nieżelaznych, *Górnictwo i Geoinżynieria*, Vol. 28, No.2/1.
- WYRWICKI, R., 2004. Analiza termogravimetryczna - niedoceniana metoda określania rodzaju i jakości kopaliny, *Górnictwo Odkrywkowe*, Vol. 46, No. 3/4, pp. 120-125.

- ZAENIA, A., BANDYOPADHYAYA, S., YU, A., RIDER, J., SORRELL, C.S., DAIN, S., BLACKBURN, D. and WHITE, C., 2010. Colour control in fly ash as a combined function of particle size and chemical composition, *Fuel*, Vol. 89, No. 2, pp. 399-404.
- ZHAO, D.J., KOLBEINSEN, L., van der EIJK, C. and TRANELL, G.M., 2008. Reduction of Ilmenite Pellets Under a CO-N<sub>2</sub> Gas Mixture, in *Proceedings of XXIV International Mineral Processing Congress* (ed: Duo, W D, Yao, S C, Hang, W F, Cheng, Z L and Long, H), pp. 2235-2241 (Beijing China).

**Szponder, D.K., Trybalski, K.,** *Określenie metodyki badań surowców i odpadów mineralnych z zastosowaniem nowoczesnych metod i urządzeń pomiarowych*, *Physicochem. Probl. Miner. Process.*, 46 (2011) 191-206, (w jęz. ang), <http://www.minproc.pwr.wroc.pl/journal>

W ostatnich latach obserwuje się dynamiczny rozwój różnorodnych dziedzin naukowych związany z wprowadzeniem nowych, doskonalszych urządzeń badawczych. Należą do nich między innymi: mikroskop elektronowy skaningowy, mikroanalizator rentgenowski, derywatograf, dyfraktometr rentgenowski, granulometr laserowy, piknometr helowy, aparat Blaine'a. Mogą być one wykorzystane przez praktycznie każdą dziedzinę nauki zajmującą się ciałami stałymi. Te nowoczesne metody znalazły również zastosowanie w badaniach właściwości surowców i odpadów mineralnych. Wykonywanie takich pomiarów może przyczynić się do stworzenia kompleksowych procedur badania surowców i odpadów mineralnych w skali laboratoryjnej. W publikacji podjęty został problem określenia metodyki badań właściwości zarówno fizycznych jak i chemicznych surowców i odpadów mineralnych na przykładzie popiołów lotnych, z zastosowaniem nowoczesnych metod i urządzeń pomiarowych. W części teoretycznej została przedstawiona charakterystyka poszczególnych metod badawczych, a także zasada działania urządzeń badawczych. Natomiast w części praktycznej omówiono metodykę wykonywania poszczególnych badań, a także przedstawiono przykładowe wyniki..

*słowa kluczowe: popioły lotne, właściwości mineralogiczne, rentgenowska analiza dyfrakcyjna, mikroanaliza rentgenowska, analiza termiczna, analiza granulometryczna, pomiar powierzchni właściwej*

Katarzyna OCHROMOWICZ \*, Tomasz CHMIELEWSKI\*

## **SOLVENT EXTRACTION IN HYDROMETALLURGICAL PROCESSING OF POLISH COPPER CONCENTRATES**

*Received June 15, 2010; reviewed; accepted July 30, 2010*

Recently, very unfavorable trends of decreasing copper content and increasing complexity of the Polish copper ores as well as lowering quality of final concentrates and metals recovery from concentration plants have been observed. This is also a major problem for the Polish copper smelters, which capabilities are not adapted to the complex and declining deposit conditions. The solution of this problem should be sought in hydrometallurgical methods (Leach-SX-EW). This paper focuses on the role of solvent extraction (SX) in recovering valuable metals from pregnant leach solutions. The problems related to the separation of undesirable and toxic metals are also discussed.

keywords: copper sulphides, copper ores, leaching, solvent extraction

### 1. INTRODUCTION

The most important operation in hydrometallurgy is leaching of properly prepared raw material by means of a specific chemical compound – leaching agent. Usually leaching agents and process conditions are selected depending on the material type and mineralization, in order to selectively and effectively extract the valuable elements to the solution and to avoid emission of dangerous or toxic gases to the atmosphere. The purification of solutions after leaching and subsequent recovery of useful elements requires application of appropriate separation processes. Among many separation processes used in hydrometallurgy, solvent extraction (SX) deserves special attention and is widely used on an industrial scale.

---

\* Division of Chemical Metallurgy, Faculty of Chemistry, Wrocław University of Technology, Wybrzeże Wyspiańskiego 23, 50-370 Wrocław, Poland

Solvent extraction is an important operation in many hydrometallurgical technologies, because it enables extraction of valuable metals from pregnant leach solutions (PLS) and acquisition of concentrated and purified solutions directed afterwards to appropriate unit operations (electrowinning, crystallization or precipitation of hard-soluble compounds). One of SX merits is the possibility of sulphuric acid waste management and isolation of sulphur as elementary sulphur (Apostoluk and Walkowiak, 2009).

SX is a process of transfer of soluble metal compounds occurring between aqueous and organic phase, in the liquid multicomponent two-phase system. Extraction is a chemical reaction between extracted metal ion existing in the aqueous phase and extractant from the organic phase. Here, the pregnant leach solution (PLS) constitutes the aqueous phase. Its composition has an enormous impact on the SX performance. The presence of valuable metals is as important as the presence of undesirable constituents. Therefore, the metals recovery will largely depend also on the mineralogical composition of the starting copper ore.

All over the world, leaching followed by SX/EW has been a rapidly developing technology in recent years. The role of SX in copper production is irrefutable. International Copper Study Group estimates that solvent extraction – electrowinning (SX-EW) production of copper is expected to increase by 4.4% annually to reach 5.2 Tg (megatonnes) in 2013 (ICSG Press Release, 2010). It is around 25% of the total copper production in the world.

Hydrometallurgical methods may be applied when high copper content standards are not fulfilled. This is also currently an issue in the Polish copper smelters which capabilities are not adapted to the complexity of ores and declining deposit qualities, including observed decrease in the copper content.

This paper brings some data on the unique nature of the Polish copper deposits. It also discusses several factors that must be considered in operating a copper SX-EW plant.

## 2. DESIGN FACTORS

In operation of a copper SX-EW plant many important factors have to be considered. The most crucial are the nature and metals content in the pregnant leach solution which depend on specifics and composition of the processed material, leaching medium, its type and concentration and other leaching parameters. The composition of PLS is diversified and differ in pH, Cu(II) and other valuable metals (Zn, Ni, Co, Fe etc.) concentration, as well as unwanted contaminants, like Fe(III), arsenic compounds, colloidal silica etc. Typically leach solutions contain from 20 to 80 g/dm<sup>3</sup> Cu, 0 to 30 g/dm<sup>3</sup> Fe, a host of other metals (Co, Ni, Zn, As) and a pH from < 1 to > 2 at relatively elevated temperatures (Kordosky, 2002).

The Polish copper ores exhibit very favourable mineralogical composition in terms of leachability. Chalcocite ( $\text{Cu}_2\text{S}$ ) and bornite ( $\text{Cu}_5\text{FeS}_4$ ), easily leachable minerals predominate in the Polish ores, while content of chalcopyrite ( $\text{CuFeS}_2$ ) and covellite ( $\text{CuS}$ ) is significantly lower (Chmielewski, 2007, Chmielewski, 2009). Mineralogical analyses of concentrate samples indicated, that the content of chalcopyrite was within 17-20%, while only the traces of chalcopyrite were detected in the shale by-product (middlings). In this material copper practically exists as chalcocite and bornite.

Copper containing sulphide materials (ores and concentrates) have different mineralogical and metallic compositions. Zinc, nickel, cobalt, silver, gold and platinum group metals, as valuable metals, are economically important components of polymetallic sulphide materials. Iron and arsenic are the most unwanted contaminants of the sulphide copper ores and concentrates. The hydrometallurgical processing of such materials consists of copper (main component) extraction, recovery of accompanying valuable metals (Ni, Co, Zn), and effective removal of arsenic and iron, as undesired and difficult to process elements.

Leaching experiments (Chmielewski, 2009) showed that the shale by-products (middlings) from the Lubin Concentrator (ZWR Lubin) can be effectively processed using hydrometallurgical methods (non-oxidative and atmospheric leaching) in order to recover copper and accompanying metals. Non-oxidative leaching is a fast, selective and easy controllable process. Atmospheric leaching with sulphuric acid was found to be surprisingly efficient for copper, zinc and cobalt recovery from the by-product (middlings) – tailings from the 1<sup>st</sup> cleaning flotation of the 1<sup>st</sup> technological circuit at ZWR Lubin. For nickel removal it is necessary to grind coarse grains to obtain granulation below 40  $\mu\text{m}$ . Moreover, the introduction of Fe(III) ions to the leaching solution causes a significant and beneficial change in the leaching kinetics. An increase of the leaching rate of Cu(II), Co(II), Ni(II) was observed.

Atmospheric leaching extracts also arsenic to the solution. Its concentration at 90°C reaches 45  $\text{mg}/\text{dm}^3$  in single-step leaching. Therefore, this element has to be separated from the leaching solutions and isolated in an environmentally safe form. The PLS, after atmospheric leaching of the Lubin concentrate, usually contains: Cu 15-23  $\text{g}/\text{dm}^3$ , Zn 0.7-1.1  $\text{g}/\text{dm}^3$ , Ni 4-21  $\text{mg}/\text{dm}^3$ , Co 16-76  $\text{mg}/\text{dm}^3$ , Fe 10-30  $\text{g}/\text{dm}^3$  and its pH is around 1.

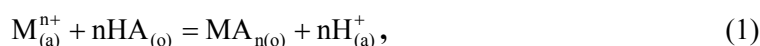
### 3. EXTRACTION OF VALUABLE METALS

The most important part of a solvent extraction circuit is a proper selection, and preparation of organic solution containing extractant. The choice of organic diluent will also influence process and operational variables such as pH and temperature. Depending on application, extractants have different chemical nature: acidic, basic and organic salts, chelating, solvating etc.

Beside extractant, an important component of the organic phase is organic diluent. Practical importance (in extraction used in hydrometallurgical technologies) has only

hydrocarbonaceous diluents. Kerosene containing heavier aliphatic hydrocarbons can be used as a diluent, for example the C<sub>12</sub>-C<sub>14</sub> fraction, which does not show solvating extractant features. Aromatic hydrocarbons show relatively weak solvating ability. Usually, hydrocarbonaceous diluents are mixtures of different types of hydrocarbons. High boiling and flash-points are desired features for good diluents because they allow lowering their losses due to evaporating and minimize fire hazard.

Aromatic hydroxyoximes (HA) extract metal cations (M<sup>n+</sup>), forming hydrogen ions according to the chemical reaction:



where subscripts (a) and (o) are related to aqueous and organic phase, respectively. According to Eq. 1, extraction of different metal cations with HA extractant depends on acidity of aqueous phase, measured by the pH value. The pH of the aqueous phase corresponding to extraction of given metal with efficiency of 50% is defined as half extraction (pH<sub>50</sub>) (Szymanowski, 1990). Metal cations extracted with different extractants under similar experimental conditions can be ranked according to their increasing pH<sub>50</sub> value. This, the so called selectivity series of metal's extraction, allows estimating the possibility of metal ions separation. It is assumed that a pair of chosen metals can be effectively separated when their pH<sub>50</sub> values differ at least by one unit.

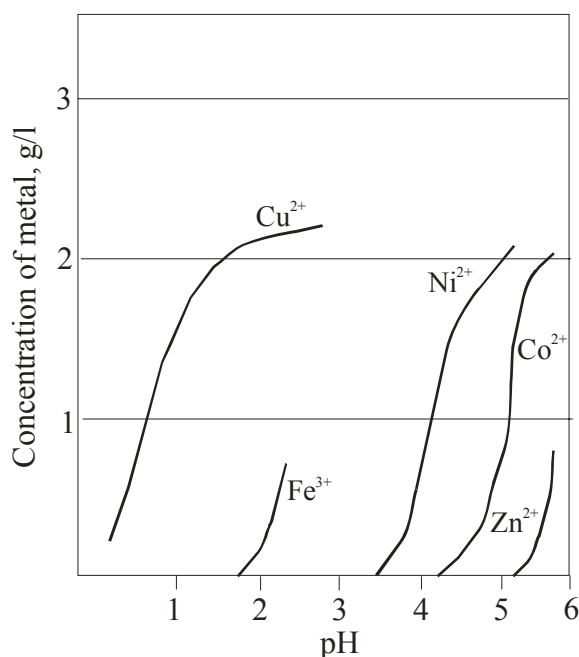
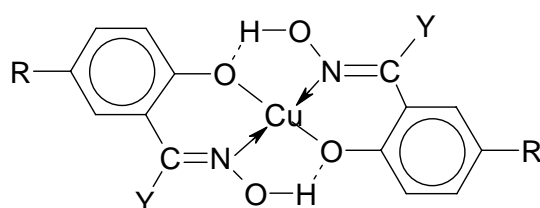


Fig. 1. The effect of pH on metals extraction with LIX 84 (Szymanowski, 2003)

From Fig. 1 the following series can be seen: Cu(II) > Fe(III) > Ni(II) > Co(II) > Zn(II). For extractants belonging to other chemical group of compounds, Fe(III) usually precedes Cu(II), while Zn(II) precedes Ni(II) and Co(II). In some cases Co(II) precedes Ni(II), where differences between the pH<sub>50</sub> values are usually small, which means that effective separation is difficult or impossible. An example of an extraction sequence of metals with carboxylic acids is given below:



The complexing ability of copper ions by hydroxyoxime group from acidic sulphate solutions decreases in the following series of substituent Y: H > CH<sub>3</sub> > C<sub>6</sub>H<sub>5</sub> (Szymanowski, 2003). Therefore, complexation of copper ions with increasing acidity of aqueous phase is more effective.

A negative feature of hydroxyoxime extractant solutions in hydrocarbonaceous diluents used for copper(II) extraction is their low extraction capacity (maximum copper concentration to obtain in loaded organic phase), which reaches from 6 to 8 g Cu(II)/dm<sup>3</sup> (Szymanowski, 1990). According to Eq. 1, the extraction reaction of metal cations is reversible towards hydrogen ions. Equilibrium state of the reaction (Eq. 1) is shifted towards products, when hydrogen ions concentration in aqueous phase is low, while high H<sup>+</sup> concentration in aqueous phase favours reextraction, shifting equilibrium towards substrates. However, in solutions, such as concentrate pressure oxidation liquors, where copper concentrations can be in excess of 40 g/dm<sup>3</sup>, Eq. 1 adds a significant amount of acid to the PLS. This in turn can shift the equilibrium towards stripping. The simplest and most expensive solution to this problem is a direct neutralization of acid in the mixers:



This requires no additional equipment or flowsheet changes, but reagent costs can be prohibitive. Another solution is to adsorb acid with ion exchange resins. However, this yields a relatively useless dilute acid (Grinbaum, 2007). In the case of Polish copper ores, by-products or concentrates, the excess of acid, which is formed during extraction, can be utilized in non-oxidative decomposition of carbonates, which are the major component of barren rocks.

Reextraction has two basic goals: getting cleaned and concentrated aqueous

solution of valuable metal salt and regeneration of extractant solution in organic diluent. Loaded organics contain usually a series of impurities, mainly as fine suspended mineral substances, dust and dispersed aqueous phase. Therefore, loaded organics should be first rinsed with water and then subjected to reextraction. For stripping of copper(II) from organic phase, sulphuric acid solutions are used. Usually, they are spent electrolytes retreated from electrolysis.

Preliminary extraction studies of valuable metals from PLS after leaching of middlings from the Lubin Concentrator exhibited promising results (Rotuska and Chmielewski, 2007). PLS contained 4300 ppm of copper, 4.7 ppm of nickel, 8.7 ppm of cobalt, 2060 ppm of iron, 115 ppm of zinc and 13.5 ppm of arsenic. Aromatic hydroxyoximes: LIX 84, 612 and 984 were investigated as copper(II) extractants. D2EHPA was used for zinc(II) and Cyanex 272 for nickel(II) and cobalt(II) extraction.

It was demonstrated that application of aromatic hydroxyoximes for copper(II) extraction can give satisfying results. The best extraction power exhibited LIX 984 with yield of extraction  $E = 99.4\%$  at A/O 1:1. Under the same conditions LIX 84 appeared to be less effective ( $E=85\%$ ). In each case the increase of extractant concentration in the organic phase increases yield of copper(II) extraction. When A/O ratio was equal to 2:1 the yield of extraction was lower for LIX 84 (around 57%) but still high for LIX 612 and LIX 984, respectively. However, none of these extractants were selective enough and other metal ion species present in leach solutions were also transferred to the organic phase.

Copper(II) reextraction from loaded organic with 1M  $H_2SO_4$  was not satisfactory. Moreover, the stronger Cu(II) extractant used in extraction stage the lower efficiency obtained in reextraction stage. Probably, reextraction of copper(II) could be facilitated by higher concentration of  $H_2SO_4$  in a strip solution or by addition to the organic phase of an appropriate quantity modifier, e.g. tridecanol or nonylphenol.

Recovery of the remaining metal was very low. Cyanex272 was used as Co(II) and Ni(II) extractant and was able to extract only 16.5% and 14% of cobalt(II) and nickel(II), respectively. Probably, the use of another extractant or its combination with some modifier could increase those metals recovery. Separation selectivity of such ion pair like Ni(II) and Co(II) extracted with carboxylic acid can be improved by modification of organic phase composition. Introduction of additional compound, called synergetic agent, causes a significant increase of extraction of one metal, even at low pH conditions, and does not have significant impact on extraction of the other metal.

In extraction systems of Ni(II) and Co(II) with carboxylic acids, aldehyde oxime or aliphatic ketone can be used as the synergetic agent. It is illustrated by extraction curves of these metals with naphthenic acids mixture and the same mixture in presence of iso-tridecane aldehyde oxime (Fig. 2).

Concentration of metal in the organic phase is a function of its concentration in

aqueous phase, acid concentration in aqueous phase and extractant concentration in organic phase and also type and structure of extractant, organic diluent and different additives existing in both phases (modifiers in organic phase and electrolytes in aqueous phase). Therefore, additional experiments are necessary to establish the optimal conditions of Cu(II), Co(II), Ni(II), Zn(II) extraction and reextraction processes.

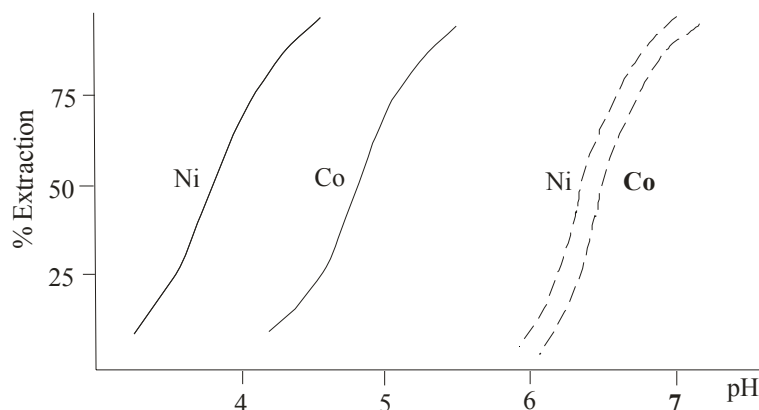


Fig. 2. Co(II) and Ni(II) extraction with 0.5 M solution of naphthenic acids in xylene (dashed lines) and mixture of 0.5 M naphthenic acids with 0.1M iso-tridecane aldehyde oxime (solid lines)

#### 4. EXTRACTION OF UNDESIRABLE AND TOXIC METALS FROM PLS

##### 4.1. IRON

Iron, which is a major component of pregnant leach solution is particularly inconvenient in solvent extraction circuits. It affects the design and operation of a solvent extraction plant in several ways. Very often, iron concentration in solutions reaches a much higher level than those of useful compounds, which seriously complicates the process of selective extraction of these metals. Moreover, its presence in electrolyte introduced to electrolysis is highly unwanted, because it negatively affects current efficiency (Szymanowski, 1990). Unfortunately, PLS will contain iron and its concentration will be increasing as a result of leaching of minerals such as  $\text{CuFeS}_2$ ,  $\text{Cu}_5\text{FeS}_4$  and  $\text{FeS}_2$ . Therefore, it has to be reduced from the circuits and separated from the remaining metals.

In copper extraction from acidic solutions (pH between 1 and 2), selectivity of copper extraction over iron is very important. Currently, the application of ester modified reagents offers the best copper/iron selectivity (Szymanowski, 1990). Good effects can be achieved also by using carboxylic acids, for example a mixture of naphthenic acids,  $\text{H}_2\text{A}_2$ , which are effective and selective towards iron, extracting iron at much lower pH than other useful metals (Fig. 3).

Iron(III) can also be removed from solutions after atmospheric or pressure leaching with sulphuric acid by means of mixed extractants based on amines and solvating diluents and also organophosphorous acids, tributyl phosphate and phosphine oxides. Besides extraction, the most frequently used and the cheapest method of iron(III) removal from acidic solutions is precipitation of hardly soluble iron hydroxide -  $\text{Fe}(\text{OH})_3$ , goethite -  $\text{FeO}(\text{OH})$ , hematite -  $\text{Fe}_2\text{O}_3$  or jarosite -  $\text{MFe}_3(\text{SO}_4)_2(\text{OH})_6$ , where  $\text{M} = \text{H}, \text{Na}, \text{K}, \text{NH}_4, 1/2\text{Pb}$ , precipitated from sulphatic solutions. In each case, partial neutralization is necessary, for example with milk of lime, in order to obtain optimal pH value:



Another solution is the use of ion exchange resins to treat a bleed from the electrolyte and selectively remove iron. This is the Fenix Iron Control Process and it was effective at controlling iron in the Mount Gordon copper plant (Shaw et al., 2006).

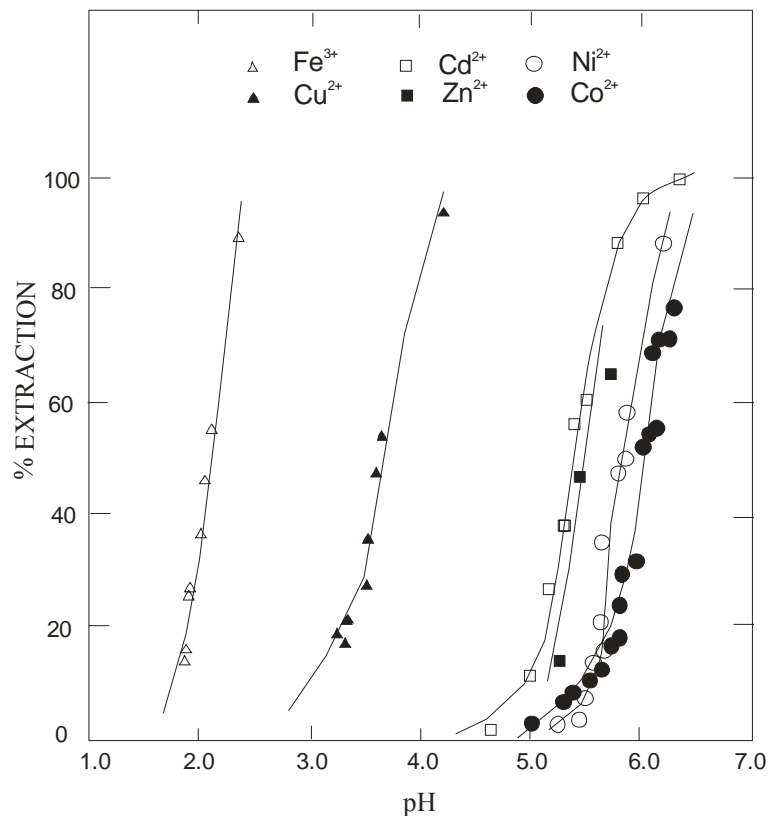


Fig. 3 The effect of pH on selectivity of metals extraction with naphthenic acids

#### 4.2. ARSENIC

In hydrometallurgy, close attention is paid to soluble arsenic compounds, which are very toxic and dangerous. Arsenic is an element which is almost always present in copper ores and its separation from technological circuits or stabilization in ecologically acceptable form became the key concern in copper industry. In solutions after leaching of ores, concentrates, dusts and slag, and also in spent electrolytes, liquors and wastes, different amounts of As(III) and As(V) occur. Significant amounts of arsenic sulphides occur in copper sulphide concentrates containing enargite ( $\text{Cu}_3\text{AsS}_4$ ) and tenantite ( $\text{Cu}_{12}\text{As}_4\text{S}_{13}$ ). Selective leaching of this concentrates with sodium sulphide leads to chalcocite concentrates with small content of arsenic, directed then to smelter (Apostoluk, 2005). In the Lubin Concentrator the content of arsenic reaches 3.3 kg/Mg of concentrate and is currently not acceptable for technical and environmental reasons.

It is worth mentioning that in the case of hydrometallurgical processing of copper-arsenic sulphide concentrates, there is no known solution with application of solvent extraction of arsenic. From solutions after leaching, containing excess of acids and contaminated with Fe(III) and As(V), compounds with optimal ratio of Fe/As can be precipitated in the form of scorodite ( $\text{FeAsO}_4 \cdot 2\text{H}_2\text{O}$ ) after appropriate correction of pH with milk of lime. Elevated temperature and pressure are recommended for precipitation of crystalline scorodite, which exhibits the lowest solubility among arsenic compounds.

In practice, only extractive removal of As(V) from spent electrolytes is used. In spite of a vast number of extractants effective in extraction of As(V), tributyl phosphate is used worldwide to remove arsenic from the spent electrolytes. Its drawback is relatively high solubility in raffinates. Hydrophobic oxides of trialkylphosphines, like TOPO, Cyanex 921, mixtures of these oxides (Cyanex 923 and 925) and di(2,4,4-trimethylpentyl) ditiophosphinic acid are free of this drawback and are efficient for removal of As(III) and As(V) from solutions in sulphuric acid (Iberhan and Wiśniewski, 2002).

Another method for arsenic separation from spent electrolytes is adsorption. The ability for effective adsorption of arsenic compounds from diluted solutions is possible by activated carbon, pyrite and metal's oxides or hydroxides like dioxide of manganese, tin, titanium, magnetite, iron(III) and magnesium(II) oxides.

#### 4.3. SILICA

Silica can also be present in the copper leach solution as a result of presence of sandstone in the copper ore or in the host rock. The presence of silica in the copper leach solution can be problematic in the solvent extraction circuit. Main difficulties are related to poor phase disengagement, high levels of entrainment and poor organic

recovery in the flotation columns. These issues were recognized in Girilambone copper SX-EW plant (Miller et al., 1997). It was found that running the operation in aqueous continuous mode caused crud formation throughout the organic phase. Significant build up of crud was occurring in the strip stage. There were a gelatinous film and solids observed. To solve those problems the operation was conducted in organic continuous regime. The reduction of aqueous entrainment in the organic and decreased silica levels were observed.

#### 4.4. LEACHING ADDITIVES

Occasionally, leaching requires addition of different agents which are able to elevate recovery or kinetics of this stage. Usually, leaching additives are surfactants, which can improve the penetration of the leach solution into the pores of ground minerals by reducing the surface tension of the leach solution (Kordosky and Virnig, 2007).

Unfortunately, these chemicals are still present in the PLS when entering the SX-EW segment of the circuit. Therefore, they can significantly affect further performance. A low surface tension of the aqueous phase can help in stabilization of dispersions, increasing the time for settling and phase separation. In the organic phase surfactants may cause formation of reverse micelles, which will carry impurities from the leach solution to the electrolyte (Kordosky and Virnig, 2007). Therefore, it is important to consider the possible negative effects of leaching aids on the SX-EW process and how to best mitigate them.

#### 4.5. CALCIUM AND MAGNESIUM

This case can be expected in leaching and extraction of metals from the Polish copper ores and concentrates containing elevated amounts of Ca and Mg carbonates as a gangue.

In sulphate solutions containing Co(II) and Ni(II), small amounts of Ca(II) and Mg(II) can also be present. During Co(II) and Ni(II) extraction with Cyanex 272, Mg(II) and Ca(II) are co-extracted to organic phase. Cobalt(II) and nickel(II) reextraction with spent electrolytes causes precipitation of relatively sparingly soluble calcium sulphate and contamination of these electrolytes with calcium and magnesium.

To prevent this situation, 2-methyl-2-ethylheptane acid (Versatic 10) with the addition of tributylphosphate (TBP) was suggested for Ni(II) and Co(II) extraction from almost neutral (pH=6.5) sulphatic solutions containing calcium and magnesium (Apostoluk, 2005).

## 5. CONCLUSION

Solvent extraction is permanently related with hydrometallurgical technologies of copper polymetallic sulphide concentrates processing. The main fields of application of this operation are cleaning of pregnant leach solutions from unwanted additives and recovery, separation and concentration of valuable metals.

The effectiveness of selective recovery of ions is determined by many factors starting from deposit and feed characteristics, leaching method and leach solution properties, the properties of used chemical compounds, which enables efficient, selective and fast recovery of appropriate metal ions.

Having in mind unfavourable trend of lowering quality of concentrates and metals output at Lubin Concentrator, the solution of this problem should be sought in hydrometallurgical methods. The preliminary studies indicate that application of Leach SX-EW technology will help to overcome this negative trend.

## REFERENCES

- APOSTOLUK W., 2005, Ekstrakcja rozpuszczalnikowa w technologiach otrzymywania metali towarzyszących siarczkowym rudom miedzi, X Seminarium "Hydrometalurgia metali towarzyszących", Lubin, 95-114.
- APOSTOLUK W., WALKOWIAK W., 2009, XII seminarium: referaty, Lubin, 17 lutego 2009. Wrocław: Oficyna Wydawnicza Politechniki Wrocławskiej, 2009, 77-100.
- CHMIELEWSKI T., 2007, Atmospheric leaching of shale by-product from Lubin Concentrator, Physicochemical Problems of Minerals Processing, 41, 337-348
- CHMIELEWSKI T., 2009, Ługowanie atmosferyczne frakcji łupkowej jako alternatywa zmian technologicznych w ZWR Lubin, Materiały XII Seminarium "Metody hydrometalurgiczne a rozwój produkcji w KGHM "POLSKA MIEDŹ" S.A.", 37-53.
- GRINBAUM B., 2007, Optimization of Cu SX by control of the acidity, Copper, Toronto, Canada, 26-29 August 2007. Ed. P.A. Riveros, D.G. Dixon, D.B. Dreisinger, M.J. Collins. Montreal, Quebec: Canadian Institute of Mining Metallurgy and Petroleum, 81- 87.
- IBERHAN L., WIŚNIEWSKI M., 2002, Extraction of arsenic(III) and arsenic(V) with Cya-nex 925, Cyanex 301 and their mixtures, Hydrometallurgy, 63, 23-30.
- ICSG Press Release, 2010, New Edition of Directory of Copper Mines and Plants, (I.II.2010).
- KORDOSKY G., 2002, Copper solvent extraction for concentrate leach solutions, Alta Conference.
- KORDOSKY G., VIRNIG M., 2007, Copper Leaching Aids – Compatibility with the copper SX process", Toronto, Canada, 26-29 August 2007, Ed. P.A. Riveros, D.G. Dixon, D.B. Dreisinger, M.J. Collins. Montreal, Quebec: Canadian Institute of Mining Metallurgy and Petroleum, 15-24.
- MILLER G.M., READETT D.J. HUTCHINSON P., 1997, Experience in operating the Girilambone copper SX-EW plant in changing chemical environments, Minerals Engineering, Vol. 10, 467-481.
- ROTUSKA K., CHMIELEWSKI T., 2007, Solvent extraction of valuable metals from preg-nant leach

solutions of cupriferous shale, *Physicochemical Problems of Mineral Processing*, 41, 365-372.

SHAW R., VANCE S., ILLESCAS J., DREISINGER D., WASSINK B., 2006, Ion exchange for iron impurity control in the base metal industry, *Iron Control Technologies*, Montreal, Canada, Ed. J.E.

DUTRIZAC AND P.A. RIVEROS, 757-769.

SZYMANOWSKI J., 1990, *Ekstrakcja miedzi hydroksyoksymami*, PWN, Warszawa – Poznań.

SZYMANOWSKI J., 2003, Wybrane fizykochemiczne aspekty wydzielania jonów metali, *Membrany teoria i praktyka, Membrany Teoria i Praktyka*, R. Wódzki, Ed., UMK Toruń, 30-46.

**Ochromowicz, K., Chmielewski, T.,** *Ekstrakcja rozpuszczalnikowa w hydrometalurgicznym przetwarzaniu polskich koncentratów miedzi*, *Physicochem. Probl. Miner. Process.*, 46 (2011) 207-218, (w jęz. ang), <http://www.minproc.pwr.wroc.pl/journal>

Od kilkunastu lat obserwuje się bardzo niekorzystny trend obniżania zawartości miedzi i wzrostu zawartości metali towarzyszących i węgla organicznego w polskich złożach miedzi LGOM oraz zmniejszania jakości koncentratów z zakładów wzbogacania. Stanowi to ogromny problem dla polskich hut miedzi, których zdolności nie są dostosowane do trudnych i pogarszających się warunków złożowych. Rozwiązaniem tych problemów może być wprowadzenie nowoczesnych metod hydrometalurgicznych (ługowanie – ekstrakcja rozpuszczalnikowa – elektroliza). W pracy omówiono rolę ekstrakcji rozpuszczalnikowej w odzyskiwaniu cennych metali z roztworów po ługowaniu. Omówiono także problemy związane z separacją metali toksycznych lub niepożądanych z tych roztworów

*słowa kluczowe:* siarczki miedzi, ruda miedzi, ługowanie, ekstrakcja rozpuszczalnikowa

Andrzej OBRANIAK\*, Tadeusz GLUBA\*

## A MODEL OF GRANULE POROSITY CHANGES DURING DRUM GRANULATION

*Received May 10, 2010; reviewed; accepted August 1, 2010*

A model equation to determine mean inner porosity of granules  $\varepsilon$  is proposed. The equation is based on the size analysis of bed particles (agglomeration kinetics) and the measurement of bulk density of feed. Bulk density of a granulated product depends on properties of the raw materials (density, particle size distribution), properties of the wetting liquid, particle concentration in the formed granules (porosity of the granules), as well as on the obtained particle size distribution on which interparticle space volume depends. In order to verify the proposed model, the process of drum granulation was tested for the following range of changing parameters: drum diameter  $D = 0.25$  to  $0.4$  m, filling of the drum with granular material  $k = 5$  to  $20\%$  of the inner volume, relative rotational speed of the drum  $n_r = 0.15$  to  $0.375$  of critical velocity. The granular bed was wetted drop-wise during the drum rotations, at constant liquid supply rate  $Q = 1$  cm<sup>3</sup>/s. During the process, at constant time intervals, samples were taken from the drum and on their basis values of bulk density of the feed as well as its particle size distribution, and inner porosity of the granules for a given size fraction were determined. The volume of liquid accumulated in the inner pores of the granules was specified basing on the mass balance before and after drying. Results of the research confirmed validity of the proposed model.

*keywords: agglomeration, bulk density, drum granulation, porosity*

### 1. INTRODUCTION

The process of tumbling granulation is usually described basing on the analysis of its kinetics (Kapur and Fuerstenau, 1966; Newitt and Conway-Jones, 1958) The particle size distribution of the processed bed does not provide information on its

---

\* Faculty of Process and Environmental Engineering, Technical University of Lodz, Wolczanska 213, 90-094 Lodz, obraniak@wipos.p.lodz.pl

many important properties, but on the other hand it determines the choice of some statistical parameters which characterise selectively the properties of tested granulated product. Heim et al. (2002) claimed that the parameter which well described granular bed properties was its bulk density  $\rho$ , a parameter easy to measure and frequently used in practice. This parameter, however, does not reflect either many significant features of agglomerates being formed. Additionally, it is not known if changes in bulk density of the granulated material are a result of changes in packing of individual granules in the bed, or changes in the porosity of granules as such. The porosity well characterises the structure of formed granules and could supplement the product description but unfortunately it is difficult to determine, especially online. For this reason, a new model of tumbling agglomeration was proposed to enable estimation of mean porosity of granules based on the measurement of bulk density of the granulated bed and its particle size analysis.

## 2. AIM OF THE WORK

The aim of this research was to develop a mathematical model of fine-grained bed granulation while wetting in a rotary drum. The model combines the agglomeration kinetics with changes in bulk density of the bed and porosity of granules in reference to air content in the processed bed.

## 3. EQUIPMENT AND INVESTIGATION RANGE

A schematic diagram of the experimental rig is shown in Fig. 1. Drum (1) was driven by motoreducer (3) through a belt transmission and a coupling. The rotational speed of the drum was changed smoothly using inverter (4). A granular bed placed in the drum was wetted drop-wise by means of sprayer (2), inserted axially to the drum.

The wetting liquid was supplied at constant flow rate  $Q = 1 \text{ cm}^3/\text{s}$  from tank (6) placed on the level of 2.5 m from the drum axis. The liquid flow rate was settled by means of rotameter (7). The sprayer was mounted on a separate stand (5). For the whole time of the experiment a constant level of liquid in the tank was maintained which ensured constant pressure of liquid supplied. The wetting liquid was distilled water.

The process of granulation was carried out batch-wise in drum granulators of the same length  $L = 0.24 \text{ m}$  and diameters ranging from  $D = 0.25$  to  $0.4 \text{ m}$ . The filling of the drum with granular material  $k$  was changed from 5 to 20% of the inner volume, and relative rotational speed of the drum  $n_w$  from 0.15 to 0.375 of the critical velocity.

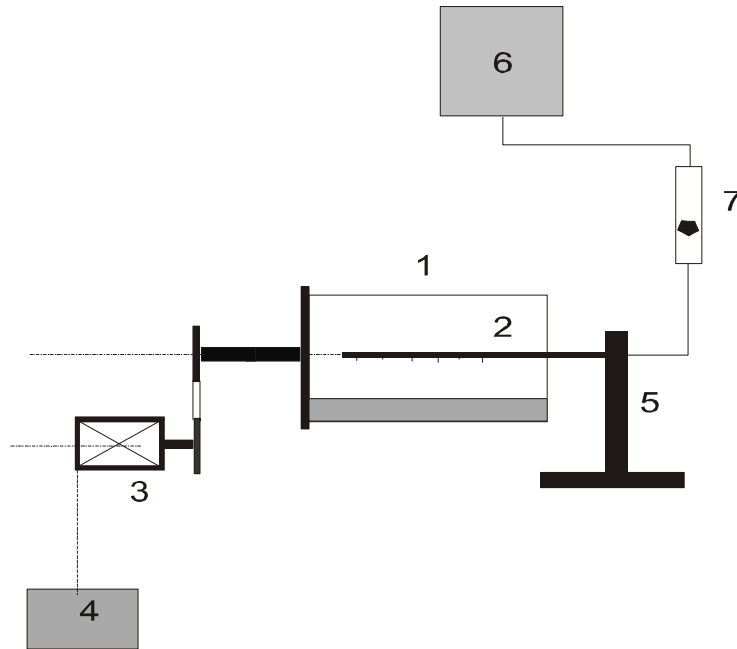


Fig. 1. Schematic diagram of the experimental rig

#### 4. MEASURING METHODS

In preliminary studies basic properties of the experimental material (foundry bentonite) were identified. Particle size distribution of the raw material was determined using a FRITSCH laser particle size analyser and on this basis an average size was calculated. The size of bentonite particles was  $<0.16$  mm, and their mean volumetric size was  $d_m = 0.056$  mm. Density of the material measured by a pycnometer, was  $\rho_s = 2150$  kg/m<sup>3</sup>, and mean bulk density determined as an arithmetic mean from the bulk density of material both loose and concentrated to a minimum volume in a shaker, was  $\rho_{ns} = 865$  kg/m<sup>3</sup>.

To identify properties of the granulated product obtained in the process, representative samples were taken from the drum at constant time intervals (every 60 or 120 s). On this basis bulk density and particle size distribution of the feed were specified. After making appropriate measurements the sample was returned to further granulation. Based on the results of sieve analysis, mass fraction with particles  $< d_o = 1$  mm was estimated. The fraction consisted mainly from not granulated particles of the raw material. For the entire process duration the instantaneous values of torque were measured every 1 s on the granulator shaft.

## 5. MODEL

Based on the analysis of a definition of bulk density Gluba et al. (2004) related changes in the bulk density of a granulated bed during wetting to moisture content of the feed  $w$ , density of raw material  $\rho_s$  and wetting liquid  $\rho_w$ , mass of raw material  $m_s$  and the volume of air contained in the bed  $V_p$ . The following relation (Eq.1) was obtained:

$$\rho = \frac{1 + \frac{m_w}{m_s}}{\frac{1}{\rho_s} + \frac{m_w}{\rho_w \cdot m_s} + \frac{V_p}{m_s}} = \frac{1 + w}{\frac{1}{\rho_s} + \frac{w}{\rho_w} + \frac{V_p}{m_s}}, \quad (1)$$

where  $m_w$  is the mass of binding liquid, kg. The feed mass in the granulator  $m_s$ , specific density of powder  $\rho_s$  and wetting liquid density  $\rho_w$  do not changed in the process.

The above relation shows that changes in bulk density of the granulated bed  $\rho$  depend only on its moisture content  $w$  and the volume of air accumulated in the bed  $V_p$ . At continuous liquid supply, moisture content of the bed is directly proportional to time, and the only unknown value is air volume  $V_p$ . This volume is related to inner porosity of formed granules ( $V_{pg}$ ), and to the volume of pores between the granules and unprocessed feed particles ( $V_{pmg}$ ).

Taking this into Eq. 1, we obtain:

$$\rho = \frac{1 + w}{\frac{1}{\rho_s} + \frac{w}{\rho_w} + \frac{V_{pg}}{m_s} + \frac{V_{pmg}}{m_s}}. \quad (2)$$

Further considerations were preceded by some simplifying assumptions. It was assumed that each droplet falling down on the bed formed a nucleus that accumulated wetting liquid and during the further process its dimension increased. This means that during wetting the whole water supplied to the bed was accumulated in the nuclei or granules being formed. Additionally, it was assumed that the considerations would refer to this stage only at which granulated product was formed, when not granulated material still remained between the granules, although with time its amount was decreasing. To describe the mechanism of changes in the volume of air accumulated inside the granulated bed and in the formed granules, the process of batch granulation was analysed at continuous wetting, from the initial point, i.e. dry powder material, until the moment when all raw material will become the form of granules.

The process discussed in the paper was initiated by sprinkling the bed which tumbled in a horizontal rotary drum. Liquid droplets of dimension about 3 mm fell down onto free surface of the tumbling bed inclined due to drum rotations, penetrated

it and formed nuclei of future granules. At the beginning of the process, when only a few droplets have entered the bed, in the powder material single granules (nuclei) appeared, which were not in contact with one another. They formed single agglomerates suspended in a powder medium. When the process proceeded, the number of granules increased at the cost of unprocessed material, however for a fairly long time they constituted a few centres separated from each other by the powder material. At this stage of the process the granules were quite dry on the surface. This lasted until the moment when an increase of the number and size of the agglomerates led to a situation when individual granules got in contact, although spaces between them were still filled up by material that had not been granulated yet. A continuation of the agglomeration process resulted in a gradual granulation of the whole powder material, at a simultaneous increase of dimensions of the previously formed granules.

The initial air volume  $V_{pp}$  accumulated in the dry bed of feed, can be determined by subtracting from the total volume of the powder bed  $V_{cs}$  the volume of feed particles (bentonite)  $V_s$ , which formed this bed:

$$V_{pp} = V_{cs} - V_s = \frac{m_s}{\rho_{ns}} - \frac{m_s}{\rho_s} = m_s \left( \frac{1}{\rho_{ns}} - \frac{1}{\rho_s} \right). \quad (3)$$

Due to the fact that with the formation of subsequent granules the fraction of not granulated material (bentonite powder) decreased, the above relation could be applied after taking into account the fraction of not granulated material  $U_m$  in any time interval (arbitrary bed moisture content) of the discussed granulation period. Then, we got the following relation:

$$V_{pmg} = U_m \cdot m_s \left( \frac{1}{\rho_{ns}} - \frac{1}{\rho_s} \right). \quad (4)$$

Substituting it to (2), the following form of bulk density relation is obtained:

$$\rho(w, U_m) = \frac{1 + w}{\frac{1}{\rho_s} + \frac{w}{\rho_w} + \frac{V_{pg}}{m_s} + U_m \left( \frac{1}{\rho_{ns}} - \frac{1}{\rho_s} \right)}. \quad (5)$$

Fraction  $U_m$  is a function of bed moisture content. Upon transformation we get:

$$V_{pg} = m_s \cdot \left[ \frac{1 + w}{\rho(w, U_m)} - \frac{1}{\rho_s} - \frac{w}{\rho_w} - U_m \left( \frac{1}{\rho_{ns}} - \frac{1}{\rho_s} \right) \right]. \quad (6)$$

If then a bed is formed from porous particles, e.g. granules composed of solid particles (Fig. 2), the total bed porosity depends both on the volume of intragranular spaces and pore volume in the granules themselves. Inner porosity of granules  $\varepsilon$  can be determined from the relation:

$$\varepsilon = \frac{V_{pg}}{V_g} = \frac{V_{pg}}{V - V_{ns}}, \quad (7)$$

where:  $V_g$  – total volume of granules,  $m^3$ .

Substituting Eq. (6) to (7) we have:

$$\varepsilon = \frac{m_s \cdot \left[ \frac{1+w}{\rho} - \frac{1}{\rho_s} - \frac{w}{\rho_w} - U_m \left( \frac{1}{\rho_{ns}} - \frac{1}{\rho_s} \right) \right]}{V - V_{ns}}. \quad (8)$$

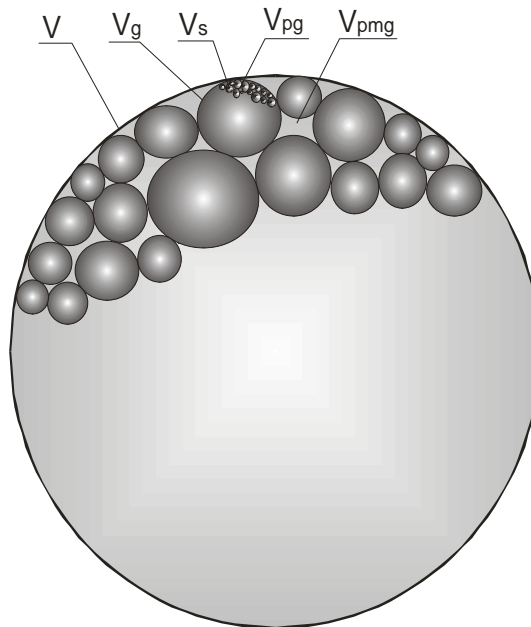


Fig. 2. Schematic diagram of a granular system formed by porous particles

The volume of not granulated raw material in the process moment  $V_{ns}$  is calculated from:

$$V_{ns} = U_m \cdot V_s = U_m \cdot \frac{m_s}{\rho_{ns}} \quad (9)$$

and

$$V = \frac{m_w + m_s}{\rho} \quad (10)$$

hence, after transformations, we obtain the equation:

$$\varepsilon = 1 - \frac{\frac{(1-U_m) + w}{\rho_s} - \frac{\rho_w}{\rho}}{\left(\frac{U_m}{\rho_{ns}}\right)} \quad (11)$$

### 6. RESULTS AND DISCUSSION

The results of our studies shown in Fig. 3 reveal that at the stage of granule formation, the mean porosity of agglomerates calculated from model relation given in Eq. 10 does not change with wetting time (bed moisture content).

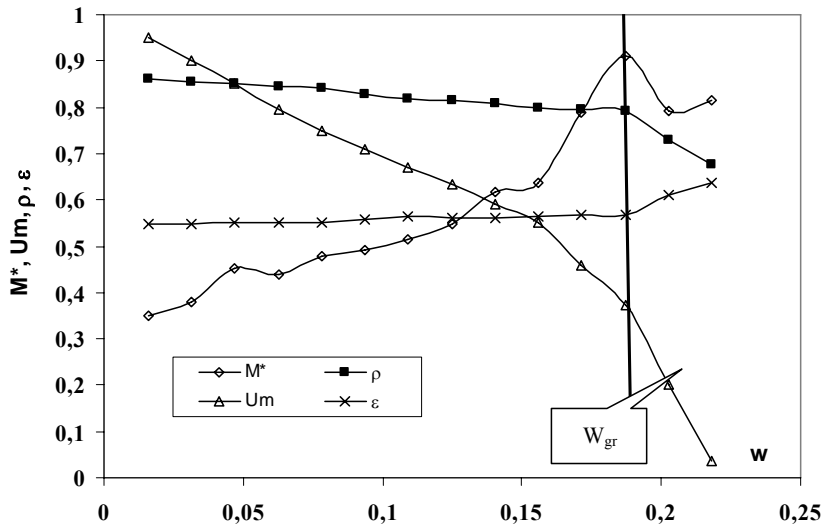


Fig. 3. Changes in the mass fraction of not granulated bed  $U_m$ , bulk density  $\rho$ , mean granule porosity  $\varepsilon$  and reduced moment  $M^*$  as a function of moisture content

When analysing the mechanisms of granulated material formation at the discussed stage of the process and taking into account the type of wetting, it can be stated that the results obtained reflect with high probability the properties of produced agglomerates. It can be expected that the granules formed at the beginning of the process, which are first suspended in the powder material and then are enveloped in it, due to the lack of mutual interactions, do not condense and until the end of this stage their porosity is approximately constant. Measurements of bulk density of the

granulated bed  $\rho$  during the process (with the growth of feed moisture content), shown for instance in Fig. 3, confirmed that changes of this parameter were decreasing linearly. Similar tendencies were observed by Heim et al. (2002a). Online measurements of torque changes carried out during the granulation process (Fig. 3) confirm conclusions presented by other authors (Heim et al., 2002b) that the torque is an indicator of process realisation. When analysing relations illustrated in Fig. 3, it was found that the upper limit of the feed moisture content for the range assumed in the discussed model corresponded to a maximum value of the reduced moment. In this range the mass fraction of not granulated raw material  $U_m$  decreased linearly with the increase of moisture content.

To generalise this conclusion, changes of  $U_m$  were analysed for all granulation trials performed (Fig. 4). The results obtained in the assumed range were approximated by the linear function:

$$U_m(w) = -a \cdot w + 1, \quad \text{where } a > 0. \quad (12)$$

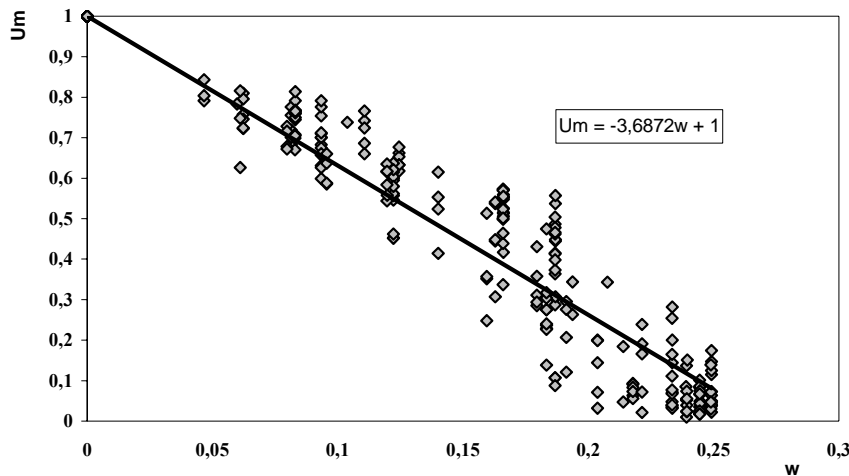


Fig. 4. Changes in mass fraction of not granulated bed  $U_m$  as a function of moisture content for all experimental runs

This relation describes changes of  $U_m$  during drum granulation in a broad range of changes in drum diameters, rotational speed and degree of drum filling, but it refers only to the agglomeration of a selected material, i.e. bentonite. It is also limited by the range of moisture content (the first period). When the results are to be generalised to other powder materials, a universal form of linear Eq. 12 should be assumed.

The form of relation (Eq. 11) and a linear character of changes in the mass fraction  $U_m$  and bulk density of the bed  $\rho$  allow us to expect that in the discussed range of

bentonite granulation the effect of bed moisture content on mean inner porosity of the agglomerates  $\varepsilon$  is reduced. A consequence of this can be a constant value of mean porosity of agglomerates  $\varepsilon$  calculated from the model equation.

Completion of the presented model with relations characteristic for the second stage of granulation (the growth of agglomerates and their condensation) will enable a quick identification of changes in the properties of granules at any time of the process.

#### REFERENCES

- GLUBA T., OBRANIAK A., GAWOT-MŁYNARCZYK E., 2004. The effect of granulation conditions on bulk density of a product; *Physicochemical Problems of Mineral Processing*; 38, 177-186.
- HEIM A., GLUBA T., OBRANIAK A., 2002a. The effect of process and equipment parameters on bulk density of a bed during drum granulation; *Proceedings of the 15th International Congress of Chemical and Process Engineering CHISA, CD-ROM*; P5. 217, 1-10.
- HEIM A., GLUBA T., OBRANIAK A., 2002b. Torque as an indicator of the advance of drum granulation process; *Proceedings of the 29th Inter. Conference of the Slovak Society of Chemical Engineering CD-ROM*; P.130, 1-7.
- KAPUR P. C., FUERSTENAU D. W., 1966. Size distribution and kinetic relationship in the nuclei region of wet pelletization, *Ind. Eng. Chem. Process Design Develop.*, 5, 5-10.
- NEWITT D. M., CONWEY-JONES J. M., 1958. A contribution to the theory and practice of granulation, *Trans. Inst. Chem. Engrs.*, 36, 422-442.

#### ACKNOWLEDGMENTS

The study was carried out within research work for promotion N N209 096135 in our Department of Process Equipment.

**Obraniak, A., Gluba, T.,** *Model zmian porowatości agregatów podczas granulacji bębnowej*, *Physicochem. Probl. Miner. Process.*, 46 (2011) 219-228, (w jęz. ang), <http://www.minproc.pwr.wroc.pl/journal>

Zaproponowano modelowe równanie do wyznaczania średniej wewnętrznej porowatości granulowanych materiałów. Równanie to oparto o analizę kinetyki agregacji oraz pomiary gęstości materiału poddawanego agregacji. Gęstość zgranulowanego produktu zależy od właściwości nadawy (gęstość, skład ziarnowy), właściwości cieczy zwilżającej, koncentracji ziarn w utworzonych granulach (porowatości), jak również od składu ziarnowego otrzymanych granul, od którego zależy objętość pustek. W celu zweryfikowania modelu, testowano proces granulacji bębnowej dla następujących parametrów: średnica bębna  $D = 0.25$  do  $0.4$  m, wypełnienie bębna z granulowanym materiałem  $k = 5$  do  $20\%$  objętości wewnętrznej, względna prędkość obrotowa bębna  $n_w = 0.15$  do  $0.375$  wartości krytycznej. Granulowane złożo było zwilżane kroplami cieczy w trójwymiarowym obrocie bębna przy stałej szybkości

wkraplania  $Q = 1 \text{ cm}^3/\text{s}$ . Podczas procesu, przy stałych interwałach czasowych, pobierano próbki z bębna i na podstawie gęstości materiału nadawy i jej składu ziarnowego wyznaczano wewnętrzną porowatość granuli dla danej klasy ziarnowej. Objętość cieczy akumulowanej w porach wewnętrznych granul były specyfikowane w oparciu o bilans masowy przed i po suszeniu. Wyniki badań potwierdziły ważność proponowanego modelu.

*słowa kluczowe: aglomeracja, gęstość, granulacja bębnowa, porowatość*

Lotta RINTALA \*, Kristian LILLKUNG\*, Jari AROMAA \*

## THE USE OF DECISION AND OPTIMIZATION METHODS IN SELECTION OF HYDROMETALLURGICAL UNIT PROCESS ALTERNATIVES

*Received April 12, 2010; reviewed; accepted August 12, 2010*

The hydrometallurgical process routes development has traditionally been made based on personnels' experiences and preferences. This tacit knowledge has been very difficult to communicate to other people. For this reason an attempt has been made to develop a tool that could be used as a selection tool or a decision support method when making process route decisions. A description of the decision problem is the most important element in decision making. That is discussed via human decision making and decision support and optimization methods. In addition, a typical hydrometallurgical process chain and decisions made in different stages at the chain are discussed. The main focus in this study is to establish what kind of tool would help in the rough selection between the different unit processes. The optimization of the process chain would be the next stage of development work but that is not discussed here.

*keywords: hydrometallurgical unit processes, decision and optimization methods, human decision making*

### 1. INTRODUCTION

When a new hydrometallurgical process is designed, decisions and comparison between process alternatives are made by human. This is somehow ineffective way since there is inexpensive and effective artificial intelligence available. There are not many cases where computers can beat the intelligence and creativity of human. But when the task is to classify and perform comparative analysis by factors that can be described by mathematical models, it is worthwhile to use computers to support the

---

\* Aalto University, Department of Materials Science and Engineering, PO Box 16200, FIN-00076 Aalto, Finland. email: [lotta.rintala@tkk.fi](mailto:lotta.rintala@tkk.fi)

decision making. This situation exists exactly when designing a hydrometallurgical process route consisting of different unit processes and their alternatives. When selecting a processing step the number of alternatives is probably between 10 and 100 taking into account different techniques and different process parameter ranges.

There are lot of information and tacit knowledge about suitable processes, but it is not usually easily available. That knowledge should be collected, preferably in numerical form. Then a decision making tool or procedure could be developed. That would enable other people to get access to this information. If the decision making tool could predict the suitable process chain as early as possible, it would help to decrease expensive and time consuming laboratory tests made to new raw materials.

A description of the decision problem is the most important element in decision making. The decision problem must be clearly defined and limited. The decision problem in this study is limited so that process development starts from pretreatment processes of raw material, i.e. grinding, beneficiation or chemical treatment before leaching.

Selection of unit processes and process optimization are very closely connected. The main difference is that process optimization is typically used to mean the variation of certain process parameters in order to achieve as good process output as possible. The emphasis of process selection is on determining, which unit processes would be suitable in general, based on the knowledge of similar cases already accomplished or which have been found to be working in the laboratory scale. Based on the selection process the optimum process parameters cannot of course be discovered. For this reason the selected process routes should be more thoroughly inspected and optimized with proper tools after the selection.

## 2. HUMAN DECISION MAKING

Human reasoning and decision making depend on many levels of neural operation, some of which are conscious and overly cognitive. The cognitive operations depend on support processes such as attention, working memory and emotion. According to Bechara et al. individuals make judgments not only by assessing the severity of outcomes and their probability of occurrence, but also and primarily in terms of their emotional quality (Bechara et al., 2000).

One factor affecting the decision making is so called decision situation. Decision situation is a broad term including the following (Sage and Armstrong, 2000):

- the objectives to be achieved
- the needs to be fulfilled
- constraints and variables associated with the decision
- people affected by the decision
- the decision options or alternative courses of action themselves
- the environment in which all of these are embedded

- the experience and familiarity of the decision maker with all of the previous.

The decision situation is therefore very dependent upon contingency variables. Some of the most important elements affecting the decision making are shown in Fig. 1.

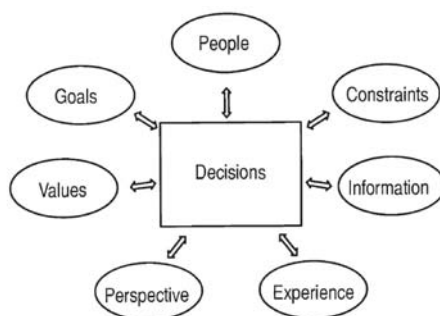


Fig. 1. Key elements affecting the decision making situation (Sage and Armstrong, 2000)

The most important element in decision making should be the goal of the decision, which is the main underlying reason the decision is being made. Besides the goals, there are very often values that the decision should also comply with. These can be personal values or for example corporate values. There are always present also some sorts of constraints like for example maximum available time or cost (Sage and Armstrong, 2000).

Perspectives of the decision maker and other people involved can often be in a major role considering the result of the decision. There are four human rationality perspectives that must always be considered in almost every decision situation: emotional, organizational, political, and technoeconomical. In this report, the focus will be only on technical and economic factors. The use of a certain process might, for example, cause more resistance among the locals (political factor). These kinds of factors may be difficult to evaluate properly with a numerical tool (Sage and Armstrong, 2000).

Previous experience in similar decision situations makes decision making much easier. Through similar experiences, the decision maker is already familiar with the type of problems. These experiences form part of the individual's tacit knowledge. This means that the individual has gained experience to act as an expert and make conclusions without precise qualitative information on which to base the conclusion. Typical for this kind of knowledge is that it is difficult to pass on to others or even express in words.

### 3. HYDROMETALLURGICAL PROCESS CHAIN

The hydrometallurgical process chain can be roughly divided in three stages (Fig. 2). Pretreatment and leaching stages are separate stages in real processes, but should

be considered as a single stage when comparing different process chains. Different types of leaching processes require very different pretreatments, which can raise the costs of certain processes significantly (Hayes, 1985).

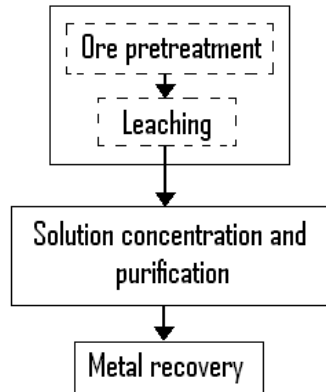


Fig. 2. Three stages of process chain

### 3.1. HYDROMETALLURGICAL PROCESS CHAIN

The ore pretreatment is needed for enhancing the metal recovery and improving the kinetics of the reactions. The pretreatment processes can be classified in three different broad categories (Hayes, 1985):

- comminution and beneficiation
- chemical changes in the minerals
- structure modification.

Comminution is used to increase the surface area of the ore of certain mass. By increasing the surface area more mineral grains are exposed to solvent. In the leaching process it is not necessary to completely liberate all the mineral grains as long as direct contact between some portion of mineral grain and the leach solution is achieved. The volume of reagent required and the consumption of solvent by the reaction is reduced when the mineral feed is concentrated before leaching. Metal concentrations in leach liquor becomes at the same time higher (Hayes, 1985).

Chemical treatments may be necessary to obtain the metal in a form, which is more easily taken into solution. In most cases this involves pyrometallurgical treatments but also hydrometallurgical processes are possible. Pyrometallurgical processes often result also in a change in microstructure of the minerals (Hayes, 1985).

The reactivity of minerals can be improved also by small changes in the ratio of the elements present in mineral. The various defects in the material can increase the kinetics of the reaction by providing preferential sites for chemical reactions (Hayes, 1985). The dislocations and micro cracks in the mineral enhance the dissolution rates and exposes fresh grains, which would not be otherwise in contact with the liquid.

## 3.2. LEACHING

In Figure 3 different hydrometallurgical processing techniques are presented. Based on the scale factors the leaching can be done in four alternative ways. The main factors affecting the selection of the leaching process are the grade of the ore, the dissolution rate of the metals and the amount of raw material to be processed. In practice the selection of the leaching process is an optimization problem, where the maximum amount of the metal content is attempted to dissolve in as short time as possible and with as small expenses as possible.

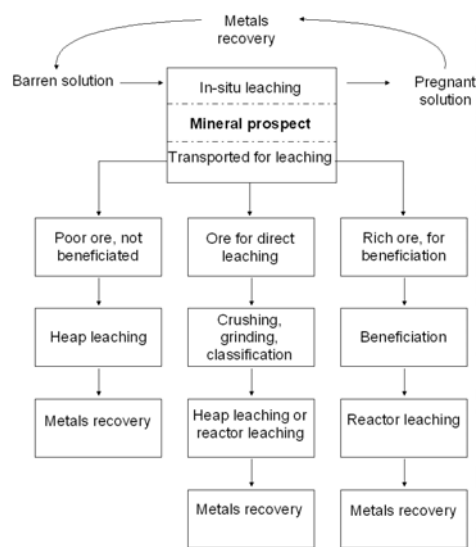


Fig. 3. Hydrometallurgical leaching techniques (Wadsworth, 1987)

As the grade of ore decreases the energy consumption per amount of metal produced increases. For every raw material there is a cut-off grade, which is the lowest grade of ore that can be economically processed. The cut-off grade can be estimated by comparing the earnings of the produced metal with the production costs. Production costs to get metals into solution include mining, crushing, ore beneficiation and leaching, but all the steps are not used in every case. The lower the grade of the ore, the simpler the process has to be and the lower the operating costs have to be.

When choosing the leaching technique, the first decision is whether the ore is transported for leaching or not. If not, the leaching method is the In-situ-leaching, where the ore is not extracted, instead the solvent is pumped into the ore body and the metal containing solution is collected for the metals recovery. In-situ -leaching is used for example in the extraction of uranium.

If the metal is transported for leaching, the second decision is whether to do ore

beneficiation. If there will be no beneficiation, leaching is done by heap leaching, where the coarse ore is stacked in large dumps or heap pads. In all heap leaching methods the leaching reagent flows through the ore. If beneficiation is made before the leaching, the choice will be reactor leaching. In the reactor leaching the processed ore is leached in a specifically designed reactor using agitation, temperature, pressure, solvent concentration, etc. to increase the reaction kinetics. The recovery is better in reactor leaching than in heap leaching, but the processing costs increase as well.

### 3.3. SOLUTION PURIFICATION AND RECOVERY

The objective in the solution purification is to remove the impurities or increase the concentration of the prospective metal. There are lots of hydrometallurgical unit processes available for solution purification, some of them are based on transport of the dissolved element from a liquid phase to another and some of them are based on forming a solid phase (Fig. 4). When choosing a process for solution purification the proper order of alternatives is:

- crystallization, chemical precipitation or liquid-liquid extraction
- cementation or ion exchange
- electrolysis or adsorption.

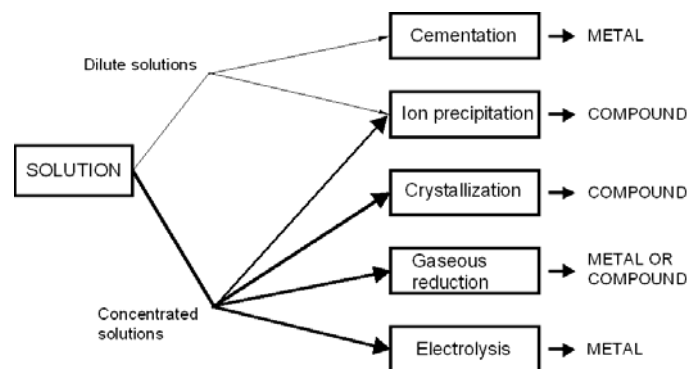


Fig. 4. Different solution purification processes and consisting products

After the leaching stage, impurities in the solvent are removed in the solution concentration and purification stage. In the solution purification the aim can be in transferring the desired metal into a pure solution or removing unwanted metals and anions while the remaining solution is ready for further processing. The used solution purification process depends on the properties of the solution.

Separating the metal from the solution can be done by crystallization, precipitation, cementation or electrolysis. Crystallization and precipitation are based on solubilities and reaction equilibrium, whereas the cementation and electrolysis are based on reduction reaction. Changing the metal from one solution phase to another can be done

by adsorption, ion exchange or liquid-liquid extraction and in these methods the metal is bonded temporarily to a transmitting agent.

When choosing the solution purification processes the key factors are the volume of solution and the grade of the metal recovered. Process selection is also affected by the place of the process in the process chain, where the solution purification is done and what is the targeted level of purification. The target level can be determined either by the acceptable level of impurities or by the desired recovery of the wanted metal from the solution.

#### 4. DECISION AND OPTIMIZATION METHODS

At first, it is important to point out the difference between process optimization and decision optimization. In this case, the emphasis is on the decision optimization. The main focus in this study is to establish what kind of tools would help in the rough selection between the different unit processes. The optimization of the process chain is the next stage of development work and is not discussed here. There are two different approaches identified for the decision optimization: decision support tool and optimization. The number of potential mathematical methods that can be used is high.

Decision methods can be classified generally in two different categories, decision making and decision support methods. The former are meant to make decision making as automatic as possible and the latter ones for supporting the decision making process and making it easier. Different methods have been developed for different purposes. Knowing the purpose is essential to achieve the optimum result. Various decision support and decision making methods have different names in different fields although the methods themselves are quite similar. Three different decision support systems have been identified as promising for this kind of use (Sage and Armstrong, 2000):

- Decision tree / Decision forest (DT/DF)
- Multi-criteria decision making (MCDM)
- Case based reasoning (CBR).

In addition to decision methods, there are numerous different optimization methods available. These are mainly useful when trying to search for a minimum or maximum of a function already known. None of the methods is able to achieve the optimum point in every situation. Optimization methods can be divided into traditional and modern methods. The former includes for example the traditional linear and nonlinear optimization. The latter includes for example genetic algorithm, ant colony optimization and neural networks (Rao, 2009). Some of these optimization methods could be fairly used in decision making. These include the following:

- Artificial neural network (ANN)
- Ant colony optimization (ACO)
- Genetic algorithm (GA).

The problem with some of the optimization methods is that they sometimes find

only the local minimum so the user has to know the magnitude of the result to verify it. This can be challenging especially when the number of parameters affecting the variable is high (Rao, 2009). Also different methods based on different algorithms may give different results.

## 5. CHOOSING UNIT PROCESS ALTERNATIVES BY OPTIMIZATION AND DECISION SUPPORT METHODS

When choosing unit processes, the main focus should not be on process optimization right from the beginning as the number of potential unit process chains is high and therefore the number of parameters to be optimized would be high. This would require the models to simplify many things, which would lead to a situation that the achieved optimum could greatly differ from the actual case. Alternatively, the comparison would require a lot of manual labour in modelling the processes and would lead to high calculating capacity demands. One goal of the tool development should be the low need for manual work and moderate capacity demands. By creating a model of every possible process and its variation the optimum process would most probably be found, but the amount of work compared with the achieved benefits would be high. Because of the high level of manual work the usability would be poor and would not bring any substantial improvement to the situation at present.

A better way would be to first narrow down the number of optimizable processes using certain criteria. One alternative would be to create a model that could predict the potential unit processes based on the composition and other classifying properties of the ore or mineral. Process decision about the first pretreatment and leaching stage narrows down the possible unit processes in the later stages. The number of choices of process chains to be simulated should be narrowed down to 3-5. Simulating all the process chain variants is not a realistic option because of the high need for manual work and high calculating capacity demand. One key factor considering the tool is that two different users should be able to get the same answer with the same input data. Also in evaluation of different unit processes the scale has to be considered. One unit process is more usable in a small scale whereas some other is at its best when the material flows are high.

After narrowing down the number of possible process chains the remaining processes should be simulated in a process simulator, such as the HSC Sim by Outotec Oyj (Oyj, 2010). Optimum detailed parameters can then be found and the decision between the process chains can be made based on simulated results.

Different methods for choosing hydrometallurgical unit process alternatives are compared in Table 1. Comparing totally different decision methods is however not straightforward. By pointing out different properties any method can be shown in a more attractive way than the others. For this reason the focus should be on the main topics. Main difference between the methods is the possibility to use database for

decision making instead of a function describing the relationships between the different parameters. According to Table 1, it seems that CBR could be the most suitable method for this kind of decision making.

Table 1. Comparison of different decision methods

Properties	Methods					
	ANN	ACO	GA	DT/DF	MCDM	CBR
requires a function to be optimized		x	x		x	
can be used without knowing the exact parameter relations (function)	x			x		x
possibility to form (optimize) process chains		x				
decisions based on a database of similar cases	x					x
weighting of different parameters possible	x	x	x		x	x
possibility to use method with lacking data						x

In the following part we have discussed the suitability of the different methods for the selection of the unit process alternatives more deeply. Firstly the decision methods (Decision tree/forest, Multi-criteria decision making and Case based reasoning) are discussed and secondly the optimization methods (Artificial neural network, Ant colony optimization and Genetic algorithm) are considered.

The Decision tree is a method, which makes data classifying fairly easy. Starting from the root, analysis ends up in the leaf by choosing in every knot the most suitable option according to the decision criteria (Fig. 5). The order of defined decision criteria greatly affects the outcome of the tree. By changing the places of two sequential criteria the achieved result can be totally different. For this reason all unit processes should be handled as separate trees to decide, whether the unit process is suitable or not. Building an utmost complex tree consisting of all possible processes and ending up to a one single process is not possible or at least the result is not reliable (Quinlan, 1986; Sage and Armstrong, 2000). A group of decision trees (decision forest) would better give the potentially suitable unit processes as a result. Main issue with the decision tree is the building of the tree, i.e. the order of the decision criteria. If something has to be adjusted later on, the whole tree should be reconsidered. The information about potential processes could in some cases narrow down the number of processes significantly but in some other case the number could still remain high. Decision tree cannot also give information about the superiority of the processes. Decision forests are already used in different kinds of selection applications. One application is a software called CDMS (Clinical decision modeling system), which can be used to define what clinical examinations should be done and in which order to

achieve the optimum result when certain resource restrictions apply (Shi and Lyons-Weiler, 2007).

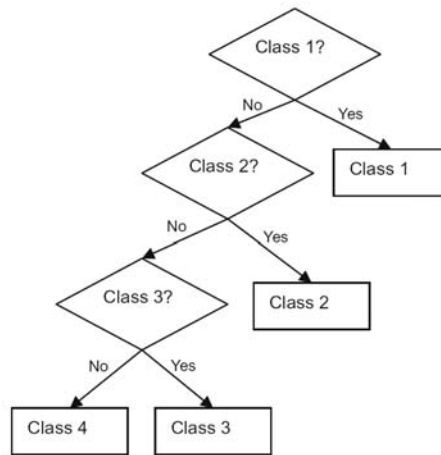


Fig. 5. A typical structure of the decision tree (Ghiassi and Bumley, 2010)

In the Multi-Criteria decision making (MCDM) the number of alternatives is first narrowed down by using certain predetermined rules. The narrowing of the alternatives reduces the need for calculation capacity. The remaining short list is then put in order using a scoring method. This can be done by very different means. TOPSIS for example is an approach where the parameters are compared with the best and worst possible values (Agrawal et al., 1991; Tong et al., 2003). The best alternative is the one closest to the optimum solution and farthest from the most undesirable solution.

Scoring of the short list seems to be a good way to compare the alternatives as long as the limits of the unit processes can be reasonably defined and there are properties that can be reliably compared using numerical scoring. The narrowing criteria have to be defined very carefully and most likely it has to be done differently for different kinds of raw materials. The same principle of narrowing down the number of alternatives based on some numerical criteria could be used with some of the other decision support methods.

The Case based reasoning (CBR) is a decision support method which uses the knowledge of past similar cases and predicts the likely outcome based on the data (Fig. 6) (Pal and Shiu, 2004; Xu, 1995). Often there is no exact match found in the previous cases so it is necessary to define, how to compare the similarity of different cases. With proper definitions, the CBR method can provide very accurate results in optimum conditions. The CBR method requires a sufficient database of similar cases than the one currently examined, otherwise the prediction is not reliable. There is no benefit in modelling analogy between generic data and unknown parameters.

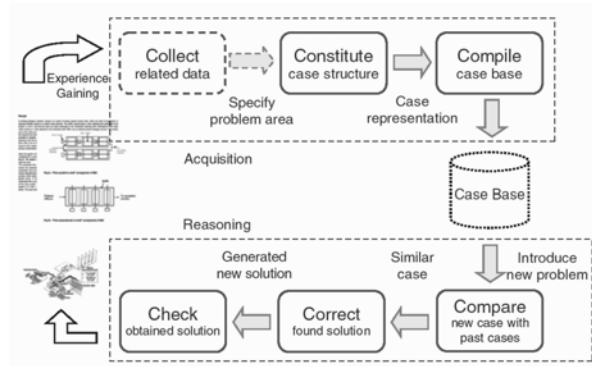


Fig. 6. The six stages of the CBR method (Avramenko and Kraslawski, 2008)

The neural network is most suitable for fairly simple optimization problems whether they are linear and nonlinear (Hassoun, 1995). It is a net consisting of an input layer, output layer and hidden layers between them (Fig. 7). The method can be used to predict for example process output with certain input if an adequate number of inputs and their outputs are known. The method can be used for example predicting the recovery with certain particle size if the recovery is known with a few other particle sizes. The level of calculating capacity demand rises rapidly with growing number of parameters affecting the situation. Positive side is that the relations between the variables do not have to be clear in order to predict the outcome (Cilek, 2002).

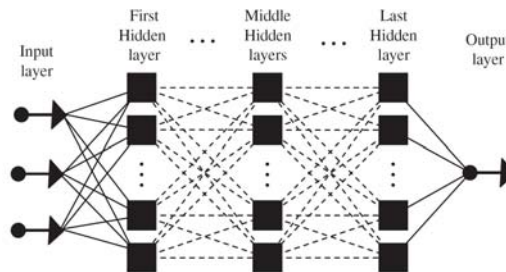


Fig. 7. Typical structure of the Neural network (Mjalli et al., 2007)

The Ant colony optimization is used to find the shortest path from “nest” to the “food”, or from the first node to the last (Dorigo and Stützle, 2004; Dorigo and Blumb, 2005). A graphic illustration of the Ant colony optimization is shown in the Fig. 8. All possible routes through the different nodes are first being tried but the shortest ones stand out. The nodes can be considered as unit processes, and then the same principle could probably be used for defining the optimum process chain. The main problem that arises is what should be the optimized parameter (or parameters), i.e. what the length of the path should represent. One alternative is to optimize a function consisting of the different variables. The variables differ however from one

ore to another, so the function should be adjusted for every new ore individually and the result would be dependent on this. Different people would value different parameters differently, so the end result would most likely not be the same.

The Genetic algorithm is an efficient method used in different kinds of optimization problems. The GA alone does not however help the decision making process, instead it should be used as a part of some of the decision support methods. The GA can achieve the maximum or minimum of difficult nonlinear functions in relatively short time (Reeves and Rowe, 2002). GA can only be used to optimize a known function. It cannot find the optimum without knowing the relations of the parameters.

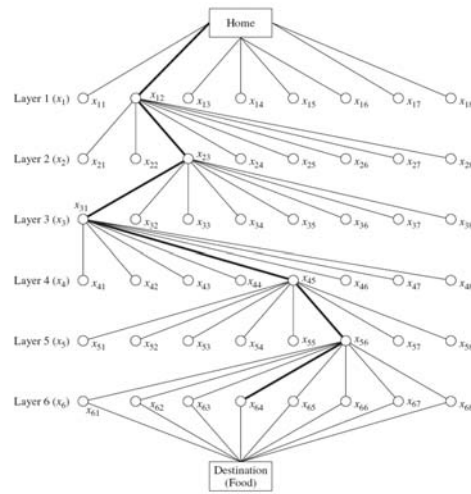


Fig. 8. A graphic illustration of the ant colony optimization (Rao, 2009)

## 6. DISCUSSION

A human makes judgements not only by assessing the severity of outcomes and their probability of occurrence, but also and primarily in terms of their emotional quality (Bechara et al., 2000). Because the human decisions are always based also on emotions, human brains are not objective in classifying and performing comparative analysis to factors that can be described by mathematical models. In these cases it is worthwhile to use computers to support decision making.

Each of the mentioned methods could be used in the decision making process but some methods seem to be more suitable than the others. The order of superiority depends on the viewpoint and on the data available. Different parameters act differently on different ores, so the creation of a model that would give one unquestionably best process chain is very likely impossible. Instead it would be reasonable to compare few processes or process chains that appear to be most

promising based on model in a process simulator. This way the processes could be modelled detailed enough and a realistic order of superiority could be defined. The recovery of the process for example depends greatly on how optimal process conditions can be achieved. Narrowing down the alternative unit processes should be done on a reasonably high level, maybe even on category level. Comparing very similar processes without detailed modelling can result in unreliable results.

In general all the information required in decision making must be in numerical form. Therefore it can be fairly easily handled by different decision methods. It is positive that nearly all necessary information is measurable data and no subjective opinions are needed to be taken into account, except for some possible adjustable weighting coefficients. When comparing different alternatives and variables the order of magnitude also has to be taken into account. There is no point calculating for example pH and temperature on a wide range as the processes run in rather tight process envelopes.

## 7. CONCLUSION

The human decision making can be limited due to cognitive limitations. A person's decision making capability improves as expertise is gained, but it will take many years. Typically, the problem solving and decision making skills are reached after ten years of relevant work experience. To assist the decision making procedure different tools are available and the tools can be used, if the problem can be described in mathematical formulas or by using a set of rules.

The design phase of a hydrometallurgical process starts with analysis of the raw materials to be treated, i.e. mineralogy, chemistry, size etc. Based on this information suitable unit processes for leaching, solution purification and product recovery are designed. In this phase the traditional way has relied on design team's experience. However, for improving this first phase a decision making tool for screening of suitable process alternatives can be useful.

In this work we have studied and compared some of the known decision support and optimization methods. Based on the method descriptions the following methods are suited for development of a process selection procedure: Case based reasoning and Multi-criteria decision making.

## REFERENCES

- AGRAWAL, V.P., KOHLI, V., GUPTA, S., Computer aided robot selection: The multiple attribute decision making approach. *International Journal of Production Research* 29(1991) 8, 1629-1644.
- AVRAMENKO, Y., KRASLAWSKI, A., Case based design: applications in process engineering. Springer, 2008.
- BECHARA, A., DAMAISO, H., DAMAISO, A.R., Emotion, Decision Making and the Orbitofrontal Cortex. *Cerebral Cortex* 10(2000) 3, 295-307.

- CILEK, E.C., Application of neural networks to predict locked cycle flotation test results. *Minerals Engineering* 15(2002), 1095-1104.
- DORIGO, M., BLUMB, C., Ant colony optimization theory: A survey. *Theoretical Computer Science* 344(2005), 243 – 278.
- DORIGO, M., STÜTZLE, T., *Ant Colony Optimization*. MIT Press, 2004, 320.
- GHIASSI, M., BURNLEY, C., Measuring effectiveness of a dynamic artificial network algorithm for classification problems. *Expert Systems with Applications* 37(2010), 3118-3128.
- HASSOUN, M.H., *Fundamentals of Artificial Neural Networks*. Massachusetts Institute of Technology, 1995.
- HAYES, P., *Process Selection in Extractive Metallurgy*. Hayes Publishing Co, Brisbane, 1985, 406.
- OYJ, O., 2010, Sim – Process Simulation. [www.outotec.com/pages/Page.aspx?id=35374](http://www.outotec.com/pages/Page.aspx?id=35374) &epslanguage=EN. Viitattu
- MJALLI, F.S., L-ASHEH, S., ALFADALA, H.E., Use of artificial neural network black-box modeling for the prediction of wastewater treatment plants performance. *Journal of Environmental Management* 83(2007) 329-338.
- PAL, S., SHIU, S., *Foundations of Soft Case-Based Reasoning*. John Wiley & Sons, 2004, 298.
- QUINLAN, J.R., *Induction of Decision Trees*. *Machine Learning* 1(1986), 81-106.
- RAO, S.S., *Engineering Optimization - Theory and Practice*. John Wiley & Sons, 2009.
- REEVES, C.R., ROWE, J.E., *Genetic Algorithms - Principles and Perspectives : A Guide to GA Theory*. Kluwer Academic Publishers 2002, 345.
- SAGE, A.P., ARMSTRONG, J. E. Jr., *Introduction: Types of Decisions*. In: *Introduction to Systems Engineering*. John Wiley & Sons, 2000, 547.
- SHI, H., Lyons-Weiler, J., *Clinical decision modeling system*. *BMC Medical Informatics and Decision Making* 7(2007) 23, 17.
- TONG, K.W., KWONG, C.K., IP, K.W., Optimization of process conditions for the transfer molding of electronic packages. *Journal of Materials Processing Technology* 138(2003), 361-365.
- WADSWORTH, M., *Leaching - Metals Applications*. In: *Handbook of Separation Process Technology*, ed. Rousseau, R. John Wiley & Sons, New York, 1987, 500-539.
- XU, L.D., *Case based reasoning*. *Potentials*, IEEE 13(1995) 5, 10-13.

**Rintala, L., Lillkung, K., Aromaa, J.,** *Zastosowanie naukowych metod podejmowania decyzji oraz optymalizacji do wyboru alternatywnych jednostkowych procesów hydrometalurgicznych*, *Physicochem. Probl. Miner. Process.*, 46 (2011) 229-242, (w jęz. ang), <http://www.minproc.pwr.wroc.pl/journal>

Rozwój linii technologicznej w hydrometalurgii opiera się zwykle na doświadczeniu i preferencjach personelu. Doświadczenie i nabyta wiedza w tej dziedzinie są bardzo trudne do przekazania. Dlatego też podjęto próbę opracowania metody wspomagania procesu podejmowania decyzji i wyboru przy planowaniu linii technologicznych. Najważniejszym elementem procesu decyzyjnego jest opis problemu. Ta część procesu dyskutowana jest w oparciu o metody wspomagania procesu decyzyjnego. Dodatkowo przedyskutowano przebieg procesu decyzyjnego w przypadku typowych dla hydrometalurgii linii technologicznych. Praca ta zogniskowana jest na zagadnieniu znalezienia odpowiednich narzędzi, które mogłyby pomóc w zgrubnym wyborze pomiędzy różnymi procesami jednostkowymi. Optymalizacja technologii byłaby następnym krokiem jej rozwoju, ale problem ten nie jest w pracy dyskutowany.

*słowa kluczowe: procesy hydrometalurgiczne, metody decyzji i optymalizacji, podejmowanie decyzji*

Aleksandra KORKOSZ\*, Marcin NIEWIADOMSKI\*, Jan HUPKA \*

## INVESTIGATION OF PROPERTIES OF SWIMMING POOL WATER TREATMENT SEDIMENTS

*Received July 8., 2010; reviewed; accepted August 18, 2010*

Two sediments resulting from swimming pool operation are characterized and the data discussed, namely the flocs which accumulated and were backwashed from deep bed filter, and bottom sediment collected from the pool by vacuum cleaner. Better understanding of sediments' structure and properties should allow for improvement of *Cryptosporidium* oocysts removal from pool water and as a consequence - increase the safety of pool users. Zeta potential, nano-size and micro-size of particles/flocs and derivatographic measurements were performed. The zeta potential data indicated easy flocculation and size distribution measurements revealed varied effectiveness of deep bed filtration. Derivatographic analysis indicated differences between sediments from filters backwashing and pool bottom sediments.

*keywords: water treatment sediments, zeta potential, Cryptosporidium oocysts, floc particle size distribution, thermal analysis, swimming pools*

### 1. INTRODUCTION

Swimming pools are becoming increasingly popular. Many hotels, motels, holiday resorts, schools and single-family homes are recently equipped with pools. In spas, hospitals and sanatoria they are used for therapy and rehabilitation (Angenent et al., 2005; Lumb et al., 2004). In our previous paper (Korkosz et al., 2010) selected aspects of water filtration in deep bed filters were considered with respect to rehabilitating

---

\* Department of Chemical Technology, Gdansk University of Technology, 80-233 Gdansk, Narutowicza 11/12, Poland, [jhupka@pg.gda.pl](mailto:jhupka@pg.gda.pl)

swimming pool facility. Besides instrumental analysis of water, and sand grain size analysis, the investigation considered particle size distribution and thermal analysis of the sediment collected in the sand bed of depth filters, and removed during the process of washing.

Functioning of a swimming pool and treatment of pool water results in formation of two kinds of sediments:

- coagulant flocs residing mainly within the top layer of the deep bed filter,
- flocculated particles collecting at the bottom of the pool basin.

While filter backwash water with suspended flocs already received attention in the available literature (Bing-Mu and Hsuan-Hsien, 2003; Greinert et al., 2004; Goeres et al., 2004; Schets et al., 2005), mainly with respect to water recycle (Wyczarska-Kokot and Piechurski, 2001; Wyczarska-Kokot and Piechurski, 2002; Reißmann et al., 2005), the basin bottom sediment composition and properties remain unknown. Comparison of properties of both sediments indirectly provides also insight into functioning of deep bed filters.

In this paper we concentrated on characterization of these two sediments with respect to separation of *Cryptosporidium* protozoa oocysts. Unlike other microbial contaminants, inactivation and removal of oocysts can occur only in water passing through filters and special treatment reactor, e.g. using ozone (Gregory et al., 2002). A pool - involving steady circulation of water - is a mixed and not a plug flow system, therefore the rate of reduction in concentration in the pool volume is slow. Effective functioning of a depth filter, with regard to removal of colloids and fine suspension, is dependent on appropriate metering of coagulant and flocculant.

## 2. EXPERIMENTAL

Aqueous sediment suspensions were procured from two swimming pools: 75 m<sup>3</sup> small pool used for children swimming lessons (sample code: PG), and 470 m<sup>3</sup> regular pool for sport and recreation (sample code: K). Samples originating from backwashing of filters are marked with letter “f” and samples collected by water vacuum cleaner are marked “vc.”

The small swimming pool uses aluminum hydroxychloroide as coagulant, sulfuric acid for pH correction and sodium hypochlorite as disinfecting agent. The recreational swimming pool uses aluminum sulfate as coagulant and similarly sulfuric acid and hypochlorite. Less frequently an agent against growth of algae, fungi and bacteria is used. The small pool applies N,N Dimethyl-2-hydroxypropylammoniumchlorid. Sporadically sodium thiosulphate is applied to reduce excessive chlorine.

Electrophoretic mobility and nano-size particle diameter distribution measurements were performed in Zetasizer instrument (model: Zeta Plus) from Malvern. Flocs/particle size distribution in micro-size range was performed with Mastersizer X

laser diffraction particle sizing instrument manufactured by Malvern. This system allows measurements in two specific ranges: 0.5-180  $\mu\text{m}$  and 1.2-600  $\mu\text{m}$ . Apart from flocs size distribution of freshly collected samples, changes of flocs when exposed to shear forces were monitored, 200  $\text{cm}^3$  of examined sediment suspension was circulated through measuring cell in the closed cycle.

Thermal analysis, including TG, DTG and DTA curves, of 50 mg of sediments from backwashing of filters and vacuum cleaning of pool bottom was carried out by means of derivatograph Q-1500 D, from MOM Budapest. First, the deposit was separated from the washing water in a centrifuge at 5000 rpm for 5 minutes, and next dried at 105°C to the constant mass. The temperature increase rate was set at 10°C/min. TG sensitivity was 50 mg, while DTA sensitivity was 250  $\mu\text{V}$ . Samples were heated up to 750°C. The reference sample was  $\alpha\text{-Al}_2\text{O}_3$ .

### 3. RESULTS AND DISCUSSION

#### 3.1. ZETA POTENTIAL

Selected sediment samples were investigated for the electrophoretic mobility of suspended particles and flocs. Zeta potential together with basic data for the aqueous phase such as pH (actual pH of pool water) and conductivity are presented in Table 1. Small pool washing water samples showed negative potential of -10.6 and -11.7 mV, while vacuum cleaner samples had around 2 mV more negative potential. Considering zeta potential deviation between 3.2 and 6.5 mV for small swimming pool, the values are comparable. The recreational swimming pool sediment sample from washing water had positive potential of + 7.7 mV and vacuum cleaner sediment sample was -8.9 mV.

Table 1. Electrophoretic mobility data

Sample	pH	Conductivity, mS	Zeta Potential, mV	Zeta Potential Deviation, mV
Backwashing water sediment samples				
PG-f-25	6.6	0.85	-10.6	4.2
PG-f-28	7.4	0.48	-11.7	3.2
K-f-3	6.9	0.42	7.7	5.0
Water vacuum cleaner sediment samples				
PG-vc-1	7.5	0.37	-13.6	3.7
PG-vc-2	7.3	0.65	-13.7	6.5
K-vc-3	7.3	0.28	-8.9	6.8

According to measurements of electrophoretic mobility of oocysts of *Cryptosporidium* p. by Considine et al. (2002), they exhibit an isoelectric point below pH 3, and the zeta-potentials are negative at pH > 3. The pH of samples presented in Table 1 varies from pH 6.6 to pH 7.5. The corresponding zeta potential of oocysts can be found between -10 and -40 mV. In most cases samples from the examined swimming pools exhibited negative zeta-potential of coagulated flocs, and one can expect electrostatic repulsion between oocysts and flocs. In addition to electrostatic repulsion, steric forces due to hairy layer of surface proteins pose additional obstacle for oocysts to be adhered to sand particles.

Zeta potential smaller than 15 mV indicates destabilized system, therefore easy flocs formation.

### 3.2. PARTICLE SIZE DISTRIBUTION

Particle size distribution was investigated in both micro-size and nano-size ranges. Figure 1 presents small swimming pool micro-size range distribution of particles originating from sediments (A through C) separated from three backwashed filters and one from water vacuum cleaner sediment (D). On all graphs the initial distribution is shown with a dashed line, while distribution after 30 minutes of suspension circulation is shown with a solid line. The first sediment A initially contained two peaks around 50 and 300  $\mu\text{m}$ . After circulation 50  $\mu\text{m}$  peak shifted to around 20  $\mu\text{m}$  and the 300 micron peak vanished, which indicates flocs decreasing their size. In the case of sediment B, there are initially two peaks, 30  $\mu\text{m}$  and 320  $\mu\text{m}$ . After 30 minutes, flocs/particles of size 320  $\mu\text{m}$  almost entirely are sheared into 30  $\mu\text{m}$  particles or are agglomerated to flocs of size above 500  $\mu\text{m}$ . Sediment C exhibited the ability for agglomeration. 40  $\mu\text{m}$  flocs slightly decreased and agglomerated forming 300  $\mu\text{m}$  flocs. Obtained from water vacuum cleaner sediment (D) had initially two flocs sizes: 80  $\mu\text{m}$  and 300  $\mu\text{m}$ . After 30 minutes of suspension circulation, 80  $\mu\text{m}$  peak significantly diminished and another strong peak, around 35  $\mu\text{m}$  appeared. At the same time increased amount of 300  $\mu\text{m}$  flocs.

Figure 2 presents sediments from recreational swimming pool. Washing water sediment (A) underwent shearing of flocs to smaller sizes as well as agglomeration. Peak 60  $\mu\text{m}$  decreased and shifted to size around 55  $\mu\text{m}$ , while peak 300  $\mu\text{m}$  shifted to size 350  $\mu\text{m}$  and increased its volume several times. Water vacuum cleaner sediment (B) initially had three size peaks: very weak 30 and 300  $\mu\text{m}$  and strong 120  $\mu\text{m}$ . After 30 minutes of circulation peak 300  $\mu\text{m}$  decreased and 30  $\mu\text{m}$  was no longer recognizable under strong and broad peak of around 70  $\mu\text{m}$ , that replaced 120  $\mu\text{m}$  peak. One can conclude, that observed in this case is only shearing of flocs and decrease of their size.

Sediment flocs from backwashing of filters from small swimming pool exhibited broad range of responses to shearing flow. Presented three distributions show three

different behaviours, flocs shearing to smaller size, flocs agglomeration to larger size and both phenomena together. Investigated sample from the same pool originating from water vacuum cleaner exhibited behavior of both shearing and agglomeration. In the case of recreational swimming pool, sample from backwashing of filters showed agglomeration and only very slight shearing, while water vacuum cleaner coagulated sediments were clearly sheared to smaller sizes only. This behavior might be attributed to the fact that recreational swimming pool had positive zeta potential of sediment flocs, therefore they were mostly agglomerating, while negatively charged flocs from vacuum cleaner sediments were sheared to smaller size.

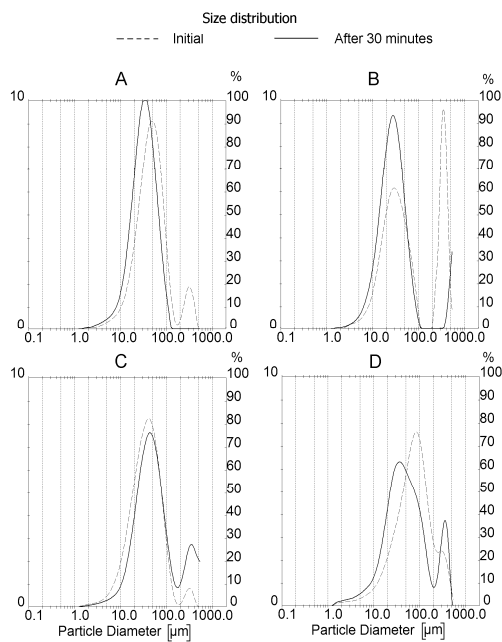


Fig. 1. Particle size distribution in micro-size range, small swimming pool sediments. A: PG-f-1; B: PG-f-3; C: PG-f-14; D: PG-vc-1

Two sediments from water vacuum cleaners were additionally investigated in nano-size range (Fig. 3). Both exhibited dual distribution characteristics. The small swimming pool sediment had a medium peak in range 80 to 90 nm size and strong peak at 500 nm. The recreational swimming pool sediment sample has only a weak peak at around 92 nm and strong peak at 1000 nm. Investigations of backwashing water from filters is further planned.

One can see on nano-size distribution mostly not coagulated particles such as bacteria, which are of size around 500 to 1000 nm. Since recreational swimming pool has a peak at larger size compared to small pool, one can speculate, that the recreational pool has particles to some degree coagulated. This would correlate well with the zeta potential measurement, that suggested larger dose of coagulant, aluminum sulfate, that charged flocs positively.

Particles of size below 100 nm can be attributed to organic macromolecules

originating from human colloidal excretions. One can speculate, that other particles were trapped in water from the atmosphere or were released from water filtering installation.

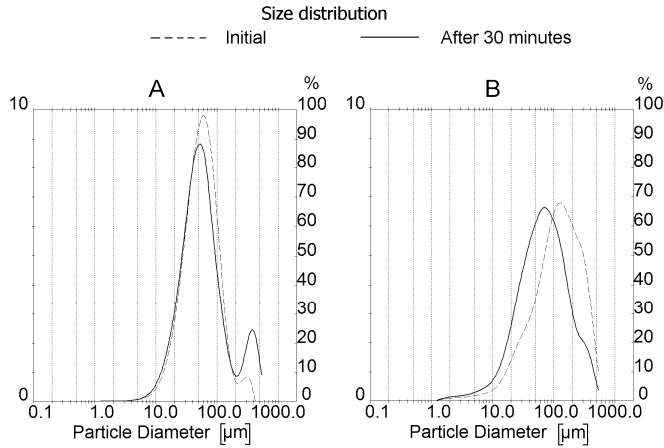


Fig. 2. Particle size distribution in micro-size range, recreational swimming pool sediments. A: K-f-3; B: K-vc-3

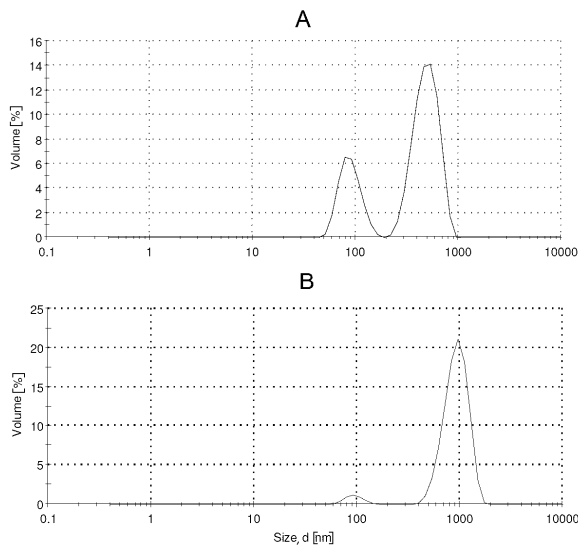


Fig. 3. Particle size distribution by volume in nano-size range, water vacuum cleaner from: A: small swimming pool, sample PG-vc-1; B - Recreational swimming pool, sample K-vc-3

### 3.3. DERIVATOGRAPHY

Table 2 shows mass lost in derivatographic analysis. Samples contained various amounts of sand and silt, therefore, the mass loss varied from 51.6 to 81.5 %. In order to compare samples based on material that could be combusted or volatilized during the analysis, mass losses in the specific temperature intervals are referred to the mass loss only and all four values in a given column from A to D add up to 100 %. The intervals are (Siewert, 2004):

- A, up to 200°C, water region
- B, 200–450°C, thermolabile organic region
- C, 450–550°C, stable organic region
- D, 550°C and above, inorganic region.

One can notice, that washing water samples had higher water and thermolabile organic matter losses, while sediments obtained from water vacuum cleaner showed few percent more stable organic matter.

Table 2. Mass loss in derivatographic measurements

Temp. Interval	Backwashing water samples				Water vacuum cleaner samples		
	PG-f-1	PG- f-3	PG- f-4	PG- f-5	PG-vc-1	K-vc-1	K-vc-2
Total Mass Loss, (wt. %)							
Total Loss	66.8	58.8	59.4	61.2	79.6	51.6	81.5
Absolute Mass Loss by Temperature Interval, (wt. %)							
A	11.1	10.1	11.0	7.9	10.0	4.8	6.1
B	42.6	37.6	39.3	40.6	47.7	33.8	51.2
C	10.0	7.7	6.6	10.3	17.6	11.7	21.8
D	3.0	3.4	2.6	2.3	4.2	1.3	2.4
Relative Mass Loss by Temperature Interval, (wt. %)							
A	16.6	17.2	18.5	12.9	12.6	9.3	7.5
B	63.8	63.9	66.1	66.4	59.9	65.5	62.8
C	15.0	13.1	11.1	16.8	22.1	22.7	26.7
D	4.5	5.8	4.3	3.8	5.3	2.5	3.0
Total A - D	100.0	100.0	100.0	100.0	100.0	100.0	100.0

Table 3 presents comparison of exothermic and endothermic peaks. water washing from filters sample exhibit strong exothermic peak around 350°C, while around 450°C only sample PG-1 shows a strong peak. The remaining samples have only weak exothermic peak. Characteristic for water vacuum cleaner samples is a strong exothermic peak around 500°C, in stable organics region. Endothermic peaks, that were broad and weak could be explicitly visible only in two backwashing water samples from small swimming pool and in vacuum cleaner sample. Figures 4 and 5 show two derivatographic samples, washing water sediment and vacuum cleaner sediment respectively.

There is evident difference between sediments from backwashing of filters and sediments from water vacuum cleaner. It is speculated, that higher molecular organic matter may more easily remain in the pool avoiding circulation through filters. Also, substances remaining in the pool and later picked up by water vacuum cleaner were longer exposed to higher concentration of chlorine.

Table 3. Exothermic and endothermic peaks in derivatographic analysis

Sample	Peaks (deg C)			
	Exothermic		Endothermic	
PG- f-1	347	strong	160	broad
	455	strong	630	broad
PG- f-3	350	strong	155	broad
	440	medium	670	broad
	520	weak		
PG- f-4	315	very strong		
	400	very weak		
	445	weak		
	490	weak		
PG- f-5	352	strong		
	450	strong		
PG-vc-1	350	medium	105	very weak broad
	400	weak	175	weak broad
	495	strong	600	broad
K-vc-1	330	strong		
	425	weak		
	503	very strong		
K-vc-2	270	very strong		
	425	strong		
	490	weak		
	505	strong		

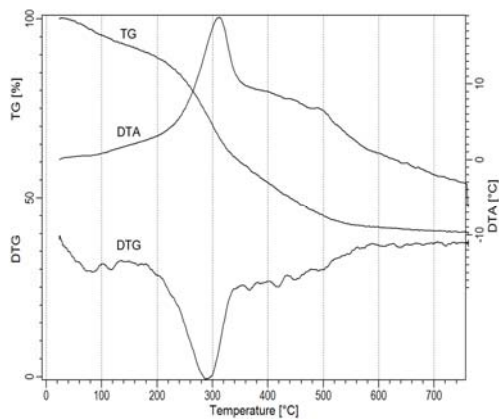


Fig. 4. Backwashing water sediments from small swimming pool filters

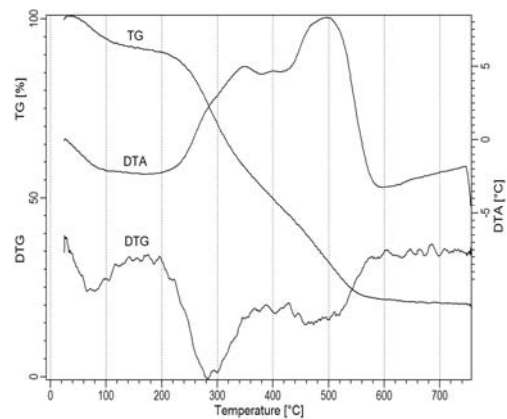


Fig. 5. Water vacuum cleaner sediments from pool bottom from small swimming pool

#### 4. FINAL COMMENTS

A comparison of pool bottom sediment and filter washing sediment can be a new indicator of proper functioning of swimming pool water treatment. Floccs present in both sediments are vulnerable to a different degree to the shear force field, which should correspond to the effectiveness of deep bed functioning. Derivatographic data indicates that higher molecular organic matter may more easily remain in the pool avoiding circulation through filters. The zeta potential shows, that all samples used for the research indicate easy flocculation and rather destabilized contaminant particles as evidenced by zeta potential smaller than -13 mV and for some suspensions even in the positive charge range.

#### ACKNOWLEDGEMENTS

This research was partially supported by the Voivodeship Fund for Environmental Protection and Water Management, grant No. RX-10/2009, the Gdansk University of Technology, contract DS No. 014668/03, by the European Union in the framework of the European Social Fund and the system project of the Pomorskie Voivodeship InnoDoktorant - Scholarships for PhD students, II edition.

#### REFERENCES

- ANGENENT L. T., KELLEY S. T., AMAND A. S., PACE, N. R., HEMANDEZ M. T. (2005), Molecular identification of potential pathogens in water and air of a hospital therapy pool, *Proceedings of the National Academy of Sciences of the United States of America*, 102(13), 4860–4865.
- BING-MU HSU, HSUAN-HSIEN YEH (2003), Removal of Giardia and Cryptosporidium in drinking water treatment: a pilot-scale study, *Water Research*, 37, 1111-1117.
- CONSIDINE R. F., DIXON D. R., DRUMMOND C. J. (2002), Oocysts of Cryptosporidium parvum and model sand surfaces in aqueous solutions: an atomic force microscope (AFM) study, *Water Research*, 36, 3421-3428.
- GOERESA D. M., PALYS T., SANDEL B. B., GEIGER J. (2004), Evaluation of disinfectant efficacy against biofilm and suspended bacteria in a laboratory swimming pool model, *Water Research*, 38(13), 3103-3109.
- GREINERT J., FURTADO D., SMITH J., MONTE BARARDI C., SIMÖ ES C. (2004), Detection of Cryptosporidium oocysts and Giardia cysts in swimming pool filter backwash water concentrates by flocculation and immunomagnetic separation, *International Journal of Environmental Health Research*, 14 (6) 395-404.
- GREGORY R. (2002), Bench-marking Pool Water Treatment for coping with Cryptosporidium, *Journal of Environmental Health Research*, 1 (1), 11-18.
- LUMB R., STAPLEDON R., SCROOP A., BOND P., CUNLIFFE D., GOODWIN, A., DOYLE R., BASTIAN I. (2004), Investigation of spa pools associated with lung disorders caused by Mycobacterium avium complex in immunocompetent adults, *Applied and Environmental Microbiology*, 70(8), 4906-4910.

- KORKOSZ A., JANCZAREK M., ARANOWSKI R., RZECUŁA J., HUPKA J. (2010), Efficiency of deep bed filtration in treatment of swimming pool water, *Physicochemical Problems of Mineral Processing*, 44, 103-115.
- REIßMANN F.G., SCHULZE E., ALBRECHT V. (2005), Application of a combined UF/RO system for the reuse of filter backwash water from treated swimming pool water, *Desalination*, 178, 41-49.
- SCHETS F. M., ENGELS G. B., EVERS E. G. (2004), *Cryptosporidium* and *Giardia* in swimming pools in the Netherlands, *J Water Health*. 2:191–200.
- SIEWERT C., (2004) Rapid Screening of Soil Properties using Thermogravimetry, *Soil Science Society of America Journal*, 68, 1656-1661.
- TWARDOWSKA I., ALLEN H. E., HÄGGBLÖM M. M. (2010), *Soil and Water Pollution Monitoring, Protection and Remediation*, NATO Science Series, 369-385.
- WYCZARSKA-KOKOT J., PIECHURSKI F. (2002), Ocena skuteczności filtracji wody i jakości wód popłucznych w instalacjach basenowych, *Ochr. Środow.*, 1(84), 33-36.
- WYCZARSKA-KOKOT J., PIECHURSKI F. (2001), Ocena skuteczności filtracji wody i jakości wód popłucznych w instalacjach basenowych, *Instalacje Basenowe. III Sympozjum naukowo-techniczne*, Ustroń, marzec 2001, Gliwice: Zakład Wodociągów i Kanalizacji. Instytut Inżynierii Wody i Ścieków. Politechnika Śląska, 103-116.

**Korkosz, A., Niewiadomski, M., Hupka, J.,** *Badania właściwości osadów pochodzących z uzdatniania wody basenowej.*, *Physicochem. Probl. Miner. Process.*, 46 (2011) 243-252, (w jęz. ang), <http://www.minproc.pwr.wroc.pl/journal>

Dwa rodzaje osadów pochodzących z instalacji basenowych zostały scharakteryzowane i otrzymane wyniki przedyskutowane, w szczególności flokuły, które zatrzymały się na filtrze piaskowo-żwirowym i następnie zostały usunięte w płukaniu zwrotnym oraz osady z dna niecki basenowej zebrane tzw. odkurzaczem wodnym. Lepsze zrozumienie struktury i właściwości osadów powinno usprawnić usuwanie cyst *Cryptosporidium* z basenów i w efekcie podnieść bezpieczeństwo kąpiących się użytkowników. Przeprowadzono pomiary potencjału dzeta, rozkładu wielkości cząstek/flokuł w zakresach nano i mikro oraz pomiary derywatograficzne. Potencjał dzeta wskazał na łatwość flokulacji cząstek w układzie, a rozkłady wielkości ujawniły różnorodną efektywność filtracji. Analiza derywatograficzna wskazała na wyraźne różnice składu pomiędzy osadami z filtracji a osadami z dna basenu.

*słowa kluczowe: potencjał dzeta, cysta, analiza termiczna, baseny kąpielowe, rozmiar flokuł*

Yuksel ABALI\*, Salih U. BAYCA \*\*, Kadir ARISOY \*\*, Ali I. VAIZOGULLAR\*\*\*

## OPTIMIZATION OF DOLOMITE ORE LEACHING IN HYDROCHLORIC ACID SOLUTIONS

*Received May 15, 2010; reviewed; accepted August 20, 2010*

In this study, the Taguchi method was used to determine the optimum conditions for leaching of dolomite ore in hydrochloric acid solutions. The experimental parameters were leaching temperature, solid-to-liquid ratio, acid initial concentration, leaching time and stirring speed. The following optimum leaching parameter levels were found: temperature 50°C, solid-to-liquid ratio 2%, acid concentration 20 g/cm<sup>3</sup> (2 mol/dm<sup>3</sup>), stirring speed 450 rpm, leaching time 5 min. Under the optimum process conditions, the dolomite ore leaching efficiency was about 83%.

*keywords: optimization, dolomite ore, hydrochloric acid, leaching, Taguchi method*

### 1. INTRODUCTION

Dolomite (CaCO<sub>3</sub>·MgCO<sub>3</sub>, carbonate of calcium and magnesium) is different from limestone and contains minimum 45% of MgCO<sub>3</sub>. Dolomite occurs either as coarse, granular mass or in fine-grained compact form. The crystal structure of dolomite is hexagonal-rhombohedral. Dolomite is naturally white, but may, due to impurities to be creamy gray, pink, green or black (Brady et al., 1997).

Dolomite leaching has been rarely studied in the past. However, the determination of optimum conditions for leaching of dolomite in hydrochloric acid has not been studied yet. Lund et al. (1977) carried out a work on leaching of dolomite in hydrochloric acid. They reported that at 25°C the dissolution process is surface

\* Celal Bayar University, Science and Arts Faculty, Department of Chemistry, Manisa, Turkey

\*\* Celal Bayar University, Soma Vocational School, Soma, 45500 Manisa, Turkey, salihbayca@gmail.com, phone: +902366120063, fax: +902366122002.

\*\*\* Mugla University, Science and Arts Faculty, Department of Chemistry, Mugla, Turkey

reaction rate limited. As the temperature is increased to 100°C, the dissolution process approaches diffusion limitation even at relatively high (500 min<sup>-1</sup>) stirring speeds. The rate of reaction was found to be proportional to a temperature dependent fractional power on the hydrochloric acid concentration. Herman and White (1985) investigated leaching of dolomite in CO<sub>2</sub>-undersaturated water. They reported that at lower temperatures the rate was lower and grain size effects were insignificant. Chou et al. (1989) investigated the dissolution of various carbonates (including calcite, magnesite and dolomite) in HCl solutions at 25°C using a continuous fluidized bed reactor and samples of relatively coarse particle size. Busenberg and Plummer (1989) carried out a work on the leaching of dolomite in CO<sub>2</sub>-undersaturated water. Abali et al. (1992) reported that the activation energy for dissolution kinetics of magnesite in water saturated by SO<sub>2</sub> gas was 81 kJ/mol and the reaction was controlled by the surface chemical reaction. Ozbek et al. (1990) investigated the dissolution kinetics of magnesite with Cl<sub>2</sub> gas in water. They found that the reaction diffusion was controlled through the fluid layer. Gautlier et al. (1999) carried out a work on influence of pH on the rate of dissolution of dolomite. They reported that the rate increases from 0.63 at 25°C to 0.80 at 80°C. Harris et al. (1988) studied the production of magnesium from concentrated magnesium chloride solutions. Also, Abali et al. (2006) investigated the optimum conditions for dissolution of magnesite with H<sub>2</sub>SO<sub>4</sub> solutions. They reported that the optimum conditions were found to be 65°C, 5/100 g/cm<sup>3</sup>, 2M, 60 min and 300 rpm. Optimization for the dissolution of ores in different acidic media has been investigated by a great number of authors (Abali et al., 1997; Demirbas et al., 1999; Copur et al., 2004; Demir et al., 2003; Ata et al., 2001; Yartasi et al., 1999).

The aim of this study was to investigate the optimization of dolomite leaching in hydrochloric acid solutions. The Taguchi method was used to determine the optimum conditions. An experimental plan was used based on parameters and their levels to determine the leaching rate of dolomite in HCl solutions. *F* test was carried out to the leaching results to determine the most effective and the least effective parameters. Each of the parameter of signal-noise graphics was drawn to determine the optimum conditions. The maximum leaching performance of dolomite was predicted by calculation of the optimum conditions.

## 2. THEORY OF THE TAGUCHI METHOD

The use of a quantitative design in the Taguchi method in order to optimize a process with multiple performance characteristics includes the following steps: (a) identification of the performance characteristics and selection of process factors to be evaluated; (b) determination of the number of quantity levels for the process and possible interaction between the process parameters; (c) selection of the appropriate orthogonal array and assignment of process factors to the orthogonal array; (d) conduction of the experiments based on the arrangement of the orthogonal array; (e)

calculation of the performance characteristics; (f) analyzing the experimental result using the performance characteristic and ANOVA; (h) selection of the optimal levels of process factors; and (i) verifying the optimal process factors through the confirmation experiment (Copur et al., 1997; Phadke, 1989).

The orthogonal array (OA) experimental design was chosen as the most suitable method to determine experimental plan,  $L_{25} (5^5)$ , five parameters, each of five values (Phadke, 1989). In order to observe the effects of noise sources on the leaching process, each experiment was repeated twice under the same conditions at different times. The performance characteristics were chosen as the optimization criteria. There are three categories of performance characteristics, the larger-the-better, the smaller-the-better and the nominal-the-better. The performance statistics was evaluated using Eq. (1) (Phadke 1989; Pignatiello, 1988):

$$SN = -10 \log \left( \frac{1}{n} \sum \frac{1}{Y_i^2} \right), \quad (1)$$

where larger-the-better  $SN$  is performance characteristics,  $n$  number of repetition done for an experimental combination, and  $Y_i$  performance value of  $i^{\text{th}}$  experiment.

In the Taguchi method the experiment corresponding to optimum working conditions might not been done during the whole period of the experimental stage. In such cases the performance value corresponding to optimum working conditions can be predicted by utilizing the balanced characteristic of OA. For this the following additive model may be used (Phadke et al., 1983):

$$Y_i = \mu + \sum X_i + \varepsilon_i \quad (2)$$

where  $\mu$  is the overall mean of performance value,  $X_i$  the fixed effect of the quantity level combination used in  $i^{\text{th}}$  experiment, and  $\varepsilon_i$  the random error in  $i^{\text{th}}$  experiment. Because Eq. (2) is a point estimation, which is calculated using experimental data in order to determine whether results of the confirmation experiments are meaningful or not, the confidence interval must be evaluated. The confidence interval at chosen error level may be calculated by (Taguchi, 1987):

$$Y_i \pm \sqrt{F_{\alpha;1, dfMSe} MSe \left( \frac{1+m}{N} + \frac{1}{n_i} \right)} \quad (3)$$

where  $F$  is the value of  $F$  table,  $\alpha$  the error level,  $dfMSe$  the degrees of freedom of mean square error,  $m$  the degrees of freedom used in the prediction of  $Y_i$ ,  $N$  the number of total experiments, and  $n_i$  the number of repetitions in the confirmation experiment.

If experimental data are in percent (%), before evaluating Eq. (2), transformation of percent values should be applied first, using Eq. (3) due to which values of interest are later determined by carrying out reverse transformation using the same Eq. (4) (Taguchi, 1987):

$$\Omega_i = -10 \cdot \log\left(\frac{P_i}{1-P_i}\right) \quad (4)$$

where  $\Omega$  is the value of percentage value subject to omega transformation and the percentage of the product obtained experimentally.

### 3. MATERIALS AND METHODS

The dolomite ore used in the present experiments was obtained from Kutahya Fertilizer Plant Co., Kutahya, Turkey. The dolomite ore was initially crushed with a jaw crusher. The sample was then sieved using  $-200 +160 \mu\text{m}$  ASTM Standard sieves. The chemical composition of the dolomite ore was determined by volumetric and gravimetric methods (Scott, 1963) and the results are given in Table 1.

Table 1. The chemical composition of dolomite ore

Component	wt %
MgO	16.93
CaO	23.68
Fe <sub>2</sub> O <sub>3</sub>	2.80
SiO <sub>2</sub>	16.80
Al <sub>2</sub> O <sub>3</sub>	2.79
Ignition Loss	36.89

The leaching experiments were carried out in a 250 cm<sup>3</sup> glass reactor equipped with a mechanical stirrer having a digital controller unit and timer, thermostat and cooler. The temperature of the reaction medium could be controlled within  $\pm 0.5$  °C. In the leaching process, 100 cm<sup>3</sup> HCl of known concentration was introduced into the reactor. After the desired leaching temperature was reached, a predetermined amount of the sample was added into the solution while the content of the vessel was stirred at a certain speed. At the end of the experiment, the content of the vessel was filtered by a filter paper of Filtrak 391 and the filtrate solution was analyzed volumetrically for Ca + Mg. The leaching ratio (in percent)  $Y$  was calculated from:

$$Y = \frac{M_1}{M_o} \cdot 100, \quad (5)$$

$M_1$  is the percent of Ca+Mg in the solution,  $M_o$  is the percent of Ca+Mg in the original sample.

A robust design method is developed for reducing cost and improving leaching dolomite ore in HCl. In the experiments, an  $L_{25}$  orthogonal array is employed to determine the effect of five process parameters on the dolomite ore leaching rate. For each factor, five levels are chosen to cover the wide region of variation.

Table 2. Parameters and their values corresponding to their levels

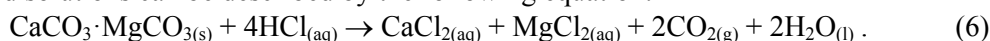
Parameters	Parameter levels				
	1	2	3	4	5
A Leaching temperature, °C	20	32	50	65	74
B Solid-to-liquid ratio, %	0.5	1	2	5	10
C Acid concentration, mol/dm <sup>3</sup>	0.2	0.5	1	2	5
D Stirring rate, min <sup>-1</sup>	50	300	450	600	750
E Leaching time, minutes	5	10	20	30	45

In this study the following parameters were selected: leaching temperature, solid-to-liquid ratio, acid initially concentration, stirring speed and leaching time. These parameters can potentially affect leaching rate of dolomite ore in HCl. Experimental factors and their levels, determined in the preliminary tests, are given in Table 2.

Since five parameters were investigated in the research, five levels of each parameter were considered. Therefore, a  $L_{25}$  orthogonal array ( $L_{25} 5^5$ ) was selected for this study. The total of  $25 \times 5 = 125$  data values were collected, which were conducted for analysis in this study.

#### 4. RESULT AND DISCUSSION

To determine the optimum conditions for leaching of dolomite ore in hydrochloric acid solutions were investigated. The leaching reaction of dolomite ore in hydrochloric acid solutions can be described by the following equation:



In this study, a  $L_{25}$  orthogonal array with five columns and 25 rows was used. Each leaching parameter was assigned to a column, 25 leaching-parameter combinations being available. Therefore, only 25 experiments were required to study the entire parameter space using the  $L_{25}$  orthogonal array. The experimental layout for the five leaching parameters using the  $L_{25}$  orthogonal array is shown in Table 3.

$F$  factors were calculated and given in Table 4. As seen from Table 4, acid concentration parameters were significant for dolomite ore leaching rate.  $F$  test is a tool to see which process parameters have a significant effect on the leaching. The  $F$ -value for each process parameters is simply a ratio of mean of the squared deviations to mean of the squared error. Usually, the larger the  $F$ -value, the greater effect of process parameter on leaching. With the leaching rate characteristics and ANOVA analyses, the optimum combination of process parameters can be predicted.

Table 3. Chosen  $L_{25}(5^5)$  experimental plan

Experiment number	Parameters and levels					Exp. 1	Exp. 2
	A	B	C	D	E	$Y_1$	$Y_2$
1	1	1	1	1	1	22.75	27.36
2	1	2	2	2	2	45.25	43.64
3	1	3	3	3	3	66.33	70.69
4	1	4	4	4	4	80.31	74.63
5	1	5	5	5	5	85.23	78.52
6	2	1	2	4	3	85.65	86.29
7	2	2	3	5	4	84.43	70.76
8	2	3	4	1	5	90.83	83.51
9	2	4	5	2	1	77.43	69.07
10	2	5	1	3	2	07.64	08.52
11	3	1	3	2	5	88.41	98.85
12	3	2	4	3	1	89.85	75.76
13	3	3	5	4	2	86.13	76.82
14	3	4	1	5	3	15.98	17.01
15	3	5	2	1	4	20.08	17.17
16	4	1	4	5	2	84.29	78.48
17	4	2	5	1	3	87.86	96.74
18	4	3	1	2	4	31.24	27.06
19	4	4	2	3	5	41.59	34.87
20	4	5	3	4	1	42.39	41.76
21	5	1	5	3	4	77.93	79.10
22	5	2	1	4	5	78.34	85.98
23	5	3	2	5	1	81.29	70.49
24	5	4	3	1	2	85.45	71.96
25	5	5	4	2	3	69.70	72.98

To obtain optimum leaching rate, the-higher-the-better leaching rate characteristic shown in Eq. (1) has been used for leaching of Ca+Mg. The  $SN$  for the-larger-the-better for leaching rate were calculated. The level, which has a higher value, determines the maximum level of each factor. For example, level five for temperature has the highest  $SN$  value (Fig. 1).

Increasing the temperature up to 65°C does not influence the rate of dissolution. However, a rapid increase in the rate of leaching was observed between 65 and 74°C.

The effect of solid-to-liquid ratio on the performance statistics for dolomite ore is given in Figure 2. The dissolution rate increases with decreasing the solid-to-liquid ratio. As seen in Figure 3, the leaching rate rapidly increases as acid concentration increases up to 3.0 mol/dm<sup>3</sup> and then leaching rate slowly increases as acid concentration increases from 3.0 to 5.0 mol/dm<sup>3</sup>. The leaching rate has not changed

with the stirring speed up to  $450 \text{ min}^{-1}$ . Further on the leaching rate increases (Fig. 4). From 5 up to 30 minutes leaching time, no significant change in the leaching rate is observed. However from 45 minutes, leaching rate increased, as can be seen in Fig. 5.

Consequently, the maximum leaching conditions were determined as  $A_5, B_2, C_5, D_4$  and  $E_5$ . Then, the maximum leaching parameter levels will be temperature:  $74^\circ\text{C}$ , solid-to-liquid ratio: 1.0 %, acid concentration:  $5 \text{ mol/dm}^3$ , stirring speed:  $600 \text{ min}^{-1}$ , leaching time: 45 min on leaching process. The predicted leaching rate using maximum  $SN$  conditions can be calculated by Eq. (3).

The selection of optimum leaching conditions for Ca+Mg production is done according to the conditions of maximum amount with minimum cost, as given in Table 5. The optimum process conditions were selected as  $A_2, B_3, C_4, D_4$  and  $E_3$ . As a result, the optimum leaching parameter levels will be temperature:  $32^\circ\text{C}$ , solid-to-liquid ratio: 2 %, acid concentration:  $20 \text{ g/dm}^3$ , stirring speed:  $600 \text{ min}^{-1}$ , leaching time: 20 minutes. The predicted leaching rate using optimum  $SN$  conditions were also calculated by equation (3).

Table 4. The results of variance analysis (ANOVA)

Parameters	Degree of freedom	Sum of Squares	Mean Squares	Test Statistic, F
A Temperature	4	1433.825	358.456	1.290
B Solid-to-liquid ratio	4	3374.577	843.644	3.035
C Acid concentration	4	8845.756	2211.439	7.957
D Stirring speed	4	979.757	244.939	1.220
E Leaching time	4	1356.249	339.062	0.881
Error	4	1111.734	277.934	
Total	24	17101.898		

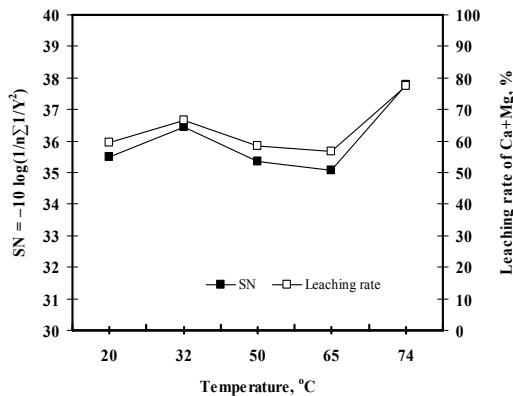


Fig. 1. The effect of leaching temperature on the performance statistics for dolomite ore

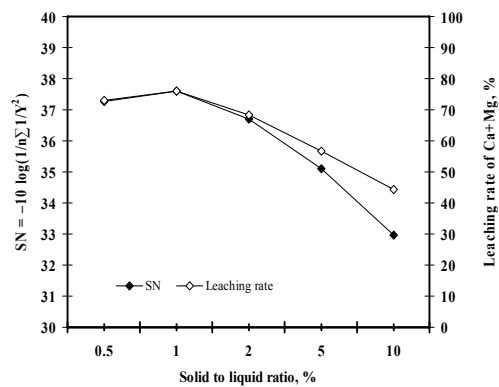


Fig. 2. The effect of solid-to-liquid ratio on the performance statistics for dolomite ore

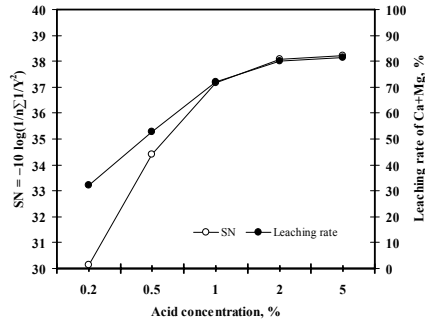


Fig. 3. The effect of acid concentration on the performance statistics for dolomite ore

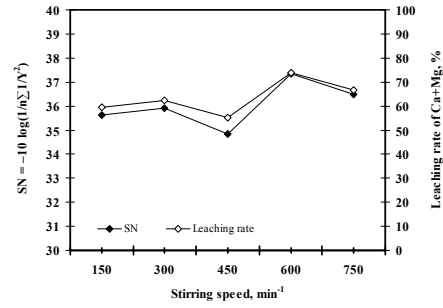


Fig. 4. The effect of stirring speed on the performance statistics for dolomite ore

Table 5. Chosen L<sub>25</sub>(5<sup>5</sup>) experimental plan

Parameters	Parameters level	Performance statistic, <i>SN</i>	Cost	Maximum <i>SN</i>	Optimum <i>SN</i>
A Leaching temperature, °C	20	35.49	Min. ↓ Max.	A <sub>5</sub>	A <sub>2</sub>
	32	36.45			
	50	35.36			
	65	35.06			
	74	37.77			
B Solid-to-liquid ratio, %	0.5	37.26	Min. ↑ Max.	B <sub>2</sub>	B <sub>3</sub>
	1	37.60			
	2	36.71			
	5	35.09			
	10	32.95			
C Acid concentration, mol/dm <sup>3</sup>	0.2	30.15	Min. ↓ Max.	C <sub>5</sub>	C <sub>4</sub>
	0.5	34.42			
	1.0	37.16			
	2.0	38.07			
	5.0	38.22			
D Stirring speed, min <sup>-1</sup>	150	35.62	Min. ↓ Max.	D <sub>4</sub>	D <sub>4</sub>
	300	35.90			
	450	34.84			
	600	37.36			
	750	36.48			
E Leaching time, min	5	35.54	Min. ↓ Max.	E <sub>5</sub>	E <sub>3</sub>
	10	35.39			
	20	36.51			
	30	35.01			
	45	37.69			

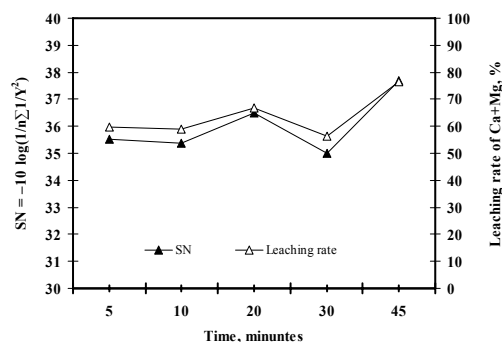


Fig. 5. The effect of dissolution time on the performance statistics for dolomite ore

### 3. CONCLUSION

In this study, the optimum conditions for leaching of dolomite ore in hydrochloric acid solutions were determined by the Taguchi method. The leaching rate increases with decreasing solid-to-liquid ratio and increasing acid concentration. The most significant parameter affecting leaching of dolomite ore is acid concentration.

Optimum reaction conditions were determined as 32°C leaching temperature, 2% for solid-to-liquid ratio, 20 g/dm<sup>3</sup> for acid concentration, 600 rpm for stirring speed and 20 minutes for leaching time. Under these optimum process conditions, the dolomite ore leaching rate in HCl solution was about 83%.

The findings of the present study may be very useful for leaching on the industrial scale since the optimum conditions determined by the Taguchi method in laboratory environment is reproducible in real production environments as well. Leaching reaction products were found to be calcium chloride and magnesium chloride.

### REFERENCES

- ABALI, Y., COLAK, S. and EKMEKYAPAR, A., 1992, Magnezit mineralinin sulu ortamda kukurt dioksit gazı ile çözünme kinetiği, (in Turkish), *Doga-Tr. J. Eng. Environ. Sci.*, 16: 319-326.
- ABALI, Y., COPUR, M. and YAVUZ, M., 2006, Determination of optimum conditions for dissolution of magnesite with H<sub>2</sub>SO<sub>4</sub> solutions, *Indian Journal of Chemical Technology*, 13: 391-397.
- ABALI, Y., COLAK, S. and YAPICI, S., 1997, The optimisation of the dissolution of phosphate rock with Cl<sub>2</sub>-SO<sub>2</sub> gas mixtures in aqueous medium, *Hydrometallurgy*, 46: 27 – 35.
- ATA, O. N., COLAK, S., EKINCI, Z. and COPUR, M. 2001, Determination of the optimum conditions for the dissolution of stibnite in HCl solution, *Chem Biochem. Eng. Q.*, 24: 409.
- BRADY, G. S., CLAUSER, H. R., VACCARI, J. A., 1997, *Materials Handbook*, McGraw-Hill, New York.
- BUSENBERG, E., PLUMMER, L. N., 1989, Thermodynamics of magnesian calcite solid-solutions at 25°C and 1 atm total pressure, *Geochimica et Cosmochimica Acta*, 53: 1189–1208.
- CHOU, L., GARRELS, R. M. and WOLLAST, R., 1989, Comparative study of the kinetics and mechanism of dissolution of carbonate minerals, *Chem. Geology*, 78: 269 – 282.

- COPUR, M., PEKDEMIR, T., CELIK, C. and COLAK, S., 1997, Determination of the optimum conditions for the dissolution of stibnite in HCl solutions, *Ind. Eng. Chem. Res.*, 36: 682.
- COPUR, M., OZMETIN, C., OZMETIN, E., KOCAKERIM, M. M., 2004, Optimization study of the dissolution of roasted zinc sulphide concentration with sulfuric acid solution, *Chemical Engineering and Processing*, 43: 1007 – 1014.
- DEMIR, F., DONMEZ, B. and COLAK, S., 2003, Dissolution kinetics of magnesite in citric acid solutions, *J. Chem. Eng. Jpn.*, 6: 683.
- DEMIRBAS, A., ABALI Y. and MERT, E., 1999, Recovery of phosphate from calcinated bone by dissolution in hydrochloric acid solutions, *Resources, Conservation and Recycling*, 26: 251-258.
- GAUTLIER, M., OELKERS, E. H., SCHOTT, J., 1999, An experimental study of dolomite dissolution rates as a function of pH from -0.5 to 5 and temperature from 25 to 80 °C, *Chemical Geology*, 157: 13 – 26.
- HARRIS, G. B., PEACEY, J. G. and Monette, S., 1988, Manufacture of concentrated magnesium chloride solution from magnesite for production of magnesium, *Chem. Abst.*, 109: 24855c.
- HERMAN, J. S., WHITE, W. B., 1985, Dissolution kinetics of dolomite: Effects of lithology and fluid flow velocity, *Geochimica et Cosmochimica Acta*, 49: 2017 – 2026.
- KHOEI, A. R., MASTERS, I., GETHIN, D. T., 2002, Design optimization of aluminum recycling processes using Taguchi technique, *J. of Materials Processing Technology*, 127: 96.
- LUND, K., FOGLER, H. S. and MCCUNE, C. C., 1977, Acidization-1. The dissolution of dolomite in hydrochloric acid, *Chem. Eng. Sci.*, 28: 691 – 700.
- OZBEK, H., ABALI, Y., ÇOLAK, S., CEYHUN, I. and KARAGOLGE, Z., 1999, Dissolution kinetics of magnesite mineral in water saturated by chlorine gas, *Hydrometallurgy*, 51: 173.
- PHADKE, M. S., 1989, *Quality Engineering Using Robust Design*, Prentice Hall: New Jersey, 61–292.
- PHADKE, M. S., KACKAR, R. N., SPEENEY, D. V., GRIECO, M. J., 1983, Off-line quality control in integrated circuit fabrication using experimental design, *Bell System Technical Journal*, 62: 1273.
- PIGNATIELLO, J. J., 1988, An overview of strategy and tactics of Taguchi, *I.I.E. Transactions.*, 20: 247 – 254.
- SCOTT, W. W., 1963, *Standard Methods of Chemical Analysis*, Van Nostrand, New York.
- TAGUCHI, G., 1987, *System of Experimental Design*, *Quality Resources*, New York, 108.
- YARTASI, A., COPUR, M., OZMETIN, C., KOCAKERIM, M. M. and TEMUR, H., 1999, An optimization study of dissolution of oxidized copper ore in NH<sub>3</sub> solutions, *Energy Educ. Sci. Techn.*, 3: 77.

**Abali, Y., Bayca, S.U., Arisoy, K., Vaizogullar, A.I.,** *Optymalizacja ługowania rudy dolomitowej w roztworach kwasu solnego*, *Physicochem. Probl. Miner. Process.*, 46 (2011) 253-262, (w jęz. ang), <http://www.minproc.pwr.wroc.pl/journal>

Wykorzystano metodę Taguchi do określenia optymalnych warunków ługowania rudy dolomitowej w roztworach kwasu solnego. Badano takie parametry jak temperatura, stosunek fazy stałej do ciekłej, początkowe stężenie kwasu, czas ługowania i prędkość mieszania. Ustalono, że optymalnymi parametrami są: stosunek fazy stałej do ciekłej 2%, początkowe stężenie kwasu 20 g/cm<sup>3</sup> (2 mol/dm<sup>3</sup>), prędkość mieszania 450 rpm, czas ługowania 5 min. W tych warunkach wyługowanie dolomitu było około 83%

*słowa kluczowe: optymalizacja , ruda dolomitowa, kwas solny, ługowanie, metoda Taguchi*

Mari LUNDSTRÖM\*, Jari AROMAA\*\*, Olof FORSÉN\*\*

## MICROSCOPY AND XRD INVESTIGATIONS OF THE PRODUCT LAYER FORMED DURING CHALCOPYRITE LEACHING IN COPPER(II) CHLORIDE SOLUTIONS

*Received May 15, 2010; reviewed; accepted August 21, 2010*

This study presents a microscopy investigation of chalcopyrite surface product layers formed in concentrated cupric chloride solutions, similar to those used in the HydroCopper® process. The physical appearance as well as chemical composition of chalcopyrite reaction product layer was studied as a function of pH (from 1 to 3) and leaching time. Microscopic methods, such as stereo-optical microscopy, scanning electron microscopy (SEM) analyses and X-ray diffraction analyses were applied. To study the chalcopyrite reaction product layers, mineral surface was leached either at open circuit potential (OCP) or treated by anodic polarization. It was shown that at lower pH values a gray elemental sulfur layer was the prevailing phase in the reaction product layer even with longer (22 h) leaching times. With increasing pH (up from 2 to 3) the reaction product layer became more yellow-brown, and consisted mainly of FeOOH. However, also elemental sulfur was observed at higher pH. At pH 1 the thickness of the reaction product layer increased from ca. 1 to 9 µm with increasing leaching time up to 22 hours. At pH 2 the layer grew up to ca. 10 µm and at pH 3, up to ca. 14 µm.

*keywords: chalcopyrite, chloride leaching, reaction product layer, sulphur, iron compounds*

### 1. INTRODUCTION

Chalcopyrite, CuFeS<sub>2</sub>, is the most common mineral in copper production. It is available in large quantities and with widespread distribution across the globe. There

---

\* Outotec Oyj, Base Metals P.O. Box 86, 02201 Espoo, Finland, mari.lundstrom@iki.fi

\*\* Aalto University, Department of Materials Science and Engineering, P.O. Box 16200, 00076 Aalto, Finland

is a great environmental incentive to develop alternative, economically beneficial processes to produce copper from sulfide minerals. Hydrometallurgical process routes may also offer the possibility to economically utilise small ore bodies and concentrates with low metal contents. HydroCopper<sup>®</sup> (Hyvärinen et al., 2005) is a chloride based process, which operates at ambient pressure and at temperatures near to the boiling point of the solution at pH between 1.5 and 2.5. The copper (II) ion ( $\text{Cu}^{2+}$ ), used as the oxidant in the process, converts the sulfur content of sulfide minerals into elemental sulfur instead of the usual sulfur dioxide. Although in a commercial process with particle collisions or a high degree mixing, chalcopyrite reaction product layer can be removed, a basic knowledge about the reaction product layer formation and composition is of a great importance.

In chalcopyrite leaching, a solid reaction product layer forms on the mineral surface. The reaction product layer on chalcopyrite has conventionally been suggested to be elemental sulfur, a polysulfide (e.g.  $\text{CuS}_2$ ) or an iron precipitate (e.g. ferric oxyhydroxide or jarosite) (Hiroyoshi et al., 2004; Kinnunen et al., 2006). On a solid chalcopyrite electrode or in heap leaching, the forming layer can hinder the transfer of the metal ions into the solution. The passivation of chalcopyrite has caused problems, specifically in sulfate leaching and bioleaching. The slow dissolution kinetics of chalcopyrite has also limited the number of commercial applications of the mineral. In sulfate media, at temperatures below 110 °C, chalcopyrite is mentioned to leach slowly, having a tendency to accumulate elemental sulfur and iron precipitate product layers, which can hinder the diffusion (Dreisinger, 2003). It has been shown, however (Lu et al., 2000), that the addition of sodium chloride to a sulfate solution (0.5 M NaCl, 0.8 M  $\text{H}_2\text{SO}_4$ ,  $T = 95$  °C) changed the amorphous or cryptocrystalline sulfur film into a crystalline and porous sulfur layer that increased remarkably the dissolution rate of chalcopyrite.

The reaction product layer forming in ferric and copper(II) chloride solutions has generally been suggested to be a more porous sulfur layer, which does not act as a diffusion barrier, but is a less protective and easily removable layer (Table 1). Formation of interference films such as iron oxides has also been observed (Parker et al., 2003). In ferric chloride media, iron precipitates as hematite at higher temperatures ( $>100^\circ\text{C}$ ) and as akaganeite ( $\beta\text{-FeOOH}$ ) at lower temperatures (Riveros et al., 1997; Dutrizac et al., 1999). In the presence of hematite seed however, hematite can already form at lower temperatures.

This article presents microscopy and XRD investigations of the chalcopyrite reaction product layer, formed in concentrated cupric chloride solution,  $[\text{NaCl}] = 250 - 280 \text{ g/dm}^3$ ,  $[\text{Cu}^{2+}] = 17.9 - 30 \text{ g/dm}^3$  and  $T = 85 - 90^\circ\text{C}$ . The topic has been studied earlier (Lundström et al., 2005; 2008; 2009), but this article aims to give a deeper microscopic view on the composition of the reaction product layer formed on stationary chalcopyrite in copper(II) chloride solution.

Table 1. Reaction product layers forming on chalcopyrite in ferric and cupric chloride solutions

LAYER	SOLUTION	T, °C	SOURCE
Elemental sulfur	0.5 – 1.0 M FeCl <sub>3</sub> , 1 M HCl	40 – 80	(Havlík et al., 1995)
Intermediate sulfides	1.0 M FeCl <sub>3</sub> , 0.2 M HCl	3.5 – 45	(Havlík et al., 1995)
Amorphous non-stoichiometric, S <sub>4</sub> predominating	0.4 M FeCl <sub>3</sub> , 1.0 M HCl		(Mikhlin et al. 2004)
Fine grained sulfur mat with globules and sulfur crystals (8h), sulfur globules with small porosity (24h), partly protective	0.1 M FeCl <sub>3</sub> , 0.3 M HCl	95	(Dutrizac, 1990)
Sulfur formation at crystal boundary sites and fractures. Interference films (iron oxides, sulfates) removing sulfur.	0.03 M FeCl <sub>3</sub> , 0.1 M HCl		(Parker, 2005)
Porous non-protective sulfur	0.02 - 0.50 M FeCl <sub>3</sub> , 1 M HCl, 3 M NaCl	96	(Palmer et al., 1981)
Porous elemental sulfur	1.0 M CuCl <sub>2</sub> , 0.2 M HCl	90	(Hirato et al., 1987)
Elemental sulfur	0.1– 0.5 M CuCl <sub>2</sub> , 0.1 M HCl, 4 M NaCl	65– 104	(Bonan et al., 1981)

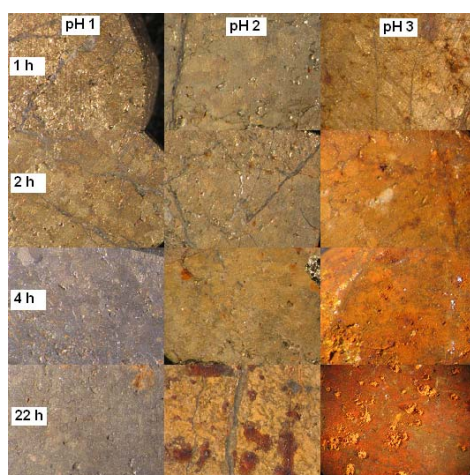


Fig. 1. Reaction product layer with respect to pH from 1 to 3 and leaching time from 1 to 22 h  
 $[\text{NaCl}] = 280 \text{ g/dm}^3$ ,  $[\text{Cu}^{2+}] = 30 \text{ g/l}$ ,  $T = 90^\circ\text{C}$

## 2. MATERIALS AND METHODS

### 2.1. CHALCOPYRITE MINERAL

The chalcopyrite used was from two sources: (i) chalcopyrite mineral used to make cubic chalcopyrite samples was from North America, samples obtained from a local Finnish gemstone shop, (ii) chalcopyrite mineral used to make electrodes originated from Pyhäsalmi mine, Finland. The average composition of the chalcopyrite in Pyhäsalmi concentrate is Cu 34.3%, Fe 30.4%, S 34.9%, Zn 0.04% and Ag 0.02%. However, no concentrate was used, but the chalcopyrite samples were chosen carefully from the liberated grains. The chosen chalcopyrite samples, examined both using microscope and visually, did not contain other phases on the polished electrode surface. The average elemental composition of samples used was analyzed with SEM/EDS from eight North American samples (in wt. %: Cu  $34.5 \pm 0.8$ , Fe  $30.2 \pm 0.5$  and S  $35.9 \pm 1.0$ ) and six Finnish samples (in wt. %: Cu  $33.4 \pm 0.2$ , Fe  $30.5 \pm 0.8$  and S  $36.0 \pm 0.7$ ). The analyzed compositions were near to the theoretical composition of chalcopyrite (i.e., Cu 34.6t, Fe 30.4 and S 34.9).

### 2.2. ELECTROCHEMICAL SETUP

In anodic polarization experiments of chalcopyrite electrodes a standard three-electrode electrochemical cell with a thermostated water jacket was used. Chalcopyrite electrodes were polarized from OCP to 1.2 V vs. SHE at pH 1.5 and pH 3. The solution contained  $[\text{NaCl}] = 250 \text{ g/dm}^3$ ,  $[\text{Cu}^{2+}] = 17.9 \text{ g/dm}^3$  and  $T = 85^\circ\text{C}$ . The electrolyte solution was stirred with a magnetic stirrer at 500 rpm. No purging of gases was done. The counter electrode was a platinum sheet, the reference electrode was saturated Ag/AgCl (REF201, Radiometer Analytical, France) placed in a sintered glass tube containing a gel of agar powder, potassium chloride and distilled water. The reference electrode junction was positioned in an external beaker and connected to the cell via a liquid bridge and a Luggin capillary.

### 2.3. STEREO-OPTICAL MICROSCOPY

For the Stereo-optical microscopy analysis, twelve cubic chalcopyrite samples ( $1 \text{ cm}^3$ ) were leached at OCP for 1, 2, 4 and 22 hours at pHs 1, 2 and 3 ( $[\text{NaCl}] = 280 \text{ g/dm}^3$ ,  $[\text{Cu}^{2+}] = 30 \text{ g/dm}^3$  and  $T = 90^\circ\text{C}$ ). pH was varied by addition of HCl and NaOH. The solution was stirred at 500 rpm and the samples were placed into a mesh basket to be able to avoid collisions. After determined leaching time, each sample was rinsed with deionised water, then ethanol and then dried. The sample surfaces were photographed with a Leica MZ6 stereomicroscope and were later cast in epoxy resin for cross-sectional analysis using the SEM line scan analysis.

#### 2.4. SEM ANALYSIS

For the SEM analysis, two type of samples were used (i) cubic samples leached at OCP and (ii) anodically polarized chalcopyrite electrodes. The cubic samples (i) were rinsed, dried and cast in epoxy resin and polished to give a cross-section of the leached surface. To enhance conductivity, the samples were coated with carbon by vapour deposition. A LEO 1450 SEM/Oxford Instruments® INCA EDS was used to analyze the structure and composition of the reaction product layer. The anodically polarized electrodes (ii) were coated by carbon as such and analyzed. Additionally one cross-sectional analysis was carried out from a polarized chalcopyrite electrode. These were analyzed at Outotec Research Centre with a Cambridge S360 scanning electron microscope equipped with and Oxford INCA EDS analyzer.

#### 2.5. X-RAY DIFFRACTION ANALYSES

Samples for X-ray diffraction analyses were treated similar to those used in the Stereo-optical microscopy analysis. Three cubic chalcopyrite samples ( $1 \text{ cm}^3$ ) were leached at OCP for 22 hours at pH 1, 2 and 3 ( $[\text{NaCl}] = 280 \text{ g/dm}^3$ ,  $[\text{Cu}^{2+}] = 30 \text{ g/dm}^3$  and  $T = 90^\circ\text{C}$ ). After leaching, the samples were washed and dried and forwarded to Outotec Research in Pori, Finland, for analysis. There the reaction product layer formed was separated from the mineral sample by careful scraping with a scapel blade and the sample was analyzed by XRD.

### 3. RESULT AND DISCUSSION

#### 3.1. STEREO-OTICAL MICROSKOPY

Twelve cubic chalcopyrite samples ( $1 \text{ cm}^3$ ) were leached in a copper(II) chloride solution for 1, 2, 4 and 22 hours at pH 1, 2 and 3. The sample surfaces were photographed with a Leica MZ6 stereomicroscope. Figure 1 shows the photographs of the chalcopyrite surface after leaching for 1 to 22 hours at pH from 1 to 3. It can be seen that at pH 1 the chalcopyrite surface becomes grayer with increasing time, suggesting the presence of elemental sulfur on the mineral surface. At pH 2, the surface becomes more yellow, even brown, with increasing time. At pH 3, the chalcopyrite surface becomes more yellow-orange with increasing time. Goethite ( $\alpha\text{-FeOOH}$ ) has been shown to be a strong yellowish brown, akaganeite ( $\beta\text{-FeOOH}$ ) a strong brown, lepidocrocite ( $\gamma\text{-FeOOH}$ ) a moderate orange and hematite ( $\alpha\text{-Fe}_2\text{O}_3$ ) a moderate reddish brown (Scheinost et al., 1999). Thus, the presence of FeOOH with increasing pH can be suggested.

#### 3.2. SCANNING ELECTRON MICROSCOPY ANALYSES

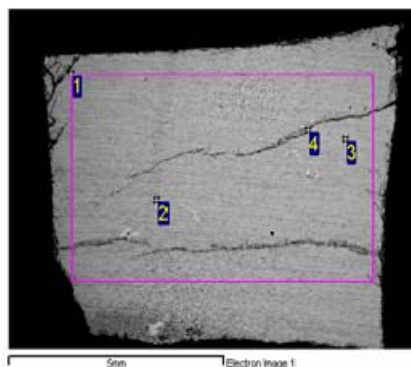
SEM analyses were firstly (area analyses, point analyses) carried out on chalcopyrite electrode surfaces, which had been anodically polarized from OCP to

1.2 V vs. SHE at pH 1.5 and at pH 3 (Figs. 2–4). Additionally, one cross-sectional analysis (Fig. 5) was carried out from a polarized chalcopyrite electrode. Furthermore, twelve cubic chalcopyrite samples were analysed using line scan analysis (Figure 6).

### 3.2. POINT ANALYSES FOR CHALCOPYRITE ELECTRODES

The SEM images for chalcopyrite electrodes can be seen in detail in Figs. 2 - 5. The average EDS analyses from the selected area and some point analyses are presented. The EDS data (weight percentages) were normalized in order to find an empirical formula for the surface composition. The normalized mass of each element was divided by the atomic weight, giving the number of moles in the empirical formula. It must be taken into account that SEM/EDS analyses have a drop shape volume and if the surface layer is thin, it also counts the elements under the reaction product layer. However, the analyzed values before and after the polarization can be compared. The changes in composition can be used to estimate the composition of the surface product layer.

Figures 2 to 4 show the surface before and after polarization at pH 1.5 and 3. It can be seen that before polarization, the mineral composition is near to the theoretical composition of chalcopyrite (Cu:Fe:S was 5:5:11). After polarization at pH = 1.5, a slight excess of sulfur was detected (Cu:Fe:S was 5:5:12). The analysis after polarization at pH = 3 showed a dramatic change in the surface composition, no copper was detected; instead the surface was mainly composed of iron, sulfur and oxygen and (Fe:S:O:Cl was 6:12:13:1). This layer was assumed to be a hematite, goethite, or iron hydroxide type layer.

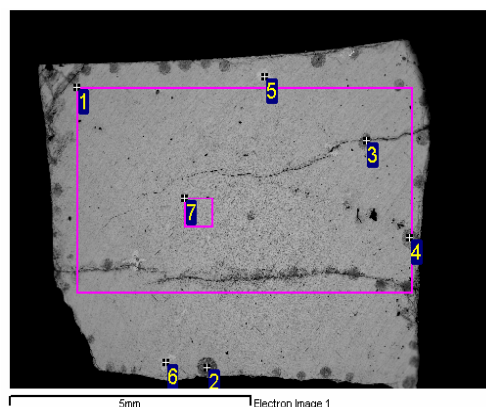


Processing option: all elements analyzed (normalized).

All results in wt. %

Spectrum	S	Mn	Fe	Cu	Zn	Total
1	36.1		30.00	33.21	0.69	100
2	34.64	0.43	8.11	1.16	55.68	100
3	34.41	0.51	12.31	7.21	45.56	100
4	34.52	0.34	7.48	0.68	56.97	100

Fig. 2. SEM images of the polished  $\text{CuFeS}_2$  electrode. The area analysis of chalcopyrite sample Cu = 33.21, Fe = 30.00 and S = 36.10 (in wt. %), with small sphalerite inclusions. Ratio of elements (Cu:Fe:S) was 5:5:11 when calculated quantitatively from area 1



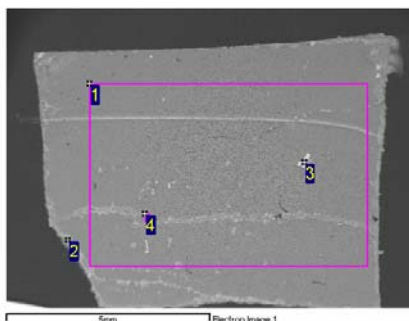
Processing option: All elements analyzed (normalized). All results in weight percent

Spectrum	O	Na	Si	S	Cl	Mn	Fe	Cu	Zn	Ag	Total
1				32.12			29.60	32.28			100
2	22.31	1.82		22.90	9.35		28.88	14.73			100
3	21.31			19.68	4.18		36.32	18.51			100
4	17.62			23.31	4.23		33.53	21.31			100
5				35.61			28.55	31.02		4.83	100
6			0.03	37.37		0.46	6.93		55.22		100
7			0.01	37.26			30.03	32.69			100

Fig. 3. SEM images of the  $\text{CuFeS}_2$  electrode. The area analysis of chalcopyrite dissolved at pH 1.5 is sulfur rich, Cu = 32.38, Fe = 29.60 and S = 38.12 (in wt. %), with chlorine – oxygen rich aggregates, sphalerite and silver rich inclusion. Ratio of elements (Cu:Fe:S) was 5:5:12 when calculated quantitatively from area 1. The solution contained  $[\text{NaCl}] = 250 \text{ g/dm}^3$ ,  $[\text{Cu}^{2+}] = 17.9 \text{ g/dm}^3$ ,  $T = 85^\circ\text{C}$

The crosscut of anodically polarized chalcopyrite electrode (Fig. 5) showed a two phase structure forming during anodic polarization. The layer, seen in Fig.5, consisted mainly of iron and oxygen (in ratio from 1:2 to 1:3). Low concentrations of chloride and sulfur were also present in the reaction product layer, but no copper or sodium were detected.

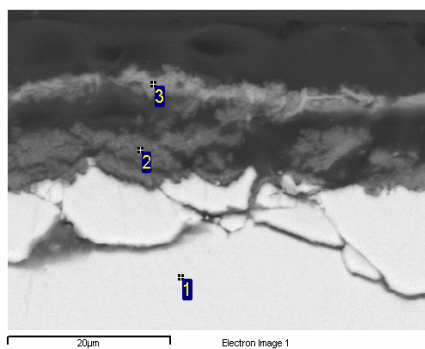
The SEM images of the chalcopyrite electrode surface (Fig. 2) showed an indication of excess sulfur at lower pH and of iron, oxygen and sulfur at higher pHs (Figs. 3 and 4). However, the potentials in the anodic polarization experiment were high (1.2 V vs. SHE) and were not directly related to chalcopyrite dissolution at OCP.



Processing option: all elements analyzed (normalized). All results in weight percent

Spectrum	O	P	S	Cl	Fe	Cu	Zn	Total
1	22.41		38.76	3.74	33.61	2.48		100
2	22.50		23.27	5.97	34.12	14.14		100
3	3.61		33.64		7.88		54.87	100
4	17.88	0.55	30.62	2.79	33.42	14.75		100

Fig. 4. SEM images of the  $\text{CuFeS}_2$  electrode. The area analysis of chalcopyrite dissolved at pH 3.0 is iron-oxygen rich, Cu = 2.48, Fe = 33.61, S = 38.76 and O = 22.41 ( in wt. %), with small chlorine excess. Ratio of the elements at pH 3 Fe:S:O:Cl was 6:12:13:1. The solution contained  $[\text{NaCl}] = 250 \text{ g/dm}^3$ ,  $[\text{Cu}^{2+}] = 17.9 \text{ g/dm}^3$ ,  $T = 85^\circ\text{C}$



Processing option: all elements analyzed (normalized). All results in weight percent

Spectrum	O	Si	P	S	Cl	Fe	Cu	Total
1				35.96		30.89	33.15	100
2	36.24	0.76		3.22	9.99	53.39		100
3	37.52	1.52	0.44	2.50	7.80	50.23		100

Fig. 5. A crosscut-section SEM picture of an  $\text{CuFeS}_2$  electrode made at Outotec Research Oy after anodic polarization at pH 3. The solution had  $[\text{NaCl}] = 250 \text{ g/dm}^3$ ,  $[\text{Cu}^{2+}] = 17.9 \text{ g/dm}^3$ ,  $T = 85^\circ\text{C}$

## 3.3. LINE SCAN FOR CUBIC SAMPLES

To get a better crosscut-section examination of the reaction product layers on stationary chalcopyrite formed at OCP, SEM analyses were carried out on the leached cubic samples (Fig. 1). Originally, an elemental analysis of the reaction product layer was carried out using point analysis. However, it was observed that the reaction product layer was only  $\leq 5 \mu\text{m}$  thick at leaching times  $\leq 4 \text{ h}$ , which made it difficult to make a point analysis of the reaction product layer. Also, when polishing the sample leached at pH 1, grey particles were observed in the epoxy and the polishing wheel, indicating that the grey reaction product layer formed at pH 1 was easily removable. For that reason, the line scan was applied.

The line scan was used to give a better indication of the thickness and the composition of the reaction product layer for all samples. The thickness of the layer was determined following the pulse signals – epoxy resin gives either very low signals (as in Fig. 6 at pH 3 for 22 hour) or O and Cl pulses if air bubbles or Cl resins are present (as in Fig. 6 at pH 1 for 22 hours). The base material chalcopyrite gives pulses of S, Fe and Cu. If the chalcopyrite sample was fragile or uneven, the base material did not give even pulses (as in Fig. 6 at pH 2 for 22 h).

Between the epoxy and the base chalcopyrite material there was a reaction product layer, which gave pulses of the elements present in the layer. The thickness of the layer was also estimated based on this. It must be noted that the number of pulses does not directly describe the concentration of a certain element, but the trends in the number of pulses indicate if the concentration of an element at a certain point is increasing or decreasing. Figure 6 shows the line scans of samples at pH 1, 2 and 3 after 22 hours leaching. Line scans were also carried out at each pH after 1, 2 and 4 hours of leaching. The curves on the base materials side from top to bottom are S, Fe, Cu, O and Cl.

It was observed that the reaction product layer at pH 1 gave pulses for sulfur and grew from a thickness of ca.  $1 \mu\text{m}$  to ca.  $9 \mu\text{m}$ . At pH 2, for  $t = 1\text{-}2 \text{ h}$  sulfur pulses and sulfur together with iron and oxygen pulses ( $t$  from 4 to 22 h) were found, the thickness increasing from ca.  $1 \mu\text{m}$  to ca.  $10 \mu\text{m}$ . At pH 3, there were indications for both oxygen and iron for all times measured and the layer thickness increased from ca.  $1 \mu\text{m}$  to ca.  $14 \mu\text{m}$ . At all pH values the chalcopyrite reaction product layer thickness (from 9 to  $14 \mu\text{m}$ ) after 22 hours of leaching was 5 to 8 times higher than the layer thickness of  $1.7 \mu\text{m}$ , reported by Parker (2005) in 0.1 M HCl solution after 22 hours of leaching at the OCP.

Line scans agreed with the earlier SEM study for polarized chalcopyrite electrodes (Fig. 2 to Fig. 5). At pH 1, only sulfur pulses were observed at the reaction product layer, but no iron or oxygen. This suggests the presence of  $\text{S}^0$  (Fig. 6, pH 1). At pH 2, sulfur pulses were observed at short leaching times ( $\leq 2 \text{ h}$ ), but also iron and oxygen pulses for leaching times longer than 2 hours (Fig. 6, pH 2). At pH 3, strong oxygen

and iron peaks were observed in the reaction product layer, and the presence of sulfur also became evident with increasing leaching time,  $t = 22$  h.

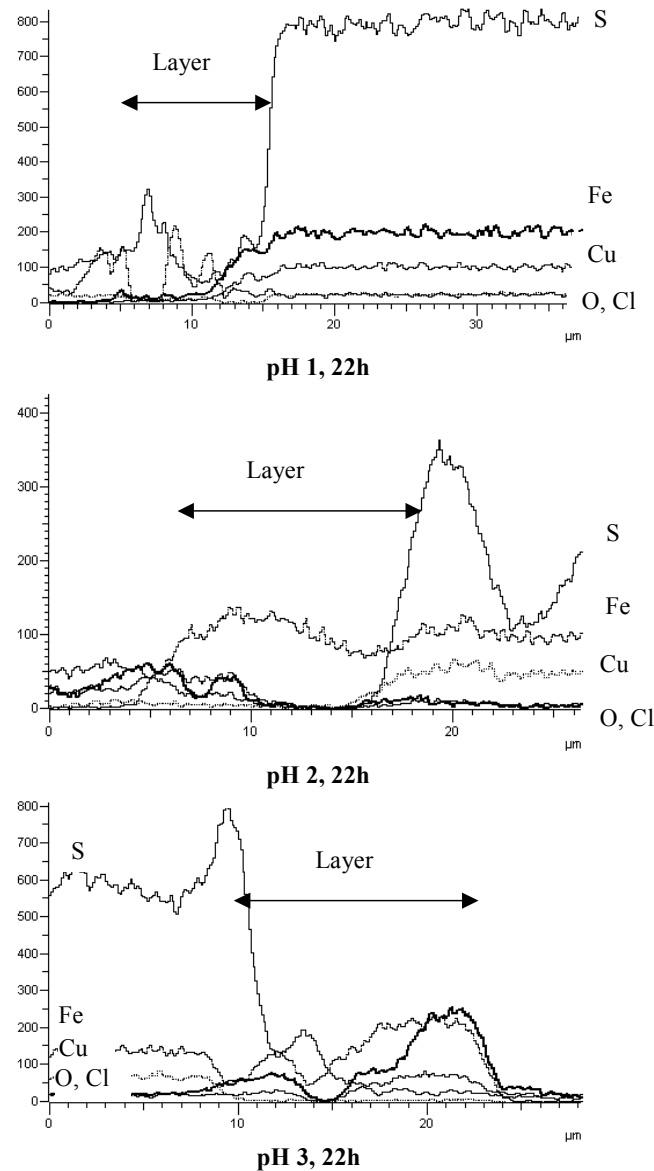


Fig. 6. SEM analysis of chalcopyrite samples. Line scan of the polished  $\text{CuFeS}_2$  samples, leached at pHs 1 – 3 for 22 hours in  $[\text{NaCl}] = 280 \text{ g/dm}^3$ ,  $[\text{Cu}^{2+}] = 30 \text{ g/dm}^3$  and  $T = 90^\circ\text{C}$ . The curves on the base materials side from top to bottom are S, Fe, Cu, O and Cl. The side of the chalcopyrite base material varies: on the right at pH 1 and 2, and on the left at pH 3

### 3.4. X-RAY DIFFRACTION ANALYSES

To confirm the presence of phases on the chalcopyrite surface, X-ray diffraction (XRD) analyses were carried out on the reaction product layers formed on cubic ( $1\text{ cm}^3$ ) chalcopyrite samples leached at the OCP. Figure 7 shows that after 22 hours leaching at pH 1, the reaction product layer consisted of elemental sulfur and a trace amount of goethite (analyzed as  $\alpha\text{-Fe}_2\text{O}_3\cdot\text{H}_2\text{O}$ ). At pH 2 the amount of FeOOH ( $\beta\text{-FeOOH}$ , akaganeite) had increased, and  $\text{S}^0$  was still present. At pH 3 (Fig. 8), the reaction product layer consisted of FeOOH (akaganeite  $\text{Fe}^{3+}\text{O}(\text{OH})$ , synthetic) and there were indications of  $\text{S}_8$ , where sulfur forms an eight-membered ring of sulfur atoms (Dreisinger, 2003). Also chalcopyrite was detected in all XRD analyses.

With increasing pH, iron forms various iron oxide or iron oxide-hydroxide compounds. The XRD spectrum agreed with that of goethite (pH 1),  $\beta\text{-FeOOH}$  (pH 2) and synthetic akaganeite (pH 3), generally discussed as FeOOH. This is intended to describe more of an iron compound, where iron is present as a trivalent species with two oxygen atoms and one hydrogen atom, than the exact phase structure. Earlier (Dutrizac and Riveros, 1999; Riveros and Dutrizac, 1997) in ferric chloride media, FeOOH was found to occur in the form of  $\beta\text{-FeOOH}$  (akaganeite).

## 4. CONCLUSIONS

The analyses indicate that during copper(II) chloride leaching of chalcopyrite elemental sulfur is the main reaction product at pH = 1 and iron compounds at pH = 3. Microscopic observation suggests formation of elemental sulfur at pH = 1, and at pH = 2 and 3 formation of FeOOH. The SEM surface analysis showed slight excess of sulfur at pH = 1.5 (Cu:Fe:S was 5:5:12). At pH = 3 the surface was mainly iron, sulfur and oxygen (Fe:S:O:Cl was 6:12:13:1). This layer was assumed to be hematite, goethite, or iron hydroxide. Crosscut section analysis confirmed a two-phase layer, consisting of mainly of iron and oxygen in ratio 1:2 to 1:3.

Based on SEM line scan analysis of reaction product layers only sulfur was observed at pH = 1 and the thickness of the layer increased from ca.  $1\ \mu\text{m}$  to  $9\ \mu\text{m}$  within 22 hours. At pH = 2 there was sulfur at leaching times 1 – 2 h with iron and oxygen after 4 - 22 h. The thickness increased from ca.  $1\ \mu\text{m}$  to  $10\ \mu\text{m}$ . At pH = 3 there was oxygen and iron for all times measured and the layer thickness increased from ca.  $1\ \mu\text{m}$  to  $14\ \mu\text{m}$ .

The X-ray analysis showed that at lower pH the reaction product layer consisted of elemental sulfur and a trace amount of goethite. With increasing pH the amount of FeOOH increased, but sulfur was still present.

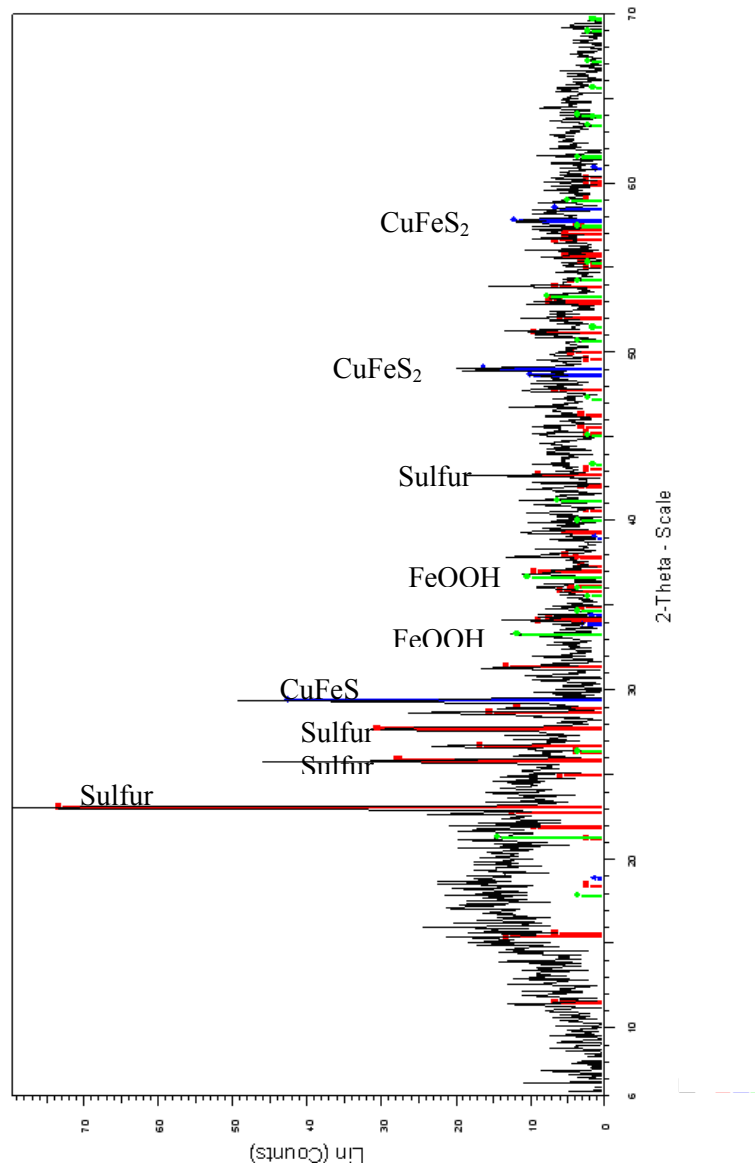


Fig. 7. XRD spectrum and analysis of the chalcopyrite reaction product layer after leaching at pH 1 for 22 hours at OCP. Solution had  $[\text{NaCl}] = 280 \text{ g/dm}^3$ ,  $[\text{Cu}^{2+}] = 30 \text{ g/dm}^3$  and  $T = 90^\circ\text{C}$

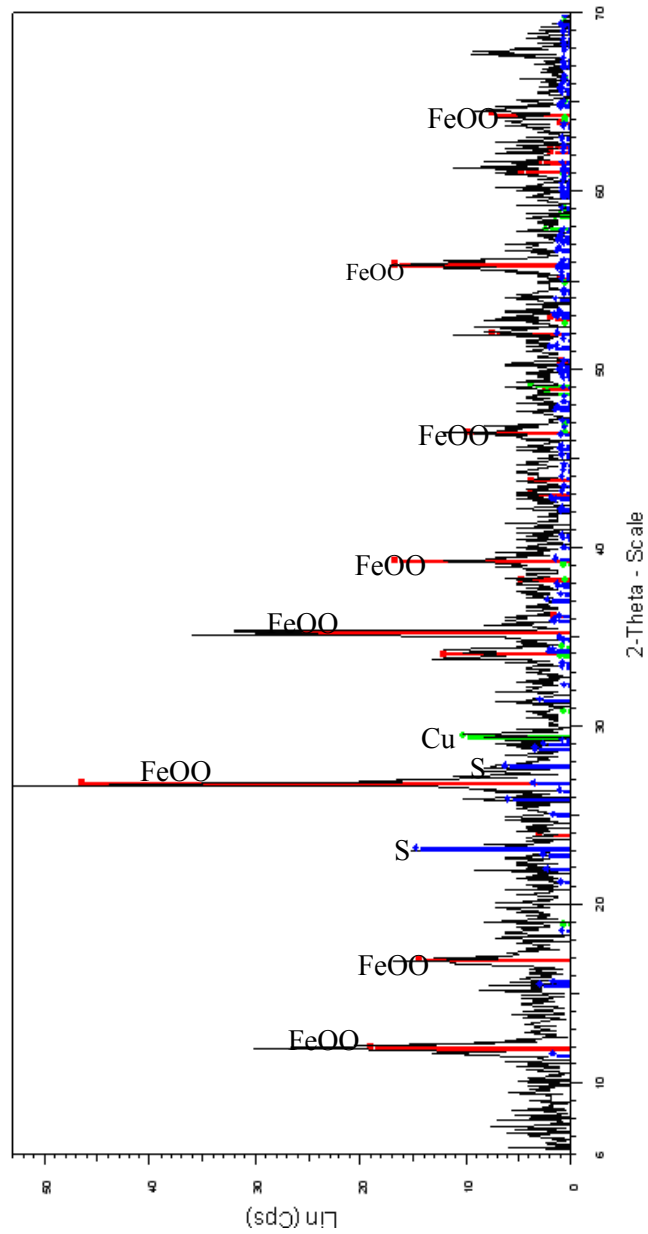


Fig. 8. XRD spectrum and analysis of the chalcopyrite reaction product layer after leaching at pH 3 for 22 hours at OCP. Solution had  $[\text{NaCl}] = 280 \text{ g/dm}^3$ ,  $[\text{Cu}^{2+}] = 30 \text{ g/dm}^3$  and  $T = 90^\circ\text{C}$

## REFERENCES

- BONAN, M., DEMARTHE, J. M., RENON, H. & BARATIN, F. (1981). Chalcopyrite Leaching by  $\text{CuCl}_2$  in Strong  $\text{NaCl}$  Solutions. *Metallurgical Transactions* 12B: pp. 269-274.
- DREISINGER, D. (2003). New Developments in the Leaching of Base and Precious Metal Ores and Concentrates. XXII International Mineral Processing Congress, Cape Town, South Africa, The South African Institute of Mining and Metallurgy.
- DUTRIZAC, J. (1990). Elemental Sulphur Formation During the Ferric Chloride Leaching of Chalcopyrite. *Hydrometallurgy* 23: pp. 153-176.
- DUTRIZAC, J. & RIVEROS, P. (1999). The Precipitation of Hematite from Ferric Chloride Media at Atmospheric Pressure. *Metallurgical and Materials Transactions* 30B: pp. 993-1001.
- HAVLÍK, T. & KAMMEL, R. (1995). Leaching of Chalcopyrite with Acidified Ferric Chloride and Carbon Tetrachloride addition. *Mineral Engineering* 8(10): pp. 1125-1134.
- HAVLÍK, T., SKROBIAN, M., BALÁZ, P. & KAMMEL, R. (1995). Leaching of Chalcopyrite Concentrate with ferric chloride. *International Journal of Mineral Processing* 43: pp. 61-72.
- HIRATO, T., MAJIMA, H. & AWAKURA, Y. (1987). The Leaching of Chalcopyrite with Cupric Chloride. *Metallurgical Transactions B* 18: pp. 31-39.
- HIROYOSHI, N., KUROIWA, S., MIKI, H., TSUNEKAWA, M. & HIRAJIMA, T. (2004). Synergistic effect of cupric and ferrous ions on active-passive behavior in anodic dissolution of chalcopyrite in sulfuric acid solutions. *Hydrometallurgy* 74: pp. 103-116.
- HYVÄRINEN, O. & HÄMÄLÄINEN, M. (2005). HydroCopper — a new technology producing copper directly from concentrate. *Hydrometallurgy* 77: pp. 61-65.
- KINNUNEN, P. H.-M., HEIMALA, S., RIEKKOLA-VANHANEN, M.-L. & PUHAKKA, J. A. (2006). Chalcopyrite Concentrate Leaching with Biologically Produced Ferric Sulphate. *Bioresource Technology* 97: pp. 1727-1734.
- LU, Z. Y., JEFFERY, M. I. & LAWSON, F. (2000). The effect of chloride ions on the dissolution of chalcopyrite in acidic solutions. *Hydrometallurgy* 56: pp. 189-202.
- LUNDSTRÖM, M., AROMAA, J. & FORSÉN, O. (2009). Transient Surface Analysis of Dissolving Chalcopyrite in Cupric Chloride Solution. *Canadian Metallurgical Quarterly* 48(1): pp. 53-60.
- LUNDSTRÖM, M., AROMAA, J., FORSÉN, O. & BARKER, M. (2008). Reaction Product Layer on Chalcopyrite in Cupric Chloride Leaching. *Canadian Metallurgical Quarterly* 47(3): pp. 245-252.
- LUNDSTRÖM, M., AROMAA, J., FORSÉN, O., HYVÄRINEN, O. & BARKER, M. (2005). Leaching of Chalcopyrite in Cupric Chloride Solution. *Hydrometallurgy* 77: pp. 89-95.
- MIKHLIN, Y. L., TOMASHEVICH, Y. V., ASANOV, I. P., OKOTRUB, A. V., VARNEK, V. A. & VYALIKH, D. V. (2004). Spectroscopic and Electrochemical Characterization of the Surface Layers of Chalcopyrite ( $\text{CuFeS}_2$ ) Reacted in Acidic Solutions. *Applied Surface Science* 225: pp. 395-409.
- PALMER, B. R., NEBO, C. O., RAU, M. F. & FUERSTENAU, M. C. (1981). Rate Phenomena Involved in the Dissolution of Chalcopyrite in Chloride-Bearing Lixiviants. *Metallurgical Transactions B* 12B: pp. 595-561.
- PARKER, A., KLAUBER, C., KOUKIANOS, A., WATLING, H. R. & VAN BROSWIJK, W. (2003). An X-ray Photoelectron Spectroscopy Study of the Mechanism of Oxidative Dissolution of Chalcopyrite. *Hydrometallurgy* 71(1-2): pp. 265-276.
- PARKER, G. K. (2005). Spectroelectrochemical Investigation of Chalcopyrite Leaching. Faculty of Science, Griffith University. Doctor of Philosophy: 131 p.
- RIVEROS, P. & DUTRIZAC, J. (1997). The Precipitation of Hematite From Ferric Chloride Media. *Hydrometallurgy* 46: pp. 85-104.
- SCHEINOST, A. & SCHWERTMANN, U. (1999). Color Identification of Iron Oxides and Hydroxysulfates: Use and Limitations. *Soil Science Society of America Journal* 63: pp. 1463-1471.

**Lundström, M., Aromaa, J., Forsén, O.,** *Badania mikroskopowe oraz rentgenowskie XRD produktów utworzonych podczas ługowania chalkopirytu w roztworach chlorków Cu(II)*, Physicochem. Probl. Miner. Process., 46 (2011) 263-277, (w jęz. ang), <http://www.minproc.pwr.wroc.pl/journal>

W pracy przedstawiono badania mikroskopowe warstw powierzchniowych na chalkopirycie utworzonych w stężonych roztworach chlorku miedzi(II), które stosuje się w procesie HydroCopper®. Badano fizyczną postać oraz skład chemiczny produktów reakcji na chalkopirycie jako funkcji pH (od pH 1 do 3) oraz czasu ługowania. Zastosowano metody mikroskopowe takie jak stereo-optyczną, scanningowo-electronową (SEM) oraz rentgenowską. W celu zbadania produktów reakcji, powierzchnia mineralna była ługowana przy otwartym obwodzie potencjału (OCP) lub traktowana przez anodową polaryzację. Wykazano, że przy niskich wartościach pH dominującą wśród produktów reakcji fazą jest szara siarka elementarna istniejąca nawet po długich (22 godziny) czasach reakcji. Wraz ze wzrostem pH (do 2 lub 3) produkty reakcji stawały się bardziej żółto-brązowe i składały się głównie z FeOOH, jednakże siarkę elementarną obserwowano także przy wyższych pH. Przy pH 1 grubość warstwy wzrastała do około 1-9  $\mu\text{m}$  i rosła wraz z czasem ługowania do 22 godzin. Przy pH 2 grubość warstwy rosła do około 10  $\mu\text{m}$ , a przy pH 3 do około 14  $\mu\text{m}$ .

*słowa kluczowe: chalkopiryt, ługowanie chlorkowe, produkty reakcji, siarka, związki żelaza*



Filip CIESIELCZYK\*, Teofil JESIONOWSKI\*

## CHARACTERISATION OF HIGHLY DISPERSED MAGNESIUM SILICATES PREPARED FROM SILICA SOLS AND SELECTED MAGNESIUM SALTS

*Received May 10, 2010; reviewed; accepted August 25, 2010*

A process of obtaining synthetic magnesium silicate by a precipitation method with the use of silicic acid sols and selected magnesium salts was analysed in order to establish the optimum parameters of the process ensuring getting a product of desired properties. The influence of the following parameters was taken into regard: concentration and type of magnesium salt, concentration of silicic acid sol and direction of reagents supply. The synthetic magnesium silicate was subjected to physico-chemical analysis. The chemical compositions of the products and their crystalline structures were determined. Moreover, the morphology, dispersion and adsorption properties of the products were characterised. The magnesium silicate obtained according to the procedure proposed is highly dispersed, homogeneous and of well-developed surface area.

*key words: magnesium silicate, silica sol, precipitation, dispersive characteristics, surface area*

### 1. INTRODUCTION

Silicates belong to the widest spread minerals on the Earth making about 25% of all known minerals. The rocks-forming silicates include: quartz, amphiboles, pyroxenes and micas. Besides their rock-forming role, silicates are the sources of many valuable metals such as nickel, zinc, zircon and lithium and form deposits of many important minerals.

Silicates and aluminosilicates are important raw materials for many industries. They are used in construction, ceramic, paper, rubber, food, pharmaceutical and

---

\* Poznan University of Technology, Institute of Chemical Technology and Engineering  
M. Skłodowskiej-Curie 2, 60-965 Poznan, Poland, [filip.ciesielczyk@put.poznan.pl](mailto:filip.ciesielczyk@put.poznan.pl)

cosmetic industries. Because of their unique physico-chemical properties they are used as selective active adsorbents or polymer fillers (Başçetin, 2010; Carretero, 2010; Villanueva, 2010).

Increasing demand for synthetic silicates of special parameters and properties has stimulated development of new technologies of their production.

One of the best known and documented methods of silica gel production is the sol-gel method. It needs relatively low temperatures and gives products of high purity and homogeneity (Mc Kenzie, 1988). This method belongs to wet ones and requires hydrolysis and condensation of metal alkoxides and inorganic salts.

Another well-known method is based on the ion exchange between the basic ions and protons contained in  $\equiv\text{Si-OH}$ , which permits formation of  $\equiv\text{Si-O-A}$  type bonds (where A is the alkaline metal e.g. Na). The course of hydrolysis and ion exchange depend on the concentration of protons and basic ions in the reaction mixture and influence the concentration of  $\equiv\text{Si-O-A}$  bonds in oligomers. The amorphous  $\text{Na}_2\text{O-SiO}_2$  powder obtained by the ion-exchange method is the initial product for synthesis of magnesium silicate. The ion exchange between alkali earth ions and sodium in  $\text{Na}_2\text{O-SiO}_2$  leads to formation of  $\equiv\text{Si-O-M}$  (where M stands for magnesium or calcium ions) (Suda, 1999).

Quite often used are the methods of obtaining synthetic silicates in water systems (Modrzejewska-Sikorska, 2010; Ciesielczyk, 2004). One of them is the standard reaction of precipitation from water-soluble alkaline silicates, e.g. sodium silicate, by addition of a reagent such as mineral acid or magnesium hydroxide (Brew, 2005; El-Naggar, 2007; Ciesielczyk, 2007). A method for obtaining forsterite and enstatite by the two different water processes has been proposed by Andre Douy (Douy, 2002). Irrespective of the type of procedure, the main reaction is hydrolysis of tetraethoxysilane (TEOS) in an aqueous solution of magnesium nitrate.

An alternative method for production of synthetic silicates is that of precipitation in emulsion systems (Kurc, 2008). A typical procedure for obtaining nanoparticle silicates involves preparation of two emulsions (microemulsions); one with metal salt (sodium silicate) and the other with the reducing agent, and their mixing (Bruch, 1997)

Other literature methods for obtaining magnesium silicates described include the hydrothermal method (Goluber, 2005), condensation of gaseous phase to solid state (Brucato, 2002), laser ablation (Fabian, 2000), recovery of magnesium silicate from geothermal brine and that based on the use of A type zeolites (Strack, 1987).

Although silicates occur naturally in many sites over the world, not all deposits are suitable for exploitation because of too high cost and technical difficulties. Moreover, the natural deposits tend to be exhausted, so the interest in production of synthetic magnesium silicate is still vivid. Much effort is made to facilitate their production, decrease the cost and make their production environmentally neutral.

Development of new processes of synthetic magnesium silicate production is aimed at getting products of desired tailored physicochemical properties. The aim of our study was to propose and characterise a new precipitation method of magnesium silicate production.

## 2. EXPERIMENTAL

### 2.1. MATERIALS

The main substrate used in the process of magnesium silicate precipitation was silicic acid sol of the commercial name LUDOX<sup>®</sup> HS-40, purchased from SIGMA-ALDRICH. It is a 40% water solution of SiO<sub>2</sub>. The ratio of silica to sodium oxide was 89/101, while the maximum content of SO<sub>4</sub><sup>2-</sup> in Na<sub>2</sub>SO<sub>4</sub> was 0.08%. The concentrations of the silicic acid sol used in our study were 5, 10, 20, 30 and 40%.

The precipitating reagents used were solutions of magnesium sulphate (MgSO<sub>4</sub>·7H<sub>2</sub>O) of 1.67 g/cm<sup>3</sup> in density, magnesium nitrate (Mg(NO<sub>3</sub>)<sub>2</sub>·6H<sub>2</sub>O) of 1.46 g/cm<sup>3</sup> in density and magnesium chloride (MgCl<sub>2</sub>·6H<sub>2</sub>O) of 1.57 g/cm<sup>3</sup> in density, all made by POCh SA. The magnesium salts were used in the form of solutions of 5, 10, 20, 30 and 40% concentrations.

### 2.2. METHODS OF STUDIES

Precipitation of synthetic highly dispersed magnesium silicates was conducted at room temperature in a reactor of 1000 cm<sup>3</sup> in volume, equipped with a mechanical stirrer CAT R18 (1000-1600 rpm.). Silicic acid sol (200 cm<sup>3</sup>) was supplied at the constant rate of 5 cm<sup>3</sup>/min to the reactor already containing a proper magnesium salt (200 cm<sup>3</sup>) with the help of a peristaltic pump type ISM 833A, made by ISMATEC. The effect of the reverse direction of supply on the final product properties was also studied. At the second stage of the process the product was filtered off under reduced pressure. To remove the traces of the salts the precipitate was twice washed with hot water. After filtration the product was dried in a stationary drier at 105°C for 24 h.

The first step of the products characterisation was determination of their chemical composition. To this aim magnesium silicate was leached in a solution of HCl/H<sub>2</sub>O (1/1) to remove MgCl<sub>2</sub>. The solution obtained contained the silica precipitate which was separated by gravitational method and washed with distilled water. The content of silicon dioxide was determined by the weight analysis. In the filtrate obtained after leaching the percent contents of magnesium and some small amounts of calcium, sodium and potassium coming from the silicic acid sol solution, were determined by the absorption atomic spectrometry (AAS) on a PU 9100X spectrophotometer made by UNICAM. The crystalline structures of the magnesium silicate samples obtained were established by the WAXS method on a horizontal diffractometer TUR-M-62. Morphology and microstructure of the silicates were assessed on the basis of SEM

photographs taken with a VO40 type scanning electron microscope made by Zeiss. SEM images permit concluding about the character of agglomerations and degree of dispersion. The particle size distributions (dispersion degree) were determined with the use of a Mastersizer 2000 instrument, made by Malvern Instruments Ltd.

The adsorption properties of the samples were estimated with the help of an ASAP 2020 instrument made by Micromeritics Instruments Co.

### 3. RESULT AND DISCUSSION

Results of determination of the chemical composition of the samples obtained by the AAS method and weight analysis are given in Table 1. According to the results the main components of synthetic magnesium silicates are silicon dioxide and magnesium oxide. The other components are the trace amounts of the salts used ( $K_2O$ ,  $Na_2O$ ,  $CaO$ ) left after washing. The chemical composition of the samples obtained was compared with that of the natural magnesium silicate – the natural talc contained  $SiO_2$  46.4÷63.4%,  $MgO$  24.3÷31.9%,  $CaO$  0.4÷13%.

Analysis of the data characterising the samples obtained has shown that only sample 2, that is magnesium silicate obtained from a 5% magnesium sulphate and 30% sol, has the composition similar to that of the natural magnesium silicate. Such a chemical composition ensures good quality of the precipitated samples. Samples 1, 3 (obtained with the use of magnesium sulphate(VI)) and samples 11, 12 (obtained with the use of magnesium chloride) have compositions different from that of the natural talc, but their content of main oxides ( $SiO_2$  and  $MgO$ ) is comparable. The lowest percent content of  $SiO_2$  (44.4%) and the highest percent contribution of  $MgO$  (52.1%) were found in sample 13 obtained with the use of 5%  $MgCl_2$  and 20%  $SiO_2$ . The highest content of  $SiO_2$  (77.2%) was found in sample 28 obtained with the use of 10%  $Mg(NO_3)_2$  and 20%  $SiO_2$ . In this sample the content of  $MgO$  was 19.3% and the moisture content was 8.5%. The moisture content in all samples varied from 8.5 to 9.4%.

On the basis of the WAXS studies (intensity distribution curves  $I=f(\Theta)$ ) the maximum intensity for the samples studied is a few tens times lower than for the crystalline samples. This observation means that the magnesium silicates obtained are fully amorphous. An exemplary WAXS pattern recorded for sample 5 is shown in Fig. 1.

At the next stage of the study, the particle size distributions were determined for the magnesium silicate samples obtained. The curves for the samples precipitated from magnesium sulphate and 10% solution of  $SiO_2$  sol shown in Fig. 2a indicate that these samples contain particles of diameters varying in a very wide range. A similar result was observed for the samples whose curves are shown in Fig. 2. The particle size distribution curves obtained for samples precipitated with the use of 5%  $MgCl_2$  (sample 14) and with the use of 10%  $Mg(NO_3)_2$  solutions (sample 29) were found to

coincide to a large degree. The particle size distribution obtained for sample 19 obtained with 10%  $\text{MgCl}_2$  solution was found significantly different from that of sample 14 obtained with 5%  $\text{MgCl}_2$  solution. Analysis of the values of  $D[4,3]$  (mean diameter by volume) reveals that the diameter of particles in the whole sample volume increases (the sample is less homogeneous) with increasing concentration of the salt used for precipitation of this sample. This relation was observed for the samples obtained using magnesium sulphate (in sample 4 the mean diameter was  $27.46 \mu\text{m}$ , while in sample 9 it was  $32.7 \mu\text{m}$ ) and using magnesium chloride (in sample 14 the mean diameter is  $18.9 \mu\text{m}$ , while in sample 19 it is  $24.5 \mu\text{m}$ ). No such relation was found for the samples obtained using magnesium nitrate as magnesium silicate was not obtained using 5%  $\text{Mg}(\text{NO}_3)_2$  and 10%  $\text{SiO}_2$  solutions.

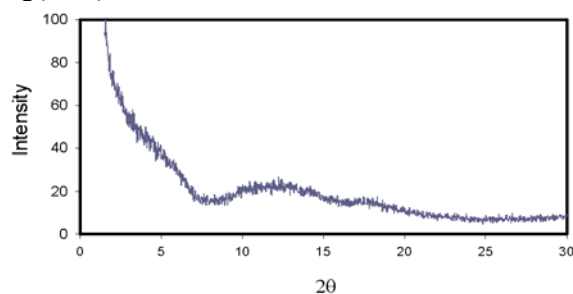


Fig.1. WAXS pattern of magnesium silicate – sample 5 (precipitated from 5%  $\text{MgSO}_4$  and 5%  $\text{SiO}_2$  sol)

As follows from Fig. 2, the particle size distributions obtained for the samples produced with the use of 20%  $\text{SiO}_2$  and 5%  $\text{Mg}(\text{NO}_3)_2$  (sample 23), 5%  $\text{MgCl}_2$  (sample 13) and 10%  $\text{MgSO}_4$  (sample 8) are similar. For sample 23 the mean particle diameter in the whole sample volume is  $21.9 \mu\text{m}$ , for sample 13 it is  $22.5 \mu\text{m}$ , while for sample 8 is  $23.6 \mu\text{m}$ . In sample 23, 10% volume contribution is brought by the particles of diameter below  $4.1 \mu\text{m}$ , for samples 13 and 8 the same volume contribution is brought by the particles of diameters below  $3.9 \mu\text{m}$  and  $3.9 \mu\text{m}$ , respectively, 50% volume contribution is brought by the particles of diameters below  $15.0 \mu\text{m}$ , for samples 13 and 8 the analogous values are  $14.9 \mu\text{m}$  and  $15.7 \mu\text{m}$  and 90% volume contribution is brought by agglomerates of the diameters below  $50.3 \mu\text{m}$ , for samples 13 and 8 the analogous values are  $52.7 \mu\text{m}$  and  $55.3 \mu\text{m}$ , respectively. A narrow range of particle diameters was obtained for magnesium silicate obtained with the use of 20% or 10%  $\text{SiO}_2$  sol and 10% solutions of magnesium chloride or magnesium nitrate, Fig. 2a.

Interesting results were obtained for the product obtained with the use of 30% sol and the magnesium salts studied in different concentrations. Practically all particle size distribution curves overlapped (Fig. 2c), which means that high concentration of sol causes that the particles of magnesium silicate vary in the same range irrespective of the use of different salts in different concentrations.

Figure 2d presents particle size distributions obtained for synthetic magnesium

silicate precipitated from a solution of 40% SiO<sub>2</sub> sol and different magnesium salts. For all samples narrow ranges of particle diameters variation were noted. Similarly as for the products precipitated with the use of 5, 10 and 30% of SiO<sub>2</sub> sol, also when using 40% sol solution the greatest mean diameter in the whole sample volume (of 25.5 μm) was obtained for sample 1 precipitated with 5% solution of MgSO<sub>4</sub>. In this sample the particles of diameters below 4.9 μm brought 10% volume contribution, those of diameters below 18.8 μm 50% contribution, while the agglomerations of diameters below 56.1 μm a 90% contribution. For the other products obtained with the use of 40% sol solution, the volume contributions of particular fractions were different than for sample 1.

Morphology of the magnesium silicate samples obtained was evaluated on the basis of SEM images. Selected images of MgO·SiO<sub>2</sub> are shown in Fig. 3. The SEM images presented confirm that the samples are built of particles whose sizes correspond to those indicated by the relevant particle size distributions and whose shapes are irregular.

Adsorption properties of the samples studied were characterised on the basis of the nitrogen adsorption/desorption isotherms. Figure 4 presents the relation between the volume of nitrogen adsorbed on samples 5, 19 and 29 versus relative pressure. The isotherms recorded for sample 5 precipitated with 5% MgSO<sub>4</sub> and 5% SiO<sub>2</sub> and sample 29 precipitated with the use of 10% Mg(NO<sub>3</sub>)<sub>2</sub> and 10% SiO<sub>2</sub> are very similar. The amount of nitrogen adsorbed increases slowly up to p/p<sub>0</sub> of 0.8. For higher p/p<sub>0</sub> values the adsorption of nitrogen rapidly increases to reach a maximum of 570 cm<sup>3</sup>/g at p/p<sub>0</sub>=1 for sample 5, while for sample 29 to reach a maximum of 540 cm<sup>3</sup>/g at p/p<sub>0</sub>=1. The isotherm recorded for sample 19 precipitated with the use of 10% MgCl<sub>2</sub> and 10% SiO<sub>2</sub> solutions has a different character. The amounts of adsorbed nitrogen are initially much smaller than for samples 5 and 29, but for relative pressure values greater than p/p<sub>0</sub>=0.8 this amount rapidly increases to reach a maximum of 470 cm<sup>3</sup>/g at p/p<sub>0</sub>=1. The adsorption capacity of sample 19 is much smaller than that of sample 5, for which the maximum amount of adsorbed nitrogen is 570 cm<sup>3</sup>/g.

The greatest porosity and thus largest specific surface area was found for the samples precipitated with the use of magnesium sulphate and magnesium chloride. All the samples of synthetic magnesium silicate were classified as mesoporous. The largest specific surface area of 513 m<sup>2</sup>/g and the greatest pore volume of 0.7 cm<sup>3</sup>/g were determined for sample 5, which indicates that this silicate shows the greatest surface activity. The same pore volume was found for sample 29, but its specific surface area was smaller 412 m<sup>2</sup>/g. The smallest specific surface area was measured for sample 19 precipitated with the use of 10% magnesium chloride and 10% SiO<sub>2</sub> sol. The pore volume of this sample was also smaller than those of the samples precipitated with magnesium sulphate or magnesium chloride. The mean pore diameter found for these three samples was similar and varied from 5.0 to 5.4 nm.

Table 1. Chemical composition of synthetic magnesium silicates

Sample no.	Concentration of magnesium salt (%)	Concentration of SiO <sub>2</sub> sol (%)	Precipitation direction	Contents (%)		
				SiO <sub>2</sub>	MgO	H <sub>2</sub> O
1	5	40	Silica sol to MgSO <sub>4</sub>	59.1	36.8	9.1
2	5	30		62.7	33.2	9.1
3	5	20		58.2	37.8	9.0
4	5	10		75.2	21.3	8.5
5	5	5		69.6	26.6	8.8
6	10	40		77.1	19.3	8.6
7	10	30		70.7	25.3	9.0
8	10	20		70.4	25.5	9.1
9	10	10		71.0	24.9	9.1
10	10	5		55.8	40.2	9.0
11	5	40	Silica sol to MgCl <sub>2</sub>	58.5	37.5	9.0
12	5	30		66.2	30.0	8.8
13	5	20		44.4	52.1	8.5
14	5	10		72.4	24.1	8.5
15	5	5		49.8	46.2	9.0
16	10	40		47.8	48.3	8.9
17	10	30		45.7	50.4	8.9
18	10	20		71.5	24.5	9.0
19	10	10		49.2	47.3	8.5
20	10	5		-	-	-
21	5	40	Silica sol to Mg(NO <sub>3</sub> ) <sub>2</sub>	-	-	-
22	5	30		76.4	18.8	8.9
23	5	20		52.9	43.1	9.0
24	5	10		-	-	-
25	5	5		-	-	-
26	10	40		76.5	19.7	8.8
27	10	30		73.6	22.9	8.5
28	10	20		77.2	19.3	8.5
29	10	10		75.9	19.7	9.4
30	10	5		-	-	-

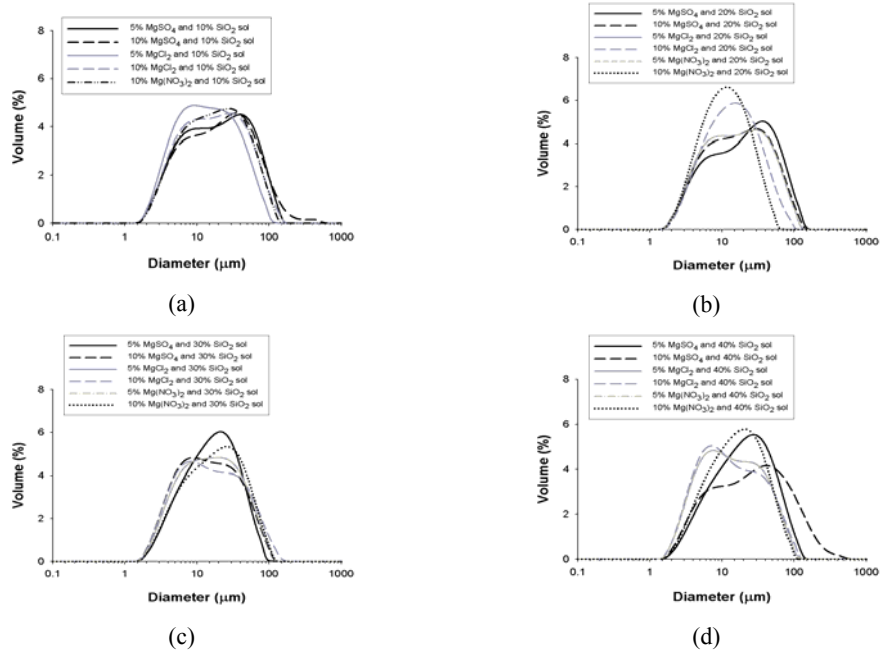


Fig. 2. PSD's of magnesium silicate – samples precipitated from (a) 10, (b) 20, (c) 30 and (d) 40% silica sol solution and different types and concentrations of magnesium salts

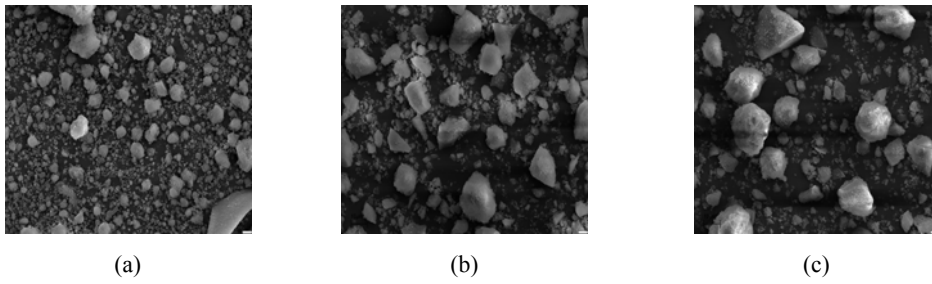


Fig. 3. SEM photographs of magnesium silicate – samples (a) 5, (b) 19 and (c) 29

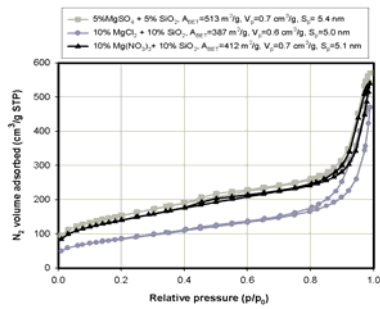


Fig. 4. N<sub>2</sub> adsorption/desorption isotherms of synthetic magnesium silicates (samples 5, 19 and 29)

### 3. CONCLUSION

According to the presented and discussed results, the character of synthetic magnesium silicate obtained by the method of precipitation based on silica sols is determined by the type of magnesium salt used. The process performed for SiO<sub>2</sub> sols of low concentrations permits getting products of higher degree of dispersion. The best physico-chemical properties have been revealed by sample 5 (obtained with the use of 5% MgSO<sub>4</sub> and 5% SiO<sub>2</sub> sole solutions), sample 19 (10% MgCl<sub>2</sub> and 10% SiO<sub>2</sub> sol) and sample 29 (10% Mg(NO<sub>3</sub>)<sub>2</sub> and 10% SiO<sub>2</sub> sol). The experiments performed for the reversed direction of reagents supply, i.e. when sol was supplied to a proper magnesium salt, have proved that under such conditions the method does not guarantee obtaining the product desired, and moreover, when the precipitating agent is magnesium nitrate or magnesium chloride, the product is impossible to get.

The dispersion character of the synthetic magnesium silicate obtained has been shown to be determined by the type of magnesium salt used in the process of precipitation and its concentration. The use of magnesium salt at a lower concentration leads to obtaining a more dispersed product. It has been shown that synthetic magnesium silicates of particles whose diameters vary in a narrow range are obtained when using SiO<sub>2</sub> sol of high concentrations, 30 or 40%. The best-developed specific surface area (BET) and the greatest pore volume (513 m<sup>2</sup>/g) have been found for sample 5, which shows the highest surface activity. The results have confirmed the possibility of using magnesium silicates as selective adsorbents.

### ACKNOWLEDGEMENTS

This work was supported by the Ministry of Science and Higher Education research grant no. N N205 109735 (2008-2010).

### REFERENCES

- BAŞÇETİN E., ATUN G., 2010, Adsorptive removal of strontium by binary mineral mixtures of montmorillonite and zeolite, *J. Chem. Eng. Data*, 55, 783-788.
- BREW D.R.M., GLASSER F.P., 2005, Synthesis and characterization of magnesium silicate hydrate gels, *Cem. Concr. Res.*, 35, 85-98.
- BRUCATO J.R., MENNELLA V., COLANGELI L., ROTUNDI A., PALUMBO P., 2002, Production and processing of silicates in laboratory and in space, *Planet. Space Sci.*, 50, 829-837.
- BRUCH C., KRUGER J.K., UNRUH H.G., KRAUSS W., ZIMMERMEIER B., BECK C., HAMPELMANN R. 1997, Inelastic light scattering and phonon-confinement in nanocrystalline Y<sub>2</sub>O<sub>3</sub>, *J. Phys. Chem.*, 101(11), 1761-1764.
- CARRETERO M.I., POZO M., 2010, Clay and non-clay minerals in the pharmaceutical and cosmetic industries Part II. Active ingredients, *Appl. Clay Sci.*, 47, 171-181.
- CIESIELCZYK F., KRYSZTAFKIEWICZ A., JESIONOWSKI T., 2004, Influence of precipitation parameters on physicochemical properties of magnesium silicates, *Physicochem. Problems Mineral. Proc.*, 38, 197-205.

- CIESIELCZYK F., KRYSZTAFKIEWICZ A., JESIONOWSKI T., 2007, Physicochemical studies on precipitated magnesium silicates, *J. Mater. Sci.*, 42, 3831-3840.
- DOUY A., 2002, Aqueous synthesis of forsterite ( $Mg_2SiO_4$ ) and enstatite ( $MgSiO_3$ ), *J. Sol-Gel Sci. Technol.*, 24, 221-228.
- EL-NAGGAR I.M., ABOU-MESALAM M.M., 2007, Novel inorganic ion exchange materials based on silicates; synthesis, structure and analytical applications of magnesio-silicate and magnesium alumino-silicate sorbents, *J. Hazard. Mater.*, 149, 686-692.
- FABIAN D., JÄGER C., HENNING Th., DORSCHNER J., MUTSCHKE H., 2000, Steps toward interstellar silicate mineralogy. - V. Thermal evolution of amorphous magnesium silicates and silica, *Astron. Astrophys.*, 364, 282-292.
- GOLUBERA O., KORYTKOVA E.N., GUSAROV V.U., 2005, Hydrothermal synthesis of magnesium silicate montmorillonite for polymer-clay nanocomposites, *Russ. J. Appl. Chem.*, 78(1), 26-32.
- KURC B., JESIONOWSKI T., KRYSZTAFKIEWICZ A., 2008, Formation and physicochemical properties of silica fillers precipitated in emulsion medium, *Physicochem. Problems Mineral. Proc.*, 42, 67-74.
- Mc KENZIE J.D., 1988, Applications of the sol-gel process, *J. Non-Cryst. Solids*, 100(1-3), 162-168.
- MODRZEJEWSKA-SIKORSKA A., CIESIELCZYK F., KRYSZTAFKIEWICZ A., JESIONOWSKI T., 2010, Synthesis and characterization of precipitated copper(II) silicates, *Physicochem. Problems Mineral. Proc.*, 44, 157-168.
- STRACK H., KLEINSCHMIT P., 1987, Magnesium-silicate bound zeolite granulates of the type of zeolite A, process for their production and use, U.S. Patent No. 4668648.
- SUDA S., TASHIRO T., UMEGAKI T., 1999, Synthesis of  $MgO-SiO_2$  and  $CaO-SiO_2$  amorphous powder by sol-gel process and ion exchange, *J. Non-Cryst. Solids*, 255, 178-184.
- VILLANUEVA M.P., CABEDO L., LAGARÓN J.M., GIMÉNEZ E., 2010, Comparative study of nanocomposites of polyolefin compatibilizers containing kaolinite and montmorillonite organoclays, *J. Appl. Polym. Sci.*, 115, 1325-1335.

**Ciesielczyk F., Jesionowski T.,** *Charakterystyka wysoko zdyspergowanych krzemianów magnezu otrzymanych w oparciu o zole kwasu krzemowego i wybrane sole magnezu*, *Physicochem. Probl. Miner. Process.*, 46 (2011) 279-288, (w jęz. ang), <http://www.minproc.pwr.wroc.pl/journal>

Przedstawiono rezultaty badań nad otrzymywaniem syntetycznego krzemianu magnezu metodą strącaniową w oparciu o zole kwasu krzemowego i wybrane związki magnezu. Istotnym zagadnieniem realizowanej tematyki było dobranie podstawowych parametrów prowadzenia procesu strącania, celem uzyskania produktu o jak najlepszych właściwościach fizykochemicznych. W trakcie badań przeanalizowano następujące parametry procesu: stężenie i rodzaj soli magnezu, stężenie zolu kwasu krzemowego, kierunek dozowania reagentów. Dodatkowo otrzymany syntetyczny krzemian magnezu poddany został analizie fizykochemicznej.

*słowa kluczowe: krzemian magnezu, zol krzemionkowy, wytrącanie, charakterystyka dyspersji, pole powierzchni*

Bernadeta GAJDA\*, Andrzej SKRZYPCZAK\*\*, Mariusz B. BOGACKI\*\*\*

## SEPARATION OF COBALT(II), NICKEL(II), ZINC(II) AND CADMIUM(II) IONS FROM CHLORIDE SOLUTION

*Received June 12, 2010; reviewed; accepted August 30, 2010*

Selective distribution of cobalt(II), nickel(II), zinc(II) and cadmium(II) ions from chloride solutions through polymer inclusion membranes (PIM) has been studied. The carrier was 1-decylimidazole. The effect of chloride ion concentration on the ion permeation was analysed. The results suggest that some of metal ions change for the worse selectivity of separation process. Especially zinc(II) and cadmium(II) ions decreased five-fold selectivity of ion separation process.

*keywords: zinc(II), cobalt(II), nickel(II) cadmium(II); polymer inclusion membranes; solvent extraction; 1-decylimidazole*

### 1. INTRODUCTION

Cobalt, nickel, zinc and cadmium are important elements known as industry useful metals. Main sources of them are sulfide and oxide ores. Other source of them is ocean in which many metal ions are dissolved or present in the concrete form. That source will be very useful in the future when traditional ores of many metals are exhausted (Gajda and Bogacki, 2010).

Also many industrial processes produce liquid or solid wastes containing metal

---

\* Department of Metal Extraction and Recirculation, Częstochowa University of Technology, Armii Krajowej 19, 42-200 Częstochowa, Poland

\*\* Division of Organic Technology, Poznań University of Technology, Pl. M. Skłodowskiej-Curie 2, 60-965 Poznań

\*\*\* Division of Process Engineering, Poznań University of Technology, Pl. M. Skłodowskiej – Curie 2, 60-965 Poznań. e-mail: Mariusz.Bogacki@put.poznan.pl

ions. That kind of wastes are produced in chemical metallurgy, industrial metallurgy and industrial electronics. A next potential source of heavy metal waste is battery and accumulator recycling (Rudnik and Nikiel, 2007). Ecological and economical regulations caused recycling of all wastes, especially containing cadmium, nickel and even cobalt ions.

Today the most important processes to obtain such metals as cobalt, nick, zinc and cadmium are: ion-exchange, hydrometallurgy, especially solvent extraction and liquid membrane ion transportation.

During the last two decades we observe growing interest in application polymer inclusive membranes (PIM) for metal ion separation. The PIM membranes have better mechanical strength and chemical resistance than liquid membranes. Plasticizing additive in polymer membrane causes their good or even very good flexibility. Membrane containing plasticizers has also good ability to miscible ion carrier in polymer. Today several ion carriers are used as metal extractants such as phosphoric acids (Reddy et al., 2005; Aouad et al., 1998; Ulewicz and Walkowiak, 2005; Kozłowski et al., 2002), trioctylamine (Pośpiech and Walkowiak, 2007), and coronene ethers (Walkowiak et al., 2000).

In the last ten years some imidazolium derivatives were also used for ion separation (Radzymińska-Lenarcik, 2008; du Preez et al., 2001; Radzymińska-Lenarcik, 2007). Imidazolium compounds have two nitrogen atoms in the aromatic ring. One nitrogen atom has a free electron pair, efficient for a coordinate bond and we observe reactions of complex formation of imidazolium compounds with metal chlorides  $MCl_2$ .

The aim of the work is to study selective separation process of Ni(II), Co(II), Zn(II) and Cd(II) ions from chloride solutions using 1-decylimidazole.

## 2. EXPERIMENTAL

1-Decylimidazole was synthesized in the reaction of imidazole and 1-bromodecane in the solution of sodium methylate in methanol – Fig. 1.

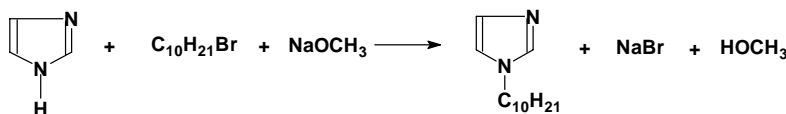


Fig. 1. 1-decylimidazole synthesis

After dissolving all substrates, the mixture was stirred and heated under reflux for 2 hours. After cooling the solution to room temperature, the crude product was separated from the solid sodium bromide, extracted with hexane and dried in vacuum. 1-decylimidazole was twice distilled under reduced pressure. The yield of the reaction was 91%.

The polymeric inclusive membranes (PIM) were prepared mixing solutions: 1.25 g

of cellulose triacetate (CTA) in 100 cm<sup>3</sup> dichloromethane, 10% solution of o-nitrophenyloctyl ether (ONPOE, Fluka) in dichloromethane and 0.1M of ion carrier (1-decylimidazole) also in dichloromethane. After careful stirring, the solution was poured into 4 cm diameter glass ring, placed on a glass horizontal plate. After 12 h, dichloromethane has evaporated the membrane was ready and immediately dipped for next 12 h into distilled water. The working membrane contained 8.0 cm<sup>3</sup> ONPOE/1.0 g CTA and 1.0 M carrier. Molar concentration of ion carrier in the membrane was calculate for the volume of the plasticizer

The measurement vessel for membrane test contained two 50 cm<sup>3</sup> in volume cells separated by 4.9 cm<sup>2</sup> surface membrane (Fig. 2).

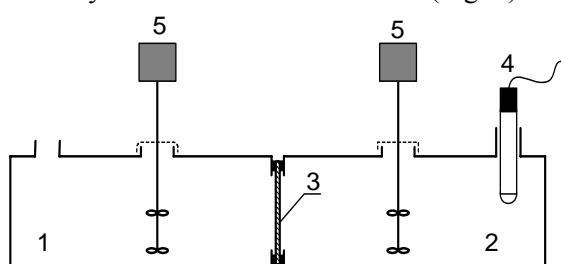


Fig. 2. Measurement system for PIM membrane metallic ion transportation  
1– receiver solution, 2– feed solution,  
3– membrane, 4– pH electrode, 5– stirrer

The feeding phase was 10<sup>-2</sup> M chloride solution of appropriate Co(II), Ni(II), Zn(II) and 5·10<sup>-3</sup> M chloride solution of Cd(II) ions. To have 2 M solution of chloride anions, NaCl was added. Four chloride solutions of metal ions were tested: 1) Co(II) – Ni(II); 2) Co(II) – Ni(II) – Zn(II); 3) Co(II) – Ni(II) – Cd(II); 4) Co(II) – Zn(II) – Cd(II); 4) Co(II) – Ni(II) – Zn(II) – Cd(II).

The receiver solution was distilled water. Prepared solutions were stirred by a 600 rpm rotating mixer. During transportation process 0.20 cm<sup>3</sup> samples were taken from the feed and receiver solutions. After dilution, samples were quantitative analyzed for ion metallic concentration using atomic absorbing spectrophotometer (ASA, Solar 939, Unicam).

The kinetics of transport across the PIMs was described as first-order process in relation to the metal ion concentration:

$$\ln\left(\frac{c}{c_i}\right) = -kt \quad (1)$$

where  $c$  – metal ions concentration,  $c_i$  – initial metal ions concentration in source phase,  $k$  – rate coefficient, 1/s, and  $t$  – time of transport, s. The initial flux,  $J_i$  (mol·m<sup>-2</sup>·s<sup>-1</sup>) is equal to:

$$J_i = \frac{V}{A} kc_i, \quad (2)$$

where  $V$  – volume of aqueous source phase, m<sup>3</sup>;  $A$  – effective area of membrane, m<sup>2</sup>. The permeability coefficient,  $P$ , (m/s) was calculated according to equation:

$$P = \frac{V}{A}k. \quad (3)$$

The selectivity coefficient was defined as a ratio of initial fluxes for to the metal ions:

$$S_{M_I / M_{II}} = \frac{J_{M_I}}{J_{M_{II}}}. \quad (4)$$

### 3. RESULTS AND DISCUSSION

An exemplary relationship between  $\ln(c/c_0)$  and time for Co(II), Zn(II), Ni(II) and Cd(II) ions transport across the PIM membranes are shown in Figs 3 and 4.

Looking at Figs 3 and 4 we can state that there is big difference between tested ion transportation coefficients for appropriate metal ions. From Table 1 we can see that the values of feeding phase for starting streams of metal ions differ even three order of magnitude from  $6.13 \cdot 10^{-7}$  for nickel ions in solution of Co – Ni – Zn and  $1.31 \cdot 10^{-4}$  for cobalt ions in solution of Co – Ni.

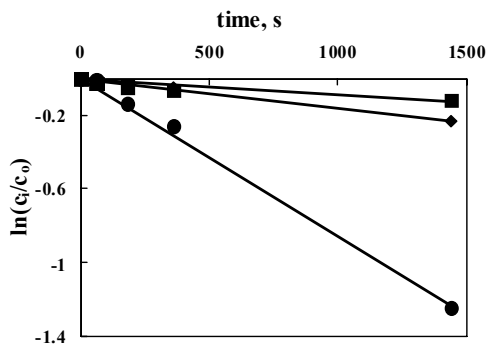


Fig. 3. Ion concentration change as a function of time in the feeding phase  $\diamond$  – Co(II),  $\blacksquare$  – Ni(II)  $\bullet$  – Cd(II). Ion carrier 1-decyloimidazol. Chloride concentration in feeding phase – 2 M. Receiver solution – distilled water. Starting ion concentration: Co, Ni –  $10^{-2}$  M, Cd –  $5 \cdot 10^{-3}$  M

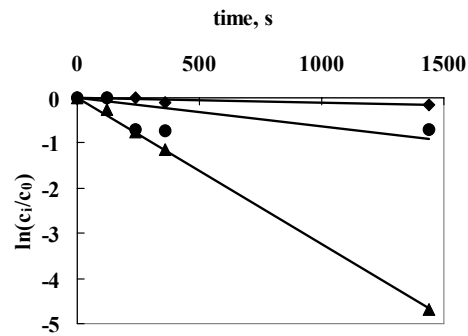


Fig. 4. Ion concentration change as a function of time in the feeding phase  $\diamond$  – Co(II),  $\blacktriangle$  – Zn(II) and  $\bullet$  – Cd(II). Ion carrier 1-decyloimidazol. Chloride concentration in feeding phase – 2 M. Receiver solution – distilled water. Starting ion concentration: Co, Zn –  $10^{-2}$  M, Cd –  $5 \cdot 10^{-3}$  M

As we can see from Tables 1 and 2 the highest value of rate the ion transport is for zinc(II) ion. Measured values ( $10^{-4}$ ) of starting stream do not depend on feeding phases. Also the rate ion transport for zinc(II) ion does not depend on the feeding phase composition. But the ion rate transport for Ni(II) and Co(II) depends on the feeding phase composition because Zn(II) and Cd(II) in tested composition highly lowered their ion transportation rate.

Presented in Table 2 selectivity coefficients show that presence of Zn(II) or Cd(II) ions in the tested solutions lowered selectivity of ion partition coefficient of Ni(II) and Co(II) ions. For instance, the selectivity coefficient for solution contained only Ni(II)

and Co(II) ions is 8.1. When Zn(II) and Cd(II) ions were added, selectivity coefficient lowered 4-5 times. We observed similar behavior for other ion pairs. The selectivity coefficient for solution containing only Zn(II) and Co(II) ions also was lowered when Cd(II) ions were added. In that case selectivity coefficient was lowered 5 times.

Table 1. Starting stream of metal ions ( $J_i$ , mol/(m<sup>2</sup>s)) for three different solutions of feeding phase. Ion carrier – 1-decylimidazole. Chloride concentration in feeding phase – 2 M. Receiver solution – distilled water. Metal ion concentration: Co, Ni, Zn – 10<sup>-2</sup> M, Cd – 5·10<sup>-3</sup> M

Ion	Feeding phase				
	Co – Ni	Co – Ni – Zn	Co – Ni – Cd	Co – Zn – Cd	Co – Ni – Zn – Cd
Co	1.31·10 <sup>-4</sup>	1.19·10 <sup>-6</sup>	1.50·10 <sup>-5</sup>	1.24·10 <sup>-5</sup>	8.33·10 <sup>-6</sup>
Ni	1.63·10 <sup>-5</sup>	6.13·10 <sup>-7</sup>	9.14·10 <sup>-6</sup>	-	1.17·10 <sup>-5</sup>
Zn	-	1.32·10 <sup>-4</sup>	-	2.78·10 <sup>-4</sup>	1.12·10 <sup>-4</sup>
Cd	-	-	4.59·10 <sup>-5</sup>	3.64·10 <sup>-5</sup>	8.03·10 <sup>-6</sup>

Table 2. Selectivity coefficient of metal ions ( $S_{M_i/M_j}$ ) for different solutions of feeding phase. \* indicates the reverse value ( $S_{M_j/M_i}$ ). Ion carrier – 1-decylimidazole. Chloride concentration in feeding phase – 2 M. Receiver solution – distilled water. Metal ions concentration: Co, Ni, Zn – 10<sup>-2</sup> M, Cd – 5·10<sup>-3</sup> M

Ion	Feeding phase				
	Co – Ni	Co – Ni – Zn	Co – Ni – Cd	Co – Zn – Cd	Co – Ni – Zn – Cd
Co/Ni	8.10	1.94	1.64	-	1.41*
Co/Zn	-	9.05*	-	2.24*	1.35*
Co/Cd	-	-	3.07*	2.94*	1.04
Ni/Zn	-	2.15*	-	-	9.59*
Ni/Cd	-	-	5.03*	-	6.86
Zn/Cd	-	-	-	1.31	1.40

#### 4. CONCLUSION

Many industrial processes produce wastes containing polymetallic ion solutions. Our measurements proved that metal ions – especially zinc(II) and cadmium(II) ions – present in the feeding phase, can improve or sometimes lower the efficiency of ion separation.

#### ACKNOWLEDGMENTS

This work was carried out in part in the framework of Statutory Research 32-126/2010-DS and 32-007/2010 –DS conducted at the Poznań University of Technology.

## REFERENCES

- AOUAD N, MIQUEL-MERCIER G., BIENVENUE E., TRONEL-PEYROZ E. (1998), Lasalocid (X537A) as a selective carrier for Cd(II) in supported liquid membranes, *J. Membr. Sci.*, 139, 167.
- dU PREEZ J.G.H., GERBER T.I.A., EDGE W., MTOTYWA V.L.V., VAN BRECHT B.J.A.M. (2001), Nitrogen reagents in metal ion separation. XI. The synthesis and extraction behavior of a new imidazole derivative, *Solvent Extr. Ion Exch.*, 19(1), 143–154.
- GAJDA, B., BOGACKI M.B. (2010), Polimetaliczne konkrecje oceaniczne jako potencjalne źródło surowców metalicznych, *Przem. Chem.*, 89(7), 824-830.
- KOZŁOWSKI C. A., WALKOWIAK W., PELLOWSKI W., KOZIOŁ J. (2002), Competitive transport of toxic metal ions by polymer inclusion membranes, *J. Radioanal. Nuclear Chem.*, 253(3), 389.
- POŚPIECH B., WALKOWIAK W. (2007), Separation of copper(II), cobalt(II) and nickel(II) from chloride solutions by polymer inclusion membranes, *Separation and Purific. Technol.*, 57, 461-465.
- RADZYMIŃSKA-LENARCIK E. (2007), The Influence of the Alkyl Chain Length on Extraction Equilibrium of Cu(II) Complexes with 1-Alkylimidazoles in Aqueous Solution/Organic Solvent Systems, *Solvent Extraction and Ion Exchange*, 25, 53–64.
- RADZYMIŃSKA-LENARCIK E. (2008), Influence of the Steric Hindrance, Ligand Hydrophobicity, and DN of solvents on Structure and Extraction of Cu(II) Complexes of 1-Alkyl-2-Ethylimidazoles, *Separation Science and Technology*, 43, 794–814.
- REDDY B. R., PRIYA, D. N., RAO, S. V., RADHIKA, P.(2005), Solvent extraction and separation of Cd(II), Ni(II) and Co(II) from chloride leach liquors of spent Ni-Cd batteries using commercial organo-phosphorus extractants, *Hydrometallurgy*, 77, 253 – 261.
- RUDNIK, E., NIKIEL M. (2007), Hydrometallurgical recovery of cadmium and nickel from spent Ni–Cd batteries, *Hydrometallurgy*, 89, 61–71.
- ULEWICZ M. WALKOWIAK W. (2005), Selective removal of transition metal ions in transport through polymer inclusion membranes with organophosphorus acids, *Environment Protection Engineering*, 31(3-4), 73-81.
- WALKOWIAK, W., BARTSCH, R. A., KOZŁOWSKI, C., GEGA, J., CHAREWICZ, W. A., AMIRI-ELIASI, B. (2000), Separation and removal of metal ionic species by polymer inclusion membranes, *J. Radioanal. Nuclear Chem.*, 246(3), 643-650.

**Gajda, B., Skrzypczak, A., Bogacki, M.B.,** *Separacja jonów kobaltu(II), niklu(II), cynku(II) i kadmu(II) z roztworów chlorkowych*, *Physicochem. Probl. Miner. Process.*, 46 (2011) 289-294, (w jęz. ang), <http://www.minproc.pwr.wroc.pl/journal>

W pracy przedstawiono wyniki badań selektywnego rozdziału jonów kobaltu(II), niklu(II), cynku(II) i kadmu(II) z roztworów chlorkowych w procesie selektywnego ich rozdziału w procesie membranowym przez polimerowe membrany inkluzyjne (PIM). Jako przenośnik zastosowano 1-decyloimidazol. Uzyskane wyniki wskazują, że obecność jonów niektórych metali pogarszać może selektywność rozdziału. Szczególnie znaczenie mają tutaj jony cynku(II) oraz kadmu(II), które prawie 5-krotnie pogarszają selektywność rozdziału jonów niklu(II) od kobaltu(II).

*słowa kluczowe: nikiel(II), kobalt(II), cynk(II), kadm(II), ekstrakcja rozpuszczalnikowa, polimerowe membrany inkluzyjne, 1-decyloimidazol*

Ayman A. EL-MIDANY \*, Suzan S. IBRAHIM \*\*

## INTERFACIAL ROLE OF COMPATIBILIZERS TO IMPROVE MECHANICAL PROPERTIES OF SILICA- POLYPROPYLENE COMPOSITES

*Received May 10, 2010; reviewed; accepted July 30, 2010*

Polymers have tremendous applications from household to high technology applications. The polymers are easy to produce, light, and flexible. However, mechanical properties of polymers, in some industries, is a point of its weakness. Therefore, a mineral, as a bulk filler, was used to overcome this limitation and to reduce the cost of polymer composites and their manufacturing. In this study, the silica flour was introduced into the polypropylene (PP) matrix to enhance its mechanical properties. In addition, the styrene-ethylene/butylene-styrene (SEBS) triblock copolymer and its grafted maleic anhydride (SEBS-g-MA) were used as silica/ PP compatibilizers. The results showed an improvement in mechanical properties after the addition of silica to the PP matrix. However, silica addition led to drop in strain measures. On the other hand, the addition of the compatibilizer enhances the interfacial bonding and smoothen the transfer of the stresses between filler particles and the polymeric matrix.

*keywords: polymers, silica, polypropylene, mechanical properties, fillers*

### 1. INTRODUCTION

Minerals represent the most important filling materials. Their advantages are twofold; firstly, as functional filler because the mineral addition is incorporated to achieve a specific performance attribute to the end-product. While in the second case the mineral represents merely a bulk filler or an extender for the costly polymer base matrix (Trivedi et al., 1994; Lee, 2000; DeArmitt, 2000; Nielsen, 1974; Lindsey et al., 1974; Haddout, 1992; Chuang et al., 1985; Leidner et al., 1974).

---

\* Mining, Petroleum, and Metallurgical Engineering Dept, Faculty of Engineering, Cairo University, Egypt

\*\* Central Metallurgical R&D Institute (CMRDI), Cairo, Egypt, [suzansibrahim@gmail.com](mailto:suzansibrahim@gmail.com)

Silica is one of the most extensively and cheapest mineral commodity used as a filler [Lofthouse 1979]. Silica application ranges from using as an extender to a functional filler. In plastics, it is used to increase abrasion, heat, corrosion and scratch resistance, to improve compressive, flexural strength, and dielectric properties. However, the compatibility of the silica flour with polymeric matrices is constrained by its siliceous surface properties and its high degree of hydrophilicity (Bryk, 1991; Scherbakoff, 1993; Payne, 1985; Zhang et al., 1993; Shang et al., 1994; Leempoel, 1997; Sahnoune et al., 1997; Kauly et al., 1997; Lyman, 1991; Krysztalkiewicz et al., 1992; Malewski et al., 2010).

Different compatibilizers were used to improve the adhesion between the filler and the matrix and accordingly enhance the mechanical properties of the end-product (Kolarik et al., 1990; Osch et al., 1994). Styrene-Ethylene/Butylene-Styrene (SEBS) and its grafted maleic anhydride (SEBS-g-MA) have already been used as efficient interfacial agents in PE/PS blends (Karrad et al., 1997; Sahnoune et al., 1997).

In this paper, the addition of silica flour to the PP matrix with and without SEBS and SEBS-g-MA compatibilizers was investigated in terms of the mechanical properties of silica/PP composites. Furthermore, the compatibilizing mechanism was proposed.

## 2. EXPERIMENTAL

### 2.1. MATERIALS

A representative white silica sand sample was used. Polypropylene (KM 6100, abbreviated PP) of density  $0.91\text{g/cm}^3$  as the base matrix was used in this study. Two thermoplastic elastomers (TPE) were used. The first was triblock copolymer [poly(styrene)-poly(ethylene, butylene)-poly(styrene)], (SEBS). The second was its corresponding grafted 2 wt. % maleic anhydride (SEBS-g-MA). Both the two triblock copolymers were of density  $0.90\text{g/cm}^3$ .

### 2.2. METHODS

#### 2.2.1. PREPARATION AND CHARACTERIZATION OF SILICA FLOUR

The original sample was chemically analysed. The sample was subjected to dry beneficiation process. At first, sieving was carried out to reject both +0.6mm and -0.1mm fractions which contain the free particles of heavy oxides and most of the soft clayey material, respectively. The -0.6 + 0.1mm sand sample was directed to dry high intensity magnetic separation using "Magnaroll" magnetic separator to remove magnetic impurities. The cleaned sample was ground in a porcelain Fritsch ball mill to produce silica flour. The sand sample was also characterized by microscopic examination under visible as well as polarized light.

## 2.2.2. BLENDING AND COMPOUNDING

Different batches of compositions were prepared. Polypropylene alone (as the base matrix), polypropylene with 3% by volume silica flour, and batches with surface compatibilizers (SEBS and SEBS-g-MA) addition to silica/PP blend in two dosages: 2.5% and 5% by volume. Each batch was thoroughly mixed for 15 min in a plastic tumbling mixer and dried at 110°C for 2 hr. The blends were subjected to compounding using a Collin twin screw extruder at 200°C. The materials were fed by a horizontal metering screw hopper with 2 kg/hr feeding rate. A Collin granulator was connected to cut the compounded film samples into short specimens of 1 cm in length.

## 2.2.3. PREPARATION OF SPECIMEN FOR MECHANICAL TESTING

Milacron K-TEC 40 injection moulder was used for preparation of 60 mm x 10 mm x 4 mm rectangular bars for mechanical testing. Meanwhile, 10 mm x 6 mm x 2 mm rectangular bars were moulded for Izod impact strength measures. At least six readings were taken for each test and the average measure was reported. Tests were performed at ambient temperature (25°C) and humidity.

# 3. RESULTS AND DISCUSSION

## 3.1. SILICA FLOUR PREPARATION AND CHARACTERIZATION

Microscopic examination of the white sand sample showed the presence of ferroginated reddish-brown inclusions above 0.6 mm, where traces of color particulates of Fe<sub>2</sub>O<sub>3</sub>, Cr<sub>2</sub>O<sub>3</sub>, and TiO<sub>2</sub>, below 0.1 mm. Rejection of both +0.6mm and -0.1mm fractions removed most of these undesirables. Dry high intensity magnetic separator was used to reject iron oxides in -0.6+0.1 mm. Chemical analysis of sand sample before and after cleaning was given in Table 1. It showed the high grade of prepared sample. D<sub>98</sub> and D<sub>50</sub>, μm of the ground sample as well as its main physical measures were depicted also in Table 1.

## 3.2. MECHANICAL PROPERTIES

### 3.2.1. EFFECT OF FILLER ADDITION

Figure 1 shows the mechanical properties of the silica/PP blend after adding 3% silica to PP matrix. It is obvious that the silica filler improves the yield and impact strengths, and negatively affects the tensile strength. In case of tensile stress the elongation of PP without silica is higher than in the presence of silica. This behaviour can be attributed to the rigidity of the silica particle because of its higher resistance to plastic deformation (Järvelä et al., 2001).

Table 1. Chemical and physical characterization of Ground Silica Sample

Chemical analysis		Physical properties	
Oxide	Wt. %	Property	Measure
SiO <sub>2</sub>	99.85	Refractive Index	1.55
MgO	-	Specific Gravity	2.65
Al <sub>2</sub> O <sub>3</sub>	0.020	Hardness	7.0
CaO	0.026	Oil Absorption, %	35
Fe <sub>2</sub> O <sub>3</sub>	0.016	Surface Area, m <sup>2</sup> /g	4.75
Na <sub>2</sub> O	-	Dry Brightness, %	88
TiO <sub>2</sub>	0.017	<i>D</i> <sub>98</sub> <i>D</i> <sub>50</sub> , μm	20 10

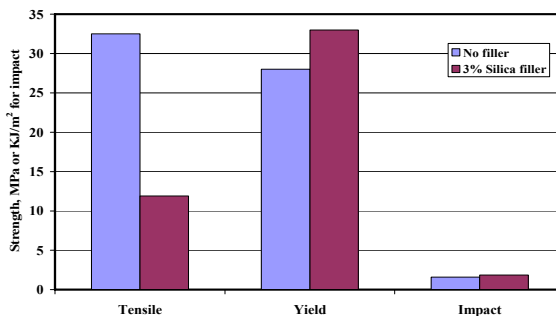


Fig. 1. Effect of the silica addition on the blend strength

### 3.2.2. TENSILE STRENGTH

SEBS, (styrene-ethylene-butylene-styrene) triblock copolymer, is mainly a nonpolar polymer and is extensively used as a compatibilizer (Legge et al., 1987). It is not compatible with a polar substance unless it has been modified. The well-known modification is grafting with MA.

Figure 2 shows the effect of compatibilizer on tensile strength of silica/PP composite. It was noticed that the addition of styrene-ethylene/butylene-styrene block and its grafted maleic anhydride as silica/PP surface compatibilizers was positively affects the tensile strength of the blend as shown in Figure 2.

One the other hand, increasing the SEBS-g-MA concentration from 2.5% to 5%

increases the number of MA groups responsible for the bonding with hydroxyl groups on the Silica surfaces and consequently increase the blend strength.

The abovementioned results indicated that both compatibilizers SEBS and SEBS-g-MA enhanced the interfacial compatibility of silica-PP composites. The higher tensile strengths are attributed to the formation of an interfacial adhesion layer in presence of compatibilizers. This layer facilitates the stress transfer between the matrix and the filler interface (Nielsen 1966; Pukanszky, 1990). The presence of suitable layer thickness with a good interfacial adhesion provide many advantages such as a filler wetting, enhance the contact between the filler and matrix at their interface, bear and transfer of the applied load from/to polymeric matrix during deformation under applied stresses (Dekkers 1985).

This finding agrees with what is reported in the literature (Du et al., 2002). However, it is worth to mention that the improvement was observed up to 5% after which a decrease in tensile strength was observed due to the lower tensile strength of the SEBS-g-MA.

### 3.2.3. YIELD STRENGTH

Figure 2 shows the effect of compatibilizer on yield strength of silica/PP composite. It was noticed that the silica/PP composite showed the highest yield strength. While the addition of both surface compatibilizers to the silica/PP system was inversely affected the yield strength (Fig. 2). The higher the concentration of the compatibilizer is the lower the yield strength. The higher yield strength at lower concentration of SEBS and SEBS-g-MA may be explained by the molecules flexibility, their freedom, and higher probability of taking a proper orientation in the force field. While the reduction in the yield strength at compatibilizers higher concentrations can be attributed to the molecules coiling and lose its effect at the interfacial region. Furthermore, it may render the interfacial region stiffer (less flexible), therefore, lower in the yield strength.

The same trend of both grafted and ungrafted SEBS indicates the absence of sufficient number of polar sites on the silica surface that can participate in the adhesion layer between silica and SEBS-g-MA.

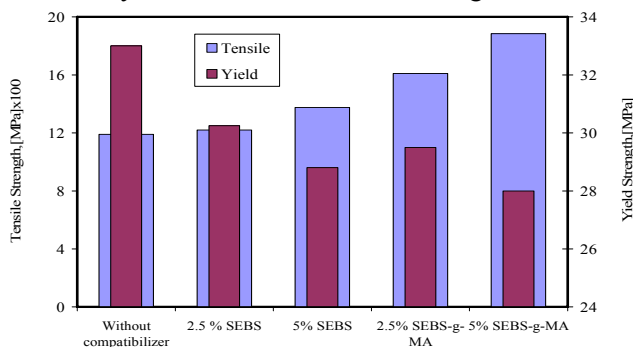


Fig. 2. Effect of the compatibilizer type and amount on the tensile and yield strengths of silica / PP composite

## 3.2.4. IZOD IMPACT STRENGTH

Figure 3 depicts the effect of compatibilizer on Izod impact strength of silica/PP composite. It was noticed that the addition of either compatibilizers improves the impact strength. A gradual increase in impact strength from  $1.85 \text{ kJ/m}^2$  without compatibilizer to  $2.7 \text{ kJ/m}^2$  in case of adding a compatibilizer (5% SEBS-g-MA).

The impact strength can be enhanced either by good adhesion between the filler and the matrix or the formation of the elastic interlayer between the filler and the matrix or both reasons together. In our case, the encapsulation of silica inside the SEBS enhances the impact strength due to the good adherence of the silica to the matrix, elasticity of the interfacial layer which leads to minimization of cracks initiation. On the other hand, the good adhesion between silica and PP can prevent coiling of the compatibilizer molecules and the formation of agglomerates.

The superior performance of SEBS-g-MA impact modifiers may be attributed to the interaction of the polar groups in the grafted MA with the silica surface resulting in better interfacial adhesion and substantially formation of small dispersed particles. It was recorded that the inclusion of small well-dispersed particles has a very positive influence on the impact strength of PP matrices (Valji, 1999; Hawley, 2000; Fellahi et al., 1993; Gaskell, 1997).

## 3.2.5. STRAIN

The effect of type and amount of compatibilizer on strain of silica/PP blends was shown in Fig. 3. It was noticed that both compatibilizers positively affected the strain. Yet some studies followed the influence of processing behavior of the mineral/polymer inside the extruder on the strain. This was carried out by controlling sample stretching during the process (Fourty, 1997). It was concluded that the increase in the orientation of the blend during melting i.e. the extrusion stage, could improve the strain. Moreover it was supposed that a better mineral filler orientation in injection molded parts could improve not only the strain, but also its impact strength (Fourty, 1997).

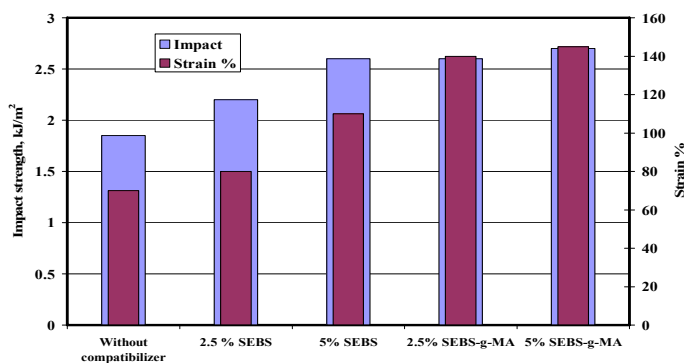


Fig. 3. Effect of the compatibilizer type and amount on the izod impact strength and strain of silica / PP composite

Also, it is obvious from the strain results (Fig. 3) that the formation of adhesive layer and the elasticity of the interface layer leads to the elongation of the composite in percentages higher than the original matrix alone. In case of the ungrafted SEBS the encapsulation of silica within coiled SEBS molecules is the reason behind the formation of a layer with a reasonable elasticity. In case of SEBS-g-MA, the superior performance was referred to the formation of adhesive layer in addition to presence of MA polar groups which enhance the elasticity.

### 3.3. SUGGESTED COMPATIBILIZATION MECHANISMS

Addition of filler particles, as rigid particles, into polymeric matrix represents spots of stress concentration and induces local micromechanical deformation processes. From one hand, presence of filler particles is advantageous for increasing plastic deformation and impact resistance, but on the other hand, deterioration in the properties of the composite may be occurred. Stress distribution around the filler particle can be modified by encapsulating the filler particles by a compatibilizer layer especially when functionalized compatibilizer was used.

The simultaneous introduction of both filler and compatibilizer is beneficial. It was reported that the PP has a poor impact strength at low temperatures, which is frequently improved by the introduction of elastomers (Karger-Kocsis et al., 1984, Trivedi, N. C., Hagemeyer, R.W., 1994, and Valji, S.E., 1999). However, it may affect other mechanical properties such as elastic modulus, which cannot be accepted in certain applications. Therefore, filler is added to compensate this effect.

Figure 4 represents a schematic representation of the mode of filler and compatibilizer distribution in the matrix in case of the SEBS and SEBS-g-MA which reflects the change in the composite behaviour to applied stresses.

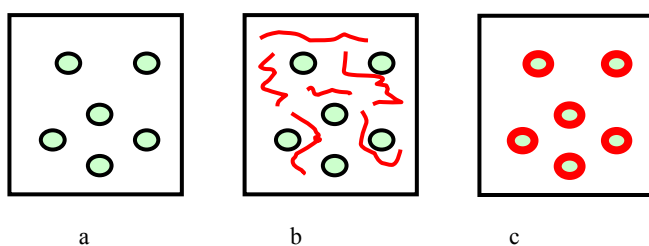


Fig.4. Schematic distribution of the compatibilizer around the filler particles, (a) no compatibilizer, (b) unmodified compatibilizer, and (c) modified compatibilizer

Since SEBS-g-MA has a polar nature and PP is non-polar, the adhesive interaction of the SEBS-g-MA with both filler particles and the polymeric matrix may be described by three mechanisms: (1) the inter-diffusion and entanglement of the poly(ethylene-butylene) segments within the polypropylene matrix that may lead to a good physical anchoring of ungrafted SEBS and the SEBS-g-MA into the PP matrix. (2) presence of ionic interaction between the SEBS-g-MA and the filler surface. First reason may explain a good performance of ungrafted SEBS while both reasons may



3. The effect of surface modifiers e.g. SEBS and SEBS-g-MA was studied at two different additions (e.g. 2.5 and 5%). The results showed that the structure of the surface modifier plays a significant role in forming an adhesion layer between the filler particles and the polymeric matrix. It was found that the SEBS-g-MA performs better due to the presence of MA functional groups that can bond the modifier molecule to the silica surface and at the same time the rest of the molecule as a hydrocarbon chain can bond the modifier molecule to the polymeric matrix. This bonding behaviour helps in the stress transfer between the filler and matrix and consequently the improvement in the mechanical properties.
4. Finally, the working mechanism of the compatibilizer was suggested according to the effect of the compatibilizer on the mechanical properties of the final blend as well as the structure of compatibilizer and filler particles surface.

#### ACKNOWLEDGMENTS

The authors would like to express their great gratitude to Prof. Friedrich, Dr. Nitz and all the assistance staff of Freiburger Materialforschungszentrum, der Albert-Ludwigs-Universität, Germany for supporting this work through the DFG programm.

#### REFERENCES

- Bryk, M. T., 1991, Degradation of Filled Polymers Ellis Horwood, London.
- Chuang, H., and Han, C. D., 1985, Mechanical properties of blends of nylon 6 with a chemically modified polyolefin, *Journal of Applied Polymer Science* 30, 165–177.
- DeArmitt, C., 2000, Filled-PP Possibilities and Optimization, International Conference of Alternative White Pigments and TiO<sub>2</sub> Extenders for Coatings, Paper and Plastics, Orlando, USA.
- Dekkers, M.J.E., Heikens, D., 1985, *Journal of Applied Polymer Science* v 30, n 6, p 2389-2400. Tensile behavior of polycarbonate and polycarbonate-glass bead composites.
- Du L L, Jin Y, Zheng T L, 2002, Advance in application of SEBS in blends of PP. *China Synthetic Resin Plast*, 19(5): 60–64 (in Chinese)
- Fellahi, S.; Boukobbal, F., 1993, Study of the Effect of Fumed Silica on Rigid PVC Properties, *Journal of Vinyl Technology*, USA, Vol. 15, No. 1, pp. 17-21.
- Fourty, G., 1997, Talc in Polypropylene, International Conference of Filled Polymers and Fillers, Manchester, UK.
- Gaskell, P., 1997, Mineral Fillers for Polypropylene, International Conference of Filled Polymers and Fillers, 8-11 Sept. Manchester, UK, 281-284.
- Haddout, A., 1992 Etude thermomécanique de l'écoulement de composites-alliages thermoplastiques dans des géométrie déterminées, Doctoral Thesis, Conservatory of Arts and Crafts.
- Hawley, G.C., 2000, Opacifiers in Paint & Plastics - an Overview, International Conference of Alternative White Pigments and TiO<sub>2</sub> Extenders for Coatings, Paper and Plastics, Orlando, USA.
- Järvelä, P. A. Enqvist, J. Järvelä P. and O.Tervala, 2001, Mechanical strength and thermal stability of magnesium silicate filled polypropylenes, *Composite Interfaces*, Vol. 8, No. 3,4, 189–206.
- Karger-Kocsis J, Kalló A, Kuleznev VN, 1984, phase structure of impact-modified polypropylene blends, *Polymer* 25, 279-286

- Karrad, S., Lopez-Cuesta J.M., Crespy, A., 1997, *Plast. Rub. Comp. Proc. Appl.* 26, 193. Compatibilizing ability of styrene hydrogenated styrene/butadiene triblock copolymer in high density polyethylene-polystyrene blends, v 26, n 5, p 193-198
- Kauly, T.; Karen, B.; Siegmann, A., Narkis, M., 1997, Highly Filled Particulate Thermoplastic Composites, *Journal of Material Science*, vol. 32 (3).
- Kolarik, J., Lednicky, F., Jancar J., Pukansky, B., 1990, *Polym. Commun.* 31, 201. Phase structure of ternary composites consisting of polypropylene/elastomer/filler. Effect of functionalized components. Kolarik, Jan (Czechoslovak Acad of Sciences, Czech Republic); Lednicky, Frantisek; Jancar, Josef; Pukanszky, Bela Source: *Polymer communications Guildford*, v 31, n 5, p 201-204, May 1990
- Krysztafkiewicz, A., Maik, M., Rager, B., 1992, Comparison of Waste Silica Fillers Modified With Various Proadhesive Compounds, *Journal of Material Science*, UK, Vol. 27, No. 13, pp. 3581-3588.
- Lee, S., 2000, Thermal, Mechanical and Morphological Characterization of Highly Filled Polyethylene Film, *Int. Conference of Alternative White Pigments and TiO<sub>2</sub> Extenders for Coatings, Paper and Plastics*, Orlando, USA.
- Leempoel, P., 1997, Filler/Polymer Interface and Performance of Silicon Elastomers, Filled Polymers and Fillers Conference, Manchester, UK.
- Legge, N.R. Holden, G., Schroeder H.E. (eds.), 1987, *Thermoplastic Elastomers: A Comprehensive Review* (Oxford University Press, New York.
- Leidner, J., and R. T. Woodhams, 1974, Strength of polymeric composites containing spherical fillers, *Journal of Applied Polymer Science*, v 18, n 6, p 1639-1654, June 1974.
- Lindsey, C. R., Paul, D. R. Barlow, W., 1981, Mechanical properties of HDPE-PS-SEBS blends, *Journal of Applied Polymer Science* 26, 1-8.
- Lofthouse, C.H., 1997, Production of Mineral Fillers, *International Conference of Filled Polymers and Fillers "Eurofillers 97"* Manchester, UK.
- Lyman, MJ, 1991, Silica Improves Thermoset Properties, *Plastic Compounding*, USA, Vol. 14, No. 7, pp. 61-63.
- Malewski, W., Jesionowski, T., Ciesielczyk, F., Krysztafkiewicz, A., Dispersion characterisation of colloidal silica at subsequent stages of silica sol preparation, *FPM*, 44(2010), 143-150.
- Nelsen, L. E., 1974, *Mechanical Properties of Polymer and Composites*, Chapter One, Marcel Dekker, New York, 1974.
- Nielsen, L. E., 1966,. Simple theory of stress-strain properties of filled polymers *J. Appl. Polym. Sci.* vol. 10(1), 97-103.
- Payne, H. F., 1985, *Organic Coating Technology*, John Willey and Sons Publications, New York.
- Pukanszky B, 1990, *Composites* 21, 255. Influence of interface interaction on the ultimate tensile properties of polymer composites *Composites*, v 21, n 3, p 255-262, 1990
- Rösch J.R , Barghoorn P, Ulhaupt, R.M., Mülhaupt R, 1994, The role of compatibilizers and elastomeric interlayers in glass-bead-reinforced poly(propylene) *Macromolecular Rapid Communications*, 15 (9), 691-696.
- Sahnoune, F. Karrad, S. Lopez-Cuesta, J.M., Crespy, A., 1997, *Proceedings of International Conference Eurofillers'97*, Manchester, September.
- Sahnoune, F., Karrad, S., Lopez-Cuesta, J.M., Crespy, A., 1997, Effect of Fillers and Interfacial Agents on the Mechanical and Morphological Properties of HDPE/PS Blends, *International Conference of Filled Polymers and Fillers*, Manchester, UK.
- Scherbakoff, N., 1993, Rheological, Interfacial and Morphological Changes Produced By Fillers in Immiscible blends, *Diss. Abstr. Int.*, Vol. 54, No. 4, pp.257.
- Shang, S. W., Williams, J. W., Soderholm, K-J. M., 1994, How the Work of Adhesion Affects the Mechanical Properties of Silica-Filled Polymer Composites, *Journal of Material Science*, UK, Vol. 29, No. 9, pp. 2406-2416.
- Tjng, S.C., Xu, S., Mai, Y., 2003, Tensile deformation mechanism of polyamide 6,6/SEBS-g-MA blend

- and its hybrid composites reinforced with short glass fibers, *Journal of Materials Science* 38, 207–215
- Trivedi, N. C., Hagemeyer, R.W., 1994, *Fillers and Coatings*, Industrial Minerals and Rocks, 6 th Edition, Senior Editor Donald D. Carr.
- Valji, S.E., 1999, *Processing Technology*, Increasing Profits in Industrial Minerals, *Industrial Mineral Journal*.
- Yang, R.T., 2003, *Adsorbents: fundamentals and applications*, John Wiley & Sons, Inc. Hoboken, New Jersey.
- Zhang, Y., Cameron, J., 1993, *Silica Particle/Glass Fibre-Reinforced Polyester Resin*, *Journal of Composite Materials*, USA, Vol. 27, No. 11, pp. 1114-1127.

**El-Midany, A.A., Ibrahim, S.S.,** *Międzyfazowa rola substancji stabilizującej stosowanej dla poprawy właściwości mechanicznych kompozytów krzemionka-polipropylen*, *Physicochem. Probl. Miner. Process.*, 46 (2011) 295-305, (w jęz. ang), <http://www.minproc.pwr.wroc.pl/journal>

Polimery znajdują szerokie zastosowanie od przedmiotów użytku domowego do aplikacji technologicznych. Polimery są łatwe w produkcji, lekkie i elastyczne. Jednakże, mechaniczne właściwości polimerów są niewystarczające w pewnych przemysłowych zastosowaniach. Dla tego, sproszkowane materiały są wprowadzane jako wypełnienie. Pozwala to na pokonanie wspomnianych ograniczeń i zredukowania kosztów wytwarzania rzeczy z plastiku. W przedstawionych badaniach, mączka kwarcowa była dodawana do propylenu dla podwyższenia jego mechanicznej wytrzymałości. Dodatkowo, trój-blokowy polimer (styren-etylen/butylen-styren i anhydryt maleinowy (SEBS-g-MA) były użyte jako odczynniki łączące krzemionkę z PP.

Otrzymane wyniki wskazują na poprawę właściwości mechanicznych po dodaniu krzemionki do matrycy polimerowej (PP). Jednakże, nadmierne dodanie krzemionki prowadzi do zmniejszenia naprężenia. Odwrotne działanie mają odczynniki łączące. Powodują one intensyfikację wiązań ich zwiększenie oraz niweluje naprężenia między cząstkami wypełniacza a matrycą polimerową.

*słowa kluczowe: polimery, krzemionka, polipropylen, właściwości mechaniczne, wypełniacze*



## **Dr. Eng. Zofia Blaschke**

**A tribute on her 70<sup>th</sup> birthday**



In October 2010 Dr Eng. Zofia Blaschke will celebrate her 70th birthday. Between 1990-2004 she was a member of the Editorial Board of the Physicochemical Problems of Mineral Processing annual. The Editorial Board would like to introduce Zofia Blaschke to our younger colleagues on the occasion of her birthday.

Zofia Blaschke was born on 22 October 1940 in Lipnica, near Kolbuszowa. She attended primary school in Lipnica and secondary school in Kolbuszowa. She then attained the highest results in the entrance exam to the Mining Faculty of the University of Mining and Metallurgy in Krakow to study mineral processing (1958 – 1963). In September 1963 she was awarded the title of Master of Science and Engineer, after successfully defending her Master's Thesis entitled "The determination of the most economic method of the mechanical processing of run-of-mine coal from the Murcki mine".

After graduating, she began an annual apprenticeship as an assistant at the department of Silicate Chemistry at the Faculty of Ceramics and later started working at the Main Research Laboratory of the Jaworzno-Mikołów Coal Industry Union at the Wesola Coal Mine, where she focussed on the study of coal quality, desulphurisation

and beneficiation.

In 1968 a doctoral study on mineral processing was established at the Mining Faculty. Zofia Blaschke was seconded to this study while still working for the Main Research Laboratory. In 1972 she defended her doctoral thesis entitled "Water and slurry management in processing pyrite-bearing coal waste". On the basis of an agreement between the AGH University and the Wesola Coal Mine, in 1972 she was officially transferred to work at the AGH Chair of Mineral Processing.

Dr Eng. Zofia Blaschke specializes in water and slurry management in coal preparation plants, in coal beneficiation and desulphurisation technologies, in selective flocculation and in oil agglomeration. She has published more than 110 papers in these fields and has written two textbooks for university students. As a co-author, Zofia Blaschke wrote 26 chapters on "mechanical preparation" for 14 textbooks of the Surowce mineralne swiata (The World's Mineral Raw Materials) series. She advises on newly designed coal preparation plants and the modernisation of existing ones and conducts research work needed for designing technologies of coal beneficiation and water and wastewater treatment.

Dr Blaschke has presented the results of her work at national and international conferences and congresses (Sydney, New Delhi, Tokyo, Halifax, Ankara, Seoul, Aachen, Acapulco, Kosice, Las Vegas, Lisbon). She was also a contributor to the IVth International Conference of Women Engineers and Scientists in 1975. In addition, she translated from Bulgarian a book entitled "Selective Flocculation" for the Śląsk Publishers (1987). Dr Blaschke is also the author of three patents.

Between 1979-1992 Zofia Blaschke was the head of the Division of Special Methods of Beneficiation and the Preparation of Mineral Raw Materials at the AGH University. From 1982 to 1986 she was also a deputy director, and from 1996 to 1999 the director of this Institute (which at that time was named the Division of Mineral Processing, Environmental Protection and Waste Utilisation). Currently she is a retired faculty member of the AGH University of Science and Technology.

Dr Blaschke is an active member of numerous organisations. Since 1966 she has been a member of the Association of Mining Engineers and Technicians and from 1979 to 1996 was the chairperson of the Mineral Preparation Commission in the Krakow Division Management Board. From 1996 to 2000 she was a member of the Commission for the analysis of Raw Materials and Mineral Products at the Analytical Chemistry Committee at the Polish Academy of Sciences. From 1991 to 2006 she was a member of the Section of the Committee for the Use of Mineral Raw Materials at the Mining of the Polish Academy of Sciences. In 1994, she became a member of the Standardization Commission for Mechanical Coal Preparation and remained so for many years. She is also a member of the AGH Alumni Association.

Since 1995 Zofia Blaschke has been working for the Polish Association of Mineral Processing and is one of its founder members. In 2001-2007 she was Vice President of the Association and in 2004 the President (annual tenure) The Journal of the Polish

Mineral Engineering Society is published bi-annually and has an international readership. Dr Blaschke has been its Editor in Chief since its establishment in 2000.

Between 1979-1994 she edited proceedings of the Krakow Mineral Processing Conferences, which in 1995 were transformed into International Mineral Processing Conferences and Dr Zofia Blaschke continued to be a member of their organizing committees for many years afterwards.

In 1994 the XIII International Coal Preparation Congress was held in Krakow. Nominated by the Minister of Industry, Dr Z. Blaschke was a member of the Congress Programme Committee and chaired the Flocculation and Agglomeration section.

For her scientific activity, Dr Blaschke received awards from Ministers of Higher Education, Science and Education in 1980, 1982, 1986 and 1990 and also 18 awards from the Rector of AGH (the University of Mining and Metallurgy). She received numerous state, regional and associations' distinctions, such as the Cross of Merit (bronze in 1981 and gold in 1990), a Medal commemorating the 40th anniversary of the People's Republic of Poland in 1984, the Badge of Merit for services for to the Mining Industry (bronze in 1986, silver in 1994, gold in 1997), the badge of merit for services to the Krakow Province in (gold in 1982) and for community work for the City of Krakow (gold 1987); Distinguished Activist of the Association of Mining Engineers and Technicians in 1980, Honorary Badge of the Polish Federation of Engineering Associations (silver in 1984, gold in 1992).

Dr Blaschke is still involved in scientific work. After preparing for print "A Small Encyclopaedia of Mineral Engineering" (published in Mineral Engineering in 2006), she is currently preparing "The Encyclopaedia of Mineral Processing Technology". Her hobby is gardening and house plants. She has two children, Zbigniew and Ewa, and five grandchildren, Dorotka, Kasia, Michał, Basia and Ola.

#### LIST OF PUBLICATION

- Blaschke Z.: Przegląd metod odsiarczania węgla. Inf. Techn. Ekon. JMZPW 1965, nr 1.
- Blaschke Z., Blaschke W.: Graficzna metoda określania wielkości odjemników przy przeliczaniu ciepła spalania na wartość opałową. Inf. Techn. Ekon. JMXPW Mysłowice 1966. z. 2, s.31-37.
- Blaschke Z., Blaschke W.: Niektóre ekonomiczne zagadnienia wzbogacania węgla dla potrzeb energetyki. VII Krakowska Konferencja Przeróbki Mechanicznej Kopalni. Inf. Techn. Ekon. JMZPW Mysłowice 1968. z. 5, s.112-127.
- Blaschke Z., Długosz W., Ociepa Z., Stachurski J.: Flotacyjne wzbogacanie odpadów węglowych. Materiały XXI Sesji Naukowej AGH, t. I. Kraków 1971.s.II-1 – II-8.
- Pilch W., Blaschke Z.: Wzbogacanie elektrostatyczne i termomagnetyczne pirytonośnych odpadów węgla energetycznego. Materiały XXI Sesji Naukowej AGH, t. I. Kraków 1971, s. XXVII-1 – XXVII-24.
- Blaschke Z., Blaschke W., Wzbogalniki strumieniowo-wachlarzowe. Rudy Żelaza 1971. nr 7-8, s. 8-15.
- Blaschke Z.: Koagulacja i flokulacja zawiesin mineralnych za pomocą nieorganicznych elektrolitów. Zeszyty Naukowe AGH nr 38. Górnictwo z. 39. Kraków 1972. s. 83-91.
- Blaschke Z.: Badania własności flokulacyjnych wysokocząsteczkowych politenków etylenu. Zeszyty Naukowe AGH nr 38. Górnictwo z. 39. Kraków 1972, s. 93-103.

- Blaschke Z.: Wpływ odczynników flokulacyjnych na proces flotacji węgla. Materiały VIII Krak. Konf. Nauk. Techn. Przer. Mech. Kopaln nt. Flokulacja i jej zastosowanie w obiegach wodno-mułowych. Kraków 1972, s. 89-100.
- Blaschke Z.: Warunki selektywnej flokulacji mułów węglowych. Materiały VIII Krak. Konf. Nauk. Techn. Przer. Mech. Kopaln nt. Flokulacja i jej zastosowanie w obiegach wodno-mułowych. Kraków 1972, s. 101-116.
- Blaschke Z., Blaschke W.: Wstępne badania nad sedimentacją brunkitu z kopalni Olkusz. Materiały VIII Krakowskiej Konferencji Przeróbki Mechanicznej Kopaln. Wyd. AGH. Kraków 1972, s. 179-193.
- Pilch W., Blaschke Z.: Zastosowanie separacji magnetycznej do wydzielenia pirytu z węgla. Przegląd Górniczy 1972, nr 4, s. 149-152.
- Blaschke Z.: Możliwości wykorzystania zawartych w wodzie jonów metali do flokulacji zawiesin ilastych w projektowanym zakładzie przeróbki pirytosytnych odpadów węgla energetycznego. Materiały IX Krak. Konf. Nauk. Techn. Przer. Mech. Kopaln. nt. Stan i perspektywy projektowania zakładów przeróbki kopaln. Kraków. 1973, s. 137-143.
- Pilch W., Blaschke Z.: Odsiarczanie węgla metodą separacji magnetycznej po uprzednim termicznym przygotowaniu nadawy. Sesja Naukowa nt. Odsiarczanie węgla i spalin, z. 1. s. 101-110, COBPWiUK Separator. Katowice 1973.
- Blaschke Z., Sztaba K.: Możliwości zastosowania odczynników flokulacyjnych w obiegu wodno-mułowym zakładu przeróbki kaolinu. Zeszyty Naukowe AGH nr 462. Górnictwo z. 63. Kraków 1974, s. 45-51.
- Blaschke Z., Sanak S.: Wydzielanie frakcji ilastej z mułu węglowego metodą flokulacji selektywnej. Zesz. Nauk. AGH nr 473. Górnictwo z. 66. Kraków 1975, s. 19-30.
- Blaschke Z.: Flocculation of Suspension in Processing-bearing waste of Power Coal. IV Int. Conf. od Women Engineers and Scientistits. Section 6. Raw materials and power engineering. 1975, s. 640-648.
- Blaschke Z.: Wpływ ilości i rodzaju odczynnika flokulującego na prędkość sedimentacji zawiesiny w strefie kompresji. Zeszyty Naukowe AGH nr 523. Górnictwo z. 77. Kraków 1975. s. 37-44.
- Blaschke W., Blaschke Z.: Beryl. Przeróbka mechaniczna. s. 200-205. W: Surowce Mineralne Świata. Tom Al-Be-Li-Mg. Pod red. A. Bolewskiego. Wydawnictwo Geologiczne. Warszawa. 1976.
- Blaschke W., Blaschke Z.: Lit. Przeróbka mechaniczna. s. 252-261. W: Surowce Mineralne Świata. Tom Al-Be-Li-Mg. Pod red. A. Bolewskiego. Wydawnictwo Geologiczne. Warszawa. 1976.
- Blaschke Z.: Możliwości utylizacji surowców ilastych otrzymanych w procesie przeróbki pirytosytnych odpadów węgla energetycznego. Zesz. Nauk. AGH. Górnictwo z. 82. Kraków 1976, s. 21-34.
- Blaschke Z.: Benefication of Coal Fines by Selective Flocculation. VII Int. Coal Preparation Congress, Paper F2, t.2. Sydney 1976, s. 1-16.
- Długosz W., Blaschke Z., Ociepa Z.: Flotacja pirytu z odpadów węglowych w zależności od udziału skały płonnej. Zesz. Nauk. AGH nr 551. Górnictwo z. 83, s. 73-82. Kraków 1977.
- Blaschke Z.: Wzbogacanie szlamów węglowych metodą flokulacji selektywnej. Zesz. Nauk. AGH nr 551. Górnictwo z. 83, s. 109-118. Kraków 1977.
- Marciniak J., Blaschke Z.: Wpływ dodatku odczynników flokulacyjnych na wydajność filtracji ciśnieniowej. Zeszyty Naukowe AGH nr 551. Górnictwo z. 83. Kraków 1977, s. 119-128.
- Blaschke W., Blaschke Z.: Cyna. Przeróbka mechaniczna. s. 102-117. Surowce Mineralne Świata. Tom Sn. Pod red. A. Bolewskiego. Wydawnictwo Geologiczne. Warszawa. 1977.
- Blaschke W., Blaschke Z., Mączka W.: Miedź. Przeróbka mechaniczna. s. 176-206. Surowce Mineralne Świata. Tom Cu. Pod red. A. Bolewskiego. Wydawnictwo Geologiczne. Warszawa. 1977.
- Blaschke Z.: Odwadnianie produktów wzbogacania i utylizacji odpadów przeróbki surowców mineralnych. Skrypt AGH nr 590. Kraków 1977. s. 142.
- Blaschke Z.: Systematyka odczynników flokulacyjnych. Zeszyty Naukowe AGH nr 589. Górnictwo z. 90. Kraków 1978. s. 33-54.
- Blaschke W., Blaschke Z.: Cynk – ołów. Przeróbka mechaniczna. s. 258-274. Surowce Mineralne Świata. Tom Zn-Pb. Pod red. A. Bolewskiego. Wydawnictwo Geologiczne. Warszawa. 1978.
- Blaschke Z.: Optymalne warunki flokulacji olejowej mułów węglowych z KWK „Jaworzno”. Materiały XII. Krak. Konf. nt. Przeróbka kopaln. Kraków 1978. s. 163-167.
- Blaschke W., Blaschke Z., Siwiec A.: Żelazo. Przeróbka mechaniczna. s. 306-322. Surowce Mineralne Świata. Tom

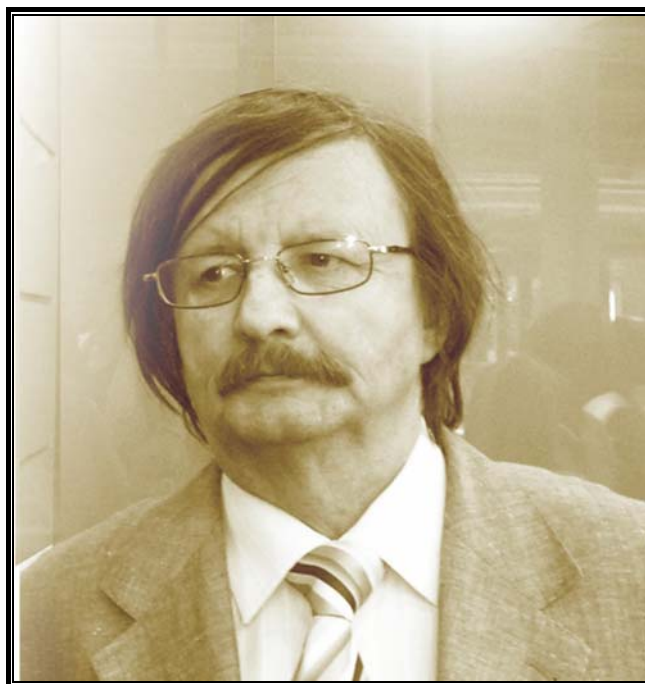
- Fe. Pod red. A. Bolewskiego. Wydawnictwo Geologiczne. Warszawa. 1978.
- Blaschke Z.: Flokulacja selektywna szlamów węglowych. Materiały XXIII Sesji Nauk. AGH. XLIII Zjazd naukowy Wychowanków Uczelni. Kraków 1978, s. 265-272.
- Blaschke W., Blaschke Z.: Bar. Przeróbka mechaniczna. s. 84-88. Surowce Mineralne Świata. Tom Ba – B – F – Sr. Pod red. A. Bolewskiego. Wydawnictwo Geologiczne. Warszawa. 1978.
- Blaschke W., Blaschke Z.: Bor. Przeróbka mechaniczna. s. 181-183. Surowce Mineralne Świata. Tom Ba – B – F – Sr. Pod red. A. Bolewskiego. Wydawnictwo Geologiczne. Warszawa. 1978.
- Blaschke W., Blaschke Z.: Przeróbka mechaniczna kopaliny fluorytowych. s. 284-290. Surowce Mineralne Świata. Tom Ba – B – F – Sr. Pod red. A. Bolewskiego. Wydawnictwo Geologiczne. Warszawa. 1978.
- Blaschke W., Blaschke Z.: Niektóre problemy przeróbki mechanicznej węgla brunatnego. Mat. I Konf. Zagadnienia surowców energetycznych w gospodarce krajowej. Kraków. 1979. s. 335-354.
- Sztaba K., Blaschke Z., Marchewczyk E., Cybulska J.: Wpływ wybranych mikroorganizmów na zmiany prędkości sedimentacji odpadów flotacyjnych rud Zn-Pb. XII Krakowska Konferencja Przeróbki Kopaliny. Kraków 1979. s. 973-979.
- Blaschke Z.: Możliwości oraz aktualny stan prac badawczo-wdrożeniowych nad wzbogacaniem najdrobniejszych ziarn węgla kamiennego metodami flokulacji. Sympozjum PAN. Komitet Górniczo-Hutniczy, Sekcja Wykorzystania Kopaliny. Katowice 1980, s. 171-180.
- Blaschke W., Blaschke Z.: Torf. Przeróbka mechaniczna. s. 170-173. Surowce Mineralne Świata. Tom Torf. Pod red. A. Bolewskiego. Wydawnictwo Geologiczne. Warszawa. 1980.
- Blaschke Z.: Próba oceny jakości odpadów węglowych ze względu na straty energetyczne spowodowane zawartością w nich węgla. Materiały XIV Krak. Konf. nt. Przeróbka surowców odpadowych i wtórnych w aspekcie ochrony środowiska i zasobów surowcowych. Jaszowiec 1980, s. 157-170.
- Blaschke Z.: Możliwości wykorzystania mułów węglowych w energetyce. Materiały II Konf. z cyklu Zagadnienia surowców energetycznych w gospodarce krajowej. Kraków 1981, s. 280-299.
- Blaschke Z., Brożek M., Mokrzycki E., Ociepa Z., Tumidajski T.: Górniczo-Hutniczo. Cz. V. Zarys technologii procesów przerobczych. Skrypt AGH nr 768, Kraków 1981, s. 249.
- Blaschke W., Blaschke Z.: Węgiel brunatny. Przeróbka mechaniczna. s. 119-130. Surowce Mineralne Świata. Tom Węgiel brunatny. Pod red. A. Bolewskiego. Wydawnictwo Geologiczne. Warszawa 1981.
- Blaschke Z.: Wzbogacanie mułów węgla energetycznego metodą aglomeracji olejowej. XV Krak. Konf. Przer. Kopaliny. Kraków 1981. s. 76-86.
- Blaschke Z.: Oil Agglomeration of Coal Slimes. Coal Symposium. Proc. Conf. Coal, Phoenix of the 80's, CIC Congress. Halifax, Nova Scotia 1981. Vol. 1. s. 229-234.
- Blaschke W., Blaschke Z.: Mangan. Przeróbka mechaniczna. s. 93-106. Surowce Mineralne Świata. Tom Mn - Cr. Pod red. A. Bolewskiego. Wydawnictwo Geologiczne. Warszawa 1981.
- Blaschke W., Blaschke Z.: Chrom. Przeróbka mechaniczna. s. 218-227. Surowce Mineralne Świata. Tom Mn - Cr. Pod red. A. Bolewskiego. Wydawnictwo Geologiczne. Warszawa 1981.
- Blaschke Z.: The Method of Determining the Optimum of Power Coal Dressing with a View to the Amount of Energy Obtainable from It. Intern. Coal. Prep. Congress, New Delhi. 1982. Paper E2. s. 1-26.
- Blaschke W., Blaschke Z.: Wanad. Przeróbka mechaniczna. s. 76-80. Surowce Mineralne Świata. Tom V – Ti – Zr – Hf. Pod red. A. Bolewskiego. Wydawnictwo Geologiczne. Warszawa 1982.
- Blaschke W., Blaschke Z.: Tytan. Przeróbka mechaniczna. s. 229-244. Surowce Mineralne Świata. Tom V – Ti – Zr – Hf. Pod red. A. Bolewskiego. Wydawnictwo Geologiczne. Warszawa 1982.
- Blaschke W., Blaschke Z.: Cyrkon. Przeróbka mechaniczna. s. 348-357. Surowce Mineralne Świata. Tom V – Ti – Zr – Hf. Pod red. A. Bolewskiego. Wydawnictwo Geologiczne. Warszawa 1982.
- Sztaba K., Blaschke Z., Marchewczyk E., Ociepa Z., Kuczyńska I.: Działalność w zakresie kształtowania i ochrony środowiska w pracach Instytutu Przeróbki i Wykorzystania Surowców Mineralnych Akademii Górniczo-Hutniczej. Zesz. Nauk. AGH. Sozologia i Sozotechnika, z. 17, Kraków 1982, s. 123-136.
- Blaschke Z.: Wzbogacanie mułów węglowych metodą aglomeracji olejowej. Budownictwo węglowe. Projekty – Problemy 1982, nr 6, s. 22-25.

- Blaschke Z.: Sposób określania optymalnej głębokości wzbogacania węgla energetycznego ze względu na możliwą do uzyskania z niego ilość energii. *Budownictwo Węglowe. Projekty – Problemy* 1983, nr 6, s. 20-25.
- Blaschke Z., Marciniak-Kowalska J., Dryś S.: Sedymentacja mułów węglowych z KWK „Janina”. *Materiały XVII Krak. Konf. Nauk.-Techn. Przer. Kopaln. Kraków – Zakopane* 1983, s. 251-259.
- Blaschke Z., Brożek M., Mokrzycki E., Ociepa Z., Tumidajski T.: *Zarys technologii procesów przerobczych*. Wyd. II. Skrypt AGH nr 931. Kraków 1983.
- Blaschke W., Blaschke Z.: Nikiel. Przeróbka mechaniczna. s. 152-165. *Surowce Mineralne Świata. Tom Ni – Co*. Pod red. A. Bolewskiego. Wydawnictwa Geologiczne. Warszawa. 1984.
- Blaschke W., Blaschke Z.: Kobalt. Przeróbka mechaniczna. s. 253 –263. *Surowce Mineralne Świata. Tom Ni – Co*. Pod red. A. Bolewskiego. Wydawnictwa Geologiczne. Warszawa. 1984.
- Blaschke Z., Kuc S., Kuczyńska I., Ociepa Z., Siwiec A., Sztaba K., Tora B.: Wykorzystanie odpadów powstających przy przeróbce miałów węgla kamiennych. *Materiały I. Kongresu Utylizacji Odpadów. Katowice* 1985.
- Blaschke W., Blaschke Z.: Molibden. Przeróbka mechaniczna. s. 104-114. *Surowce Mineralne Świata. Tom Mo – W – Re – Sc*. Pod red. A. Bolewskiego. Wydawnictwa Geologiczne. Warszawa 1985.
- Blaschke W., Blaschke Z.: Wolfram. Przeróbka mechaniczna. s. 264-294. *Surowce Mineralne Świata. Tom Mo – W – Re – Sc*. Pod red. A. Bolewskiego. Wydawnictwa Geologiczne. Warszawa 1985.
- Czerwenka C., Blaschke Z.: Siarka rodzima – przeróbka mechaniczna. s. 201-211. *Surowce Mineralne Świata. Tom Siarka*. Pod red. A. Bolewskiego. Wydawnictwa Geologiczne. Warszawa 1985.
- Blaschke W., Blaschke Z.: Piryty. Przeróbka mechaniczna. s. 310-327. *Surowce Mineralne Świata. Tom Siarka*. Pod red. A. Bolewskiego. Wydawnictwa Geologiczne. Warszawa 1985.
- Blaschke W., Blaschke Z.: Przeróbka kopaliny apatytu. s. 192-201. *Surowce Mineralne Świata. Tom Fosfor*. Pod red. A. Bolewskiego. Wydawnictwa Geologiczne. Warszawa 1985.
- Blaschke W., Blaschke Z.: Przeróbka fosforytów. s. 201-215. *Surowce Mineralne Świata. Tom Fosfor*. Pod red. A. Bolewskiego. Wydawnictwa Geologiczne. Warszawa 1985.
- Blaschke W., Blaschke Z.: Organizacja, zaplecze naukowe, zaplecze projektowo-badawcze oraz szkolenie kadr dla zakładów przeróbki mechanicznej kopaln. *Mat. III Jugosławiańsko-Polskiego Sympozjum Górniczego. Opatija – Jugosławia*. 1986. Wydawnictwo ZG SITG. s. 74-78.
- Blaschke Z.: Wzbogacanie mułów różnych typów węgla kamiennych metodą aglomeracji olejowej. *Fizykochemiczne problemy mineralurgii. Zeszyt 19*. Wrocław 1987. s. 177-182.
- Sztaba K., Blaschke Z., Siwiec A.: Wielostadialne wzbogacanie grawitacyjne miałów energetycznych węgla kamiennych. *Materiały IX seminarium nauk.-przem. nt. Wzbogacanie grawitacyjne węgla. GIG-RJGW-SITG. Katowice, Jastrzębie Zdrój* 1987, s. 57-81.
- Sztaba K., Blaschke Z., Kuczyńska I.: Potrzeby i uwarunkowania w zakresie rozwoju metod gospodarki wodno-mułowej i procesów pomocniczych. *Zeszyty Naukowe AGH nr 1130. Górnictwo 130. Kraków* 1987. s. 131-148.
- Sztaba K., Blaschke Z.: Wzbogacanie miałów energetycznych węgla kamiennych w aspekcie zagospodarowania odpadów i ochrony środowiska naturalnego. *Materiały sympozjum nauk.-techn. SIMMEX'87 Sekcja „Energetyka”*. Katowice 1987, s. 20-23.
- Blaschke Z., Karcz A., Leśniak K.: Analiza możliwości rozszerzenia bazy surowcowej koksownictwa poprzez właściwe wykorzystanie węgla gazowo-płomiennych. *Materiały Sympozjum PAN. Wyd. AGH, Zakopane* 1988. s. 16-33.
- Blaschke Z.: Ocena możliwości poprawy jakości węgla dla potrzeb energetyki. *Materiały sympozjum nt. Optymalizacja wykorzystania surowców mineralnych w procesach przeróbki i przetwórstwa. Zakopane* 1988, s. 364-376.
- Blaschke Z., Karcz A., Leśniak K.: Zastosowanie miałów węgla typu 32 do produkcji koksu przemysłowo-opałowego systemem ubijanym. *Przegląd Górniczy nr 10. Katowice* 1988. s. 18-23.
- Blaschke Z., Nowakowski K., Pilch W., Siwiec A.: Nowe możliwości otrzymywania niskopopiołowych koncentratów węglowych. *Fizykochemiczne problemy mineralurgii, z. 20, Wrocław* 1988. s. 59-67.
- Blaschke Z.: Ocena wzbogacalności miałów węgla energetycznych. *Gospodarka Surowcami Mineralnymi. Zeszyt 3. Kraków* 1989. s. 627-645.

- Blaschke Z.: Influence the Carbon Content, King and Gangue and of Diesel Oil on the Results of Coal Beneficiation by Oil Agglomeration. Proceedings of the 11th ICPC. Tokyo 1990. s. 257-260.
- Blaschke W., Mokrzycki E., Blaschke S.A., Grudziński Z., Blaschke Z.: Oplacalność wzbogacania węgla energetycznego w nowym systemie cen na węgiel. XXII Krakowska Konf. Przer. Kopalin. Bukowina Tatrzańska, 1991, s. 89-108.
- Blaschke Z.: Wpływ ziarn skrajnie drobnych na wyniki wzbogacania miału węgla energetycznego w osadzarce OM12-2. Gospodarka Surowcami Mineralnymi. t. 7. z. 1, 1991, s. 141-152.
- Blaschke W., Blaschke Z., Blaschke S.A.: Wpływ parametrów jakościowych węgla energetycznego na efektywność jego użytkowania. Przegląd Górniczy. 1991. Nr 8. s. 1-6.
- Blaschke W., Mokrzycki E., Blaschke S.A., Grudziński Z., Karcz A., Blaschke Z., Jaworski A.: System cen na węgiel kamienny. Przegląd Górniczy nr 2. Katowice 1991, s. 18-26.
- Blaschke Z.: The Effect of Extremely Fine Grains on Cleaning Results of Power Fine Coal in the OM 12-2 Jig. Proc. of the Int. Conf. "Environment and Mineral Processing". Ostrava 1992. s. 151-160.
- Blaschke Z., Siwiec A.: State of the Art. at Coal Cleaning and Coal Separation Technique in Poland. Materiały XXIV. Cracovian Mineral Processing Conference. Zakopane 1992, s. 193-201.
- Blaschke Z., Gawlik L.: Optimal Quality of Coal Concentrates for Power Industry. Proceedings Intern. Symp. Energex'93. Korea.Seul. 1993
- Blaschke Z.: Influence the Carbon Content, King and Gangue and of Diesel Oil on the Results of Coal Beneficiation by Oil Agglomeration. Gospodarka Surowcami Mineralnymi. Zeszyt 4. Kraków 1993. s. 661-668.
- Blaschke W., Blaschke Z.: Krakowskie Konferencje Przeróbki Kopalin. Mat. XXV Krakowskiej Konferencji Przeróbki Kopalin. Szczawnica 1993. Sympozja i Konferencje Nr 8. Wyd. CPPGSMiE PAN. Kraków. s. 5-29.
- Sztaba K., Blaschke Z.: Założenia technologii usuwania siarki zawartej w energetycznych węglach kamiennych z uwzględnieniem wykorzystania wybranych składników urobku. Materiały Sympozjum Nauk.- Techn. SIMMEX'93. Katowice 1993.
- Blaschke Z.: Aglomeracja olejowa i flokulacja selektywna mulów węglowych. Sympozja i Konferencje CPPGSMiE PAN nr 11 tom 3. Kraków 1994. s. 139-153.
- Blaschke Z., Kisielowska E., Konopka E., Gładysz Z.: Wykorzystanie biomasy wybranych mikroorganizmów jako flokulanta biologicznego w procesie flokulacji selektywnej. Sympozja i Konferencje CPPGSMiE PAN nr 11 tom 3. Kraków 1994. s. 187-193.
- Blaschke Z., Blaschke Z., Gawlik L.: Pokongresowe wycieczki techniczne do Zakładów Przeróbki Węgla. Sympozja i Konferencje CPPGSMiE PAN nr 11 tom 6. Kraków 1994. s. 151-159.
- Blaschke Z., Sztaba K.: The Present Quality of Power Coal and Possibilities and Conditions of its Improvement. Gospodarka Paliwami i Energią 42 (9). 1994. s. 13-15.
- Blaschke Z., Sanak-Rydlowska S.: Selective Flocculation in Silt Separation from Coal Slimes. Gospodarka Surowcami Mineralnymi. t. 10. z. 2. Kraków 1994. s. 305-313.
- Sztaba K., Blaschke Z.: The of Enrichment of Power Coal on the Condition and Shaping of Natural Environment. Materials of the Seminar Ecological New Power Technologies. University of Mining and Metallurgy. Department of Power Machines and Equipment. Consulate General of Austria in Cracow. Kraków 1994. s. 80-87.
- Blaschke Z.: Oil Agglomeration and Selective Flocculation of Coal Slurries. Preprint of the 12th ICPC. Vol. 2. Cracow 1994. s. 763-776.
- Blaschke Z., Kisielowska E., Konopka E., Gładysz Z.: Utilization of the Biomass of Selected Microorganisms Flocculant in Selective Flocculation. Preprint of the 12th ICPC. Vol. 2. Cracow 1994. s. 803-807.
- Blaschke Z., Gawlik L.: Optimal quality of coal concentrates for power industry. Gospodarka Surowcami Mineralnymi. t. 11. z. 4. Kraków 1995. s. 579-588.
- Sztaba K., Blaschke Z.: O podstawowych uwarunkowaniach podnoszenia jakości koncentratów węglowych. Prace naukowe GIG seria Konferencje nr 12. Katowice 1996. s. 261-271.
- Blaschke Z.: Oil Agglomeration and Selective Flocculation of Coal Slurries. Proceedings of the 12th International Coal Preparation Congress. Cracow 1994. s. 483-492. Gordon and Breach Publishers 1996.
- Blaschke Z., Kisielowska E., Konopka E., Gładysz Z.: Utilization of the Biomass of Selected Micro-organisms

- Flocculant in Selective Flocculation. Proceedings of the 12th ICPC. Cracow 1994. s. 511-514. Gordon and Breach Publisher. 1996.
- Blaschke Z., Blaschke Z., Gawlik L.: The Congress Technical Tours to Coal Preparation Plants. Proceedings of the 12th ICPC. Cracow 1994. s. 9783-979. Gordon and Breach Publisher 1996.
- Sztaba K., Blaschke Z.: O podstawowych uwarunkowaniach podnoszenia jakości koncentratów węglowych. Przegląd Górniczy nr 12. Katowice 1996. s. 16-22.
- Blaschke Z.: Technologia odsiarczania węgla. Materiały Szkoły Gospodarki Odpadami. Wyd. PAN. Kraków 1997.
- Sztaba K., Blaschke Z.: The possibilities and principles of application of enriched coal as ecological fuels in average Polish conditions. Gospodarka Surowcami Mineralnymi. t.13. z. 4. Kraków 1997. s. 461-469.
- Blaschke Z.: Jakość kamiennego węgla energetycznego w świetle przepisów dotyczących ochrony środowiska. Kompleksowe wykorzystanie surowców a ochrona środowiska. Wyd. AGH. Kraków 1998. s.47-56.
- Blaschke Z.: The quality of hard power coal in the light of environment protection regulations. Gospodarka Surowcami Mineralnymi. t.15. z. 4. Kraków 1999. s. 59-70.
- Blaschke Z.: Coal preparation in Poland: Present practice and perspectives. Proceedings of the American – Polish mining symposium: Mining in the New Millennium Challenges and Opportunities. Wyd. Balkema, Rotterdam. 2000. s. 231-236.
- Blaschke Z.: Gospodarka wodno-mułowa i operacje odwadniania w zakładach przeróbki węgla. Prace GIG. Seria Konferencje nr 34. Katowice 2000. s. 51-59.
- Blaschke Z., Blaschke W.: Evaluation of the efficiency for coal slime beneficiation and desulfurisation in spirals. Zbornik prednasok I Medzinárodná Konferencia „Mineralurgia a environmentalne technologie”. BERG TU Kosice. Herlany 2000. pp. 4-9.
- Blaschke Z.: Ocena skuteczności wzbogacania i odsiarczania mułów węglowych we wzbogacalnikach zwojowych. Inżynieria Mineralna. t.1 z. 2. Wyd. PTPK, Kraków 2000. s. 33-36.
- Blaschke Z.: Wzbogacanie węgla kamiennego w Polsce. Inżynieria Mineralna. t. 2. z. 1(3), Wyd. PTPK, Kraków 2001. s. 3-9.
- Blaschke Z., Blaschke W.: Sposób określania energetycznie optymalnych parametrów jakościowych węgla na przykładzie zakładu wzbogacania PPMW Biskupice. XVI Konferencja z cyklu „Zagadnienia surowców energetycznych i energii w gospodarce krajowej”. Zakopane, 6-9 października 2002. Sympozja i Konferencje nr 57. Wyd. Instytutu GSMiE PAN. Kraków, s. 589-599.
- Blaschke Z.: Wybrane technologie wzbogacania fizykochemicznego materiałów bardzo drobno uziarnionych. Inżynieria Mineralna. t.3. z. 1(7). Kraków 2002. s. 145-155.
- Blaschke Z.: Metoda określania najkorzystniejszych parametrów jakościowych węgla z punktu widzenia optymalnego wykorzystania jego energii chemicznej. Inżynieria Mineralna. t.4. z. 3(10). Kraków 2003. s. 166-175.
- Blaschke Z., Blaschke W.: Ocena celowości wzbogacania węgla na potrzeby energetyki w samodzielnych zakładach przerobczych. Studia, Rozprawy, Monografie nr 116. Wyd. Instytutu GSMiE PAN. Kraków 2003. s. 1-70.
- Blaschke Z., Blaschke W., Blaschke S.: Determination of the most favourable parameters of coal concentrates allowing optimal utilisation of chemical energy of coal. 8 Conference on environment and mineral Processing. Wyd. VSB-Technical University of Ostrava 2004, Part II s. 327-332.
- Blaschke W., Blaschke Z., Blaschke S.: The Method of Determination of the Most Favourable Parameters of Coal Concentrates Regarding Maximum Electricity Production. Energex 2004 – 10th International Energy Forum. Wyd. Universidade Nova de Lisboa. Portugal 2004, s. 181-186.
- Blaschke W., Blaschke Z., Future of Hard Coal Designed for Utilisation in Power Industry. Conference. Současnost a perspektivy úpravy nerostných surovin. Wyd. VŠB-TU. Ostrava 2005, s. 19-35.
- Blaschke S., Blaschke Z., Blaschke W., Blaschke J., Blaschke S.A.: Mała Encyklopedia Inżynierii Mineralnej. Inżynieria Mineralna. t. 7.z. S4 (17). Wyd. PTPK, Kraków. S. 3-163.

## **Professor Andrzej Krysztafkiewicz, Ph.D., D.Sc. (1947-2010)**



6 October 1947 – 31 January 2010

Professor Andrzej Krysztafkiewicz was born on the 6th of October 1947 in Gniezno. He studied at the Faculty of Mathematics, Physics and Chemistry, Adam Mickiewicz University, from which he graduated in 1970 with the degree of master of chemical sciences. The same year he joined the Faculty of Chemistry, presently the Faculty of Chemical Technology, at the Poznań University of Technology. In 1978 he got the degree of doctor of chemical sciences conferred by the Faculty of Chemistry, Adam Mickiewicz University in Poznań. In 1991, he presented his habilitation dissertation entitled “Active highly dispersed silica and silicate fillers from waste post-fluorine silica” and after completion of the habilitation procedure at the Faculty of Chemical Technology and Engineering of the Szczecin University of Technology, he was awarded the habilitation degree (D.Sc.) of technical sciences in chemical technology. In 2001 the President of the Republic of Poland awarded him the title of professor. Since 2003 he had been employed as a full professor at the Poznań University of Technology.

Scientific interests of Professor Andrzej Krysztafkiewicz concerned three research disciplines closely related in the cognitive and application aspects: inorganic chemical technology, material engineering, and protection of natural environment. His main

subject of study was directed to obtaining silicas and silicates, highly dispersed materials of particles in the size of nanometers. The substances are widely applied in many fields, e.g. in polymer processing, production of composites, production of new generations of paints and lacquers. In recent years he had extended the area of his interest by the processes of obtaining colourful silicas and silicates making inorganic pigments of high degree of dispersion. In the processes of their production he used the post-galvanic waste solutions of salts of non-ferrous metals.

His best known achievements include:

- modification of the precipitation of highly dispersed silica by introduction of organic compounds to the classical precipitation system (e.g. mono- or multihydroxide alcohols of short or long carbon chains),
- development of a new method for silica surface modification during the process of precipitation,
- comparison of the effects of surface modification of silica and silicates performed by classical dry methods and in the precipitation process – the wet method,
- establishment of conditions of modification; selection of solvent, optimisation of amount of modifier, optimisation of process temperature, etc.
- obtaining silica-carbonate fillers from nanocomposite powders by precipitation with the use of calcium hydroxide or calcium salts, sodium carbonate or sodium hydroxide, sodium metasilicate and carbon dioxide,
- obtaining pigment composites by deposition of organic dyes on highly dispersed silica,
- use of modern research technologies for evaluation of the synthesised silicas and silicates and also natural silicates such as bentonites, kaolins and talc.

He was the author or co-author of over 300 scientific papers, published in *Dyes and Pigments*, *Journal of Materials Science*, *Colloids and Surfaces A: Physicochemical and Engineering Aspects*, *Journal of Adhesion Technology*, *Powder Technology*, *Environmental Science and Technology*, *Advanced Powder Technology*, *Colloid and Polymer Science*, *Physicochemical Problems of Mineral Processing*, *Pigment and Resin Technology* and *Przemysł Chemiczny*, and other journals as well as many industrial implementations and patents.

Professor Andrzej Krysztafkiewicz cooperated with many companies, e.g., CIECH S.A. Chemical Group (mainly with VITROSILICON S.A. and SODA Polska S.A.), Zakłady Chemiczne POLICE S.A., Zakłady Chemiczne LUBOŃ Sp. z o.o. (presently LUVENA S.A.), Zakład Surowców Chemicznych i Mineralnych PIOTROWICE II Sp. z o.o., Poznańskie Zakłady Zielarskie HERBAPOL SA, PAROC Trzemeszno Sp. z o.o., VOLKSWAGEN Poznań Sp. z o.o., Gestamp Polska Sp. z o.o., REXAM Szkło Gostyń S.A.) and with many research and scientific institutions.

Professor Krysztafkiewicz supervised 12 doctoral dissertations, over 130 Master of Science and Bachelor of Science theses. Four associates of Professor Krysztafkiewicz

are active academics at the Poznań University of Technology, Adam Mickiewicz University, and the State Vocational College in Gniezno. One former associate is completing his doctoral dissertation at Kent State University and one is writing thesis at Universidad Autonoma de Madrid.

Professor Andrzej Krysztafkiewicz was a member of the Scientific Board of the Physicochemical Problems of Mineral Processing journal and other Scientific Committees and Associations (e.g. PTChem and IACIS – International Association of Colloid and Interface Scientists). He was a leader of many projects, many of them co-financed from European Structural Funds.

He was awarded distinctions and medals for his research and teaching, e.g. the prize of the Minister of National Education, the prize of the Minister of Higher Education and Technology for achievements in teaching (1980) and for research on Chemistry and technology of white mineral highly dispersible fillers used in the processing of plastomers and elastomers (1989). Professor Krysztafkiewicz received many distinctions for research and teaching and many prizes of vice-Chancellor of the Poznań University of Technology.

Professor Andrzej Krysztafkiewicz performed many important administrative functions (Dean's Representative for Work Placement; Deputy Director of Institute of Chemical Technology and Engineering, Poznań University of Technology (1981-2004); vice-Chancellor's Representative, Poznań University of Technology for contacts with the Board of the Town of Gniezno regarding organization of training in applied sciences in Gniezno (1996-2004); Director, Institute of Chemical Technology and Engineering, Poznań University of Technology (2004-2008); Head, Department of Chemical Technology, Poznań University of Technology (2008-2010).

He was a lover of the history of art and travel. Professor Krysztafkiewicz was not a craftsman but an artist of science and a great writer. He disliked technological gadgets except for a phone, which he could not live without as he could not live without a great number of friends and colleagues with whom Professor Krysztafkiewicz was in touch.

Everyday Professor Andrzej Krysztafkiewicz welcomed his associated with warm words, supported them with useful advice. He knew life... It is difficult to express our grief and sorrow. And although He is no longer with us, our memory of Him and His teaching will remain...

We thank Him for the strength and hope He has given us. He has shown us how we can live our lives in dignity. He used to say that wisdom and nobleness must be considered the art of life. He was a great, wise, and noble Man, very understanding and very close to our hearts, has left us. He was our pillar of strength. Our Friend and Master.

*Non omnis moriar*

## LIST OF PUBLICATION

- KRANZ M., DOMKA L., KRYSZTAFKIEWICZ A., MAIK M., 1979, Zastosowanie organicznych związków krzemu jako czynników sprzęgających w układzie napelniacz – elastomer, *Polimery*, 24, 3, 86-90.
- DOMKA L., KRYSZTAFKIEWICZ A., 1980, Wpływ własności fizykochemicznych tlenku cynkowego na jego przydatność jako aktywatora w procesie wulkanizacji, *Polimery*, 25, 3, 102-104.
- DOMKA L., KRYSZTAFKIEWICZ A., WIECZOREK W., 1980, Przerób odpadowego fosfogipsu z produkcji kwasu fosforowego na czysty siarczan amonowy, *Przem. Chem.*, 59, 6, 346-348.
- KRYSZTAFKIEWICZ A., KRANZ M., DOMKA L., 1980, Badania nad możliwością otrzymywania wysoko zdyspergowanych krzemionek strączanych jako napelniaczy aktywnych dla przemysłu gumowego, *Polimery*, 25, 12, 452-456.
- KRYSZTAFKIEWICZ A., WIECZOREK W., DOMKA L., 1981, Zastosowanie mikroskopii elektronowej w badaniach napelniaczy krzemionkowych, *Polimery*, 26, 5, 175-178.
- KRYSZTAFKIEWICZ A., DOMKA L., WIECZOREK W., 1981, Zastosowanie odpadowej krzemionki po fluorowej jako napelniacza w przemyśle gumowym, *Polimery*, 26, 6, 221-224.
- MAIK M., KRYSZTAFKIEWICZ A., 1981, Wpływ napelniaczy na własności poliuretanów, *Polimery*, 26, 7, 245-247.
- KRYSZTAFKIEWICZ A., DOMKA L., 1982, Zastosowanie chromatografii cienkowarstwowej do oznaczania siarki nie związanej chemicznie w wulkanizatach i mieszkach gumowych, *Polimery*, 27, 11, 437-439.
- MARCINIEC B., KRYSZTAFKIEWICZ A., DOMKA L., 1983, Wettability of silane films on silica fillers, *Colloid Polym. Sci.*, 261, 4, 306-311.
- KRYSZTAFKIEWICZ A., 1984, Krzemiany wapniowe o dużym stopniu dyspersji jako napelniacze elastomerów, *Przem. Chem.*, 63, 6, 312-315.
- KRYSZTAFKIEWICZ A., MAIK M., 1984, Waste cement dusts as activating agents for rubber compound, *Cem. Concr. Res.*, 14, 5, 615-621.
- KRYSZTAFKIEWICZ A., MAIK M., 1984, Waste cement dusts as fillers for rubber compounds, *Cem. Concr. Res.*, 14, 6, 776-784.
- KRYSZTAFKIEWICZ A., 1984, Otrzymywanie jednorodnego roztworu metakrzemianu sodowego z odpadowych krzemionek po fluorowych, *Chemia Stosowana*, 28, 3 – 4, 477-488.
- KRYSZTAFKIEWICZ A., DOMKA L., WIECZOREK W., 1985, The modified talcs as semi-active fillers of rubbers, *Colloid Polym. Sci.*, 263, 10, 804-811.
- KRYSZTAFKIEWICZ A., MAIK M., MIEDZIŃSKI M., BŁASZCZAK J., RAGER B., 1986, Wpływ fosforanów na krystalizację uwodnionego fluorku glinowego, *Przem. Chem.*, 65, 4, 207-209.
- KRYSZTAFKIEWICZ A., DOMKA L., 1986, Effect of silane coupling in filled rubber Vulcanizates, *Plast. Rubber Compos. Process. Appl.*, 6, 3, 197-203.
- KRYSZTAFKIEWICZ A., MAIK M., MIEDZIŃSKI M., BŁASZCZAK J., RAGER B., 1986, Wpływ warunków otrzymywania uwodnionego fluorku glinowego na jego strukturę krystaliczną, *Przem. Chem.*, 65, 11, 616-618.
- KRYSZTAFKIEWICZ A., 1986, Krzemian cynkowy – efektywny napelniacz kauczuków, *Przem. Chem.*, 65, 12, 677-679.
- KRYSZTAFKIEWICZ A., 1987, Modified calcium silicates as active rubber fillers, *J. Mater. Sci.*, 22, 2, 478-482.
- KRYSZTAFKIEWICZ A., 1987, Roztwory metakrzemianu sodowego z odpadowych krzemionek po fluorowych jako substraty do otrzymywania napelniaczy o wysokim stopniu dyspersji, *Chemia Stosowana*, 31, 1, 127-138.
- KRYSZTAFKIEWICZ A., DOMKA L., 1987, Effect of surfactants on the properties of talc used as a filler in rubber compound, *Tenside Surfact., Det.*, 24, 4, 227-231.
- KRYSZTAFKIEWICZ A., MAIK M., 1987, Modified precipitated silicas as polyurethane fillers, *Colloid Polym. Sci.*, 265, 8, 704-710.
- KRYSZTAFKIEWICZ A., 1987, Metody oceny mineralnych napelniaczy elastomerów, *Chemia Stosowana*, 31, 3, 443-461.
- KRYSZTAFKIEWICZ A., WIECZOREK W., 1988, Krzemionka odpadowa z produkcji fluorku glinowego jako

- napelniacz kauczuku, *Przem. Chem.*, 67, 1, 29-31.
- KRYSZTAFKIEWICZ A., 1988, Modification of waste silicas by silanes and titanates and their uses as reinforcing fillers in elastomer composites, *J. Adhes. Sci. Technol.*, 2, 3, 203-213.
- KRYSZTAFKIEWICZ A., RAGER B., 1988, NIR studies of the surface modification in silica fillers, *Colloid Polym. Sci.*, 266, 6, 485-493.
- BLASZCZAK J., KRYSZTAFKIEWICZ A., MAIK M., RAGER B., 1988, Wpływ środków powierzchniowo czynnych na krystalizację fluorku glinowego, *Przem. Chem.*, 67, 7, 345-346.
- KRYSZTAFKIEWICZ A., 1988, Otrzymywanie roztworów metakrzemianu sodowego o podwyższonych modułach – surowca do wytwarzania wysoko zdyspergowanych krzemionek, *Przem. Chem.*, 67, 8, 384-386.
- KRYSZTAFKIEWICZ A., 1988, Modified zinc silicate – an active rubber filler, *J. Mater. Sci.*, 23, 2407-2414.
- KRYSZTAFKIEWICZ A., 1988, Surface – modified fillers for reinforcing elastomers, *Surf. Coat. Technol.*, 35, 151-170.
- KRYSZTAFKIEWICZ A., 1989, Modified silica precipitated in the medium of organic solvents – an active rubber filler, *Colloid Polym. Sci.*, 267, 5, 399-408.
- KRYSZTAFKIEWICZ A., 1989, Otrzymywanie silnie zdyspergowanej krzemionki z roztworów metakrzemianu sodowego w środowisku rozpuszczalnika organicznego, *Przem. Chem.*, 68, 4, 183-185.
- KRYSZTAFKIEWICZ A., 1989, Filterability of sodium metasilicate solutions, *Tenside Surfact. Det.*, 26, 6, 420-423.
- KRYSZTAFKIEWICZ A., 1989, Czynniki wiążące w układzie napelniacz – polimer, *Chemia Stosowana*, 33, 4, 561-584.
- BLASZCZAK J., KRYSZTAFKIEWICZ A., MAIK M., 1990, Wpływ warunków produkcji fluorku glinowego na uziarnienie wytrącającej się krzemionki odpadowej, *Przem. Chem.*, 69, 1, 38-40.
- KRYSZTAFKIEWICZ A., MAIK M., RAGER B., 1990, Odpadowe krzemionki po fluorowe jako napelniacze elastomerów, *Inżynieria Materiałowa*, 11, 5, 125-129.
- KRYSZTAFKIEWICZ A., 1990, Use of highly dispersed, precipitated carbonate – silicate powders as fillers for elastomers, *Powder Technol.*, 63, 1, 1-11.
- KRYSZTAFKIEWICZ A., BLASZCZAK J., 1991, Effect of surfactants on the process of obtaining aluminium fluoride and silica from fluorosilicic acid solution, *Tenside Surfact. Det.*, 28, 4, 260-263.
- BLASZCZAK J., KRYSZTAFKIEWICZ A., MAIK M., 1991, Badania nad krystalizacją uwodnionego fluorku glinowego, *Przem. Chem.*, 70, 4, 185-187.
- BLASZCZAK J., KRYSZTAFKIEWICZ A., 1992, Otrzymywanie pigmentów cynkowo –kobaltowych o dużym stopniu rozdrobnienia na nośniku krzemionkowym, *Przem. Chem.*, 71, 4, 145-147.
- KRYSZTAFKIEWICZ A., MAIK M., RAGER B., 1992, Comparison of waste silica fillers modified with various proadhesive compounds, *J. Mater. Sci.*, 27, 3581-3588.
- KRYSZTAFKIEWICZ A., MAIK M., RAGER B., WIECZOREK W., 1993, Highly dispersed precipitated silicas as agents improving products made on the base of polymers and as thickening agents in toothpastes, *Powder Technol.*, 75, 1, 29-41.
- KRYSZTAFKIEWICZ A., RAGER B., MAIK M., 1993, Utylizacja krzemionki odpadowej z produkcji kwasu fluorowodorowego, *Fizykochemiczne Problemy Mineralurgii*, 27, 163-178.
- KRYSZTAFKIEWICZ A., RAGER B., MAIK M., 1994, Wpływ modyfikacji powierzchni na właściwości fizykochemiczne krzemionki strącanej, *Fizykochemiczne Problemy Mineralurgii*, 28, 177-186.
- KRYSZTAFKIEWICZ A., RAGER B., MAIK M., SZYMANOWSKI J., 1994, Model hydrophobing compounds with nitrogen and sulphur atoms in oxyethylene structures, as modifiers of silica filler, *Colloid Polym. Sci.*, 272, 12, 1526-1535.
- KRYSZTAFKIEWICZ A., RAGER B., MAIK M., 1994, Surface modification of highly dispersed rubber fillers and pigments by titanate proadhesive and hydrophobic compounds, *Colloid Polym. Sci.*, 272, 12, 1547-1559.
- BLASZCZAK J., KRYSZTAFKIEWICZ A., MAIK M., 1995, Otrzymywanie czystego siarczanu glinu z popiołów turoszowskich, *Przem. Chem.*, 74, 10, 384-386.
- KRYSZTAFKIEWICZ A., MAIK M., RAGER B., 1995, Modyfikowane odpadowe pyły cementowe – napelniacze mieszanek gumowych, *Fizykochemiczne Problemy Mineralurgii*, 29, 169-181.

- KRYSZTAFKIEWICZ A., RAGER B., MAIK M., WIECZOREK W., 1995, Novel alumino – silicate powders and their use as fillers and pigments, *Pol. J. Appl. Chem.*, 39, 2, 73-85.
- KRYSZTAFKIEWICZ A., RAGER B., MAIK M., 1996, Silica recovery from waste obtained in hydrofluoric acid and aluminum fluoride production from fluorosilicic acid, *J. Hazard. Mater.*, 48, 1, 31-49.
- JESIONOWSKI T., KRYSZTAFKIEWICZ A., 1996, Production of the highly dispersed sodium – aluminium silicate to be used as a white pigment or as a polymer filler, *Pigment Resin Technol.*, 25, 3, 4-14. Praca uznana za publikację roku 1996r. w brytyjskim czasopiśmie "Pigment and Resin Technology"
- KRYSZTAFKIEWICZ A., RAGER B., WIECZOREK W., 1996, Metody modyfikacji powierzchni napelniaaczy mineralnych stosowanych w tworzywach sztucznych, *Fizykochemiczne Problemy Mineralurgii*, 30, 107-117.
- KRYSZTAFKIEWICZ A., RAGER B., MAIK M., WALKOWIAK J., 1996, Modified sodium – aluminium silicate – a highly dispersed polymer filler and a pigment, *Colloids Surf. A*, 113, 203-214.
- DOMKA L., KRYSZTAFKIEWICZ A., MARCINIEC B., GULIŃSKI J., URBANIAK W., 1996, Napelniaacze krzemionkowe i krzemianowe modyfikowane krajowym silanowymi związkami proadhezyjnymi, *Przem. Chem.*, 75, 10, 376-378.
- DOMKA L., KRYSZTAFKIEWICZ A., GULIŃSKI J., URBANIAK W., MACIEJEWSKI H., 1997, Krzemionki i krzemiany modyfikowane krajowymi silanowymi związkami proadhezyjnymi – napelniaacze poliuretanów i PCW, *Przem. Chem.*, 76, 3, 96-98.
- KRYSZTAFKIEWICZ A., RAGER B., JESIONOWSKI T., 1997, The effect of surface modification on physicochemical properties of precipitated silica, *J. Mater. Sci.*, 32, 1333-1339.
- KRYSZTAFKIEWICZ A., JESIONOWSKI T., RAGER B., 1997, Reinforcing of synthetic rubber with waste cement dust modified by coupling agents, *J. Adhes. Sci. Technol.*, 11, 4, 507-517.
- KRYSZTAFKIEWICZ A., DOMKA L., 1997, Specific area and activity of highly dispersed silicas – fillers of synthetic rubbers, *Pol. J. Appl. Chem.*, 41, 1-2, 3-16.
- RAGER B., KRYSZTAFKIEWICZ A., 1997, Effect of electrolytes and surfactants on physicochemical properties and porous structure of hydrated silicas, *Colloids Surf. A*, 125, 121-130.
- KRYSZTAFKIEWICZ A., DOMKA L., 1997, Surface – modified microporous talcs as fillers of polymers and pigments, *J. Mater. Chem.*, 7, 8, 1655-1659.
- KRYSZTAFKIEWICZ A., RAGER B., JESIONOWSKI T., 1997, Otrzymywanie barwnych pigmentów - krzemianów o dużym stopniu rozdrobnienia, *Fizykochemiczne Problemy Mineralurgii*, 31, 165-173.
- KRYSZTAFKIEWICZ A., JESIONOWSKI T., DUL J., DOMKA L., 1997, Krzemionki, krzemiany sodowo-glinowe i strącane węglany wapnia - napelniaacze kauczuku SBR, *Elastomery*, 2, 211-219.
- KRYSZTAFKIEWICZ A., MICHALSKA I., JESIONOWSKI T., WIECZOREK W., 1998, Odpadowe sole chromu i żelaza - potencjalne źródło otrzymywania pigmentów krzemianowych, *Fizykochemiczne Problemy Mineralurgii*, 32, 77-85.
- KRYSZTAFKIEWICZ A., JESIONOWSKI T., WALKOWIAK J., 1998, Silicates of green colour – highly dispersed pigments, *Pigment Resin Technol.*, 27, 81-87.
- JESIONOWSKI T., KRYSZTAFKIEWICZ A., 1999, Properties of highly dispersed silicas precipitated in an organic medium, *J. Dispersion Sci. Technol.*, 20, 1609-1623.
- KRYSZTAFKIEWICZ A., MICHALSKA I., JESIONOWSKI T., BOGACKI M., 1999, Wysoko zdyspergowane syntetyczne krzemiany cynku - przyszłościowe pigmenty ekologicznych farb krzemianowych, *Fizykochemiczne Problemy Mineralurgii*, 33, 83-92.
- GRODZKA J., KRYSZTAFKIEWICZ A., JESIONOWSKI T., RAGER B., 1999, Otrzymywanie i modyfikacja napelniaaczy węglanowo-krzemianowych, *Fizykochemiczne Problemy Mineralurgii*, 33, 45-54.
- JESIONOWSKI T., KRYSZTAFKIEWICZ A., 1999, Postęp w technologii modyfikacji powierzchni wysoko zdyspergowanych krzemionek, *Prace Naukowe Instytutu Technologii Nieorganicznej i Nawozów Mineralnych Politechniki Wrocławskiej*, 48 (28), 200-204.
- KRYSZTAFKIEWICZ A., JESIONOWSKI T., BINKOWSKI S., 2000, Precipitated silicas modified with 3-aminopropyltriethoxysilane, *Colloids Surf. A*, 173, 73-84.
- JESIONOWSKI T., KRYSZTAFKIEWICZ A., 2000, Comparison of the techniques used to modify amorphous

- hydrated silicas, *J. Non-Cryst. Solids*, 277, 45-57.
- BINKOWSKI S., JESIONOWSKI T., KRYSZTAFKIEWICZ A., 2000, Preparation of pigments on modified precipitated silicas, *Dyes Pigments*, 47, 247-257.
- JESIONOWSKI T., KRYSZTAFKIEWICZ A., 2000, Wpływ kationowych związków powierzchniowo czynnych na aktywność napełniaczy krzemionkowych, *Prace Naukowe Katedry Budowy Maszyn Politechniki Śląskiej*, 1, 127-130.
- JESIONOWSKI T., KRYSZTAFKIEWICZ A., SKRZYPCZAK A., 2000, Wpływ kationowych związków powierzchniowo czynnych na wielkość cząstek i polidispersyjność strąconych krzemionek aktywnych, *Prace Naukowe Instytutu Technologii Organicznej i Tworzyw Sztucznych Politechniki Wrocławskiej*, 48 (22), 273-276.
- KRYSZTAFKIEWICZ A., JESIONOWSKI T., SKRZYPCZAK A., 2000, Hydrofobizacja powierzchni krzemionek za pomocą kationowych związków powierzchniowo czynnych z ugrupowaniem imidazoliowym, *Prace Naukowe Instytutu Technologii Organicznej i Tworzyw Sztucznych Politechniki Wrocławskiej*, 48 (22), 285-288.
- WIECZOREK M., KRYSZTAFKIEWICZ A., JESIONOWSKI T., 2000, Bentonity modyfikowane czwartorzędowymi ZPC oraz silanowymi czynnikami pro adhezyjnymi, *Prace Naukowe Instytutu Technologii Organicznej i Tworzyw Sztucznych Politechniki Wrocławskiej*, 48 (22), 337-340.
- KRYSZTAFKIEWICZ A., WIECZOREK M., JESIONOWSKI T., 2000, Modyfikacja piasku kwarcytowego surowca do produkcji roztworów metakrzemianów alkalicznych, *Prace Naukowe Instytutu Górnictwa Politechniki Wrocławskiej*, 88, 65-74.
- GRODZKA J., KRYSZTAFKIEWICZ A., JESIONOWSKI T., 2000, Wpływ silanowych związków wiążących na właściwości napełniaczy węglanowo-krzemianowych, *Prace Naukowe Instytutu Górnictwa Politechniki Wrocławskiej*, 88, 95-104.
- KRYSZTAFKIEWICZ A., JESIONOWSKI T., 2000, Krzemionki modyfikowane bezpośrednio w trakcie strącania – aktywne napełniacze polimerów, *Prace Naukowe Katedry Budowy Maszyn Politechniki Śląskiej*, 1, 138-144.
- JESIONOWSKI T., KRYSZTAFKIEWICZ A., 2001, Influence of silane coupling agents on surface properties of precipitated silicas, *Appl. Surf. Sci.*, 172, 18-32.
- KRYSZTAFKIEWICZ A., WERNER R., LIPSKA K.L., JESIONOWSKI T., 2001, Effect of silane coupling agents on properties of precipitated sodium-aluminium silicates, *Colloids Surf. A*, 182, 73-84.
- JESIONOWSKI T., KRYSZTAFKIEWICZ A., SKRZYPCZAK A., 2001, Effects of quaternary ammonium chlorides on the surface properties of precipitated silicas, *Tenside Surfact. Det.*, 38, 158-163.
- JESIONOWSKI T., KRYSZTAFKIEWICZ A., 2001, Silicas modified with amino- and mercaptosilanes – fillers of urethane elastomers, *Compos. Interfaces*, 8, 243-248.
- JESIONOWSKI T., KRYSZTAFKIEWICZ A., 2001, Silicas modified with silane proadhesive compounds – active fillers of rubbers, *Compos. Interfaces*, 8, 221-225.
- KRYSZTAFKIEWICZ A., GRODZKA J., JESIONOWSKI T., RAGER B., 2001, Carbonate-silicate fillers: their production, properties and application in plastic and paper industries, *Compos. Interfaces*, 8, 227-232.
- KRYSZTAFKIEWICZ A., MICHALSKA I., JESIONOWSKI T., 2001, Zinc, chromium and iron silicates as fillers and inorganic colour pigments, *Compos. Interfaces*, 8, 257-262.
- JESIONOWSKI T., BULA K., JURGA J., KRYSZTAFKIEWICZ A., 2001, Effect of amorphous precipitated silica on properties and structure of poly(p-phenylene sulphide) (PPS), *Colloid Polym. Sci.*, 297, 983-989.
- WERNER R., KRYSZTAFKIEWICZ A., JESIONOWSKI T., JĘCZALIK J., 2001, Silane modified sodium-aluminium silicates – fillers used in polyurethane elastomers, *J. Adhes. Sci. Technol.*, 15, 1711-1724.
- WIECZOREK M., KRYSZTAFKIEWICZ A., JESIONOWSKI T., 2001, Utilisation of refuse ashes from mineral wool production processes, *Polish J. Chem. Technol.*, 3, 36-37.
- JESIONOWSKI T., KRYSZTAFKIEWICZ A., ŻURAWSKA J., 2001, Potassium metasilicate as a substrate in precipitation technology of unmodified and modified active silicas, *Polish J. Chem. Technol.*, 3, 3-5.
- GRODZKA J., KRYSZTAFKIEWICZ A., JESIONOWSKI T., 2001, Comparison of carbonate-silicate fillers modified with various proadhesion compounds, *Physicochem. Problems Mineral Proc.*, 35, 73-81.
- JESIONOWSKI T., KRYSZTAFKIEWICZ A., DEC A., 2001, Modified titanium white – characteristics and application, *Physicochem. Problems Mineral Proc.*, 35, 195-205.

- BINKOWSKI S., KRYSZTAFKIEWICZ A., JESIONOWSKI T., ŻURAWSKA J., 2001, Fyzykochemiczne właściwości ekologicznych pigmentów nieorganicznych, *Chemia i Inżynieria Ekologiczna*, 8, 1025-1030.
- ŻURAWSKA J., JESIONOWSKI T., KRYSZTAFKIEWICZ A., 2001, Mechanizm adsorpcji chemicznej w układzie silanowy związek wiążący-krzemionka uwodniona, *Chemia i Inżynieria Ekologiczna*, 8, 1086-1091.
- KRYSZTAFKIEWICZ A., GRODZKA J., JESIONOWSKI T., 2001, Modified carbonate-silicate fillers as components of dispersive paints, *Pigment Resin Technol.*, 30, 348-356.
- KRYSZTAFKIEWICZ A., JESIONOWSKI T., 2001, Wpływ krzemianów cynku na eliminację aktywatorów z wulkanizatów gumowych, *Prace Naukowe Katedry Budowy Maszyn Politechniki Śląskiej*, 1, 91-96.
- JESIONOWSKI T., KRYSZTAFKIEWICZ A., 2001, Porównanie wpływu różnych czynników modyfikujących na parametry fizykochemiczne wysoko zdyspergowanych proszków, *Zeszyty Naukowe Politechniki Śląskiej, seria Chemia*, 142, 85-94.
- JESIONOWSKI T., KRYSZTAFKIEWICZ A., ŻURAWSKA J., 2001, Surface properties and chemical modification of hydrated silicas, *Chemia ANNALES*, LVI, 66-79.
- WERNER R., KRYSZTAFKIEWICZ A., DEC A., JESIONOWSKI T., 2001, Effect of surface modification on physicochemical properties of precipitated sodium-aluminium silicate used as a pigment in acrylic paints, *Dyes Pigments*, 50, 41-54.
- JESIONOWSKI T., ŻURAWSKA J., KRYSZTAFKIEWICZ A., 2002, Surface properties and dispersion behaviour of precipitated silicas, *J. Mater. Sci.*, 37, 1621-1633.
- ŻURAWSKA J., KRYSZTAFKIEWICZ A., JESIONOWSKI T., 2002, Studies on precipitation of highly dispersed silica from sodium metasilicate-sodium hydrogencarbonate system, *J. Chem. Technol. Biot.*, 77, 917-924.
- JESIONOWSKI T., KRYSZTAFKIEWICZ A., 2002, Preparation of the hydrophilic/hydrophobic silica particles, *Colloids Surf. A*, 207, 49-58.
- DOMKA L., JESIONOWSKI T., MORAWSKA A., KOZAK M., 2002, Influence of pyridinium chlorides on the physicochemical character, morphology and particle size distribution of natural chalk, *Tenside Surf. Det.*, 39, 33-39.
- KRYSZTAFKIEWICZ A., BINKOWSKI S., JESIONOWSKI T., 2002, Adsorption of dyes on a silica surface, *Appl. Surf. Sci.*, 199, 31-39.
- WIECZOREK M., KRYSZTAFKIEWICZ A., JESIONOWSKI T., 2002, Charakterystyka bentonitów – potencjalnych ekologicznych adsorbentów i wypełniaczy, *Chemia i Inżynieria Ekologiczna*, 9, 667-672.
- JESIONOWSKI T., KRYSZTAFKIEWICZ A., DEC A., 2002, Modified Al<sub>2</sub>O<sub>3</sub>-treated titanium whites as pigments of acrylic paints, *Physicochem. Problems Mineral Proc.*, 36, 307-316.
- GRODZKA J., KRYSZTAFKIEWICZ A., JESIONOWSKI T., 2002, Carbonate-silicate fillers modified with two types of proadhesive compounds, *Physicochem. Problems Mineral Proc.*, 36, 89-99.
- JESIONOWSKI T., KRYSZTAFKIEWICZ A., DEC A., 2002, Modified titanium white covered by Al<sub>2</sub>O<sub>3</sub> and SiO<sub>2</sub> – characteristics and application in acrylic paints, *Pigment Resin Technol.*, 31, 290-296.
- JESIONOWSKI T., ŻURAWSKA J., KRYSZTAFKIEWICZ A., POKORA M., WASZAK D., TYLUS W., 2003, Physicochemical and morphological properties of hydrated silicas precipitated following alkoxy silane surface modification, *Appl. Surf. Sci.*, 205, 212-224.
- MICHALSKA I., KRYSZTAFKIEWICZ A., BOGACKI M.B., JESIONOWSKI T., 2003, Preparation and characterization of precipitated zinc silicate, *J. Chem. Technol. Biot.*, 78, 452-460.
- ŻURAWSKA J., KRYSZTAFKIEWICZ A., JESIONOWSKI T., 2003, Active silicas obtained in processes of precipitation from solutions of sodium metasilicate and ammonium chloride, *J. Chem. Technol. Biot.*, 78, 534-541.
- JESIONOWSKI T., POKORA M., TYLUS W., DEC A., KRYSZTAFKIEWICZ A., 2003, Effect of N-2-(aminoethyl)-3-aminopropyltrimethoxysilane surface modification and C.I. Acid Red 18 dye adsorption on physicochemical properties of silicas precipitated in an emulsion route, used as a pigment and filler in acrylic paints, *Dyes Pigments*, 57, 29-41.
- WIECZOREK M., KRYSZTAFKIEWICZ A., JESIONOWSKI T., 2003, Comparative characteristics of local and foreign bentonites, *Macromol. Symp.*, 194, 345-350.
- KLAPISZEWSKA B., KRYSZTAFKIEWICZ A., JESIONOWSKI T., 2003, Highly dispersed green silicate and oxide

- pigments precipitated from model systems of postgalvanic waste, *Environ. Sci. Technol.*, 37, 4811-4818.
- ŻURAWSKA J., KRYSZTAFKIEWICZ A., JESIONOWSKI T., 2003, Effect of ammonium salts on dispersive and adsorptive parameters of silicas precipitated from sodium metasilicate solution, *Colloids Surf. A*, 223, 201-214.
- JESIONOWSKI T., KRYSZTAFKIEWICZ A., SKRZYPCZAK A., 2003, Influence of quaternary ammonium chlorides on dispersion of silica and on morphological properties of its surface, *Tenside Surf. Det.*, 40, 155-161.
- KRYSZTAFKIEWICZ A., JESIONOWSKI T., 2003, Układy hybrydowe krzemionka – barwnik organiczny: otrzymywanie i zastosowanie, *Przem. Chem.*, 82, 844-846.
- ŻURAWSKA J., KRYSZTAFKIEWICZ A., JESIONOWSKI T., 2003, Rola związków amonu w procesie kształtowania nanometrycznych cząstek krzemionek, *Przem. Chem.*, 82, 878-881.
- ŻURAWSKA J., KRYSZTAFKIEWICZ A., JESIONOWSKI T., 2003, Physicochemical properties, surface morphology and particle size distribution of precipitated silicas, *Surf. Interface Anal.*, 35, 914-921.
- KRYSZTAFKIEWICZ A., BINKOWSKI S., KACZMAREK A., JESIONOWSKI T., 2003, Properties of amorphous silicas as modified by adsorbed silane coupling agents and organic dyes, *Pigment Resin Technol.*, 32, 149-159.
- ANDRZEJEWSKA A., KRYSZTAFKIEWICZ A., JESIONOWSKI T., 2003, Synthetic silicas – adsorbents of organic dyes, *Polish J. Chem. Technol.*, 5, 29-31.
- KLAPISZEWSKA B., KRYSZTAFKIEWICZ A., JESIONOWSKI T., 2003, Application of reduced chromate solutions for precipitation of silicate pigments, *Polish J. Chem. Technol.*, 5, 31-33.
- GRODZKA J., KRYSZTAFKIEWICZ A., JESIONOWSKI T., PAUKSZTA D., 2003, Carbonate-silicate fillers precipitated from solutions of alkaline silicates and calcium hydroxide using carbon dioxide, *Physicochem. Problems Mineral Proc.*, 37, 123-130.
- WIECZOREK M., JESIONOWSKI T., KRYSZTAFKIEWICZ A., 2003, Influence of organic polymer modification on physicochemical properties of bentonites, *Physicochem. Problems Mineral Proc.*, 37, 131-140.
- WIECZOREK M., KRYSZTAFKIEWICZ A., JESIONOWSKI T., 2004, Influence of modification by N-2-(aminoethyl)-3-aminopropyltrimethoxysilane on physicochemical properties of bentonite, *J. Phys. Chem. Solids*, 65, 447-452.
- ANDRZEJEWSKA A., KRYSZTAFKIEWICZ A., JESIONOWSKI T., 2004, Adsorption of organic dyes on the aminosilane modified TiO<sub>2</sub> surface, *Dyes Pigments*, 62, 121-130.
- KRYSZTAFKIEWICZ A., LIPSKA L.K., CIESIELCZYK F., JESIONOWSKI T., 2004, Amorphous magnesium silicate – synthesis, physicochemical properties and surface morphology, *Adv. Powder Technol.*, 15, 549-565.
- ANDRZEJEWSKA A., KRYSZTAFKIEWICZ A., JESIONOWSKI T., 2004, Influence of solvents during the silica surface modification with 3-aminopropyltriethoxysilane on dispersive characteristics of the obtained products as a filler for plastic and paint systems, *Pigment Resin Technol.*, 33, 142-151.
- CIESIELCZYK F., KRYSZTAFKIEWICZ A., JESIONOWSKI T., 2004, Influence of precipitation parameters on physicochemical properties of magnesium silicate, *Physicochem. Problems Mineral Proc.*, 38, 197-205.
- BŁASZCZAK J., JESIONOWSKI T., KRYSZTAFKIEWICZ A., 2004, Porównanie właściwościdyspersyjnych krzemionek strączanych w środowisku nieorganicznym lub organicznym, *Inżynieria i Aparatura Chemiczna*, 4-5, 17-18.
- ANDRZEJEWSKA A., KRYSZTAFKIEWICZ A., JESIONOWSKI T., 2004, Modified silicas – adsorbents for decontamination of waste solutions from production of organic dyes, *Polish J. Chem. Technol.*, 6, 1-3.
- KLAPISZEWSKA B., KRYSZTAFKIEWICZ A., JESIONOWSKI T., 2004, Utilization of nickel(II) salt-containing industrial waste, *Polish J. Chem. Technol.*, 6, 27-30.
- KRYSZTAFKIEWICZ A., GRODZKA J., BULA K., JESIONOWSKI T., 2004, Wpływ napelnaczy węglanowo-krzemianowych na właściwości fizykomechaniczne wulkanizatów, *Elastomery*, 8, 21-26.
- ANDRZEJEWSKA A., KRYSZTAFKIEWICZ A., JESIONOWSKI T., 2004, Efektywne oczyszczanie roztworów zanieczyszczonych barwnikiem organicznym za pomocą krzemionek modyfikowanych, *Prace Naukowe Akademii Ekonomicznej we Wrocławiu*, 1041, 183-188.
- KLAPISZEWSKA B., KRYSZTAFKIEWICZ A., JESIONOWSKI T., 2004, Możliwości wykorzystania odpadów pogalwanicznych do otrzymywania wysoko zdyspergowanych pigmentów nieorganicznych, *Prace Naukowe*

- Akademii Ekonomicznej we Wrocławiu, 1041, 189-193.
- JAKUCZEK L., ŻUCHOWSKA D., JESIONOWSKI T., KRYSZTAFKIEWICZ A., 2004, Composites based on styrenic thermoplastic elastomer SBS and new type of precipitated silica, *Annals of the Polish Chemical Society*, 3(3), 975-978.
- JESIONOWSKI T., BINKOWSKI S., KRYSZTAFKIEWICZ A., 2005, Adsorption of the selected organic dyes on the functionalized surface of precipitated silica via emulsion route, *Dyes Pigments*, 65, 183-283.
- GRODZKA J., KRYSZTAFKIEWICZ A., JESIONOWSKI T., 2005, Physicochemical and structural evaluation of carbonate-silicate fillers, *Adv. Powder Technol.*, 16, 181-192.
- KLAPISZEWSKA B., KRYSZTAFKIEWICZ A., JESIONOWSKI T., 2005, Nickel(II) silicates and oxides – highly dispersed green pigments, *Pigment Resin Technol.*, 34, 139-147.
- CIESIELCZYK F., KRYSZTAFKIEWICZ A., JESIONOWSKI T., 2005, Influence of surface modification on morphology and physicochemical parameters of synthetic magnesium silicate, *Physicochem. Problems Mineral Proc.*, 39, 155-164.
- KRYSZTAFKIEWICZ A., ŚWIT Z., JESIONOWSKI T., 2005, Evaluation of waste silica precipitated in the process of hydrofluoric acid production from fluosilicic acid, *Physicochem. Problems Mineral Proc.*, 39, 165-176.
- KLAPISZEWSKA B., KRYSZTAFKIEWICZ A., JESIONOWSKI T., 2005, Emulsion systems used to obtain synthetic silicates by highly dispersed pigments, *Physicochem. Problems Mineral Proc.*, 39, 140-148.
- MALEWSKI W., KRYSZTAFKIEWICZ A., JESIONOWSKI T., 2006, Zastosowanie silnie kwaśnego mikroporowatego jonitu Amberlyst®15 w procesie otrzymywania rozcieńczonych roztworów zolu kwasu meta krzemowego, *Przem. Chem.*, 85, 851-853.
- CIESIELCZYK F., KRYSZTAFKIEWICZ A., JESIONOWSKI T., 2006, Syntetyczne krzemiany magnezu modyfikowane organofunkcyjnymi silanami, *Przem. Chem.*, 85, 806-809.
- POKORA M., KRYSZTAFKIEWICZ A., JESIONOWSKI T., CIESIELCZYK F., 2006, Ocena stopnia modyfikacji strąconych krzemionek i krzemianów metodą spektroskopii FT-IR, *Przem. Chem.*, 85, 1349-1352.
- KLAPISZEWSKA B., KRYSZTAFKIEWICZ A., JESIONOWSKI T., 2006, Precipitation methods of coloured silicates and oxides – highly dispersed pigments, *Polish J. Chem. Technol.*, 8, 106-108.
- SIWIŃSKA-STEFAŃSKA K., KRYSZTAFKIEWICZ A., JESIONOWSKI T., 2006, Modification of silica surface using latex emulsions, *Polish J. Chem. Technol.*, 8, 45-47.
- TEPPER B., JESIONOWSKI T., KRYSZTAFKIEWICZ A., 2006, Preparation of spherical silicas in aliphatic hydrocarbons systems, *Polish J. Chem. Technol.*, 8, 48-50.
- ANDRZEJEWSKA A., KRYSZTAFKIEWICZ A., JESIONOWSKI T., 2006, Production of pigments on functionalized silica carriers, *Polish J. Chem. Technol.*, 8, 100-102.
- CIESIELCZYK F., KRYSZTAFKIEWICZ A., JESIONOWSKI T., 2006, Magnesium silicates – potential adsorbents and polymer fillers, *Polish J. Chem. Technol.*, 8, 103-105.
- CIESIELCZYK F., KRYSZTAFKIEWICZ A., JESIONOWSKI T., 2006, Sedimentation and wettability of synthetic magnesium silicates, *Physicochem. Problems Mineral Proc.*, 40, 255-263.
- SIWIŃSKA-STEFAŃSKA K., KRYSZTAFKIEWICZ A., JESIONOWSKI T., 2006, Physicochemical analysis of silicas coated with natural latex milk, *Physicochem. Problems Mineral Proc.*, 40, 275-286.
- MALEWSKI W., KRYSZTAFKIEWICZ A., JESIONOWSKI T., 2006, Preparation of polysilic acid sols by ion exchange method, *Physicochem. Problems Mineral Proc.*, 40, 265-273.
- ANDRZEJEWSKA A., KRYSZTAFKIEWICZ A., JESIONOWSKI T., 2007, Treatment of textile dye wastewater using modified silica, *Dyes Pigments*, 75, 116-124.
- CIESIELCZYK F., KRYSZTAFKIEWICZ A., JESIONOWSKI T., 2007, Physicochemical studies on precipitated magnesium silicates, *J. Mater. Sci.*, 42, 3831-3840.
- CIESIELCZYK F., KRYSZTAFKIEWICZ A., JESIONOWSKI T., 2007, Magnesium silicates – adsorbents of organic compounds, *Appl. Surf. Sci.*, 253, 8435-8442.
- BULA K., JESIONOWSKI T., KRYSZTAFKIEWICZ A., JANIK J., 2007, The effect of filler surface modification and processing conditions on distribution behaviour of silica nanofillers in polyesters, *Colloid Polym. Sci.*, 285, 1267-1273.

- JESIONOWSKI T., TEPPER B., KRYSZTAFKIEWICZ A., 2007, Characterization of spherical silicas obtained from sodium silicate and hydrochloric acid in emulsion medium using hexane as the organic phase, *Surf. Interface Anal.*, 39, 948-957.
- CIESIELCZYK F., KRYSZTAFKIEWICZ A., JESIONOWSKI T., 2007, Adsorptive properties of synthetic magnesium silicate, *Physicochem. Problems Mineral Proc.*, 41, 185-193.
- TEPPER B., JESIONOWSKI T., KRYSZTAFKIEWICZ A., 2007, Colloidal silicas obtained via co-precipitation method using cyclohexane as an organic phase, *Physicochem. Problems Mineral Proc.*, 41, 195-203.
- SIWIŃSKA-STEFAŃSKA K., KRYSZTAFKIEWICZ A., JESIONOWSKI T., 2007, Modification of hydrophilic/hydrophobic character of TiO<sub>2</sub> surface using selected silane coupling agents, *Physicochem. Problems Mineral Proc.*, 41, 205-214.
- KLAPISZEWSKA B., KRYSZTAFKIEWICZ A., JESIONOWSKI T., 2007, Pigments precipitated from chromate post-galvanic solutions in emulsion systems, *Polish J. Chem. Technol.*, 9(2), 27-29.
- JESIONOWSKI T., TEPPER B., KRYSZTAFKIEWICZ A., 2007, Evaluation of colloidal silica obtained via the co-precipitation method using octane as an organic phase, *Polish J. Chem. Technol.*, 9(4), 1-4.
- JESIONOWSKI T., SIWIŃSKA-STEFAŃSKA K., KRYSZTAFKIEWICZ A., SÓJKA-LEDAKOWICZ J., KOPROWSKA J., LEWARTOWSKA J., 2007, The morphological and dispersive characterization of commercial titanium dioxides, *Polish J. Chem. Technol.*, 9(4), 28-35.
- SÓJKA-LEDAKOWICZ J., KOPROWSKA J., PEĆZKOWSKA B., 2007, Characterization of TiO<sub>2</sub> surface following the modification with silane coupling agents, *Polish J. Chem. Technol.*, 9(4), 72-76.
- SIWIŃSKA-STEFAŃSKA K., WALKOWIAK J., KRYSZTAFKIEWICZ A., JESIONOWSKI T., 2008, Polymer adsorption on the surface of highly dispersed silica, *Appl. Surf. Sci.*, 254, 3591-3600.
- JESIONOWSKI T., ANDRZEJEWSKA A., KRYSZTAFKIEWICZ A., 2008, Adsorption of basic dyes from model aqueous solutions onto novel spherical silica support, *Color Tech.*, 124, 165-172.
- KRYSZTAFKIEWICZ A., KLAPISZEWSKA B., JESIONOWSKI T., 2008, Precipitated green pigments: products of chromate postgalvanic waste utilization, *Environ. Sci. Technol.*, 42(19), 7482-7488.
- SÓJKA-LEDAKOWICZ J., LEWARTOWSKA J., KUDZIN M., JESIONOWSKI T., SIWIŃSKA-STEFAŃSKA K., KRYSZTAFKIEWICZ A., 2008, Modification of textile materials with micro- and nano-structural metal oxides, *Fibres Text. East. Eur.*, 16(5), 112-116.
- KURC B., JESIONOWSKI T., KRYSZTAFKIEWICZ A., 2008, Formation and physicochemical properties of silica fillers precipitated in emulsion medium, *Physicochem. Problems Mineral Proc.*, 42, 67-74.
- SIWIŃSKA-STEFAŃSKA K., KRYSZTAFKIEWICZ A., JESIONOWSKI T., 2008, Effect of inorganic oxides treatment on the titanium dioxide surface properties, *Physicochem. Problems Mineral Proc.*, 42, 141-152.
- BŁASZCZAK J., JESIONOWSKI T., KRYSZTAFKIEWICZ A., 2008, Wpływ charakteru hydrofilowo-hydrofobowego związków powierzchniowo czynnych na właściwości fizykochemiczne krzemionek strączanych, *Chemik*, LXI (10), 499-501.
- KURC B., JESIONOWSKI T., KRYSZTAFKIEWICZ A., 2008, Porównanie właściwości powierzchniowych i dyspersyjnych amorficznych krzemionek strączanych w skali laboratoryjnej i wielkolaboratoryjnej, *Chemik*, LXI (10), 509-511.
- SIWIŃSKA-STEFAŃSKA K., KRYSZTAFKIEWICZ A., JESIONOWSKI T., 2008, Wpływ warunków strącania na właściwości bieli tytanowej, *Chemik*, LXI (10), 523-525.
- JESIONOWSKI T., KRYSZTAFKIEWICZ A., ŻURAWSKA J., BULA K., 2009, Novel precipitated silicas – an active filler of synthetic rubber, *J. Mater. Sci.*, 44, 759-769.
- SIWIŃSKA D., KOŁODZIEJCZAK-RADZIMSKA A., KRYSZTAFKIEWICZ A., JESIONOWSKI T., 2009, Adsorption of octylamine on titanium dioxide, *Appl. Surf. Sci.*, 255, 7337-7342.
- SÓJKA-LEDAKOWICZ J., LEWARTOWSKA J., GAJDZICKI B., KUDZIN M., JESIONOWSKI T., SIWIŃSKA-STEFAŃSKA K., KRYSZTAFKIEWICZ A., 2009, Functionalization of textile materials by alkoxy-silane-grafted titanium dioxide, *J. Mater. Sci.*, 44, 759-769.
- JESIONOWSKI T., KURC B., KRYSZTAFKIEWICZ A., 2009, Otrzymywanie pigmentów na nośnikach krzemionkowych strączanych w układach emulsyjnych w środowisku oktanu, *Przem. Chem.*, 88(7), 838-844.

- CIESIELCZYK F., KRYSZTAFKIEWICZ A., JESIONOWSKI T., MODRZEJEWSKA-SIKORSKA A., 2009, Porównanie właściwości fizykochemicznych i użytkowych talku oraz syntetycznych kompozytów tlenkowych MgO-SiO<sub>2</sub>, *Przem. Chem.*, 88(8), 930-933.
- MALEWSKI W., KRYSZTAFKIEWICZ A., JESIONOWSKI T., 2009, Wpływ metod otrzymywania roztworów polikrzemianu litu na ich strukturę i charakterystykę dyspersyjną, *Przem. Chem.*, 88(8), 924-928.
- SIWIŃSKA-STEFAŃSKA K., KRYSZTAFKIEWICZ A., JESIONOWSKI T., 2009, Kompozyty tlenkowe TiO<sub>2</sub>-SiO<sub>2</sub> impregnowane emulsjami lateksu kauczuku naturalnego, *Przem. Chem.*, 88(9), 1037-1044.
- KOŁODZIEJCZAK-RADZIMSKA A., JESIONOWSKI T., KRYSZTAFKIEWICZ A., 2010, Obtaining zinc oxide from aqueous solutions of KOH and Zn(CH<sub>3</sub>COO)<sub>2</sub>, *Physicochem. Problems Mineral Proc.*, 44, 93-102.
- MALEWSKI W., JESIONOWSKI T., CIESIELCZYK F., KRYSZTAFKIEWICZ A., 2010, Dispersion characterization of colloidal silica at subsequent stages of silica preparation, *Physicochem. Problems Mineral Proc.*, 44, 143-150.
- MODRZEJEWSKA-SIKORSKA A., JESIONOWSKI T., CIESIELCZYK F., KRYSZTAFKIEWICZ A., 2010, Synthesis and characterization of precipitated copper(II) silicate, *Physicochem. Problems Mineral Proc.*, 44, 157-168.
- SIWIŃSKA-STEFAŃSKA K., KRYSZTAFKIEWICZ A., CIESIELCZYK F., PAUKSZTA D., SÓJKA-LEDAKOWICZ J., JESIONOWSKI T., 2010, Physicochemical and structural properties of TiO<sub>2</sub> precipitated in an emulsion system, *Physicochem. Problems Mineral Proc.*, 44, 231-244.
- JESIONOWSKI T., CIESIELCZYK F., KRYSZTAFKIEWICZ A., 2010, Influence of selected alkoxysilanes on dispersive properties and surface chemistry of spherical silica precipitated in emulsion media, *Mater. Chem. Phys.*, 119, 65-74.

Teofil Jesionowski, Poznań, January 31, 2010

Our books are available in Tech bookstore  
plac Grunwaldzki 13  
50-377 Wrocław, D-1 PWr., tel. (071) 320 32 52  
Orders can also be sent by post

ISSN 1643-1049

**Physicochemical Problems of Mineral Processing, 46 (2011)**